VNIVERSITAT DE VALÈNCIA

Escola Tècnica Superior d'Enginyeria

Ph.D Thesis

Doctoral Program in Chemical, Environmental and Process Engineering

Microalgae-bacteria consortia for urban wastewater treatment

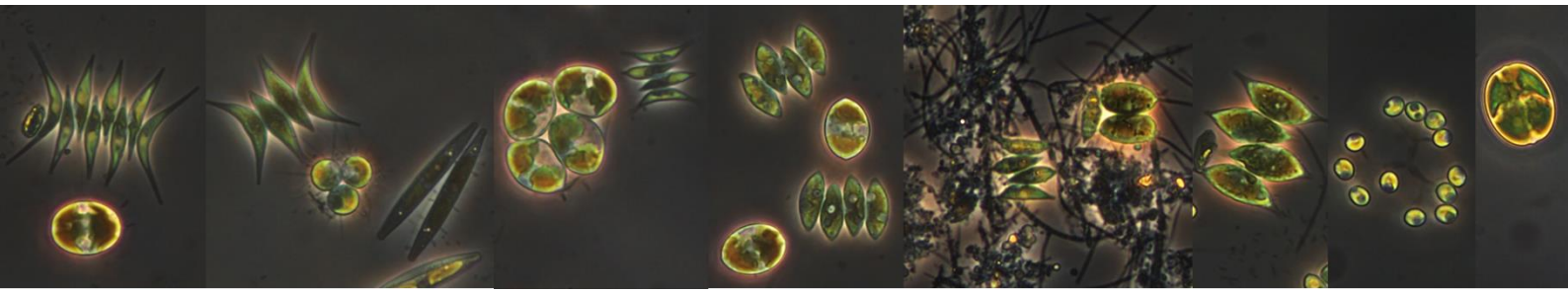

Stéphanie Aparicio Antón

December 2021

Supervisors:

Dr. Aurora Seco Torrecillas

Dr. Luis Borrás Falomir

Dña. AURORA SECO TORRECILLAS, catedrática del Departament d'Enginyeria Química de la Universitat de València, y

D. LUIS BORRÁS FALOMIR, profesor titular del Departament d'Enginyeria Química de la Universitat de València

CERTIFICAN:

que la presente memoria, titulada "**MICROALGAE-BACTERIA CONSORTIA FOR URBAN WASTEWATER TREATMENT**", corresponde al trabajo realizado bajo su dirección por **Dña. STÉPHANIE APARICIO ANTÓN**, para supresentación como tesis doctoral en el programa de doctorado en Ingeniería Química, Ambiental y de Procesos de la Universitat de València.

Los artículos presentados en la tesis doctoral no se han utilizado ni se utilizarán en ninguna otra tesis doctoral.

Y para que conste firma/n el presente certificado en Valencia,a 17 de diciembre de 2021

MARIA AURORA\| SECO\| TORRECILLAS Firmado digitalmente por MARIA AURORA\| SECO\|TORRECILLAS Fecha: 2021.12.17 16:49:33 +01'00'

Fdo. Aurora Seco Torrrecillas

LUIS\| BORRAS\| FALOMIR Firmado digitalmente por LUIS\|BORRAS\| FALOMIR Fecha: 2021.12.17 16:15:31 +01'00'

Fdo. Luis Borrás Falomir

Acknowledgements

Después de tantos años y tanto trabajo, ha llegado, por fin, el momento de cerrar una etapa. Pese que, en la portada ponga mi nombre, esta tesis tiene muchos más autores, por ello quiero utilizar este espacio para dar las gracias a todas las personas, que, de algún modo u otro, me han ayudado y apoyado. No obstante, los que me conocen saben que tengo ciertas rarezas y que nunca pierdo ocasión para expresarlas, y esta vez no va a ser una excepción.

Empiezo, obviamente, por los artífices directos de este trabajo, mis directores. Sólo me conocía de ser su alumna de máster, de ser mi profesora en la asignatura de tratamiento de aguas, y, aun así, confió en mí y me ofreció la oportunidad de empezar mi carrera como investigadora. Parecerá una tontería, pero son estas pequeñas decisiones las que te cambian la vida. Y aunque en la primera cena oficial del grupo llegué tarde y en la segunda me presente con un jersey navideño feo con luces, siempre me ha ayudado y apoyado. Por las reuniones, en las que de repente todos los datos cobraban sentido y por brindarme esta oportunidad, Aurora, muchísimas gracias.

A Luis, sin embargo, lo conocía de antes, de cuando las modas capilares eran más “rebeldes”. Te escogí para hacer el trabajo final de máster, te escogí para ser mi director de tesis, y volvería a escogerte una y mil veces. Gracias por ser siempre tan positivo y empujarme hacia delante, incluso cuando pensaba que era imposible que llegase a tiempo a depositar. He aprendido muchas cosas junto a ti. La microbiología para mí era una gran desconocida, y gracias a ti poco a poco, voy entendiéndola. Espero poder seguir aprendiendo contigo.

Siguiendo dentro del grupo hay dos personitas a las que les debo muchísimo también, Josué y Ángel. Aunque al principio del todo, prácticamente ni me hablaba, Josué es la persona de la que más he aprendido y no sólo a nivel técnico sino también a nivel de vida. El primer día que llegué a la depuradora y me encontré con la planta piloto, con el cuadro eléctrico, con aparatejos que ni sabía que existían, quería llorar, estaba

completamente aterrorizada. Josué fuiste mi gran maestro y contigo me di cuenta de que todo es posible incluso la imposible. Rememorando nuestros grandes momentos en planta me vienen dos. El primero, el día en que tú abriste una válvula del reactor, yo abrí otra, y cuando nos dimos cuenta el reactor estaba prácticamente vacío. No nos dijimos nada, nos sentamos delante de la planta y nos quedamos fijamente mirando el reactor. El segundo, el día que dije que era buena idea cambiar de membranas un viernes, creo que me sigues odiando por ello.

A Ángel en realidad, lo conocí de rebote, un gran sabio me dijo: “acércate a Ángel que es el que más publica”, y así lo hice. Tuve la gran suerte de que nuestros campos de investigación confluyeran en las algas, y así poder “aprovecharme” de esa cabeza aguda y gran saber. Entre los caminitos del despacho al coche (a las nueve de la noche) y la comida de cabeza para que entrase en los YWP, pude conocerte un poco más y que descubriera que eres un friki de Marvel y DC, como yo. Aunque tengas un gusto pésimo por las películas (te parece buena la de la Liga de la Justicia), muchísimas gracias por toda tu ayuda y todo tu apoyo.

Hay muchas más personas en el grupo, pero si les dedico a cada una de ellas un párrafo, esto acabaría siendo un capítulo más de la tesis, así que muchas gracias a todos mis compañeros (Miguel, Guille, Juan, Jesús, Nuria, Berta, Eladio, Dani, Óscar, Rebecca, Pau, Antonio Patri e Ivana) y a todos mis superiores, que de una manera u otra me habéis ayudado y enseñado (Jose, María, Joaquín, Ramón, Daniel, Alberto, Vicky, Nuria, Juan, Ana y Josep). Si me he dejado a alguien, lo siento, mis neuronas no son lo que eran.

Hay una personita, a la que no he nombrado, pero ella se merece una mención especial. Adri, mi compañera del “chemita”. Has sido uno de mis grandes apoyos tanto en el trabajo como fuera de él. Lo que ha unido el “chemita” que no lo separe el hombre.

Y si bien he tenido mucho apoyo dentro del trabajo, fuera, en la vida “real” también.

Mis dos apoyos incondicionales, Úrsula y Jose. Ese viaje a Madrid fue para mí un antes y un después. Desde entonces, sois mis confidentes más absolutos. Si este último año he conseguido centrarme en la tesis, ha sido gracias a vosotros. Gracias por demostrarme que de verdad hay personas por las que vale la pena derretirse. Me queréis y aceptáis sin pretender cambiarme. Gracias por recordarme quien soy.

Isabel, dentro de ese gran caos que a veces eres, me has demostrado en muchos momentos, que eres un gran apoyo y que siempre podré contar contigo. Gracias por confiar en mí y nunca darme la espalda.

Ana, a ti te conocí en un mal momento, pero después de tres años aquí seguimos. Sólo te diré una cosa. Creo que sí que estás completamente loca, pero te cuento un secreto entre nosotras, las mejoras personas lo están. Gracias, por abrirme las puertas a un nuevo mundo, el mundo del “Forma Sport”, donde he conocido personas tan maravillosas como, Rocío, Vanesa, Álex, Jesús e Ismael.

Hay una personita, que apareció en mi vida, hará menos de un año, que se dedica a hacerme sufrir seis días a la semana, y que, si no llega a ser por él, no habría mantenido mi salud física y mental. Alejandro, muchas gracias por tu motivación, por confiar en que puedo hacer águilas con cinco kilos y por dedicarme esas palabras tan bonitas, que de vez en cuando me dices. Por primera vez en años, estoy empezando a ser mi mejor versión.

Y como mi vida está con quien amo más, cierro estos larguísimos agradecimientos con mi “Ohana”. Mi madre y mi hermana son las que han sufrido directamente todos mis momentos críticos, mi mal humor y mis malas contestaciones. No, obstante, siempre han estado ahí, para recogerme y levantarme, para distraerme, para apoyarme y para que nunca me sintiera sola. Gracias por aguantarme, os quiero.

Gracias a mi padre por siempre confiar en mis aptitudes. A mi tatie preferida por ser siempre la niña de sus ojos. A los nenes por siempre pensar que podía con esto y más.

A mi tío Iván por burlarse de mí. Y a mi mamie y mi papi por recordarme que yo puedo con todo.

Cierro, con mi chico gordito que se ha pasado las horas muertas a mi lado mientras estudiaba y trabajaba. Gizmo, por mucho que vueles lejos de aquí, seguirás siempre junto a mí.

Al inicio de los agradecimientos, he comentado que tengo ciertas rarezas y que no iba a perder la oportunidad de plasmarlas aquí. Pues bien, ahí va, en los agradecimientos he ido colando frases de películas que han marcado mi vida. Eternamente agradecida.

ABSTRACT

Microalgae-bacteria consortia appears as an ideal option within the framework of sustainable technologies for wastewater treatment. Pollutants removal mechanisms result from direct and/or indirect ecological interactions between microalgae and indigenous wastewater bacteria. Effectively designed systems that incorporate microalgae-bacteria consortia require an understanding of ecological interactions between microalgae and bacteria within wastewater treatment processes.

The main objective of this research work is therefore study and explore the ecological interactions to improve microalgae-bacteria based-wastewater treatment. This thesis addresses from the operation of an outdoor membrane high rate algal pond (MHRAP) pilot plant to the development of a mathematical model that reproduces the ecological interactions observed experimentally. The common thread between the different chapters of the thesis is specifically the interaction between microalgae and nitrifying bacteria.

The feasibility of wastewater treatment by microalgae-bacteria consortium was assessed at the MHRAP pilot plant by varying the hydraulic retention time (HRT) and the incoming wastewater stream. Both HRT and wastewater stream influenced the relationship between microalgae and nitrifying bacteria. Negative interactions, such as nitrite inhibition of photosynthesis and competitive interactions, were observed. The influence of nitrite on photosynthesis was then studied under laboratory conditions. Nitrite effectively had an inhibitory effect on the light-dependent phase of photosynthesis. Kinetic expression which reproduces nitrite inhibition was proposed and validated.

Competitive processes reduce the potential of microalgae and bacteria consortia to recover nutrients from wastewater, therefore, a guide to identify and reduce these negative interactions was developed.

Additionally, microbial ecology of five operational periods of the MHRAP pilot plant was evaluated. Massive sequencing of 16S/18S rDNA biomarkers have been applied to identify the main bacteria and microalgae communities and to detect the influence on operational and environmental parameters on bioreactor microbiology. *Coelastrella* and *Desmodesmus* were the dominant genera of microalgae, while *Verrucomicrobiota* and *Proteobacteria* were the dominant bacterial phylum in the five operating periods.

All the knowledge gathered during the development of this thesis was used to develop a mathematical model, which faithfully reproduces the main interactions between microalgae and bacteria. As the literature review revealed, the metabolism of microalgae cannot be considered a well-characterized process, since some parameters of the mathematical models are uncertain and speciation-dependent. Thus, the more influential factors on microalgae kinetics and the uncertainty of the model outputs were analyzed by a global sensitivity analysis and an uncertainty analysis, respectively. The 34 parameters of the microalgae kinetics model were reduced to 11 influential factors, which should be calibrated for each microalgae culture to reduce model uncertainty. An integral microalgae-bacteria model was developed, which includes crucial physical, chemical and biokinetic processes observed during the thesis development. The model was used to reproduce microalgae and nitrifying bacteria interactions that occur in an outdoor membrane photobioreactor (MPBR) pilot plant. Moreover, nitrification control strategies were also simulated to improve both microalgae activity and nutrient recovery rates.

RESUMEN

Los consorcios de microalgas y bacterias surgen como una opción idónea en el marco de las tecnologías sostenibles para el tratamiento de aguas residuales. Los mecanismos de eliminación de contaminantes son el resultado de interacciones ecológicas directas y/o indirectas entre las microalgas y las bacterias autóctonas de las aguas residuales. Para diseñar sistemas eficaces que incorporen consorcios de microalgas y bacterias es necesario comprender las interacciones ecológicas entre ambas comunidades dentro de los procesos de tratamiento de aguas residuales.

El objetivo principal de este trabajo de investigación es, por tanto, estudiar y explorar las interacciones ecológicas para mejorar el tratamiento de aguas residuales basado en el consorcio de microalgas y bacterias. Esta tesis aborda desde el funcionamiento de un raceway acoplado a un sistema de membranas (MHRAP), hasta el desarrollo de un modelo matemático que reproduce las interacciones ecológicas observadas experimentalmente. El hilo conductor entre los diferentes capítulos de la tesis es concretamente, la interacción entre las microalgas y las bacterias nitrificantes.

Se evaluó la viabilidad del tratamiento de aguas residuales mediante un consorcio de microalgas y bacterias en la planta piloto MHRAP, variando el tiempo de retención hidráulico (TRH) y la corriente de agua residual a tratar. Tanto el TRH como la corriente de agua residual influyeron en la relación entre las microalgas y las bacterias nitrificantes. Se observaron procesos competitivos entre ambas comunidades, así como interacciones negativas, como la inhibición de la fotosíntesis debida a los nitritos. A continuación, se estudió la influencia del nitrito en la fotosíntesis en condiciones de laboratorio. El nitrito tuvo efectivamente un efecto inhibidor en la fase lumínica de la fotosíntesis. Se propuso y validó una expresión cinética que reproduce la inhibición de la fotosíntesis por nitritos.

Los procesos competitivos reducen el potencial de los consorcios de microalgas y bacterias para eliminar nutrientes del agua residual, por lo que se desarrolló una guía para identificar y reducir estas interacciones negativas.

Por otro lado, se evaluó la ecología microbiana de cinco períodos operativos de la planta piloto MHRAP. Se ha aplicado la secuenciación masiva de los biomarcadores 16S/18S rDNA para identificar las principales comunidades de bacterias y de microalgas, además de esclarecer la influencia de los parámetros operativos y ambientales en la microbiología del biorreactor. *Coelastrella* y *Desmodesmus* fueron los géneros de microalgas dominantes, mientras que *Verrucomicrobiota* y *Proteobacteria* fueron los filos bacterianos dominantes en los cinco periodos operativos.

Todos los conocimientos recopilados durante el desarrollo de la tesis se utilizaron para desarrollar un modelo matemático capaz de reproducir las principales interacciones entre las microalgas y las bacterias. Como resultado de la revisión bibliográfica, se observó que el metabolismo de las microalgas no puede considerarse un proceso bien caracterizado, ya que algunos parámetros de los modelos matemáticos, ya publicados, son inciertos y dependen del tipo de microalga. Por ello, se realizó un análisis de sensibilidad global de los factores más influyentes de la cinética de las microalgas y un análisis de incertidumbre de los resultados del modelo matemático. Los 34 parámetros de las cinéticas de las microalgas se redujeron a 11 factores influyentes, los cuales se recomienda calibrar para cada cultivo de microalgas, con el objetivo de reducir la incertidumbre del modelo. Se desarrolló un modelo integral de microalgas y bacterias, que incluye procesos físicos, químicos y biocinéticos cruciales observados durante el desarrollo de la tesis. El modelo se utilizó para reproducir las interacciones entre las microalgas y las bacterias nitrificantes que se producen en una planta piloto de fotobiorreactores de membrana (MPBR). Además, también se simularon estrategias de control de la nitrificación para mejorar tanto la actividad de las microalgas como la tasa de recuperación de nutrientes.

RESUM

Els consorcis de microalgues i bacteris sorgeixen com una opció idònia en el marc de les tecnologies sostenibles per al tractament d'aigües residuals. Els mecanismes d'eliminació de contaminants són el resultat d'interaccions ecològiques directes i/o indirectes entre les microalgues i els bacteris autòctons de les aigües residuals. Per a dissenyar sistemes eficaços que incorporen consorcis de microalgues i bacteris és necessari comprendre les interaccions ecològiques entre totes dues comunitats dins dels processos de tractament d'aigües residuals.

L'objectiu principal d'aquest treball de recerca és, per tant, estudiar i explorar les interaccions ecològiques per a millorar el tractament d'aigües residuals basat en el consorci de microalgues i bacteris. Aquesta tesi aborda des del funcionament d'un raceway acoblat a un sistema de membranes (MHRAP), fins al desenvolupament d'un model matemàtic que reprodueix les interaccions ecològiques observades experimentalment. El fil conductor entre els diferents capítols de la tesi és concretament, la interacció entre les microalgues i els bacteris nitrificants.

Es va avaluar la viabilitat del tractament d'aigües residuals mitjançant un consorci de microalgues i bacteris en la planta pilot MHRAP, variant el temps de retenció hidràulic (TRH) i el corrent d'aigua residual a tractar. Tant el TRH com el corrent d'aigua residual van influir en la relació entre les microalgues i els bacteris nitrificants, encara que l'activitat nitrificant va ser deguda majoritàriament a les microalgues. Es van observar processos competitius entre totes dues poblacions, així com interaccions negatives, com la inhibició de la fotosíntesi deguda als nitrits. A continuació, es va estudiar la influència del nitrit en la fotosíntesi en condicions de laboratori. El nitrit va tindre efectivament un efecte inhibidor en la fase lumínica de la fotosíntesi. Es va proposar i validar una expressió cinètica que reprodueix la inhibició de la fotosíntesi per nitrits.

Els processos competitius redueixen el potencial dels consorcis de microalgues i bacteris per a eliminar nutrients de l'aigua residual, per la qual cosa es va desenvolupar una guia per a identificar i reduir aquestes interaccions negatives.

D'altra banda, es va avaluar l'ecologia microbiana de cinc períodes operatius de la planta pilot MHRAP. S'ha aplicat la seqüenciació massiva dels biomarcadors 16S/18S rDNA per a identificar les principals comunitats de bacteris i de microalgues, a més d'esclarir la influència dels paràmetres operatius i ambientals en la microbiologia del bioreactor. *Coelastrella* i *Desmodesmus* van ser els gèneres de microalgues dominants, mentre que *Verrucomicrobiota* i *Proteobacteria* van ser els talls bacterians dominants en els cinc períodes operatius.

Tots els coneixements recopilats durant la realització de la tesi es van utilitzar per a desenvolupar un model matemàtic capaç de reproduir les principals interaccions entre les microalgues i els bacteris. Com a resultat de la revisió bibliogràfica, es va observar que el metabolisme de les microalgues no pot considerar-se un procés ben caracteritzat, ja que alguns paràmetres dels models matemàtics, ja publicats, són incerts i depenen del tipus de microalga. Per això, es va realitzar un anàlisi de sensibilitat global dels factors més influents de la cinètica de les microalgues i un anàlisi d'incertesa dels resultats del model matemàtic. Els 34 paràmetres de les cinètiques de les microalgues es van reduir a 11 factors influents, els quals es recomana calibrar per a cada cultiu de microalgues, amb l'objectiu de reduir la incertesa del model. Es va desenvolupar un model integral de microalgues i bacteris, que inclou processos físics, químics i biocinètics crucials observats durant la realització de la tesi. El model es va utilitzar per a reproduir les interaccions entre les microalgues i els bacteris nitrificants que es produeixen en una planta pilot amb fotobiorreactors de membrana (MPBR). A més, també es van simular estratègies de control de la nitrificació per a millorar tant l'activitat de les microalgues com la recuperació de nutrients.

Table of contents

CHAPTER I

1. INTRODUCTION

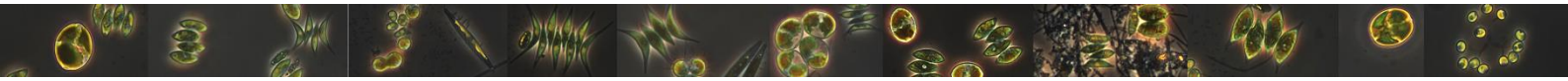

1. INTRODUCTION

1.1. WASTEWATER TREATMENT

The rise in world population has demanded an increase in water resources, and consequently large volumes of wastewater are produced and discharged into the aquatic environment (Choudhary et al., 2020). Although natural aquatic ecosystems have the self-purification capacity, some of wastewater pollutant can get into natural biochemical cycles and negatively impact the receiving environment (Preisner, 2020). High organic-pollutant loads or organic enrichment can deplete the dissolved oxygen (DO) form water ecosystems, thus reducing both species richness and biological diversity. In addition, emission of nutrients, such as nitrogen and/or phosphorus can cause a nutrient over-enrichment in the water body, commonly referred to as eutrophication. The most notable effect of eutrophication is the proliferation of opportunistic photosynthetic organism (adapted to the new environmental conditions), inducing changes in the structure and functioning of all biological communities. These proliferations, or blooms, produce large amounts of biomass. Their degradation by aerobic bacteria results in an oxygen depletion (hypoxia or anoxia) in the aquatic ecosystem and emission of toxic gasses, reducing water quality (Le Moal et al., 2019). The wastewater treatment has had a significant role in reducing the discharge of pollutants into the natural aquatic ecosystem (Cooper et al., 2020). In this respect, in conventional wastewater treatment plants (WWTPs), a primary treatment is used to physically remove wastewater particulate pollutants, followed by an aerobic biological treatment (the so-called secondary treatment) to degrade organic pollutants form wastewater and a tertiary treatment to disinfect water. Some WWTPs also incorporate chemical and biological processes to remove nitrogen and phosphorus from wastewater, decreasing eutrophication potential (Rahman et al., 2016).

Nowadays, conventional urban WWTPs are highly effective in terms of human health and pollutant removal, but a high energy input is required (Rahman et al., 2016) and

nutrients are not recovered (Acién et al., 2016). Wastewater treatment therefore appears as a key sector where the circular economy concept can be applied to address the urgency for more sustainable technologies (Puyol et al., 2017). Within the circular economy concept, wastewater is considered a source of resources rather than waste (Sfez et al., 2019).

Conventional nutrient removal technologies in WWTPs spend approximately 50% of their energy demand in aeration system (Foley et al., 2010), implying a global warming potential of 0.6−0.9 kg CO_2 eq. per m^3 (Rahman et al., 2016). From these technologies, nitrogen is released to the atmosphere (Meng et al., 2016) and phosphorus is lost within the sludge as a metal salt, which avoids its possible reuse (Szabó et al., 2008). Nitrogen and phosphorus contained in wastewater can account for approximately 20% of the manufactured nutrients (Puyol et al., 2017). Nutrient recovery from wastewater is therefore of great interest nowadays, especially as agriculture faces a phosphorus-scarce future (Solovchenko et al., 2016), and because nitrogen production as ammonia is energy-intensive (Matassa et al., 2015). Emerging water resource recovery facilities (WRRFs) focus not only on wastewater treatment per se, but also on the recovery of nutrients and energy (Seco et al., 2018). In this respect, microalgae-based wastewater treatments have been receiving increasing interest from the scientific community since they are able to recover nutrient with low energy consumption (Acién et al., 2016; González-Camejo et al., 2021; Guldhe et al., 2017).

1.2. MICROALGAE

The definition of microalgae covers unicellular and simple multicellular microorganism, including eukaryotic microalgae and prokaryotic cyanobacteria (Zhang et al., 2020). Eukaryotic microalgae contain membrane-bounded organelles such as chloroplast, mitochondria, vacuoles, Golgi body and a nucleus that contains the genetic material. Prokaryotic cyanobacteria lack an organized nucleus and membrane-bound organelles, but they contain *Chlorophyll a* (*Chl a*) and high protein content. In this thesis, the word

“microalgae” will be used to describe eukaryotic microalgae. Taxonomic classification of microalgae is based on their light-harvesting photosynthetic pigments: *Chlorophyta* (green algae), *Rhodophyta* (red algae), *Chrysophyta* (golden algae) and *Phaeophyceae* (brown algae) (Masojıdek et al., 2003). Microalgae can bee also classified according to their metabolism. Generally, microalgae are photoautotrophic organisms, i.e. they use inorganic carbon source, such as carbon dioxide (CO_2), and light as energy source. However, microalgae can also be photoheterotrophic, i.e. they use organic carbon and light as carbon and energy source, respectively, or even heterotrophic and, therefore, energy and carbon sources are provided from organic compounds. Depending on the substrate availability and light conditions, microalgae can combine both autotrophic and heterotrophic metabolisms, commonly referred to as mixotrophic metabolism (Pang et al., 2019). However, heterotrophic and mixotrophic metabolisms are restricted to few microalgae and, therefore, the most common pathway is the photoautotrophic metabolism (Perez-Garcia et al., 2011; Shandilya and Pattarkine, 2019). Nutrient recovery ability and photo-oxygenation through photosynthesis (avoiding the need for external aeration (Foladori et al., 2018)) has sparked scientific interest in microalgae biotechnology, with a 20-fold increase in the number of publications since 2005 (Garrido-Cardenas et al., 2018).

1.2.1. Microalgae metabolism

This section focuses on describing the processes of photosynthesis and nutrient assimilation pathways, specifically nitrogen and phosphorus.

1.2.1.1. Photosynthesis

Photosynthesis is the only energy conversion process of sunlight. In this process, inorganic compounds and light energy are transformed into organic matter by microalgae (Figure I. 1). Oxygenic photosynthesis comprises a series of redox reaction driven by light energy, in which carbon dioxide and water are converted to organic compounds and oxygen.

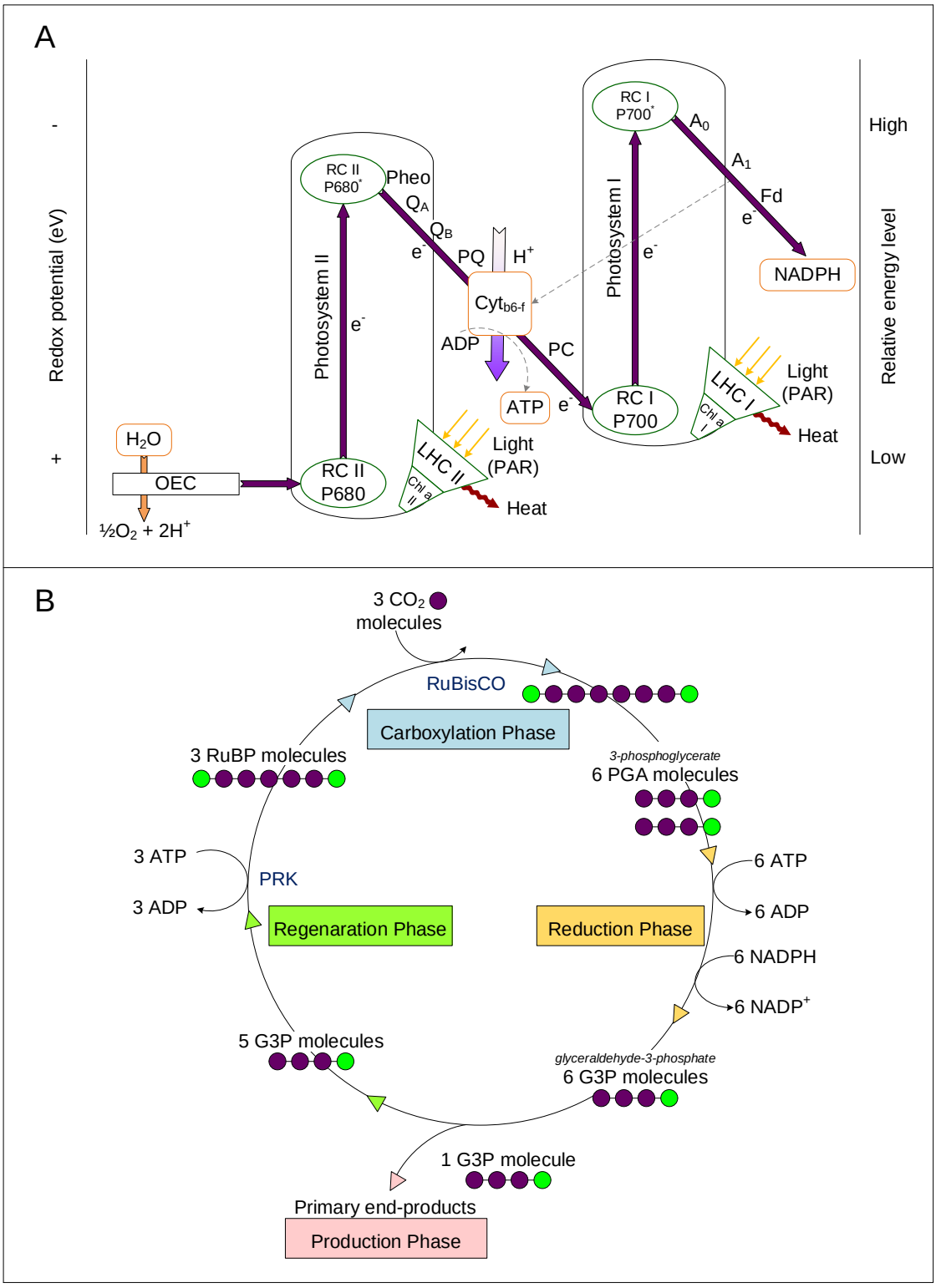

Figure I. 1. Simplified and adapted Z-scheme of the photosynthetic electron transport chain (A) and Calvin Cycle (B). Abbreviations: OEC, oxygen-evolving complex; RC, reaction center; Q_A, PSII primary quinone acceptor; Q_B, PSII secondary quinone acceptor; cyt_{b6f}, complex cytochrome b6f; LHC II, light-harvesting complex of PS II; LHC I, light-harvesting complex of PS I; *Chl a* II, *Chlorophyll a* of PS II; and *Chl a* I, *Chlorophyll a* of PS I; RuBisCO, ribulose bisphosphate carboxylase/oxygenase; RuBP, ribulose 1,5-bisphosphate; PGA, 3-phosphoglycerate; G3P, glyceraldehyde-3-phosphate; and PRK, phosphoribulokinase.

It is traditionally divided into two stages, the so-called light-dependent reactions (Figure I. 1A) and light-independent reactions or dark reactions (Figure I. 1B) (Masojıdek et al., 2003). In the light-dependent reactions, the light energy is converted into chemical energy by providing a biochemical reductant, nicotinamide-adenine dinucleotide phosphate reduced (NADPH), and an energy compound, adenosine triphosphate (ATP) (Reynolds, 2006). The photosynthetic light-dependent reactions are located in the thylakoid membranes (Masojıdek et al., 2003). In the thylakoid membranes are contained five major complexes: light-harvesting antennae, photosystem II (PS II), photosystem I (PS I), cytochrome b_6f (cyt_{b6-f}) and ATP synthase.

The main function of the antenna system is light-harvesting and energy transfer to photosynthetic reaction centers of PS II and PS I where it is utilized for photochemistry. The light harvested corresponds to wavelength range of 400-750 nm, which is called photosynthetically active radiation (PAR) (Masojıdek et al., 2003). All photosynthetically pigments (*chlorophylls*, *carotenoids* and *phycobilins*) are associated with proteins. The light-harvesting pigment-protein complexes are accommodated within structures known as light harvesting complexes (LHC) and are these which act as antennae in harvesting incoming photons (Reynolds, 2006). One group of LHC serves PS II (LHC II), and a genetically and biochemically distinct group is associated with PS I (LHC I) (Reynolds, 2006). LCH II and LHC I contain *Chl a*, *Chlorophyll b* (*Chl b*) and carotenoids (Masojıdek et al., 2003).

The PS II complex can be divided into three major functional units: the PS II core complex, surrounded by the LHC II and the oxygen-evolving complex (OEC). The core complex contains six polypeptides and four *Chl a* molecules, two of which form the reaction center. These two molecules of *Chl a* have an absorption maximum of 680 nm and are known as P_{680}. The PS I is a pigment-containing protein complex than can also be divided into a core complex and LHC I. The reaction center contains two chlorophyll molecules, which have an absorption maximum of 700 (P_{700}) (Wayne, 2019).

It is at P_{680} that PS II reactions are initiated, when the complex is exposed to PAR. Light energy is absorbed by LHC II and is passed to P_{680} by resonance transfer (Wayne, 2019). Once light is absorbed by P_{680}, the energy of an electron raises a P_{680} from its ground-states to its oxidated-states orbital (P_{680}^{+}) and that energy is then passed to pheophytin (usually referred to as Pheo) acceptor molecule (Wayne, 2019). The electron is passed from Pheo to a further bound form of plastoquinone known as Q_A, and then to a freely diffusing form of plastoquinone Q_B (Reynolds, 2006; Wayne, 2019). After accepting two electrons, plastoquinone Q_B binds two protons (H^+) from the stroma and passes the electron to the $cyt_{b6\text{-}f}$ complex. The P_{680}^{+} becomes a stronger oxidizing agent and an electron is extracted from water, leading to the formation of H^+ in the lumen and the evolution of ½ oxygen (O_2) (Wayne, 2019). The P_{680}^{+} is reduced by action of manganese ions, via a redox-active tyrosine (Reynolds, 2006). Until the P_{680}^{+} molecule is re-reduced, the reaction centre is "closed", i.e. the reaction centre is unable to accept further electrons. It remains so until Q_A is reoxidized. The electron is serially transported toward PS I. Once it has accepted two electrons, the $cyt_{b6\text{-}f}$ complex oxidizes the reduced plastoquinone (PQH_2) and reduces the plastocyanin oxidized. Plastocyanin (PC), located in the thylakoid lumen, carries the electrons to P_{700} (Masojıdek et al., 2003; Reynolds, 2006).

Light is also absorbed by LHC I where the energy is passed by resonance transfer in a random manner to P_{700} (Wayne, 2019). Once it reaches P_{700}, an electron is raised to a higher energy level and it is passed through a series of carriers (usually denoted A) to ferredoxin, resulting in its reduction (Masojıdek et al., 2003; Reynolds, 2006). The oxidized P_{700} (P_{700}^{+}) can take an electron from PC. The last electron carrying enzyme, ferredoxin-$NADP^+$ oxidoreductase, is able to reduce $NADP^+$ to NADPH by the oxidation of two ferredoxin molecules and a H^+ from the stroma. The NADPH formation thus causes an alkalinization of the stroma and contributes to the electrochemical gradient across the thylakoid membrane (Wayne, 2019).

The electron transport chain described is usually visualized in a so-called “Z-scheme” (Figure I. 1A). In this scheme, the redox components are represented by their midpoint equilibrium potentials and the electron transport reactions proceed energetically downward from a lower to a higher redox potential (Trebst, 1974).

In the electron transport process, an electrochemical gradient of H^+ is produced across the thylakoid membrane. The energy made available by gradient is used for the synthesis of ATP from adenosine diphosphate (ADP) and inorganic phosphate (P_i) (Wayne, 2019) in a process called photophosphorylation. Photosynthetic phosphorylation proceeds by mainly two alternative electron-transport pathway: non-cyclic and cyclic electron transport. The Z-scheme (Figure I. 1A) explains both non-cyclic and cyclic reactions. Cyclic phosphorylation involves only PS I. In contrast, non-cyclic phosphorylation requires both photosystems, PS II and PS I, which are linked in series. This linkage produces net oxidation of an electron donor (i.e. of water to oxygen) and reduction of $NADP^+$ to NADPH as described above, while cyclic phosphorylation produces only ATP. Allen (2003) described that photosynthetic organisms used both; the interplay between pathways could meet different metabolic demands for ATP. However, the description of photosynthesis and phosphorylation are usually linked to the non-cyclic electron transport chain. Three molecules of ATP and two molecules of NADPH produced in the non-cyclic electron transport chain (light-dependent reactions) are used to fix carbon dioxide into simple organic compounds in the stroma. The subsequent reactions of carbon dioxide fixation are not directly dependent upon light and can be synthesized as follows (Reaction I. 1):

$$CO_2 + 4H^+ + 4e^- \xrightarrow{2\ NADPH+3ATP} \underbrace{(CH_2O)}_{\text{simple organic compound}} + H_2O \qquad \text{Reaction I. 1}$$

Fixation of carbon dioxide is carried out by a cyclic series of reactions called the Calvin cycle (Figure I. 1B). There are four major phases in the Calvin Cycle: Carboxylation, Reduction, Production and Regeneration Phases (Masojıdek et al., 2003). The initial

incorporation of carbon dioxide (carboxylation phase) is catalyzed by the enzyme ribulose bisphosphate carboxylase/oxygenase, usually called RuBisCO. In this phase, carbon dioxide is added to five-carbon compound, ribulose 1,5-bisphosphate (RuBP) to form two molecules of 3-phosphoglycerate (PGA). Energy and reducing power from ATP and NADPH, respectively, are used to reduce PGA to glyceraldehyde-3-phosphate (G3P) in the reduction phase. Energy of ATP is also needed in the Regeneration Phase to regenerate original five-carbon compound, RuBP from further carbon dioxide fixations in a complex series of reactions combining 3-, 4-, 5-, 6- and 7-carbon sugar phosphates and by the action of the enzyme phosphoribulokinase (PRK). Primary end-products of photosynthesis are considered simples molecules of glucids, but amino acids and organic acids can be also synthetized in the Production Phase (Masojıdek et al., 2003). Three rounds of the Calvin Cycle lead to fixation of 3 CO_2 molecules and production of one G3P molecule, which can be converted into glucose and other primary end-products (Wang and Lan, 2010)

Photosynthesis comprises both light-dependent and –independent reactions, which can be summarized in a simple reaction (Reaction I. 2):

$$H_2O + CO_2 + \text{photons} \rightarrow {}^{1}/_{6}\,(C_6H_{12}O_6) + O_2 \qquad \text{Reaction I. 2}$$

1.2.1.2. Nutrient assimilation

Nitrogen is a constituent of amino acids and, therefore, of all proteins from which they are synthesized. Intracellular nitrogen accounts for no less than 3% of dry weight. However, nitrogen content can rise to about 7.0-8.5% in nitrogen-replete microalgal cells (Reynolds, 2006). A wide variety of nitrogen compounds of different oxidation states are available in wastewater and used by microalgae: ammonium (NH_4-N), nitrite (NO_2-N) and nitrate (NO_3-N) nitrogen, and organic nitrogen forms as urea can also be considered (Eustance et al., 2013; Larsdotter, 2006). NH_4-N is considered to be the preferred form of nitrogen for microalgae because its assimilation and incorporation is energetically more efficient (Barbera et al., 2018; Eustance et al., 2013). Transport across the cell

membrane of NH_4-N and NO_3-N/NO_2-N are performed by ammonium and nitrate/nitrite transporter proteins (AMTs and NRTs, respectively) (Rogato et al., 2015).

Nitrogen pathways in microalgae are summarized in Figure I. 3. After translocated across the cell membrane, NH_4-N can directly be incorporated into amino acids required for metabolic functions. In contrast, NO_3-N and NO_2-N must be reduced to NH_4-N. NO_3-N is reduced stepwisely to NO_2-N in the cytoplasmic matrix by nitrate reductase (NR) (Collos and Berges, 2009) and to NH_4-N by the enzyme Fd-dependent nitrite reductase (NiR) in chloroplast (Collos and Berges, 2009; Eustance et al., 2013). Both enzymatic reactions require reducing power, NADPH, as the electron donor (Raven and Giordano, 2016).

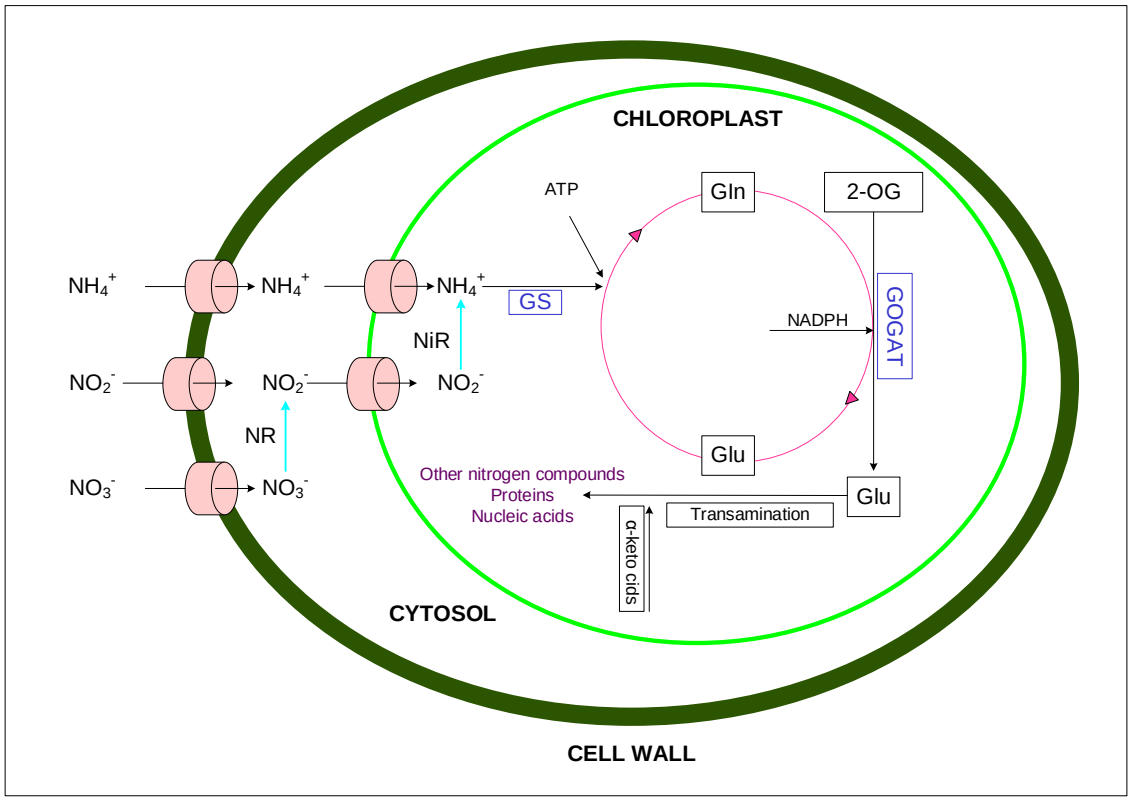

Figure I. 2. Nitrogen pathways in microalgae. Abbreviations: NR, nitrate reductase; NiR, nitrite reductase; GS, glutamine synthetase; GOGAT, glutamine 2-oxoglutarate amino transferase; Glu, glutamate; Gln, glutamie; and 2-OG, 2-oxoglutarate.

The assimilation of inorganic nitrogen in microalgae is interconnected with carbon metabolism, requiring carbon skeletons to incorporate nitrogen into organic compounds (Falkowski and Raven, 2007). The integration of NH_4-N as the primary nitrogen donor molecule (either derived from NO_2-N reduction in chloroplast or direct uptake from culture broth) is catalyzed by the sequential action of the enzymes glutamine synthetase (GS)

and glutamine 2-oxoglutarate amino transferase (GOGAT) (Eustance et al., 2013). GS fixes NH_4-N on a glutamate (Glu) molecule to produce glutamine (Gln) and the added amino group can then act as a nitrogen-donor to 2-oxoglutarate (2-OG) in NADPH-dependent conversion, to produce two combinations of Glu catalyzed by GOGAT (Inokuchi et al., 2002). One of these two molecules is recycled back by GS, and the other is at the base of amino acids formation by transamination of the amino nitrogen of glutamate to some α-keto acids (Eustance et al., 2013).

Concerning urea ($CO(NH_2)_2$), once inside the cytoplasmic matrix, the molecule is splited to ammonia/ammonium and assimilated. The carbon moiety (carbon dioxide) is released to the extracellular medium, or sometimes used as a carbon source (Collos and Berges, 2009).

Phosphorus is an essential element for innumerable metabolic pathways and structural component of nucleotides, phospholipids and ATP. Phosphorus content is generally close to 1-1.2% of dry weight. However, microalgae can accumulate phosphorus in excess of their metabolic needs and store it as acid-insoluble polyphosphate (Poly-P) granules, which can be used for cell growth when external phosphorus concentration becomes limiting (Powell et al., 2009; Ruiz-Martinez et al., 2014; Ruiz-Martínez et al., 2015). Intracellular phosphorus can therefore rise in some species to >3% of dry weight (Reynolds, 2006). This storage process is widely termed “luxury uptake” (Powell et al., 2009; Ruiz et al., 2013).

Inorganic phosphorus in wastewater is present in several ionic states, which are pH-dependent (H_3PO_4, pH < 2.15; $H_2PO_4^-$, pH from 2.15 to 7.20; HPO_4^{2-}, pH from 7.20 to 12.33; and PO_4^{3-}, pH >12.33) (Shen et al., 2015). Inorganic phosphorus (P_I, including $H_2PO_4^-$, HPO_4^{2-} and PO_4^{3-}) is generally considered the most bioavailable form of phosphorus source, and microalgae preferentially assimilate $H_2PO_4^-$ and HPO_4^{2-}. Phosphorus pathways in microalgae are summarized in Figure I. 3. Multiple P_I transporters located in the plasma membrane are involved in P_I uptake. The forms and

abundance of P_I transporters are regulated by P_I availability and concentration: low-rate but high-affinity P_I transporters are predominant under P-deplete conditions and high-rate but low-affinity P_I transporters accumulate under P-replete conditions (Su, 2021).

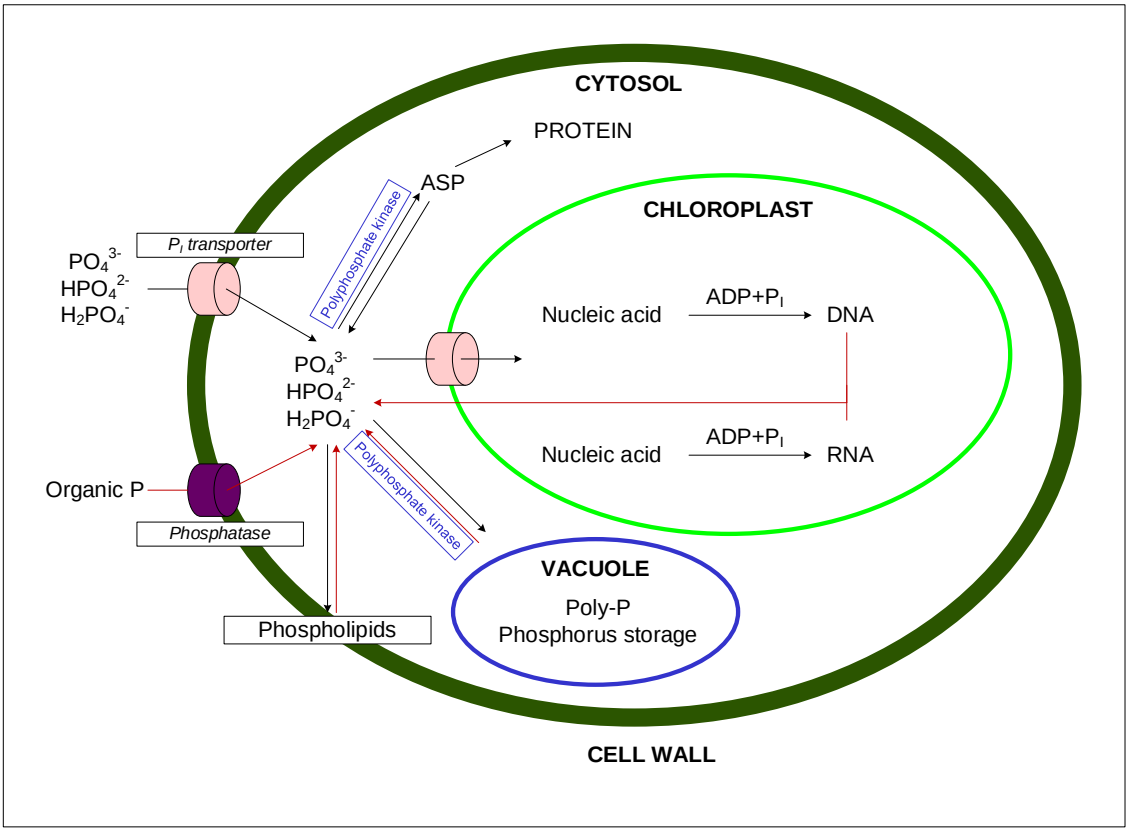

Figure I. 3. Phosphorus pathways in microalgae. Black and red lines under P_I-replete and –deplete conditions, respectively.

Phosphorus transfer from the enveloping boundary layer into cell membrane is performed by an active transport through a symporter channel (i.e. two substances are transported in the same direction across the membrane) with H^+ or Na^+ ions providing the driving force, set by a plasma membrane H^+-ATPase pump (Falkowski and Raven, 2007). Phosphorus organic compounds are also a source of bioavailable phosphorus, which are accessible through the expression of extracellular membrane-bound as well as free phosphatases, which hydrolyze bound PO_4^{3-} groups (Borowitzka et al., 2016). Acid-soluble polyphosphate and Poly-P are synthesized by polyphosphate kinase (also called ATP-polyphosphate) to transfer P_I from ATP to elongate polyphosphate (ATP + $(phosphate)_n \leftrightarrow$ ADP + $(phosphate)_n$. ASP is used for deoxyribonucleic acid (DNA) and

protein synthesis during photosynthesis process. Ribonucleic acid (RNA) and phospholipids are synthesized from cellular P_I after being obtained from the extracellular P source. The transfer of phosphate to RNA is a light-inhibited process. The excess phosphorus can be accumulated and stored as Poly-P in vacuoles. Microalgae synthesize several low P_I-regulated phosphatases to utilize external organic phosphorus in response to phosphorus deprivation. Different strategies for phosphorus saving and recycling are adopted by microalgae under conditions of phosphorus-deplete conditions. For instance, the breakage of compounds as DNA, RNA and phospholipids releases phosphorus that can be reused in processes such as phosphorylation.

Restated, microalgal metabolism processes are a promising and suitable approach to simultaneously realize wastewater treatment and nitrogen and phosphorus recovery, without the need for external aeration. However, in real systems, microalgae-based wastewater treatments are performed not only by microalgae cultures but by microalgae-bacteria consortia (Acién et al., 2016; González-Camejo et al., 2020a). Microalgal-bacterial biotechnology is envisioned as a preferably sustainable and commercially feasible option as compared to those based on individual microorganisms (Subashchandrabose et al., 2011).

1.3. MICROALGAE-BACTERIA CONSORTIA

Microalgal-bacterial processes have demonstrated to be an effective option for wastewater treatment (Foladori et al., 2018; Mantovani et al., 2020; Rada-Ariza et al., 2017; Robles et al., 2020). This is achieved through direct and/or indirect ecological interactions between microalgae and indigenous wastewater bacteria. Effectively designed systems that incorporate microalgae-bacteria consortia require an understanding of ecological interactions between microalgae and bacteria within wastewater treatment processes.

Ecological interactions between microalgae and bacteria cover a wide range of relationship from mutualism/commensalism to competition/amensalism (Zhang et al., 2020). Substrate exchange constitutes the basis of mutualistic relationship. In a simplified scheme, microalgae produce oxygen through photosynthesis that aerobic bacteria can use as an electron acceptor to oxidize biodegradable organic matter, and the carbon dioxide released during bacterial mineralization is readily available for photosynthesis. The interdependence of substrates/metabolites promotes faster growth of microalgae and bacteria, provides robustness to oscillations of abiotic conditions (environmental and operational parameters), minimizes invasion by other microorganisms and improves overall nutrient uptake. Mutualism is not only restricted to a self- sustaining oxygen-carbon dioxide gas exchange. Microalgae can also supply organic carbon compounds to mutualistic bacteria, and bacteria in return, supply dissolved inorganic carbon along with low molecular organic carbon for microalgal consumption (Cho et al., 2015; González-Camejo et al., 2020).

Commensalism is an ecological relationship in which only one-partner benefits unlike mutualism. However, a thin line separates commensalism, mutualism, competition and amensalism. In most cases of commensalism, mutualism, competition and amensalism the thin line, which not only delimits but also determines these relationships, are the abiotic boundary factors (Hu et al., 2010; Valiente-Banuet and Verdú, 2008). Interrelationship between microalgae and ammonia-oxidizing bacteria (AOB) can be favorable or unfavorable for both communities according to abiotic parameters. Under high pH values (commonly associated to photosynthetic processes), high temperatures (due to weather and climatic conditions) and high total ammoniacal nitrogen (i.e. sum of ammonia and ammonium) the equilibrium reaction between free ammonia nitrogen (FAN) and NH_4-N shift towards FAN, which is a strong inhibitor of microalgae (Rossi et al., 2020). In these specific conditions, photo-oxygenation would support nitrification, i.e NH_4-N oxidation to NO_2-N and NO_3-N, results in a decrease of FAN concentrations and its inherent inhibitory pressure on microalgae metabolism (mutualism). However, under

these same conditions, NO_2-N accumulation due to inhibition of nitrite-oxidizing bacteria (NOB) has been widely observed (González-Camejo et al., 2020b; Kim et al., 2008, 2006; Philips et al., 2002; Sui et al., 2016; Yang et al., 2003). NO_2-N can inhibit microalgal metabolism (González-Camejo et al., 2020b), and interaction between partners and therefore, it would be amensalistic. The third interaction is competition for NH_4-N between microalgae and AOB, resulting in a slower growth of the outcompeted-partner. Eventually, after several generations, the better competitor outlive the existence of the outcompeted-partner in the system. In an NH_4-N-limited system, temperature and light intensity play a key role on microalgae-AOB competition. Temperatures above 30°C and light intensities below 40 $\mu mol \cdot m^{-2} \cdot s^{-1}$ negatively affected microalgal metabolism, resulting in a competitive displacement of microalgae by AOB (González-Camejo et al., 2018; González-Camejo et al., 2019a). In non-limiting ammonium systems and suitable abiotic boundary conditions (i.e. light, temperature, pH suitable for biomass growth and low FAN concentrations), microalgae can supply oxygen for nitrification, so that only AOB can benefit from these interactions (commensalism). Although under specific conditions some interactions between partners can be considered as commensalism, this relationship is not usually in the forefront in microalgae-bacteria interactions. Mutualism, competition and amensalism are the main interactions in microalgae-bacteria consortia and may change between them depending on abiotic conditions, as illustrated through the microalgae and AOB example. These interactions are therefore a continuous and non-discrete interface (Ramanan et al., 2016).

A suitable biological community, able to remove pollutants from wastewater and to recover nutrients through different biological mechanisms, can develop resulting from all the possible interactions involved in a microalgae-bacteria consortium and abiotic conditions.

1.3.1. Microalgae-bacteria consortia for wastewater treatment

Wastewater treatments based on microalgae-bacteria consortia have emerged as a sustainable option due to the biomass's ability to remove organic pollutants and recover nutrients (Acién et al., 2016). Organic matter, total nitrogen and total phosphorus removal efficiencies range from 84-87%, 87-98% and 57-99%, respectively, depending on abiotic boundary conditions (Foladori et al., 2018; Posadas et al., 2015; Toledo-Cervantes et al., 2019). The use of microalgae-bacteria systems allows recovering up to 90% of the nutrients contained in wastewater (Acién et al., 2018; Posadas et al., 2015). Data from Aqualia, Europe's third largest wastewater treatment company, indicate that average energy consumption of reactor operation in systems based on microalgae-bacteria and conventional wastewater treatment plant (WWTP) is 0.030 and 0.49 kWh/m^{-3}, respectively, resulting in an energy consumption reduction of 94% (Acién et al., 2016). Advantages described are principally centered on suitable microalgae-bacteria consortium growth conditions. Microalgae-bacteria consortium can remove wastewater pollutants by multiple pathways due to the complex interactions.

1.3.1.1. Nutrient and organic matter removal mechanisms

Knowledge of the removal mechanisms involved in microalgae-bacteria interaction can help in the design of wastewater treatment systems.

Ammonium removal from wastewater

The main biological removal pathways using microalgae-bacteria consortia are nitrification, NH_4-N uptake by biomass and FAN stripping (González-Fernández et al., 2011). Coupled activity of AOB and NOB oxidizes NH_4-N to NO_2-N and then to NO_3-N according the Reaction I. 3Reaction I. 4.

$$2NH_4^+ + 3O_2 \rightarrow 2NO_2^- + 2H_2O + 4H^+$$ Reaction I. 3

$$2NO_2^- + O_2 \rightarrow 2NO_3^- + 2H_2O + 4H^+$$ Reaction I. 4

Nitrification consumes almost 4.6 mg of dissolved oxygen per mg NH_4-N oxidized. Both Bankston et al. (2020) and Karya et al. (2013) found that microalgal photosynthesis support full nitrification of ammonium without mechanical aeration. Kwon et al. (2019) reported that the amount of electricity consumption associated with mixing and aeration was reduced by 57-99% in co-cultures of enriched microalgae and nitrifying bacteria compared to activated sludge-only cultures.

Besides nitrification, NH_4-N assimilation is also a key mechanism during nitrogen removal (Posadas et al., 2015; Toledo-Cervantes et al., 2019). Bankston et al. (2020) showed that NH_4-N removal by biomass assimilation was almost 2 times higher than that removed by nitrification. Indeed, presence of activated sludge induced higher nitrogen content in biomass. Therefore, aside from a higher growth rate of biomass, it may lead to faster ammonium uptake in microalgae-bacteria consortium compared to those of isolates microalgae cultures. Sepehri et al. (2020) showed that the consortium of nitrifying bacteria with microalgae *Chlorella vulgaris* led to the maximum NH_4-N removal rate, mainly due to the oxygen supplied by the microalgae. In this study, microalgae played a minor and supported nitrification.

Due to the uptake of inorganic carbon by autotrophic organism, pH of the culture medium increases. Indeed, pH values close to 9 have been frequently recorded (Foladori et al., 2018; González-Fernández et al., 2011; Posadas et al., 2015). Alkalinity conditions combined with high temperatures that can be reached in outdoor systems contribute to enhance FAN stripping ($\mathrm{NH_3 + H^+ \leftrightarrow NH_4^+}$; pK_a = 9.25). Abiotic removal by stripping can result in a loss of up to 40% of the ammonium present in the wastewater (González-Fernández et al., 2011).

Nitrite/Nitrate removal from wastewater

NO_2-N and NO_3-N contamination of aquatic ecosystem results in a drop in environmental quality (eutrophication). In addition, nitrite can induce inhibition of microalgae and most bacteria activity (Ciji and Akhtar, 2020; González-Camejo et al., 2020b; Philips et al.,

2002). Biological pathways are considered the most suitable and promising approaches for oxidized nitrogen removal. NO_2-N and NO_3-N removal is achieved either by assimilation pathway fueling the growth of biomass, or by the dissimilation pathway in which NO_2-N and NO_3-N is reduced to nitrogen gas (N_2) via denitrification (Ashadullah et al., 2021; Boelee et al., 2014; Toledo-Cervantes et al., 2019).

Assimilatory nitrite/nitrate removal involves the reduction of oxidized nitrogen to ammonium for cell synthesis and it is independent of the DO concentration (Krapp et al., 2014). Heterotrophic bacteria degrade organic matter to drive nitrite/nitrate reduction. Autotrophic bacteria need a significant amount of energy to reduce both NO_2-N/NO_3-N and inorganic carbon for cell synthesis, resulting in a low rate of autotrophic biomass production and thus a low NO_2-N/NO_3-N removal rate (Fallahi et al., 2021). Oxidized forms of nitrogen can also be consumed by microalgae (Section 1.2.1.2), using photosynthesis to power reductive processes. Unlike autotrophic bacteria, microalgae can contain 5-10% (Reynolds, 2006) intracellular nitrogen, resulting in high removal rate.

Denitrification is a process in which NO_2-N/NO_3-N is used as the final electron acceptor (instead of DO) for oxidation of organic matter. Denitrification occurs mainly in anoxic conditions. Nitrite/nitrate reductions proceeds through the Reaction I. 5.

$$NO_3^- \rightarrow NO_2^- \rightarrow NO \rightarrow N_2O \rightarrow N_2$$ Reaction I. 5

Denitrification occurs under anoxic conditions. However, microalgal photosynthesis produces oxygen promoting aerobic conditions, which can inhibit activity of nitrate reductase enzyme (Rezvani et al., 2019). Petrovič and Simonič (2015) reported that denitrification process in presence of microalgae was slower than without them, but still more than 95 % of the NO_3-N was removed in 24 h. Microalgae respiration can lead to even greater DO depletion under night or dark conditions compared to isolate bacterial processes (Holmes et al., 2020), promoting low-oxygen conditions needed for denitrification. With this framework, nitrification occurs under light conditions (sunlight or

artificial light) when DO levels are high due to photo-oxygenation of the culture medium, and denitrification occurs at night or under dark conditions when DO has been consumed by biomass respiration. Coupled nitrification-denitrification process can be regulated in sequence batch reactor. For instance, denitrifying bacteria were strongly mutualistic with *Scenedesmus sp*. and *Chlorella sp*., achieving 100% removal of oxidized nitrogen at dark conditions (Zhang et al., 2020). Operating parameters can be modified to promote coupled nitrification-denitrification process in microalgae-bacteria consortia. Van Den Hende et al. (2016) achieved a nitrification-denitrification cycle coupled to daytime and nighttime hours in an outdoor microalgal bacterial floc raceway pond.

In microalga-bacteria consortia, the coupled nitrification-denitrification process requires careful culture management to control the DO concentration.

Phosphate removal from wastewater

Soluble reactive phosphorus (orthophosphate, PO_4-P) is the most available fraction of phosphorus for microalgae assimilation (Patel et al., 2012). Microalgae-bacteria consortia remove PO_4-P from wastewater through assimilation and abiotic processes including precipitation (Larsdotter et al., 2010) and adsorption both to the surface of cells and the bioreactor (Martínez et al., 2000). In addition to the assimilation of essential phosphorus for biomass growth, both microalgae and heterotrophic bacteria, called polyphosphate-accumulating organisms (PAO), can uptake large amounts of PO_4-P and store it as Poly-P (Barat et al., 2008; Ruiz-Martínez et al., 2015). Ji et al. (2020) observed an effective mutualistic relationship between microalgae and PAO, which resulted in 86% of PO_4-P removed, and more than 70% of phosphorus could potentially be recovered as Poly-P.

Phosphate can also be removed from wastewater through precipitation with calcium and magnesium at alkaline pH (Barat et al., 2010, 2008), and through surface adsorption by hydrogen bonds formation with extracellular polysaccharides secreted (EPS) by microalgae and bacteria (Li et al., 2013). Organic phosphorus is hydrolyzed to PO_4-P by

extracellular enzymes secreted by bacteria and then assimilated (Li et al., 2013). Similar to phosphate, organic phosphorus can combine with EPS and adsorb on the biomass and reactor wall (Lu et al., 2016). Overall, phosphorus removal pathways of microalgae-bacteria consortium make them a suitable alternative platform for advanced phosphorus removal.

Organic matter removal from wastewater

Chemical and biological oxygen demand (COD and BOD) are used to characterize the degree and type of organic matter pollution by wastewater. Aerobic heterotrophic bacteria use the oxygen produced by microalgae for cellular respiration and organic matter oxidation. The gas exchange between bacteria and microalgae facilitates each other's growth and promotes organic matter removal from wastewater. COD and BOD removal efficiencies in microalgae and bacterial consortia were reported to be over 90% (Anbalagan et al., 2016; Ashadullah et al., 2021; Posadas et al., 2015). Bankston et al. (2020) observed that co-cultivation of microalgae and bacteria was better than bacterial monoculture in removing COD from wastewater.

Figure I. 4 compiles the biological pathways of nitrogen, phosphorus and organic matter removal, described in Section 1.3.1.1.

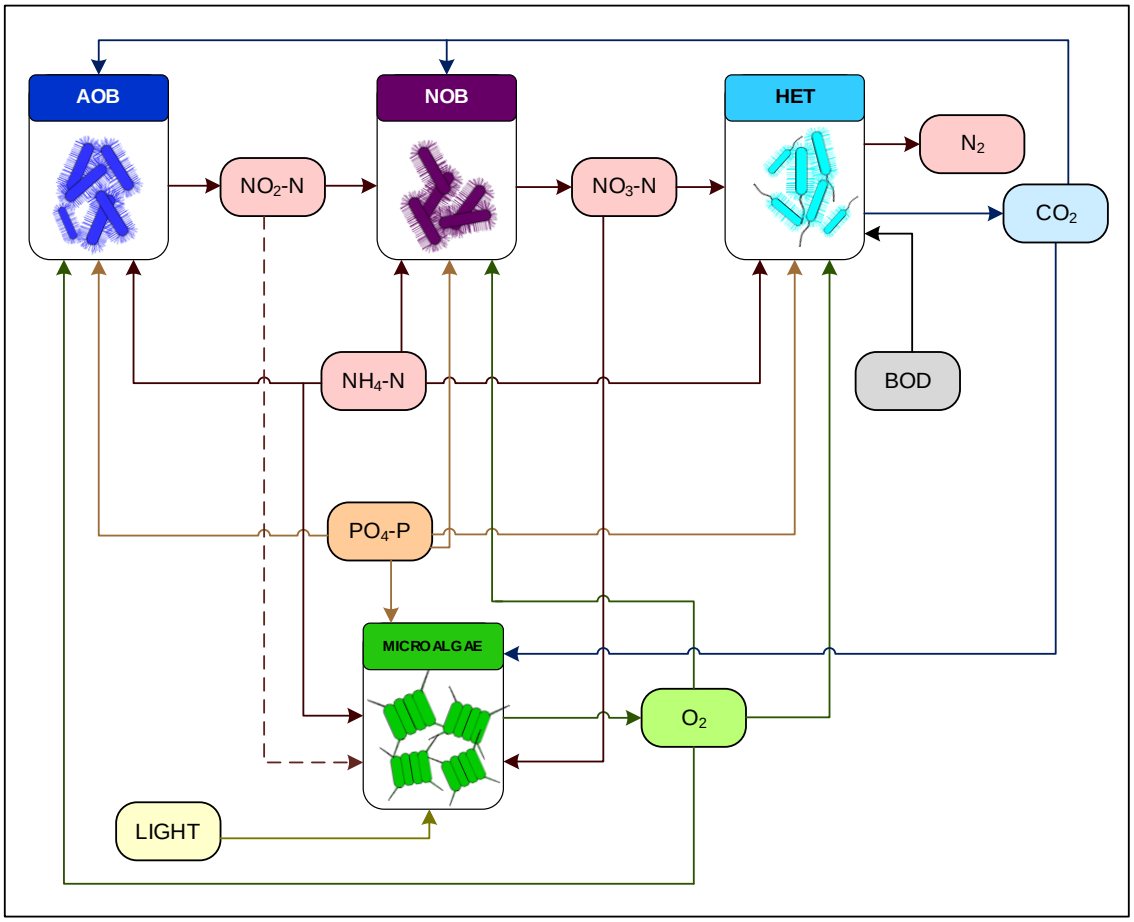

Figure I. 4. Possible interactions between microalgae and bacteria. The dotted straight arrow shows inhibition process.

1.3.1.2. Factors affecting the performance of treatment efficiency

Phototrophic consortia of microalgae and bacteria can certainly be applied to meet European discharge limits for COD, total nitrogen and phosphorus (Directive 98/15/CEE), with the benefits of using natural sunlight and the energy savings of mechanical aeration (Leong et al., 2019). Considering the large-scale outdoor application of microalgae-bacteria technology, optimization of abiotic factors is considered an effective approach to achieve desirable performance in wastewater treatment. Therefore, several key abiotic factors (i.e. environmental and operational parameters), such as light intensity, light period, hydraulic retention time (HRT), biomass retention time (BRT), wastewater composition, etc., are described in the following sections.

Light intensity and photoperiod

Photoautotrophic growth of microalgae is driven by the supply of light (PAR), as this is the energy source used to convert dissolved inorganic carbon (DIC), usually CO_2, into organic carbon (Section 1.2.1.1). Photosynthetic activity is proportional to light intensity until it reaches light saturation point (Reynolds, 2006). However, for light intensities above the saturation point LHCs can be damaged, resulting in the inhibition of photosynthesis, and thus a reduction in photosynthetic efficiency and microalgae growth (photoinhibition process) (Murata et al., 2007; Nishiyama et al., 2006).

Light has emerged as a brand-new operating parameter, due to the biological regulation of the anaerobic/anoxic and aerobic periods under dark and light conditions, respectively, which supports continuous removal of nutrients and organic matter. For instance, through sophisticated illumination management, a novel Phototrophic - Enhanced Biological Phosphorus Removal (Photo-EBPR) system, was developed to achieve superior net PO_4-P removal, during which it was operated for a period of 3 hours of darkness - 4 hours of lighting - 1 hour of idle time (Carvalho et al., 2018). Similarly, by introducing a specific light-dark cycle, denitrification efficiency increased significantly (Jia and Yuan, 2018). Operating at different light intensities also significantly affected the DO concentration in the reactor and the removal efficiencies of wastewater pollutants, specifically nitrogen (Akizuki et al., 2020). However, excessive light irradiance not only can inhibit microalgal photosynthesis but can also engender oxidative stress and damage bacteria. Excessive light irradiance exposure damaged cytochrome-c and enzymes of AOB and NOB, inhibiting the activities of AOB and NOB and further restricting nitrogen elimination (Kwon et al., 2020). Although, both AOB and NOB were photoinhibited, Vergara et al. (2016) suggested a higher light sensitivity of NOB, resulting in partial-nitrification and NO_2-N accumulation.

Outdoor microalgae-bacteria consortium systems are also influenced by light availability of the culture. Reactor depth, sunlight intensity, microalgae biomass and microalgae's pigments increase light attenuation within the culture (Abu-Ghosh et al., 2016; Huang et

al., 2017; Wágner et al., 2018). Light attenuation implies that microalgae and light-sensitive bacteria close to the illuminated surface are exposed to high light intensities and can be photoinhibited (Pires et al., 2017), while biomass deeper in the reactor remain in darkness (Raeisossadati et al., 2019). Only some reactor zones will receive light at the saturation point, attaining microalgal maximum photosynthetic rate. A well-mixed reactor provides a rapid transition of biomass between lighting and dark zones, thus being exposed to an average light irradiance, i.e. total light integration, which depends on reactor depth, culture extinction coefficient and the reactor solids content.

Temperature

Temperature also have a significant impact on microalgae-bacteria consortium (Xu et al., 2021). Optimal temperature of microalgae and bacteria is species specific (Bernard and Rémond, 2012; Grunditz and Dalhammar, 2001). However, similar to light intensity, temperatures below and above the optimal value reduce biomass growth due to lower rate of enzymatic processes and protein degradation, respectively (Ras et al., 2013; Ratkowsky et al., 2005; Van Derlinden et al., 2008).

Overall, microalgae-bacteria consortia can grow at temperatures between 11 to 37 ºC based on the existing scientist sources (García et al., 2000; Godos et al., 2009; Gutzeit et al., 2005; Ji et al., 2021; Posadas et al., 2015; Wang et al., 2021). Operating temperature can also affect interaction between microalgae and bacteria. González-Camejo et al. (2019) AOB outcompeted microalgae at 30-35ºC, while temperatures below 30 ºC favored microalgae activity over AOB activity. In addition, temperature affects other parameters related to biomass growth, as gas solubility (oxygen, carbon dioxide, FAN, etc.) and equilibrium of chemical species (Solimeno et al., 2015). Although temperature is a parameter that has a strong impact on the activity of microalgae and bacteria, it cannot be controlled. Since temperature control for such high volumes would be economically unfeasible. It is therefore recommended to operate open systems that favor evaporation, reducing excessive temperature rise.

pH

Daily assessment of culture pH can be used to monitor photosynthetic activity (González-Camejo et al., 2020b). Value of pH of 7-9 is the growing range of most of microalgae and indigenous wastewater bacteria (Moheimani, 2013; Nwoba et al., 2019; Park et al., 2007; Saravanan et al., 2021). The CO_2 concentration supplied acidifies the culture pH. However, pH values increase due to the absorption of CO_2 as a source of inorganic carbon for photosynthesis (Section 1.2.1.1). This is especially relevant in reactors operated in outdoor conditions, since the pH can increase above values of 9 during peaks of maximum solar irradiance (Acién et al., 2016). High pH values negatively affect microalgae and bacterial activity. Barceló-Villalobos et al. (2019) reported that pH has a negative effect on the electron transport chain between PS II to PS I at values above 8. Value of pH above 8.2 can also inhibit nitrifying activity, as NOB are more sensitive to alkaline pH, leading to NO_2-N accumulation (Park et al., 2007), which is a potential inhibitor of microalgae (González-Camejo et al., 2020b). Increasing pH also affects the availability of nitrogen and phosphorus in the culture for biomass (Ruiz-Martínez, 2015). Values of pH above 9 favor FAN in the ammonium-ammonia equilibrium ($\mathrm{NH_3 + H^+ \leftrightarrow NH_4^+}$; pK_a = 9.25). This is not convenient since FAN can inhibit the photosynthetic process (Rossi et al., 2020) and nitrogen can be removed from the medium by FAN stripping (González-Fernández et al., 2011). Regarding phosphorus, a pH higher than 9 leads to phosphorus precipitation (Barat et al., 2008), which reduces phosphorus bioavailability and decreases light dispersion in microalgae-bacteria consortium (Muñoz and Guieysse, 2006).

Hydraulic and Biomass retention time

HRT is a common operating parameter that can help identify nutrients, organic matter, and light requirements to support microalgae-bacteria communities (Anbalagan et al., 2016). Long HRT enables optimization of operating conditions during cold periods to achieve better nutrient removal (Sutherland et al., 2015). However, during warm periods,

longer HRT can lead to nutrients starvation (Larsdotter, 2006). Similar, BRT is a more assertive operating parameter to control and select biological community that comprises microalgae-bacteria consortia, and thus efficiently regulate nutrient removal. For instance, the biomass of the microalgae-bacteria consortium improved significantly (almost 5 times) when BRT was increased from 0.55 d to 2.5 d, removing 80 and 70% of nitrogen and phosphorus, respectively (Sforza et al., 2018).

Other important factors

Composition of wastewater is another important factor involved in microbial interactions and can influence on the efficiency of wastewater treatment. Wastewater systems based on microalgae-bacteria consortia have been widely used for the treatment of different wastewater streams, such as raw urban wastewater, primary and secondary effluents, centrate, agricultural and industrial wastewater, etc. (Anbalagan et al., 2016; Godos et al., 2009; Guldhe et al., 2017; Posadas et al., 2015). Each wastewater stream presents different characteristics, such as varying concentrations of nutrients and organic matter, presence of toxic substances, inhibitors, etc.(Guldhe et al., 2017).

Urban wastewater (or sewage) is composed of a mixture of domestic wastewater (about 80-95%) and industrial wastewater (about 5-20%) (Guldhe et al., 2017). Raw urban wastewater can exhibit high variations in its characteristics depending on the wastewater source (Komolafe et al., 2014), including toxics, heavy metals and pathogens (Cai et al., 2013). High-suspended solids concentrations in raw wastewater can also have a negative effect on phototrophic organisms due to reduced light availability in the culture (Guldhe et al., 2017). Primary-treated effluents are expected to be a more suitable microalgae-bacteria consortium media due to their lower suspended solids concentrations but high nutrients and organic matter concentrations. Anbalagan et al. (2016) reported high removal efficiencies of organic matter and nutrients using effluent from primary settling. Secondary effluents present a low amount of suspended solids, but also a low organic matter concentration, limiting heterotrophic activity (Guldhe et al.,

2017). Secondary effluents are also used to microalgae growth (AlMomani and Örmeci, 2016; Eida et al., 2018; Gómez-Serrano et al., 2015; Ruiz et al., 2013). However, they often present low nutrient concentration and NO_3-N is the nitrogen source, which can reduce microalgae activity (Guldhe et al., 2017). In this case, the incoming wastewater flow can be increased using membranes to ensure biomass retention (Acién et al., 2016). Centrate from the anaerobic digestion of activated sludge contains high nitrogen, phosphorus and organic matter concentration (Acién et al., 2016; Morales-Amaral et al., 2015). The carbon footprint of the overall wastewater treatment process can be reduced by treating centrate with microalgae-bacteria consortia (Guldhe et al., 2017). However, it is often required prior dilution to avoid biomass inhibition by an excess of ammonium, urea, organic acids and pesticides (Acién et al., 2016; Djelal et al., 2014). Microalgae-bacteria consortia can also be grown in other wastewater streams, such as agro-industrial or industrial wastewater (García et al., 2018; Godos et al., 2009; Guldhe et al., 2017; Van Den Hende et al., 2016). However, both wastewater streams can present high variability in nutrient concentration (Rogato et al., 2015), limited inorganic carbon, high turbidity, reducing light irradiance availability, and a high amount of antibiotics, pesticides, heavy metals nanoparticles or other toxics (Guldhe et al., 2017).

Mixing is another important operating parameter, as it promotes culture homogenization, improve gas mass transfer and prevent biomass sedimentation (Huang et al., 2017). In addition, mixing also prevents microalgal photorespiration due to excessive oxygen accumulation (above saturation) (Almomani et al., 2019).

Similarly, inoculation profile of microalgae and bacteria is also considered an important factor, which affect directly nutrients and organic matter removal. A higher inoculum ratio of microalgae can improve DO concentration at the initial stage of biological community, improving nitrifying efficiency (Sepehri et al., 2020). Nitrification rate gradually increase, along with the increase in the concentration of microalgae (Zhang et al., 2021). Notably, microalgae species is also a critical factor. Kwon et al. (2020) reported that FAN and NO_2-N oxidation rates were higher with a relatively low proportion of bacteria and

microalgae (*Chlorella vulgaris* and *Scenedesmus quadricauda*). However, NH_4-N oxidation rate decreased when microalgae-bacteria consortium exceeded 2000 $g \cdot m^{-3}$, due to low oxygen production rate, caused in turn by self-shading effect. Additionally, ammonium removal mechanisms could be modified when the inoculum ratio of microalgae and bacteria changed (Bankston and Higgins, 2020). For instance, primary NH_4-N removal mechanism change from biomass assimilation to nitrification when ratio of microalgae-bacteria changed from 5:1 to 1:1 (Su et al., 2012). Microalgae and bacteria inoculation ratio influences both nutrients removal efficiently and mutualistic interaction (Zhang et al., 2021).

1.3.1.3. Outdoor microalgae-bacteria cultivation

Microalgae-bacteria consortia can grow in two main outdoor-systems: open raceway pond (Figure I. 5A) and closed photobioreactor (PBR) (Figure I. 5B). Outdoor-systems should be designed and operated to achieve optimal light penetration (high surface area/volume ratio) and provide good mixing and favor gas transfer, while minimizing construction and operating costs (Bosma et al., 2014).

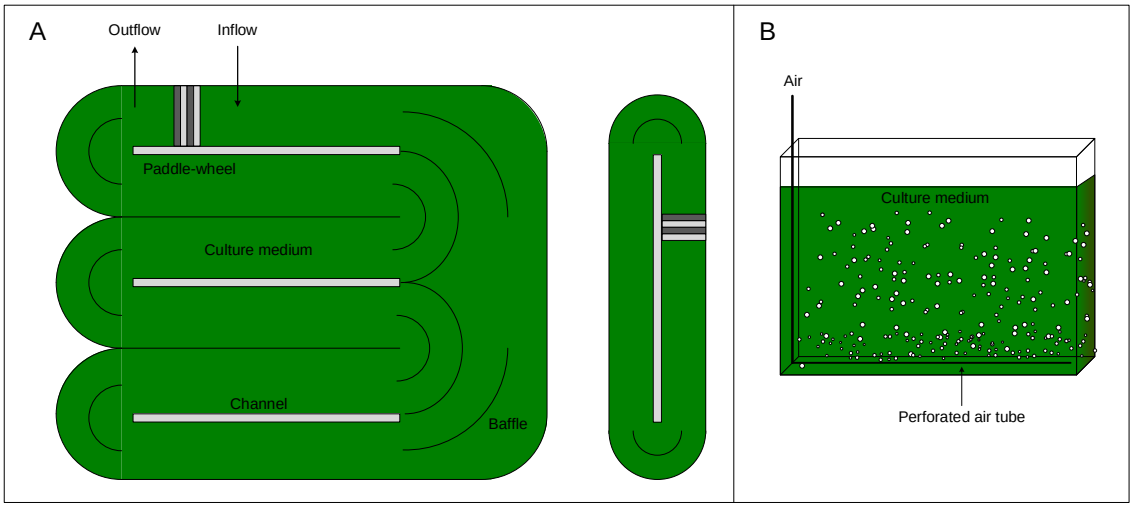

Figure I. 5. Scheme of (A) Open pond and (B) closed Photobioreactor.

Although open systems are generally more cost-efficient and easier to operate than closed PBR (Bosma et al., 2014; Xu et al., 2019), they are also significantly more affected by environmental conditions. Moreover, biological contamination and colonization by

non-indigenous microorganisms are difficult to avoid (Lam et al., 2018; Vo et al., 2019). Both increased sensitivity to environmental conditions and biological contamination negatively affect microalgae performance and thus wastewater treatment (García-Galán et al., 2018). In addition, open systems present the risk of pollutant volatilization, which can account, for instance, for up to 73% of nitrogen losses (Romero-Villegas et al., 2018). Open reactors usually operate at a depth of between 0.15 and 0.40 m and HRTs of 5-10 days (Acién et al., 2016; Arbib et al., 2017), and are equipped with a paddle-wheel, which provide mixing and continuous circulation to prevent sedimentation and stabilize microalgae and bacterial growth (Muñoz and Guieysse, 2006).

Closed systems have been designed to overcome some of the main drawbacks related to open production systems, achieving higher photosynthetic efficiencies, better control to environmental conditions and lower risk of pollutant volatilization and biological contamination. However, although closed systems are more efficient than open systems, they are expensive to build and operate (Muñoz and Guieysse, 2006).

Regardless of the microalgae-bacteria growth system selected, biomass-harvesting process appears as a key factor of the system (Alkarawi et al., 2018). Indeed, harvesting process is needed because: (I) effluent can contain microalgae and bacteria that needs to be removed prior to water discharge, and (II) harvesting process can increase biomass concentration in the culture. Generally, biomass harvesting is challenging due to their high capital and operational costs (Alkarawi et al., 2018), which can reach 20 to 30% to the overall production costs (Molina-Grima et al., 2003). Biomass separation from outgoing wastewater can be attained by sedimentation, flocculation, flotation, centrifugation or filtration. Membrane filtration appears as one of the most competitive of all the harvesting systems (Mata et al., 2010; Robles et al., 2020b). Membrane technology allows retaining most of the biomass on one side of the membrane, thus achieving higher biomass concentrations in the culture and a high quality permeate (González-Camejo et al., 2020a; Robles et al., 2020a). In addition, HRT and BRT can

be decoupled using membrane technology, thus enhancing biomass productivity and nutrient removal from microalgae-bacteria consortia (González-Camejo et al., 2020a, 2018).

1.4. MODELING MICROALGAE-BACTERIA CONSORTIUM FOR WASTEWATER TREATMENT

Physical, chemical and biological processes (described in Section 1.3.1) that take place in reactors (open or closed systems) occur simultaneously and they are interdependent (García et al., 2006). The rate of these processes depend on abiotic processes, i.e. operating conditions and the ever-changing environmental conditions, such as HRT, light intensity, temperature and pH. In this framework, a deep and realistic knowledge about microalgae-bacteria interactions is needed to predict system performance and optimize reactor design. Mathematical models represent a powerful tool to understand complex systems such as microalgae-bacterial consortia-based wastewater treatment systems.

Mechanistic bacteria mathematical models for wastewater treatment systems have been successfully developed and validated, and nowadays are widely used and accepted. For instance, Biological Nutrient Removal Model No. 2 (BNRM2) includes the most important physical, chemical and biological interactions taking place in a WWTP (Barat et al., 2013). The physical processes included comprise: (I) settling and clarification processes, (II) volatile fatty acids elutriation, and (III) gas-liquid transfer. The chemical interactions are: (I) acid-base and ion-pairing processes, and (II) precipitation processes. The biological processes included comprise: (I) organic matter and nutrient removal, acidogenesis, acetogenesis and methanogenesis. The model BNRM2 considers the possible growth of bacterial groups included in the model (Acetogenic bacteria, Acidogenic bacteria, Heterotrophic organisms, AOBs, NOBs, Methanogenic acetoclastic organisms, Methanogenic hydrogenotrophic organisms and PAOs) in each operation unit. Aerobic, anoxic or anaerobic conditions determine the bacterial groups that can

proliferate. This "natural selection" observed in WWTPs is modeled by adding switching functions for the different electron acceptors in the kinetic expressions.

In contrast to well-established bacterial models, mechanistic models describing the internal complexity of microalgae-bacteria consortia-based wastewater treatment systems are not well consolidated and are still under development and testing. Microalgae-bacteria models are more complex due to the multiple factors involved, as well as the numerous interactions between the organisms. In next Section (1.4.1), the main integral mechanistic mathematical models are described.

1.4.1. Microalgae-bacteria models

Different mathematical models have been proposed as a solid scientific basis for optimizing wastewater treatment with microalgae-bacteria consortia. Some of the mathematical models are described in the following sections.

1.4.1.1. River Water Quality Model No. 1

The mathematical model River Water Quality Model No. 1 (RWQM1) was developed by a defined IWA (formerly IAWQ) task group (Reichert et al., 2001). Although, RWQM1 was developed for river water quality modeling, it is also used as a basic model for microalgae and bacteria treatment systems, since both groups of microorganisms are included. Particulate organic matter sedimentation and chemical equilibrium of carbon, nitrogen and phosphorus species are also considered in this model.

The mechanistic model is based on organisms elemental composition (C, H, N, O and P) and on the stoichiometry of biochemical conversion processes. It considers 26 process and 24 components. The soluble fraction is composed by: inert soluble organic matter (S_I), readily biodegradable soluble organic matter (S_S), ammonium nitrogen (S_{NH4}), ammonia nitrogen (S_{NH3}), nitrite nitrogen (S_{NO2}), nitrate nitrogen (S_{NO3}), inorganic dissolved phosphorus ($S_{HPO4} + S_{H2PO4}$), dissolved oxygen (S_{O2}), sum of dissolved carbon dioxide and H_2CO_3 (S_{CO2}), bicarbonate (S_{HCO3}), dissolved carbonate (S_{CO3}), hydrogen

ions (S_H), hydroxyl ions ions (S_{OH}) and dissolved calcium (S_{Ca}). The particulate fraction is composed by: heterotrophic bacteria (X_H), AOB (X_{N1}), NOB (X_{N2}), algae and macrophytes (X_{ALG}), consumers (X_{CON}), biodegradable particulate organic matter (X_S), inert particulate organic matter (X_I), phosphate adsorbed to particles (X_P) and particulate inorganic material (X_{II}).

The biokinetic expressions are based on switching functions of nutrients, light and temperature, specifically, Monod function, Lambert and Beer's Law and Arrhenius equation, respectively.

1.4.1.2. Zambrano's model

Zambrano et al. (2016) developed a simplified mechanistic model to describe microalgae-bacteria consortia growth in a PBR. The model considered 6 processes and 6 components. The soluble components are nitrogen fractions (S_{NH4} and S_{NO3}), oxygen (S_{O2}) and dissolved carbon dioxide (S_{CO2}), while as particulate components only considered bacteria biomass (X_{BAC}), which, according to its kinetic expression, refers to the AOBs, and microalgae (X_{ALG}).

The model was calibrated by matching ammonium, nitrate and oxygen data from lab-scale batch experiments with urban wastewater. Effects of light intensity, temperature and other abiotic parameters such as pH were not considered.

1.4.1.3. ASM-A

The mathematical model ASM-A (Wágner et al., 2016) was developed as an extension of the well-established Activated Sludge Model, ASM-2d (Henze et al., 2015) for describing microalgae metabolism in waste stabilization ponds (WSPs), high rate algal ponds (HRAPs) and closed PBRs fed with wastewater. It considered 6 processes and 11 components. The soluble components are ammonium (S_{NH4}), nitrite and nitrate (S_{NO}), inorganic phosphate (S_{PO4}), alkalinity (S_{ALK}), dissolved oxygen (S_{O2}) and acetate (S_A). The particulate components are microalgae biomass (X_{ALG}), inert particulate organic matter (X_I) and biodegradable particulate organic matter (X_S). In particulate fraction, the

internal cell quota of nitrogen and phosphorus ($X_{ALG,N}$ and $X_{ALG,PP}$, respectively) was also considered. Nitrogen and phosphorus limitations of microalgae growth are described according to the Droop model, while Monod kinetic is used to simulate inorganic carbon consumption. Light limitation was implemented using the Steele equation (Steele, 1962).

The model was calibrated and validated with lab-scale airlift PBR operated in batch with synthetic culture medium. The model was able to predict microalgal biomass growth, nutrient uptake and storage by minimizing the relative normalized mean square error (RMSNE).

1.4.1.4. BIO_ALGAE 2

The model BIO_ALGAE 2 (Solimeno et al., 2019) was developed mainly by coupling RWQM1 (Reichert et al., 2001) with the modified ASM3 (Iacopozzi et al., 2007) to describe the growth of microalgae and bacteria in WSPs, HRAPs and PBRs. The model considered 25 processes and 19 components. The soluble components included are: inert soluble organic matter (S_I), readily biodegradable soluble organic matter (S_S), ammonium nitrogen (S_{NH4}), ammonia nitrogen (S_{NH3}), nitrite nitrogen (S_{NO2}), nitrate nitrogen (S_{NO3}), dissolved phosphate phosphorus (S_{PO4}), dissolved oxygen (S_{O2}), carbon dioxide (S_{CO2}), bicarbonate (S_{HCO3}), carbonate (S_{CO3}), hydrogen ions (S_H) and hydroxide ions (S_{OH}). The particulate components included are: heterotrophic bacteria (X_H), AOB (X_{AOB}), NOB (X_{NOB}), microalgae (X_{ALG}), biodegradable particulate organic matter (X_S) and inert particulate organic matter (X_I).

Carbon and nutrients limitation were included by Monod type function. The model also included pH, temperature dependence for bacteria and microalgae using cardinal sub-models. The dynamic model of Eilers and Peters (Eilers and Peeters, 1988) was included to simulate the effect of light intensity on photosynthesis. Moreover, the mathematical model also included an on-demand carbon dioxide injection for pH control.

The model was calibrated and validated using data from a laboratory reactor fed with real wastewater. It was able to match experimental data and simulate microalgae and bacteria dynamics.

1.4.1.5. ABACO

The mathematical model ABACO (Sánchez-zurano et al., 2021) was developed as an extension to the Activated Sludge Model, ASM-2d (Henze et al., 2015) for including microalgae metabolism. The model equations were inspired in the mechanistic BIO_ALGAE model (Solimeno et al., 2017), integrating kinetic processes and components. BIO_ALGAE model was improved by considering the nutrient concentration influence (carbon dioxide (S_{CO2}), ammonium nitrogen (S_{NH4}), nitrate nitrogen (S_{NO3}), dissolved phosphate phosphorus (S_{PO4}) and readily biodegradable soluble organic matter (S_S)) in the microalgae and bacteria kinetic parameters.

The model was calibrated and validated with data obtained from two lab-scale PBRs fed with pig slurry (diluted at 20%). Calibrated values were optimized by the Genetic Algorithm Optimization Toolbox (GAOT).

1.4.1.6. ALBA

The ALBA model (Casagli et al., 2021) described growth and interaction between microalgae, heterotrophic and nitrifying bacteria in a raceway pond. It considered 19 processes and 17 components. The soluble components are: inert soluble organic matter (S_I), readily biodegradable soluble organic matter (S_S), total ammoniacal nitrogen (S_{NH}), organic nitrogen (S_{ND}), nitrous nitrogen (S_{NO2}), nitric nitrogen (S_{NO3}), nitrogen gas (S_{N2}) dissolved inorganic phosphorus (S_{PO4}), dissolved oxygen (S_{O2}), total inorganic carbon (S_{IC}) and water (S_{H2O}). The suspended fraction are: heterotrophic bacteria (X_H), AOB (X_{AOB}), NOB (X_{NOB}), microalgae (X_{ALG}), biodegradable particulate organic matter (X_S) and inert particulate organic matter (X_I).

Substrate for each biological group were included by Monod type function. Light dependence of microalgae growth was simulated by a Haldane-type function, choosing

the parametrization proposed by Bernard and Rémond (2012). Such as BIO_ALGAE2 and ABACO, the temperature and pH dependence of biomass growth of ALBA model are based on Cardinal temperature and pH sub-model.

The model was calibrated and validated over the four seasons (fifteen months), with data obtained from an outdoor raceway pond fed with synthetic wastewater.

1.4.1.7. Microalgae-bacteria models comparison

In general, the corrective factors that limit the maximum growth rate of microalgae are included by Monod functions. Only the ASM-A model (briefly described above) used the internal cell quota according to Droop model. The Droop model accounts for luxury uptake (Section 1.2.1.2) and nutrient storage for growth under nutrient-starved conditions through intracellular concentration (Powell et al., 2009; Ruiz et al., 2013). The rest of the models described above assumed that wastewater systems are inherently nutrient-rich and that intracellular storage of nutrients is a minor process that can be neglected. However, the autotrophic microalgae model developed by Viruela et al. (2021) observed that, depending on the operating and environmental parameters, microalgae growth can be limited by phosphorus concentration in urban wastewater. Luxury uptake can be also simulated by the Hill-type function as proposed Ruiz-Martínez et al. (2015) and Viruela et al. (2021).

The description of bacteria processes is quite complete in RWQM1, BIO_ALGAE2, ABACO and ALBA models, although certain simplifications have been made to better control the biochemical processes. Phosphorus uptake by PAOs was omitted because of the relatively oxidized nature of microalgae-bacteria systems. However, zero-dissolved oxygen concentration can be reached at nighttime or in dark conditions, and therefore, organisms such as PAOs could grow.

In addition, phosphorus removal by chemical precipitation was not considered in any modeled described. A consequence of photosynthetic activity is the increase of culture pH up to values close to 9 and can lead phosphorus precipitation (Foladori et al., 2018;

González-Fernández et al., 2011; Posadas et al., 2015). The chemically induced phosphorus removal process can become significant at pH values above 9 and, therefore, this process should be included in microalgae-bacteria models.

In comparison to well-established bacterial models, such as BNRM2, the presented microalgal-bacterial models focus on a very specific group of bacteria. Furthermore, chemical precipitation processes are considered as a minor removal pathway and are not included. A single model bringing together the processes described in the BNRM2 model and microalgae metabolism, along with microalgae-bacteria interactions should be developed.

1.4.2. Global sensitivity analysis and Uncertainty analysis

The use of mathematical model has become widespread in the design and optimization of microalgae-bacteria consortia-based wastewater treatment systems. However, microalgae kinetic parameters of these models are usually prone to uncertainty resulting from simplifying assumptions, poor knowledge of kinetic processes, etc. These sources of uncertainty propagate through the mathematical model and lead to uncertainty in the resulting simulations. Uncertainties resulting from model output have negative impacts on model reliability in practical applications. Addressing this issue involves two interrelated aspects: (I) the quantification of the uncertainties in the model outputs that arise from the propagation of the input uncertainties through the mathematical model, and (II) the allocation of the uncertainties in the model outputs to the different sources of uncertainty in the model inputs (Mannina et al., 2018). The first aspect needs an uncertainty analysis (UA), and the second aspect needs a global sensitivity analysis (GSA). Both UA and GSA should be performed concurrently, since are essential parts of the model development process. However, the mathematical models described in Section 1.4.1 do not include UA and GSA. Only Zambrano's model, BIO_ALGAE2 and ALBA model performed a GSA to obtain the most influential parameters. Thus, there are gaps in the investigation of UA and GSA for modeling microalgae-bacteria systems.

Studies should be conducted to address these gaps by concurrently performing a detailed UA and a GSA.

To reduce model uncertainty, understand and predict biomass growth and microalgae-bacteria interactions, information coming from biological studies should be linked to mathematical models. To enable this linkage, measurements of biomass concentration and activity are essential.

1.4.3. Measuring microalgae and bacteria concentrations

In chemical engineering and ecological assessments, the fundamental parameter that should be calculated to quantify the wastewater pollutant impact is the biomass (dry weight) and microbial community composition. Most of the methods traditionally used to measure microorganisms are based solely on biomass dry weight concentration, measured as total and volatile suspended solids (TSS and VSS, respectively). However, the average cell dry weight is not a constant value for a microalgal species, and can change depending on abiotic conditions. For instance, the average cell weight of *Scenedesmus obliquus, Chlorella sp. and Haematococcus pluvialis* increases approximately 2-fold under nitrogen starvation conditions (Baroni et al., 2019; Di Caprio et al., 2018). In contrast, a decrease of approximately two fold in the average dry weight of different heterotrophic bacteria during the stationary phase has been found (Cermak et al., 2017; Gray et al., 2019). In addition, microalgae are usually the dominant organism in microalgae-bacteria consortia mainly due to their larger cell size. Luo et al. (2018) reported that only 0.2 to 3.5% of the dry weight was accounted for by bacteria in a laboratory-scale microalgae culture system. Microalgae-bacteria consortium is often determined and quantified as TSS or VSS, without distinction of species and genera and microalgae-bacteria ratio (Mantovani et al., 2020; Toledo-Cervantes et al., 2019; Van Den Hende et al., 2016). Nevertheless, other analytical methods should be used to quantify microalgae-bacteria populations.

Optical microscope

Optical microscope is one of the most selective and reliable methods to quantify microorganisms in microalgae-bacteria consortium (Di Caprio, 2020). This methodology offers the advantage of measuring the microorganisms directly in their natural environment, with minimal or no pretreatment. Expert researchers can use this method to separately count different morphologies of microalgae using the same analysis (Assemany et al., 2015; Riaño et al., 2012). Contrary, researchers with limited knowledge can make mistakes if the foreign microalgae are similar from the target strain. Aggregate cells in multicellular structures (e.g., coenobium) or small colonies can also be counted. However, in the case of large colonies or flocs, significant errors can result from non-random distribution of cells in the counted area, and from the difficulty of viewing the cells within a floc.

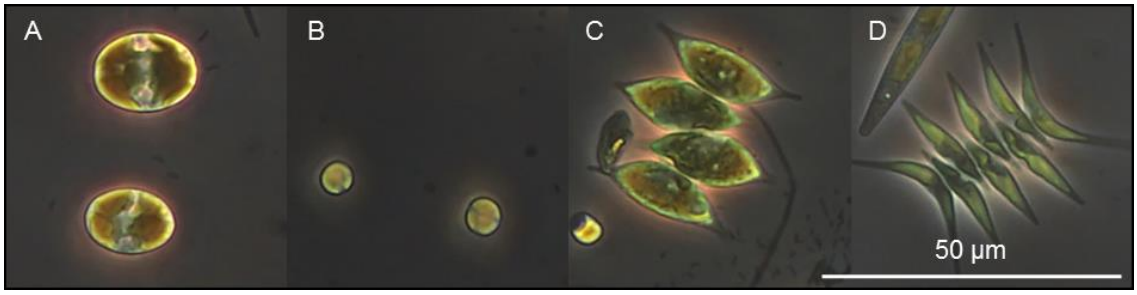

Figure I. 6. Common green microalgae for wastewater treatment: (A-B) microalgae with morphology similar to genus *Chlorella*, and (C-D) microalgae with morphology similar to genus *Scenedesmus.*

The main morphologies identified as *Chlorella* and *Scenedesmus* genus (Figure I. 6) have been widely reported as suitable genera for wastewater treatment (Arias et al., 2019; González-Camejo et al., 2019b; Pachés et al., 2020; Vo et al., 2019).

Direct cell counting is widely used to quantify bacteria in microalgae-bacteria consortium (Di Caprio, 2020). To clearly see the small bacterial cells, an epifluorescence microscope is often used after staining the cells with DNA fluorescence dyes. However, it should be noted that microalgae have autofluorescent pigments, such as *Chl a*, which should be carefully considered in the choice of fluorescence dyes to avoid signal interference (Sato et al., 2004).

Electron microscopy

Transmission electron microscopy (TEM) and scanning electron microscopy (SEM) are the most sensitive techniques for morphological analysis of microalgae and bacteria. Microalgal and bacterial cells can be seen at nanometer resolution. However, such techniques are expensive and time-consuming, making them hardly applicable for analyzing large numbers of cells (Di Caprio, 2020).

Flow cytometry

Flow cytometry (FCM) is a high-throughput technique that enables the analysis of a large number of cells (1000-35,000 events/s), in a relatively short time (Di Caprio, 2020). Similar to microscopic observations, FCM enables microorganisms to be measured directly in the sample, but with the advantage of using an automated fluid-optical system, rather than a single biased observation by the researcher (Hyka et al., 2013). In FCMs, cells are separated by a fluidic system and analyzed one at a time at the point of interrogation by an incident laser, producing two output scattering signals (side scattering (SSC) and forward scattering (FSC)) along with different fluorescence emissions detected by various optical filters and light detectors. One of the main drawbacks of FCM is cell aggregation (flocs) and multicellular systems (coenobium), which should be excluded by filtration or broken into single cells. Several genera of microalgae, such as Scenedesmus, frequently live in heterogeneous conditions in which single cells coexist with double cells, four cells (coenobium) or other multi-cell structures, making identification and counting difficult (Borowitzka et al., 2016). In addition, bacteria can live attached to microalgae cells, which are not detected by the FCM (Lee et al., 2013).

Imaging flow cytometry (IFC) is a specific technology of FCM, in which biomass cells passing through the interrogation point are detected by photographic imaging (Di Caprio, 2020). Conventional FCM produces a single pixel (a single value) for each parameter measured in each event, while IFC produces multi-pixel 2D images for each parameter analyzed in each event (Dashkova et al., 2017; Hildebrand et al., 2016). IFC is more

efficient than conventional FCM for samples containing cellular aggregates and complex multicellular structures because each readout event can be analyzed using the 2D stored images. However, IFC throughput is typically between 300 and 1,000 events/s, lower than conventional FCM (Di Caprio, 2020). The relevant issues limiting the IFC system throughput are the exposure time of the camera and the large amount of data to be processed. Collecting one or more photos for each detected event produces a larger amount of data to process and store compared to conventional FCM, which produces 10-20 numbers per event (Rane et al., 2017).

Genetic biomarkers

Genetic analyses are the most sensitive and specific for identification of microorganisms. Genetic biomarkers can be used to determine a specific nucleic acid molecule, due to polymerase chain reaction (PCR)-based amplification tools, ideally enabling identification of each different species of microalgae and bacteria in the sample. Sample collection and storage may affect the results due to DNA degradation. The main steps in DNA analysis are: (I) sample collection and storage; (II) DNA extraction; (III) DNA amplification; (IV) DNA sequences identification; (V) data analysis. Both collection and storage should therefore be performed according to a standard procedure (Thomas et al., 2012).

Several commercial kits have been developed to extract DNA from microalgae-bacteria samples (Ferrero et al., 2012; Lakaniemi et al., 2012). DNA extraction is an important step because if the selected kit is not able to extract DNA with the same efficiency from all cells, it can be a source of systematic errors (Thomas et al., 2012). DNA extraction is an important step because if the selected kit is not able to extract DNA with the same efficiency from all cells, it can be a source of systematic errors (Thomas et al., 2012).

DNA molecular analyses can be qualitative and quantitative. Both qualitative and quantitative analyses are based on PCR amplification of 18S rDNA or small ribosomal DNA fragments (for microalgae) and 16S rRNA genes (for bacteria analysis) (Kowalska

et al., 2019). Qualitative genetic analyses provide information on the presence/absence of species in a sample and on the relative increase/decrease of species between different samples, but without a quantitative indication of the actual concentration in the samples. After amplification, the amplified DNA sequences can be detected and assigned to a known species by comparison with known sequences stored in genetic databases (e.g. GenBank) (Thomas et al., 2012). It should be emphasized that the percentage of DNA abundance measured in a single sample is usually not the true percentage of abundance. Indeed, different biases are involved: (I) different extraction efficiency, (II) different ration from DNA concentration in the sample and DNA concentration after amplification, (III) primers used for DNA amplification, (IV) sequences available in the genetic databases, and the algorithms used for data analysis. For these reasons, a more robust assessment is the relative comparison between different samples (analyzed with the same protocol), looking for qualitative variations of DNA sequences as a function of abiotic parameters.

Non-genetic biomarkers analysis

Non-genetic biomarker analysis is based on production or uptake of specific non-genetic molecules from one or several groups of organisms to indirectly measure microorganism concentration. For microalgae, the most used molecule is *Chl a*, which is quantified by spectrophotometer analysis Jeffrey and Humphrey's Equation (APHA-AWWA-WPCF, 2012; Di Caprio, 2020). Several researcher sources quantify microalgae by *Chl* a concentration (Michelon et al., 2010; Rada-Ariza et al., 2017; Solmaz and Işık, 2020; M. Zhang et al., 2020). However, *Chl a* content in microalgae depends on abiotic conditions, such as light irradiance, temperature or nutrients availability (da Silva Ferreira and Sant'Anna, 2017), the assumption of a constant *Chl a* content is therefore generally not valid. Other possible biases associated with *Chl a* analysis result from the extraction efficiency and the presence of other colored molecules adsorbed from the wastewater,

which can lead to interferences during spectrophotometric analysis. *Chl a* analysis cannot be therefore considered a reliable microalgae concentration indicator.

Non-genetic biomarkers analysis is not a suitable tool for comparing microalgal and bacterial cells concentration due to the main limits of *Chl a* (described above), and the lack of common biomarkers for heterotrophic and nitrifying wastewater indigenous bacteria.

1.4.4. Measuring microalgae and bacteria activities

Activity of microalgae and bacteria can be also exploited for monitoring microalgae-bacteria systems, as well as to assess relative increase/decrease of their activities in a mixed culture. Respirometry could play a useful role in this perspective, as it can be adapted to be applicable to both oxygen-consuming and oxygen-producing biomass. Photo-respirometric test in microalgae-bacteria consortium consists of batch essays with light and dark (L/D) phases to obtain oxygen production rate by phototrophic organism (OPR) and oxygen consumption rate (OUR) by aerobic respiration (Rossi et al., 2020). Different substrates (organic matter, ammonium or nitrite) along with inhibitors (allylthiourea (ATU) or potassium chlorate ($KClO_3$)) can be combined to obtain different oxygen profiles: (I) OPR by microalgae and cyanobacteria, (II) OUR by microalgae respiration coupled with endogenous consumption, (III) OUR by nitrification, (IV) OUR by aerobic heterotrophic organism respiration (Rossi et al., 2018; Sánchez-Zurano et al., 2020). However, estimation of oxygen balance can be quite influenced by abiotic parameters (light intensity, temperature, pH, nutrients availability, etc.). Photo-respirometric test should be therefore performed with the same protocol to compare the activity between different samples (Rossi et al., 2020).

Although not applicable to bacteria, another useful technique for measuring microalgal activity is the *Chl a* fluorescence method. *Chl a* fluorescence is a widely used technique to monitor photosynthetic (specifically PS II) yield, as it is considered an easy, fast and non-invasive tool that provides much information on the PS II yield of microalgae under

diverse abiotic conditions (Hernández-Zamora et al., 2014; Ji et al., 2018; Markou et al., 2016; Perales-Vela et al., 2007; Sun et al., 2020).

1.5. PERSPECTIVES OF MICROALGAE-BACTERIA SYSTEMS

The use of microalgae-bacteria cultures for treating wastewater constitutes a sustainable approach. As it has been developed throughout this chapter, the efficiency of pollutants removal from wastewater depends on the interactions between microalgae and indigenous bacteria. However, limited knowledge of the interactions occurring between microalgae and bacteria still limits its full exploitation. New research on microalgae-bacteria cultivation technology should therefore focus on:

- Evaluating the optimal operating conditions to enhance mutualism interactions between microalgae and bacteria.
- Evaluating how bacterial community growth impacts microalgal metabolism.
- Avoiding the proliferation of competing organisms without damaging microalgae.
- Detecting and modeling factors and processes that limit or inhibit the development of an effective microalgae-bacteria consortium to remove pollutants from wastewater.
- Studying the biological community structure to optimize wastewater treatment processes.
- Performing a detailed uncertainty analysis and a global sensitivity analysis to detect the uncertainty sources of the model.
- Developing a mathematical model including the most relevant biological, chemical and physical processes to optimize the operation and design of microalgae-bacteria consortia-based systems.

Some of these research lines are further discussed in this PhD thesis.

REFERENCES

Abu-Ghosh, S., Fixler, D., Dubinsky, Z., Iluz, D., 2016. Flashing light in microalgae biotechnology. Bioresour. Technol. 203, 357–363. https://doi.org/10.1016/J.BIORTECH.2015.12.057

Acién, F.G., Gómez-Serrano, C., Morales-Amaral, M.M., Fernández-Sevilla, J.M., Molina-Grima, E., 2016. Wastewater treatment using microalgae: how realistic a contribution might it be to significant urban wastewater treatment? Appl. Microbiol. Biotechnol. 2016 10021 100, 9013–9022. https://doi.org/10.1007/S00253-016-7835-7

Acién Fernández, F.G., Gómez-Serrano, C., Fernández-Sevilla, J.M., 2018. Recovery of Nutrients From Wastewaters Using Microalgae. Front. Sustain. Food Syst. 2, 59. https://doi.org/10.3389/FSUFS.2018.00059/BIBTEX

Akizuki, S., Kishi, M., Cuevas-Rodríguez, G., Toda, T., 2020. Effects of different light conditions on ammonium removal in a consortium of microalgae and partial nitrifying granules. Water Res. https://doi.org/10.1016/j.watres.2019.115445

Alkarawi, M.A.S., Caldwell, G.S., Lee, J.G.M., 2018. Continuous harvesting of microalgae biomass using foam flotation. Algal Res. 36, 125–138. https://doi.org/10.1016/J.ALGAL.2018.10.018

Allen, J.F., 2003. Cyclic, pseudocyclic and noncyclic photophosphorylation: new links in the chain. Trends Plant Sci. 8, 15–19. https://doi.org/10.1016/S1360-1385(02)00006-7

Almomani, F., Judd, S., Bhosale, R.R., Shurair, M., Aljaml, K., Khraisheh, M., 2019. Intergraded wastewater treatment and carbon bio-fixation from flue gases using Spirulina platensis and mixed algal culture. Process Saf. Environ. Prot. 124, 240–250. https://doi.org/10.1016/j.psep.2019.02.009

AlMomani, F.A., Örmeci, B., 2016. Performance Of Chlorella Vulgaris, Neochloris Oleoabundans, and mixed indigenous microalgae for treatment of primary effluent, secondary effluent and centrate. Ecol. Eng. 95, 280–289. https://doi.org/10.1016/J.ECOLENG.2016.06.038

Anbalagan, A., Schwede, S., Lindberg, C.F., Nehrenheim, E., 2016. Influence of hydraulic retention time on indigenous microalgae and activated sludge process. Water Res. 91, 277–284. https://doi.org/10.1016/j.watres.2016.01.027

APHA-AWWA-WPCF, 2012. Standard Methods for the Examination of Water and Wastewater, 22nd edition, American P. ed. Washington DC, USA.

Arbib, Z., de Godos, I., Ruiz, J., Perales, J.A., 2017. Optimization of pilot high rate algal ponds for simultaneous nutrient removal and lipids production. Sci. Total Environ. 589, 66–72. https://doi.org/10.1016/j.scitotenv.2017.02.206

Arias, D.M., Rueda, E., García-Galán, M.J., Uggetti, E., García, J., 2019. Selection of cyanobacteria over green algae in a photo-sequencing batch bioreactor fed with wastewater. Sci. Total Environ. 653, 485–495. https://doi.org/10.1016/J.SCITOTENV.2018.10.342

Ashadullah, A.K.M., Shafiquzzaman, M., Haider, H., Alresheedi, M., Azam, M.S., Ghumman, A.R., 2021. Wastewater treatment by microalgal membrane bioreactor: Evaluating the effect of organic loading rate and hydraulic residence time. J. Environ. Manage. 278, 111548. https://doi.org/10.1016/J.JENVMAN.2020.111548

Assemany, P.P., Calijuri, M.L., Couto, E. de A. do, de Souza, M.H.B., Silva, N.C., Santiago, A. da F., Castro, J. de S., 2015. Algae/bacteria consortium in high rate ponds: Influence of solar radiation on the phytoplankton community. Ecol. Eng. 77, 154–162. https://doi.org/10.1016/j.ecoleng.2015.01.026

Bankston, E., Wang, Q., Higgins, B.T., 2020. Algae support populations of heterotrophic, nitrifying, and phosphate-accumulating bacteria in the treatment of poultry litter anaerobic digestate. Chem. Eng. J. 2020, Vol. 398, Page 125550 398, 125550. https://doi.org/10.1016/J.CEJ.2020.125550

Bankston, E.M., Higgins, B.T., 2020. Anaerobic microbial communities can influence algal growth and nutrient removal from anaerobic digestate. Bioresour. Technol. 297, 122445. https://doi.org/10.1016/J.BIORTECH.2019.122445

Barat, R., Montoya, T., Borrás, L., Ferrer, J., Seco, A., 2008. Interactions between calcium precipitation and the polyphosphate-accumulating bacteria metabolism. Water Res. 42, 3415–3424. https://doi.org/10.1016/J.WATRES.2008.05.003

Barat, R., Montoya, T., Seco, A., Ferrer, J., 2010. The Role of Potassium, Magnesium and Calcium in the Enhanced Biological Phosphorus Removal Treatment Plants. https://doi.org/10.1080/09593332608618485 26, 983–992.

Barat, R., Serralta, J., Ruano, M. V., Jiménez, E., Ribes, J., Seco, A., Ferrer, J., 2013. Biological Nutrient Removal Model No. 2 (BNRM2): a general model for wastewater treatment plants. Water Sci. Technol. 67, 1481–1489. https://doi.org/10.2166/WST.2013.004

Barbera, E., Bertucco, A., Kumar, S., 2018. Nutrients recovery and recycling in algae processing for biofuels production. Renew. Sustain. Energy Rev. https://doi.org/10.1016/j.rser.2018.03.004

Barceló-Villalobos, M., Serrano, C.G., Zurano, A.S., García, L.A., Maldonado, S.E., Peña, J., Fernández, F.G.A., 2019. Variations of culture parameters in a pilot-scale thin-layer reactor and their influence on the performance of Scenedesmus almeriensis culture. Bioresour. Technol. Reports 6, 190–197. https://doi.org/10.1016/J.BITEB.2019.03.007

Baroni, É.G., Yap, K.Y., Webley, P.A., Scales, P.J., Martin, G.J.O., 2019. The effect of nitrogen depletion on the cell size, shape, density and gravitational settling of Nannochloropsis salina, Chlorella sp. (marine) and Haematococcus pluvialis. Algal Res. 39, 101454. https://doi.org/10.1016/J.ALGAL.2019.101454

Bernard, O., Rémond, B., 2012. Validation of a simple model accounting for light and temperature effect on microalgal growth. Bioresour. Technol. 123, 520–527. https://doi.org/10.1016/j.biortech.2012.07.022

Boelee, N.C., Temmink, H., Janssen, M., Buisman, C.J.N., Wijffels, R.H., 2014. Balancing the organic load and light supply in symbiotic microalgal–bacterial biofilm reactors treating synthetic municipal wastewater. Ecol. Eng. 64, 213–221. https://doi.org/10.1016/J.ECOLENG.2013.12.035

Borowitzka, M.A., Beardall, J., Raven, J.A., 2016. The Physiology of Microalgae, The Physiology of Microalgae. Springer International Publishing. https://doi.org/10.1007/978-3-319-24945-2

Bosma, R., de Vree, J.H., Slegers, P.M., Janssen, M., Wijffels, R.H., Barbosa, M.J., 2014. Design and construction of the microalgal pilot facility AlgaePARC. Algal Res. 6, 160–169. https://doi.org/10.1016/J.ALGAL.2014.10.006

Cai, T., Park, S.Y., Li, Y., 2013. Nutrient recovery from wastewater streams by microalgae: Status and prospects. Renew. Sustain. Energy Rev. 19, 360–369. https://doi.org/10.1016/J.RSER.2012.11.030

Carvalho, V.C.F., Freitas, E.B., Silva, P.J., Fradinho, J.C., Reis, M.A.M., Oehmen, A., 2018. The impact of operational strategies on the performance of a photo-EBPR system. Water Res. 129, 190–198. https://doi.org/10.1016/j.watres.2017.11.010

Casagli, F., Zuccaro, G., Bernard, O., Steyer, J.P., Ficara, E., 2021. ALBA: A comprehensive growth model to optimize algae-bacteria wastewater treatment in raceway ponds. Water Res. 190, 116734. https://doi.org/10.1016/j.watres.2020.116734

Cermak, N., Becker, J.W., Knudsen, S.M., Chisholm, S.W., Manalis, S.R., Polz, M.F., 2017. Direct single-cell biomass estimates for marine bacteria via Archimedes' principle. ISME J. 11, 825–828. https://doi.org/10.1038/ismej.2016.161

Cho, D.H., Ramanan, R., Heo, J., Lee, J., Kim, B.H., Oh, H.M., Kim, H.S., 2015. Enhancing microalgal biomass productivity by engineering a microalgal–bacterial community. Bioresour. Technol. 175, 578–585. https://doi.org/10.1016/J.BIORTECH.2014.10.159

Choudhary, M., Peter, C.N., Shukla, S.K., Govender, P.P., Joshi, G.M., Wang, R., 2020. Environmental Issues: A Challenge for Wastewater Treatment. Springer, Cham, pp. 1–12. https://doi.org/10.1007/978-3-030-17724-9_1

Ciji, A., Akhtar, M.S., 2020. Nitrite implications and its management strategies in aquaculture: a review. Rev. Aquac. 12, 878–908. https://doi.org/10.1111/raq.12354

Collos, Y., Berges, J.A., 2009. Nitrogen metabolism in phytoplankton, in: Duarte, C.M., Lott Helgueras, A. (Eds.), Marine Ecology.

Cooper, R.J., Hawkins, E., Locke, J., Thomas, T., Tosney, J., 2020. Assessing the environmental and economic efficacy of two integrated constructed wetlands at mitigating eutrophication risk from sewage effluent. Water Environ. J. 34, 669–678. https://doi.org/10.1111/wej.12605

da Silva Ferreira, V., Sant'Anna, C., 2017. Impact of culture conditions on the chlorophyll content of microalgae for biotechnological applications. World J. Microbiol. Biotechnol. 33, 1–8. https://doi.org/10.1007/S11274-016-2181-6/TABLES/2

Dashkova, V., Malashenkov, D., Poulton, N., Vorobjev, I., Barteneva, N.S., 2017. Imaging flow cytometry for phytoplankton analysis. Methods 112, 188–200. https://doi.org/10.1016/j.ymeth.2016.05.007

Di Caprio, F., 2020. Methods to quantify biological contaminants in microalgae cultures. Algal Res. https://doi.org/10.1016/j.algal.2020.101943

Di Caprio, F., Pagnanelli, F., Wijffels, R.H., Van der Veen, D., 2018. Quantification of Tetradesmus obliquus (Chlorophyceae) cell size and lipid content heterogeneity at single-cell level. J. Phycol. 54, 187–197. https://doi.org/10.1111/JPY.12610

Djelal, H., Tahrani, L., Fathallah, S., Cabrol, A., Mansour, H. Ben, 2014. Treatment process and toxicities assessment of wastewater issued from anaerobic digestion of household wastes. Environ. Sci. Pollut. Res. Int. 21, 2437–2447. https://doi.org/10.1007/S11356-013-2158-Z

Eida, M.F., Darwesh, O.M., Matter, I.A., 2018. Cultivation of Oleaginous Microalgae Scenedesmus obliquus on Secondary Treated Municipal Wastewater as Growth Medium for Biodiesel Production. J. Ecol. Eng. Vol. 19, 38–51. https://doi.org/10.12911/22998993/91274

Eilers, P.H.C., Peeters, J.C.H., 1988. A model for the relationship between light intensity and the rate of photosynthesis in phytoplankton. Ecol. Modell. 42, 199–215. https://doi.org/10.1016/0304-3800(88)90057-9

Eustance, E., Gardner, R.D., Moll, K.M., Menicucci, J., Gerlach, R., Peyton, B.M., 2013. Growth, nitrogen utilization and biodiesel potential for two chlorophytes grown on ammonium, nitrate or urea. J. Appl. Phycol. 25, 1663–1677. https://doi.org/10.1007/s10811-013-0008-5

Falkowski, P.G., Raven, J.A., 2007. Aquatic photosynthesis. 2nd Edition. Princet. Univ. Press 484.

Fallahi, A., Rezvani, F., Asgharnejad, H., Khorshidi, E., Hajinajaf, N., Higgins, B., 2021. Interactions of microalgae-bacteria consortia for nutrient removal from wastewater: A review. Chemosphere 272, 129878. https://doi.org/10.1016/J.CHEMOSPHERE.2021.129878

Ferrero, E.M., de Godos, I., Rodríguez, E.M., García-Encina, P.A., Muñoz, R., Bécares, E., 2012. Molecular characterization of bacterial communities in algal–bacterial photobioreactors treating piggery wastewaters. Ecol. Eng. 40, 121–130. https://doi.org/10.1016/J.ECOLENG.2011.10.001

Foladori, P., Petrini, S., Andreottola, G., 2018. Evolution of real municipal wastewater treatment in photobioreactors and microalgae-bacteria consortia using real-time parameters. Chem. Eng. J. 345, 507–516. https://doi.org/10.1016/J.CEJ.2018.03.178

Foley, J., de Haas, D., Hartley, K., Lant, P., 2010. Comprehensive life cycle inventories of alternative wastewater treatment systems. Water Res. 44, 1654–1666. https://doi.org/10.1016/j.watres.2009.11.031

García-Galán, M.J., Gutiérrez, R., Uggetti, E., Matamoros, V., García, J., Ferrer, I., 2018. Use of full-scale hybrid horizontal tubular photobioreactors to process agricultural runoff. Biosyst. Eng. 166, 138–149. https://doi.org/10.1016/j.biosystemseng.2017.11.016

García, D., Posadas, E., Blanco, S., Acién, G., García-Encina, P., Bolado, S., Muñoz, R., 2018. Evaluation of the dynamics of microalgae population structure and process performance during piggery wastewater treatment in algal-bacterial photobioreactors. Bioresour. Technol. 248, 120–126. https://doi.org/10.1016/j.biortech.2017.06.079

García, J., Green, B.F., Lundquist, T., Mujeriego, R., Hernández-Mariné, M., Oswald, W.J., 2006. Long term diurnal variations in contaminant removal in high rate ponds treating urban wastewater. Bioresour. Technol. 97, 1709–1715. https://doi.org/10.1016/J.BIORTECH.2005.07.019

García, J., Mujeriego, R., Hernández-Mariné, M., 2000. High rate algal pond operating strategies for urban wastewater nitrogen removal, in: Journal of Applied Phycology. Springer Netherlands, pp. 331–339. https://doi.org/10.1023/a:1008146421368

Garrido-Cardenas, J.A., Manzano-Agugliaro, F., Acien-Fernandez, F.G., Molina-Grima, E., 2018. Microalgae research worldwide. Algal Res. 35, 50–60. https://doi.org/10.1016/j.algal.2018.08.005

Godos, I. de, Blanco, S., García-Encina, P.A., Becares, E., Muñoz, R., 2009. Long-term operation of high rate algal ponds for the bioremediation of piggery wastewaters at high loading rates. Bioresour. Technol. 100, 4332–4339. https://doi.org/10.1016/J.BIORTECH.2009.04.016

Gómez-Serrano, C., Morales-Amaral, M.M., Acién, F.G., Escudero, R., Fernández-Sevilla, J.M., Molina-Grima, E., 2015. Utilization of secondary-treated wastewater for the production of freshwater microalgae. Appl. Microbiol. Biotechnol. 99, 6931–6944. https://doi.org/10.1007/S00253-015-6694-Y/FIGURES/10

González-Camejo, J., Aparicio, S., Jiménez-Benítez, A., Pachés, M., Ruano, M. V, Borrás, L., Barat, R., Seco, A., 2020a. Improving membrane photobioreactor performance by reducing light path: operating conditions and key performance indicators. Water Res. 172. https://doi.org/10.1016/j.watres.2020.115518

González-Camejo, J., Aparicio, S., Ruano, M. V., Borrás, L., Barat, R., Ferrer, J., 2019a. Effect of ambient temperature variations on an indigenous microalgae-nitrifying bacteria culture dominated by Chlorella. Bioresour. Technol. 290, 121788. https://doi.org/10.1016/j.biortech.2019.121788

González-Camejo, J, Barat, R., Pachés, M., Murgui, M., Seco, A., Ferrer, J., 2018. Wastewater nutrient removal in a mixed microalgae–bacteria culture: effect of light and temperature on the microalgae–bacteria competition. Environ. Technol. (United Kingdom) 39, 503–515. https://doi.org/10.1080/09593330.2017.1305001

González-Camejo, J., Barat, R., Ruano, M. V., Seco, A., Ferrer, J., 2018. Outdoor flat-panel membrane photobioreactor to treat the effluent of an anaerobic membrane bioreactor. Influence of operating, design, and environmental conditions. Water Sci. Technol. 78, 195–206. https://doi.org/10.2166/WST.2018.259

González-Camejo, J., Ferrer, J., Seco, A., Barat, R., 2021. Outdoor microalgae-based urban wastewater treatment: Recent advances, applications, and future perspectives. Wiley Interdiscip. Rev. Water. https://doi.org/10.1002/wat2.1518

González-Camejo, J., Jiménez-Benítez, A., Ruano, M. V., Robles, A., Barat, R., Ferrer, J., 2019b. Optimising an outdoor membrane photobioreactor for tertiary sewage treatment. J. Environ. Manage. 245, 76–85. https://doi.org/10.1016/j.jenvman.2019.05.010

González-Camejo, J., Montero, P., Aparicio, S., Ruano, M. V., Borrás, L., Seco, A., Barat, R., 2020b. Nitrite inhibition of microalgae induced by the competition between microalgae and nitrifying bacteria. Water Res. 172, 115499. https://doi.org/10.1016/j.watres.2020.115499

González-Camejo, J, Pachés, M., Marín, A., Jiménez-Benítez, A., Seco, A., Barat, R., 2020a. Production of microalgal external organic matter in a Chlorella-dominated culture: influence of temperature and stress factors. Environ. Sci. Water Res. Technol. 6, 1828–1841. https://doi.org/10.1039/D0EW00176G

González-Camejo, J, Robles, A., Seco, A., Ferrer, J., Ruano, M. V, 2020b. On-line monitoring of photosynthetic activity based on pH data to assess microalgae cultivation. J. Environ. Manage. 276. https://doi.org/10.1016/j.jenvman.2020.111343

González-Fernández, C., Molinuevo-Salces, B., García-González, M.C., 2011. Nitrogen transformations under different conditions in open ponds by means of microalgae-bacteria consortium treating pig slurry. Bioresour. Technol. 102, 960–966. https://doi.org/10.1016/j.biortech.2010.09.052

Gray, D.A., Dugar, G., Gamba, P., Strahl, H., Jonker, M.J., Hamoen, L.W., 2019. Extreme slow growth as alternative strategy to survive deep starvation in bacteria. Nat. Commun. 2019 101 10, 1–12. https://doi.org/10.1038/s41467-019-08719-8

Grunditz, C., Dalhammar, G., 2001. Development of nitrification inhibition assays using pure cultures of nitrosomonas and nitrobacter. Water Res. 35, 433–440. https://doi.org/10.1016/S0043-1354(00)00312-2

Guldhe, A., Kumari, S., Ramanna, L., Ramsundar, P., Singh, P., Rawat, I., Bux, F., 2017. Prospects, recent advancements and challenges of different wastewater streams for microalgal cultivation. J. Environ. Manage. 203, 299–315. https://doi.org/10.1016/J.JENVMAN.2017.08.012

Gutzeit, G., Lorch, D., Weber, A., Engels, M., Neis, U., 2005. Bioflocculent algal–bacterial biomass improves low-cost wastewater treatment. Water Sci. Technol. 52, 9–18. https://doi.org/10.2166/WST.2005.0415

Henze, M., Gujer, W., Mino, T., van Loosedrecht, M., 2015. Activated Sludge Models ASM1, ASM2, ASM2d and ASM3. Water Intell. Online 5, 9781780402369–9781780402369. https://doi.org/10.2166/9781780402369

Hernández-Zamora, M., Perales-Vela, H.V., Flores-Ortíz, C.M., Cañizares-Villanueva, R.O., 2014. Physiological and biochemical responses of Chlorella vulgaris to Congo red. Ecotoxicol. Environ. Saf. 108, 72–77. https://doi.org/10.1016/j.ecoenv.2014.05.030

Hildebrand, M., Davis, A., Abbriano, R., Pugsley, H.R., Traller, J.C., Smith, S.R., Shrestha, R.P., Cook, O., Sánchez-Alvarez, E.L., Manandhar-Shrestha, K., Alderete, B., 2016. Applications of imaging flow cytometry for microalgae. Methods Mol. Biol. 1389, 47–67. https://doi.org/10.1007/978-1-4939-3302-0_4

Holmes, B., Paddock, M.B., VanderGheynst, J.S., Higgins, B.T., 2020. Algal photosynthetic aeration increases the capacity of bacteria to degrade organics in wastewater. Biotechnol. Bioeng. 117, 62–72. https://doi.org/10.1002/BIT.27172

Hu, B., Du, J., Zou, R. yang, Yuan, Y.J., 2010. An Environment-Sensitive Synthetic Microbial Ecosystem. PLoS One 5, e10619. https://doi.org/10.1371/JOURNAL.PONE.0010619

Huang, Q., Jiang, F., Wang, L., Yang, C., 2017. Design of Photobioreactors for Mass Cultivation of Photosynthetic Organisms. Engineering 3, 318–329. https://doi.org/10.1016/J.ENG.2017.03.020

Hyka, P., Lickova, S., Přibyl, P., Melzoch, K., Kovar, K., 2013. Flow cytometry for the development of biotechnological processes with microalgae. Biotechnol. Adv. https://doi.org/10.1016/j.biotechadv.2012.04.007

Iacopozzi, I., Innocenti, V., Marsili-Libelli, S., Giusti, E., 2007. A modified Activated Sludge Model No. 3 (ASM3) with two-step nitrification–denitrification. Environ. Model. Softw. 22, 847–861. https://doi.org/10.1016/J.ENVSOFT.2006.05.009

Inokuchi, R., Kuma, K.I., Miyata, T., Okada, M., 2002. Nitrogen-assimilating enzymes in land plants and algae: phylogenic and physiological perspectives. Physiol. Plant. 116, 1–11. https://doi.org/10.1034/J.1399-3054.2002.1160101.X

Ji, B., Zhang, M., Wang, L., Wang, S., Liu, Y., 2020. Removal mechanisms of phosphorus in non-aerated microalgal-bacterial granular sludge process. Bioresour. Technol. 312, 123531. https://doi.org/10.1016/J.BIORTECH.2020.123531

Ji, B., Zhu, L., Wang, S., Liu, Y., 2021. Temperature-effect on the performance of non-aerated microalgal-bacterial granular sludge process in municipal wastewater treatment. J. Environ. Manage. 282, 111955. https://doi.org/10.1016/J.JENVMAN.2021.111955

Ji, X., Cheng, J., Gong, D., Zhao, X., Qi, Y., Su, Y., Ma, W., 2018. The effect of NaCl stress on photosynthetic efficiency and lipid production in freshwater microalga—Scenedesmus obliquus XJ002. Sci. Total Environ. 633, 593–599. https://doi.org/10.1016/J.SCITOTENV.2018.03.240

Jia, H., Yuan, Q., 2018. Nitrogen removal in photo sequence batch reactor using algae-bacteria consortium. J. Water Process Eng. 26, 108–115. https://doi.org/10.1016/J.JWPE.2018.10.003

Karya, N.G.A.I., van der Steen, N.P., Lens, P.N.L., 2013. Photo-oxygenation to support nitrification in an algal–bacterial consortium treating artificial wastewater. Bioresour. Technol. 134, 244–250. https://doi.org/10.1016/J.BIORTECH.2013.02.005

Kim, D.-J., Lee, D.-I., Cha, G.-C., Keller, J., 2008. Analysis of Free Ammonia Inhibition of Nitrite Oxidizing Bacteria Using a Dissolved Oxygen Respirometer. Environ. Eng. Res. 13, 125–130. https://doi.org/10.4491/eer.2008.13.3.125

Kim, D.J., Lee, D.I., Keller, J., 2006. Effect of temperature and free ammonia on nitrification and nitrite accumulation in landfill leachate and analysis of its nitrifying bacterial community by FISH. Bioresour. Technol. 97, 459–468. https://doi.org/10.1016/J.BIORTECH.2005.03.032

Komolafe, O., Velasquez Orta, S.B., Monje-Ramirez, I., Noguez, I.Y., Harvey, A.P., Orta Ledesma, M.T., 2014. Biodiesel production from indigenous microalgae grown in wastewater. Bioresour. Technol. 154, 297–304. https://doi.org/10.1016/J.BIORTECH.2013.12.048

Kowalska, Z., Pniewski, F., Latała, A., 2019. DNA barcoding – A new device in phycologist's toolbox. Ecohydrol. Hydrobiol. https://doi.org/10.1016/j.ecohyd.2019.01.002

Krapp, A., David, L.C., Chardin, C., Girin, T., Marmagne, A., Leprince, A.S., Chaillou, S., Ferrario-Méry, S., Meyer, C., Daniel-Vedele, F., 2014. Nitrate transport and signalling in Arabidopsis. J. Exp. Bot. 65, 789–798. https://doi.org/10.1093/JXB/ERU001

Kwon, G., Kim, H., Song, C., Jahng, D., 2019. Co-culture of microalgae and enriched nitrifying bacteria for energy-efficient nitrification. Biochem. Eng. J. 152, 107385. https://doi.org/10.1016/j.bej.2019.107385

Kwon, G., Le, L.T., Jeon, J., Noh, J., Jang, Y., Kang, D., Jahng, D., 2020. Effects of light and mass ratio of microalgae and nitrifiers on the rates of ammonia oxidation and nitrate production. Biochem. Eng. J. 161, 107656. https://doi.org/10.1016/J.BEJ.2020.107656

Lakaniemi, A.M., Intihar, V.M., Tuovinen, O.H., Puhakka, J.A., 2012. Growth of Chlorella vulgaris and associated bacteria in photobioreactors. Microb. Biotechnol. 5, 69–78. https://doi.org/10.1111/J.1751-7915.2011.00298.X

Lam, T.P., Lee, T.M., Chen, C.Y., Chang, J.S., 2018. Strategies to control biological contaminants during microalgal cultivation in open ponds. Bioresour. Technol. 252, 180–187. https://doi.org/10.1016/j.biortech.2017.12.088

Larsdotter, K., 2006. Wastewater treatment with microalgae – a literature review. Vatten 62, 31–38.

Larsdotter, K., La Cour Jansen, J., Dalhammar, G., 2010. Phosphorus removal from wastewater by microalgae in Sweden – a year-round perspective. http://dx.doi.org/10.1080/09593330903382815 31, 117–123. https://doi.org/10.1080/09593330903382815

Le Moal, M., Gascuel-Odoux, C., Ménesguen, A., Souchon, Y., Étrillard, C., Levain, A., Moatar, F., Pannard, A., Souchu, P., Lefebvre, A., Pinay, G., 2019. Eutrophication: A new wine in an old bottle? Sci. Total Environ. https://doi.org/10.1016/j.scitotenv.2018.09.139

Lee, J., Cho, D.H., Ramanan, R., Kim, B.H., Oh, H.M., Kim, H.S., 2013. Microalgae-associated bacteria play a key role in the flocculation of Chlorella vulgaris. Bioresour. Technol. 131, 195–201. https://doi.org/10.1016/j.biortech.2012.11.130

Leong, W.H., Azella Zaine, S.N., Ho, Y.C., Uemura, Y., Lam, M.K., Khoo, K.S., Kiatkittipong, W., Cheng, C.K., Show, P.L., Lim, J.W., 2019. Impact of various microalgal-bacterial populations on municipal wastewater bioremediation and its energy feasibility for lipid-based biofuel production. J. Environ. Manage. 249, 109384. https://doi.org/10.1016/J.JENVMAN.2019.109384

Li, S.S., Li, J.H., Xia, M.S., Meng, Y.Y., Zhang, H., 2013. Adsorption of nitrogen and phosphorus by intact cells and cell wall polysaccharides of Microcystis. J. Appl. Phycol. 25, 1539–1544. https://doi.org/10.1007/s10811-013-9992-8

Lu, H., Feng, Y., Wu, Y., Yang, L., Shao, H., 2016. Phototrophic periphyton techniques combine phosphorous removal and recovery for sustainable salt-soil zone. Sci. Total Environ. 568, 838–844. https://doi.org/10.1016/j.scitotenv.2016.06.010

Luo, Y., Le-Clech, P., Henderson, R.K., 2018. Assessment of membrane photobioreactor (MPBR) performance parameters and operating conditions. Water Res. 138, 169–180. https://doi.org/10.1016/j.watres.2018.03.050

Mannina, G., Cosenza, A., Viviani, G., Ekama, G.A., 2018. Sensitivity and uncertainty analysis of an integrated ASM2d MBR model for wastewater treatment. Chem. Eng. J. 351, 579–588. https://doi.org/10.1016/j.cej.2018.06.126

Mantovani, M., Marazzi, F., Fornaroli, R., Bellucci, M., Ficara, E., Mezzanotte, V., 2020. Outdoor pilot-scale raceway as a microalgae-bacteria sidestream treatment in a WWTP. Sci. Total Environ. 710, 135583. https://doi.org/10.1016/J.SCITOTENV.2019.135583

Markou, G., Depraetere, O., Muylaert, K., 2016. Effect of ammonia on the photosynthetic activity of Arthrospira and Chlorella: A study on chlorophyll fluorescence and electron transport. Algal Res. 16, 449–457. https://doi.org/10.1016/j.algal.2016.03.039

Martínez, M.E., Sánchez, S., Jiménez, J.M., El Yousfi, F., Muñoz, L., 2000. Nitrogen and phosphorus removal from urban wastewater by the microalga Scenedesmus obliquus. Bioresour. Technol. 73, 263–272. https://doi.org/10.1016/S0960-8524(99)00121-2

Masojıdek, J., Koblızek, M., Torzillo, G., 2003. 2 Photosynthesis in Microalgae. Handb. microalgal Cult. Biotechnol. Appl. Phycol. 20–39. https://doi.org/https://doi.org/10.1002/9780470995280.ch2

Mata, T.M., Martins, A.A., Caetano, N.S., 2010. Microalgae for biodiesel production and other applications: A review. Renew. Sustain. Energy Rev. 14, 217–232. https://doi.org/10.1016/J.RSER.2009.07.020

Matassa, S., Batstone, D.J., Hü, T., Schnoor, J., Verstraete, W., 2015. Can Direct Conversion of Used Nitrogen to New Feed and Protein Help Feed the World? https://doi.org/10.1021/es505432w

Meng, L., Li, W., Zhang, S., Wu, C., Jiang, W., Sha, C., 2016. Effect of different extra carbon sources on nitrogen loss control and the change of bacterial populations in sewage sludge composting. Ecol. Eng. 94, 238–243. https://doi.org/10.1016/j.ecoleng.2016.05.013

Michelon, W., Luis Busi Da Silva, M., Paola Mezzari, M., Pirolli, M., Michel Prandini, J., Moreira Soares, H., 2010. Effects of Nitrogen and Phosphorus on Biochemical Composition of Microalgae Polyculture Harvested from Phycoremediation of Piggery Wastewater Digestate. Appl. Biochem. Biotechnol. 178, 1407–1419. https://doi.org/10.1007/s12010-015-1955-x

Moheimani, N.R., 2013. Inorganic carbon and pH effect on growth and lipid productivity of Tetraselmis suecica and Chlorella sp (Chlorophyta) grown outdoors in bag photobioreactors. J. Appl. Phycol. 25, 387–398. https://doi.org/10.1007/S10811-012-9873-6/TABLES/3

Molina Grima, E., Belarbi, E.H., Acién Fernández, F.G., Robles Medina, A., Chisti, Y., 2003. Recovery of microalgal biomass and metabolites: process options and economics. Biotechnol. Adv. 20, 491–515. https://doi.org/10.1016/S0734-9750(02)00050-2

Morales-Amaral, M. del M., Gómez-Serrano, C., Acién, F.G., Fernández-Sevilla, J.M., Molina-Grima, E., 2015. Production of microalgae using centrate from anaerobic digestion as the nutrient source. Algal Res. 9, 297–305. https://doi.org/10.1016/j.algal.2015.03.018

Muñoz, R., Guieysse, B., 2006. Algal–bacterial processes for the treatment of hazardous contaminants: A review. Water Res. 40, 2799–2815. https://doi.org/10.1016/J.WATRES.2006.06.011

Murata, N., Takahashi, S., Nishiyama, Y., Allakhverdiev, S.I., 2007. Photoinhibition of photosystem II under environmental stress. Biochim. Biophys. Acta - Bioenerg. 1767, 414–421. https://doi.org/10.1016/J.BBABIO.2006.11.019

Nishiyama, Y., Allakhverdiev, S.I., Murata, N., 2006. A new paradigm for the action of reactive oxygen species in the photoinhibition of photosystem II. Biochim. Biophys. Acta - Bioenerg. 1757, 742–749. https://doi.org/10.1016/J.BBABIO.2006.05.013

Nwoba, E.G., Parlevliet, D.A., Laird, D.W., Alameh, K., Moheimani, N.R., 2019. Light management technologies for increasing algal photobioreactor efficiency. Algal Res. 39, 101433. https://doi.org/10.1016/j.algal.2019.101433

Pachés, M., Martínez-Guijarro, R., González-Camejo, J., Seco, A., Barat, R., 2020. Selecting the most suitable microalgae species to treat the effluent from an anaerobic membrane bioreactor. Environ. Technol. (United Kingdom) 41. https://doi.org/10.1080/09593330.2018.1496148

Pang, N., Gu, X., Chen, S., Kirchhoff, H., Lei, H., Roje, S., 2019. Exploiting mixotrophy for improving productivities of biomass and co-products of microalgae. Renew. Sustain. Energy Rev. 112, 450–460. https://doi.org/10.1016/J.RSER.2019.06.001

Park, S., Bae, W., Chung, J., Baek, S.C., 2007. Empirical model of the pH dependence of the maximum specific nitrification rate. Process Biochem. 42, 1671–1676. https://doi.org/10.1016/j.procbio.2007.09.010

Patel, A., Barrington, S., Lefsrud, M., 2012. Microalgae for phosphorus removal and biomass production: A six species screen for dual-purpose organisms. GCB Bioenergy 4, 485–495. https://doi.org/10.1111/j.1757-1707.2012.01159.x

Perales-Vela, H.V., González-Moreno, S., Montes-Horcasitas, C., Cañizares-Villanueva, R.O., 2007. Growth, photosynthetic and respiratory responses to sub-lethal copper concentrations in Scenedesmus incrassatulus (Chlorophyceae). Chemosphere 67, 2274–2281. https://doi.org/10.1016/J.CHEMOSPHERE.2006.11.036

Perez-Garcia, O., Escalante, F.M.E., de-Bashan, L.E., Bashan, Y., 2011. Heterotrophic cultures of microalgae: Metabolism and potential products. Water Res. 45, 11–36. https://doi.org/10.1016/J.WATRES.2010.08.037

Petrovič, A., Simonič, M., 2015. Effect of Chlorella sorokiniana on the biological denitrification of drinking water. Environ. Sci. Pollut. Res. 22, 5171–5183. https://doi.org/10.1007/s11356-014-3745-3

Philips, S., Laanbroek, H.J., Verstraete, W., 2002. Origin, causes and effects of increased nitrite concentrations in aquatic environments. Rev. Environ. Sci. Biotechnol. https://doi.org/10.1023/A:1020892826575

Pires, J.C.M., Alvim-Ferraz, M.C.M., Martins, F.G., 2017. Photobioreactor design for microalgae production through computational fluid dynamics: A review. Renew. Sustain. Energy Rev. 79, 248–254. https://doi.org/10.1016/J.RSER.2017.05.064

Posadas, E., Morales, M. del M., Gomez, C., Acién, F.G., Muñoz, R., 2015. Influence of pH and CO2 source on the performance of microalgae-based secondary domestic wastewater treatment in outdoors pilot raceways. Chem. Eng. J. 265, 239–248. https://doi.org/10.1016/J.CEJ.2014.12.059

Powell, N., Shilton, A., Chisti, Y., Pratt, S., 2009. Towards a luxury uptake process via microalgae - Defining the polyphosphate dynamics. https://doi.org/10.1016/j.watres.2009.06.011

Preisner, M., 2020. Surface Water Pollution by Untreated Municipal Wastewater Discharge Due to a Sewer Failure. Environ. Process. 7, 767–780. https://doi.org/10.1007/s40710-020-00452-5

Puyol, D., Batstone, D.J., Hülsen, T., Astals, S., Peces, M., Krömer, J.O., 2017. Resource recovery from wastewater by biological technologies: Opportunities, challenges, and prospects. Front. Microbiol. https://doi.org/10.3389/fmicb.2016.02106

Rada-Ariza, A.M., Lopez-Vazquez, C.M., van der Steen, N.P., Lens, P.N.L., 2017. Nitrification by microalgal-bacterial consortia for ammonium removal in flat panel sequencing batch photo-bioreactors. Bioresour. Technol. 245, 81–89. https://doi.org/10.1016/j.biortech.2017.08.019

Raeisossadati, M., Moheimani, N.R., Parlevliet, D., 2019. Luminescent solar concentrator panels for increasing the efficiency of mass microalgal production. Renew. Sustain. Energy Rev. 101, 47–59. https://doi.org/10.1016/J.RSER.2018.10.029

Rahman, S.M., Eckelman, M.J., Onnis-Hayden, A., Gu, A.Z., 2016. Life-Cycle Assessment of Advanced Nutrient Removal Technologies for Wastewater Treatment. Environ. Sci. Technol. 50, 3020–3030. https://doi.org/10.1021/acs.est.5b05070

Ramanan, R., Kim, B.H., Cho, D.H., Oh, H.M., Kim, H.S., 2016. Algae–bacteria interactions: Evolution, ecology and emerging applications. Biotechnol. Adv. 34, 14–29.

https://doi.org/10.1016/J.BIOTECHADV.2015.12.003

Rane, A.S., Rutkauskaite, J., deMello, A., Stavrakis, S., 2017. High-Throughput Multi-parametric Imaging Flow Cytometry. Chem 3, 588–602. https://doi.org/10.1016/J.CHEMPR.2017.08.005

Ras, M., Steyer, J.P., Bernard, O., 2013. Temperature effect on microalgae: A crucial factor for outdoor production. Rev. Environ. Sci. Biotechnol. 12, 153–164. https://doi.org/10.1007/s11157-013-9310-6

Ratkowsky, D.A., Olley, J., Ross, T., 2005. Unifying temperature effects on the growth rate of bacteria and the stability of globular proteins. J. Theor. Biol. 233, 351–362. https://doi.org/10.1016/J.JTBI.2004.10.016

Raven, J.A., Giordano, M., 2016. Combined Nitrogen. Physiol. Microalgae 143–154. https://doi.org/10.1007/978-3-319-24945-2_7

Reichert, P., Borchardt, D., Henze, M., Rauch, W., Shanahan, P., Somlyódy, L., Vanrolleghem, P., 2001. River Water Quality Model no. 1 (RWQM1): II. Biochemical process equations, in: Water Science and Technology. pp. 11–30. https://doi.org/10.2166/wst.2001.0241

Reynolds, C.S., 2006. Ecology of phytoplankton. Cambridge University Press, Cambridge. https://doi.org/10.1017/CBO9780511542145

Rezvani, F., Sarrafzadeh, M.-H., Ebrahimi, S., Oh, H.-M., 2019. Nitrate removal from drinking water with a focus on biological methods: a review. Korea Env. Sci Pollut Res 26, 1124–1141. https://doi.org/10.1007/s11356-017-9185-0

Riaño, B., Hernández, D., García-González, M.C., 2012. Microalgal-based systems for wastewater treatment: Effect of applied organic and nutrient loading rate on biomass composition. Ecol. Eng. 49, 112–117. https://doi.org/10.1016/J.ECOLENG.2012.08.021

Robles, Á., Capson-Tojo, G., Galès, A., Ruano, M.V., Sialve, B., Ferrer, J., Steyer, J.P., 2020a. Microalgae-bacteria consortia in high-rate ponds for treating urban wastewater: Elucidating the key state indicators under dynamic conditions. J. Environ. Manage. 261. https://doi.org/10.1016/j.jenvman.2020.110244

Robles, Á., Capson-Tojo, G., Galès, A., Ruano, M.V., Sialve, B., Ferrer, J., Steyer, J.P., 2020b. Microalgae-bacteria consortia in high-rate ponds for treating urban wastewater: Elucidating the key state indicators under dynamic conditions. J. Environ. Manage. 261. https://doi.org/10.1016/j.jenvman.2020.110244

Rogato, A., Amato, A., Iudicone, D., Chiurazzi, M., Ferrante, M.I., D'Alcalà, M.R., 2015. The diatom molecular toolkit to handle nitrogen uptake. Mar. Genomics. https://doi.org/10.1016/j.margen.2015.05.018

Romero-Villegas, G.I., Fiamengo, M., Acién Fernández, F.G., Molina Grima, E., 2018. Utilization of centrate for the outdoor production of marine microalgae at pilot-scale in flat-panel photobioreactors. J. Biotechnol. 284, 102–114. https://doi.org/10.1016/j.jbiotec.2018.08.006

Rossi, S., Bellucci, M., Marazzi, F., Mezzanotte, V., Ficara, E., 2018. Activity assessment of microalgal-bacterial consortia based on respirometric tests. Water Sci. Technol. 78, 207–215. https://doi.org/10.2166/wst.2018.078

Rossi, Simone, Díez-Montero, R., Rueda, E., Castillo Cascino, F., Parati, K., García, J., Ficara, E., 2020. Free ammonia inhibition in microalgae and cyanobacteria grown in wastewaters: Photo-respirometric evaluation and modelling. Bioresour. Technol. 305, 123046. https://doi.org/10.1016/j.biortech.2020.123046

Rossi, S., Sforza, E., Pastore, M., Bellucci, M., Casagli, F., Marazzi, F., Ficara, E., 2020. Photo-respirometry to shed light on microalgae-bacteria consortia—a review. Rev. Environ. Sci. Biotechnol. https://doi.org/10.1007/s11157-020-09524-2

Ruiz-Martinez, A., Serralta, J., Pachés, M., Seco, A., Ferrer, J., 2014. Mixed microalgae culture for ammonium removal in the absence of phosphorus: Effect of phosphorus supplementation and process modeling. Process Biochem. 49, 2249–2257. https://doi.org/10.1016/j.procbio.2014.09.002

Ruiz-Martínez, A., Serralta, J., Romero, I., Seco, A., Ferrer, J., 2015. Effect of intracellular P content on

phosphate removal in Scenedesmus sp. Experimental study and kinetic expression. Bioresour. Technol. 175, 325–332. https://doi.org/10.1016/j.biortech.2014.10.081

Ruiz, J., Álvarez-Díaz, P.D., Arbib, Z., Garrido-Pérez, C., Barragán, J., Perales, J.A., 2013. Performance of a flat panel reactor in the continuous culture of microalgae in urban wastewater: Prediction from a batch experiment. Bioresour. Technol. 127, 456–463. https://doi.org/10.1016/J.BIORTECH.2012.09.103

Sánchez-Zurano, A., Gómez-Serrano, C., Acién-Fernández, F.G., Fernández-Sevilla, J.M., Molina-Grima, E., 2020. A novel photo-respirometry method to characterize consortia in microalgae-related wastewater treatment processes. Algal Res. 47, 101858. https://doi.org/10.1016/j.algal.2020.101858

Sánchez-zurano, A., Rodríguez-miranda, E., Guzmán, J.L., Acién-fernández, F.G., Fernández-sevilla, J.M., Grima, E.M., 2021. Abaco: A new model of microalgae-bacteria consortia for biological treatment of wastewaters. Appl. Sci. 11, 1–24. https://doi.org/10.3390/app11030998

Saravanan, A., Kumar, P.S., Varjani, S., Jeevanantham, S., Yaashikaa, P.R., Thamarai, P., Abirami, B., George, C.S., 2021. A review on algal-bacterial symbiotic system for effective treatment of wastewater. Chemosphere 271, 129540. https://doi.org/10.1016/J.CHEMOSPHERE.2021.129540

Sato, M., Murata, Y., Mizusawa, M., 2004. A Simple and Rapid Dual-fluorescence Viability Assay for Microalgae 20.

Seco, A., Aparicio, S., González-Camejo, J., Jiménez-Benítez, A., Mateo, O., Mora, J.F., Noriega-Hevia, G., Sanchis-Perucho, P., Serna-García, R., Zamorano-López, N., Giménez, J.B., Ruiz-Martínez, A., Aguado, D., Barat, R., Borrás, L., Bouzas, A., Martí, N., Pachés, M., Ribes, J., Robles, A., Ruano, M. V., Serralta, J., Ferrer, J., 2018. Resource recovery from sulphate-rich sewage through an innovative anaerobic-based water resource recovery facility (WRRF). Water Sci. Technol. 78, 1925–1936. https://doi.org/10.2166/wst.2018.492

Sepehri, A., Sarrafzadeh, M.H., Avateffazeli, M., 2020. Interaction between Chlorella vulgaris and nitrifying-enriched activated sludge in the treatment of wastewater with low C/N ratio. J. Clean. Prod. 247, 119164. https://doi.org/10.1016/J.JCLEPRO.2019.119164

Sfez, S., De Meester, S., Vlaeminck, S.E., Dewulf, J., 2019. Improving the resource footprint evaluation of products recovered from wastewater: A discussion on appropriate allocation in the context of circular economy. Resour. Conserv. Recycl. 148, 132–144. https://doi.org/10.1016/J.RESCONREC.2019.03.029

Sforza, E., Pastore, M., Santeufemia Sanchez, S., Bertucco, A., 2018. Bioaugmentation as a strategy to enhance nutrient removal: Symbiosis between Chlorella protothecoides and Brevundimonas diminuta. Bioresour. Technol. Reports 4, 153–158. https://doi.org/10.1016/J.BITEB.2018.10.007

Shandilya, K.K., Pattarkine, V.M., 2019. Using microalgae for treating wastewater, in: Advances in Feedstock Conversion Technologies for Alternative Fuels and Bioproducts: New Technologies, Challenges and Opportunities. Woodhead Publishing, pp. 119–136. https://doi.org/10.1016/B978-0-12-817937-6.00007-2

Shen, H., Wang, Z., Zhou, A., Chen, J., Hu, M., Dong, X., Xia, Q., 2015. Adsorption of phosphate onto amine functionalized nano-sized magnetic polymer adsorbents: mechanism and magnetic effects. RSC Adv. 5, 22080–22090. https://doi.org/10.1039/C4RA14630A

Solimeno, A., Gómez-Serrano, C., Acién, F.G., 2019. BIO_ALGAE 2: improved model of microalgae and bacteria consortia for wastewater treatment. Environ. Sci. Pollut. Res. 26, 25855–25868. https://doi.org/10.1007/s11356-019-05824-5

Solimeno, A., Parker, L., Lundquist, T., García, J., 2017. Integral microalgae-bacteria model (BIO_ALGAE): Application to wastewater high rate algal ponds. Sci. Total Environ. 601–602, 646–657. https://doi.org/10.1016/j.scitotenv.2017.05.215

Solimeno, A., Samsó, R., Uggetti, E., Sialve, B., Steyer, J.P., Gabarró, A., García, J., 2015. New mechanistic model to simulate microalgae growth. Algal Res. https://doi.org/10.1016/j.algal.2015.09.008

Solmaz, A., Işık, M., 2020. Optimization of membrane photobioreactor; the effect of hydraulic retention time on biomass production and nutrient removal by mixed microalgae culture. Biomass and Bioenergy 142, 105809. https://doi.org/10.1016/J.BIOMBIOE.2020.105809

Solovchenko, A., Verschoor, A.M., Jablonowski, N.D., Nedbal, L., 2016. Phosphorus from wastewater to crops: An alternative path involving microalgae. Biotechnol. Adv. 34, 550–564. https://doi.org/10.1016/J.BIOTECHADV.2016.01.002

Steele, J.H., 1962. ENVIRONMENTAL CONTROL OF PHOTOSYNTHESIS IN THE SEA. Limnol. Oceanogr. 7, 137–150. https://doi.org/10.4319/lo.1962.7.2.0137

Su, Y., 2021. Revisiting carbon, nitrogen, and phosphorus metabolisms in microalgae for wastewater treatment. Sci. Total Environ. 762, 144590. https://doi.org/10.1016/j.scitotenv.2020.144590

Su, Y., Mennerich, A., Urban, B., 2012. Synergistic cooperation between wastewater-born algae and activated sludge for wastewater treatment: Influence of algae and sludge inoculation ratios. Bioresour. Technol. 105, 67–73. https://doi.org/10.1016/J.BIORTECH.2011.11.113

Subashchandrabose, S.R., Ramakrishnan, B., Megharaj, M., Venkateswarlu, K., Naidu, R., 2011. Consortia of cyanobacteria/microalgae and bacteria: Biotechnological potential. Biotechnol. Adv. 29, 896–907. https://doi.org/10.1016/J.BIOTECHADV.2011.07.009

Sui, Q., Liu, C., Zhang, J., Dong, H., Zhu, Z., Wang, Y., 2016. Response of nitrite accumulation and microbial community to free ammonia and dissolved oxygen treatment of high ammonium wastewater. Appl. Microbiol. Biotechnol. 2016 1009 100, 4177–4187. https://doi.org/10.1007/S00253-015-7183-Z

Sun, C., Xu, Y., Hu, N., Ma, J., Sun, S., Cao, W., Klobučar, G., Hu, C., Zhao, Y., 2020. To evaluate the toxicity of atrazine on the freshwater microalgae Chlorella sp. using sensitive indices indicated by photosynthetic parameters. Chemosphere 244, 125514. https://doi.org/10.1016/J.CHEMOSPHERE.2019.125514

Sutherland, D.L., Howard-Williams, C., Turnbull, M.H., Broady, P.A., Craggs, R.J., 2015. Enhancing microalgal photosynthesis and productivity in wastewater treatment high rate algal ponds for biofuel production. Bioresour. Technol. 184, 222–229. https://doi.org/10.1016/J.BIORTECH.2014.10.074

Szabó, A., Takács, I., Murthy, S., Daigger, G.T., Licskó, I., Smith, S., 2008. Significance of Design and Operational Variables in Chemical Phosphorus Removal. Water Environ. Res. 80, 407–416. https://doi.org/10.2175/106143008X268498

Thomas, T., Gilbert, J., Meyer, F., 2012. Metagenomics - a guide from sampling to data analysis. Microb. Inform. Exp. 2, 1–12. https://doi.org/10.1186/2042-5783-2-3/FIGURES/1

Toledo-Cervantes, A., Posadas, E., Bertol, I., Turiel, S., Alcoceba, A., Muñoz, R., 2019. Assessing the influence of the hydraulic retention time and carbon/nitrogen ratio on urban wastewater treatment in a new anoxic-aerobic algal-bacterial photobioreactor configuration. Algal Res. 44, 101672. https://doi.org/10.1016/J.ALGAL.2019.101672

Trebst, A., 1974. Energy Conservation in Photosynthetic Electron Transport of Chloroplasts. Annu. Rev. Plant Physiol. 25, 423–458. https://doi.org/10.1146/annurev.pp.25.060174.002231

Valiente-Banuet, A., Verdú, M., 2008. Temporal shifts from facilitation to competition occur between closely related taxa. J. Ecol. 96, 489–494. https://doi.org/10.1111/J.1365-2745.2008.01357.X/FORMAT/PDF

Van Den Hende, S., Beelen, V., Julien, L., Lefoulon, A., Vanhoucke, T., Coolsaet, C., Sonnenholzner, S., Vervaeren, H., Rousseau, D.P.L., 2016. Technical potential of microalgal bacterial floc raceway ponds treating food-industry effluents while producing microalgal bacterial biomass: An outdoor pilot-scale study. Bioresour. Technol. 218, 969–979. https://doi.org/10.1016/J.BIORTECH.2016.07.065

Van Derlinden, E., Bernaerts, K., Van Impe, J.F., 2008. Accurate estimation of cardinal growth temperatures of Escherichia coli from optimal dynamic experiments. Int. J. Food Microbiol. 128, 89–100. https://doi.org/10.1016/J.IJFOODMICRO.2008.07.007

Vergara, C., Muñoz, R., Campos, J.L., Seeger, M., Jeison, D., 2016. Influence of light intensity on bacterial nitrifying activity in algal-bacterial photobioreactors and its implications for microalgae-based

wastewater treatment. Int. Biodeterior. Biodegradation 114, 116–121. https://doi.org/10.1016/J.IBIOD.2016.06.006

Viruela, A., Aparicio, S., Robles, Á., Falomir, L.B., Serralta, J., Seco, A., Ferrer, J., 2021. Kinetic modeling of autotrophic microalgae mainline processes for sewage treatment in phosphorus-replete and -deplete culture conditions. Sci. Total Environ. 149165. https://doi.org/10.1016/J.SCITOTENV.2021.149165

Vo, H.N.P., Ngo, H.H., Guo, W., Nguyen, T.M.H., Liu, Yiwen, Liu, Yi, Nguyen, D.D., Chang, S.W., 2019. A critical review on designs and applications of microalgae-based photobioreactors for pollutants treatment. Sci. Total Environ. 651, 1549–1568. https://doi.org/10.1016/j.scitotenv.2018.09.282

Wágner, D.S., Valverde-Pérez, B., Plósz, B.G., 2018. Light attenuation in photobioreactors and algal pigmentation under different growth conditions – Model identification and complexity assessment. Algal Res. 35, 488–499. https://doi.org/10.1016/j.algal.2018.08.019

Wágner, D.S., Valverde-Pérez, B., Sæbø, M., Bregua de la Sotilla, M., Van Wagenen, J., Smets, B.F., Plósz, B.G., 2016. Towards a consensus-based biokinetic model for green microalgae – The ASM-A. Water Res. 103, 485–499. https://doi.org/10.1016/j.watres.2016.07.026

Wang, B., Lan, C.Q., 2010. Biofixation of carbon dioxide (CO2) by microorganisms. Dev. Innov. Carbon Dioxide (Co 2, 411–432. https://doi.org/10.1533/9781845699581.4.411

Wang, S., Zhu, L., Ji, B., Hou, H., Ma, Y., 2021. Microalgal-Bacterial Granular Sludge Process in Non-Aerated Municipal Wastewater Treatment under Natural Day-Night Conditions: Performance and Microbial Community. Water 2021, Vol. 13, Page 1479 13, 1479. https://doi.org/10.3390/W13111479

Wayne, R., 2019. Chloroplasts. Plant Cell Biol. 235–267. https://doi.org/10.1016/B978-0-12-814371-1.00013-8

Xu, K., Zou, X., Xue, Y., Qu, Y., Li, Y., 2021. The impact of seasonal variations about temperature and photoperiod on the treatment of municipal wastewater by algae-bacteria system in lab-scale. Algal Res. 54, 102175. https://doi.org/10.1016/J.ALGAL.2020.102175

Xu, X., Gu, X., Wang, Zhongyang, Shatner, W., Wang, Zhenjun, 2019. Progress, challenges and solutions of research on photosynthetic carbon sequestration efficiency of microalgae. Renew. Sustain. Energy Rev. 110, 65–82. https://doi.org/10.1016/j.rser.2019.04.050

Yang, W., Vollertsen, J., Hvitved-Jacobsen, T., 2003. Nitrite accumulation in the treatment of wastewaters with high ammonia concentration, in: Water Science and Technology. IWA Publishing, pp. 135–141. https://doi.org/10.2166/wst.2003.0182

Zambrano, J., Krustok, I., Nehrenheim, E., Carlsson, B., 2016. A simple model for algae-bacteria interaction in photo-bioreactors. Algal Res. 19, 155–161. https://doi.org/10.1016/j.algal.2016.07.022

Zhang, B., Li, W., Guo, Y., Zhang, Z., Shi, W., Cui, F., Lens, P.N.L., Tay, J.H., 2020. Microalgal-bacterial consortia: From interspecies interactions to biotechnological applications. Renew. Sustain. Energy Rev. 118, 109563. https://doi.org/10.1016/J.RSER.2019.109563

Zhang, C., Li, S., Ho, S.H., 2021. Converting nitrogen and phosphorus wastewater into bioenergy using microalgae-bacteria consortia: A critical review. Bioresour. Technol. 342, 126056. https://doi.org/10.1016/J.BIORTECH.2021.126056

Zhang, M., Leung, K.T., Lin, H., Liao, B., 2020. The biological performance of a novel microalgal-bacterial membrane photobioreactor: Effects of HRT and N/P ratio. Chemosphere 261, 128199. https://doi.org/10.1016/J.CHEMOSPHERE.2020.128199

CHAPTER II

2. Aims and objectives

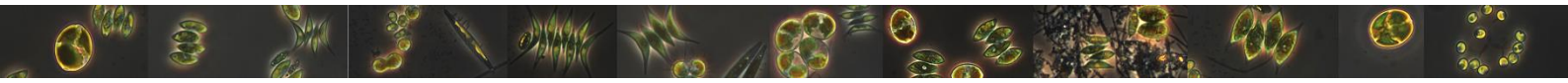

2. AIMS AND OBJECTIVES

This PhD thesis is aimed the knowledge of urban wastewater treatment based on microalgae-bacteria consortia. This research work has been approached from different knowledge areas, including microbiological analysis, experimental study in a pilot-scale plant and modelling, among others, with the main objective of evaluating the potential of microalgae-bacteria systems for wastewater treatment under the Circular Economy Principles.

Specifically, the project key objectives are:

- Assessing the effect of hydraulic retention time and type of influent wastewater on microalgae-bacteria growth in an outdoor membrane high rate algal pond (Chapter 5).

- Evaluating and identifying the inhibition mechanism of nitrite on photosynthesis and describing a mathematical photo-oxygenation model for nitrite inhibition in microalgae-bacteria consortia-based systems (Chapter 6).

- Developing a guide to identify and reduce competitive interactions between nitrifying bacteria and microalgae (Chapter 7).

- Understanding the changes in microalgal and bacterial community structures through the evaluation of different operational parameters (Chapter 8).

- Evaluating the sensitivity and uncertainty of a microalgae model outputs with respect to a subset of the key input parameters (Chapter 9).

- Developing, calibrating and validating an integrated microalgae-bacteria mechanistic model in outdoor membrane photobioreactor pilot plant and an outdoor membrane high rate algal pond (Chapter 10).

CHAPTER III

3. Thesis plan

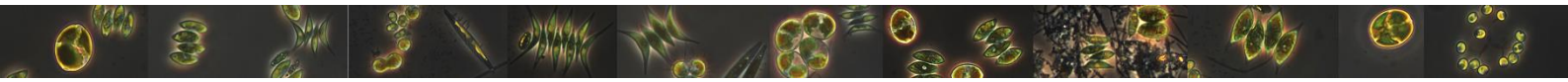

3. THESIS PLAN

This PhD thesis document is presented in a paper format composed of three published chapters and three additional chapters, also structured as a paper. The experimental design of the chapters has been elaborated to accomplish the aim and objectives of this research work.

Chapter 5. Prepared for imminent submission.

This chapter is focused on the effect of hydraulic retention time and wastewater influent on the effectiveness of wastewater treatment by microalgae-bacteria consortia in an outdoor high rate algal pond. The main interaction between microalgae and indigenous wastewater bacteria is described and analyzed. The outcome of Chapter 5 was used to support the experimental design of Chapters 8 and 10.

Chapter 6. Published in Science of the Total Environment*.

This chapter identifies nitrite as a photosynthesis inhibitor compound. The effect of nitrite in oxygen production and *Chlorophyll a* fluorescence is described and analyzed at lab-scale assays. Besides, nitrite inhibition of photosynthesis is modeled. The outcome of Chapter 6 was used to support the experimental design of Chapters 7, 8 and 10.

Chapter 7. Published in Algal Research*.

This chapter makes an overall assessment of competition between microalgae and ammonia-oxidizing bacteria. Biotic and abiotic factors influencing competition, methods to measure concentration and activity of both communities within the mixed culture and nitrification control strategies were explored. The outcome of Chapter 7 was used to evaluate Chapter 8.

Chapter 8. Prepared for submission.

This chapter identifies the microbiological composition of microalgae-bacteria acclimated community for wastewater treatment. The effect of hydraulic retention time and the wastewater influent in an outdoor high rate algal pond over microbial structure is here

evaluated. The outcome of Chapter 8 was used to support the experimental design of Chapter 10.

Chapter 9. Published in Science of the Total Environment*.

This chapter identifies the most influential parameters and uncertainty sources of a mechanistic microalgae model. Results of a global sensitivity and uncertainty analyses were here described. Besides, a calibration protocol for the most influential parameters was also established. The outcome of Chapter 9 was used to support the experimental design of Chapter 10.

Chapter 10. Prepared for future submission.

This chapter describes an integrate microalgae-bacteria mechanistic model. Validation of the mathematical model in an outdoor membrane photobioreactor pilot plant and an outdoor membrane high rate algal pond is here reported.

Chapter 11.

This chapter discusses and synthetizes the overall Ph.D. research outputs and compiles the contribution to the knowledge of this work.

This dissertation finalizes with the Conclusions. Finally, an extended abstract written in Spanish (Appendix A) has been included to in accordance with the regulation of the Universitat de València.

**Journal Editor has permitted the use of the article in this dissertation document.*

CHAPTER IV

4. Materials and Methods

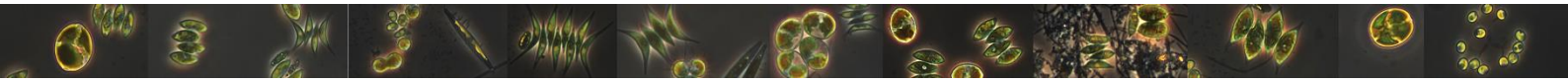

4. MATERIALS AND METHODS

4.1. MPBR and MHRAP pilot plant

The outdoor membrane photobioreactos (MPBR) pilot plant consisted of two flat-panel photobioreactors (PBRs) connected to one membrane tank (MT) (Figure IV. 1). The MPBR pilot plant was located at “Cuenca del Carraixet” Waste Water Treatment Plant (WWTP) (39°30′04.0’’N 0°20′00.1’’W, Valencia, Spain) and fed with effluent from an anaerobic membrane bioreactor (AnMBR) pilot plant (Table IV. 1). Further details of the AnMBR pilot plant can be found in Seco et al. (2018).

The influent wastewater was fed into the MPBR pilot plant by a centrifugal pump (P1) and mixed with recirculated biomass culture (R) in a distribution chamber (DC1) to be fed to the PBRs by gravity. The biomass culture from the PBRs then fell into a second distribution chamber (DC2), from where it was pumped to the MT. The biomass culture was recirculated from the MT to the PBRs by a progressing cavity pump (P2). Permeate was obtained from the MT of a rotary lobe vacuum pump (P3) and stored in the clean-in-place (CIP) tank. The biomass retention time (BRT) was controlled by extracting a specific volume of the biomass culture from the MT with a centrifugal pump (P4). The PBRs had a sun-exposed surface area of 2.3 m^2 (1.15 x 2 m). Two PBR with different width were operated: 0.25-m width PBRs (working volume of 0.550 m^3) and 0.10-m width PBRs (working volume of 0.220 m^3). The PBRs were continuously air-stirred for mixing the culture medium and avoiding fouling. Pure dioxide carbon (CO_2) was injected into the air system to set pH at 7.5 and ensure culture conditions rich in inorganic carbon. Uncontrolled phosphorus precipitation and free ammonia nitrogen (FAN) stripping were effectively reduced. A temperature control system was implemented consisting of a cooling device equipped with a thermostat (Daikin R410A inverter). The set point temperature was 20ºC. The cooled fluid was supplied to the MPBR plant through a 20-m long spiral tube immersed in the PBRs.

Online sensors were installed in the MPBR plant to obtain real-time information on the process performance: one pH sensor (pHD sc DPD1R1, Hach Lange) and one dissolved oxygen-temperature sensor (LDO Hach Lange) in each PBR. A light irradiance sensor (Apogee Quantum SQ-200) was set up on the surface of the PBRs to monitor and measure the photosynthetic active radiation (PAR). Besides sunlight, PBRs were constantly lit by twelve LED lamps (Unique Led IP65 WS-TP4S–40W-ME) placed on the back of the PBRs, providing a continuous light irradiation of 300 $\mu mol \cdot m^{-2} \cdot s^{-1}$ (measured on the PBR surface).

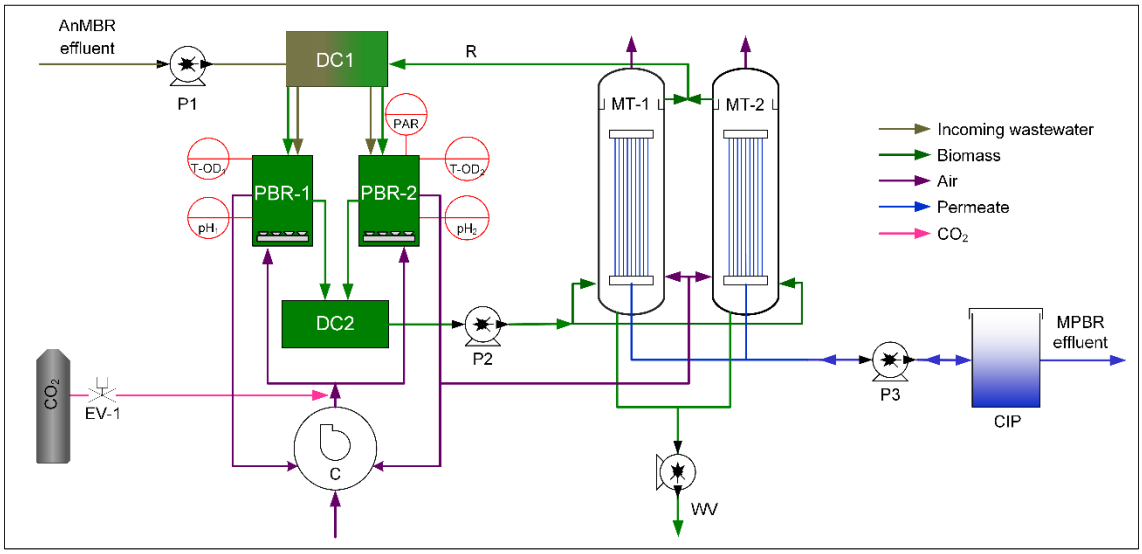

Figure IV. 1. Flow diagram of the MPBR pilot plant. Nomenclature: P: pump, DC: distribution chamber, PBR: photobioreactor, C: compressor, MT: membrane tank, R: recirculation, WV: wasting volume and CIP: clean-in-place.

The outdoor membrane high rate algal pond (MHRAP) was also located at the “Cuenca del Carraixet” WWTP. It consisted in one high rate algal pond (HRAP) connected to one MT, as shown schematically in Figure IV. 2. The HRAP had a working volume of 318.75 L, a solar irradiance area of 1.275 m^2 (2.55 x 0.5 m) and a liquid depth of 0.25 m. The reactor was continuously stirred by a single paddle wheel (six blades). The MHRAP pilot plant was fed with primary settling and pre-treatment effluent from the “Cuenca del Carraixet” WWTP (Table IV. 1).

The influent was fed into the HRAP by a centrifugal pump (P1). The biomass culture was pumped to the MT and recirculated by progressing cavity pump (P2). Permeate was

obtained from the MT from a rotary lobe vacuum pump (P3) and stored in the clean-in-place (CIP) tank. The BRT was controlled by extracting a specific volume of the biomass culture from the HRAP by overflow.

The on-line sensors were installed in the MHRAP pilot plant were: a pH sensor (pHD sc DPD1R1, Hach Lange), a dissolved oxygen-temperature sensor (LDO Hach Lange), an oxidation reduction potential (ORP) sensor (ORP DRD1P5.99, Hach Lange), an AN-ISE sensor (AN-ISE LXV440.99.00001, Hach Lange) to record ammonium (NH_4-N) and NO_X-N (sum of nitrite (NO_2-N) and nitrate (NO_3-N)), and a light irradiance sensor (Apogee Quantum SQ-200) set up on the surface of the HRAP for measuring PAR.

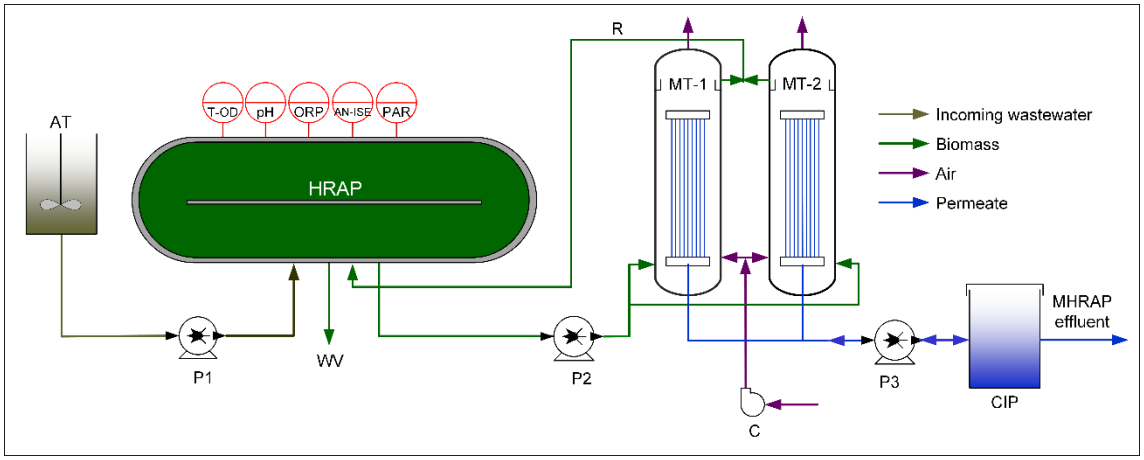

Figure IV. 2. Flow diagram of the HRAP pilot plant. Nomenclature: P: pump, DC: distribution chamber, HRAP: high rate algal pond, C: compressor, MT: membrane tank, R: recirculation, WV: wasting volume and CIP: clean-in-place.

Both pilot plants were connected to two MT modules (one spare and one operating). Each MT consisted of a hollow-fiber ultrafiltration membrane bundle extracted from an industrial-scale membrane unit (PURON® Koch Membrane Systems (PUR-PSH31), 0.03 µm pores). It had a total working volume of 14 L and a filtration area of 3.4 m^2. For membrane scouring, air was introduced to the MT through its bottom.

4.1.1. MPBR and MHRAP operation

Membrane filtration technology enables decoupling both BRT and hydraulic retention time (HRT). The corresponding amount of biomass was purged from the system and the incoming wastewater (AnMBR, primary settling or pre-treatment effluent) was fed into

the system. To control HRT, the corresponding amount of permeate was extracted from the system as effluent. The same amount of substrate was introduced into the system to replace the volume taken out of the system. A fraction of the biomass culture was fed into the MT at a flowrate of 300 $L \cdot h^{-1}$ in both pilot plants. The rejection of the membrane unit was recycled to the PBRs and HRAP, as shown in Figure IV. 1Figure IV. 2.

Membrane operation for both pilot plants consisted of a combination of the classical stages of filtration–relaxation (F–R) and back-flushing. Ventilation and degasification stages were also considered (Robles et al., 2013). The membrane operating mode followed a sequence of 300 s basic F-R cycle (250 s filtration and 50 s relaxation), 40 s of back-flush every 10 F–R cycles, 60 s of ventilation every 20 F–R cycles and 60 s of degasification every 50 F–R cycles. The gross 20ºC-standardised transmembrane flux (J_{20}) was kept around 22-30 LMH. The average specific gas demand per unit of membrane area (SGD_m) was kept around 0.3-0.4 $Nm^3 \cdot h^{-1} \cdot m^{-2}$. This gave an average specific gas demand per volume of produced permeate (SGD_P) of around 8-12 Nm^3 of gas per m^3 of permeate.

No active inoculation of the HRAP was needed, implying that a natural process of initial ecological succession of the indigenous microorganisms occurred. This approach facilitates a possible industrial application of this technology.

4.1.2. Incoming wastewater streams

The AnMBR effluent along with primary settling and pre-treatment effluent from the “Cuenca del Carraixet” WWTP were used as MPBR and MHRAP influent. The main characteristics of three incoming wastewater streams are displayed in Table IV. 1.

The AnMBR effluent consisted of a nutrient-rich permeate with a negligible concentration of total suspended solids and very low concentration of biodegradable organic matter (0 g TSS m^{-3} and 27 ± 2 g BOD m^{-3}, respectively) making it a suitable culture medium for microalgae growth. Low biodegradable organic matter concentration limits heterotrophic

activity, and therefore the synergetic interactions between microalgae and heterotrophic bacteria become less effective. A biomass culture dominated by microalgae is suitable for calibrating parameters and kinetics expressions related to photosynthetic organisms. Primary settling and pre-treatment effluents contained biodegradable organic matter, which depending on operating parameters can provide favorable conditions for developing self-sustaining microalgae-bacteria consortia.

Table IV. 1. Characteristics and composition of AnMBR, primary settling and pre-treatment effluent. Nomenclature: NH_4-N: ammonium, NO_2-N: nitrite, NO_3-N: nitrate, T-N: total nitrogen, PO_4-P: phosphate, T-P: total phosphorus, T-COD: total chemical oxygen demand, S-COD: soluble chemical oxygen demand, T-BOD: total biochemical oxygen demand, S-BOD: soluble biochemical oxygen demand, TSS: total suspended solids, VSS: volatile suspended solids and L.D: limit of detection.

Parameter	Unit	AnMBR effluent	Primary settling effluent	Pre-treatment effluent
NH_4-N	g $N \cdot m^{-3}$	49 ± 7	37 ± 8	39 ± 3
NO_2-N	g $N \cdot m^{-3}$	< LD[1]	0.8 ± 0.7	0.5 ± 0.2
NO_3-N	g $N \cdot m^{-3}$	< LD[1]	2.4 ± 1.4	1.2 ± 0.8
T-N	g $N \cdot m^{-3}$	53 ± 7[1]	40 ± 10	47 ± 4
PO_4-P	g $P \cdot m^{-3}$	5.7 ± 1.4	3.7 ± 0.9	4.4 ± 1.3
T-P	g $P \cdot m^{-3}$	5.7 ± 1.4[1]	4.2 ± 1.2	7.7 ± 1.4
T-COD	g $COD \cdot m^{-3}$	67 ± 7[1]	252 ± 71	692 ± 139
S-COD	g $COD \cdot m^{-3}$	67 ± 7	107 ± 61	308 ± 86
T-BOD	g $O_2 \cdot m^{-3}$	27 ± 2[1]	105 ± 18	290 ± 30
S-BOD	g $O_2 \cdot m^{-3}$	27 ± 2	36 ± 5	106 ± 21
TSS	g $TSS \cdot m^{-3}$	< LD[1]	107 ± 61	308 ± 86
VSS	g $VSS \cdot m^{-3}$	< LD[1]	92 ± 46	258 ± 73

[1]AnMBR permeate effluent did not contain particulate fraction, thus no differences between total and soluble fractions were observed. TSS and VSS were therefore not detected in the permeate effluent.

4.2. LAB-SCALE ASSAYS

The lab-scale PBR consisted of a cylindrical transparent reactor with a working volume of 8 L (20 cm internal diameter). The culture was air-stirred at a flowrate of 0.7 vvm through four fine bubble diffusers placed crosswise at the bottom to achieve biomass homogenization and avoid biofilm formation on the walls. The reactor was placed in a thermostatic chamber keeping the culture temperature at 25 ºC. Pure CO_2 (99.9%) was

injected from a pressurized cylinder at 1.5-2.0 bar pressure to keep reactor pH constant at 7.5 (Figure IV. 3). An on-off electro-valve synchronized with the pH measurements recorded by the data acquisition system (a temperature-pH probe connected to a multiparametric analyzer, CONSORT C832, Belgium) was opened for 2s when the pH exceeded the set point value of 7.5. Dissolved oxygen (DO) was measured by a Cellox 330i electrode (WTW, Germany) connected to an oximeter (Oxi 320, SET WTW, Germany). The lab-scale PBR was litted by five cool-white LED lamps (T8 LED-Tube 9 W) to supply a light intensity of 150 µmol·m^{-2}·s^{-1} measured at the PBR surface. The PBR was operated in a semi-continuous mode (BRT ≡ HRT). Incoming wastewater was driven by a peristaltic pump. The wasting volume was purged by overflow.

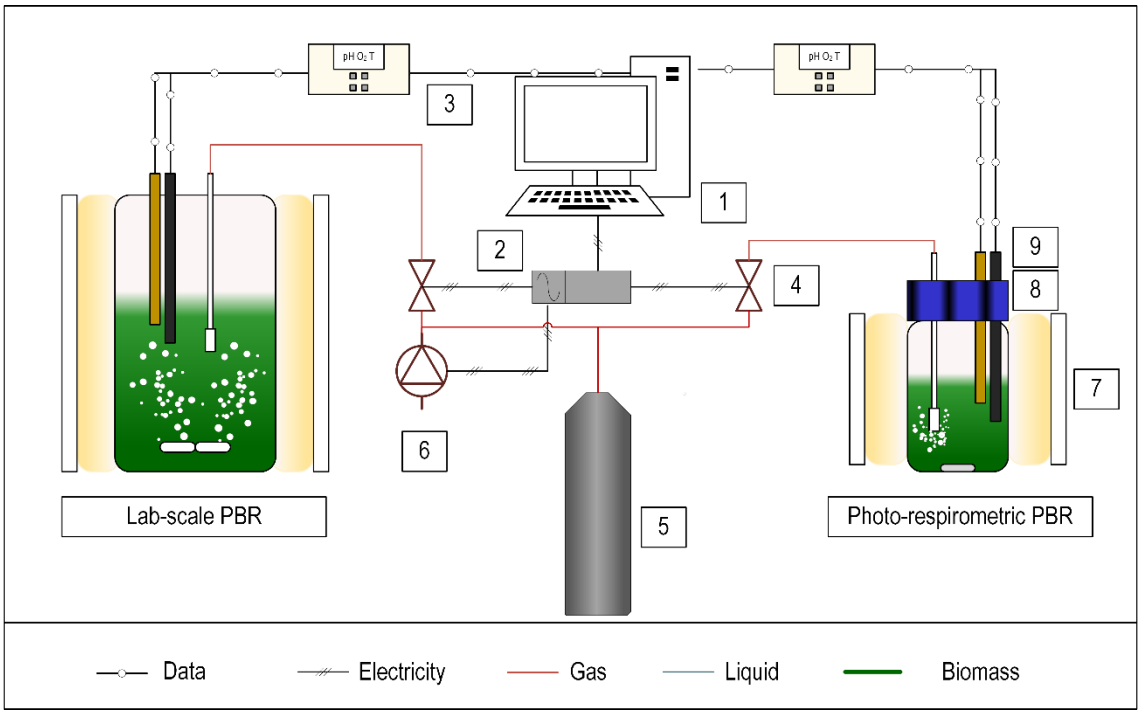

Figure IV. 3. Scheme of Lab-scale PBR and photo-respirometric PBR. Legend: 1 = Industrial grade PC, 2 = relay box, 3 = multiparametric consort, 4 = on-off electro-valve, 5 = pure CO_2 gas bullet, 6 = air compressor, 7 = light source, 8 = DO and 9 = pH and temperature probes.

4.2.1. Photo-respirometric tests

A 0.5-L cylindrical closed PBR was lit by two LED lamps (Seven ON LED 11 W) to supply a light intensity of 150 µmol·m^{-2}·s^{-1} on the surface (Figure IV. 3). It was placed inside a climate chamber to perform photo-respirometric tests at a constant temperature of

around 25 ºC. A temperature-pH probe was connected to a multiparametric analyzer (CONSORT C832, Belgium). An on-off valve was used to add pure CO_2 (99.9%) for 1 s when the pH recorded by pH probe exceeded the set point value of 7.5. The biomass culture was stirred at 250 rpm to ensure homogenization and avoid biomass sedimentation.

The DO concentration was monitored during the time that each test lasted by an oxygen probe (Cellox 330i electrode (WTW, Germany)). Data was retrieved and used to obtain net oxygen production rate (OPR_{NET}) and oxygen uptake rate (OUR). DO evolution can be used as an indirect measurement of microalgae and bacteria activities (Rossi et al., 2018; Sánchez-Zurano et al., 2020).

Both OPR_{NET} and OUR were obtained by performing photo-respirometric tests using a protocol adapted from Rossi et al. (2018) and Sánchez-Zurano et al. (2020):

- Samples of biomass culture were subjected to nutrient and organic matter starvation (continuous light of 200 $\mu mol \cdot m^{-2} \cdot s^{-1}$ and an aeration rate of 0.2 vvm). According to main objective of photo-respirometric tests, this step could be omitted (Chapter 5).
- Culture samples were placed inside the PBR and DO variations over time were measured under different conditions.
- Biomass culture was diluted or concentrated (depending on its concentration) to achieve an optical density at 680 nm (OD_{680}) around 0.5.
- OPR_{NET} ($mg\ O_2 \cdot g \cdot VSS^{-1} \cdot h^{-1}$): Biomass culture was exposed to 5-min light-dark cycles (both lasted 2.5 minutes and 4 cycles were performed) to record DO concentration every 10 s performing between 80 and 120 %Sat. The first minute of light and dark exposure was disgregaded as it was considered the adaptation time (Sánchez-Zurano et al., 2020).

  The OPR_{NET} was calculated as the sum between the monitored values (i.e., specifying whether the slope is positive or negative) of the oxygen production rate (OPR) slope in the light phase and the OUR slope in the dark phase, divided by volatile suspended

solids (VSS) (Equation IV. 1) (i.e. volatile suspended solids (VSS), which were measured according to the Standard Methods).

$$\mathrm{OPR_{NET}} = \frac{\mathrm{OPR} + \mathrm{OUR}}{\mathrm{VSS}} \qquad \text{Equation IV. 1}$$

where OPR_{NET} is the net oxygen production rate (g $O_2 \cdot g\ VSS^{-1} \cdot h^{-1}$), OPR is the oxygen production rate (g $O_2 \cdot m^{-3} \cdot h^{-1}$), OUR is the oxygen uptake rate, value (g $O_2 \cdot m^{-3} \cdot h^{-1}$), VSS is the volatile suspended solids (g $VSS \cdot m^{-3}$).

- Heterotrophic OUR (OUR_{HET}) (mg $O_2 \cdot g \cdot VSS^{-1} \cdot h^{-1}$): Another culture sample was used to measure heterotrophic activity. Substrate solution of sodium acetate was dosed under dark conditions to achieve a substrate concentration of 30 $g \cdot m^{-3}$. Heterotrophic activity was measured as the sum between OUR measured after substrate addition ($OUR_{HET\text{-}TOT}$) and the endogenous OUR ($OUR_{HET\text{-}END}$), specifying whether the slope is positive or negative (Equation IV. 2).

$$\mathrm{OUR_{HET}} = \frac{\mathrm{OUR_{HET-TOT}} + \mathrm{OUR_{HET-END}}}{\mathrm{VSS}} \qquad \text{Equation IV. 2}$$

where OUR_{HET} is the oxygen uptake rate by heterotrophic bacteria (g $O_2 \cdot g\ VSS^{-1} \cdot h^{-1}$), $OUR_{HET\text{-}TOT}$ is the oxygen uptake rate associated with substrate consumption and endogenous respiration (g $O_2 \cdot m^{-3} \cdot h^{-1}$), $OUR_{HET\text{-}END}$ is the oxygen uptake rate associated with endogenous respiration (g $O_2 \cdot m^{-3} \cdot h^{-1}$), and VSS is the volatile suspended solids (g $VSS \cdot m^{-3}$).

- Ammonia-oxidizing bacteria oxygen uptake rate (OUR_{AOB}) (mg $O_2 \cdot g\ VSS^{-1} \cdot h^{-1}$): A sample of biomass culture was placed inside the PBR and a substrate solution of ammonium chloride (NH_4Cl) was dosed to achieve an NH_4-N concentration of 10 g N m^{-3}. NOB activity was inhibited by dosing an inhibitor solution of potassium chlorate ($KClO_3$) to achieve 1.2 $g \cdot L^{-1}$ in biomass culture (Rossi et al., 2018). OUR_{AOB} was measured as the sum between OUR measured after substrate ($OUR_{AOB\text{-}TOT}$) addition

and the endogenous OUR ($OUR_{AOB\text{-}END}$), specifying whether the slope is positive or negative (Equation IV. 3).

$$OUR_{AOB} = \frac{OUR_{AOB-TOT} + OUR_{AOB-END}}{VSS} \quad \text{Equation IV. 3}$$

where OUR_{AOB} is the oxygen uptake rate by AOB (g $O_2 \cdot g\ VSS^{-1} \cdot h^{-1}$), $OUR_{AOB\text{-}TOT}$ is the oxygen uptake rate associated with substrate consumption and endogenous respiration (g $O_2 \cdot m^{-3} \cdot h^{-1}$), $OUR_{AOB\text{-}END}$ is the oxygen uptake rate associated with endogenous respiration (g $O_2 \cdot m^{-3} \cdot h^{-1}$) and VSS is the volatile suspended solids (g $VSS \cdot m^{-3}$).

- Nitrite-oxidizing bacteria oxygen uptake rate (OUR_{NOB}) (mg $O_2 \cdot g\ VSS^{-1} \cdot h^{-1}$): A new sample from biomass culture was placed inside the PBR and nitrite standard solution (sodium nitrite) of 1000 g $NO_2 \cdot m^{-3}$ was dosed to achieve an NO_2-N concentration of 10 g N m^{-3}. AOB activity was inhibited by dosing an inhibitor solution of allylthiourea (ATU) to achieve 5 g m^{-3} in the culture (González-Camejo et al., 2019). OUR_{NOB} was measured as the sum between OUR measured after substrate ($OUR_{NOB\text{-}TOT}$) addition and the endogenous OUR ($OUR_{NOB\text{-}END}$), specifying whether the slope is positive or negative (Equation IV. 4).

$$OUR_{AOB} = \frac{OUR_{AOB-TOT} + OUR_{AOB-END}}{VSS} \quad \text{Equation IV. 4}$$

where OUR_{NOB} is the oxygen uptake rate by NOB (g $O_2 \cdot g\ VSS^{-1} \cdot h^{-1}$), $OUR_{NOB\text{-}TOT}$ is the oxygen uptake rate associated with substrate consumption and endogenous respiration (g $O_2 \cdot m^{-3} \cdot h^{-1}$), $OUR_{NOB\text{-}END}$ is the oxygen uptake rate associated with endogenous respiration (g $O_2 \cdot m^{-3} \cdot h^{-1}$) and VSS is the volatile suspended solids (g $VSS \cdot m^{-3}$).

Experimental DO data were matched to a model, which considers oxygen mass transfer and DO biological production or consumption (Equation IV. 4). The DO mass balance in the photorespirometric test is therefore obtained with Equation IV. 4 and 6.

The oxygen mass transfer (K_La) coefficient was evaluated by performing an abiotic test in distilled water in the same chemical-physical conditions set during the experiments. Destilled water was placed in the batch reactor and oxygen concentration was increased to 130%Sat by bubbling air. Then, aeration was stopped and oxygen concenrtation was recorded during 3 hours. The minimum residual sum of squared errors was used to match dynamic mass balance for DO with Equation IV. 4.

$$\frac{d(DO)}{dt} = K_La \cdot (DO_{SAT} - DO) + OR \qquad \text{Equation IV. 5}$$

$$DO_{SAT} = pO_2 \cdot K_{H,O_2}(T) = pO_2 \cdot K_{H,O_2,REF} \cdot \exp\left(-\frac{-\Delta_{SOL}H}{R} \cdot \left(\frac{1}{T} - \frac{1}{T_{REF}}\right)\right) \qquad \text{Equation IV. 6}$$

where OR is the oxygen production or uptake rate, K_La is the oxygen mass transfer coefficient (h^{-1}), DO_{SAT} is the DO saturation concentration (g O_2 m^{-3}) at tempertature T (K) and the partial pressure of oxygen in atmosphere pO_2 (Atm), and $K_{H,O2}(T)$ = 40.5 (mg O_2 L^{-1} Atm^{-3}) is the Henry's law solubility constant for DO at experimental temperature (Sander, 2015) and $\Delta_{SOL}H/R$ = 1200 (K) (tabulated) is the enthalpy of dissolution divided for the univeral gas constant (Sander, 2015). The reference temperature (T_{REF}), and pO_2 were 298.15 K and 0.21 atm.

4.2.2. Chlorophyll a fluorescence

Chlorophyll a (*Chl a*) fluorescence provides plenty of information about the Photosystem II (PS II) performance and electron transport chain (Strasser et al., 2004). Electron transport rate (ETR) curve, non-photochemical quenching (NPQ) and the fluorescence transient kinetics were measured.

The ETR curve was recorded in dark-adapted samples (20 min) using the Light curve test (LC1) protocol of the fluorometer AquaPen-C AP-C 100 (PSI (Photon Systems Instruments), 2017). This protocol is based on successive measurements of the sample exposed to a stepwise increase in actinic light intensity (red-light diode). The effective quantum yields of PS II are determined under 6 actinic light intensities: 10, 20, 50,100,

300 and 500 μmol·m^{-2}·s^{-1}, with 60 s phase. The ETR curve was calculated using the quantum yields of photosynthesis derived from the LC1 protocol and the number of absorbed photons per *Chl a* and time according to Equation IV. 7.

$$\mathrm{ETR} = \Phi_{\mathrm{PS\,II}} \cdot \mathrm{E} \cdot 0.5 \qquad \text{Equation IV. 7}$$

where $\Phi_{\mathrm{PS\,II}}$ is the quantum yield of PS II, E is the irradiance of the actinic light (μmol·m^{-2}·s^{-1}) and 0.5 is the fraction of absorbed quanta direct to PS II, i.e. the radiant energy is absorbed by PS I and PS II equally (Yamori et al., 2011).

The nonlinear model described by Serôdio et al. (2013) (Equation IV. 7) was applied to match the ETR curves and to estimate the following key parameters: (I) maximum photosynthetic rate ($\mathrm{ETR_{MAX}}$, Equation IV. 7), the maximum electron transport rate through the PS II (μmol·m^{-2}·s^{-1}); (II) the initial slope of ETR curve (α, Equation IV. 7), the quantum efficiency of photosynthetic electron transport (electrons/photon); and (III): the saturating irradiance of photosynthesis (E_K, Equation IV. 7) (μmol·m^{-2}·s^{-1}).

$$\mathrm{rETR} = \frac{\mathrm{E}}{\mathrm{aE^2 + bE + c}} \qquad \text{Equation IV. 8}$$

$$\alpha = \frac{1}{\mathrm{c}}, \mathrm{ETR_{MAX}} = \frac{1}{\mathrm{b} + \sqrt{\mathrm{ac}}} \text{ and } \mathrm{E_K} = \frac{\mathrm{c}}{\mathrm{b} + \sqrt{\mathrm{ac}}} \qquad \text{Equation IV. 9}$$

NPQ was measured in dark-adapted samples (20 min) following the AquaPen-C AP-C 100 NPQ2 protocol (PSI (Photon Systems Instruments), 2017). The NPQ protocol is divided in two parts, one measuring fluorescence under dark-adapted and a second under light-adapted conditions. The protocol begins by giving a measuring light to obtain the minimum fluorescence level in a dark-adapted state (F_o). A short saturating light flash is then applied to reduce the plastoquinone (PQ) pool and the maximum fluorescence is measured in the dark-adapted state (F_m). After a short-term relaxation in the dark, the microalgae sample is exposed to light actinic for hundreds of seconds to elicit a transient

of the Kautsky effect measuring the instantaneous *Chl* fluorescence in the light-adapted phase (F_tL) (Stirbet and Govindjee, 2011). An additional saturating flash sequence is applied on top of the actinic light to measure NPQ and the effective quantum yield of photosynthesis in the light-adapted state (F_ML). After exposure to continuous illumination, NPQ relaxation is determined by saturating pulses applied in the dark, measuring maximum Chl fluorescence and instantaneous Chl fluorescence in the dark adapted phase (F_tD and F_MD, respectively).

Transient *Chlorophyll* fluorescence induction in dark-adapted samples was measured using the AquaPen-C AP-C 100 JIP-test (PSI (Photon Systems Instruments), 2017). The fast fluorescence induction curve was recorded in 50 µs - 2 s time range with a saturating light of 3000 µmol·m^{-2}·s^{-1} of red-orange light (620 nm). The fluorescence transient starts at the phase O (at 50 µs), passes through two intermediate, phases J and I, (at 2 and 60 ms, respectively) and reaches the maximum fluorescence in the phase P. The set of phases is called the OJIP curve (Figure IV. 3).

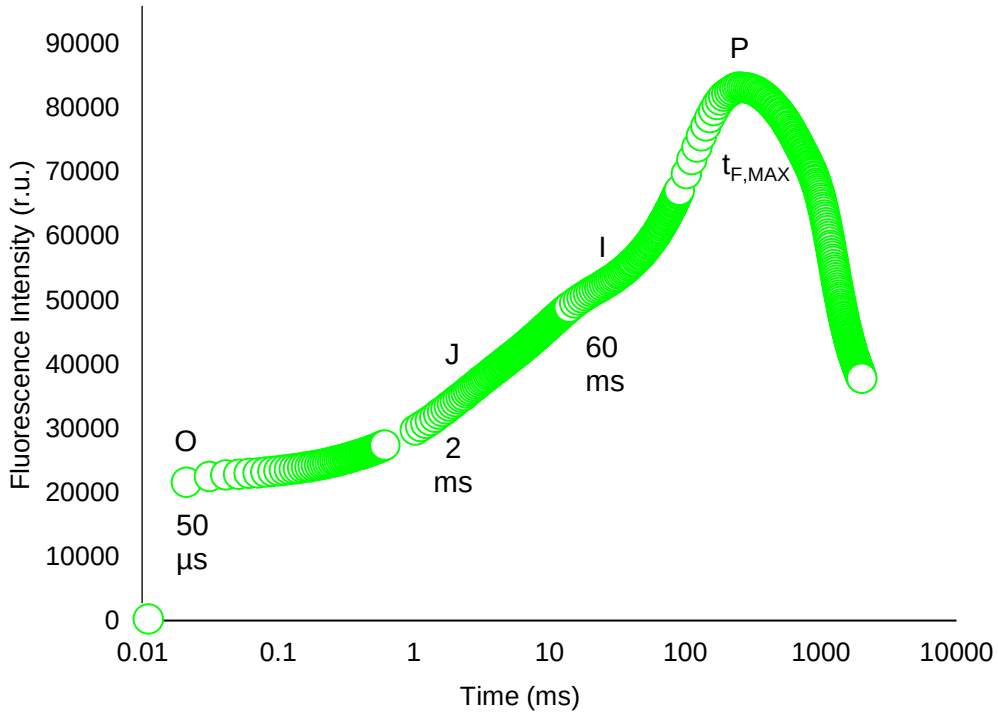

Figure IV. 4. Example of OJIP curve and the phases O, J, I and P.

To better evaluate the events reflected in the OJIP curve and between the O-J, J-I and I-P phases, the fluorescence data were normalized (between the minimum and maximum fluorescence intensity, F_o and F_m, respecitvely) and presented as the relative variable fluorescence kinetics at any time (Equation IV. 7) and as a kinetic profile of the difference between the control reactor and the other two batch reactors in the same set (Equation IV. 7) (Gomes et al., 2012).

$$V_{OP} = \frac{(F_t - F_o)}{(F_m - F_o)}$$ Equation IV. 10

$$\Delta V_{OP} = (V_{OP} - V_{OP-\text{control reactor}})$$ Equation IV. 11

where F_t is the instantaneous chlorophyll fluorescence at any time t (relative units); F_o is the minimum chlorophyll fluorescence (relative units); F_m is the maximum chlorophyll fluorescence (relative units); and V_{OP} is the relative variable fluorescence (relative units).

4.3. SEQUENCING-BASED TECHNIQUES

4.3.1. Sample collection and DNA extraction

Microalgae-bacteria samples were collected from the MHRAP pilot plant and were concentrated tenfold and stored in 50 mL Eppendorf tube at -20ºC to characterize bacterial and microalgal communities involved in ecological interactions. Extraction of bacterial DNA was performed with an E.Z.N.A.® Soil DNA Kit (Omega-Biotek), according to the manufacturer's protocol. Microalgal DNA extraction were performed with a E.Z.N.A.® Plant DNA Kit (Omega-Biotek) also according to the manufacturer's protocol. Extractions were performed from 1 mL of homogenized sample. Concentration and purity of DNA was determined by wavelengths of 260, 230 and 280 nm using a Nanodrop 2000 spectrophotometer (Thermo Scientific).

4.3.2. Illumina amplicon sequencing

The V3-4 hyper-variable region of the 16S rDNA gene was amplified using the universal prokaryotic indexed primers 515F (5'-GTGCCAGCMGCCGCGGTAA-3') and 806R (5'-GGACTACHVGGGTWTCTAAT-3') to identify bacterial communities (Klindworth et al., 2013). The V4 hyper-variable region of the 18S rDNA gene was amplified using the universal primer set TAReuk454FWD1 (5′- CCA GCA SCY GCG GTA ATT CC-3′) and TAReukREV3P (5′-ACT TTC GTT CTT GAT YRA-3′) to identify microalgal communities (Krug et al., 2019). Amplification conditions were: denaturing stage at 95ºC during 30 seconds, 28 cycles of 30 seconds steps at 95, 55 and 72ºC, successively; and final elongation stage at 72ºC during 5 minutes. The resulting amplicons were multiplexed in a Nextera XT Index kit (Illumina) and sequencing was performed according to the Illumina manufacturer's protocol on a MiSeq V3 reagent kit on a MiSeq sequencer in a 2x300 bp paired-end run, in the genomic department of the "Fundación para el Fomento de la Investigación Sanitaria y Biomédica de la Comunidad Valenciana" (FISSABIO).

4.3.3. Downstream sequencing analysis: diversity and biostatistics

The resulting raw sequences retrieved from Illumina sequencing were then sequentially processed using an open-source *mothur* software (v.1.46.1). The taxonomy was assigned according to the v138.1 release of SILVA database. The contingency table generated was used as the input for microbial ecology analysis using R-studio v.2021.09.0 software and vegan packages. For bacteria quantification, Chloroplast were not considered for microbial ecology analysis as they were supposed to belong to eukaryotic microalgae and not to the bacteria domain.

Alpha diversity was calculated through the evenness and richness index indicators (Shannon-Wiener and Simpson) using IBM SPSS Statistics 26 software (Armonk, NY: IBM Corp). A principal co-ordinate analysis (PCoA) based on the Bray-Curtis distances matrix was performed in mothur to explore the beta diversity of the different samples processed for bacteria and microalgae quantification.

The microbial and operational results obtained were statistically analysed by IBM SPSS Statistics 26 software (Armonk, NY: IBM Corp). An analysis of variance (ANOVA) was performed to evaluate the significance of the differences in the mean values. Differences were considered statistically significant when p-value was below 0.01.

4.4. SAMPLING AND ANALYTICAL METHODS

Samples were collected in duplicate three times a week. NH_4-N, NO_2-N, NO_3-N and phosphorus phosphate (PO_4-P) were analyzed according to methods 4500-NH3-G, 4500-NO2-B, 4500-NO3-H and 4500-P-F, respectively, of Standard Methods (APHA-AWWA-WPCF, 2012), using an automatic analyzer (Smartchem 200, WestcoScientific Instruments, Westco). TSS, VSS, total and soluble chemical oxygen demand (T-COD and S-COD, respectively) concentrations were also measured three times a week in duplicate, according to methods 2540-TSS-D, 2540-VSS-E, 5220-COD-C and 522-COD-D, respectively of Standard Methods (APHA-AWWA-WPCF, 2012).

Once a week, total and soluble biological oxygen demand (T-BOD and S-BOD, respectively), along with total nitrogen and phosphorus (T-N and T-P, respectively) were also measured. BOD were performed according to method 5210-BOD-C (APHA-AWWA-WPCF, 2012). T-N concentration was measured by colorimetric analysis using the nitrogen total cell test kit (Merckoquant 1.14537.001, Merck, Germany). T-P concentration was measured after a total digestion at 150 ºC for two hours, followed by PO_4-P determination according to Standard Methods, 4500-P-F, (APHA et al., 2005), using the aforementioned automatic analyser (Smartchem 200, WestcoScientific Instruments, Westco).

OD_{680} and *Chl a* fluorescence parameters were measured with a portable fluorometer AquaPen-C AP-C 100 (Photon Systems Instruments). Wavelength spectrum (400-700 nm) was measured by a spectrophotometer (Spectroquant® Pharo 100, Merck,

Germany) and was used to obtain the extinction coefficient of the biomass culture (González-Camejo et al., 2020) (Equation IV. 20).

4.5. CALCULATIONS

4.5.1. Nutrient and organic matter removal

The nutrient and organic matter removal capacity of the system were assessed by removal rate (RR) ($g \cdot m^{-3} \cdot d^{-1}$) and removal efficiency (RE) (%), which were calculated by Equation IV. 12 and Equation IV. 13, respectively:

$$RR = \frac{Q_I \cdot (C_I - C_F)}{V_R} \quad \text{Equation IV. 12}$$

$$RE = \frac{(C_I - C_F)}{C_I} \quad \text{Equation IV. 13}$$

where RR and RE are the removal rate ($g \cdot m^{-3} \cdot d^{-1}$) and removal efficiency (%) of the given compound (nitrogen, phosphorus, COD or BOD), respectively, Q_I is the treatment flow rate ($m^3 \cdot d^{-1}$), V_R is the reactor volume (m^3) and C_I and C_F are the concentrations of nitrogen, phosphorus, COD or BOD in the influent and the effluent ($g \cdot m^{-3}$), respectively.

The global mass balance of nitrogen and phosphorus were calculated as described in Equation IV. 14 and Equation IV. 15, respectively:

$$T_{NI} \cdot Q_I = T_{NF} \cdot Q_F + X_{NB} \cdot BP + N - NO_2 + N - NO_3 + FAN_{stripping} + N_2 + X_{N-Precip.} \quad \text{Equation IV. 14}$$

$$T_{PI} \cdot Q_I = T_{PF} \cdot Q_F + (X_{PB} - X_{P-Precip.}) \cdot BP + X_{P-Precip.} \quad \text{Equation IV. 15}$$

where the subscripts I and F are the concentrations of a given compound in the influent and effluent ($g \cdot m^{-3}$), respectively. Q is the treatment flow rate ($m^3 \cdot d^{-1}$), BP is the biomass productivity ($g\ VSS \cdot m^{-3} \cdot d^{-1}$), X_{NB} is the nitrogen content in biomass ($g\ N \cdot g\ VSS^{-1}$), X_{PB} is the phosphorus content in biomass ($g\ P \cdot g\ VSS^{-1}$), $N\text{-}NO_2$ and $N\text{-}NO_3$ ($g\ N \cdot m^{-3}$) are the nitrite and nitrate concentrations, respectively, $FAN_{stripping}$ is the FAN stripping ($g\ N \cdot m^{-3}$), N_2 is the nitrogen gas produced by denitrification ($g\ N \cdot m^{-3}$), $X_{N\text{-}Precip}$ is the precipitates containing N ($g\ N \cdot m^{-3}$) and $X_{P\text{-}Precip}$ is the precipitates containing P ($g\ P \cdot m^{-3}$). $FAN_{stripping}$

and precipitates were calculated with Visual MinteQ 3.1 software. N_2 from denitrification was calculated as the difference between T-N in the incoming wastewater and the sum of T-N in the effluent and biomass wastage.

4.5.2. Biomass productivity

The biomass productivity (BP) (g VSS·m^{-3}·d^{-1}) was calculated by Equation IV. 16:

$$BP = \frac{F_w \cdot VSS}{V}$$ Equation IV. 16

where F_w (m^3·d^{-1}) is the flow of the biomass wasted with the purge; VSS (g VSS·m^{-3}) is the volatile suspended solids concentration in the sample; and V is the volume of the culture in the pilot plant (m^3).

4.5.3. Intracellular nutrient content

The intracellular nutrient content, i.e., X_{NB} (Equation IV. 17) and X_{PB} (Equation IV. 18) (%) of biomass were estimated considering that all the VSS corresponded to microalgae-bacteria biomass:

$$X_{NB} = \frac{X_N}{VSS} \cdot 100$$ Equation IV. 17

$$X_{PB} = \frac{X_P}{VSS} \cdot 100$$ Equation IV. 18

where X_N and X_P are the suspended concentration of nitrogen (g N·m^{-3}) and phosphorus (g P·m^{-3}) of the biomass culture, respectively.

4.5.4. Optical properties

The average irradiance (I_{av}) (µmol·m^{-2}·s^{-1}) inside the reactor was calculated by the Lambert-Beer law (Equation IV. 19):

$$I_{av} = \frac{I_0}{K_a \cdot X_{TSS} \cdot L_p} \cdot (1 - e^{-K_a \cdot X_{TSS} \cdot L_p})$$ Equation IV. 19

where I_0 is the light intensity at the surface of the culture (µmol m^{-2} s^{-1}), K_a is the culture extinction coefficient (m^2·g^{-1}), X_{TSS} is the TSS concentration in the reactor (g TSS·m^{-3}) and L_P is the light path of the reactor (m).

The culture extinction coefficient, i.e. K_a, is calculated using Equation IV. 20.

$$K_a = \frac{OD_{400-700}}{TSS \cdot Lp_c}$$ Equation IV. 20

where $OD_{400-700}$ (-) is the average optical density in the range of 400-700 nm; and Lp_c (m) is the light path of the spectrophotometer´s cuvette.

4.5.5. Growth rate and nutrient uptake rates

Microalgae growth rate (µ) (d^{-1}) was calculated by applying the Verhulst logistic kinetic model (Verhulst, 1838) (Equation IV. 21):

$$\mu = \frac{X_0 X_{max} e^{t\mu_{max}}}{X_{max} - X_0 + X_0 e^{t\mu_{max}}}$$ Equation IV. 21

where X_0, and X_{MAX} are biomass concentrations (g VSS·m^{-3}) at an operating time (t) equal to zero and infinity, respectively.

The Michaelis-Menten relationship (Equation IV. 22) is an ecological model which can be applied to nutrient removal kinetics (Aslan and Kapdan, 2006).

$$r_0 = \frac{r_{max} S_0}{K_m + S_0}$$ Equation IV. 22

where r_0 is the nutrients uptake rate ($g \cdot m^{-3} \cdot d^{-1}$), r_{max} is the maximum removal rate of nutrients (d^{-1}), S_0 is the nutrient concentration at time equal zero ($g\ m^{-3}$) and K_m is the Michaelis-Menten constant ($g \cdot m^{-3}$). The kinetic coefficients r_{max} and K_m were matched and calibrated by use of the Lineweaver-Burk equation (Equation IV. 23).

$$\frac{1}{r_0} = \frac{K_m}{r_{max}} \frac{1}{S_0} + \frac{1}{r_{max}}$$ Equation IV. 23

4.6. STATISTICAL ANALYSIS

All analytical determinations were performed in duplicate or triplicate. The results are given as average values with their corresponding standard deviations.

To assess the differences between groups of variable, the Tukey's pairwise comparison of means and an analysis of variance (ANOVA) were performed using STATGRAPHICS Centurion XVI.I software. P-values < 0.05 were considered statistically significant. Correlations between microbial communities and abiotic parameters were analyzed by a PCA (IBM SPSS Statistics 26 software). Differences were considered statistically significant when p-value was below 0.01.

REFERENCES

APHA-AWWA-WPCF, 2012. Standard Methods for the Examination of Water and Wastewater, 22nd edition, American P. ed. Washington DC, USA.

Aslan, S., Kapdan, I.K., 2006. Batch kinetics of nitrogen and phosphorus removal from synthetic wastewater by algae. Ecol. Eng. 28, 64–70. https://doi.org/10.1016/j.ecoleng.2006.04.003

Gomes, M.T.G., da Luz, A.C., dos Santos, M.R., do Carmo Pimentel Batitucci, M., Silva, D.M., Falqueto, A.R., 2012. Drought tolerance of passion fruit plants assessed by the OJIP chlorophyll a fluorescence transient. Sci. Hortic. (Amsterdam). 142, 49–56. https://doi.org/10.1016/j.scienta.2012.04.026

González-Camejo, J., Aparicio, S., Jiménez-Benítez, A., Pachés, M., Ruano, M. V, Borrás, L., Barat, R., Seco, A., 2020. Improving membrane photobioreactor performance by reducing light path: operating conditions and key performance indicators. Water Res. 172. https://doi.org/10.1016/j.watres.2020.115518

González-Camejo, J., Jiménez-Benítez, A., Ruano, M. V., Robles, A., Barat, R., Ferrer, J., 2019. Optimising an outdoor membrane photobioreactor for tertiary sewage treatment. J. Environ. Manage. 245, 76–85. https://doi.org/10.1016/j.jenvman.2019.05.010

Klindworth, A., Pruesse, E., Schweer, T., Peplies, J., Quast, C., Horn, M., Glöckner, F.O., 2013. Evaluation of general 16S ribosomal RNA gene PCR primers for classical and next-generation sequencing-based diversity studies. Nucleic Acids Res. 41, e1–e1. https://doi.org/10.1093/NAR/GKS808

Krug, L., Erlacher, A., Berg, G., Cernava, T., 2019. A novel, nature-based alternative for photobioreactor decontaminations. Sci. Rep. 9, 1–10. https://doi.org/10.1038/s41598-019-39673-6

PSI (Photon Systems Instruments), 2017. AquaPen-P AP-P 100 manual [WWW Document]. URL http://www.ictinternational.com/content/uploads/2016/09/AquaPen_Manual.pdf (accessed 7.1.21).

Robles, A., Ruano, M. V., Ribes, J., Ferrer, J., 2013. Factors that affect the permeability of commercial hollow-fibre membranes in a submerged anaerobic MBR (HF-SAnMBR) system. Water Res. 47, 1277–1288. https://doi.org/10.1016/J.WATRES.2012.11.055

Rossi, S., Bellucci, M., Marazzi, F., Mezzanotte, V., Ficara, E., 2018. Activity assessment of microalgal-bacterial consortia based on respirometric tests. Water Sci. Technol. 78, 207–215. https://doi.org/10.2166/wst.2018.078

Sánchez-Zurano, A., Gómez-Serrano, C., Acién-Fernández, F.G., Fernández-Sevilla, J.M., Molina-Grima, E., 2020. A novel photo-respirometry method to characterize consortia in microalgae-related wastewater treatment processes. Algal Res. 47, 101858. https://doi.org/10.1016/j.algal.2020.101858

Sander, R., 2015. Compilation of Henry's law constants (version 4.0) for water as solvent. Atmos. Chem. Phys. 15, 4399–4981. https://doi.org/10.5194/ACP-15-4399-2015

Seco, A., Aparicio, S., González-Camejo, J., Jiménez-Benítez, A., Mateo, O., Mora, J.F., Noriega-Hevia, G., Sanchis-Perucho, P., Serna-García, R., Zamorano-López, N., Giménez, J.B., Ruiz-Martínez, A., Aguado, D., Barat, R., Borrás, L., Bouzas, A., Martí, N., Pachés, M., Ribes, J., Robles, A., Ruano, M. V., Serralta, J., Ferrer, J., 2018. Resource recovery from sulphate-rich sewage through an innovative anaerobic-based water resource recovery facility (WRRF). Water Sci. Technol. 78, 1925–1936. https://doi.org/10.2166/wst.2018.492

Serôdio, J., Ezequiel, J., Frommlet, J., Laviale, M., Lavaud, J., 2013. A method for the rapid generation of nonsequential light-response curves of chlorophyll fluorescence. Plant Physiol. 163, 1089–1102. https://doi.org/10.1104/pp.113.225243

Stirbet, A., Govindjee, 2011. On the relation between the Kautsky effect (chlorophyll a fluorescence induction) and Photosystem II: Basics and applications of the OJIP fluorescence transient. J. Photochem. Photobiol. B Biol. 104, 236–257. https://doi.org/10.1016/J.JPHOTOBIOL.2010.12.010

Strasser, R.J., Tsimilli-Michael, M., Srivastava, A., 2004. Analysis of the Chlorophyll a Fluorescence Transient 321–362. https://doi.org/10.1007/978-1-4020-3218-9_12

Verhulst, P.-F., 1838. Notice sur la loi que la population suit dans son accroissement. Correspondance Mathématique et Physique Publiée par A. Quetelet 10, 113–121.

Yamori, W., Sakata, N., Suzuki, Y., Shikanai, T., Makino, A., 2011. Cyclic electron flow around photosystem I via chloroplast NAD(P)H dehydrogenase (NDH) complex performs a significant physiological role during photosynthesis and plant growth at low temperature in rice. Plant J. 68, 966–976. https://doi.org/10.1111/J.1365-313X.2011.04747.X

CHAPTER V

5. Can microalgae-bacteria consortia effectively remove wastewater pollutants? Assessing urban wastewater treatment using microalgae and bacteria at different hydraulic retention times and using different wastewater streams

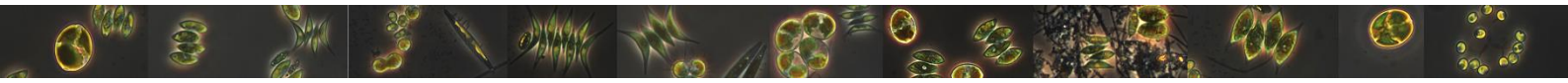

5. Can microalgae-bacteria consortia effectively remove wastewater pollutants? Assessing urban wastewater treatment using microalgae and bacteria at different hydraulic retention times and using different wastewater streams

ABSTRACT

The influence of the hydraulic retention time (HRT) and the wastewater characterization (effluent from primary settling and pre-treatment step) on microalgae and bacteria activity and the efficiency of nutrients and organic matter removal was evaluated in a membrane high rate algal pond (MHRAP) pilot plant operated at a biomass retention time of 6 days. This study was divided in two experimental sets according to the characteristics of the influent wastewater. The MHRAP was continuously fed with effluent from primary settling and operated at 6, 4 and 2 days HRT in the first experimental set. Organic loading rate (OLR) was the main limiting factor for heterotrophic bacteria growth. Nitrifying bacteria dominated the microalgal consortium community. However, abiotic boundary parameters reduced nitrite-oxidizing bacteria activity, resulting in partial-nitrification at 6 days HRT. Total nitrogen (T-N) and total phosphorus (T-P) removal efficiencies at 6 days of HRT resulted in 23.6 ± 0.6 and 32 ± 4%, respectively, affected by free ammonia nitrogen stripping and phosphorus precipitation. T-N and T-P removal efficiencies at 4 and 2 days HRT were lower than 10 and 5%, respectively, since physical and chemical processes were reduced by operational and environmental parameters and biomass uptake rate was a minor removal mechanism. In the second experimental set, the MHRAP pilot plant was fed with effluent from pre-treatment and operated at 4, 2 and 1 days of HRT. 4-day HRT resulted in the same pattern of microbial activity and removal efficiencies than the first experimental set. A suitable equilibrium between microalgae and bacteria was assessed at 2-day HRT. T-N and T-P removal efficiencies of 91 ± 5 and 71 ± 8%, respectively, enabled to meet European Union discharge limits. Nitrification-denitrification process was the main nitrogen removal mechanism (87% of T-N). Heterotrophic bacteria dominated at 1 day HRT and nutrients removal efficiencies were lower than 5%. COD removal efficiencies were higher than 86%, regardless experimental set, since ultrafiltration removed not only particulate COD but also colloids.

Keywords

Microalgae-bacteria consortia, hydraulic retention time (HRT), photo-respirometric tests and nutrient removal.

Authors

Stéphanie Aparicio, Luis Borrás, José Ferrer, Aurora Seco, Ángel Robles.

5.1. INTRODUCTION

Although it is generally accepted that conventional wastewater treatment technologies are a notable human achievement, new times require the development of novel technologies able to cope and adapt to the needs of a modern society. The development of Water Resource Recovery Facilities (WRRFs) is moving in this direction, with the aim of recovering all valuables contained in wastewater (e.g. nitrogen, phosphorus, and reclaimed water) (Cornejo et al., 2019; Seco et al., 2018).

Microalgae-bacteria consortia applied to wastewater can play a major role in WRRFs due to ecological relationships and synergic effects between microalgae and bacteria (Morillas-España et al., 2021; Robles et al., 2020). Interactions between microalgae and bacteria cover a wide range of relationships from mutualism/commensalism to amensalism/competition (Fallahi et al., 2021). A general framework of the potential interactions between biological communities is shown in Figure V. 1.

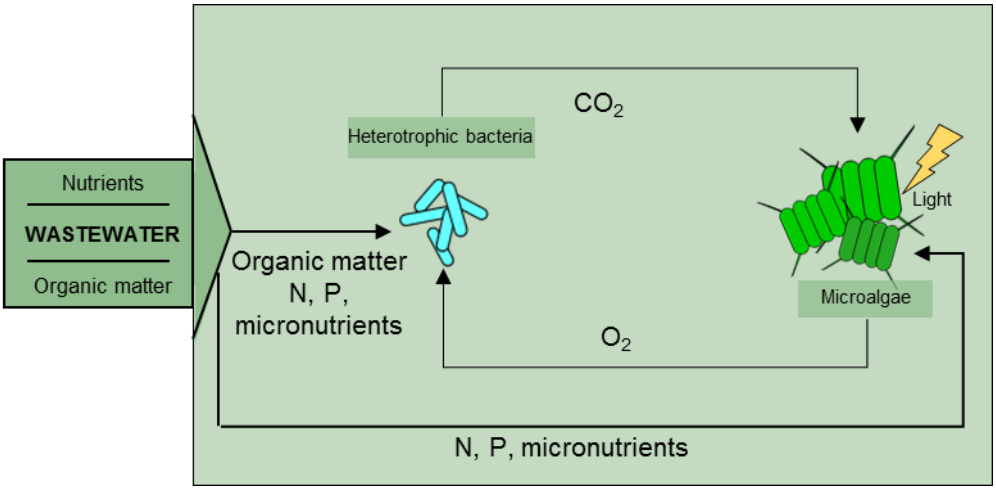

Figure V. 1. Simplified scheme of interactions between microalgae and heterotrophic bacteria. Abbreviations: nitrogen (N), phosphorus (P), carbon dioxide (CO_2) and oxygen (O_2).

Self-sustaining oxygen-carbon dioxide gas exchange constitutes the basis of the main mutualistic relationship between microalgae and aerobic heterotrophic bacteria (Figure V. 1). As a simplified scheme of ecological process, microalgae, through photosynthesis, produce oxygen (O_2) which can be used by aerobic heterotrophic bacteria as an electron acceptor to oxidize organic matter. In parallel, carbon dioxide (CO_2) released during

bacterial oxidation is used by microalgae as an inorganic carbon source for photosynthesis, completing the mutualistic interaction (Fallahi et al., 2021). In this simplified scheme, microalgae uptake nutrients (nitrogen (N) and phosphorus (P)) from wastewater in their soluble inorganic forms, namely ammonium (NH_4-N) or nitrate (NO_3-N), and phosphate (PO_4-P); and bacteria degrade organic matter. However, the reality is far more complex, with different chemical and biological processes taking place at the same time (Figure V. 2).

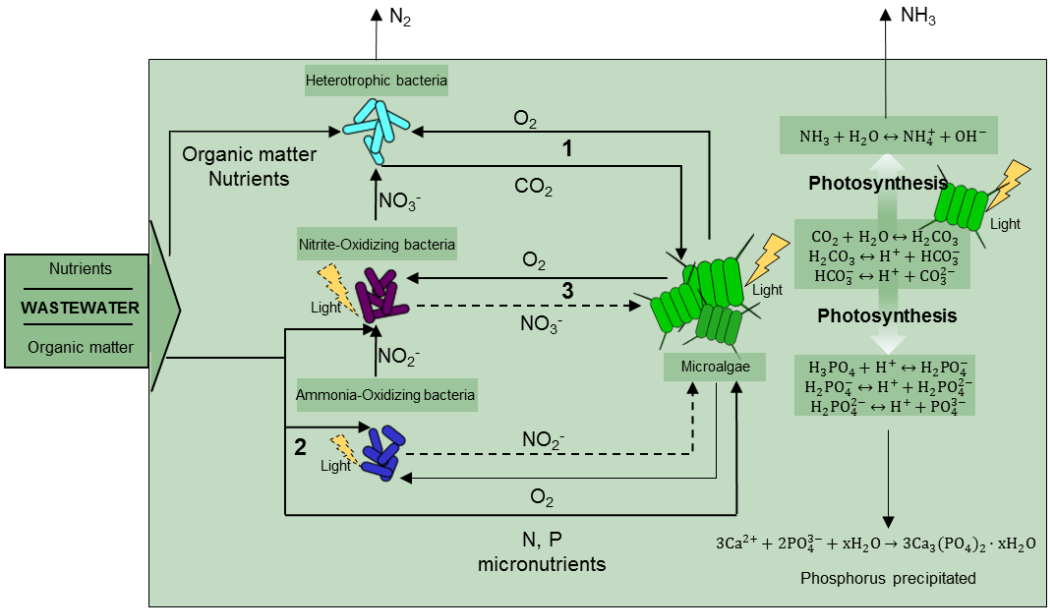

Effect of interaction on growth rate				
Interaction (+) Positive effect (-) Negative effect (0) Non-effect	Microalgae	Heterotrophic bacteria	Nitrite-Oxidizing bacteria	Ammonia-Oxidizing bacteria
1. Mutualism	+	+	+	+
2. Competition	-			-
3. Ammensalism	-			0

Figure V. 2. Scheme of interactions between microalgae, heterotrophic bacteria, and nitrifying bacteria. The main interactions were numbered: (1) mutualism, (2) competition, and (3) competition. Abbreviations: nitrogen (N), phosphorus (P), carbon dioxide (CO_2), oxygen (O_2), nitrite (NO_2^-), and nitrate (NO_3^-). Dashed lines indicate inhibition processes.

The main chemical processes occurring include bicarbonate-carbonate equilibrium shifts towards the formation of carbonate due to microalgal photosynthesis, increasing pH while boosting free ammonia nitrogen (FAN) stripping and uncontrolled P precipitation

(Morales-Amaral et al., 2015). Not only aerobic heterotrophic metabolism is supported by microalgae, photosynthesis can also provide the O_2 needed for nitrification process. During nitrification, ammonia-oxidizing bacteria (AOB) use NH_4-N as a source of electrons, producing nitrite (NO_2-N), which is further oxidized to NO_3-N by nitrite oxidizing bacteria (NOB). In high NH_4-N-loaded wastewater treatments, commensalism interaction could exist between microalgae and AOB. However, under low NH_4-N and dissolved inorganic carbon (DIC) concentrations, AOB compete for NH_4-N with microalgae (Fallahi et al., 2021). Amensalism relationships between microalgae and AOB have also been reported, e.g., photosynthesis inhibition by NO_2-N accumulation (Aparicio et al., 2022; González-Camejo et al., 2020b).

The ecological interrelationships described above depend on the O_2 released by photosynthesis during daylight hours. However, during nighttime hours, microalgae switch from photosynthesis to respiration and O_2 can be depleted according to microorganism respiration rate (both heterotrophic bacteria and microalgae). Under these conditions (depleted/low O_2 concentrations), denitrification can also take place in microalgae-bacteria consortia: i.e. NO_3-N is used as a final electron acceptor (instead of O_2) for organic matter oxidation by facultative heterotrophic bacteria (Fallahi et al., 2021). The overall set of ecological interaction described above (Figure V. 2) results in: (I) nutrients removal (uptake by biomass, nitrification/denitrification, FAN stripping and P precipitation); and (II) organic matter removal (aerobic and anoxic organic matter degradation).

The contribution of microalgae to wastewater treatment systems could reduce two of the major challenges in conventional WWTP: high energy demand due to aeration (i.e. 45-75% of total WWTP energy consumption) and nutrients recovery and conversion into valuable biomass (Acién et al., 2016). For instance, data from Aqualia, Europe's third largest wastewater treatment company, indicate that conventional WWTP involves an average energy consumption of 0.49 kWh/m^3 associated with reactor operation, while

Microalgae-bacteria consortia in a high rate algal pond (HRAP) involves an average energy consumption of 0.030 kWh/m^3 (Acién et al., 2016). On the other hand, nutrients recovery from wastewater by microalgae is of great interest nowadays, especially as agriculture faces a P-scarce future (Solovchenko et al., 2016), and because ammonia production through the Haber-Bosch process is energy-intensive (Matassa et al., 2015). Considering the intracellular nutrients content that microalgae can storage (intracellular P ranging 1-5% (Chu et al., 2019; Ruiz-Martínez et al., 2015) and intracellular N ranging 6-10% (González-Camejo et al., 2019c)), a 73 and 53% of P and N could be recovered from wastewater, respectively (González-Camejo et al., 2020a). However, benefits of microalgae-bacteria consortia implementation in WRRFs depend on the development of a desirable biocenosis. In case of not achieving the equilibrium, microalgal and bacterial communities could be adversely affected. Culture pH rise above the optimal range of bacteria (Foladori et al., 2018; Van Den Hende et al., 2016) as a consequence of microalgae bloom. Contrary, in a bacterial-dominated ecological structure, photosynthesis could not fully support bacteria activity (Foladori et al., 2018). Microalgae-bacteria consortia equilibrium change with time due to the ever-changing environmental conditions (mainly, temperature (T) (González-Camejo et al., 2019a) and light intensity (González-Camejo et al., 2020a)), besides operating parameters (hydraulic retention time (HRT) and biomass retention time (BRT) (González-Camejo et al., 2018)). Subsequently, to produce a biological culture that maximizes nutrient recovery and organics removal, control of both environmental and operational parameters would be required to achieve a desirable microalgae-bacteria community. Since outdoor HRAPs are subject to seasonal and daily weather variations (i.e. culture T and available light for photosynthesis fluctuate throughout the day and year), environmental parameters cannot be used as control tool (i.e. artificial light intensity and temperature control may result in unaffordable costs). Nonetheless, by optimizing HRT and/or BRT, requirements of N and P can be identified to support desirable microalgae-bacteria communities in the HRAP. Ashadullah et al. (2021) studied the simultaneous organic matter and nutrients

removal from synthetic wastewater in a lab-scale membrane bioreactor, under different conditions of organic loading rate (OLR) and HRT. The influence of HRT on the treatment of synthetic wastewater was also evaluated in a lab-scale anoxic-aerobic algal-bacterial photobioreactor configuration by Toledo-Cervantes et al. (2019). Anbalagan et al. (2016) investigated the integration of microalgae and activated sludge in WWTP by varying the HRT of lab-scale semi-continuous photo-bioreactor. However, none of the previous studies focused on the effect of HRT on microalgae-bacteria ecology community and the wastewater treatment efficiency within a pilot-scale outdoor reactor without external aeration, artificial light and control of culture pH and T.

In this study, the main question that arises is: Could a balance between microalgae and bacteria for pollutant removal be achieved by modifying the operating HRT? To answer this question, the performance of an outdoor pilot scale membrane HRAP (MHRAP) treating two different urban wastewater streams under different operating HRT was evaluated. Specifically, the study consisted of evaluating the effect of HRT on: (I) the DO, pH, inorganic nitrogen, and ORP profile; (II) the biological activity of microalgae, heterotrophic bacteria, AOB, and NOB by photo-respirometry tests and; (III) N, P, and COD removal.

5.2. MATERIALS AND METHODS

5.2.1. MHRAP pilot plant

This study was performed using a continuous pilot-scale MHRAP plant located in the "Cuenca del Carraixet" WWTP (39°30′04.0''N 0°20′00.1''W, Valencia, Spain). It was operated outdoors, i.e. culture temperature and sunlight irradiance were variable depending on weather conditions. The MHRAP pilot plant mainly consisted of one high rate algal pond (HRAP) connected to one membrane tank (MT) module. The HRAP had a working volume of 318.75 L, a solar irradiance area of 1.275 m^2 (2.55 x 0.5 m) and a liquid depth of 0.25 m. The reactor was continuously stirred by a single paddle wheel (six blades). The MT module had a total working volume of 14 L with a filtration area of 3.4

m^2 given by one bundle from a commercial ultrafiltration hollow-fiber membrane system (PURON® Koch Membrane Systems (PUR-PSH31), 0.03 µm pore size). Membrane filtration enabled decoupling BRT and HRT. Air-sparging was used to reduce membrane fouling by membrane scouring.

Different on-line sensors were installed in the MHRAP to obtain real-time information on the process performance: a pH sensor (pHD sc DPD1R1, Hach Lange); a dissolved oxygen-temperature sensor (LDO Hach Lange); an oxidation reduction potential (ORP) sensor (ORP DRD1P5.99, Hach Lange); an AN-ISE sensor (AN-ISE LXV440.99.00001, Hach Lange) to record NH_4-N and NO_X-N (sum of NO_2-N and NO_3-N); and a light irradiance sensor (Apogee Quantum SQ-200) set up on the surface of the HRAP for measuring the photosynthetic active radiation (PAR).

5.2.2. MHRAP pilot plant operation

The start-up of the MHRAP pilot plant consisted of the following steps:

1. Filling the MHRAP with the incoming wastewater stream. No active inoculation of the MHRAP was needed, implying that a natural process of initial ecological succession of the indigenous microorganisms occurred. This approach facilitates a possible industrial application of this technology.
2. Operating at batch mode until reaching pseudo-stationary phase (i.e. biomass concentration measured as volatile suspended solids (VSS) did not significantly vary (González-Camejo et al., 2019c)).
3. Operating with continuous feeding and biomass wastage for maintaining the desired HRT and BRT.

The second step of this start-up was used to calculate a theoretical BRT which promotes maximum biomass productivity (Ruiz et al., 2013). The last two steps were carried out at the beginning of each evaluated operating period.

The HRAP was fed with two wastewater streams from the “Cuenca del Carraixet WWTP”: effluent from primary settling and effluent from pre-treatment (screening,

degritter, and grease removal). Table V. 1 shows the main characteristics of both wastewater streams.

Table V. 1. Average characteristics of effluent from primary settling and pre-treatment from full-scale WWTP.

Parameter		Effluent from primary settling	Effluent from pre-treatment
pH		7.7 ± 0.5	7.9 ± 0.3
TSS	(g TSS·m^{-3})	107 ± 61	308 ± 86
VSS	(g VSS·m^{-3})	92 ± 46	258 ± 73
T-COD	(g COD·m^{-3})	252 ± 71	692 ± 139
S-COD	(g COD·m^{-3})	100 ± 27	123 ± 29
T-BOD	(g BOD·m^{-3})	105 ± 18	290 ± 30
S-BOD	(g BOD·m^{-3})	36 ± 5	106 ± 21
T-N	(g N·m^{-3})	40 ± 10	47 ± 4
NH_4-N	(g N·m^{-3})	37 ± 8	39 ± 3
T-P	(g P·m^{-3})	4.2 ± 1.2	7.7 ± 1.4
PO_4-P	(g P·m^{-3})	3.7 ± 0.9	4.4 ± 1.3

Microalgae-bacteria interactions were studied with two sets of independent experiments according to the incoming stream wastewater.

In the first experimental set (S1), the MHRAP pilot plant was continuously fed with effluent from primary settling of the “Cuenca del Carraixet WWTP”. The theoretical optimum BRT was 6 days. The S1 was divided in three periods according to the operating HRTs studied, which were 6, 4 and 2 days. The second set of experiment (S2) consisted of the continuous operation of the MHRAP with effluent from the pre-treatment of the same WWTP. Three HRT of 4, 2 and 1 days with a fixed BRT of 6 days (which was also obtained from batch stage of MHRAP start-up) were studied in three experimental periods. All periods were preceded by chemical cleaning of MHRAP and a start-up phase.

The following nomenclature was used to refer and identify each operating period: S(experimental set)_HRT(operating HRT), so that period operated at 6 days HRT of S1 was referred to as S1_HRT6.

5.2.3. Photo-respirometric tests

Microalgae-bacteria consortia activity was quantified using the standardized photo-respirometric protocol developed by Sánchez-Zurano et al. (2020). This protocol differentiates between microalgae, heterotrophic, and nitrifying bacteria activity using O_2 production and uptake rate. Although the photo-respirometric protocol is a valuable tool for optimizing microalgae and bacteria-based process, the protocol to obtain the nitrifying bacteria respiration rate was slightly modified to differentiate and quantify AOB and NOB activity:

- Ammonia-oxidizing bacteria oxygen uptake rate (OUR_{AOB}) (mg $O_2 \cdot g\ VSS^{-1} \cdot h^{-1}$). A sample of microalgae-bacteria culture was placed inside the photo-respirometer described in Chapter 3 and a substrate solution of NH_4Cl was dosed to achieve a NH_4-N concentration of 10 g $N \cdot m^{-3}$. NOB activity was inhibited by dosing an inhibitor solution of $KClO_3$ to achieve 1.2 g $\cdot L^{-1}$ in microalgae-bacteria culture (Rossi et al., 2018).

- Nitrite-oxidizing bacteria oxygen uptake rate (OUR_{NOB}) (mg $O_2 \cdot g\ VSS^{-1} \cdot h^{-1}$). A new sample from microalgae-bacteria culture was placed inside the same photo-respirometer and a solution of $NaNO_2$ was dosed to achieve an NO_2-N concentration of 10 g $N \cdot m^{-3}$. AOB activity was inhibited by dosing an inhibitor solution of allylthiourea (ATU) to achieve 5 g m^{-3} in microalgae-bacteria culture (González-Camejo et al., 2019c).

The effect of three nitrification inhibitors (i.e. ATU, $KClO_3$, and hydroxylamine) on photosynthesis were analyzed by the fluorometer AquaPen-C AP-C 100 (Photon Systems Instruments, Czech Republic). The net oxygen production rate (OPR_{NET}), electron transport rate (ETR) curve, non-photochemical quenching (NPQ), and the *Chlorophyll a* (*Chl a*) fluorescence transient kinetics were analyzed. From fluorescence of *Chl a*, the maximum quantum yield of Photosystem II (PS II) photochemistry (F_V/F_M)

and the performance index (PI_{ABS}) were obtained. The measurement protocols are described in detail in Chapter VI. Figure V. 3 shows that ATU and $KClO_3$ did not inhibit photosynthesis, unlike hydroxylamine, which hindered the electron transport chain. The described protocol is therefore a suitable methodology to evaluate the activity of microalgae and heterotrophic bacteria, AOB and NOB.

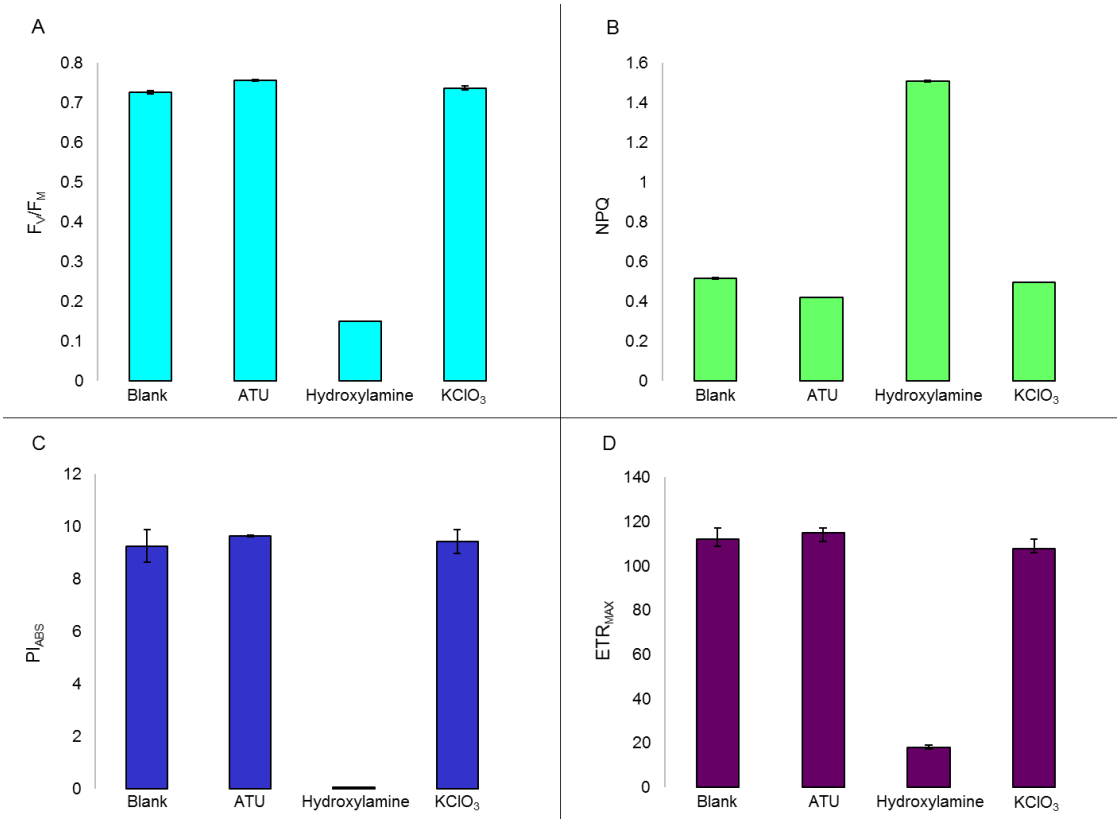

Figure V. 3. Effect of allylthiourea (ATU), hydroxylamine and $KClO_3$ on fluorescence parameters: A) Maximum quantum yield of PS II photochemistry (F_V/F_M), B) Non-photochemical quenching (NPQ), C) Performance index (PI_{ABS}) and D) Maximum photosynthetic rate (ETR_{MAX}). Blank is a control reactor, operating with the same abiotic conditions but without nitrifying bacteria inhibitors.

Microalgae net oxygen production rate (OPR_{NET}) (mg $O_2 \cdot g\ VSS^{-1} \cdot h^{-1}$) and heterotrophic bacteria oxygen respiration rate (OUR_{HET}) (mg $O_2 \cdot g\ VSS^{-1} \cdot h^{-1}$) were quantified as specified in the protocol proposed by Sánchez-Zurano et al. (2020).

5.2.4. Sampling and analytical methods

Grabbed samples of HRAP culture, MT permeate, and incoming wastewater were collected in duplicate three times a week. NH_4-N, NO_2-N, NO_3-N, and PO_4-P were analysed according to Standard Methods (APHA-AWWA-WPCF, 2012): 4500- NH3-G,

4500-NO2-B, 4500-NO3-H, and 4500-P-F, respectively), using an automatic analyser (Smartchem 200, WestcoScientifi Instruments, Westco). Total suspended solids (TSS), VSS, total and soluble COD (T-COD and S-COD) and total and soluble biological oxygen demand (T-BOD and S-BOD) were measured according to methods 2540-TSS-D, VSS 2540-VSS-E, 5220-COD-C, 522-COD-D, and 5210-BOD-C, respectively (APHA-AWWA-WPCF, 2012). Total nitrogen (T-N) concentration was measure by colorimetric analysis with a nitrogen total cell test kit (Merckoquant 1.14537.001, Merck, Germany). After total digestion of the sample at 150 ºC for 2 h, total phosphorus (T-P) concentration was measured according to 4500-P-F method (APHA-AWWA-WPCF, 2012) using the automatic analyzer.

5.2.5. Mass balance calculation and MHRAP performance indicators

The global mass balance of N and P were calculated as described in Equation V. 1Equation V. 2, respectively:

$$\mathrm{TN_I \cdot Q_I = TN_F \cdot Q_F + X_{NB} \cdot BP + NO_X - N + FAN_{stripping} + N_2 + X_{N-Precip.}} \quad \text{Equation V. 1}$$

$$\mathrm{TP_I \cdot Q_I = TP_F \cdot Q_F + (X_{PB} - X_{P-Precip.}) \cdot BP + X_{P-Precip.}} \quad \text{Equation V. 2}$$

where the subscripts I and F refers to influent and effluent concentrations ($g \cdot m^{-3}$), respectively, Q is the treatment flow rate ($m^3 \cdot d^{-1}$), BP is the biomass productivity (g $VSS \cdot m^{-3} \cdot d^{-1}$), X_{NB} is the nitrogen content in biomass (g $N \cdot g\ VSS^{-1}$), X_{PB} is the P content in biomass (g $P \cdot g\ VSS^{-1}$), NO_X-N (g $N \cdot m^{-3}$) is the sum of nitrite and nitrate concentrations, resulting from nitrification, $FAN_{stripping}$ is the free ammonia nitrogen stripping (g $N \cdot m^{-3}$), N_2 is the nitrogen gas produced by denitrification (g $N \cdot m^{-3}$), $X_{N\text{-}Precip}$ is the precipitates containing N (g $N \cdot m^{-3}$) and $X_{P\text{-}Precip}$ is the precipitates containing P (g $P \cdot m^{-3}$). $FAN_{stripping}$ and precipitates were calculated with Visual MinteQ 3.1 software and BNRM2 model. N_2 from denitrification was calculated as the difference between T-N in the incoming wastewater and the sum of T-N in the effluent and biomass wastage. P content in biomass was calculated as the difference between T-P of biomass and phosphorus precipitates simulated.

Different nitrogen and phosphorus removal mechanism were considered in this study: nitrogen and phosphorus uptake by microalgae, nitrification, denitrification, FAN stripping and P precipitation. To calculate their contribution to the net nutrient removal rate, the following mass balances were applied:

$$[TN_I - (i_{N,S_I} \cdot S_I + i_{N,X_I} \cdot X_I)] \cdot Q_I = TN_F \cdot Q_F + X_{NB} \cdot BP + NO_X - N + FAN_{stripping} + N_2 + X_{N-Precip.}$$ Equation V. 3

$$[TP_I - (i_{P,S_I} \cdot S_I + i_{P,X_I} \cdot X_I)] \cdot Q_I = TP_F \cdot Q_F + (X_{PB} - X_{P-Precip.}) \cdot BP + X_{P-Precip.}$$ Equation V. 4

where $i_{N,SI}$ (g COD·g N^{-1}), $i_{N,XI}$ (g COD·g N^{-1}), $i_{P,SI}$ (g COD·g P^{-1}) and $i_{P,XI}$ (g COD·g P^{-1}) are the nitrogen and phosphorus contained in inert particulate and soluble organic matter, respectively. Values of $i_{N,SI}$, $i_{N,XI}$, $i_{P,SI}$ and $i_{P,XI}$ were 0.01 g COD·g N^{-1}, 0.03 g COD·g N^{-1}, 0 g COD·g P^{-1} and 0.01 g·COD g P^{-1}, respectively (Viruela et al., 2021). Complete hydrolysis of biodegradable particulate organic matter (X_S) was assumed.

Removal rate (RR) (g m^{-3} d^{-1}) and removal efficiency (RE) (%) were calculated by Equation V. 5Equation V. 6, respectively:

$$RR = \frac{Q_I \cdot (C_I - C_F)}{V_R}$$ Equation V. 5

$$RE = \frac{(C_I - C_F)}{C_I}$$ Equation V. 6

RR and RE are the removal rate (g·m^{-3}·d^{-1}) and removal efficiency (%) of the given compound (N, P or COD) (g·m^{-3}·d^{-1}), Q_I is the treatment flow rate (m^3·d^{-1}), V_R is the volume reactor (m^3) and C_I and C_F are the concentrations of N, P or COD in the influent and the effluent (g·m^{-3}), respectively.

The average irradiance inside the culture (I_{av}) was calculated applying the Lambert-Beer Law (Equation V. 7) as reported by González-Camejo et al. (2020a):

$$I_{av} = \frac{I_0}{K_a \cdot X_{TSS} \cdot L_p} \cdot (1 - e^{-K_a \cdot X_{TSS} \cdot L_p})$$ Equation V. 7

where I_0 is the light intensity at the surface of the culture ($\mu mol \cdot m^{-2} \cdot s^{-1}$), K_a is the culture extinction coefficient ($m^2 \cdot g^{-1}$), X_{TSS} is the TSS concentration in the HRAP ($g \cdot TSS\ m^{-3}$) and L_P is the light path of the HRAP (m).

5.2.6. Statistical analysis

The data shown in this work is expressed as mean values and standard deviation (SD). A Tukey's pairwise comparison of means was performed to identify significant differences between samples (p-value < 0.05). A Pearson correlation analysis was performed to identify relationships between the different variables.

5.3. RESULTS AND DISCUSSION

5.3.1. Dynamics of abiotic parameters

Variations of abiotic parameters described in this Section will inherently occur in any outdoor system and impact on MHRAP pilot plant performance.

5.3.1.1. Influence of HRT treating effluent from primary settling (S1)

Three operating HRTs were studied to treat effluent from primary settling, i.e. HRT of 6, 4 and 2 days (S1_HRT6, S1_HRT4 and S1_HRT2, respectively). Effects of HRTs on microalgae-bacteria consortia were analyzed using on-line sensors installed in the MHRAP pilot plant. The average, maximum and minimum of DO saturation (DO Sat%) concentration, PAR, pH and T for periods S1_HRT6, S1_HRT4 and S1_HRT2 are shown in **¡Error! No se encuentra el origen de la referencia.**. Analysis of abiotic parameters was supported by graphical representation of one representative day of each period (Figure V. 4).

Table V. 2. Average operating parameters, abiotic boundary conditions, and composition of MHRAP permeate under steady-state operation in the three experimental periods for the first experimental set (S1). Values in bracket were the minimum and the maximum value.

Parameters		S1_HRT6	S1_HRT4	S1_HRT2
HRT	days	6.2 ± 0.4	3.9 ± 0.3	2.0 ± 0.6
BRT	days	6.2 ± 0.4	6.3 ± 0.7	5.9 ± 0.4
COD loading rate	$g \cdot m^{-3} \cdot d^{-1}$	40 ± 7	58 ± 6	123 ± 11
BOD loading rate	$g \cdot m^{-3} \cdot d^{-1}$	18 ± 9	25 ± 4	53 ± 15
Average PAR	$\mu mol \cdot m^{-2} \cdot s^{-1}$	139 ± 61	113 ± 10	110 ± 50
Maximum PAR	$\mu mol \cdot m^{-2} \cdot s^{-1}$	936 ± 209	550 ± 238	598 ± 130
Average I_{av}	$\mu mol \cdot m^{-2} \cdot s^{-1}$	16 ± 5	13 ± 5	12 ± 2
Maximum I_{av}	$\mu mol \cdot m^{-2} \cdot s^{-1}$	186 ± 33	91 ± 73	105 ± 40
OD Sat%	%	25.9 ± 1.4 [19, 38]	76 ± 8 [34, 114]	78 ± 8 [31, 96]
OD	$g\ O_2\ m^{-3}$	2.6 ± 0.6 [2.0, 3.2]	8 ± 4 [3.0, 12.3]	8 ± 4 [2.8, 10.8]
T	ºC	17 ± 5 [12, 24]	16 ± 5 [12, 21]	16 ± 5 [10, 21]
pH		8.7 ± 0.3 [7.8, 9.2]	7.4 ± 0.2 [7.0, 7.6]	7.3 ± 0.3 [6.9, 7.6]
TSS	$(g\ TSS \cdot m^{-3})^1$	175 ± 28	342 ± 20	302 ± 10
VSS	$(g\ VSS \cdot m^{-3})^1$	145 ± 8	307 ± 16	295 ± 18
T-COD	$(g\ COD \cdot m^{-3})$	21 ± 4	27 ± 3	27.6 ± 1.3
T-N	$(g\ N \cdot m^{-3})$	32 ± 3	43 ± 8	52 ± 12
NH_4-N	$(g\ N \cdot m^{-3})$	10 ± 2	0.8 ± 0.6	0.6 ± 0.3
NO_2-N	$(g\ N \cdot m^{-3})$	21 ± 3	1.1 ± 0.7	1.6 ± 0.5
NO_3-N	$(g\ N \cdot m^{-3})$	0.5 ± 0.2	41 ± 7	50 ± 4
T-P	$(g\ P \cdot m^{-3})$	3.0 ± 0.7	3.7 ± 0.8	4.9 ± 1.3
PO_4-P	$(g\ P \cdot m^{-3})$	2.8 ± 0.6	3.7 ± 0.5	4.8 ± 0.9

[1] TSS and VSS concentration in the mixed liquor. Solids concentration were negligible in the final permeate.

The OD Sat% (Pearson correlation = 0.93, p-value < 0.05) and pH (Pearson correlation = 0.79, p-value < 0.05) were correlated with the diurnal solar radiation cycle, regardless of MHRAP operational conditions (Figure V. 4A, C, and D).

An average PAR of 139 ± 61, 113 ± 10, and 110 ± 50 $\mu mol \cdot m^{-2} \cdot s^{-1}$ (p-value < 0.05) were recorded for S1_HRT6, S1_HRT4, and S1_HRT2, respectively (Table V. 2). Optimal PAR range for microalgae growth often range from 80 (Khalili et al., 2015) to 413 $\mu mol \cdot m^{-2} \cdot s^{-1}$ (Barbera et al., 2020). Daily average PAR values were thus suitable to support microalgae growth.

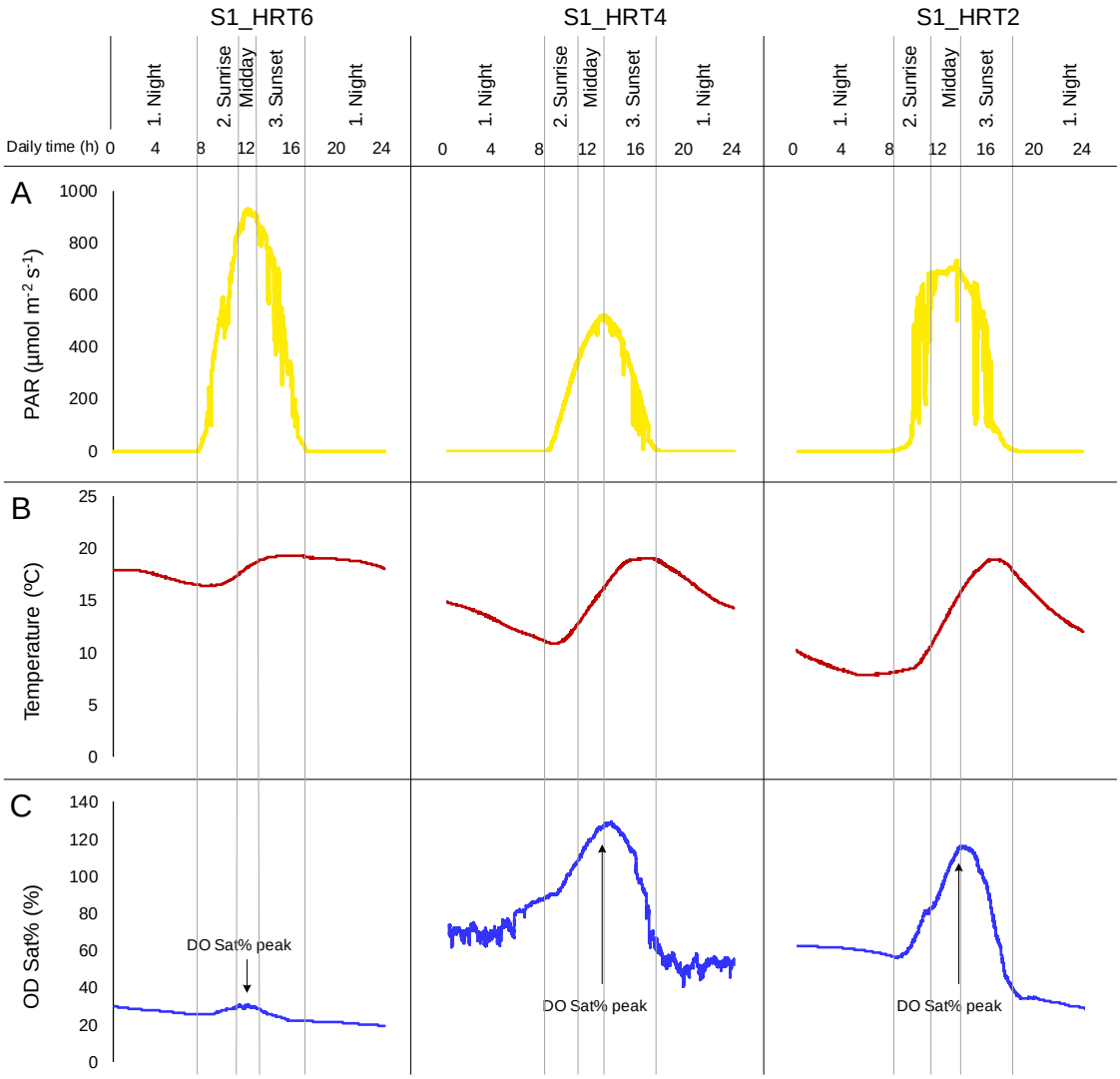

Figure V. 4. Representative day of 6, 4 and 2 days HRT (experimental set 1). (A) daily PAR (µmol·m^{-2}·s^{-1}), (B) temperature (ºC), (C) oxygen saturation (%).

Average T in the mixed liquor of S1_HRT6, S1_HRT4 and S1_HRT2 were 17 ± 5, 16 ± 5, and 16 ± 5 ºC, respectively (p-value < 0.05). Although optimal temperature for microalgae ranges between 25 and 30 ºC (González-Camejo et al., 2019a; Rossi et al., 2020a), the success in COD and nutrient removals from wastewater obtained at an average mixed liquor temperature of 9 ºC suggested that temperatures registered during S1 would also allow for an efficient microalgae-bacteria consortia for wastewater treatment (Posadas et al., 2015). Microalgae-bacteria relationship resulted in an average DO Sat% of 25.9 ± 1.4, 76 ± 8, and 78 ± 8 % during S1_HRT6, S1_HRT4, and S1_HRT2, respectively (Table V. 2). DO Sat% recorded in S1_HRT4 and S1_HRT2 did not show

statistically significant differences (p-value > 0.05), unlike that recorded between both and S1_HRT6 (p-value < 0.05). As it can be observed in Figure V. 4C and Table V. 2, available oxygen concentration for aerobic metabolism was lower in S1_HRT6. Aerobic conditions always prevailed throughout the day, even during nighttime hours, regardless the operating HRT (Table V. 2).

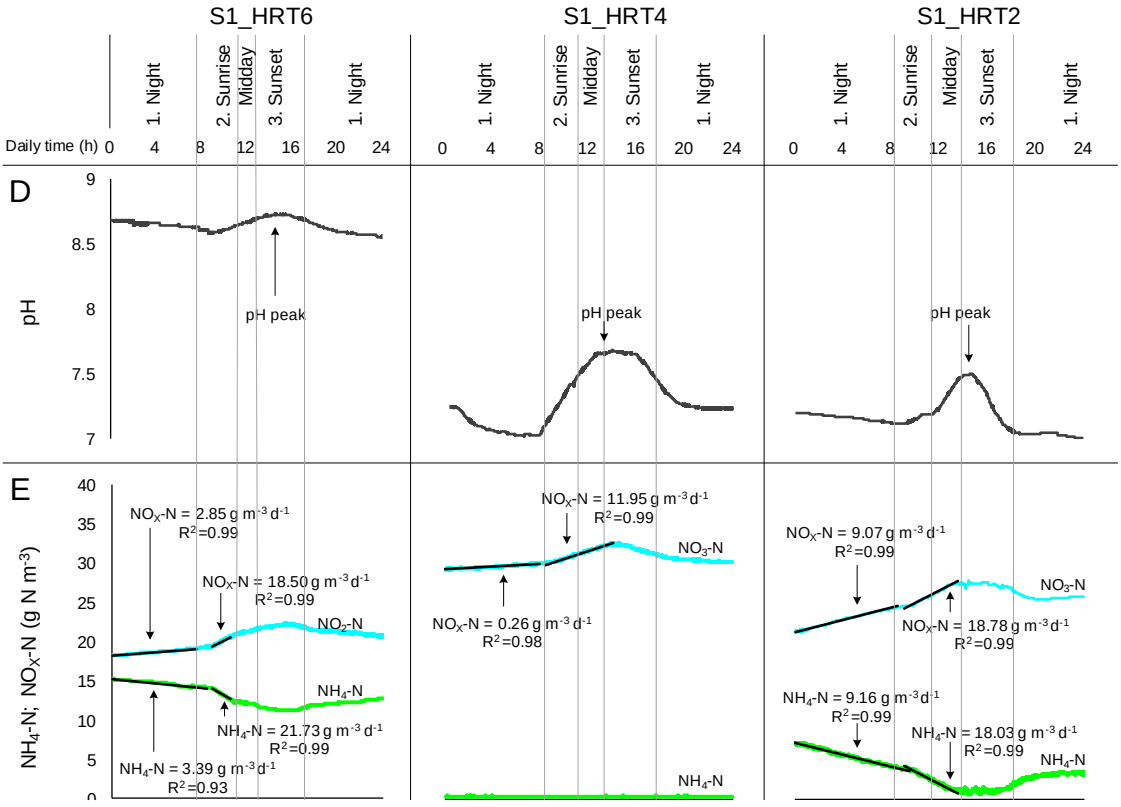

Figure V. 5. Continuation. Representative day of 6, 4 and 2 days HRT (experimental set 1). (D) pH and (E) ammonium and the sum of nitrite and nitrate (g N·m^{-3}).

Average pH values for S1_HRT6, S1_HRT4, and S1_HRT2 were 8.7 ± 0.3, 7.4 ± 0.2, and 7.3 ± 0.3, respectively. pH remained stable during nighttime hours and rose with increasing OD concentration during daylight hours, inducing in a peak of pH around midday, when available light intensity was maximum (Figure V. 4D). The same pH profile was obtained regardless of operating HRT. However, only S1_HRT6 reached values near 9. The higher the HRT, the lower the water renewal rate and the lower the DIC supply. Acid-base balance of microalgae-bacteria cultures was influenced by both DIC uptake via photosynthesis and acidification via nitrification. Decreasing HRT entailed a

reduction of the pH. Periods operated at 2 and 4 days of HRT promoted a nitrifying bacterial-dominated ecological structure (Section 5.3.2.1.), obtaining the mean pH values indicated in Table V. 2. According to Posadas et al. (2015), mean pH values for all periods were suitable to support a successful wastewater treatment. However, potential NOB and microalgae inhibition by alkaline pH in S1_HRT6 will be discussed in Section 5.3.2.1.

AN-ISE on-line sensor provided daily dynamics for NH_4-N and NO_X-N concentrations (Figure V. 4D). NO_X-N daily fluctuations follow the same pattern in the three periods regardless of operating conditions, while the concentration of NH_4-N was almost zero at S1_HRT4 throughout the day. The ever-aerobic conditions supported nitrification during all day and denitrification would be limited (see Section 5.3.3.1). Figure V. 4E shows that NH_4-N removal rate and nitrification rate in S1_HRT2 did not showed statistical differences. Thus, nitrification appears to be the main nitrogen removal mechanism, while microalgae uptake represented a minor process. Nitrification rate was correlated with T (Pearson correlation = 0.88, p-value < 0.05) and DO Sat% (Pearson correlation = 0.92, p-value < 0.05). Daily variation effects of temperature were observed in nitrification rate by Gujer (2010), which obtained that NO_3-N increased with temperature by a factor of 0.11 $^oC^{-1}$.

5.3.1.2. Influence of HRT treating effluent from pre-treatment (S2)

Three operating HRTs were studied to treat effluent from pre-treatment: i.e. 4, 2, and 1 days of HRT (S2_HRT4, S2_HRT2, and S2_HRT1, respectively).

Table V. 3 shows average, minimum and maximum values of DO Sat% concentration, T, PAR and pH. Both PAR and T average values were suitable to support microalgae photosynthesis and bacteria activities (Barbera et al., 2020; González-Fernández et al., 2011; Khalili et al., 2015) and showed no statistical differences between periods (p-value > 0.05).

Balance between O_2 uptake and production resulted in an average DO Sat% of 58 ± 9, 29 ± 7, and 2.53 ± 0.98% during S2_HRT4, S2_HRT2, and S2_HRT1 (p-value < 0.05), respectively. The OD Sat% in S2_HRT4 ranged from 23 to 82 %, prevailing aerobic conditions even during night-time and following the same pattern described for S1 periods.

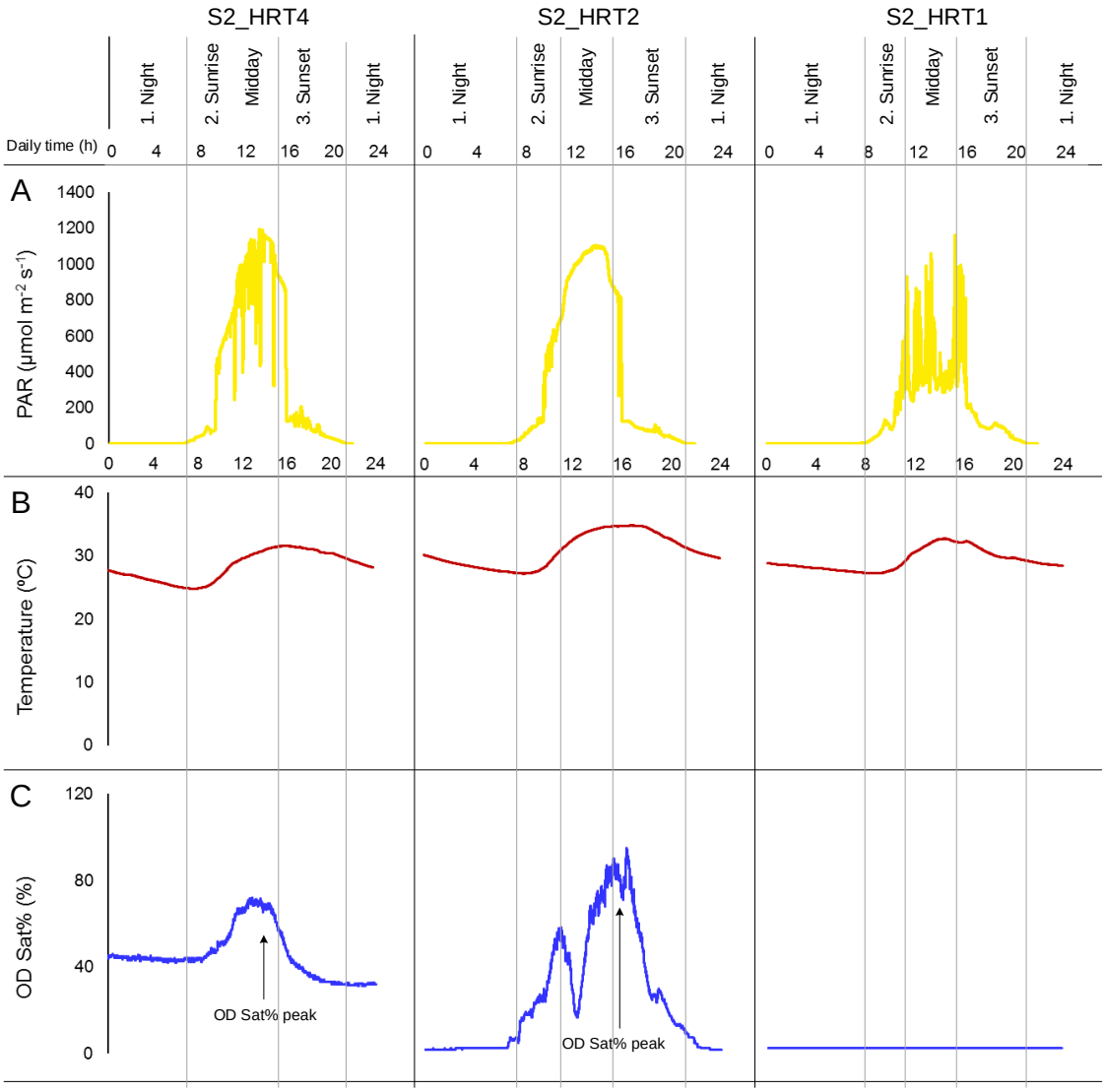

Figure V. 5. Representative day of 4, 2 and 1 days HRT (experimental set 2). (A) daily PAR (µmol·m^{-2}·s^{-1}), (B) temperature (ºC), (C) oxygen saturation (%).

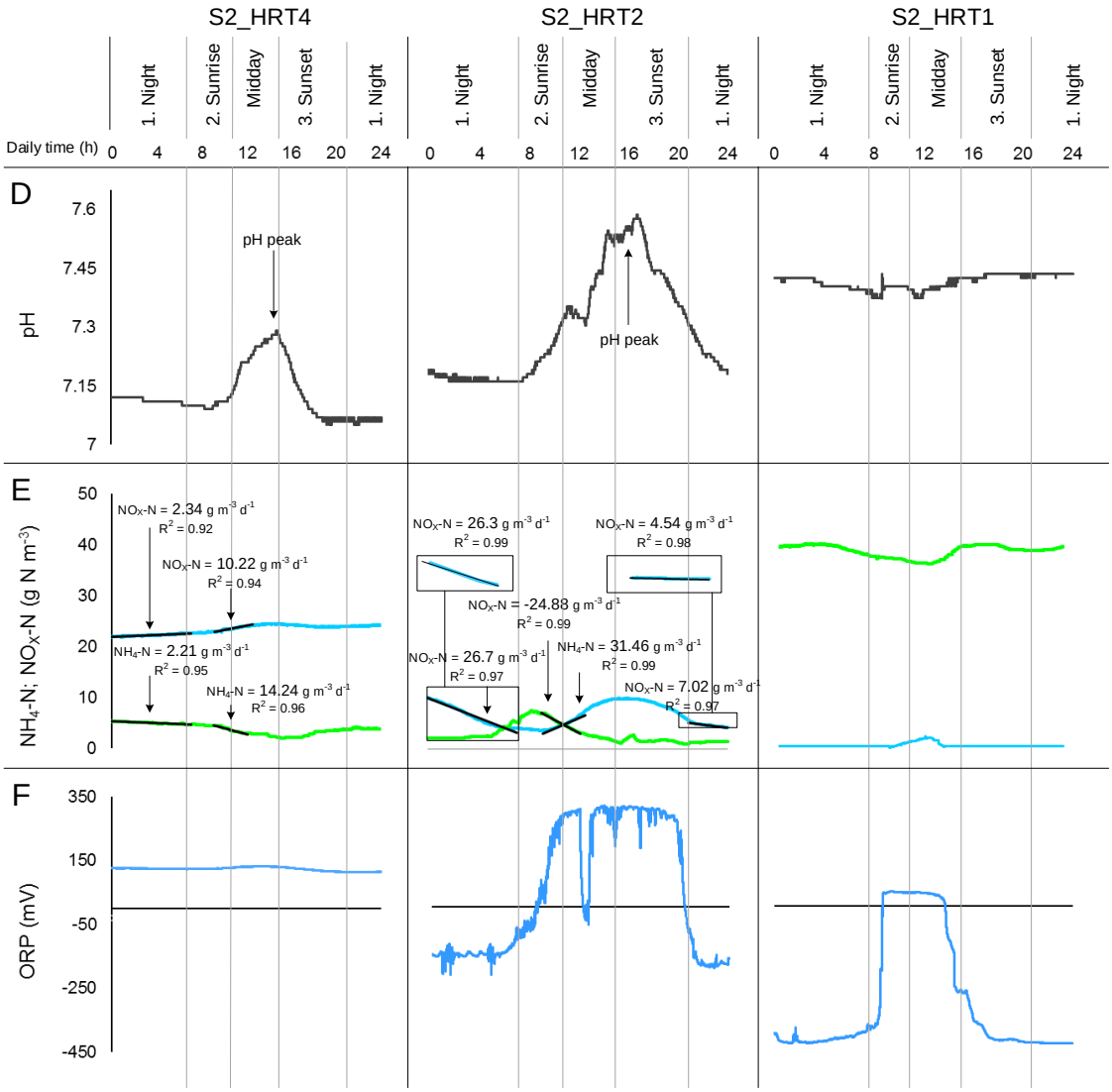

Figure V. 5. Continued. Representative day of 4, 2 and 1 days HRT (experimental set 2). (D) pH, (E) ammonium and the sum of nitrite and nitrate (g N·m^{-3}), (F) ORP (mV).

Decreasing HRT to 2 days resulted in a severe drop in average OD Sat% (Table V. 3). Figure V. 4C shows the DO Sat% profile of S2_HRT2, which can be divided in 3 phases according to diurnal solar radiation cycle:

1. Night-time. It is characterized by dark conditions and DO concentration nearly zero (0.9 ± 0.14% of DO Sat% i.e. 0.08 ± 0.02 g O_2 m^{-3}). In dark conditions, photo-oxygenation did not occur, and oxygen consumption by organism respiration resulted in zero O_2 concentration. The ORP profile remained stable at 150 mV. The O_2 depletion and the availability of NO_X-N in the MHRAP promoted anoxic

conditions (Figure V. 4C and E). Trend of NO_X-N and OPR profiles showed that denitrification of NO_3-N could occur (Figure V. 4E and F). Figure V. 4E shows NO_X-N profile corrected by dilution rate of the incoming wastewater. A steady reduction in NO_X-N concentration was observed, indicating that NO_X-N was consumed by denitrification.

2. Sunrise phase. This phase is defined by a significant increase in the DO Sat% concentration as PAR increased. The DO Sat% reached a peak according to the maximum PAR around midday. The DO Sat% peak reached oversaturation (116 ± 21 % of DO Sat% i.e. 8 ± 3 g O_2 m^{-3}) level in S2_HRT2. In this phase, the O_2 production by microalgae surpassed the O_2 consumption from biomass. Similarly, ORP also increased towards positive values (Figure V. 4F), indicating oxidative conditions. The pH profile followed the same trend and increased due to microalgal photosynthesis (Figure V. 4D). The pH increase was probably counterbalanced by acidification produced by nitrification as it can be observed by the increase in NO_3-N concentration (Figure V. 4F). NH_4-N removal rate was significantly higher (p-value < 0.05) than nitrification rate. Mass balance and boundary abiotic conditions suggested that NH_4-N was also removed by microalgae uptake.
3. Sunset phase. This phase is defined by the decline of solar light intensity along with a decrease of OD Sat% concentration. The photosynthetic activity was slowed down due to a progressive reduction of available PAR (Figure V. 4A). The MHRAP was continuously fed with pre-treatment effluent, thus COD and NH_4-N were constantly supplied to oxygen-consuming heterotrophic and nitrifying bacteria, respectively. DO consumption remained almost constant, while O_2 production decreases, resulting in a decreasing trend in OD Sat%. High positive ORP values indicated that DO was enough to maintain oxidative conditions. The pH profile decreased due to a combination of acidification from continued nitrification and reduced photosynthetic activity (Figure V. 4D). After this phase,

dark period associated with night-time would again take place along with its characteristics abiotic conditions.

At shortest HRT (S2_HRT1), DO Sat% was nearly zero during all day (Figure V. 5C):

1. Night-time. This period is defined by dark conditions and DO concentrations nearly zero (0.9 ± 0.3% of DO Sat% i.e. 0.08 ± 0.03 g O_2 m^{-3}). As in S2_HRT2, O_2 demand by wastewater indigenous organisms resulted in zero DO concentration. The ORP profile remained steadily bellow – 300 mV (Figure V. 4F), corresponding to more strongly reducing conditions compared to period operated at 2 days HRT. Indeed, NO_X-N was not detected in this phase (Figure V. 4E).
2. Sunrise phase. This period was characterized by DO Sat% values close to zero in spite of the increasing PAR. Although DO was continuously provided by photosynthesis in the system, it was not enough to satisfy oxygen demand by biomass (Figure V. 4C). In some days, a very low DO Sat% peak appeared around midday when available PAR was maximum. Photosynthetic activity increased and O_2 released momentarily surpassed biological demand. Due to the enhanced photosynthetic activity, an increase in pH was also detected, but after the maximum photosynthetic rate, the culture pH decreased because of lower DIC consumption by microalgae. This phase apparently presented conditions without O_2, but the presence of DO was recognized because the ORP profile increased toward positive values and a peak of NO_X-N was detected (Figure V. 4E and F). NH_4-N remained stable except for the short peak of NO_X-N recorded.
3. Sunset phase. This period was denoted by the decline of solar light intensity and OD Sat% values close to zero. The photosynthetic activity was slowed down due to a progressive reduction of available PAR and the ORP profile decreased toward negative values. (Figure V. 4F). Reducing conditions along with

increasing NH_4-N concentration indicated that nitrification was slowed down to a half and anoxic conditions were not reached.

Despite the pH fluctuation due to biological processes, average values (Table V. 3) were suitable to microalgae-bacteria consortia growth regardless operating HRT (Posadas et al., 2015). In S2_HRT4 and S2_HRT2, the increase recorded in NO_X-N concentration correlated positively with daily temperature fluctuations (Pearson correlation = 0.83 and 0.76, respectively, p-value < 0.05).

Table V. 3. Average operating parameters, abiotic boundary conditions and composition of MHRAP permeate under steady-state operation in the three experimental periods for the second experimental set (S2). Values in bracket were the minimum and the maximum value.

Parameters		S2_HRT4	S2_HRT2	S2_HRT1
HRT	days	4.3 ± 0.7	1.9 ± 0.2	1.06 ± 0.09
BRT	days	5.8 ± 0.5	6.1 ± 0.4	6.2 ± 0.6
COD loading rate	$g \cdot m^{-3} \cdot d^{-1}$	115 ± 13	165 ± 17	351 ± 27
BOD loading rate	$g \cdot m^{-3} \cdot d^{-1}$	73 ± 6	145 ± 10	290 ± 30
Average PAR	$\mu mol \cdot m^{-2} \cdot s^{-1}$	221 ± 62	255 ± 49	231 ± 52
Maximum PAR	$\mu mol \cdot m^{-2} \cdot s^{-1}$	1205 ± 55	1123 ± 45	1119 ± 54
Average I_{av}	$\mu mol \cdot m^{-2} \cdot s^{-1}$	5.1 ± 1.2	4.3 ± 0.8	3.1 ± 1.2
Maximum I_{av}	$\mu mol \cdot m^{-2} \cdot s^{-1}$	18.9 ± 0.7	19.7 ± 0.6	7.2 ± 0.8
OD Sat%	%	58 ± 9 [23, 82]	29 ± 7 [0.9, 116]	2.53 ± 0.98 [0.9, 9.5]
OD	$g\ O_2\ m^{-3}$	4.5 ± 1.3 [2, 5.7]	2.20 ± 0.96 [0.08, 8]	0.19 ± 0.14 [0.08, 0.66]
T	ºC	29.0 ± 0.5 [23, 35]	29.1 ± 0.8 [24, 36]	29.3 ± 0.8 [24, 35]
pH		7.36 ± 0.12 [7.2, 7.5]	7.40 ± 0.10 [7.12, 7.6]	7.44 ± 0.09 [7.3, 7.6]
TSS	$(g\ TSS \cdot m^{-3})^1$	721 ± 22	1272 ±46	1836 ± 17
VSS	$(g\ VSS \cdot m^{-3})^1$	667 ± 15	995 ± 34	1629 ± 15
T-COD	$(g\ COD \cdot m^{-3})$	33 ± 7	37 ± 2	21 ± 3
T-N	$(g\ N \cdot m^{-3})$	43 ± 2	4.2 ± 0.9	44 ± 4
NH_4-N	$(g\ N \cdot m^{-3})$	2.2 ± 0.8	1.4 ± 0.4	44 ± 2
NO_2-N	$(g\ N \cdot m^{-3})$	1.2 ± 0.7	0.9 ± 0.3	0.29 ± 0.12
NO_3-N	$(g\ N \cdot m^{-3})$	40 ± 3	1.9 ± 0.7	0.75 ± 0.5
T-P	$(g\ P \cdot m^{-3})$	2.2 ± 0.8	0.85 ± 0.06	4.2 ± 1.12
PO_4-P	$(g\ P \cdot m^{-3})$	2.33 ± 0.98	0.77 ± 0.12	4.0 ± 1.15

[1] TSS and VSS concentration in the mixed liquor. Solids concentration were negligible in the final permeate.

5.3.2. Evaluation of the biological activity of microalgae-bacteria consortia

Microalgae-bacteria community activity was assessed by photo-respirometric tests. Although they are considered as a pivotal tool for understanding metabolic mechanisms

occurring in microalgae-bacteria consortia (Rossi et al., 2020b, 2018; Sánchez-Zurano et al., 2020), the results obtained by different scientific research are usually hard to compare (mainly due to variations in light intensity, culture biomass, substrate concentration, and other abiotic parameters such as temperature (Petrini et al., 2020)). To overcome this issue, Rossi et al. (2020b) stated that the following data should be reported to make photo-respirometric protocols comparable: (I) abiotic and biotic conditions of microalgae-bacteria culture, and (II) respirometric procedure. The activity of microalgae and bacteria obtained in this study was therefore compared with the assays conducted with wastewater by Sánchez-Zurano et al. (2020), since the same protocol was used and the biotic and abiotic conditions were similar. Four biological communities were analyzed through OUR in the two experimental sets (S1 and S2): microalgae (OPR_{NET}), heterotrophic bacteria (OUR_{HET}), AOB (OUR_{AOB}) and NOB (OUR_{NOB})

5.3.2.1. Influence of HRT treating effluent from primary settling (S1)

Microalgae and bacteria activity in the three periods treating effluent from the primary settling is shown in Figure V. 4A.

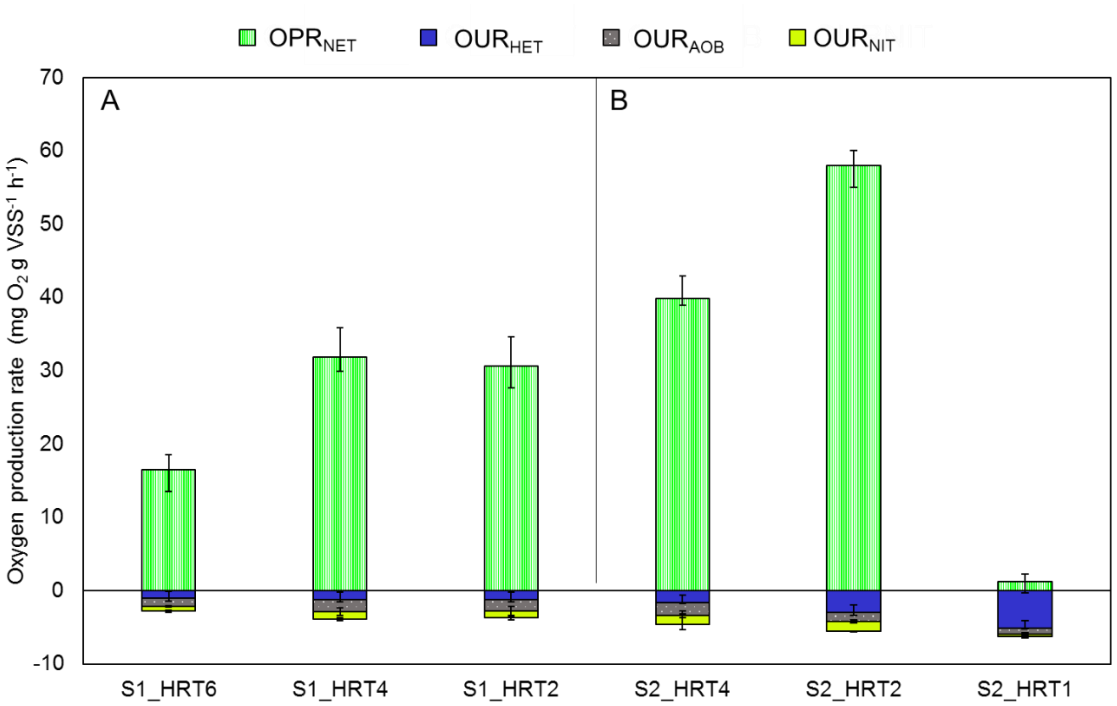

Figure V. 6. Oxygen production rate of: microalgae, (OP_{RNET}), heterotrophic bacteria (OUR_{HET}), AOB (OUR_{AOB}), and NOB (OUR_{NOB}) for (A) experimental set 1 (S1) and (B) experimental set 2 (S2)

The results from Figure V. 4A highlight that OPR_{NET} was higher than the heterotrophic and nitrifying activity in all periods, regardless the operating HRT. Photosynthetic activity of microalgae in S1_HRT4 was likewise very similar to that in microalgae-bacteria consortia produced in S1_HRT2 (32 ± 4 and 31 ± 4 mg O_2·g VSS^{-1}·h^{-1}, respectively). Sánchez-Zurano et al. (2020) reported an OPR_{NET} of about 38 mg O_2·g VSS^{-1}·h^{-1} in an outdoor HRAP using primary domestic wastewater, similar to that achieved in both periods operated at HRT of 4 and 2 days. However, oxygen production recorded in S1_HRT6 (Figure V. 4A, 17 ± 2 mg O_2·g VSS^{-1}·h^{-1}) was significantly lower than the ones obtained in the other periods and the value reported by Sánchez-Zurano et al. (2020). Four factors can limit microalgal photosynthesis: (I) nutrient and DIC supply, (II) competition between microalgae and AOB for NH_4-N and DIC, (III) high culture pH for microalgae growth (Mantovani et al., 2020), and (IV) NO_2-N accumulation which can inhibit microalgae photosynthesis (González-Camejo et al., 2020b)

Heterotrophic activities were similar (p-value > 0.05) regardless operating conditions (Figure V. 4A), showing that heterotrophic bacteria was present at similar relative levels. The OUR_{HET} measured in an outdoor HRAP culture using primary domestic wastewater has been reported at approximately 2.6 mg O_2·g VSS^{-1}·h^{-1} (Sánchez-Zurano et al., 2020), higher than the values obtained in all periods, regardless of HRT (1.1 ± 0.4, 1.2 ± 0.4, and 1.2 ± 0.2 mg O_2·g VSS^{-1}·h^{-1} for S1_HRT6, S1-HRT4, and S1_HRT2, respectively). The biodegradability of primary wastewater used in this set of experiments was 42 ± 7 %, resulting in a T-BOD concentration of 105 ± 8 g BOD·m^{-3}. Thus, heterotrophic bacteria could be substrate limited by low BOD loadings (18 ± 9, 25 ± 9, and 53 ± 15 g·m^{-3}·d^{-1} for operating periods at 6, 4, and 2 days of HRT, respectively).

Nitrifiying activity was divided into OUR_{AOB} and OUR_{NOB} (Figure V. 4A). Reducing HRT from 6 to 4 days increased significantlly OUR_{AOB} (p-value < 0.05), while a reduction from 4 to 2 days did not show statisitcally differences in AOB activity (p-value > 0.05). The higher the HRT the lower the substrates loading rates and AOB growth. However, NH_4-N concentration in the permeate from S1_HRT6 accounted for 24% of N distribution,

thus AOB were not substrate-limited. As described before (Section 5.3.1.1), the main difference in boundary abiotic conditions between S1_HRT6 and both S1_HRT4 and S1_HRT2 was the mean culture pH (8.7 ± 0.3). Despite the alkaline-tolerance of AOB cells, the average pH was slightly above the optimal growth range reported by Park et al. (2007). At high pH values ($NH_3 + H^+ \leftrightarrow NH_4^+$; pK_a = 9.25), a switch from NH_4-N to FAN occurs, which is a potential inhibitor of AOB metabolism (Torà et al., 2010). Less DIC availability could derive to a competition between nitrifying bacteria and microalgae and, therefore, growth rates of both microorganisms would be negatively affected. AOB activity could be adversely affected by culture pH combined with FAN concentration and DIC depletion in S1_HRT6. The average pH decreased (Table V. 2 and Figure V. 4) avoiding the potential pH inhibition and switch of chemical balance to FAN. By removing growth limiting factors and increasing the incoming DIC supply (by reducing the operating HRT), OUR_{AOB} increased from 1.12 ± 0.09 mg $O_2 \cdot g\ VSS^{-1} \cdot h^{-1}$ to 1.7 ± 0.6 and 1.5 ± 0.5 mg $O_2 \cdot g\ VSS^{-1} \cdot h^{-1}$ in S1_HRT6, S1_HRT4, and S1_HRT2, respectively.

The same pattern was also described for OUR_{NOB} (Figure V. 4A). OUR_{NOB} was statistically lower in S1_HRT6 (0.6 ± 0.2 mg $O_2 \cdot g\ VSS^{-1} \cdot h^{-1}$) than in S1_HRT4 (1.1 ± 0.2 mg $O_2 \cdot g\ VSS^{-1} \cdot h^{-1}$) (p-value < 0.05), while no differences were observed between S1_HRT4 and S1_HRT2 (1.0 ± 0.2 mg $O_2 \cdot g\ VSS^{-1} \cdot h^{-1}$) (p-value > 0.05). NOB are more sensitive to pH values above 8 than AOB (Park et al., 2007) and can also be limited by FAN, NO_2-N accumulation, and DIC depletion. In addition, Vergara et al. (2016) observed NO_2-N accumulation under continuous illumination of 250 $\mu mol \cdot m^{-2} \cdot s^{-1}$, suggesting that NOB can be photoinhibited and be more light-sensitive than AOB. Maximum incident light intensity was recorded in S1_HRT6 (Table V. 2). NOB growth may have been limited by the abiotic parameters described above, and also by the intensity of incident light. Reducing operating HRT from 6 to 4 and 2 days, leads to suitable conditions for NOB growth and thus NOB activity increased. In addition, due to weather conditions the maximum light intensity was reduced in S1_HRT4 and S1_HRT2 below photoinhibition levels obtained by Vergara et al. (2016) (Table V. 2).

5.3.2.2. Influence of HRT treating effluent from pre-treatment (S2)

The OPR_{NET} values were higher than heterotrophic and nitrifying activity in both S2_HRT4 and S2_HRT2, while O_2 production did not match demand in S2_HRT1 (Figure V. 4B). The OPR_{NET} measured were 40 ± 7 and 58 ± 10 mg O_2·g VSS^{-1}·h^{-1} in S2_HRT4 and S2_HRT2, respectively. The shorter operating HRT, the more nutrients and DIC supplied for microalgae growth. Reducing operating HRT from 4 to 2 days, increased BOD loading and, therefore, heterotrophic activity, releasing more DIC for photosynthesis. Oxygen production in S2_HRT4 was similar than recorded by Sánchez-Zurano et al. (2020) in microalgae-based wastewater treatment systems. The photosynthetic activity in S2_HRT2 was comparable to that in cultures produced using agricultural leachate wastes, considered a good microalgae substrate (Sánchez-Zurano et al., 2020). Contrary, OPR_{NET} of microalgae-bacteria culture in S2_HRT1 (1.2 ± 0.8 mg O_2·g VSS^{-1}·h^{-1}) was not able to match O_2 demand by heterotrophic (5.1 ± 0.2 mg O_2·g VSS^{-1}·h^{-1}) and nitrifying bacteria (1.1 ± 0.4 mg O_2·g VSS^{-1}·h^{-1}) (Figure V. 4B). The biological activity and OD profile (Section 5.3.2.1) suggest a shift in the microbiological structure of the system towards the heterotrophic activity domain (S2_HRT1).

OUR_{HET} increased from 3.0 ± 0.6 to 5.1 ± 0.2 mg O_2·g VSS^{-1}·h^{-1} (p-value < 0.05) when reducing the HRT from 2 to 1 day. In addition, OUR_{HET} of S2_HRT1 was above the O_2 consumption reported by Sánchez-Zurano et al. (2020). O_2 deficiency could be due to increased COD and BOD loading (Table V. 3), which promoted heterotrophic bacteria growth, thus increasing TSS concentration in HRAP and reducing light availability for microalgae growth (González-Camejo et al., 2020a) (Table V. 3). In S2_HRT4 and S2_HRT2, photosynthesis supply enough O_2 to support activity of oxygen-consuming organisms (Figure V. 4B). The OUR_{HET} measured in S2_HRT4 (1.67 ± 0.12 mg O_2·g VSS^{-1}·h^{-1}) was lower to that obtained by Sánchez-Zurano et al. (2020), suggesting that BOD loading was not able to promote further heterotrophic bacteria development and microalgae-bacteria consortia were BOD-limiting. Heterotrophic activity reached in S2_HRT2 (3.0 ± 0.7 mg O_2·g VSS^{-1}·h^{-1}) was similar to the OUR_{HET} measured in a HRAP

and in a tubular reactor evaluated by Sánchez-Zurano et al. (2020), where COD removal was quite efficient.

Nitrification activity did not show statistical difference between S2_HRT4 and S2_HRT2 (p-value > 0.05) (3 ± 0.2 and 2.5 ± 0.4 mg O_2·g VSS^{-1}·h^{-1}, respectively), indicating that nitrification potential was largely unaffected by HRT operation in the range of 4-2 days under these abiotic conditions. However, both AOB and NOB showed the same pattern as microalgae in S2_HRT1. The drop in nitrifying activity, probably due to OD limitation, suggested a displacement of AOB and NOB by heterotrophic bacteria, which showed a higher affinity for DO than the autotrophic bacteria in this system with these abiotic boundary conditions.

Oxygen uptake rate for heterotrophic and nitrifying bacteria exceeded oxygen production by microalgae in S2_HRT1, resulting in zero oxygen concentration (described in Section 5.3.1.2 (Figure V. 4C)).

5.3.3. Wastewater treatment. Compliance with discharge limits.

5.3.3.1. Influence of HRT treating effluent from primary settling (S1)

Average T-N removal efficiencies (TN-REs) in S1_HRT6, S1_HRT4, and S1_HRT2, accounted for 26.3 ± 0.6, 5.5 ± 0.9, and 5.5 ± 0.8%, respectively. This corresponded to a permeate T-N concentration of 32 ± 3, 43 ± 8, and 52 ± 12 g N·m^{-3}. The maximum T-N concentration permitted for effluent discharge into the environment is 15 g N·m^{-3} according to European Directive 98/15/CEE (10000 - 100000 p.e.), which was surpassed in all experimental periods regardless the operating HRT. Figure V. 4E shows that NH_4-N removal rate was higher than nitrification rate (p-value > 0.05) in S1_HRT6, therefore, another nitrogen removal mechanism was involved. Figure V. 4A shows nitrogen removal mechanism of the three operating HRT studied.

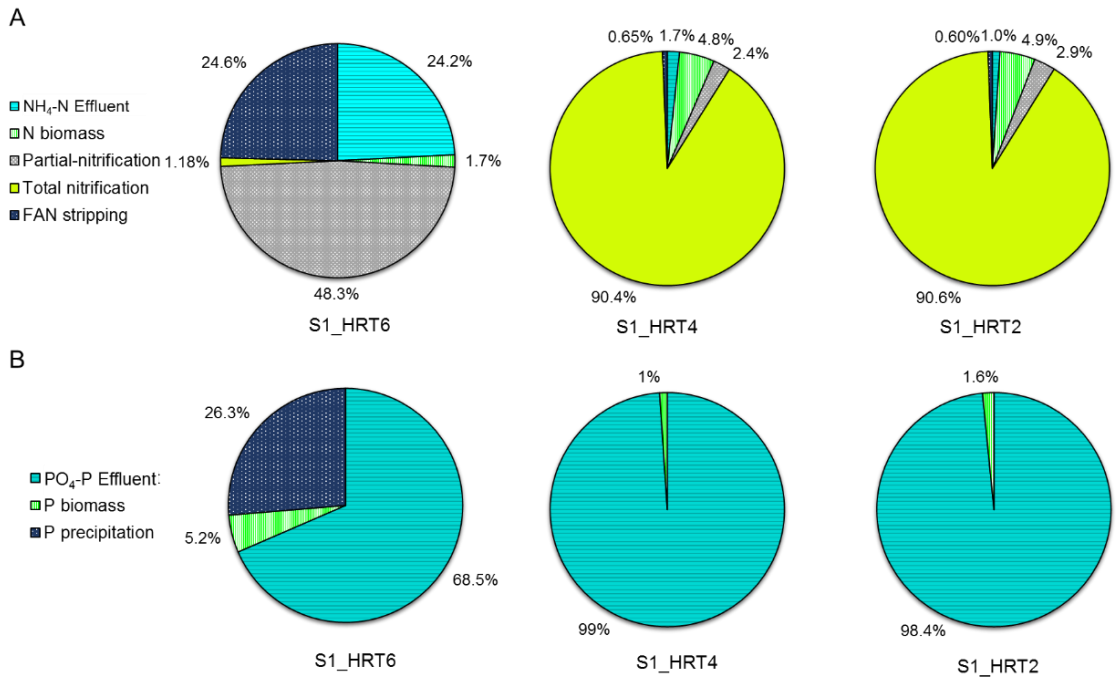

Figure V. 7. (A) Nitrogen and (B) phosphorus removal mechanism in experimental set 1 (S1).

T-N concentration removed from S1_HRT6 was related to FAN stripping due to alkaline pH (8.7 ± 0.3), which accounted for 25 ± 4%. Contrary, N removal by FAN stripping was negligible because of culture pH in S1_HRT4 and S1_HRT2. The N mass balance revealed that 1.7 ± 0.6, 4.8 ± 1.3, and 5 ± 2% of the T-N was removed by biomass uptake in S1_HRT6, S1_HRT4, and S1_HRT2, respectively. Reduced T-N assimilation by biomass in MHRAP operated at 6 days of HRT was related with a reduced microalgae activity (Section 5.3.2.1). Ammonium removal efficiencies (NH_4-N-REs) were higher than 98% in S1_HRT4 and S1_HRT2, while NH_4-N removal was 75 ± 2% in S1_HRT6 (Figure V. 4A). In S1_HRT4 and S1_HRT2, abiotic boundary conditions supported an active N-NH_4 nitrification (Table V. 2). Indeed, NH_4-N removal rate and nitrification rate obtained in Figure V. 4E (p-value > 0.05) showed that N uptake by biomass, denitrification, and stripping were minor processes at night, sunrise and even at midday, when microalgae activity theoretically reaches its maximum under suitable conditions. Partial-nitrification due to NOB inhibition by abiotic conditions (Section 5.3.2.1) accounted for 48 ± 3%, which resulted in a NO_2-N accumulation in the HRAP (Table V. 2). The N mass balance

confirmed that denitrification process did not occur due to the high OD concentration in MHRAP culture, regardless operating HRT (Table V. 2).

T-P removal efficiencies (TP-REs) in S1_HRT6, S1_HRT4, and S1_HRT2 were, respectively, 32 ± 4, 1.07 ± 0.02, and 1.6 ± 0.4%, resulting in a final permeate concentration far above the European Union (EU) discharge limit of 2 g $P \cdot m^{-3}$ (10000 to 100000 p.e.) (Table V. 2). Specific T-P removal rates (TP-RRs) were 0.23 ± 0.13, 0.010 ± 0.008, and 0.040 ± 0.003 g $P \cdot m^{-3} \cdot d^{-1}$. Contribution of T-P removal mechanism is shown in Figure V. 4B. In this context, while the pH influence on T-P removal was negligible in S1_HRT4 and S1_HRT2, the alkaline-pH of S1_HRT6 promoted uncontrolled P-PO_4 precipitation. Chemical P precipitation mainly due to calcium and magnesium ions was the main T-P removal mechanism in S1_HRT6 (Figure V. 4B). The P uptake by biomass was negligible in all periods, regardless of operating conditions and abiotic boundary conditions (Figure V. 4B).

The COD removal efficiencies (COD-REs) in S1_HRT6, S1_HRT4, and S1_HRT2 were, respectively, 89 ± 10, 88 ± 6, and 86 ± 9%. Specific COD removal rates (COD-RRs) were 28 ± 13, 48 ± 15, and 85 ± 15 g COD m^{-3} d^{-1}. The final COD permeate concentration in all periods remained lower than 125 g O_2 m^{-3} (Table V. 2), which is the maximum concentration of COD established for wastewater discharge into the environment according to the EU Directive 98/15/CEE. However, the analysis of COD concentration in supernatant obtained from a 0.45-µm membrane filter and in the permeate from MT module showed that MT physically removed a significant portion of COD (p-value < 0.05). COD-REs using a 0.45-µm membrane filter in S1_HRT6, S1_HRT4, and S1_HRT2 were, respectively, 59 ± 15, 64 ± 11, and 58 ± 13%. These results indicated that the mixed liquor in MHRAP reactor contained a significant portion of colloidal and particulate COD, which was effectively retained by the 0.03 µm hollow-fiber membrane.

Biomass concentration measured as VSS were 145 ± 8, 307 ± 16, and 295 ± 10 g $VSS \cdot m^{-3}$ in S1_HRT6, S1_HRT4, and S1_HRT2, respectively. Biomass concentration and activity suggested the development of a poorly robust microalgae-bacteria consortium,

regardless HRT, which were not able to remove pollutants from wastewater up to EU discharge limits.

5.3.3.2. Influence of HRT treating effluent from pre-treatment (S2)

Figure V. 4A shows T-N distribution of the three operating HRT studied in S2. Nutrient and COD removal rates were the result of microalgae-bacteria consortia formed by operating HRT. TN-REs of 1.8 ± 1.3, 91 ± 5, and 1.12 ± 0.7% were obtained in S2_HRT4, S2_HRT2, and S2_HRT1, respectively. This corresponded to specific TN-RRs of 0.20 ± 0.16, 20 ± 2, and 0.50 ± 0.14 g $N \cdot m^{-3} \cdot d^{-1}$. Efficiencies of nitrogen removal resulted into permeate T-N concentrations of 43 ± 2, 4.2 ± 0.9, and 44 ± 4 $g \cdot N \cdot m^{-3}$ in MHRAP operated at 4, 2, and 1 days of HRT. Hence, final T-N concentration only complied with the European limit discharge for S2_HRT2. Although permeate T-N concentration in S2_HRT4 and S2_HRT1 were similar, NH_4-N-REs was significantly higher in S2_HRT4 (95 ± 6 and 1.1 ± 0.5 respectively, p-value < 0.05). The contribution of N removal mechanisms in S2 is shown in Figure V. 4A. At 4 days of HRT, microalgae supply the O_2 needed for nitrifying kinetics and 90 ± 5% of NH_4-N was oxidized to NO_3-N, while nitrification was negligible in S2_HRT1 (Figure V. 4A) because of O_2 shortage (Section 5.3.2.2). The ever-aerobic conditions (Table V. 3) did not allowed denitrification, as well as in periods of S1. NH_4-N-RE accounted for 95 ± 4% of the T-N removed from wastewater at 2 days of HRT. NH_4-N removal rate and nitrification rate shown in Figure V. 4E were statistically different (p-value < 0.05), suggesting that more removal processes were involved in S2_HRT4. Abiotic parameters did not provide FAN stripping and aerobic conditions limited denitrification, therefore, NH_4-N-RR was due to the combination of nitrification and NH_4-N uptake by biomass. However, N removal by biomass assimilation remained a minor process (Figure V. 4A). S2_HRT2 provided abiotic boundary conditions for coupling nitrification and denitrification processes during daytime and night-time, respectively. Nitrification-denitrification was the main mechanism for N removal (Figure V. 4A). The microalgae-bacteria consortia developed

in the MHRAP at 1 day of HRT was dominated by heterotrophic organism that displaced nitrifying bacteria along with microalgae, thus the large part of the incoming N was not eliminated (Table V. 3 and Figure V. 8A).

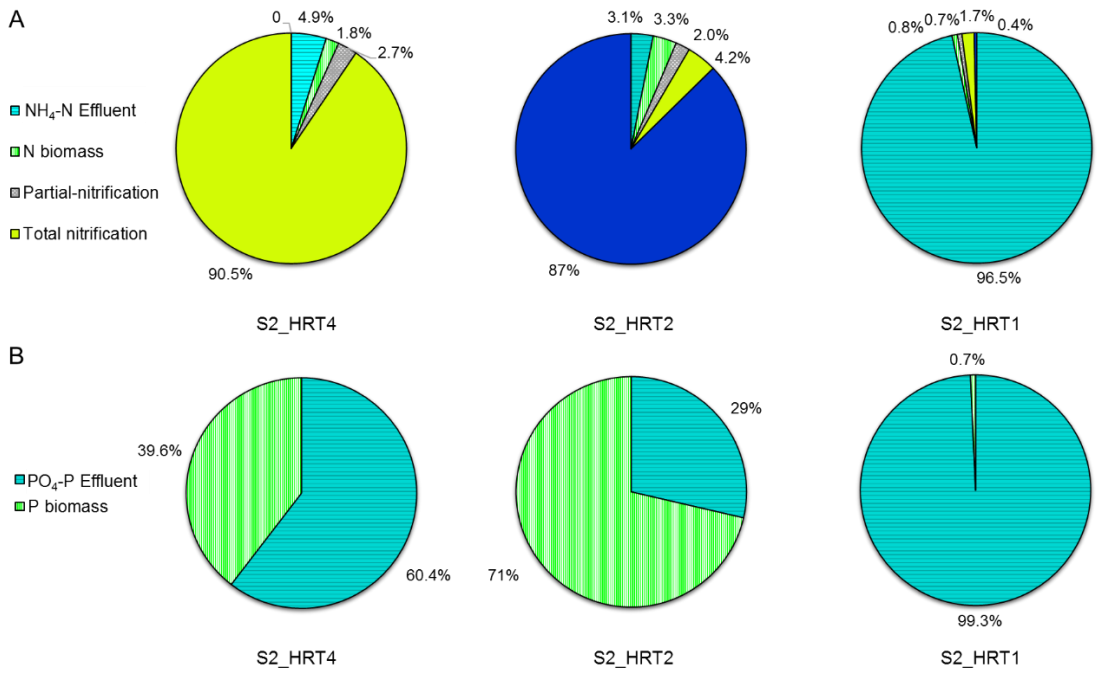

Figure V. 8. (A) Nitrogen and (B) phosphorus removal mechanism in experimental set 2 (S2).

TP-REs in S2_HRT4, S2_HRT2, and S2_HRT1 were, respectively, 40 ± 4, 71 ± 8, and 0.70 ± 0.13%, resulting in a final permeate concentration of 2.2 ± 0.8, 0.85 ± 0.06, and 4.2 ± 1.2 g $P \cdot m^{-3}$, so that only S2_HRT2 met the EU discharge limits. Specific TP-RRs were 0.7 ± 0.3, 1.06 ± 0.12, and 0.015 ± 0.005 g $P \cdot m^{-3} \cdot d^{-1}$. Contribution of P removal mechanism are described by Figure V. 4B. Chemical P precipitation was negligible at the average T and pH values observed in all periods (Table V. 3 and Section 5.3.1.2), regardless HRT. Only S2_HRT2 provided suitable conditions to enhance assimilation capacity of microalgae-bacteria consortium and comply with European discharge limits. The operating HRT did not influence the COD-RE (96 ± 1.4%) throughout the three periods studied. Filtration process by MT module was involved in COD removal mechanism as stated in Section 5.3.3.1.

The decrease in HRT brought about a significant increase in biomass concentration measured as VSS (p-value < 0.05), accounting for 667 ± 15, 995 ± 34, and 1629 ± 15 g $VSS \cdot m^{-3}$ in S2_HRT4, S2_HRT2, and S2_HRT1, respectively.

5.3.4. Overall discussion: could a suitable microalgae-bacteria consortium be achieved for efficient wastewater treatment by modifying HRT?

From the conceptual scheme of a microalgae-bacteria consortium (Figure V. 1B), achieving a self-sufficient biomass able to remove wastewater pollutants without mechanical aeration would be possible. However, can it really be achieved in a practical framework? Two real domestic wastewater inputs and different operating HRTs have been studied in this work.

The achieved microalgae-bacteria consortia from MHRAP using effluent from primary settling (S1) were not able to remove N and P. Although nitrifying bacteria activity was less than 10% of biological activity measured in the three periods in S1 (regardless the operating HRT), the equilibria reached were fully dominated by autotrophic bacteria. The difference between nitritation and nitratation activity was barely 3% in S1_HRT6, being this small margin enough to generate significant nitrite accumulation according to Philips et al. (2002). Nitrite can be highly toxic, not only to microalgae (González-Camejo et al., 2020b) but also to a wide range of bacteria, such as AOB and NOB (Philips et al., 2002). Partial-nitrification was avoided and complete oxidation of NH_4-N to NO_3-N was achieved at 4 and 2 days of HRT. The nitrifying activity accounted for less than 10% of biological activity in both S1_HRT4 and S1_HRT2. Figure V. 4A and B show that most of the incoming NH_4-N was oxidized by the coupling of AOB and NOB, resulting in an N and P uptake by biomass of less than 5%. Predominance of nitrification over nutrient assimilation by biomass, suggested that nitrifying bacteria outcompeted microalgae for substrates (such as NH_4-N and DIC), limiting nutrient assimilation ability. However, a significant reduction in nutrient uptake upon nitrifying bacteria proliferation was also reported by González-Camejo et al. (2020), which operated a Membrane

Photobiorreactor (MPBR) supplying pure CO_2. Nonetheless, despite the continuous supply of DIC, nitrifying bacteria displaced microalgae. Competitive displacement was then probably more conditioned to NH_4-N concentration than DIC availability.

Figure V. 4A shows that NH_4-N uptake by biomass was lower than 5% despite the presence of available ammonium in the MHRAP. González-Camejo et al. (2019b) observed that nitrogen uptake by microalgae was reduced at NH_4-N concentrations below 15 $g \cdot m^{-3}$. AOB not only compete for NH_4-N but also reduce its availability, with a subsequent reduction in microalgal activity.

In the microalgae-bacteria consortia ecological relationship framework, denitrification process by heterotrophic bacteria could reduce NO_3-N concentration in the MHRAP pilot plant. The ever-aerobic conditions suggested that low BOD loading limited heterotrophic activity (25 ± 9 and 53 ± 15 $g \cdot m^{-3} \cdot d^{-1}$ for S1_HRT4 and S1_HRT2, respectively).

Chemical P precipitation was the main mechanism for P removal. Indeed, abiotic conditions prevented precipitation in S1_HRT4 and S1_HRT2, leading to P-REs below 2%. Microalgae-bacteria consortia developed in S1 was therefore not able to recover phosphorus from biomass.

High average light intensity in S1_HRT6 (936 ±209 µmol m^{-2} s^{-1}), combined with low TSS (175 ± 28 g TSS m^{-3}, Table V. 2), resulted in a maximum I_{av} inside the HRAP of 186 ± 33 µmol m^{-2} s^{-1}. The maximum I_{av} of S1_HRT6 was near to NOB photoinhibition intensity observed by Vergara et al. (2016), suggesting that light intensity can be a key inhibitor factor, when light intensity reaches its maximum. On the other hand, NOB photoinhibition in S1_HRT4 and S1_HRT2 can be discarded since the maximum I_{av} were 91 ± 73 and 105 ± 40 $\mu mol \cdot m^{-2} \cdot s^{-1}$, respectively.

Answering the question posed in Section 5.1, it would not be possible to achieve the equilibrium between microalgae and indigenous wastewater bacteria in MHRAP

operating at 6, 4, and 2 days HRT using effluent from primary settling, thus the system was not able to remove wastewater nutrients and comply with EU discharge limits.

The second set of experiments (S2) was carried out in summer and with pre-treatment effluent to promote growth of microalgae and heterotrophic bacteria, respectively.
Period S2_HRT4 showed the same pattern than S1_HRT4 and S1_HRT2. Despite the more suitable abiotic boundary conditions for microalgae growth (specifically, an increase in light availability), AOB outcompeted microalgae for NH_4-N uptake. In addition, the increase in BOD loading (73 ± 6 $g \cdot m^{-3} \cdot d^{-1}$) did not promote growth of an active heterotrophic community. NO_3-N accumulation and ever-aerobic conditions were recorded, thus the MHRAP operating at 4 days of HRT did not comply with the discharge limits established by the EU Directive.

Decreasing HRT from 4 to 2 days did not promote nitrogen uptake by biomass, being nitrification the main NH_4-N removal pathway (Figure V. 4A). However, phosphorus removal was increased by the assimilation capacity of microalgae-bacteria consortium. N/P uptake ratio was 11.7 ± 1.4 (on a mass basis), similar to N/P ratio reported by Gardner-Dale et al. (2017) and Reynolds (2006). The increasing of BOD loading (145 ± 10 $g \cdot m^{-3} \cdot d^{-1}$) resulted in a shift from aerobic to anoxic conditions during daylight hours and night-time, respectively. The coupled nitrification-denitrification process accounted for 87% of total nitrogen removed (Figure V. 4B).
Overall, the decrease in the HRT from 2 to 1 days resulted in an increase in heterotrophic activity (BOD loading 290 ± 30 g m^{-3} d^{-1}) and reduced the nitrification rate due to low DO concentration prevailing during all day. Growth of heterotrophic bacteria increased TSS and reduced the maximum I_{av}, photolimiting microalgal photosynthesis.

Employing microalgae in nitrification-denitrification processes required careful culture management to control oxygen levels. Growth of heterotrophic bacteria appears to be the key to achieving aerobic and anoxic conditions. The community of heterotrophic

bacteria was limited by the amount of organic matter supplied to the system in S1 and S2_HRT4. In all periods, microalgae played a key role as oxygen supplier for aerobic bacteria. The EU nutrients limits discharge were only met at 2 days of HRT for S2, when an equilibrium between microalgae and bacteria provided suitable conditions for nitrification, denitrification, and phosphorus uptake by biomass.

5.4. CONCLUSION

This study evaluated the impact of HRT on the performance of a MHRAP pilot plant for wastewater treatment. The overall study results showed that MHRAP is a suitable option for the treatment of effluent from-pretreatment with an operating HRT of 2 days and BOD loading rate of 145 $g \cdot m^{-3} \cdot d^{-1}$. Under this specific operating conditions and abiotic boundary conditions, the achieved microalgae-bacteria consortia did not need any external source of aeration and simultaneously removed organic matter and nutrients. The main nitrogen removal mechanism was the nitrification-denitrification process. Oxygen released by microalgae under lighting conditions was used by nitrifying bacteria to oxidize ammonium to nitrate. Biomass respiration consumed oxygen during night-time and nitrate was used as electron acceptor by heterotrophic bacteria. Phosphorus was removed by biomass uptake. The use of membrane technology coupled with bacterial activity removed the organic matter in wastewater below the discharge limits, regardless operating HRT and wastewater stream. Microalgae key role was to supply oxygen for nitrifying and heterotrophic activity.

Regarding the treatment of effluent from primary settling, for the three HRT studied the biomass was not able to remove nutrients. Ecological community was dominated by nitrifying bacteria at 4 and 2 days of HRT. Microalgae released the oxygen needed to nitrification but promoted ever-aerobic conditions (even at night), resulting in a NO_3-N accumulation. Organic matter supplied by primary effluent was not enough to provide anoxic conditions and remove the oxidized nitrogen.

MHRAP operated with pre-treatment effluent (higher BOD) achieved two opposite communities. Operating at 4 days HRT it was dominated by nitrifying bacteria activity. However, the community structure shifted towards heterotrophic bacteria at 1 day HRT. The higher the organic matter loading rate, the greater the growth of heterotrophic bacteria, resulting in high TSS concentration, low light irradiance available for microalgae, and zero oxygen concentration in the MHRAP. This system operated at 1 day HRT was also not able to remove nutrients from wastewater.

The heterotrophic activity was therefore the key parameter to obtain a suitable system for wastewater treatment. A bacteria-deficient consortium did not promote microalgae growth and anoxic conditions to remove oxidized nitrogen, but an ecological structure dominated by heterotrophic bacteria reduced light for photosynthesis and resulted in zero oxygen concentration that allowed anoxic conditions for denitrifying bacteria.

REFERENCES

Acién, F.G., Gómez-Serrano, C., Morales-Amaral, M.M., Fernández-Sevilla, J.M., Molina-Grima, E., 2016. Wastewater treatment using microalgae: how realistic a contribution might it be to significant urban wastewater treatment? Appl. Microbiol. Biotechnol. 2016 10021 100, 9013–9022. https://doi.org/10.1007/S00253-016-7835-7

Anbalagan, A., Schwede, S., Lindberg, C.F., Nehrenheim, E., 2016. Influence of hydraulic retention time on indigenous microalgae and activated sludge process. Water Res. 91, 277–284. https://doi.org/10.1016/j.watres.2016.01.027

Aparicio, S., Robles, Á., Ferrer, J., Seco, A., Borrás Falomir, L., 2022. Assessing and modeling nitrite inhibition in microalgae-bacteria consortia for wastewater treatment by means of photo-respirometric and chlorophyll fluorescence techniques. Sci. Total Environ. 808, 152128. https://doi.org/10.1016/J.SCITOTENV.2021.152128

APHA-AWWA-WPCF, 2012. Standard Methods for the Examination of Water and Wastewater, 22nd edition, American P. ed. Washington DC, USA.

Ashadullah, A.K.M., Shafiquzzaman, M., Haider, H., Alresheedi, M., Azam, M.S., Ghumman, A.R., 2021. Wastewater treatment by microalgal membrane bioreactor: Evaluating the effect of organic loading rate and hydraulic residence time. J. Environ. Manage. 278, 111548. https://doi.org/10.1016/J.JENVMAN.2020.111548

Barbera, E., Sforza, E., Grandi, A., Bertucco, A., 2020. Uncoupling solid and hydraulic retention time in photobioreactors for microalgae mass production: A model-based analysis. Chem. Eng. Sci. 218. https://doi.org/10.1016/j.ces.2020.115578

Chu, F., Cheng, J., Zhang, X., Ye, Q., Zhou, J., 2019. Enhancing lipid production in microalgae Chlorella PY-ZU1 with phosphorus excess and nitrogen starvation under 15% CO2 in a continuous two-step cultivation process. Chem. Eng. J. 375, 121912. https://doi.org/10.1016/j.cej.2019.121912

Cornejo, P.K., Becker, J., Pagilla, K., Mo, W., Zhang, Q., Mihelcic, J.R., Chandran, K., Sturm, B., Yeh, D., Rosso, D., 2019. Sustainability metrics for assessing water resource recovery facilities of the future. Water Environ. Res. 91, 45–53. https://doi.org/10.2175/106143017X15131012187980

Fallahi, A., Rezvani, F., Asgharnejad, H., Khorshidi, E., Hajinajaf, N., Higgins, B., 2021. Interactions of microalgae-bacteria consortia for nutrient removal from wastewater: A review. Chemosphere 272, 129878. https://doi.org/10.1016/J.CHEMOSPHERE.2021.129878

Foladori, P., Petrini, S., Andreottola, G., 2018. Evolution of real municipal wastewater treatment in photobioreactors and microalgae-bacteria consortia using real-time parameters. Chem. Eng. J. 345, 507–516. https://doi.org/10.1016/J.CEJ.2018.03.178

Gardner-Dale, D.A., Bradley, I.M., Guest, J.S., 2017. Influence of solids residence time and carbon storage on nitrogen and phosphorus recovery by microalgae across diel cycles. Water Res. 121, 231–239. https://doi.org/10.1016/J.WATRES.2017.05.033

Gómez-Serrano, C., Morales-Amaral, M.M., Acién, F.G., Escudero, R., Fernández-Sevilla, J.M., Molina-Grima, E., 2015. Utilization of secondary-treated wastewater for the production of freshwater microalgae. Appl. Microbiol. Biotechnol. 99, 6931–6944. https://doi.org/10.1007/S00253-015-6694-Y/FIGURES/10

González-Camejo, J., Aparicio, S., Jiménez-Benítez, A., Pachés, M., Ruano, M. V, Borrás, L., Barat, R., Seco, A., 2020a. Improving membrane photobioreactor performance by reducing light path: operating conditions and key performance indicators. Water Res. 172. https://doi.org/10.1016/j.watres.2020.115518

González-Camejo, J., Aparicio, S., Ruano, M. V., Borrás, L., Barat, R., Ferrer, J., 2019a. Effect of ambient temperature variations on an indigenous microalgae-nitrifying bacteria culture dominated by Chlorella. Bioresour. Technol. 290, 121788. https://doi.org/10.1016/j.biortech.2019.121788

González-Camejo, J., Barat, R., Ruano, M. V., Seco, A., Ferrer, J., 2018. Outdoor flat-panel membrane

photobioreactor to treat the effluent of an anaerobic membrane bioreactor. Influence of operating, design, and environmental conditions. Water Sci. Technol. 78, 195–206. https://doi.org/10.2166/WST.2018.259

González-Camejo, J., Jiménez-Benítez, A., Ruano, M.V., Robles, A., Barat, R., Ferrer, J., 2019b. Preliminary data set to assess the performance of an outdoor membrane photobioreactor. Data Br. 27. https://doi.org/10.1016/j.dib.2019.104599

González-Camejo, J., Jiménez-Benítez, A., Ruano, M. V., Robles, A., Barat, R., Ferrer, J., 2019c. Optimising an outdoor membrane photobioreactor for tertiary sewage treatment. J. Environ. Manage. 245, 76–85. https://doi.org/10.1016/j.jenvman.2019.05.010

González-Camejo, J., Montero, P., Aparicio, S., Ruano, M. V., Borrás, L., Seco, A., Barat, R., 2020b. Nitrite inhibition of microalgae induced by the competition between microalgae and nitrifying bacteria. Water Res. 172, 115499. https://doi.org/10.1016/j.watres.2020.115499

González-Camejo, J, Robles, A., Seco, A., Ferrer, J., Ruano, M. V, 2020. On-line monitoring of photosynthetic activity based on pH data to assess microalgae cultivation. J. Environ. Manage. 276. https://doi.org/10.1016/j.jenvman.2020.111343

González-Fernández, C., Molinuevo-Salces, B., García-González, M.C., 2011. Nitrogen transformations under different conditions in open ponds by means of microalgae-bacteria consortium treating pig slurry. Bioresour. Technol. 102, 960–966. https://doi.org/10.1016/j.biortech.2010.09.052

Gujer, W., 2010. Nitrification and me - A subjective review. Water Res. https://doi.org/10.1016/j.watres.2009.08.038

Khalili, A., Najafpour, G.D., Amini, G., Samkhaniyani, F., 2015. Influence of nutrients and LED light intensities on biomass production of microalgae Chlorella vulgaris. Biotechnol. Bioprocess Eng. 20, 284–290. https://doi.org/10.1007/s12257-013-0845-8

Mantovani, M., Marazzi, F., Fornaroli, R., Bellucci, M., Ficara, E., Mezzanotte, V., 2020. Outdoor pilot-scale raceway as a microalgae-bacteria sidestream treatment in a WWTP. Sci. Total Environ. 710, 135583. https://doi.org/10.1016/J.SCITOTENV.2019.135583

Markou, G., Vandamme, D., Muylaert, K., 2014. Microalgal and cyanobacterial cultivation: The supply of nutrients. Water Res. https://doi.org/10.1016/j.watres.2014.07.025

Matassa, S., Batstone, D.J., Hü, T., Schnoor, J., Verstraete, W., 2015. Can Direct Conversion of Used Nitrogen to New Feed and Protein Help Feed the World? https://doi.org/10.1021/es505432w

Morales-Amaral, M. del M., Gómez-Serrano, C., Acién, F.G., Fernández-Sevilla, J.M., Molina-Grima, E., 2015. Outdoor production of Scenedesmus sp. in thin-layer and raceway reactors using centrate from anaerobic digestion as the sole nutrient source. Algal Res. 12, 99–108. https://doi.org/10.1016/J.ALGAL.2015.08.020

Morillas-España, A., Lafarga, T., Sánchez-Zurano, A., Acién-Fernández, F.G., Rodríguez-Miranda, E., Gómez-Serrano, C., González-López, C.V., 2021. Year-long evaluation of microalgae production in wastewater using pilot-scale raceway photobioreactors: Assessment of biomass productivity and nutrient recovery capacity. Algal Res. 60, 102500. https://doi.org/10.1016/J.ALGAL.2021.102500

Park, S., Bae, W., Chung, J., Baek, S.-C., 2007. Empirical model of the pH dependence of the maximum specific nitrification rate. Process Biochem. 42, 1671–1676. https://doi.org/https://doi.org/10.1016/j.procbio.2007.09.010

Petrini, S., Foladori, P., Donati, L., Andreottola, G., 2020. Comprehensive respirometric approach to assess photosynthetic, heterotrophic and nitrifying activity in microalgal-bacterial consortia treating real municipal wastewater. Biochem. Eng. J. 161. https://doi.org/10.1016/j.bej.2020.107697

Philips, S., Laanbroek, H.J., Verstraete, W., 2002. Origin, causes and effects of increased nitrite concentrations in aquatic environments. Rev. Environ. Sci. Biotechnol. https://doi.org/10.1023/A:1020892826575

Podevin, M., De Francisci, D., Holdt, S.L., Angelidaki, I., 2015. Effect of nitrogen source and acclimatization

on specific growth rates of microalgae determined by a high-throughput in vivo microplate autofluorescence method. J. Appl. Phycol. 27, 1415–1423. https://doi.org/10.1007/S10811-014-0468-2/FIGURES/5

Posadas, E., Morales, M. del M., Gomez, C., Acién, F.G., Muñoz, R., 2015. Influence of pH and CO2 source on the performance of microalgae-based secondary domestic wastewater treatment in outdoors pilot raceways. Chem. Eng. J. 265, 239–248. https://doi.org/10.1016/J.CEJ.2014.12.059

Reynolds, C.S., 2006. The ecology of phytoplankton, The Ecology of Phytoplankton. Cambridge University Press, Cambridge. https://doi.org/10.1017/CBO9780511542145

Robles, Á., Capson-Tojo, G., Galès, A., Ruano, M.V., Sialve, B., Ferrer, J., Steyer, J.P., 2020. Microalgae-bacteria consortia in high-rate ponds for treating urban wastewater: Elucidating the key state indicators under dynamic conditions. J. Environ. Manage. 261, 110244. https://doi.org/10.1016/J.JENVMAN.2020.110244

Rossi, S., Bellucci, M., Marazzi, F., Mezzanotte, V., Ficara, E., 2018. Activity assessment of microalgal-bacterial consortia based on respirometric tests. Water Sci. Technol. 78, 207–215. https://doi.org/10.2166/wst.2018.078

Rossi, S., Casagli, F., Mantovani, M., Mezzanotte, V., Ficara, E., 2020a. Selection of photosynthesis and respiration models to assess the effect of environmental conditions on mixed microalgae consortia grown on wastewater. Bioresour. Technol. 305, 122995. https://doi.org/10.1016/J.BIORTECH.2020.122995

Rossi, S., Sforza, E., Pastore, M., Bellucci, M., Casagli, F., Marazzi, F., Ficara, E., 2020b. Photo-respirometry to shed light on microalgae-bacteria consortia—a review. Rev. Environ. Sci. Biotechnol. https://doi.org/10.1007/s11157-020-09524-2

Ruiz-Martínez, A., Serralta, J., Romero, I., Seco, A., Ferrer, J., 2015. Effect of intracellular P content on phosphate removal in Scenedesmus sp. Experimental study and kinetic expression. Bioresour. Technol. 175, 325–332. https://doi.org/10.1016/j.biortech.2014.10.081

Ruiz, J., Álvarez-Díaz, P.D., Arbib, Z., Garrido-Pérez, C., Barragán, J., Perales, J.A., 2013. Performance of a flat panel reactor in the continuous culture of microalgae in urban wastewater: Prediction from a batch experiment. Bioresour. Technol. 127, 456–463. https://doi.org/10.1016/J.BIORTECH.2012.09.103

Sánchez-Zurano, A, Cárdenas, J.A.G., Serrano, C.G., Amaral, M.M., Acién-fernández, F.G., Sevilla, J.M.F., Grima, E.M., 2020. Year-long assessment of a pilot-scale thin-layer reactor for microalgae wastewater treatment . Variation in the microalgae-bacteria consortium and the impact of environmental conditions. Algal Res. 50, 101983. https://doi.org/10.1016/j.algal.2020.101983

Sánchez-Zurano, A., Gómez-Serrano, C., Acién-Fernández, F.G., Fernández-Sevilla, J.M., Molina-Grima, E., 2020. A novel photo-respirometry method to characterize consortia in microalgae-related wastewater treatment processes. Algal Res. 47, 101858. https://doi.org/10.1016/j.algal.2020.101858

Seco, A., Aparicio, S., González-Camejo, J., Jiménez-Benítez, A., Mateo, O., Mora, J.F., Noriega-Hevia, G., Sanchis-Perucho, P., Serna-García, R., Zamorano-López, N., Giménez, J.B., Ruiz-Martínez, A., Aguado, D., Barat, R., Borrás, L., Bouzas, A., Martí, N., Pachés, M., Ribes, J., Robles, A., Ruano, M. V., Serralta, J., Ferrer, J., 2018. Resource recovery from sulphate-rich sewage through an innovative anaerobic-based water resource recovery facility (WRRF). Water Sci. Technol. 78, 1925–1936. https://doi.org/10.2166/wst.2018.492

Solovchenko, A., Verschoor, A.M., Jablonowski, N.D., Nedbal, L., 2016. Phosphorus from wastewater to crops: An alternative path involving microalgae. Biotechnol. Adv. 34, 550–564. https://doi.org/10.1016/J.BIOTECHADV.2016.01.002

Toledo-Cervantes, A., Posadas, E., Bertol, I., Turiel, S., Alcoceba, A., Muñoz, R., 2019. Assessing the influence of the hydraulic retention time and carbon/nitrogen ratio on urban wastewater treatment in a new anoxic-aerobic algal-bacterial photobioreactor configuration. Algal Res. 44, 101672. https://doi.org/10.1016/J.ALGAL.2019.101672

Torà, J.A., Lafuente, J., Baeza, J.A., Carrera, J., 2010. Combined effect of inorganic carbon limitation and inhibition by free ammonia and free nitrous acid on ammonia oxidizing bacteria. Bioresour. Technol. 101, 6051–6058. https://doi.org/10.1016/J.BIORTECH.2010.03.005

Van Den Hende, S., Beelen, V., Julien, L., Lefoulon, A., Vanhoucke, T., Coolsaet, C., Sonnenholzner, S., Vervaeren, H., Rousseau, D.P.L., 2016. Technical potential of microalgal bacterial floc raceway ponds treating food-industry effluents while producing microalgal bacterial biomass: An outdoor pilot-scale study. Bioresour. Technol. 218, 969–979. https://doi.org/10.1016/J.BIORTECH.2016.07.065

Viruela, A., Aparicio, S., Robles, Á., Falomir, L.B., Serralta, J., Seco, A., Ferrer, J., 2021. Kinetic modeling of autotrophic microalgae mainline processes for sewage treatment in phosphorus-replete and -deplete culture conditions. Sci. Total Environ. 149165. https://doi.org/10.1016/J.SCITOTENV.2021.149165

CHAPTER VI

6. Assessing and modeling nitrite inhibition in microalgae-bacteria consortia for wastewater treatment by means of photo-respirometric and chlorophyll fluorescence techniques

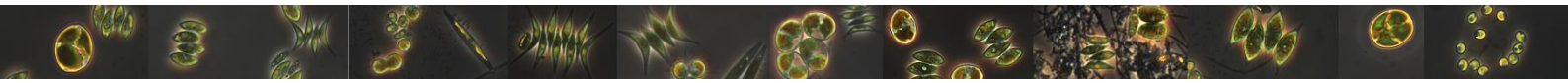

6. Assessing and modeling nitrite inhibition in microalgae-bacteria consortia for wastewater treatment by means of photo-respirometric and chlorophyll fluorescence techniques

ABSTRACT

Total nitrite ($TNO_2 = HNO_2 + NO^-_2$) accumulation due to the activity of ammonia-oxidizing bacteria (AOB) was monitored in microalgae-bacteria consortia, and the inhibitory effect of nitrite/free nitrous acid (NO_2-N/FNA) on microalgae photosynthesis and inhibition mechanism was studied. A culture of *Scenedesmus* was used to run two sets of batch reactors at different pH and TNO_2 concentrations to evaluate the toxic potential of NO_2-N and FNA. Photo-respirometric tests showed that NO_2-N accumulation has a negative impact on net oxygen production rate (OPR_{NET}). Chlorophyll a fluorescence analysis was used to examine the biochemical effects of NO_2-N stress and the mechanism of NO_2-N inhibition. The electron transport rate (ETR), non-photochemical quenching (NPQ), and JIP-test revealed that the electron transport chain between Photosystems II and I (PS II and PS I) was hindered at NO_2-N concentrations above 25 g N m^{-3}. Electron acceptor Q_A was not able to reoxidize and could not transfer electrons to the next electron acceptor, Q_B, accumulating P^+_{680} (excited PS II reaction center) and limiting oxygen production.

A semi-continuous reactor containing a *Scenedesmus* culture was monitored by photo-respirometry tests and Chlorophyll a fluorescence to calibrate NO_2-N inhibition (5 – 35 g N m^{-3}). Non-competitive inhibition and Hill-type models were compared to select the best-fitting inhibition equations. Inhibition was correctly modeled by the Hill-type model and a half inhibition constant (K_I) for OPR_{NET}, NPQ, maximum photosynthetic rate (ETR_{MAX}) and the performance index PI_{ABS} was 23.7 ± 1.2, 26.36 ± 1.10, 39 ± 2 and 26.5 ± 0.4, respectively.

Keywords

Chlorophyll a fluorescence; Hill-type model; Microalgae; Nitrite inhibition; Photo-respirometry; Wastewater treatment.

Publication

Aparicio, S., Robles, Á., Ferrer, J., Seco, A., Borrás Falomir, L., 2022. Assessing and modeling nitrite inhibition in microalgae-bacteria consortia for wastewater treatment by means of photo-respirometric and chlorophyll fluorescence techniques. Sci. Total Environ. 808, 152128. https://doi.org/10.1016/J.SCITOTENV.2021.152128

6.1. INTRODUCTION

Microalgae-bacteria based wastewater treatment systems have emerged as a sustainable and feasible alternative to remove the main pollutants from wastewater, specifically organic matter and nutrients (Bankston et al., 2020; Fito and Alemu, 2018; Mujtaba and Lee, 2017; Robles et al., 2020; Wang et al., 2017). Microalgae-bacteria consortia are supported mainly by a mutualistic interaction between microalgae and heterotrophic bacteria. The oxygen produced by photosynthesis is used to oxidize organic matter by heterotrophic bacteria, while the carbon dioxide released by organic matter oxidation is used as a carbon source for microalgae (Fito and Alemu, 2018). However, other bacterial populations e.g. ammonia-oxidizing bacteria (AOB) and nitrite-oxidizing (NOB) (nitrifying bacteria), develop in this biological community. The combined processes of ammonium (NH_4-N) assimilation by microalgae and nitrification can improve nitrogen removal rate in wastewater (Akizuki et al., 2019; Rada-Ariza et al., 2017), while negative interactions can also develop between AOB and microalgae communities. Although competition for NH_4-N is the most frequently studied negative interaction (Galès et al., 2019; González-Camejo et al., 2019; Risgaard-Petersen et al., 2004), amensalistic interactions also develop, e.g., microalgae inhibition by the final product of AOB metabolism, nitrite (NO_2-N) (Chapter 5, González-Camejo et al., 2020). Admiraal (1977) detected a decrease in the photosynthetic rate of diatoms when incubated in media with NO_2-N concentrations between 10 and 50 g N m^{-3}. González-Camejo et al. (2020) reported that an NO_2-N concentration ranging from 5 to 20 g N m^{-3} inhibits microalgae metabolism in terms of biomass productivity and nutrient removal. Although NO_2-N can be oxidized by NOB, Akizuki et al. (2019), González-Camejo et al. (2020b, 2017) and Van Den Hende et al. (2016) reported that NO_2-N can accumulate and reach concentrations of 15 to 50 g N m^{-3} in microalgae-bacteria consortia.

NO_2-N ion is related to nitrous acid (HNO_2) through acid-base equilibrium and, therefore, the relationship between NO_2-N and free HNO_2 (FNA) is highly dependent on pH ($NO_2^- +$

$H_2O \leftrightarrow HNO_2 + OH^-$; pK_a = 3.16 (Da Silva et al., 2006), for example, the concentration of HNO_2 at pH 4.5 and 8 (25ºC) accounts for 4.2% and 0.001%, respectively). Although microalgae-bacteria cultures do not provide the necessary conditions for obtaining a high FNA concentration, the protonated species has been reported to inhibit indigenous wastewater microorganisms at very low concentrations (Blackburne et al., 2007; Claros et al., 2013; Pijuan et al., 2010; Yang et al., 2003), so that FNA should be discarded as the true inhibitor of microalgae metabolism instead of NO_2-N.

The TNO_2 ($TNO_2 = HNO_2 + NO^-_2$) inhibition of photosynthesis can be assessed in the following ways: by batch growth experiments, measuring nutrient removal rate or by coupling photo-respirometry tests with *Chlorophyll a* (*Chl a*) fluorescence measures (Perales-Vela et al., 2007). Photo-respirometry tests can be successfully applied to identify potential inhibitory effects through the oxygen production rate (Rossi et al., 2020b) but they do not provide information on the inhibition mechanism in microalgal metabolism. *Chl a* concentration provides plenty of information about the Photosystem II (PS II) performance and electron transport chain (Strasser et al., 2004). In microalgae cultures, *Chl a* fluorescence measurement has been proposed as a reliable tool to study changes in primary photosynthetic processes (light-dependent reactions) due to the inhibitory compounds: free ammonia, (which negatively impacts PS II and Photosystem I (PS I), electron transport chain, the oxygen-evolving complex and dark respiration (Li et al., 2019; Markou et al., 2016)), atrazine, (damaging PS II reaction center, suppressing the electron transport chain and acting on absorption, transfer and utilization of light (Sun et al., 2020)), copper oxide nanoparticles, (which damages the oxygen-evolving complex and inhibits the electron transport chain (Che et al., 2018)), polystyrene microplastics, (which damages PS II (Li et al., 2020)), volatile organic compounds, (reducing concentration of PS II reaction centers, suppressing the electron transport chain and acting on light absorption (Zhao et al., 2016)) and herbicides, (which damages PS II

(Magnusson et al., 2008)). The combination of these techniques can thus provide a rapid and simple assessment of TNO_2 inhibition of photosynthetic processes.

Mathematical models have been widely used to study the simultaneous effects of different environmental and operational variables on the activity of microalgae-bacteria consortia (Sánchez-Zurano et al., 2021; Sánchez-Zurano et al., 2021a; Solimeno et al., 2017). However, the biokinetics of bacteria and eukaryotic organisms are developed independently and some negative interactions between the communities are not included. Inhibition processes should be included, as for example microalgae TNO_2 inhibition reported by González-Camejo et al. (2020), which must first be modeled and calibrated.

The aims of this study were: (I) to confirm that NO_2-N inhibits microalgae metabolism; (II) to analyze the inhibition mechanism of NO_2-N on photosynthesis; and (III) to propose a mathematical model to describe toxic species inhibition. To the best of the authors' knowledge, this is the first study to analyze the effect of TNO_2 on PS II and the electron transport chain activity of microalgae-bacteria consortia from an outdoor raceway pond reactor fed with real wastewater.

6.2. MATERIALS AND METHODS

6.2.1. Microorganism and wastewater

Microalgae-bacteria consortia were obtained from an outdoor pilot-scale membrane high rate algal pond (MHRAP) in the “Cuenca del Carraixet” Wastewater Treatment Plant (WWTP), Valencia (Spain). This plant mainly consisted of one HRAP connected to a membrane tank (MT). The HRAP had a surface area of 1.275 m^2 (2.55 x 0.5 m) and an operating depth of 0.25 m. A single six-blade paddle wheel was used to obtain the complete mixing of the culture medium. The MHRAP was fed with effluent from the pre-treatment of the above mentioned WWTP, having demonstrated good characteristics as the growth substrate for microalgae-bacteria consortia. The average characteristics of

the wastewater were 34 ± 5 g $N \cdot m^{-3}$ of nitrogen (mainly ammonium; i.e.>98% of total soluble nitrogen), 4.20 ± 1.04 g $P \cdot m^{-3}$ of phosphorus, 297 ± 38 g TSS m^{-3} of total suspended solids (TSS), 360 ± g $COD \cdot m^{-3}$ of soluble chemical oxygen demand (S-COD) and the alkalinity was 340 ± 49 mg $CaCO_3 \cdot L^{-1}$.

Microalgae-bacteria consortia were observed under Leica DM2500 microscope. The term “microalgae” will be used to describe eukaryotic microalgae, and therefore cyanobacteria are not included. The dominant indigenous microalgae morphology was associated with different *Scenedesmus* genera. Microalgal community was composed of >99% different *Scenedesmus* morphologies and <1% spherical unicellular microalgae cells. Mixed culture obtained by González-Camejo et al. (2020a) was composed of *Scenedesmus* and *Chlorella* using the same matrix culture, so that observed unicellular microalgae cells could be identified as *Chlorella*. No changes in microalgal community composition were observed during the study. Cyanobacteria were not observed. Microalgae were not observed forming flocs but free in the culture broth. Bacteria never accounted for more than 2% of the total biomass, resulting in a microalgae-bacteria ratio around 0.98.

6.2.2. Experimental set up

Two different sets of experiments were performed: (I) lab-scale tests to confirm the species of TNO_2 that inhibits microalgal metabolism and its mechanism of inhibition; and (II) lab-scale tests to calibrate the parameters of the model related to the inhibition process.

6.2.2.1. Inhibition tests experimental setup

Batch tests were carried out to confirm that NO_2-N inhibits photosynthesis, but mainly to analyze its inhibition mechanism: the net oxygen production rate (OPR_{NET}), electron transport rate (ETR) curve, non-photochemical quenching (NPQ) and the fluorescence transient kinetics. Three sets of three batch tests were performed with three different TNO_2 concentrations and two pH values. All the experiments were performed in triplicate.

Three TNO_2 concentrations and one pH value were studied in each test (0, 25 and 50 g $N \cdot m^{-3}$ with pH set at 4.5 or 8 (Table 1)). The following nomenclature was used to refer and identify each batch test: B(working pH)_(TNO_2 concentration), so that a batch reactor operated at a pH value of 8 and a TNO_2 concentration of 25 $g \cdot N\ m^{-3}$ was referred to as B8_25. Values of pH 4.5 and 8 were selected according to FNA concentration. The NO_2-N effect on photosynthesis can be analyzed at pH 8 since the chemical equilibrium is completely shifted towards the NO_2-N species and FNA concentration is negligible. FNA's effects on microalgal photosynthesis were studied in the batch experiments operated at pH 4.5.

In each set, 3L of microalgae-bacteria consortia culture from the MHRAP pilot plant was centrifuged at 5000xg (Eppendorf AG 22331, Hamburg) and resuspended with synthetic wastewater with the following composition (adapted medium from (Test No. 201: Alga, Growth Inhibition Test, 2006): NH_4Cl, 133.72 g m^{-3}; KH_2PO_4, 17.66 g m^{-3}; $MgSO_4 \cdot 7H_2O$, 28.99 g m^{-3}; $CaCl_2 \cdot 2H_20$, 37.67 g m^{-3}; $FeCl_3 \cdot 6H_2O$, 17.16 g m^{-3}; H_3BO_3, 1.72 g m^{-3}; $CuSO_4 \cdot 5H_2O$, 0.15 g m^{-3}; KI, 0.25 g m^{-3}; $MnCl_2 \cdot 4H_2O$, 1.02 g m^{-3}; $Na_2MoO_4 \cdot 2H_2O$, 1.07 g m^{-3}; $ZnSO_4 \cdot 7H_2O$, 4.21 g m^{-3} and $CoCl_2 \cdot 6H_2O$ 0.66 g m^{-3} and an alkalinity of 297 ± 37 mg $CaCO_3\ L^{-1}$. Allylthiourea (ATU) at 10 g m^{-3} and $KClO_3$ at 1.2 g L^{-1} (Rossi et al., 2018) were also added to the synthetic wastewater to inhibit ammonia-oxidizing bacteria (AOB) and nitrite-oxidizing bacteria (NOB) growth, respectively, and to keep TNO_2 concentration constant during the tests. ATU and $KClO_3$, did not inhibit photosynthetic activity (Chapter 5). The biomass was resuspended to set optical density at 680 nm (OD_{680}) close to 0.5, providing comparable light attenuation. 1.5 L of the resuspended culture was distributed between three batch reactors (500 mL working volume) operated in parallel. A nitrite standard solution (sodium nitrite) of 1000 $g\ NO_2 \cdot m^{-3}$ was added to the batch reactors at the beginning of the experiments to achieve an initial TNO_2 concentration of 0, 25 and 50 $g\ N \cdot m^{-3}$. As NO_2-N and FNA concentrations are highly dependent on pH, concentrations of both species were obtained (Table VI. 1) according to culture temperature and pH using Visual MINTEQ 3.1 software.

The batch reactors were equipped with: a dissolved oxygen probe (WTW CellOx 330i) connected to an oximeter (Oxi 320, WTW, Germany) recording both dissolved oxygen (DO) and temperature data every 5 s, a lighting system made of 2 cool-white LED lamps (Seven ON LED 2 x 11W) to supply a light photosynthetically active radiation (PAR) of 100 µmol m^{-2} s^{-1}, an on-off electro-valve supplied air to keep the O_2 concentration in the 80 to 120% saturation range, and a magnetic stirrer system ran at 150 rpm to ensure homogeneous conditions. The reactor was placed in a thermostatic chamber keeping the culture temperature at 26.1 ± 0.2 ºC (which is in the optimal range for microalgae growth 25-30 ºC (González-Camejo et al., 2019; Rossi et al., 2020a)).

The pH was controlled by 0.5 M HCl or 0.2 M NaOH (Pijuan et al., 2010) addition using a fuzzy-logic controller and monitored by a pH probe connected to a multiparametric analyzer (CONSORT C832, Belgium). The volume added was recorded to monitor the dilution effect.

Table VI. 1. Experimental conditions applied in each experimental test.

	Set 1			Set 2		
Batch reactor	B4.5_0 (control)	B4.5_25	B4.5_50	B8_0 (control)	B8_25	B8_50
pH	4.3 ± 0.4	4.4 ± 0.2	4.5 ± 0.3	8.0 ± 0.3	7.9 ± 0.3	8.2 ± 0.2
NO_2-N (g N·m^{-3})	0	23.96 ± 0.14	47.95 ± 0.09	0	25.3 ± 0.7	49.7 ± 0.5
HNO_2 (g N·m^{-3})	0	1.04 ± 0.11	2.04 ± 0.04	0	0.00	0.00

The sets of experiments were performed in triplicate and included a control reactor, i.e. the nitrite standard solution was not added but the reactor was operated under the same culture conditions as the other batch reactors. Photosynthetic activity was analyzed by comparing the reactors at different TNO_2 levels with the control reactor of each set. This experimental procedure reduces the variability of microalgae biomass on different experimental days and the effect of pH on the biological parameters analyzed.

Net oxygen production rate (OPR_{NET})

The 3 batch reactors described in Section 6.2.2.1 were operated for 5 days, in triplicate. The OPR_{NET} was obtained by performing photo-respirometric tests, using a protocol adapted from Rossi et al. (2018) and Sánchez-Zurano et al. (2020) (Figure VI. 1A).

1. A 500 mL aliquot of resuspended microalgae culture (at OD_{680} close to 0.5) was inoculated into each reactor.
2. Nitrite standard solution was added to achieve a TNO_2 concentration of 25 and 50 g $N \cdot m^{-3}$, taking the dilution effect into account.
3. The batch reactors were subjected to 20-min light and dark periods (in 10-min phases) throughout the 5 experimental days. DO was measured and registered every 10 s. As recommended by Sánchez-Zurano et al. (2020a), the first minute of light and dark exposure was disgregaded as was considered the adaptation time. The electro-valve was open and air was provided between the light and dark phases to keep O_2 concentration in the 80 to 120 %Sat range.

DO generation was expected in the light phases as a result of microalgae photosynthesis, while the oxygen was consumed by respiration in the dark phase. Nitrifiying bacteria activity was neglected due to the addition of AOB and NOB inhibitors (ATU and $KClO_3$, respectively), as was the aerobic activity of heterotrophic bacteria, since the used synthetic wastewater used did not contain organic matter and the biomass culture sCOD was less than 15 g COD m^{-3}. The OPR_{NET} (mg $O_2 \cdot gVSS^{-1} \cdot h^{-1}$) was calculated as the sum between the monitored values (i.e., specifying whether the slope is positive or negative) of the oxygen production rate (OPR) slope in the light phase and the oxygen uptake rate (OUR) slope in the dark phase, divided by the dry wieght of total biomass in the sample (Equation VI. 1) (i.e. volatile suspended solids (VSS), which were measured according to the Standard Methods). The OUR is the oxygen consumed by the respiration of microalgae and endogenous respiration of bacteria. The MHRAP pilot plant was monitored and controlled during all experimental periods. VSS remained stable

during the whole period at an average concentration of 325 ± 45 g VSS·m^{-3}. The biological culture was periodically examined under the microscope. Bacteria never accounted for more than 2% of the total biomass, thus, VSS were considered to represent microalgae biomass. Similary, Luo et al. (2018) reported that bactertia accounted for only 0.2-3.5% of microalgae-bacteria consortium biomass. For this reason, the whole biomass measured as VSS was considered to be composed solely of microalgae. The oxygen mass transfer coefficient (K_La) was calculated to correct the influence of oxygen desorption on the photo-respirometric measures (Equation VI. 2 andEquation VI. 3). The K_La coefficient was evaluated by performing an abiotic test in distilled water (in triplicate) in the same chemical-physical conditions set during the experiments. Destilled water was placed in the batch reactor and oxygen concentration was increased to 130%Sat by bubbling air. Then, aeration was stopped and oxygen concenrtation was recorded during 3 hours. The minimum residual sum of squared errors was used to match dynamic mass balance for DO with Equation VI. 2 (González-Camejo et al., 2020) and K_La value of 0.27 ± 0.04 h^{-1} was obtained at 25ºC.

$$\mathrm{OPR_{NET}} = \frac{\mathrm{OPR} + \mathrm{OUR}}{\mathrm{VSS}} \qquad \text{Equation VI. 1}$$

$$\frac{\mathrm{d(DO)}}{\mathrm{dt}} = \mathrm{K_L a} \cdot (\mathrm{DO_{SAT}} - \mathrm{DO}) \qquad \text{Equation VI. 2}$$

$$\mathrm{DO_{SAT}} = \mathrm{pO_2} \cdot \mathrm{K_{H,O_2}(T)} = \mathrm{pO_2} \cdot \mathrm{K_{H,O_2,REF}} \cdot \exp\left(-\frac{-\Delta_{\mathrm{SOL}}\mathrm{H}}{\mathrm{R}} \cdot \left(\frac{1}{\mathrm{T}} - \frac{1}{\mathrm{T_{REF}}}\right)\right) \qquad \text{Equation VI. 3}$$

where OPR_{NET} is the net oxygen production rate (g O_2·gVSS^{-1}·h^{-1}), OPR is the oxygen production rate, value (g O_2·m^{-3}·h^{-1}), OUR is the oxygen uptake rate, value (g O_2·m^{-3}·h^{-1}), VSS is the volatile suspended solids (g VSS·m^{-3}), K_La is the oxygen mass transfer coefficient (h^{-1}), DO_{SAT} is the DO saturation concentration (g O_2·m^{-3}) at tempertature T (K) and the partial pressure of oxygen in atmosphere pO_2 (Atm), and $K_{H,O2}$(T) = 40.5 (mg·O_2 L^{-1}·Atm^{-3}) is the Henry's law solubility constant for DO at temperature T (Sander, 2015) and Δ_{SOL}H/R = 1200 (K) (tabulated) is the enthalpy of dissolution divided for the univeral gas constant (Sander, 2015). The reference temperature (T_{REF}), and pO_2 were 298.15 K and 0.21 atm.

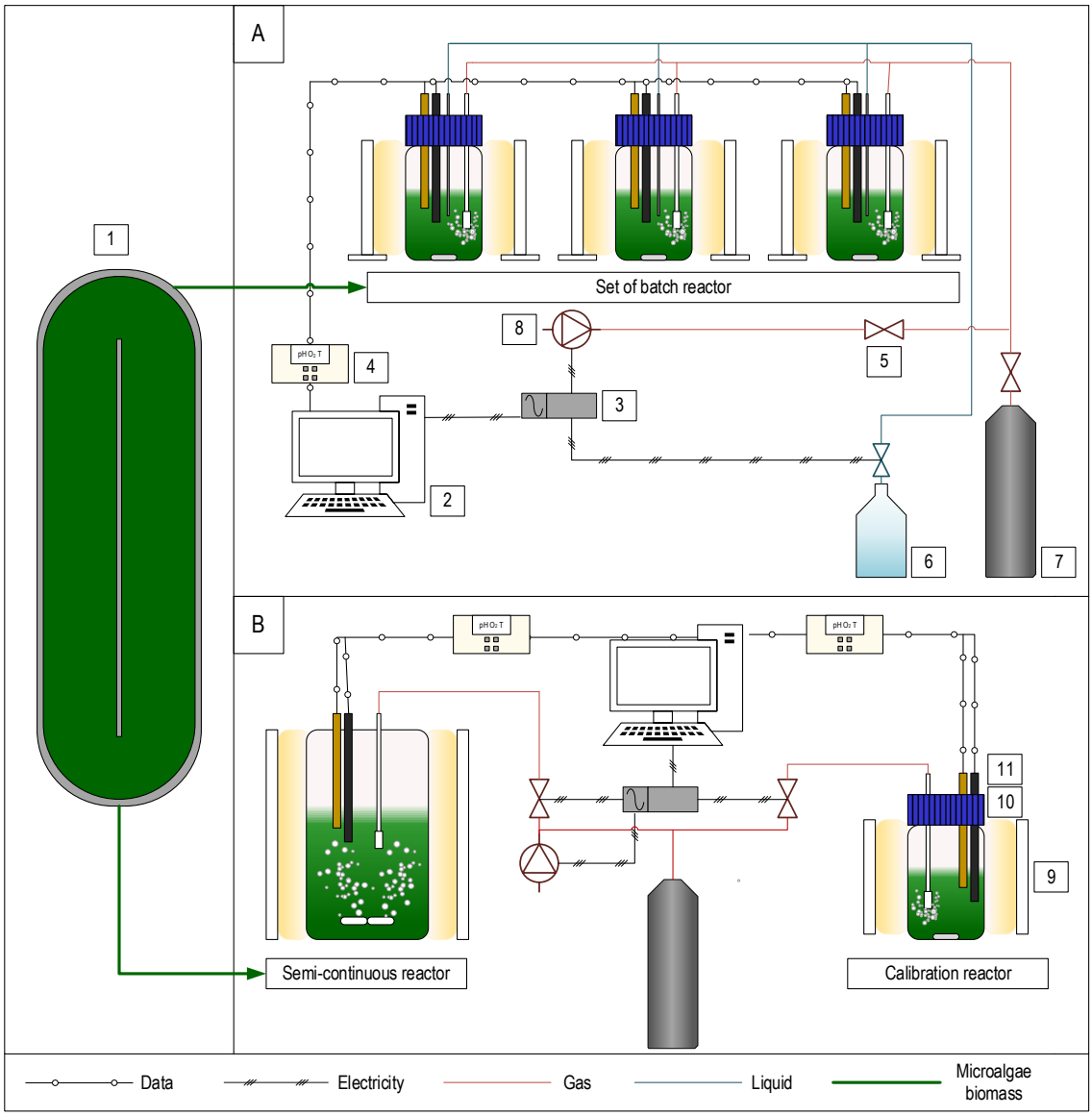

Figure VI. 1. Scheme of the experimental setups for (A) inhibition and (B) calibration tests. Legend: 1 = HRAP; 2 = Industrial grade PC; 3 = relay box; 4 = multiparametric consort; 5 = on-off electro-valve; 6 = acid/base solution; 7 = pure CO_2 gas bullet; 8 = air compressor; 9 = light source; 10 = reactor; 11 = DO, pH and temperature probes

The OPR_{NET} was used to confirm that NO_2-N inhibits microalgal photosynthesis, while *Chl a* fluoresecence was used to analyze the mechanism of inhibitor action.

Electron transport rate (ETR) curve

The ETR curve was recorded in dark-adapted samples (20 min) using the Light curve test (LC1) protocol of the fluorometer AquaPen-C AP-C 100 (Photon Systems Instruments, Czech Republic). This protocol is based on successive measurements of the microalgae sample exposed to a stepwise increase in actinic light intensity (red-light

diode). The effective quantum yields of PS II are determined under 6 actinic light intensities: 10, 20, 50,100, 300 and 500 μmol·m^{-2}·s^{-1}, with 60 s phase duration (PSI (Photon Systems Instruments), 2017). The ETR curve was calculated using the quantum yields of photosynthesis derived from the LC1 protocol and the number of absorbed photons per *Chl a* and time according to Equation VI. 4.

$$ETR = \Phi_{PS\,II} \cdot E \cdot 0.5 \qquad \text{Equation VI. 4}$$

where $\Phi_{PS\,II}$ is the quantum yield of PS II, E is the irradiance of the actinic light (μmol·m^{-2}·s^{-1}) and 0.5 is the fraction of absorbed quanta direct to PS II, i.e. the radiant energy is absorbed by PS I and PS II equally (Yamori et al., 2011).

The nonlinear model described by Serôdio et al. (2013) was applied to match the ETR curves obtained and to estimate the following key parameters: (I) maximum photosynthetic rate (ETR_{MAX}), the maximum electron transport rate through the PS II (μmol·m^{-2}·s^{-1}); (II) the initial slope of ETR curve (α), the quantum efficiency of photosynthetic electron transport (electrons/photon); and (III): the saturating irradiance of photosynthesis (E_K) (μmol·m^{-2}·s^{-1}).

After 5 experimental days, an aliquot of 3 mL from each batch reactor was kept in darkness for 20 min before applying the LC1 protocol.

Non-photochemical quenching (NPQ)

NPQ was measured in dark-adapted samples (20 min) following the AquaPen-C AP-C 100 NPQ2 protocol. The NPQ protocol is divided in two parts, one measuring fluorescence under dark-adapted and a second under light-adapted conditions. The protocol begins by giving a measuring light to obtain the minimum fluorescence level in a dark-adapted state (F_o). A short saturating light flash is then applied to reduce the plastoquinone (PQ) pool and the maximum fluorescence is measured in the dark-adapted state (F_m). After a short-term relaxation in the dark, the microalgae sample is exposed to light actinic for hundreds of seconds to elicit a transient of the Kautsky effect

measuring the instantaneous Chl fluorescence in the light-adapted phase (F_tL) (Stirbet and Govindjee, 2011). An additional saturating flash sequence is applied on top of the actinic light to measure NPQ and the effective quantum yield of photosynthesis in the light-adapted state (F_ML). After exposure to continuous illumination, NPQ relaxation is determined by saturating pulses applied in the dark, measuring maximum Chl fluorescence and instantaneous Chl fluorescence in the dark adapted phase (F_tD and F_MD, respectively) (PSI (Photon Systems Instruments), 2017).

NPQ was measured dark-adapted samples (20 min) from the batch reactors after 5 experimental days.

Fluorescence transient (JIP-test)

Transient chlorophyll fluorescence induction in dark-adapted samples was measured by the AquaPen-C AP-C 100 JIP-test. The fast fluorescence induction curve was recorded in 50 µs - 2 s time range with a saturating light of 3000 $\mu mol \cdot m^{-2} \cdot s^{-1}$ of red-orange light (620 nm). The fluorescence transient starts at the phase O (at 50 µs), passes through two intermediate, phases J and I, (at 2 and 60 ms, respectively) and reaches the maximum fluorescence in the phase P. The set of phases is called the OJIP curve. To better evaluate the events reflected in the OJIP curve and between the O-J, J-I and I-P phases, the fluorescence data were normalized (between the minimum and maximum fluorescence intensity, F_o and F_m, respecitvely) and presented as the relative variable fluorescence kinetics at any time (Equation VI. 5) and as a kinetic profile of the difference between the control reactor and the other two batch reactors in the same set (Equation VI. 6) (Gomes et al., 2012).

$$V_{OP} = \frac{(F_t - F_o)}{(F_m - F_o)} \qquad \text{Equation VI. 5}$$

$$\Delta V_{OP} = (V_{OP} - V_{OP-\text{control reactor}}) \qquad \text{Equation VI. 6}$$

where F_t is the instantaneous chlorophyll fluorescence at any time t (relative units); F_o is the minimum chlorophyll fluorescence (relative units); F_m is the maximum chlorophyll fluorescence (relative units); and V_{OP} is the relative variable fluorescence (relative units).

The JIP-test includes the determination of the photochemical parameters listed in Table VI. 2

Table VI. 2. Formula and definition of JIP-test parameters

Data extracted from the recorded fluorescence transient OJIP	
F_o	Minimal reliable recorded fluorescence at 50 μs (Relative units)
F_J	Fluorescence at the J-peak of OJIP curve (Relative units)
F_t	Fluorescence at time *t* after actinic illumination onset (Relative units)
F_m	Maximal recorded fluorescene at the peak P of OJIP curve (Relative units)
Area	Total complementary area between fluorescence induction curve and F = F_m
Fluorescence parameters derived from the extracted data	
$V_J = \frac{F_J - F_o}{F_m - F_o}$	Relative variable fluorescence at the J-peak of OJIP curve
$\frac{F_V}{F_m} = \frac{F_m - F_o}{F_m}$	Maximum quantum yield of PS II photochemistry
$M_o = \frac{4(F_{300} - F_o)}{F_m - F_o}$	Approximated initial slope (ms^{-1}) of the fluorescence transient V = f(*t*)
$S_M = \frac{Area}{F_m - F_o}$	Normalized total complementary area above the OJIP transient
Specific energy fluxes, per QA-reducing PS II reaction center (RC)	
$\frac{ABS}{RC} = M_o \cdot \left(\frac{1}{V_J}\right) \cdot \left(\frac{1}{\varphi_{Po}}\right)$	Absorption flux per RC
$\frac{TR_o}{RC} = M_o \cdot \left(\frac{1}{V_J}\right)$	Trapped energy flux per RC
$\frac{DI_o}{RC} = \left(\frac{ABS}{RC}\right) - \left(\frac{TR_o}{RC}\right)$	Dissipated energy flux per RC
Yields or flux ratio	
$\varphi_{Po} = 1 - \frac{F_o}{F_M}$	Maximum quantum yield of primary photochemistry (at *t* = 0)
$\varphi_{Eo} = \left(1 - \frac{F_o}{F_M}\right) \cdot (1 - V_J)$	Quantum yield of electron transport (at *t* = 0)
$\psi_{Eo} = 1 - V_J$	Probability (at *t* = 0) that a trapped exciton moves an electron into the electron transport chain beyong Q_A^-
$\varphi_{Do} = \left(\frac{F_o}{F_M}\right)$	Quantum yield (at *t* = 0) of energy dissipation
$\delta_{Ro} = \frac{1 - V_I}{1 - V_J}$	Efficiency/Probability with which an electron from the intersystem electron carriers moves to reduce end electron acceptors at the PS I acceptor side
$\varphi_{Ro} = \left(1 - \frac{F_o}{F_M}\right) \cdot (1 - V_I)$	Quantuym yield for reduction of end electron acceptors at the PS I acceptor side
Performance indexes (PI) at *t* = 0	
$PI_{ABS} = \frac{RC}{ABS} \cdot \frac{\varphi_{Po}}{1 - \varphi_{Po}} \cdot \frac{\psi_{Eo}}{1 - \psi_{Eo}}$	Performance index (potential) for energy conservation from exciton to the reduction of intersystem electron acceptors
$PI_{TOTAL} = \frac{PI_{ABS} \cdot \varphi_{Ro}}{(1 - \varphi_{Ro})}$	Performance index (potential) for energy conservation from exciton to the reduction of PS I end acceptors

JIP-test was recorded using a 3 mL dark-adapted sample (20 min) from the batch reactors after the 5 experimental days.

6.2.2.2. Model calibration setup

Semi-continuous reactor

A lab-scale reactor was operated in semi-continuous mode to promote controlled conditions (temperature, light intensity, pH, and nutrients and CO_2 availability) and to calibrate the parameters of the mathematical model related to photosynthesis inhibition by TNO_2 and achieve the optimal non-stressed biomass for calibration (i.e. microalgae activity was not limited by environmental conditions). The lab-scale reactor consisted of an 8-L cylindrical methacrylate tank (20-cm internal diameter) and was filled with 33% of substrate (synthetic wastewater) and 67% of microalgae-bacteria consortia from MHRAP pilot plant (see Section 6.2.1). Air-stirred at 0.7 vvm through four fine bubble diffusers on the bottom to homogenize the culture and avoid biofilm on the reactor walls and biomass sedimentation. Pure CO_2 (99.9%) was injected from a pressurized cylinder at 1.5-2.0 bar pressure into the air flow to keep reactor pH constant at 7.5 ± 0.4. An on-off electro-valve synchronized with the pH measurements recorded by the data acquisition system (a temperature-pH probe connected to a multiparametric analyzer, CONSORT C832, Belgium) was opened for 2 s when the pH exceeded the set point value of 7.5. The reactor was placed in a thermostatic chamber keeping the culture temperature at 25.3 ± 0.8 ºC. Five LED lamps (T8 LED-Tube 9 W) were placed around the reactor to provide a continuous light PAR of 154 ± 30 $\mu mol \cdot m^{-2} \cdot s^{-1}$ on the reactor surface. The reactor was sealed but not hermetic, to avoid extreme overpressure and oxygen concentration was kept close to saturation levels (111 ± 7 %Sat). DO was measured by a Cellox 330i electrode (WTW, Germany) connected to an oximeter (Oxi 320, SET WTW, Germany). The reactor was operated in semi-continuous mode, maintaining 4 days of hydraulic retention time (HRT). Every 3 hours, 0.250 L of biomass culture was taken from the reactor and replaced with synthetic wastewater (Section 6.2.2.1).

Calibration reactor

The concentration levels of the tested TNO_2 was calibrated by the semi-continuous reactor biomass culture. The calibration procedure was carried out in a 0.5 L batch reactor, inside the same thermostatic chamber as the semi-continuous reactor, providing a culture temperature of 25.7 ± 1.2 ºC. An on-off valve was used to add pure CO_2 (99.9%) for 1 s when the pH exceeded the set point value of 7.5, keeping constant pH at 7.5 ± 0.6. The microalgae culture was stirred at 250 rpm to ensure homogenization and avoid biomass sedimentation. K_La was 0.19 h^{-1} (the protocol applied is described in Section 6.2.1.1.). Two LED lamps (Seven ON LED 11 W) were placed over the reactor to provide an average light PAR of 162 ± 20 $\mu mol \cdot m^{-2} \cdot s^{-1}$ on the reactor surface. The batch reactor was equipped with a Cellox 330i electrode (WTW, Germany) connected to an oximeter (Oxi 320, SET WTW, Germany) connected to a personal computer.

Ten different experiments were performed in triplicate at different TNO_2 concentrations ranging from 2.5 to 35 g N m^{-3} (calibration TNO_2 concentrations studied were 0, 2.5, 5, 7.5, 10, 15, 20, 25, 30 and 35 g N m^{-3}). An aliquot of 0.5 L of microalgae sample was placed inside the batch reactor and nitrite standard solution was added to achieve TNO_2 levels. Concentration of NO_2 and FNA were calculated on Visual MINTEQ 3.1 software. After 20 min of adaptation to the TNO_2 concentration, the microalgae culture was exposed to 5-min light-dark cycles (both lasted 2.5 minutes and 4 cycles were performed) to record DO concentration every 10 s performed between 80 and 120 %Sat. The first minute of light and dark exposure was disgregaded as it was considered the adaptation time (Sánchez-Zurano et al., 2020). Microalgae OPR_{NET}, ETR curve, NPQ, and the JIP-test were measured as described in Section 6.2.2.1 after 20 min of NO_2/FNA addition.
The 10 inhibition assay sets were performed in triplicate. Since the culture volume of the semi-continuous reactor was limited to 8 L, the assays were carried out on different days. The stability of the semi-continous reactor was monitorized according to VSS, OD_{680} and F_V/F_m values. Calibration replicates were performed once the steady state was reached

i.e. VSS, OD_{680} and F_V/F_m values were similar between replicates. The calibration procedures included a control reactor, i.e. the nitrite standard solution was not added but the reactor was operated in the same conditions. The inihibition effect was the difference between photosyntetic activity in the control reactor and the inhibition assays. Calibration tests were attempted at a maximum of 2.5 h to ensure similar biomass from the semi-continuous reactor. The calibration setup scheme is shown in Figure VI. 1B.

Mathematical models

Two inhibition models were chosen to reproduce the effect of NO_2/FNA on photosynthesis: the non-competitive inhibition model (Equation VI. 7) used to evaluated TNO_2 inhibition in nitrifying activity models (Claros et al., 2013) and a sigmoidal logistic curve, or Hill-type model (Equation VI. 8) used to describe dose-response curve (Prinz, 2010).

$$\frac{v}{v_{MAX}} = \frac{K_I}{K_I + I} \qquad \text{Equation VI. 7}$$

$$\frac{v}{v_{MAX}} = \frac{{K_I}^n}{{K_I}^n + I^n} \qquad \text{Equation VI. 8}$$

where v/v_{MAX} is the relative photosynthesis activity rate, v_{MAX} is the non-inhibited photosynthesis activity rate, K_I is the 50% inhibitor concentration, and n is the Hill coefficient.

The minimum residual sum of squared errors was used to match the experimental data with both inhibition models. The R-squared (R^2) was calculated to evaluate goodness of fit.

6.2.3. Analytical methods

Ammonium (NH_4-N), nitrite (NO_2-N) and nitrate (NO_3-N) concentrations were analyzed on an automatic analyzer (Smartchem 200, WestcoScientific Instruments, Westco) according to the Standard Methods (APHA-AWWA-WPCF, 2012): 4500-NH3-G, 4500-NO2-B and 4500-NO3-H, respectively. Total suspended solids (TSS), VSS and sCOD

were analyzed according 2540-TSS-D, VSS 2540-VSS-E and 5220-COD-D, respectively (APHA-AWWA-WPCF, 2012).

The OD_{680} and fluorescence parameters were measured by a portable AquaPen-C AP-C 100 (Photon Systems Instruments, Czech Republic).

6.2.4. Statistical analysis

As previously mentioned, all the experiments were performed in triplicate to calculate the mean values and standard deviation. The relationships between the photosynthetic parameters and the NO_2-N or FNA concentrations were determined by an ANOVA analysis on STATGRAPHICS Centurion XVI.I software. P-values < 0.05 were considered statistically significant.

6.3. RESULTS AND DISCUSSION

6.3.1. NO_2/FNA inhibition on microalgae photosynthesis.

To determine the true inhibitory species, concentrations of TNO_2 and pH values were systematically varied in batch tests. It was expected that if NO_2-N was the inhibitor, increasing it would reduce OPR_{NET} regardless of the pH value. If the OPR_{NET} reduction were only noted at pH 4.5, then the inhibiting species would be the FNA.

Figure VI. 2A and 2B show OPR_{NET} for 5 days at different TNO_2 concentration levels evaluated in the experiments carried out at pH 4.5 and 8, respectively. DO dynamic mass balance was attributed to photosynthesis and microalgae respiration since the nitrifying and heterotrophic bacteria activity was negligible.

Microalgae activity was normalized (i.e. expressed as a percentage of the maximum OPR_{NET}) to compare the impact on microalgae metabolism of different NO_2/FNA ratios at different pH values. At pH 8, the chemical equilibrium completely shifted towards the NO^-_2 species, i.e. TNO_2 consisted of 100% NO_2-N species. The second set of three batch reactors was run at a fixed pH value of 4.5, with a species distribution of 95.86% and 4.14% of NO_2-N and FNA at 25 ºC, respectively. The FNA concentration studied (Table VI. 1) was higher than that achieved in the experimental setups described in González-

Camejo et al. (2020), in which inhibition was already observed. Although FNA concentrations were low (< 5 g $N \cdot m^{-3}$), even lower concentrations that inhibit different bacterial taxonomic groups can be found in the literature (Blackburne et al., 2007; Claros et al., 2013; Pijuan et al., 2010).

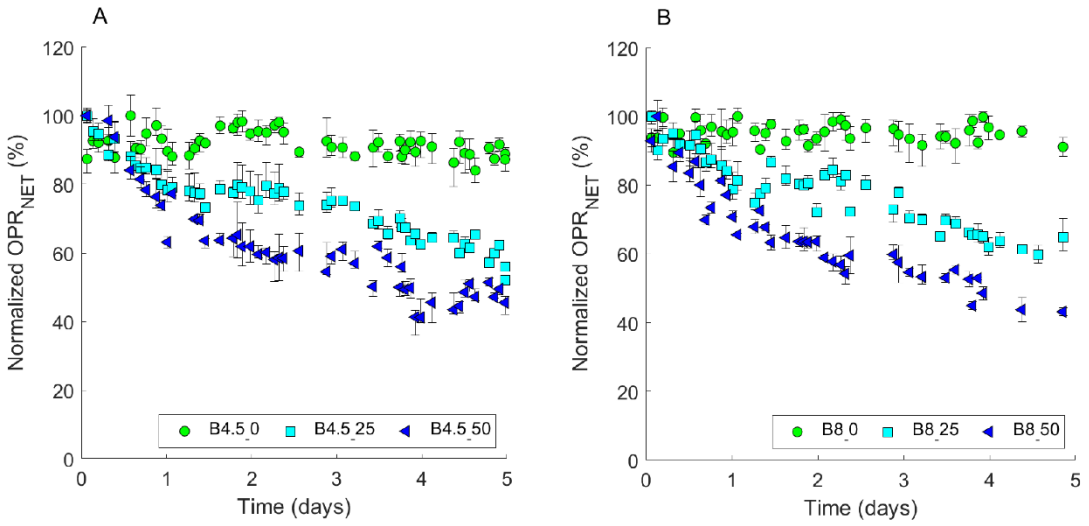

Figure VI. 2. Normalized OPR_{NET} at a pH value of (A) 4.5 and (B) 8 for different concentration of TNO_2 after 5 experimental days.

Figure VI. 2 shows a continuous reduction of OPR_{NET} in both sets of experiments compared to the control reactor (p-value < 0.05). Photosynthesis was inhibited throughout the 5 experimental days at the concentrations tested (Table VI. 1) in both sets of experiments. The results obtained in the two sets of three-batch assays confirmed that the microalgal activity inhibition was a consequence of NO_2-N accumulation and not of FNA, since increasing NO_2-N concentration significantly reduced (p-value < 0.05 obtained by ANOVA test) the ORP_{NET} regardless of the pH value. Understanding and quantifying the inhibition of photosynthetic activity by NO_2-N is of particular interest in wastewater treatments based on microalgal and bacterial consortia, since NO_2-N accumulation in the range of 15 to 50 g $N \cdot m^{-3}$ has been observed in these systems (Akizuki et al., 2019; González-Camejo et al., 2020b, 2017; Van Den Hende et al., 2016) so that, the specific effects of NO_2-N on microalgae photosynthesis were investigated using ETR, NPQ and JIP-test analyses.

6.3.2. NO_2-N inhibition mechanism

6.3.2.1. NO_2-N impact on ETR and NPQ

The impact of NO_2-N on photosynthesis activity was analyzed from the data obtained from assays performed at pH 8 rather than 4.5 due to: (I) the mean pH value in microalgae-bacteria systems dominated by microalgae and nitrifying bacteria is approximately 7.5 (daily-average) and tends towards alkaline pH values during the day-time (Mantovani et al., 2020); and (II) the optimal pH of microalgae ranges from 7 to 9 (Barceló-Villalobos et al., 2019; Rossi et al., 2020a). The results obtained from photosynthetic activity at pH 8 described NO_2-N inhibition under typical operating conditions in a microalgae-bacteria system and favorable environmental conditions for *Scenedesmus*. All the results described below were compared with the values obtained in the control reactor.

The ETR curve experimental profile and NPQ values obtained are shown in Figure VI. 3. The ETR curves were found to be highly dependent on NO_2-N concentration (Figure VI. 3A). The microalgae α, ETR_{MAX} and E_K values were negatively affected at the two concentrations tested after 5 experimental days in both sets (Table VI. 3). However, these parameters showed different inhibition patterns. The α values showed slight reduction from B8_25 to B8_50 (3%), and decrease to a maximum of 13% (p-value < 0.05) from the control reactor to B8_50. ETR_{MAX} and E_K declined significantly with a reduction of up to 35 and 25% (p-value < 0.05) in B8_50, respectively. The ETR curve response matched the type 1 photoinhibition described by Proctor and Bates (2018). At low irradiance ETR response increased with light intensity, but at higher irradiance (well below 1000 $\mu mol \cdot m^{-2} \cdot s^{-1}$) the ETR measurements sharply declined. Type 1 photoinhibition was related to an increase in NPQ on microalgae, as shown in Table VI. 3. The influence of NO_2-N approximately doubled and tripled the NPQ values in B8_25 and B8_50, increasing by up to 276% (p-value < 0.05) in B8_50 with respect to the control reactor Figure VI. 3. According to Hernández-Zamora et al. (2014) this pattern

(reduced ETR curve parameters and higher NPQ values) results from partial inhibition of the primary photosynthetic process (light-dependent reactions), reducing the capacity to process light energy. Light-driven reactions regulate the excitation energy harvested by the antenna complex, so that it can be balanced by the electron transport chain and synthesis of ATP and NADPH to reduce the potentially damaging effect on PS II by an excess of excitation energy, which can lead to a photooxidation process. On the other hand, the higher NPQ values can be interpreted as an increase in thermal energy release due to the operation of the xanthophyll cycle (photoprotection mechanism which consists of reversible and rapid conversion from pigment diadinoxanthin to energy-dissipating form diatoxanthin), or gradually reversible damage to the microalgae's photosynthetic apparatus (Jiang et al., 2008; Roach and Krieger-Liszkay, 2014; Schulze and Caldwell, 2012).

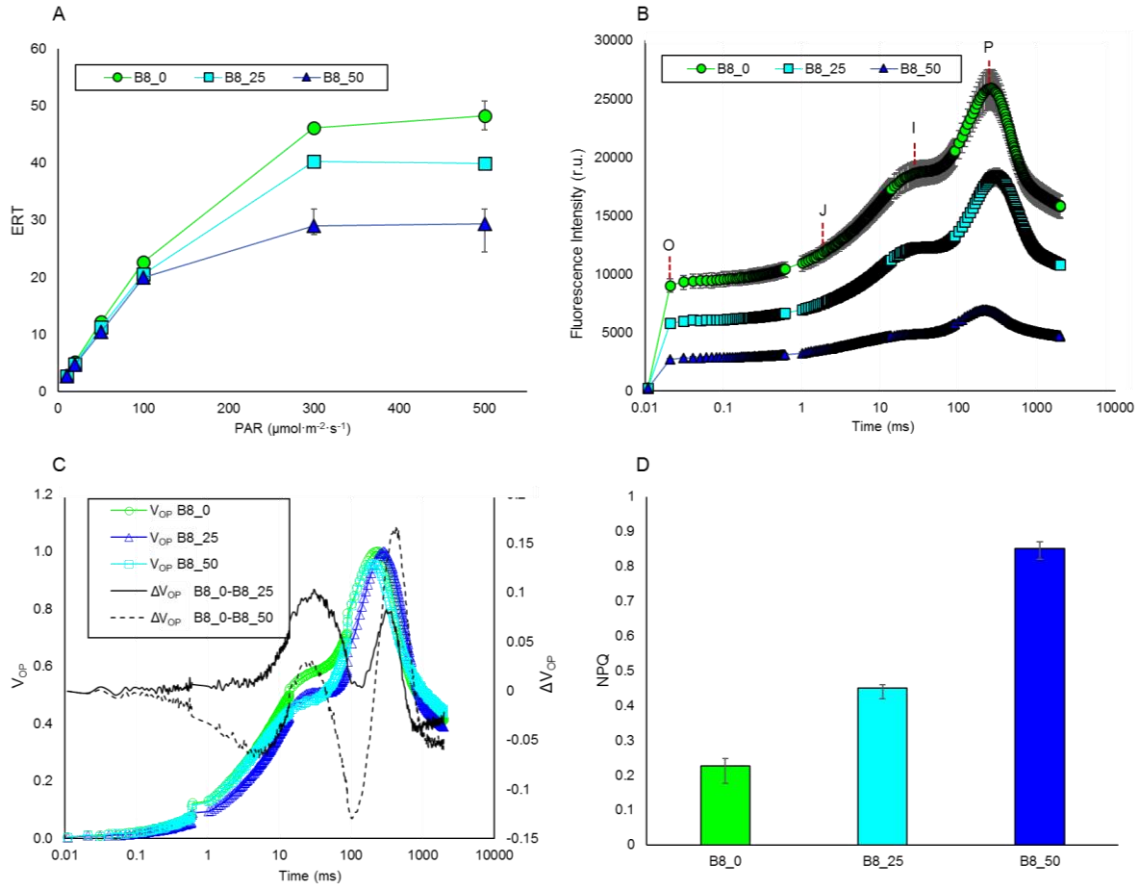

Figure VI. 3. Effect after 5 days of exposure on TNO_2 (A) ETR, (B) raw OJIP transient (C) relative variable fluorescence and kinetic difference of V_{OP} and (D) NPQ at pH value of 8 for different concentrations of TNO_2.

6.3.3. NO_2-N impact on JIP-test

According to the ETR parameters and NPQ values, NO_2-N had a significant effect on the electron transport chain and on the light energy harvesting efficiency. However, none of these provided accurate data on the effect of NO_2-N on the photochemical reactions. The polyphasic rise of *Chl a* fluorescence transients were analyzed to determine the specific inhibition mechanism (Figure VI. 3B and 3C). OJIP transients account for the sequential reduction of the electron acceptor pools of PS II. The fluorescence transient starts at phase O (at 50 µs), passes through two intermediate phases J and I (at 2 and 30 ms, respectively) and reaches the maximum fluorescence in phase P (Strasser et al., 2004). The raw fluorescence rise kinetic OJIP curves of batch reactors operated at pH 8 after 5 experimental days are shown in Figure VI. 3B. The microalgae cells exhibited a raw polyphasic OJIP rise kinetic in B8_0, similar to that described by Markou et al. (2016) and Perales-Vela et al. (2007). After 5 days of microalgae growth with NO_2-N, the raw transients gradually decreased when NO_2-N concentration increased with slightly lower (p-value < 0.05) variable fluorescence values than the control reactor ($F_v = F_m - F_0$; where F_m is the maximal fluorescence intensity and F_0 is the fluorescence intensity at 50 µs) was detected in the O- J- I- P-step in B8_25, in contrast to the sharp decrease in F_v in B8_50 (p-value < 0.05). The gradual fall of the fluorescence rise kinetic OJIP curves along with NO_2-N concentration levels resulted in the accumulation of oxidized P_{680}^{+} (PS II reaction center) (Ji et al., 2018). P_{680}^{+} accumulates when the electron transport chain after the first electron acceptor Q_A is inhibited and the oxygen-evolving complex (OEC) cannot provide electrons to PS II and reduce PQ, which is consistent with the ETR results (Figure VI. 3A). Reduction of ETR and OJIP transients in nitrite-stressed reactors could suggest that microalgae cells did not have the potential to grow due to NO_2-N (Zhang et al., 2010; Zhao et al., 2008).

A fluorescence normalization (between F_o and F_m) was performed to better evaluate the events or discrepancies reflected in the O-J, J-I and I-P phases, to obtain the relative variable fluorescence kinetics at any time, V_{OP}, (Equation VI. 5) and a kinetic profile of

differences ΔV_{OP} (Equation VI. 6) (Gomes et al., 2012). V_{OP} variation between control and B8_25 and B8_50 showed a slight reduction in the overall OJIP curve transient with increasing inhibitor concentration, but not statistical changes (p-value < 0.05) in fluorescence peaks (O, J, I, P) were detected. However, B8_25 was characterized by a reduction of ΔV_{OP} values only in the I-P phase, while in B5_50, the NO_2-N concentration considerably reduced both the O-J and I-P phases from the OJIP curve. The OJIP curve phases represent different reduction processes of the electron transport chain (Gomes et al., 2012). The first phase, O-J, is related to the photochemical reduction of the primary acceptor, Q_A, in PS II reaction centers. The J-I phase reflects the reduction of the PQ (plastoquinone) pool, while the last phase (I-P) represents the reduction of both plastocyanin and P_{700}^{+} in photosystem I (PS I). I-P phase reduction was visible in both batch reactors, but the decrease in this specific OJIP transient in B8_50 was more pronounced. The I-P phase decreased with increasing NO_2-N supply, indicating that NO_2-N showed a fractional reduction of PS I final electron acceptors ($NADP^+$) (Roach and Krieger-Liszkay, 2014). The results suggest that the higher the NO_2-N concentration, the more limited the NADPH oxidation for carbon assimilation (Roach and Krieger-Liszkay, 2014). A reduction of transient J-I phase was only found in B8_50. Deactivation of the donor side of PS II has a negative effect on the J-I phase (Schreiber and Neubauer 1987), which is related to the reduction of the PQ-pool, electrons being necessary for this process. The required electrons are only produced when there is an intact and active manganese cluster. A loss of the J-I phase at 50 g $N \cdot m^{-3}$ of NO_2-N suggested that inhibitor stress destroyed the oxygen-evolving complex due to a loss of manganese cluster activity on passing from 25 to 50 g N m^{-3} of NO_2-N.

JIP-test parameters from the OJIP kinetic curve were calculated and analyzed in detail. The ratio of variable to maximum fluorescence (F_V/F_M) represents the light absorbed by PS II to reduce Q_A, i.e. F_V/F_M is the maximum quantum efficiency of PS II. The value of F_V/F_M generally varies slightly under non-stressed conditions and is not influenced by

microalgae species or operating conditions. However, marked fluctuations in F_V/F_M values under stress have also been reported (Ji et al., 2018), making it a useful indicator of photosynthesis efficiency and stress. The performance index (PI) describes the potential for energy conservation of photons absorbed by PS II to reduce Q_A (PI_{ABS}) (Ji et al., 2018) and the reduction of the final PS I acceptor (PI_{TOT}) (Strasser et al., 2010). Significant differences were found among F_V/F_M values (p-value < 0.05) and both PI values (p-value < 0.05) for B8_25 and B8_50 compared to the control reactor (Table VI. 3). F_V/F_M, PI_{ABS} and PI_{TOT} values of microalgae grown in B8_25 were 13.49, 32.70 and 63.16% lower (p-value < 0.05), respectively, than the values obtained in the control reactor. Microalgae cells subjected to 50 g $N \cdot m^{-3}$ of NO_2-N showed a 22.23, 51.97 and 85.40% reduction (p-value < 0.05) in F_V/F_M, PI_{ABS} and PI_{TOT}, respectively. The drop in F_V/F_M, PI_{ABS} and PI_{TOT} values in reactors operated with NO_2-N indicated that the RC of PS II were damaged, the light-dependent reactions were inhibited and the electron transport chain was hindered, as reported in other studies (Ji et al., 2018). PI_{ABS} and PI_{TOT} were more sensitive than F_V/F_M to NO_2-N stress. This is consistent with previously published results (Charalampous et al., 2019; Ji et al., 2018; Sun et al., 2020) in which PIs were considered the most sensitive transient parameter for indicating inhibition processes.

The specific energy fluxes ABS/RC, TR_0/RC and DI_0/RC showed that for both B8_25 and B8_50, NO_2-N had a negative effect on photosynthetic activity. As shown in Table VI. 3 increasing NO_2-N concentration raised the specific energy flux parameters. The ABS/RC parameter is the effective antenna size per active reaction center, while TR_0/RC is the trapped energy flux per active reaction center. When microalgae were grown with 25 and 50 g $N \cdot m^{-3}$ of NO_2-N, ABS/RC values were 19.20% and 54.47% higher than for the control reactor, respectively, and TR_0/RC values were 13.34% and 21.70% higher than B8_0, both indicating a significant inhibitory effect (p-value < 0.05). On the other hand, DI_0/RC is the dissipated energy flux per active reaction center. Comparing ABS/RC and TR_0/RC with DI_0/RC, the former showed an overall sluggish upward tendency, while

DI_0/RC rose sharply, especially in the highest NO_2-N concentrations, 31.81% and 123.75% in B8_25 and B8_50, respectively (p-value < 0.05). It is worth mentioning that the term RCs refers only to the Q_A-reducing RCs (Strasser et al., 2004), so that the fact that the specific energy fluxes increased with a higher NO_2-N concentration suggests that the Q_A-reducing RCs were negatively affected due to NO_2-N damage. The ABS/RC ratio thus increased by the deactivation of some active RCs, resulting in an intracellular accumulation of energy (Ji et al., 2018) and raised DI_0/RC. The trend of increasing TR_0/RC implied that all the Q_A was reduced but was not able to reoxidize due to NO_2-N damage, i.e., reoxidation of Q_A^- was inhibited and could not efficiently transfer electrons to Q_B (Mehta et al., 2010). The higher DI_0/RC was the microalgae cells' self-protective mechanism against the damage by the excess of intracellular energy, so that the absorbed energy was dissipated instead of being used to reduce Q_A (Ji et al., 2018). This conclusion is supported by the fact that NPQ values increase on exposure to NO_2-N (when photochemistry is partially inhibited, energy dissipation through NPQ is expected to increase) (Juneau et al., 2002).

Adding NO_2-N to a microalgae culture reduces the flux ratios of the photochemistry values, φ_{Po}, φ_{Eo} and ψ_{Eo} (Table VI. 3). φ_{Po} is the excitation energy capture probability of PS II, φ_{Eo} is the quantum yield for PQ pool reduction and ψ_{Eo} is defined as the probability electron transfer from Q_A in PS II to the PQ pool (Todorenko et al., 2021). φ_{Po} values in B8_25 and B8_50 were 5% and 21.24%, respectively, lower than the results achieved in B8_0 (p-value < 0.05). The decrease in φ_{Po} indicated an inhibited light reaction. The reduction efficiency of light photochemical reactions (φ_{Po}) led to higher energy dissipation (Chen et al., 2016), this being consistent with the trends described in NPQ and DI_0/RC. The flux ratio φ_{Eo} showed a reduction of 11.57% and 29.44% in B8_25 and B8_50, respectively, while ψ_{Eo} reduction was 6.92% and 10.40% compared to the control microalgae culture (p-value < 0.05). The downward trend of φ_{Eo} and ψ_{Eo} agreed with the changes in the F_V/F_M and PI_{ABS} parameters with a higher NO_2-N concentration. The

inhibition effect of NO_2-N can reduce light absorption, hinder electron transfer efficiency and reduce the maximum electron microalgae's transfer yield.

Unlike the three flux ratios described above, φ_{Do}, δ_{Ro} and φ_{Ro} are associated with non-photochemical processes (dos Santos Farias et al., 2019). φ_{Do} is the quantum yield of energy dissipation (Sun et al., 2020), δ_{Ro} is the electron transfer probability beyond the PQ pool and φ_{Ro} is the quantum yield of electron acceptor reduction in PS I (Chen et al., 2016). φ_{Do} was 13.10% and 48.24% in B8_25 and B8_50, respectively (p-value < 0.05) higher than in the control reactor. The higher heat dissipation energy indicated that the light energy utilization efficiency decrease (φ_{Po}). δ_{Ro} fell by 15.76% and 39.40%, while φ_{Ro} was reduced by 13.10% and 48.24% in B8_25 and B8_50, respectively, compared to R8_0 (p-value < 0.05). The studied NO_2-N concentrations reduced the probability of an electron being transported to the PS I final electron acceptor (δ_{Ro}) and reduced the quantum yield for the reduction of the final electron acceptors on the acceptor side of PS I (φ_{Ro}).

The parameters directly derived from the transient OJIP curve, V_J, M_o and S_M, represent the relative variable fluorescence at peak J (Sun et al., 2020), the initial slope of the OJIP transient normalized on the maximal F_V and the electron numbers that pass through the electron transport chain, respectively (Franić et al., 2018). V_J increased by 143.27% and 215.63%, while values of M_o were 176.07% and 284.62% higher in B8_25 and B8_50, respectively, compared to the control reactor (p-value < 0.05). The increase of V_J and M_o as NO_2-N exposure rose (p-value < 0.05) reflected the accumulation of Q_A^-, while M_o indicated that the net rate of the reaction center closure was mainly in the oxidized state (Matorin et al., 2013). On the other hand, the reduced S_M values with higher NO_2-N levels (p-value < 0.05) suggested that maximum fluorescence could be reached quicker, as fewer electrons were needed to reduce PS II electron acceptors, indicating NO_2-N's inhibitory effect (Franić et al., 2018).

Up to now, the effects of NO_2-N on ETR, NPQ, polyphasic OJIP rise kinetics and transient parameters have not been reported. However, it can be concluded that the parameters' behavior described is similar to the results reported by other authors for microalgae exposed to different toxic compounds, such as free ammonia (Markou et al., 2016), herbicides (Magnusson et al., 2008; Sun et al., 2020), or heavy metals (Perales-Vela et al., 2007).

Table VI. 3. Photosynthetic parameters related to the electron transport chain and the JIP-test affected by NO_2-N concentration in batch reactors operated at pH 8.

Photosynthetic parameters	**B8_0 (control)**	**B8_25**	**B8_50**
α (electrons/photon)	0.5241 ± 0.0004	0.4715 ± 0.0004	0.458 ± 0.006
E_K (µmol·m^{-2}·s^{-1})	219 ± 10	203.6 ± 0.2	164 ± 2
ETR_{MAX} (µmol·m^{-2}·s^{-1})	115 ± 5	96 ± 2	75 ± 3
NPQ	0.227 ± 0.04	0.45 ± 0.04	0.85 ± 0.08
V_J	0.046 ± 0.002	0.112 ± 0.002	0.145 ± 0.002
F_V/F_M	0.739 ± 0.009	0.639 ± 0.006	0.57 ± 0.03
M_o	0.078 ± 0.002	0.215 ± 0.005	0.300 ± 0.003
S_M	384 ± 13	329 ± 18	267 ± 23
ABS/RC	2.50 ± 0.13	2.98 ± 0.02	3.86 ± 0.07
TR_o/RC	1.70 ± 0.07	1.922 ± 0.007	2.06 ± 0.02
DI_o/RC	0.80 ± 0.06	1.06 ± 0.02	1.80 ± 0.05
φ_{Po}	0.679 ± 0.004	0.645 ± 0.002	0.535 ± 0.004
φ_{Eo}	0.648 ± 0.003	0.573 ± 0.003	0.457 ± 0.003
ψ_{Eo}	0.954 ± 0.002	0.888 ± 0.002	0.855 ± 0.002
φ_{Do}	0.314 ± 0.006	0.355 ± 0.004	0.465 ± 0.004
δ_{Ro}	0.69 ± 0.02	0.58 ± 0.05	0.415 ± 0.004
φ_{Ro}	0.4381 ± 0.0114	0.30 ± 0.03	0.189 ± 0.002
PI_{ABS}	11.99 ± 0.98	8.1 ± 0.4	5.8 ± 0.7
PI_{TOTAL}	9.37 ± 1.13	3.5 ± 0.3	1.4 ± 0.2

6.3.4. Overall NO_2-N effects on photosynthesis

Exposure to NO_2-N produced a partial inhibition of the primary photosynthetic process (F_V/F_M, φ_{Po}, PI_{ABS}) mainly due to hindrance of the electron transport chain (ETR curve). Under non-stress conditions, i.e. no NO_2-N accumulation (Figure VI. 4A), the excitation energy obtained from light is absorbed by the reaction center (RC) of PS II, (P_{680}). The excited P_{680} is oxidized by releasing an electron which is transported across the membrane to the first electron acceptor, Q_A, then the electron passes to the second

acceptor, Q_B, and finally reduces PQ to PQH_2. Electrons passing through the electron transport chain lose energy that is used to pump H+ ions by complex Cytochrome b6f. These concentrated ions store potential energy forming an electrochemical gradient. H^+ ions “slide” down their concentration gradient. As they flow, the ion channel/enzyme ATP synthase uses its energy to produce ATP. At the end of the chain, electrons bind H^+ ions to $NADP^+$ to produce NADPH (non-cyclic photophosphorylation). The excited electrons can take an alternative path called cyclic electron flow, which only is involved the PS I. Electrons flow from the electron acceptor ferredoxin to Cytochrome b6f, with ATP being the only product (cyclic photophosphorylation). However, under NO_2-N stress conditions (Figure VI. 4B), the electron transport chain between PS II and PS I is hindered and the probability of an electron being transported to PS I is reduced (I-P phase, PI_{TOT}, δ_{Ro}, φ_{Ro} and S_M). The reduced Q_A is not able to reoxidize and cannot efficiently transfer electrons to Q_B (phase O-J and TR_0/RC), accumulating P_{680}^+ (raw kinetic OJIP curves, V_J, M_o) and PQ (φ_{Eo} and ψ_{Eo}). Therefore, the P_{680}^+ cannot be re-reduced and the oxidative splitting of water into four protons and molecular oxygen is limited (OPR_{NET}). ATP and NADPH production are negatively affected, reducing sugar building in the second stage of photosynthesis.

The preceding energy of excited electrons are accumulated and damages RCs of PS II (ABS/RC). As a self-protective mechanism, the excess of intracellular energy is dissipated as heat (NPQ, DI_0/RC and φ_{Do}).

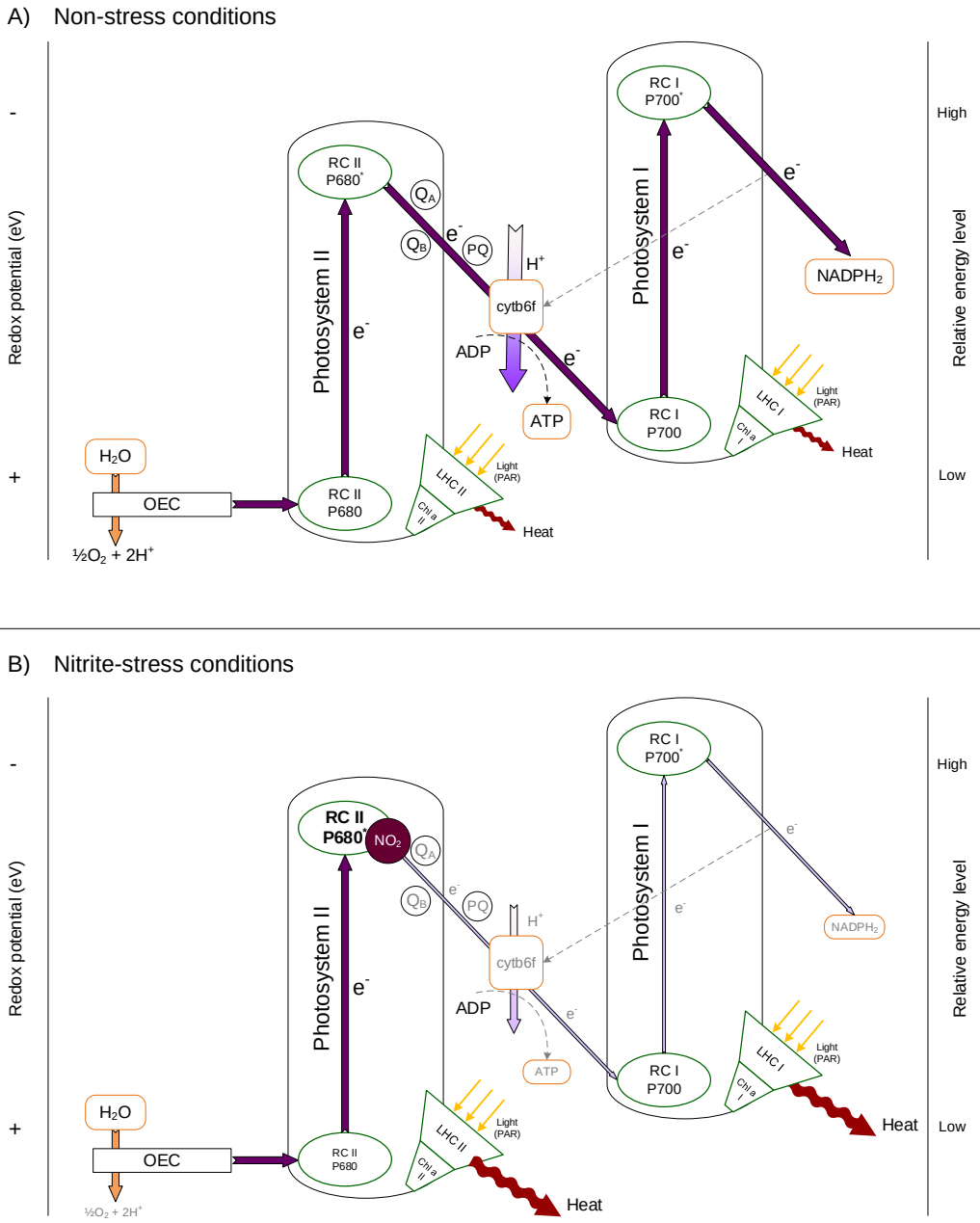

Figure VI. 4. Simplified and adapted Z-scheme of the photosynthetic electron transport chain under non-stress conditions (A) and NO_2-N-stress conditions. The scheme shows the redox reactions needed to transfer one electron from H_2O to NADPH and produce ATP. Abbreviations: OEC = oxygen-evolving complex; RC = reaction center; Q_A = PSII primary quinone acceptor; Q_B = PSII secondary quinone acceptor; cytb6f = complex cytochrome b6f; LHC II = light-harvesting complex of Photosystem II; LHC I = light-harvesting complex of Photosystem I; *Chl* a II = *Chlorophyll a* of Photosystem II; and *Chl a* I = *Chlorophyll a* of Photosystem I. The dotted straight arrow shows the pathway of non-cyclic and cyclic photophosphorylation.

6.3.5. Calibration of NO_2-N inhibition

The results described above show that the inhibition of microalgae activity is a consequence of NO_2-N concentration. A total of ten experiments were carried out at different NO_2-N concentrations to determine and calibrate the inhibitory effect on photosynthesis activity. The sets of calibration assays were carried out on different days. To properly compare and calibrate the effect of NO_2-N, inhibitory effects were thus obtained as the difference between photosynthesis activity in the control and NO_2-N stressed microalgae assays. Photosynthetic parameters were normalized and expressed as the percentage of the maximum value. Figure VI. 5 shows the photosynthetic activity parameters in terms of percentage versus total NO_2-N concentrations. The trend of OPR_{NET}, NPQ, ETR_{MAX} (the most sensitive ETR parameter) and PI_{ABS} are shown in Figure VI. 5A, B, C and D, respectively. From the OJIP transient parameters, only PI_{ABS} was used to calibrate NO_2-N damage since it was one of the most sensitive parameters for NO_2-N damage and in the literature it is commonly used to identify inhibition effects (Chen et al., 2016; Ji et al., 2018; Sun et al., 2020).

Experimental results were used to match the non-competitive inhibition model (Equation VI. 7) and the Hill-type model (Equation VI. 8). The latter can describe all the photosynthetic parameters with a high degree of accuracy (R^2 higher than 0.97, Table VI. 4), while the non-competitive model was not able to accurately describe NPQ and PI_{ABS} values (R^2 less than 0.80). The variability in the results differed according to the parameters measured, as shown by the bandwidth of the 95% confidence limits (Figure VI. 5A, B, C and D). ETR (Figure VI. 5C) and PI_{ABS} (Figure VI. 5D) values were more accurate than OPR_{NET} (Figure VI. 5A) and NPQ (Figure VI. 5B).

For all experiments, the photosynthetic parameters followed a similar decreasing trend when increasing total NO_2-N concentration. The NO_2-N inhibition constants were determined by minimizing the root mean square error between model prediction (Hill-type model) and experimental data. Values of $K_{I,NO2}$ (Figure VI. 5E) and n_{NO2} (Figure VI.

5F) and the 95% confidence limits of each parameter are listed in Table VI. 4. Values of $K_{I,NO2}$ ranged from 24.10 to 40.54 g NO_2-N m^{-3}, while n varied between 1.86 and 5.90. The least sensitive photosynthetic parameter was ETR_{MAX}, showing an inhibition constant of 40.54 g NO_2-N m^{-3}, while the remaining parameters are practically the same, ranging from 24.10 and 26.99 g NO_2-N m^{-3}. The OPR_{NET} trend could be matched with a non-competitive inhibition model with a good degree of accuracy, as the Hill constant value is near to 1 (1.86) and 0.95 of R^2. Regarding only OPR_{NET} values, there was little difference between the two models. To reduce computational cost, the non-competitive inhibition model is preferable because a similar prediction can be obtained with a single parameter. However, the Hill-type model was selected to reproduce NO_2-N inhibition since it matches the trend of the 4 photosynthetic parameters, while the non-competitive inhibition model only reproduces the OPR_{NET} results.

Up to now, inhibition parameters for microalgae related to NO_2-N toxicity effects have not been reported, so that direct comparison and analysis with previous works is not possible.

Table VI. 4. Selection criteria and Hill-type model calibrated parameters. Average data of each parameter are reported as mean value ± standard deviation; and 95% confidence intervals on calibrated parameters are reported in square brackets.

Parameter calibrated	R^2	K_I	n
OPR_{NET} (g O_2 m^{-3} d^{-1})	0.9486	23.7 ± 1.2 [21.89 25.54]	1.82 ± 0.14 [1.59 2.04]
NPQ	0.9742	26.36 ± 1.1 [24.62 28.10]	5.3 ± 0.5 [4.44 6.08]
ETR_{MAX} (µmol·m^{-2}·s^{-1})	0.9873	39 ± 2 [35.77 41.25]	2.4 ± 0.4 [1.79 2.94]
PI_{ABS}	0.9915	26.5 ± 0.4 [25.81 27.71]	4.2 ± 0.2 [3.91 4.45]

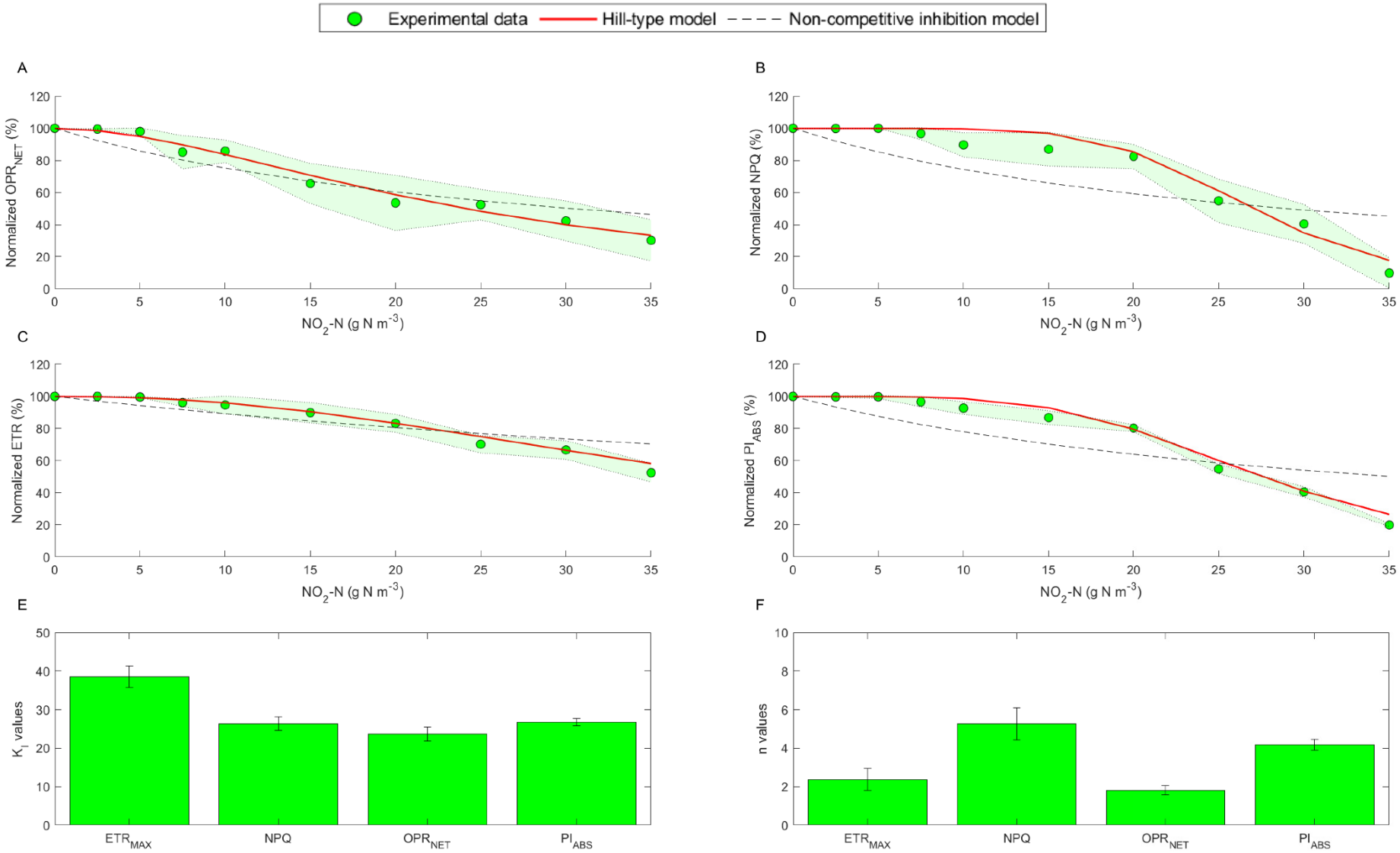

Figure VI. 5. Effect of NO_2-N on microalgae. Hill-type model and non-competitive inhibition model fit for normalized parameters: (A) OPR_{NET}, (B) NPQ, (C) ETR_{MAX} and (D) $PI_{ABS;}$ and estimated model parameters: (D) half inhibition constant (K_I) and (E) Hill constant. Shaded areas and error bars represent the 95% confidence intervals.

According to the calibrated microalgae model by Aparicio et al. (2022), the following kinetic expressions are proposed to represent the microalgae growth in the model developed in Chapter 10 (Equation VI. 9):

$$\mu_{ALG} \cdot \frac{S_{Ig,C}}{K_{Ig,C} + S_{Ig,C}} \cdot \frac{S_{NHX}}{K_{NHX} + S_{NHX}} \cdot \frac{S_{PO4}}{K_{PO4} + S_{PO4}} \cdot \frac{{K_{I,NO2}}^{n_{NO2}}}{{K_{I,NO2}}^{n_{NO2}} + {S_{NO2}}^{n_{NO2}}} \cdot X_{ALG} \cdot f_L \cdot f_{pH} \cdot f_T \quad \text{Equation VI. 9}$$

where μ_{ALG} is the maximum growth rate for microalgae (d^{-1}); $S_{Ig,C}$ is the total inorganic carbon (mol C·m^{-3}); $K_{Ig,C}$ is the half saturation parameter for inorganic carbon (mol C m^{-3}); S_{NHx} is the ammonium plus free ammonia nitrogen (g N·m^{-3}); K_{NHX} is the half saturation parameter for the ammonium plus free ammonia nitrogen (g N·m^{-3}); S_{PO4} is the total soluble inorganic phosphorus (g P·m^{-3}); K_{PO4} is the half saturation parameter for the total soluble inorganic phosphorus (g P·m^{-3}); S_{NO2} is nitrite nitrogen (g N·m^{-3}); $K_{I,NO2}$ is the inhibitor concentration that produce 50% inhibition (g N·m^{-3}); n_{NO2} is the Hill coefficient; X_{ALG} is the microalgae biomass (g COD·m^{-3}), f_L is the light factor; f_{pH} is the pH factor and f_T is the thermic factor.

As mathematical modeling of microalgae is usually based on oxygen production (Rossi et al., 2020a; Sánchez Zurano et al., 2021; Solimeno et al., 2017), it is recommended to use the $K_{I,NO2}$ value obtained in OPR_{NET} assays to introduce the NO_2-N inhibition process. González-Camejo et al. (2020) found that a short 30-min exposure to NO_2-N did not have significant effect on the photosynthetic activity of the indigenous microalgae *Chlorella*-like morphology. In this study, the calibration procedure consisted of a 20-min exposure to NO_2-N and significant results of the toxic effect on photosynthesis were achieved. Short-term exposure photosynthesis inhibition was evaluated only by the OPR_{NET} trend in the study conducted by González-Camejo et al. (2020), while in the present study inhibitory effects were analyzed through the combination of OPR_{NET} and fluorescence parameters which provided more specific results. A microalgae-bacteria culture was obtained from outdoor pilot-scale reactors in both studies. The ever-changing environmental and operating conditions promote community shift between different

biological communities, for example changes in the dominance of *Scenedesmus*-like morphology over the *Chlorella* genus. Comparing both studies, *Scenedesmus* could be more sensitive to the NO_2-N inhibitory effect than *Chlorella*, as reflected in a reduction in OPR_{NET} when exposing microalgal cells to different NO_2-N concentrations. The inhibitory effect of NO_2-N can be species-dependent.

Microalgal model, to which NO_2-N inhibition of microalgae growth has been added, was validated with different structures of microalgae communities (8% Chlorella and 92% Scenedesmus; 56% Chlorella and 44% Scenedesmus; 87% Chlorella and 13% Scenedesmus; and 96% Chlorella and 4% Scenedesmus) (Aparicio et al., 2022; Viruela et al., 2021). However, calibration procedure was performed with a community structure dominated by different *Scenedesmus*-like morphology genera. Comparing with results obtained by González-Camejo et al. (2020), it was deduced that different microalgae show different response and sensitivity to NO_2-N stress. To depict the actual condition in the biological system, NO_2-N should therefore be validated with operating periods that combine different community structures. Future work is aimed at developing a comprehensive microalgae-bacteria model, including NO_2-N inhibition and its validation with different microalgae culture technologies (membrane HRAP and membrane photobioreactor), different input wastewater streams and community structures.

6.3.6. NO_2-N scenarios in microalgae-based wastewater treatment

The use of estimated parameters for NO_2-N can be particularly useful to assess the extent of NO_2-N inhibition under common operating and environmental conditions of microalgae and bacterial cultivation. For example, nitrite was accumulated along the MHRAP operation at 6 days HRT (Chapter 5). For example, NO_2-N can accumulate from variations of light intensity, temperature and pH that promote AOB over NOB activity (partial nitrification). Although the nitrifying bacteria can be inhibited by high light intensity Akizuki et al. (2020) and Vergara et al. (2016) suggested NOB had a higher light sensitivity. Vergara et al. (2016) reported that NOB photoinhibition happened under a

continuous illumination of a 250 µmol m^{-2} s^{-1} light intensity, while NO_2-N continued to accumulate at intensities above 500 µmol m^{-2} s^{-1}. Nitrification is more strongly regulated by average daily light intensity than instantaneous incident light (Akizuki et al., 2020). The average daily light intensity recorded in the MHRAP pilot plant operated in this study ranged from 158 ± 60 to 301 ± 48 µmol m^{-2} s^{-1} in winter and summer respectively, and may promote NOB photoinhibition in summer. Temperature is also a key environmental parameter that can influence both NO_2-N and NO_3-N production rates. Partial nitrification and NO_2-N accumulation were generally promoted at temperatures between 20 – 35 ºC, at which, the specific AOB growth rate is higher than that of NOB (Gao et al., 2010; Kim et al., 2006). The culture temperature in MHRAP pilot plant was 17 ± 2 and 29.1 ± 0.8 ºC in winter and summer respectively, so that warm temperatures can influence nitrite concentration and inhibit photosynthesis.

pH values commonly increase during daylight hours due to photosynthesis. For example, the average pH value of HRAP was 7.5 ± 0.7 in winter, while in summer, it rose to 8.2 ± 0.3 when photosynthesis was higher. The optimum pH range for AOB and NOB ranges 8.2 – 8.4 and 7.7 – 7.9 respectively (Park et al., 2007). NOB are more sensitive to alkaline pH, which in microalgae cultures is usually recorded in summer.

The most favorable scenario for NO_2-N accumulation was in summer, with daily average light above 250 µmol m^{-2} s^{-1} and culture temperature and pH between 20 – 35 ºC and 8.2 – 8.4, respectively. During daylight, NO_2-N oxidation to NO_3-N was inhibited by increased light intensity, temperature and pH above NOB optimal range, resulting in an NO_2-N accumulation and inhibition of microalgal photosynthesis.

Nitrite concentration has been reported in the range of 15 to 50 g N m^{-3} in different microalgae-bacteria systems (Akizuki et al., 2019; González-Camejo et al., 2020b, 2017; Van Den Hende et al., 2016)

Different strategies can be used to limit and reduce the nitrite production rate in outdoor systems with ever-changing culture conditions. The simplest option is the complete

inhibition of AOB activity using ATU, but this requires the continuous addition of chemical substances that involves environmental impact and cost, so that alternative operating strategies based on operational and environmental conditions are recommended. González-Camejo et al. (2020) and González-Camejo et al. (2019) propose temperature ranges and biomass retention times that promote: (I) microalgae growth over AOB and NOB growth; and (II) complete nitrification.

6.4. CONCLUSIONS

The effects of nitrite and free nitrous acid on microalgae photosynthesis were studied in batch reactors operated at pH 4.5 and 8. Nitrite, rather than the free nitrous acid, has an overall negative and rapid effect on photosynthesis, affecting simultaneously different sites of the photosynthetic apparatus. The present work suggests that the nitrite inhibition mechanism was based on reducing light absorption and hindering the electron transport chain. The Q_A was not able to transfer electrons to Q_B, so that the primary photosynthetic process was limited and the maximum electron transfer yield was also reduced. The photosynthetic apparatus of microalgae responded to nitrite stress by increasing self-protective mechanism to avoid damage by the excess of intracellular energy. The proposed Hill function was able to accurately reproduce the inhibitory effect of nitrite on four photosynthetic parameters, OPR_{NET}, NPQ, ETR_{MAX}, and PI_{ABS}. The $K_{I,NO2}$ resulted in 24.10, 26.99, 40.54, and 27.55 g N m^{-3} and the Hill parameter, n, was 1.82, 5.3, 2.4 and 4.2 for the above four parameters, respectively. Comparing the results obtained in this work with other scientific investigations, it is suggested that the inhibitory effect of nitrite could be species-dependent.

REFERENCES

Admiraal, W., 1977. Tolerance of estuarine benthic diatoms to high concentrations of ammonia, nitrite ion, nitrate ion and orthophosphate. Mar. Biol. 43, 307–315. https://doi.org/10.1007/BF00396925

Akizuki, S, Cuevas-Rodríguez, G., Toda, T., 2019. Microalgal-nitrifying bacterial consortium for energy-saving ammonia removal from anaerobic digestate of slaughterhouse wastewater. J. Water Process Eng. 31. https://doi.org/10.1016/j.jwpe.2019.01.014

Akizuki, S., Kishi, M., Cuevas-Rodríguez, G., Toda, T., 2020. Effects of different light conditions on ammonium removal in a consortium of microalgae and partial nitrifying granules. Water Res. 171, 115445. https://doi.org/https://doi.org/10.1016/j.watres.2019.115445

Aparicio, S., García, R.S., Seco, A., Ferrer, J., Falomir, L.B., Robles, Á., 2022. Global sensitivity and uncertainty analysis of a microalgae model for wastewater treatment. Sci. Total Environ. 806, 150504. https://doi.org/10.1016/J.SCITOTENV.2021.150504

APHA-AWWA-WPCF, 2012. Standard Methods for the Examination of Water and Wastewater, 22nd edition, American P. ed. Washington DC, USA.

Bankston, E., Wang, Q., Higgins, B.T., 2020. Algae support populations of heterotrophic, nitrifying, and phosphate-accumulating bacteria in the treatment of poultry litter anaerobic digestate. Chem. Eng. J. 125550. https://doi.org/10.1016/j.cej.2020.125550

Barceló-Villalobos, M., Serrano, C.G., Zurano, A.S., García, L.A., Maldonado, S.E., Peña, J., Fernández, F.G.A., 2019. Variations of culture parameters in a pilot-scale thin-layer reactor and their influence on the performance of Scenedesmus almeriensis culture. Bioresour. Technol. Reports 6, 190–197. https://doi.org/10.1016/J.BITEB.2019.03.007

Blackburne, R., Vadivelu, V.M., Yuan, Z., Keller, J., 2007. Kinetic characterisation of an enriched Nitrospira culture with comparison to Nitrobacter. Water Res. 41, 3033–3042. https://doi.org/10.1016/j.watres.2007.01.043

Charalampous, N., Grammatikopoulos, G., Kourmentza, C., Kornaros, M., Dailianis, S., 2019. Effects of Burkholderia thailandensis rhamnolipids on the unicellular algae Dunaliella tertiolecta. Ecotoxicol. Environ. Saf. 182, 109413. https://doi.org/10.1016/J.ECOENV.2019.109413

Che, X., Ding, R., Li, Y., Zhang, Z., Gao, H., Wang, W., 2018. Mechanism of long-term toxicity of CuO NPs to microalgae. Nanotoxicology 12, 923–939. https://doi.org/10.1080/17435390.2018.1498928

Chen, S., Yang, J., Zhang, M., Strasser, R.J., Qiang, S., 2016. Classification and characteristics of heat tolerance in Ageratina adenophora populations using fast chlorophyll a fluorescence rise O-J-I-P. Environ. Exp. Bot. 122, 126–140. https://doi.org/10.1016/j.envexpbot.2015.09.011

Claros, J, Jiménez, E., Aguado, D., Ferrer, J., Seco, A., Serralta, J., 2013. Effect of pH and HNO2 concentration on the activity of ammonia-oxidizing bacteria in a partial nitritation reactor. Water Sci. Technol. 67, 2587–2594. https://doi.org/10.2166/wst.2013.132

Da Silva, G., Kennedy, E.M., Dlugogorski, B.Z., 2006. Ab initio procedure for aqueous-phase pKa calculation: The acidity of nitrous acid. J. Phys. Chem. A 110, 11371–11376. https://doi.org/10.1021/jp0639243

dos Santos Farias, D.B., da Silva, P.S.O., Tadeu Lucas, A.A., de Freitas, M.I., de Jesus Santos, T., Nascimento Fontes, P.T., de Oliveira Júnior, L.F.G., 2019. Physiological and productive parameters of the okra under irrigation levels. Sci. Hortic. (Amsterdam). 252, 1–6. https://doi.org/10.1016/j.scienta.2019.02.066

Fito, J., Alemu, K., 2018. Microalgae–bacteria consortium treatment technology for municipal wastewater management. Nanotechnol. Environ. Eng. 2018 41 4, 1–9. https://doi.org/10.1007/S41204-018-0050-2

Franić, M., Galić, V., Mazur, M., Šimić, D., 2018. Effects of excess cadmium in soil on JIP-test parameters, hydrogen peroxide content and antioxidant activity in two maize inbreds and their hybrid. Photosynthetica 56, 660–669. https://doi.org/10.1007/s11099-017-0710-7

Galès, A., Bonnafous, A., Carré, C., Jauzein, V., Lanouguère, E., Le, E., Pinoit, J., Poullain, C., Roques, C., Sialve, B., Simier, M., Steyer, J., Fouilland, E., 2019. Importance of ecological interactions during wastewater treatment using High Rate Algal Ponds under di ff erent temperate climates. Algal Res. 40, 101508. https://doi.org/10.1016/j.algal.2019.101508

Gao, D., Peng, Y., Wu, W.-M., 2010. Kinetic Model for Biological Nitrogen Removal Using Shortcut Nitrification-Denitrification Process in Sequencing Batch Reactor. Environ. Sci. Technol. 44, 5015–5021. https://doi.org/10.1021/ES100514X

Gomes, M.T.G., da Luz, A.C., dos Santos, M.R., do Carmo Pimentel Batitucci, M., Silva, D.M., Falqueto, A.R., 2012. Drought tolerance of passion fruit plants assessed by the OJIP chlorophyll a fluorescence transient. Sci. Hortic. (Amsterdam). 142, 49–56. https://doi.org/10.1016/j.scienta.2012.04.026

González-Camejo, J., Aparicio, S., Jiménez-Benítez, A., Pachés, M., Ruano, M. V, Borrás, L., Barat, R., Seco, A., 2020a. Improving membrane photobioreactor performance by reducing light path: operating conditions and key performance indicators. Water Res. 172. https://doi.org/10.1016/j.watres.2020.115518

González-Camejo, J., Aparicio, S., Ruano, M. V., Borrás, L., Barat, R., Ferrer, J., 2019. Effect of ambient temperature variations on an indigenous microalgae-nitrifying bacteria culture dominated by Chlorella. Bioresour. Technol. 290, 121788. https://doi.org/10.1016/j.biortech.2019.121788

González-Camejo, J., Barat, R., Pachés, M., Murgui, M., Seco, A., Ferrer, J., 2017. Environmental Technology Wastewater nutrient removal in a mixed microalgae-bacteria culture: effect of light and temperature on the microalgae-bacteria competition. Taylor Fr. 39, 503–515. https://doi.org/10.1080/09593330.2017.1305001

González-Camejo, J., Montero, P., Aparicio, S., Ruano, M. V., Borrás, L., Seco, A., Barat, R., 2020b. Nitrite inhibition of microalgae induced by the competition between microalgae and nitrifying bacteria. Water Res. 172, 115499. https://doi.org/10.1016/j.watres.2020.115499

Hernández-Zamora, M., Perales-Vela, H.V., Flores-Ortíz, C.M., Cañizares-Villanueva, R.O., 2014. Physiological and biochemical responses of Chlorella vulgaris to Congo red. Ecotoxicol. Environ. Saf. 108, 72–77. https://doi.org/10.1016/j.ecoenv.2014.05.030

Ji, X., Cheng, J., Gong, D., Zhao, X., Qi, Y., Su, Y., Ma, W., 2018. The effect of NaCl stress on photosynthetic efficiency and lipid production in freshwater microalga—Scenedesmus obliquus XJ002. Sci. Total Environ. 633, 593–599. https://doi.org/10.1016/J.SCITOTENV.2018.03.240

Jiang, H.X., Chen, L.S., Zheng, J.G., Han, S., Tang, N., Smith, B.R., 2008. Aluminum-induced effects on Photosystem II photochemistry in Citrus leaves assessed by the chlorophyll a fluorescence transient. Tree Physiol. 28, 1863–1871. https://doi.org/10.1093/treephys/28.12.1863

Juneau, P., Berdey, A. El, Popovic, R., 2002. PAM Fluorometry in the Determination of the Sensitivity of Chlorella vulgaris, Selenastrum capricornutum, and Chlamydomonas reinhardtii to Copper Environmental Contamination a n d Toxicology. Arch. Environ. Contam. Toxicol 42, 155–164. https://doi.org/10.1007/s00244-001-0027-0

Kim, D.J., Lee, D.I., Keller, J., 2006. Effect of temperature and free ammonia on nitrification and nitrite accumulation in landfill leachate and analysis of its nitrifying bacterial community by FISH. Bioresour. Technol. 97, 459–468. https://doi.org/10.1016/J.BIORTECH.2005.03.032

Li, S., Wang, P., Zhang, C., Zhou, X., Yin, Z., Hu, T., Hu, D., Liu, C., Zhu, L., 2020. Influence of polystyrene microplastics on the growth, photosynthetic efficiency and aggregation of freshwater microalgae Chlamydomonas reinhardtii. Sci. Total Environ. 714, 136767. https://doi.org/10.1016/j.scitotenv.2020.136767

Li, X., Li, W., Zhai, J., Wei, H., Wang, Q., 2019. Effect of ammonium nitrogen on microalgal growth, biochemical composition and photosynthetic performance in mixotrophic cultivation. Bioresour. Technol. 273, 368–376. https://doi.org/10.1016/j.biortech.2018.11.042

Liu, J., Wu, Y., Wu, C., Muylaert, K., Vyverman, W., Yu, H.Q., Muñoz, R., Rittmann, B., 2017. Advanced nutrient removal from surface water by a consortium of attached microalgae and bacteria: A review. Bioresour. Technol. https://doi.org/10.1016/j.biortech.2017.06.054

Luo, Y., Le-Clech, P., Henderson, R.K., 2018. Assessment of membrane photobioreactor (MPBR) performance parameters and operating conditions. Water Res. 138, 169–180. https://doi.org/10.1016/j.watres.2018.03.050

Magnusson, M., Heimann, K., Negri, A.P., 2008. Comparative effects of herbicides on photosynthesis and growth of tropical estuarine microalgae. Mar. Pollut. Bull. 56, 1545–1552. https://doi.org/10.1016/j.marpolbul.2008.05.023

Mantovani, M., Marazzi, F., Fornaroli, R., Bellucci, M., Ficara, E., Mezzanotte, V., 2020. Outdoor pilot-scale raceway as a microalgae-bacteria sidestream treatment in a WWTP. Sci. Total Environ. 710, 135583. https://doi.org/10.1016/J.SCITOTENV.2019.135583

Markou, G., Depraetere, O., Muylaert, K., 2016. Effect of ammonia on the photosynthetic activity of Arthrospira and Chlorella: A study on chlorophyll fluorescence and electron transport. Algal Res. 16, 449–457. https://doi.org/10.1016/j.algal.2016.03.039

Matorin, D.N., Todorenko, D.A., Seifullina, N.K., Zayadan, B.K., Rubin, A.B., 2013. Effect of silver nanoparticles on the parameters of chlorophyll fluorescence and P700 reaction in the green alga Chlamydomonas reinhardtii. Microbiol. (Russian Fed. 82, 809–814. https://doi.org/10.1134/S002626171401010X

Mehta, P., Allakhverdiev, S.I., Jajoo, A., 2010. Characterization of photosystem II heterogeneity in response to high salt stress in wheat leaves (Triticum aestivum). Photosynth. Res. 105, 249–255. https://doi.org/10.1007/s11120-010-9588-y

Mujtaba, G., Lee, K., 2017. Treatment of real wastewater using co-culture of immobilized Chlorella vulgaris and suspended activated sludge. Water Res. 120, 174–184. https://doi.org/10.1016/j.watres.2017.04.078

Park, S., Bae, W., Chung, J., Baek, S.C., 2007. Empirical model of the pH dependence of the maximum specific nitrification rate. Process Biochem. 42, 1671–1676. https://doi.org/10.1016/j.procbio.2007.09.010

Perales-Vela, H.V., González-Moreno, S., Montes-Horcasitas, C., Cañizares-Villanueva, R.O., 2007. Growth, photosynthetic and respiratory responses to sub-lethal copper concentrations in Scenedesmus incrassatulus (Chlorophyceae). Chemosphere 67, 2274–2281. https://doi.org/10.1016/J.CHEMOSPHERE.2006.11.036

Pijuan, M., Ye, L., Yuan, Z., 2010. Free nitrous acid inhibition on the aerobic metabolism of poly-phosphate accumulating organisms. Water Res. 44, 6063–6072. https://doi.org/10.1016/j.watres.2010.07.075

Prinz, H., 2010. Hill coefficients, dose–response curves and allosteric mechanisms. J. Chem. Biol. 3, 37. https://doi.org/10.1007/S12154-009-0029-3

Proctor, M.C.F., Bates, J.W., 2018. Chlorophyll-fluorescence measurements in bryophytes: evidence for three main types of light-curve response. J. Bryol. 40, 1–11. https://doi.org/10.1080/03736687.2017.1407280

PSI (Photon Systems Instruments), 2017. AquaPen-P AP-P 100 manual [WWW Document]. URL http://www.ictinternational.com/content/uploads/2016/09/AquaPen_Manual.pdf (accessed 7.1.21).

Rada-Ariza, A.M., Lopez-Vazquez, C.M., van der Steen, N.P., Lens, P.N.L., 2017. Nitrification by microalgal-bacterial consortia for ammonium removal in flat panel sequencing batch photo-bioreactors. Bioresour. Technol. 245, 81–89. https://doi.org/10.1016/j.biortech.2017.08.019

Risgaard-Petersen, N., Nicolaisen, M.H., Revsbech, N.P., Lomstein, B.A., 2004. Competition between Ammonia-Oxidizing Bacteria and Benthic Microalgae. Appl. Environ. Microbiol. 70, 5528 LP – 5537. https://doi.org/10.1128/AEM.70.9.5528-5537.2004

Roach, T., Krieger-Liszkay, A., 2014. Regulation of Photosynthetic Electron Transport and Photoinhibition. Curr. Protein Pept. Sci. 15, 351–362. https://doi.org/10.2174/1389203715666140327105143

Robles, Á., Capson-Tojo, G., Galès, A., Ruano, M.V., Sialve, B., Ferrer, J., Steyer, J.P., 2020. Microalgae-bacteria consortia in high-rate ponds for treating urban wastewater: Elucidating the key state indicators under dynamic conditions. J. Environ. Manage. 261. https://doi.org/10.1016/j.jenvman.2020.110244

Rossi, S., Bellucci, M., Marazzi, F., Mezzanotte, V., Ficara, E., 2018. Activity assessment of microalgal-bacterial consortia based on respirometric tests. Water Sci. Technol. 78, 207–215. https://doi.org/10.2166/wst.2018.078

Rossi, S., Casagli, F., Mantovani, M., Mezzanotte, V., Ficara, E., 2020. Selection of photosynthesis and respiration models to assess the effect of environmental conditions on mixed microalgae consortia grown on wastewater. Bioresour. Technol. 305, 122995. https://doi.org/10.1016/J.BIORTECH.2020.122995

Rossi, Simone, Díez-Montero, R., Rueda, E., Castillo Cascino, F., Parati, K., García, J., Ficara, E., 2020. Free ammonia inhibition in microalgae and cyanobacteria grown in wastewaters: Photo-respirometric evaluation and modelling. Bioresour. Technol. 305, 123046. https://doi.org/10.1016/j.biortech.2020.123046

Sánchez-Zurano, A., Gómez-Serrano, C., Acién-Fernández, F.G., Fernández-Sevilla, J.M., Molina-Grima, E., 2020. A novel photo-respirometry method to characterize consortia in microalgae-related wastewater treatment processes. Algal Res. 47, 101858. https://doi.org/10.1016/j.algal.2020.101858

Sánchez-zurano, A., Rodríguez-miranda, E., Guzmán, J.L., Acién-fernández, F.G., Fernández-sevilla, J.M., Grima, E.M., 2021. Abaco: A new model of microalgae-bacteria consortia for biological treatment of wastewaters. Appl. Sci. 11, 1–24. https://doi.org/10.3390/app11030998

Sánchez Zurano, A., Gómez Serrano, C., Acién-Fernández, F.G., Fernández-Sevilla, J.M., Molina-Grima, E., 2021. Modeling of photosynthesis and respiration rate for microalgae–bacteria consortia. Biotechnol. Bioeng. 118, 952–962. https://doi.org/10.1002/bit.27625

Sander, R., 2015. Compilation of Henry's law constants (version 4.0) for water as solvent. Atmos. Chem. Phys. 15, 4399–4981. https://doi.org/10.5194/ACP-15-4399-2015

Schreiber, U., Neubauer, C., 1987. The polyphasic rise of chlorophyll fluorescence upon onset of strong continuous illumination: II. partial control by the photosystem II donor side and possible ways of interpretation. Zeitschrift fur Naturforsch. - Sect. C J. Biosci. 42, 1255–1264. https://doi.org/10.1515/znc-1987-11-1218

Schulze, E.D., Caldwell, M.M., 2012. Ecophysiology of photosynthesis, Terrestrial Photosynthesis in a Changing Environment a Molecular, Physiological and Ecological Approach. https://doi.org/10.1007/978-3-642-79354-7

Serôdio, J., Ezequiel, J., Frommlet, J., Laviale, M., Lavaud, J., 2013. A method for the rapid generation of nonsequential light-response curves of chlorophyll fluorescence. Plant Physiol. 163, 1089–1102. https://doi.org/10.1104/pp.113.225243

Solimeno, A., Parker, L., Lundquist, T., García, J., 2017. Integral microalgae-bacteria model (BIO_ALGAE): Application to wastewater high rate algal ponds. Sci. Total Environ. 601–602, 646–657. https://doi.org/10.1016/j.scitotenv.2017.05.215

Stirbet, A., Govindjee, 2011. On the relation between the Kautsky effect (chlorophyll a fluorescence induction) and Photosystem II: Basics and applications of the OJIP fluorescence transient. J. Photochem. Photobiol. B Biol. 104, 236–257. https://doi.org/10.1016/J.JPHOTOBIOL.2010.12.010

Strasser, R.J., Tsimilli-Michael, M., Qiang, S., Goltsev, V., 2010. Simultaneous in vivo recording of prompt and delayed fluorescence and 820-nm reflection changes during drying and after rehydration of the resurrection plant Haberlea rhodopensis. Biochim. Biophys. Acta - Bioenerg. 1797, 1313–1326. https://doi.org/10.1016/J.BBABIO.2010.03.008

Strasser, R.J., Tsimilli-Michael, M., Srivastava, A., 2004. Analysis of the Chlorophyll a Fluorescence Transient 321–362. https://doi.org/10.1007/978-1-4020-3218-9_12

Sun, C., Xu, Y., Hu, N., Ma, J., Sun, S., Cao, W., Klobučar, G., Hu, C., Zhao, Y., 2020. To evaluate the toxicity of atrazine on the freshwater microalgae Chlorella sp. using sensitive indices indicated by photosynthetic parameters. Chemosphere 244, 125514. https://doi.org/10.1016/J.CHEMOSPHERE.2019.125514

Test No. 201: Alga, Growth Inhibition Test, 2006. , OECD Guidelines for the Testing of Chemicals, Section 2: Effects on Biotic Systems. OECD Publishing. https://doi.org/10.1787/9789264069923-en

Todorenko, D., Volgusheva, A., Timofeev, N., Kovalenko, I., Matorin, D., Antal, T., 2021. Multiple in vivo Effects of Cadmium on Photosynthetic Electron Transport in Pea Plants. Photochem. Photobiol. https://doi.org/10.1111/PHP.13469

Van Den Hende, S., Beelen, V., Julien, L., Lefoulon, A., Vanhoucke, T., Coolsaet, C., Sonnenholzner, S., Vervaeren, H., Rousseau, D.P.L., 2016. Technical potential of microalgal bacterial floc raceway ponds treating food-industry effluents while producing microalgal bacterial biomass: An outdoor pilot-scale study. Bioresour. Technol. 218, 969–979. https://doi.org/10.1016/J.BIORTECH.2016.07.065

Vergara, C., Muñoz, R., Campos, J.L., Seeger, M., Jeison, D., 2016. Influence of light intensity on bacterial nitrifying activity in algal-bacterial photobioreactors and its implications for microalgae-based wastewater treatment. Int. Biodeterior. Biodegradation 114, 116–121. https://doi.org/10.1016/J.IBIOD.2016.06.006

Viruela, A., Aparicio, S., Robles, Á., Falomir, L.B., Serralta, J., Seco, A., Ferrer, J., 2021. Kinetic modeling of autotrophic microalgae mainline processes for sewage treatment in phosphorus-replete and -deplete culture conditions. Sci. Total Environ. 149165. https://doi.org/10.1016/J.SCITOTENV.2021.149165

Wang, J.H., Zhang, T.Y., Dao, G.H., Xu, X.Q., Wang, X.X., Hu, H.-Y., 2017. Microalgae-based advanced municipal wastewater treatment for reuse in water bodies. Appl. Microbiol. Biotechnol. https://doi.org/10.1007/s00253-017-8184-x

Yamori, W., Sakata, N., Suzuki, Y., Shikanai, T., Makino, A., 2011. Cyclic electron flow around photosystem I via chloroplast NAD(P)H dehydrogenase (NDH) complex performs a significant physiological role during photosynthesis and plant growth at low temperature in rice. Plant J. 68, 966–976. https://doi.org/10.1111/J.1365-313X.2011.04747.X

Yang, W., Vollertsen, J., Hvitved-Jacobsen, T., 2003. Nitrite accumulation in the treatment of wastewaters with high ammonia concentration, in: Water Science and Technology. IWA Publishing, pp. 135–141. https://doi.org/10.2166/wst.2003.0182

Zhang, T., Gong, H., Wen, X., Lu, C., 2010. Salt stress induces a decrease in excitation energy transfer from phycobilisomes to photosystem II but an increase to photosystem I in the cyanobacterium Spirulina platensis. J. Plant Physiol. 167, 951–958. https://doi.org/10.1016/j.jplph.2009.12.020

Zhao, B., Wang, J., Gong, H., Wen, X., Ren, H., Lu, C., 2008. Effects of heat stress on PSII photochemistry in a cyanobacterium Spirulina platensis. Plant Sci. 175, 556–564. https://doi.org/10.1016/j.plantsci.2008.06.003

Zhao, J., Yang, L., Zhou, L., Bai, Y., Wang, B., Hou, P., Xu, Q., Yang, W., Zuo, Z., 2016. Inhibitory effects of eucalyptol and limonene on the photosynthetic abilities in Chlorella vulgaris (Chlorophyceae). Phycologia 55, 696–702. https://doi.org/10.2216/16-38.1

Zhao, Junkai, Zhao, Jianqiang, Xie, S., Lei, S., 2021. The role of hydroxylamine in promoting conversion from complete nitrification to partial nitrification: NO toxicity inhibition and its characteristics. Bioresour. Technol. 319, 124230. https://doi.org/10.1016/J.BIORTECH.2020.124230

CHAPTER VII

7. Comprehensive assessment of the microalgae-nitrifying bacteria competition in microalgae-based wastewater treatment systems: relevant factors, evaluation methods and control strategies

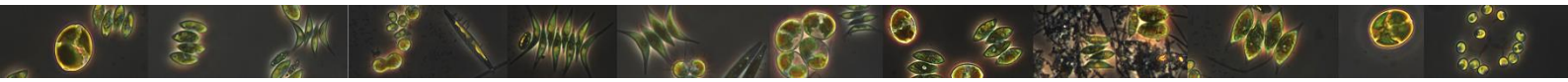

7. Comprehensive assessment of the microalgae-nitrifying bacteria competition in microalgae-based wastewater treatment systems: relevant factors, evaluation methods and control strategies

ABSTRACT

Due to their capacity to assimilate carbon dioxide and nutrients, microalgae-based cultivation systems have emerged as a green solution for intensive wastewater treatment. However, when large concentrations of ammonium are present the competition between microalgae and ammonium-oxidising bacteria (AOB) plays a significant role. Microalgae use ammonium to synthesise proteins, photosynthetic pigments and nucleic acids, while AOB use it as a source of electrons and oxidise it to nitrite.

Several authors have studied the isolated factors that influence microalgae-nitrifying bacteria competition, although a comprehensive analysis of this interesting topic is still lacking. This review makes an overall assessment of the competition between microalgae and AOB for ammonium uptake, focusing on: I) factors that influence the competition; II) methods of measuring the activity and concentrations of microalgae and nitrifying bacteria; III) useful strategies to control nitrification to improve the performance of microalgae-based wastewater treatment systems.

Keywords

Ammonium; Competition; Microalgae; Nitrification; Wastewater

Authors

Josué González Camejo, Stéphanie Aparicio, María Pachés, Luis Borrás Falomir and Aurora Seco.

González-Camejo, J., Aparicio, S., Pachés, M., Borrás, L., Seco, A., 2021. Comprehensive assessment of the microalgae-nitrifying bacteria competition in microalgae-based wastewater treatment systems: Relevant factors, evaluation methods and control strategies. Algal Res. https://doi.org/10.1016/j.algal.2021.102563

7.1. INTRODUCTION

Microalgae cultivation is attracting increasing interest as intensive green tertiary wastewater treatment from the scientific community all over the world (Acién et al., 2016; Cuevas-Castillo et al., 2020; Fallahi et al., 2021; González-Camejo et al., 2021; Goswami et al., 2021; Hussain et al., 2021; K. Li et al., 2019; Mohsenpour et al., 2021; Rajesh Banu et al., 2020; Soares et al., 2019). Phototrophic microalgae can remove large amounts of nutrients from the medium while fixing carbon dioxide to produce microalgae biomass, which can then be used to obtain by-products such as biofuels and fertilisers (Rossi et al., 2020a; Rossi et al., 2020; Shahid et al., 2020; Su, 2021). Recent studies have focused on the design of different microalgae cultivation technologies, the different wastewater streams to be treated by microalgae and the parameters affecting microalgae performance (Assunção and Malcata, 2020; González-Camejo et al., 2021; Gupta et al., 2019; X. Li et al., 2019; Mohsenpour et al., 2021; Nagarajan et al., 2020; Vo et al., 2019; Wollmann et al., 2019). However, when microalgae are cultivated outdoors, non-aseptic conditions trigger the proliferation of other microorganisms such as heterotrophic bacteria, protozoa, intrusive microalgae, fungi, etc., competing with microalgae for nutrient assimilation (Acién et al., 2016; Day et al., 2017; Di Caprio, 2020; Fallahi et al., 2021; Galès et al., 2019b; Lam et al., 2018; Lee and Lei, 2019). With wastewater from anaerobic processes such as digestates, centrates and effluents from anaerobic membrane bioreactor (AnMBR) systems or aerobic secondary effluents, heterotrophic bacteria activity is usually neglected as their organic matter content is mostly recalcitrant to biodegradation (Rossi et al., 2020a). As ammonium (NH_4) is usually present in these wastewater streams (Mantovani et al., 2020; Seco et al., 2018), the competition between microalgae and autotrophic nitrifying bacteria (specifically ammonium oxidising bacteria (AOB)) for ammonium uptake plays a significant role (Akizuki et al., 2020b; Bankston et al., 2020; Bellucci et al., 2020).

There are several ways of dealing with microalgae-nitrifying bacteria cultivation systems to treat high ammonium-loaded wastewater streams, depending on the final goal of the process:

- Maximizing microalgae activity to improve nitrogen and phosphorus removal, thus reducing the nutrient concentration of the effluent common in wastewaters with middle or low ammonium concentrations, i.e. 20-80 mg $N \cdot L^{-1}$ (González-Camejo et al., 2020a).
- Maximizing microalgae activity to increase by-products produced by microalgae biomass (Romero-Villegas et al., 2018).
- Favoring nitrification by the oxygen production of microalgae to reduce the ammonium load, which in turn reduces system aeration requirements (Mantovani et al., 2020; Rada-Ariza et al., 2017; Sepehri et al., 2020).

One or other will be more active, according to the goal of the mixed microalgae-nitrifying bacteria system.

Although many studies analyse the factors which affect microalgae (Li et al., 2019; Mohsenpour et al., 2021; Umamaheswari and Shanthakumar, 2016; Xu et al., 2019), their influence (such as temperature, light, nutrient concentration, dilution rate, etc.) on the competition between microalgae and AOB for ammonium uptake is often overlooked, given little attention, or is evaluated by only considering one of the isolated factors. For instance, Choi et al. (2010) reported that microalgae growth was favoured over AOB under appropriate lighting and nutrient-replete conditions, while González-Camejo et al. (González-Camejo et al., 2019a) suggested that high temperature peaks can make AOB growth surpass microalgae activity. Other authors have studied the metabolic routes of microalgae (Nwoba et al., 2019; Xu et al., 2019) and nitrifying bacteria (Lu et al., 2020) separately. However, a comprehensive analysis of this competition is still lacking.

It should be noted that nitrification can be the main ammonium removal pathway in microalgae cultivation systems, even if there is much less AOB biomass than microalgae. Methods of measuring the activity and the abundance of both microalgae and nitrifying bacteria are thus essential to monitor culture dynamics during continuous operation.

This review makes an overall assessment of the competition between microalgae and AOB for ammonium uptake in suspended cultures, focusing on: I) factors that influence microalgae-AOB competition; II) methods of measuring the concentration and activity of both microalgae and nitrifying bacteria within the mixed culture; III) nitrification control strategies. This is expected to be useful to wastewater treatment systems based on microalgae-AOB cultures as it could help to improve the process performance by maximising/minimising microalgae activity and/or nitrification.

7.2. MICROALGAE-AOB COMPETITION FOR AMMONIUM UPTAKE

Microalgae used ammonium for the synthesis of proteins, photosynthetic pigments and nucleic acids (Baroni et al., 2019; Shahid et al., 2020). Nitrifying bacteria use NH_4 as a source of electrons in the nitrification process, producing nitrite (NO_2) and nitrate (NO_3) (Figure VII. 1). In high NH_4-loaded wastewater treatment systems based on microalgae cultivation, an equilibrium often exists between microalgae and AOB (González-Camejo et al., 2019a; Rada-Ariza et al., 2019). However, if ammonium is not present in excess, microalgae and AOB reduce the NH_4 concentration of the culture, limiting their activities (González-Camejo et al., 2018).

As can be seen in Table VII. 1, cultures with higher nitrification usually reach lower microalgae performance in terms of nitrogen removal rate or nitrogen removal efficiency. For instance, González-Camejo et al. (González-Camejo et al., 2020c), who treated AnMBR effluent in an outdoor membrane photobioreactor (MPBR) system, obtained a nitrogen removal rate (NRR) and nitrogen removal efficiency (NRE) of 19.7 mg $N \cdot L^{-1} \cdot d^{-1}$ and 59.8%, respectively, when nitrification only accounted for 34.6% of the influent

ammonium, while they decreased to 14.5 mg $N \cdot L^{-1} \cdot d^{-1}$ and 32.6%, respectively, when nitrification rose to 57.2% of the influent NH_4 concentration. This suggests partial microalgae inhibition due to an increasing nitrification rate. Under lab-conditions, Rada-Ariza et al. (2019) reported an NRR of 5.4 mg $N \cdot L^{-1} \cdot d^{-1}$ when nitrification achieved 40% of total NH_4 removed, while it dropped to 1.6 mg $N \cdot L^{-1} \cdot d^{-1}$ when nitrification accounted for 66% of the total NH_4 removed. The factors that influence microalgae activity and nitrification thus need further study.

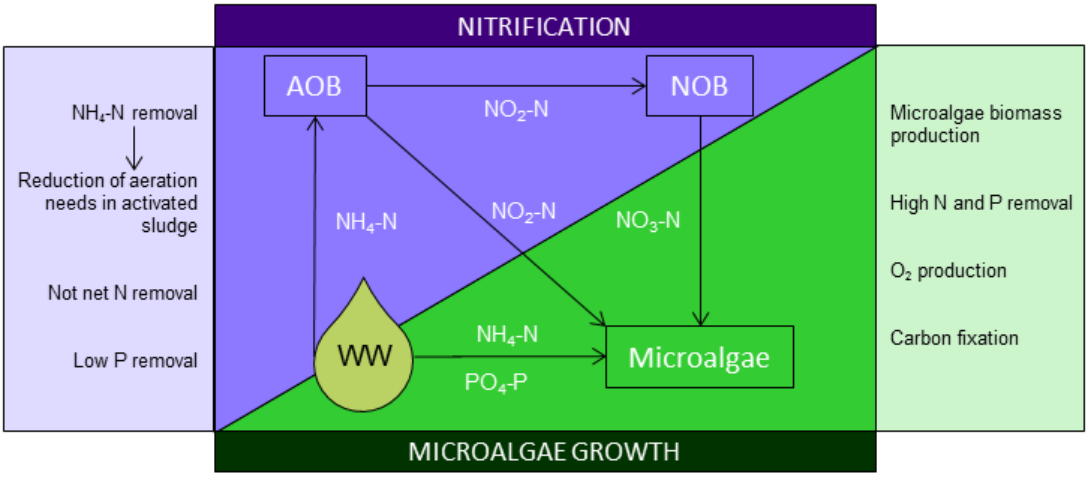

Figure VII. 1. Schematic representation of the nitrogen cycle within the microalgae-ammonium oxidising bacteria competition.

Microalgae can also have a negative impact on nitrifiers (Choi et al., 2010; Sepehri et al., 2020; Wu et al., 2020). Although some authors found no significant influence of nitrification on microalgae activity (Rada-Ariza et al., 2017), others obtained symbiotic benefits between microalgae and nitrifying organisms (Bankston et al., 2020; Vargas et al., 2016). Microalgae-AOB competition must thus be analysed in depth to fully understand the behaviour of microalgae-based wastewater treatment system.

Table VII. 1. Results obtained in previous studies related to microalgae-AOB competition for ammonium uptake. AnMBR: anaerobic membrane bioreactor; AOB: ammonium oxidising bacteria; CSTR: continuous stirred tank reactor; HRT: hydraulic retention time; HRAP: high rate algal pond; MA: microalgae; MPBR: membrane photobioreactor; $NH_{4,i}$: ammonium influent concentration; NRE: nitrogen removal efficiency; NRR: nitrogen removal rate; PBR: photobioreactor; BRT: biomass retention time.

Wastewater	Reactor (Volume)	$[NH_{4,i}]$ (g $N \cdot m^{-3}$)	Conditions	Microalgae uptake ($\%NH_{4,i}$)	Nitrification ($\%NH_{4,i}$)	Stripping (%N)	NRR (g $N \cdot m^{-3} \cdot d^{-1}$)	NRE (%)	Reference
Artificial	CSTR (1.5 L)	1400	HRT = 10 d	40	60	-	-	98[a]	(Vargas et al., 2016)
Sewage	HRAP (1900 L)	54-63	HRT = 6 d	<50%	-	-	-	>80%[a]	(Galès et al., 2019)
AnMBR effluent	PBR (550 L)	44.7	T = 18.5ºC	57.4	17.8	0.3	4.3	63.5	(González-Camejo et al. 2019)
AnMBR effluent	PBR (550 L)	44.7	T = 26.7ºC	44.4	16.3	0.4	3.3	47.0	(González-Camejo et al. 2019)
Centrate	Bubble column	147	T = 20ºC; pH = 8.6-8.7	35	34	20	20	54.1	(Marazzi et al., 2019)
Artificial	Cylindrical reactor (1 L)	23	SRT = 26 d	35	40	-	5.4	89.5[b]	(Rada-Ariza et al., 2019
Artificial	Cylindrical reactor (1 L)	23	SRT = 17 d	10	66	-	1.6	87.0[b]	(Rada-Ariza et al., 2019
AnMBR effluent	MPBR (470 L)	40.0	SRT = 2.5 d; HRT = 1.25 d.	53.7	34.6	0.1	19.7	59.8	(González-Camejo et al. 2020)
AnMBR effluent	MPBR (470 L)	51.5	SRT = 4.5 d; HRT = 1.25 d.	39.7	57.2	0.1	14.5	32.6	(González-Camejo et al. 2020)
Centrate	HRAP (1200 L)	244	HRT = 10 d; pH = 8.2	10	45	32	-	86[a]	(Mantovani et al., 2020)
Centrate	PBR (35 L)	451	HRT = 10 d; pH = 7.9; T = 25ºC	6.0	37.1	0.01	4.7	6.0	(Akizuki et al., 2020)

[a] NH_4-N removal efficiency (includes the nitrified NH_4).
[b] Includes denitrification.

7.3. FACTORS INFLUENCING MICROALGAE-NITRIFYING BACTERIA CULTIVATION

Different medium characteristics and environmental and operational conditions can greatly affect microalgae or nitrifying bacteria, and shift their equilibrium (Bellucci et al., 2020; A. Sánchez-Zurano et al., 2020). The most important factors related to both microalgae and nitrifying bacteria activity are depicted in Figure VII. 2 and discussed below. In this study, the word “microalgae” is considered to refer to eukaryotic microalgae. The most common indigenous wastewater microalgae are *Chlorella, Scenedesmus, Monoraphium, Chlamydomonas,* etc, (Pachés et al., 2020; A. Sánchez-Zurano et al., 2020).

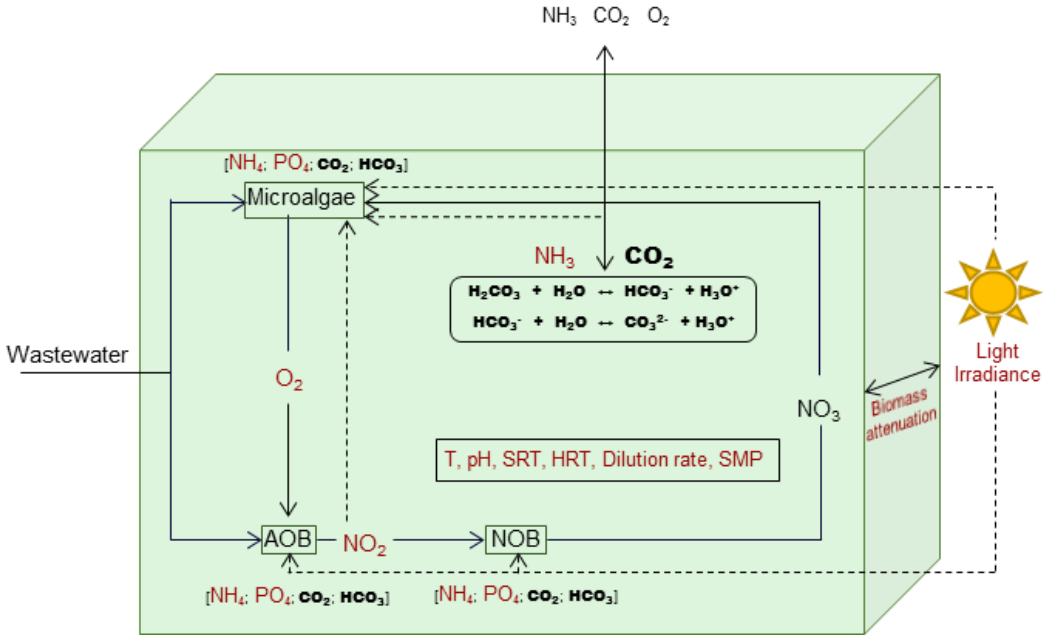

Figure VII. 2. Representation of the main parameters and interactions influencing microalgae-AOB competition. In red the main environmental and operational parameters that affect metabolism of microalgae and bacteria are highlighted. The carbon species involved in the carbonate/bicarbonate equilibrium that regulates the pH of the culture medium are represented in bold. Legend: HRT: hydraulic retention time; SMP: soluble microbial products; SRT: solids retention time; T: temperature.

7.3.1. Temperature

Temperature is a key factor in the rate of enzymatic processes (Reynolds, 2006; Serra-Maia et al., 2016). Microalgae growth increases with temperature until they reach the optimum, which is strain-specific (Ras et al., 2013). *Scenedesmus* and *Chlorella* usually have growth rates in the range of 0.3-0.9 d^{-1} (González-Camejo et al., 2020a; Ruiz et al., 2013; Tan et al., 2016; Xu et al., 2015). However, when temperature is higher than the optimum value even by only 2-4ºC, microalgae growth can fall drastically (Mazzelli et al., 2020). In the case of a mixed microalgae culture dominated by microalgae with a morphology similar to *Chlorella*, González-Camejo et al. (González-Camejo et al., 2019a) reported that microalgae viability fell significantly when temperature was over 30 ºC.

The AOB growth rate sharply increases at higher temperatures. In this respect, AOB growth has been reported to be 0.9 d^{-1} at 20 ºC but reaches 2.9 d^{-1} at 30 ºC (Jiménez, 2010), showing temperature peaks can have a noteworthy influence on microalgae-AOB competition. If high temperatures are maintained, nitrification will increase steadily, and nitrifying bacteria will outcompete the microalgae, while if temperature drops, nitrification will fall and microalgae activity will be able to recover (Faleschini et al., 2012; González-Camejo et al., 2019a).

7.3.2. Light

The importance of light irradiance on the microalgae-AOB competition is mainly due to microalgae as it is probably the main factor in phototrophic growth (Raeisossadati et al., 2019). In fact, when a culture is light-irradiated under proper conditions, microalgae are usually the dominant organism in microalgae-AOB competition (Galès et al., 2019a). However, in an open or closed photobioreactor (PBR), light intensity is exponentially reduced with PBR depth due to the scattering of the culture biomass, the inorganic matter and the microalgae pigments (Martinez et al., 2019; Sutherland et al., 2020). This light attenuation is indirectly measured by the extinction coefficient (K_a) (Romero Villegas et

al., 2017), together with other factors that affect light availability, like microalgae adaptation to light changes or the microalgae cells´ age (Romero-Villegas et al., 2018). The Lambert-Beer Law (Equation VII. S 1) is normally used to calculate average light irradiance ($I_{av,}$), which represents the average irradiance to which the microalgae culture is exposed inside the PBR (Fernández et al., 2016; Romero Villegas et al., 2017). I_{av} (better than total irradiance) is thus the factor which determines microalgae activity.

Although nitrifying bacteria do not need light for their metabolism, excessive light irradiance can affect them negatively (Lu et al., 2020; Wu et al., 2020). For instance, Akizuki et al. (Akizuki et al., 2020b) reported nitrification inhibition at incident light intensities over 450 $\mu mol \cdot m^{-2} \cdot s^{-1}$, while Merbt et al. (2012) observed photoinhibition of AOB *Nitrosomonas europaea* and *Nitrosospira multiformis* at light irradiance of 500 $\mu mol \cdot m^{-2} \cdot s^{-1}$. Meng et al. (2019) found inhibition of *Nitrospiraceae* (nitrite oxidising bacteria (NOB)) under incident light irradiances over 180 $\mu mol \cdot m^{-2} \cdot s^{-1}$. In fact, NOB are usually more sensitive to light than AOB (Akizuki et al., 2020a; Guerrero and Jones, 1996), implying that photoinhibition can lead to partial nitrification, i.e. accumulation of nitrite due to the inhibition of the second step of nitrification (Meng et al., 2019).

7.3.3. Nitrogen concentration

Of all the nitrogen sources that microalgae can assimilate, NH_4-N, NO_2-N and NO_3-N are the only ones involved in the nitrification process. The distribution of these nitrogen species in the wastewater is highly relevant in the microalgae-AOB interaction (Fallahi et al., 2021).

7.3.3.1. Ammonium/free ammonia nitrogen (NH_4-N/ NH_3-N)

Ammonium is the preferred nitrogen species for microalgae, since its uptake needs less energy than other sources (Kumar and Bera, 2020; Reynolds, 2006). In this respect, González-Camejo et al. (González-Camejo et al., 2019a) reported ammonium uptake rates of microalgae up to 15-fold higher than nitrite and nitrate uptake rates in lab-scale PBRs.

The influence of NH_4-N is analogous in both microalgae and AOB and their growth rate is limited with low ammonium availability. In the case of microalgae, ammonium concentrations under 10 mg $N \cdot L^{-1}$ have been found to significantly affect their growth (González-Camejo et al., 2019b; Pachés et al., 2020). However, AOB can support NH_4-N scarcity more efficiently than microalgae. According to Reichert et al. (Reichert et al., 2001), the semi-saturation constant of AOB growth with respect to ammonium is only 0.5 mg $N \cdot L^{-1}$. This suggests that under low ammonium concentrations, AOB can induce microalgae growth limitation (Mohsenpour et al., 2021).

It should also be noted that ammonium is in equilibrium with free ammonia nitrogen (FAN), which is toxic to both microalgae and AOB (Bankston et al., 2020; Simone Rossi et al., 2020; Sayedin et al., 2020). This equilibrium favours FAN at high nitrogen concentrations, temperature and pH (over 9) (see Equation VII. S 2). For this, ammonium-rich wastewater streams such as centrates, which can contain up to 1000 mg $N\text{-}NH_4 \cdot L^{-1}$, have often to be diluted prior to being added to microalgae-nitrifying bacteria cultures (Acién et al., 2016; Tan et al., 2016), as do other toxic substances (Bankston et al., 2020). FAN has been reported to inhibit NOB more than AOB (Su, 2021). In fact, the toxic FAN concentration for NOB has been reported to be in the range of 0.1-3 mg $N \cdot L^{-1}$, while AOB can support ammonia concentrations over 10 mg $N \cdot L^{-1}$ (Weon et al., 2004).

7.3.3.2. Nitrite/free nitrous acid (NO_2-N/HNO_2-N)

Since nitrite is the product of the first step of nitrification and a substrate for NOB, if NOB are more affected by any biotic or abiotic factor other than AOB, NO_2 can be expected to accumulate (Chapter 5; Sayedin et al., 2020). Nitrite can act as a nitrogen source for microalgae (Akizuki et al., 2021), although it can also have negative effects on photosynthesis (Chapter 6). For instance, González-Camejo et al. (2020c) reported a decay in the performance of a mixed microalgae culture dominated by microalge with a morphology similar to *Chlorella* when nitrite concentration was 5-20 mg $N \cdot L^{-1}$, and Yang

et al. (Yang et al., 2004) found reduced growth of green microalgae *Botryococcus braunii* at 70 mg $N \cdot L^{-1}$. It is assumed that this effect is in fact due to an accumulation of free nitrous acid (FNA), which is in acid-base equilibrium with nitrite. FNA has also been found to inhibit nitrifying bacteria at concentrations as low as 200 µg $N \cdot L^{-1}$ and 30 µg $N \cdot L^{-1}$ for AOB and NOB, respectively (Anthonisen et al., 1976; Blackburne et al., 2007).

7.3.3.3. Nitrate (NO_3-N)

Nitrate, the final product of nitrification, is usually more innocuous to aquatic life than ammonium and nitrite (Bankston et al., 2020; Sayedin et al., 2020). If residual nitrogen is emitted from a microalgae-AOB cultivation system, it will be less problematical if the nitrogen is in the form of nitrate. However, microalgae assimilate NO_3 less efficiently than ammonium, as they have to reduce it internally by the action of the nitrate and nitrite reductase enzymes (Kumar and Bera, 2020; Mohsenpour et al., 2021; Su, 2021).

7.3.4. pH

pH affects the microalgae-AOB culture in two aspects: I) it regulates their metabolic pathways; microalgae present optimum pH at around 7-8 (Caia et al., 2018; Eze et al., 2018), while the optimum pH range for AOB and NOB has been reported to be 7.4-7.8 (Claros et al., 2013) and 7.5-9.95 (Jiménez et al., 2011), respectively; II) pH is related to the acid-base equilibrium of the medium (Rossi et al., 2020a), so that it is related to the production of FAN and FNA (Section 7.3.3). It should be remembered that pH not only affects the biological process, but also microalgae autotrophic activity entails pH rises (Eze et al., 2018) while nitrification reduces pH due to a drop in culture alkalinity (Petrini et al., 2020).

7.3.5. BRT/HRT/Dilution rate

SRT and HRT are essential operating parameters in continuous and semi-continuous operations as they can be used to control factors related microalgae-AOB systems (González-Camejo et al., 2020b; Rada-Ariza et al., 2017). In cultivation systems with no biomass retention, HRT (or dilution rate as the inverse of HRT) controls the biomass

concentration and nutrient loads to the culture. On the other hand, when HRT and biomass retention time (BRT) are decoupled (for instance, in MPBR systems (González-Camejo et al., 2020a) or in raceway reactors coupled to membrane filtration (Robles et al., 2019)), BRT appears as the key parameter in the control of biomass concentration to improve light availability (Barbera et al., 2020; Huang et al., 2019; Luo et al., 2018) while HRT is responsible for the nutrient load to the system, thus being a key factor in the nutrient removal efficiency of the system (Arbib et al., 2013; J. González-Camejo et al., 2018).

It must be noted that shorter BRTs boost the growth of the fastest microorganisms (Winkler et al., 2017), which can favour bacteria growth with respect to microalgae (J. González-Camejo et al., 2020c).

7.3.6. Oxygen concentration

In a microalgae-nitrifying bacteria culture, oxygen is mainly produced from microalgae photosynthesis. Indeed, oxygen concentration is often used as an indirect measurement of microalgae performance (Toledo-Cervantes et al., 2019). Oxygen is needed to carry out nitrification (Fallahi et al., 2021). Depending on the microalgae activity within the culture, there will be four different situations (Akizuki et al., 2020b): I) low microalgae activity, which produces insufficient oxygen to carry out nitrification (Toledo-Cervantes et al., 2019); II) enough oxygen to develop the first step of nitrification (via nitrite); III) sufficient oxygen to carry out full nitrification (via nitrate); i.e. over 2 $g \cdot m^{-3}$; IV) production of oversaturated dissolved oxygen, i.e. over 250% (around 20-25 $g \cdot m^{-3}$), which can reduce microalgae performance (Barreiro-Vescovo et al., 2020).

7.3.7. Soluble microbial products/Extracellular polymeric substances

Soluble microbial products (SMP) and extracellular polymeric substances (EPS) include proteins, polysaccharides, nucleic acids and are a result of microalgae and bacteria activity (Delattre et al., 2016; Manhaeghe et al., 2021). It has been reported that stressing factors such as extreme temperatures and nutrient limitation can increase the release of

SMP/EPS to the culture (J González-Camejo et al., 2020a). However, microalgae do not usually take advantage of this organic matter since most microalgae species tend to grow autotrophically under lighting (Assunção and Malcata, 2020; Cuevas-Castillo et al., 2020). Excessive SMP/EPS in microalgae-bacteria cultures tends to favour the growth of competing organisms such as heterotrophic bacteria and grazers, reducing microalgae performance (Kwon et al., 2019). It can also reduce nitrifying bacteria activity due to oxygen depletion (Fallahi et al., 2021).

7.4. MEASURING CULTURE ACTIVITY

The microbial state of the culture will be defined by the activity of both microalgae and nitrifying bacteria. The most active microorganism will dominate the competition, while they will be in equilibrium if they show similar activity. Several parameters are often needed to properly assess the activity since some of these parameters are based on analysing microalgae while others focus on nitrifying bacteria. Figure VII. 3 gives a summary of the methods of measuring microalgae and nitrifying bacteria activity/concentration.

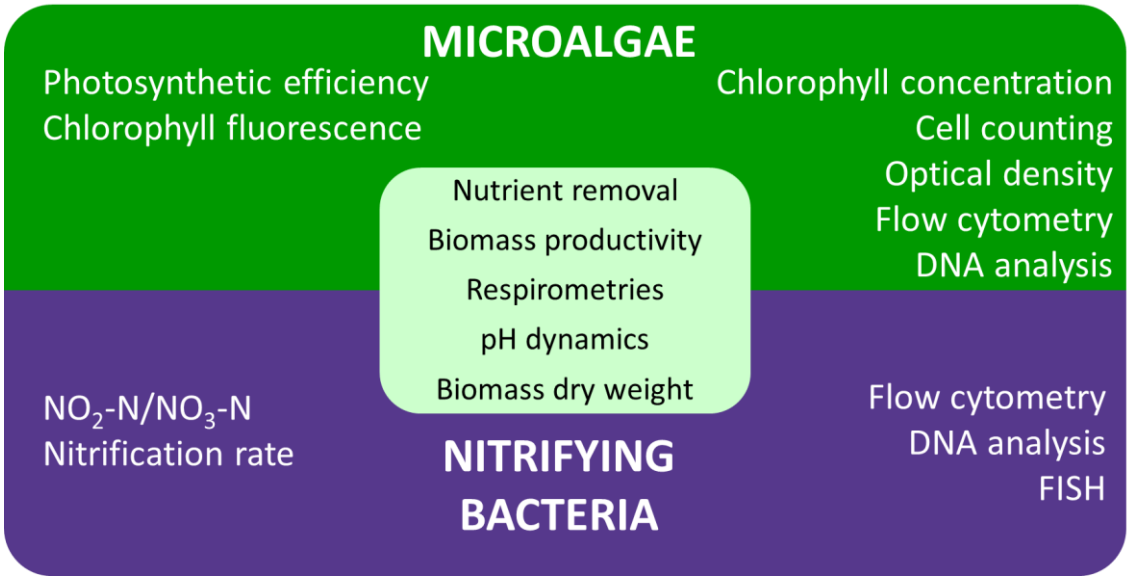

Figure VII. 3. Methodologies to measure the activity and concentration of microalgae and nitrifying bacteria.

7.4.1. Nutrient removal

The main goal of microalgae-based wastewater treatment systems is to reduce the nitrogen and phosphorus loads of the influent. This nutrient removal mainly occurs due to: I) microalgae growth; II) nitrifying bacteria growth; III) nitrogen losses due to ammonia stripping; and IV) phosphorus precipitation. During nitrification, nitrogen is not removed from the system, only changes its oxidation state. Other mechanisms of removing nutrients like phosphorus adsorption in the culture biomass or volatilisation of N_2/N_2O are often negligible (Alcántara et al., 2015).

There are two different approaches to evaluate nutrient removal: nutrient removal efficiency (NRE) and nutrient removal rate (NRR). The former considers the percentage of nutrient concentration removed from the influent (Equation VII. S 3), while the latter measures the rate at which nutrients are removed from the system (Equation VII. S 4).

7.4.2. Biomass productivity

Biomass productivity is the culture biomass produced and taken out of the PBRs (Andrade et al., 2016) and can be calculated by Equation VII. S 5. It is usually related to nutrient removal (González-Camejo et al., 2019c) so that it is a useful parameter to assess wastewater treatment processes. It also appears an essential factor in microalgae cultures designed to obtain by-products (Shahid et al., 2020).

7.4.3. Photosynthetic efficiency

As photosynthetic efficiency measures the capacity of microalgae to use the light applied to the PBRs (Equation VII. S 6), it is a useful parameter to evaluate photolimitation or photoinhibition processes (Straka and Rittmann, 2018). It is also a relevant parameter in evaluating microalgae production and designing PBRs (Morillas-España et al., 2020). Although it gives no direct information on the activity of nitrifying bacteria, a decay in photosynthetic efficiency can be due to bacteria proliferation.

7.4.4. Respirometry

Respirometry is a simple and cheap method based on dissolved oxygen (DO) profiles (Manhaeghe et al., 2021; Petrini et al., 2020). In the case of microalgae-nitrifying bacteria cultures, it consists of batch tests in which light and dark (L/D) phases alternate to obtain the oxygen production rate (OPR) or the oxygen uptake rate (OUR). The L/D phases can be repeated several times during the test to obtain replicates of the OPR and OUR values. Nutrients can be added as substrate to obtain maximum activity while substances like allylthiourea (ATU) can be injected to inhibit AOB (Rossi et al., 2020b). The oxygen profile is the result of several processes: I) OPR by microalgae; II) OUR by nitrification; III) OUR by microalgae respiration; IV) and OUR by heterotrophic bacteria respiration (Rossi et al., 2018; Rossi et al., 2020b).The gross OPR/OUR value differ according to the weight of each component and gives valuable information on the activity of the different organisms in the culture (Sánchez-Zurano et al., 2020).

Although many respirometric protocols have been reported in the literature (Table VII. 2), the results are usually hard to compare (Petrini et al., 2020). To overcome this issue, Rossi et al. (Rossi et al., 2020b) stated that the following data should be reported to make these protocols comparable:

- Microalgae cultivation system: environmental and operational conditions, composition of the microbial community and culture characteristics.
- Respirometric procedure: initial culture concentration, nutrient sources and their concentrations, setpoints for temperature, pH and dissolved oxygen, light intensity, test procedure (protocol and duration of light and dark phases) and processed OPR and OUR data.

The main advantages of respirometry are its: I) low-cost; II) possibility to obtain both OPR/OUR in the same test; III) it can measure specific kinetic parameters; and IV) good test reproducibility. However it also has some drawbacks: I) off-site test that cannot be

carried out in-situ nor continuously monitored; II) it usually includes an acclimatation phase that takes time; III) it can be affected by oxygen mass transfer from the atmosphere; and IV) it sometimes has to be supplied with external aeration or pH control (Petrini et al., 2020; Rossi et al., 2020b).

7.4.5. Chlorophyll fluorescence parameters

Chlorophyll fluorescence parameters, i.e. parameters that evaluate variations in the photosystem II (PS II) photochemistry and linear photon flux (Baker, 2008), indirectly measure the adaptability of microalgae to certain environmental and operating conditions (Rossi et al., 2020b). Maximum PS II quantum efficiency (F_v/F_m) is the most frequently used fluorescence parameter and represents the maximum efficiency at which light absorbed by PS II is used for the reduction of the primary quinone electron acceptor (Q_A). In this respect, Sánchez-Zurano et al. (2020) suggested that F_v/F_m values below 0.6 indicated photoinhibition. However, Baker (Kalyuzhnaya et al., 2006) found issues related to the accuracy of this value and its relation to the rates of linear CO_2 assimilation. These parameters give no direct information on nitrification. In fact, González-Camejo et al. (González-Camejo et al., 2020a) did not find any statistically significant relationship between F_v/F_m and microalgae-bacteria performance in the continuous operation of a mixed microalgae-AOB culture.

7.4.6. pH dynamics

pH data can monitor online the activity of mixed microalgae-bacteria cultures due to the pH variations caused by their metabolic activity. Robles et al. (2020) used pH sensors to describe the start-up phase of an outdoor raceway pond treating urban wastewater, while González-Camejo et al. (2020b) reported a good correlation between pH dynamics and performance of an outdoor MPBR plant treating AnMBR effluent.

Table VII. 2. Description of respirometric protocols.

Cultivation system					Respirometric protocol							
Wastewater	**Reactor (L)**	**HRT/BRT (d)**	**Culture**	**Nutrients ($g \cdot m^{-3}$)**	**Initial biomass ($g \cdot m^{-3}$)**	**Light ($\mu mol \cdot m^{-2} \cdot s^{-1}$)**	**T (ºC)**	**pH**	**DO ($g \cdot m^{-3}$)**	**Duration L/D phases**	**OPR/OUR ($g \cdot m^{-3} \cdot h^{-1}$)**	**References**
AnMBR effluent	Vertical PBR (7)	-	Mixed microalgae culture	-	833	Only dark	20	7-8.4	1-9	0/> 48 h	0/0.1-0.8	(Ruiz-Martinez et al., 2016)
Artificial	Flasks (0.25)	Batch	*Chlorella vulgaris*	$NaHCO_3$ (0.75 $g \cdot L^{-1}$); NH_4 (10 $mgN \cdot L^{-1}$); NO_3 (10 $mgN \cdot L^{-1}$)	1.06-2.05[a]	135	24	7-8	Non-controlled	24 h (L)/ 0 (D)	0.61 /-	(Najm et al., 2017)
Centrate	Raceway pond (1200)	20	Microalgae-bacteria	NH_4Cl (3.2 $gN \cdot L^{-1}$); $NaNO_2$ (8.2 $gN \cdot L^{-1}$)	0.4-0.6[b]	-	-	-	-	15/10 min	10-25/0-4	(Rossi et al., 2018)
Artificial	Flasks (0.25)	Batch	*Mixed Chlorella protothecoides*	$NaCO_3$ (1 $g \cdot L^{-1}$); N (247 $mgN \cdot L^{-1}$); P (5.4 $mgP \cdot L^{-1}$)	200	20-1500	24	7.5	0-11	5/5 min	-	(Sforza et al., 2019)
Primary effluent	SB-PBR (2)	5.6/65	Microalgae-bacteria	Acetate (5-10 $gCOD \cdot L^{-1}$); NH_4 (1 $gN \cdot L^{-1}$)	900-1000	90	-	-	7.5-8.5	I) based on nutrients II) based on DO	8.3/0.5	(Petrini et al., 2020)
Centrate	Raceway pond (1200)	10	Microalgae-bacteria	$NaHCO_3$ (150 $mgC \cdot L^{-1}$); NH_4Cl (30 $mgN \cdot L^{-1}$); K_2HPO_4 (10 $mgP \cdot L^{-1}$)	0.2[b]	110	20	8.5	10	10/20 min	-	(Rossi et al., 2020)
Primary effluent	Raceway (4400)	5	Microalgae-bacteria	$C_2H_3O_2^-$ (0.3 $g \cdot L^{-1}$); NH_4Cl (30 $mg \cdot L^{-1}$)	-	200	25	8.0	90-130%sat	4/4 min	16.7/1.9	(Sánchez-Zurano et al., 2020)

[a] Final biomass concentration.

[b] Measured as optical density at 680 nm (OD680)

AnMBR: anaerobic membrane bioreactor; DO: dissolved oxygen; HRT: hydraulic retention time; L/D: light-dark; SB-PBR; sequencing batch photobioreactor; BRT: solids retention time.

7.4.7. Nitrite and nitrate concentrations

Some authors have used nitrite and nitrate concentrations as an indirect measure of nitrifying bacteria activity (Akizuki et al., 2020b; Marazzi et al., 2019). However, these parameters cannot be used to directly evaluate nitrification if NO_2/NO_3 are present in the influent in relevant concentrations, since some of the nitrite and nitrate present in the culture would not be due to nitrification but to the influent in which case nitrification rate (Section 7.4.8) would be a better indicator of nitrifying bacteria activity.

7.4.8. Nitrification rate

Nitrification rate measures the production of nitrite and nitrate during nitrification (Equation VII. S 7). Microalgae can assimilate nitrite and nitrate simultaneously with ammonium (González-Camejo et al., 2019a) although the amount assimilated by microalgae cannot be assessed by the nitrification rate. When microalgae absorb relevant amounts of nitrite and nitrate, the evaluation of nitrifying bacteria activity should thus be complemented by other methods such as respirometry (Section 7.4.4).

7.5. MEASURING CULTURE CONCENTRATION

The culture biomass concentration also gives information on microalgae-AOB competition, as microalgae and bacteria concentrations are closely highly related to biomass productivity and nutrient removal rates (González-Camejo et al., 2020b; Sánchez-Zurano et al., 2020). In microalgae-bacteria cultures, microalgae are usually the dominant organism mainly due to their larger cell size. In this respect, Luo et al. (2018) reported only 0.2-3.5% of bacteria in a lab-scale microalgae cultivation system. For this reason, some methods of assessing culture biomass concentration consider the whole biomass as if it were only composed of microalgae, so that several methods should be used to measure the distribution of microalgae and bacteria and evaluate the competition between these microorganisms (Di Caprio, 2020).

7.5.1. Biomass dry weight

The common method of measuring biomass concentration is by quantifying the total (TSS) or volatile suspended solids (VSS) concentration. This is a low-cost method, although time-consuming: at least 2 hours for TSS and around 24 hours for VSS (Di Caprio, 2020).

This measure will include not only the mass of microalgae and bacteria but also any other compound present in the culture such as cell debris and SMP/EPS as it cannot distinguish between them (Rossi et al., 2020b; Sánchez-Zurano et al., 2020).

7.5.2. Chlorophyll concentration

Chlorophyll concentration has traditionally been used as an indirect measure of microalgae concentration (Galès et al., 2019a). Although it gives no information on bacteria, the relation between chlorophyll and total biomass (mg Chla·mg VSS^{-1}) can serve as a proxy for the microalgae-bacteria ratio (Di Caprio, 2020).

The trichromatic method can be used to measure chlorophyll and consists of extracting the chlorophyll from the culture biomass by solvents such as acetone. The solution composed of the extracted chlorophyll and the solvent is then measured by spectrophotometer analysis (APHA et al., 2005). Chlorophyll a concentration can then be calculated by applying Jeffrey and Humphrey's Equation (Equation VII. S 8), being a simple and inexpensive method (Di Caprio, 2020). However, chlorophyll concentration as a proxy for microalgae biomass content is somewhat controversial since microalgae can vary their intracellular chlorophyll content with the lighting conditions, showing higher chlorophyll a content when microalgae are light-limited to take full advantage of light irradiance (Chen et al., 2011). Other limitations of chlorophyll analysis lie in the incomplete efficiency of chlorophyll extraction by the solvent and the presence of molecules that can interfere with the spectrophotometric analysis. Similar limitations are present in measuring the concentration of other pigments such as carotenoids and phycocyanin (Di Caprio, 2020).

7.5.3. Optical density

Optical density (OD) is based on the linear relationship between light absorbance and particle concentration (Di Caprio, 2020). It is often used as it is fast and cheap, only requires a small sample and can be monitored online (Havlik et al., 2013). Selecting the wavelength to be measured is a critical point and should minimise absorbance from the medium, thus reducing background noise. Wavelengths in the range of 600-700 nm are usually applied in bacterial cultures (Griffiths et al., 2011). In those dominated by green microalgae, the most frequently used wavelength is 680 nm, as it coincides with the chlorophyll absorption peak (Markou et al., 2017; Nielsen and Hansen, 2019). However, some authors have employed other wavelengths to measure biomass concentration in microalgae-based systems (Table VII. 3).

Table VII. 3. Optical density used to measure biomass concentration in microalgae-based systems.

OD	Wastewater	Reactor	Microorganism	R^2	Reference
750 nm	Artificial	Airlift reactors (3.2 L)	Green microalgae	-	(Griffiths et al., 2011)
750 nm	Artificial	Flask (0.4)	Green microalgae	0.992-0.998	(Gonçalves et al., 2014)
940 nm	Artificial	ePBR	*C. sorokiniana*	0.938	(Lucker et al., 2014)
683 nm	Artificial	Flask (0.25 L)	*C. vulgaris*	0.991	(Najm et al., 2017)
680 nm	Artificial	Cylindrical PBR (1 L)	*Chlorella*	0.996-0.999	(Izadpanah et al., 2018)
550/665/750 nm	Artificial	Tubes (0.1 L)	*Rhodomonas salina*	0.952-0.979	(Nielsen and Hansen, 2019)
680 nm	AnMBR effluent	MPBR (470 L)	Microalgae-nitrifying bacteria	0.905	(González-Camejo et al., 2020)
680 nm	Centrate	Raceway (1200 L)	Microalgae-bacteria	0.87	(Mantovani et al., 2020)
680 nm	Synthetic secondary effluent	MPBR (2.5 L)	*C. vulgaris*	0.999	(Novoa et al., 2020)
680 nm	AnMBR effluent	Flask (2 L)	Green microalgae	0.891-0.992	(Pachés et al., 2020)

AnMBR: anaerobic membrane bioreactor; ePBR: environmental photobioreactor; MPBR: membrane photobioreactor; OD: optical density; R^2: coefficient of determination.

The calibration curve which relates OD and biomass concentration varies throughout the experimental period and is a drawback of using optical density, due to changes in the microalgae pigment content, the dominant microalgae species and the proportion of microalgae and bacteria. This can cause serious errors when measuring biomass concentration (Di Caprio, 2020).

7.5.4. Cell counting

Cell counting under a microscope is another common method of measuring microalgae biomass. It can quantify not only the total microalgae concentration but also distinguish between genera or species on a morphological basis (Figure VII. 4), although it gives no information on bacteria identity (Rossi et al., 2020b). A minimum of 100 microalgae cells of the most abundant genera and at least 300 total microalgae cells need to be counted to achieve less than a 20% error (Pachés et al., 2012). After counting, microalgae concentration can be correlated with dry weight as long as microalgae are the dominant organism. However, this linear relationship will not always occur as the method does not consider microalgae cell size, which can vary (Di Caprio, 2020).

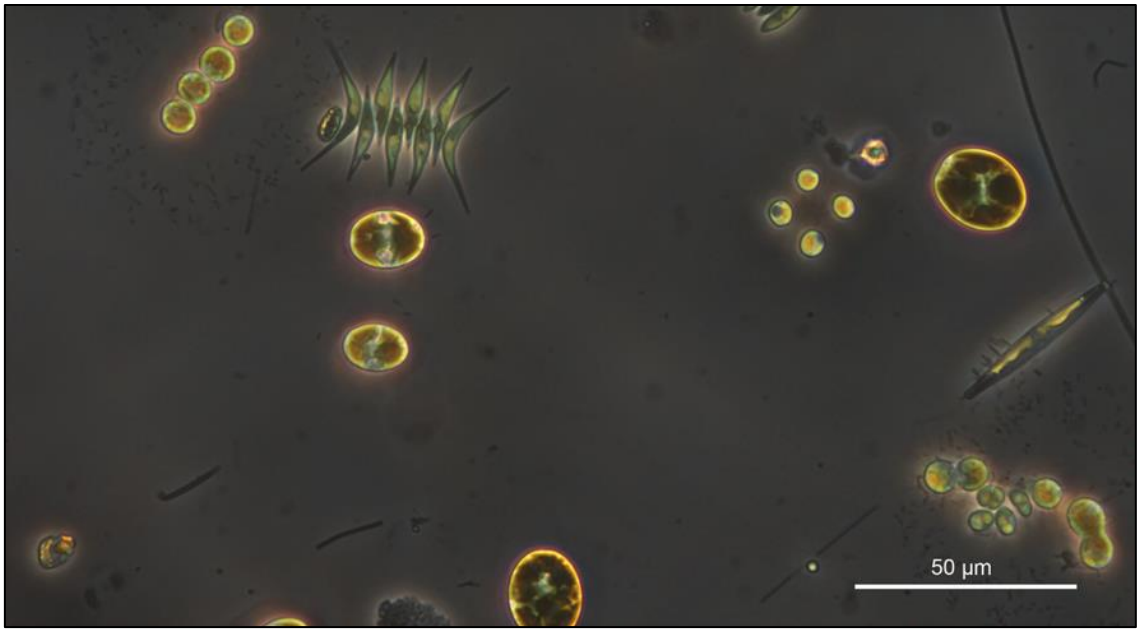

Figure VII. 4. Visualization of different microalgae genera (Chlorella, Scenedesmus and diatoms) (400x) from a Leica DM2500 microscope with N2.1 and I3 filters.

With large microalgae colonies or flocs in the sample, serious errors can occur in counting due to the difficulty of counting inside a floc and the lack of random cell distribution in the area counted (Di Caprio, 2020).

7.5.5. Autofluorescent pigments, fluorescent probes and dyes

Information on some of the most frequently used fluorophores for bacterial cells is given in the Supplementary Data. Fluorescent dyes are not needed for microalgae cells due to the autofluorescence provided by their photosynthetic pigments. Microalgae emit red fluorescence (λ_{em} = 670 nm) when the cells are illuminated by a blue-light excitation filter (λ_{ex}: 460–490 nm), as seen in Figure VII. 5. Although the fluorescent dyes included mainly focus on the detection of total bacterial cells, SYTOX Green and fluorescein diacetate (FDA) have also been used to detect non-viable cells. The simultaneous detection of live and dead microalgae or bacterial cells is therefore possible by applying double fluorescent staining.

Propidium iode (PI) stain is also widely used for cell viability staining (Medeiros et al., 2020; Wei et al., 2011). However, the maximum emission wavelength is in the same range as microalgae photosynthetic pigments, so that the two signals overlap. On the other hand, SYTOX green only penetrates non-viable cells and does not overlap with photosynthetic pigments (Sato et al., 2004), so that red autofluorescence and SYTOX green fluorescence can be used as markers for viable and non-viable microalgal cells, respectively (Figure VII. 5B).

Despite the variety of dyes, it is not possible to classify taxonomically bacteria classification by generic fluorescent dyes described in the Supplementary Data. The fluorescence in-situ hybridization (FISH) microscopic technique is widely used to identify different taxonomic groups of bacteria using probes with different non-overlapping fluorochromes (Di Caprio, 2020). The main FISH probes used to detect the bacterial domain (specifically AOB) are also compiled in the Supplementary Data. This method was used by González-Camejo et al. (González-Camejo et al., 2018) and Mantovani et

al. (Mantovani et al., 2020) to detect AOB diversity in mixed microalgae cultures. However, FISH is not normally used to identify photosynthetic organisms due to signal interference with autofluorescence given by the microalgae photosynthetic pigments. Hosoi-Tanabe and Sako (Hosoi-Tanabe and Sako, 2006, 2005) designed ribosomal RNA-based probes for the detection of phytoplanktonic organisms, specifically dinoflagellates.

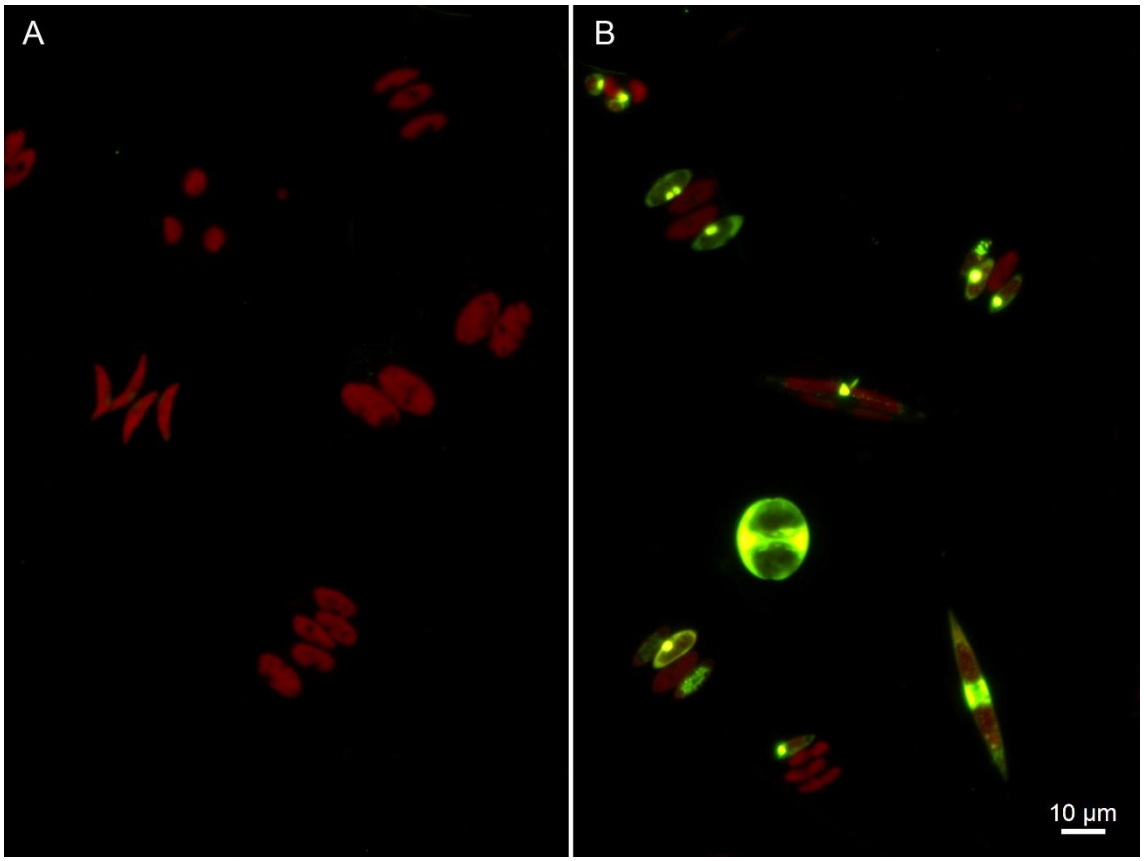

Figure VII. 5. (A) Microalgae autofluorescence; (B) Microalgae sample stains with SYTOX Green, cells with damaged membrane emit a green fluorescent signal, while cells that are considered viable emit a red fluorescent signal associated with microalgal autofluorescence. The microalgae sample was visualized (400x) through a Leica DM2500 microscope when excited with a blue-light excitation filter (λex 450–490 nm).

Target organisms in stained samples are quantified by epifluorescence microscopy with an image acquisition system and image processing, although this is a time-consuming technique (Sanz and Köchling, 2007).

7.5.6. Flow Cytometry

7.5.6.1. Conventional Flow Cytometry

Flow cytometry (FCM) is a powerful tool for single-cell analysis that can provide a rapid, direct and precise quantification of cells in samples containing heterogeneous microbial populations (Di Caprio, 2020). It can count more than 1000 cells (or events)·s^{-1} directly in the sample by using an automated fluid-optical system (Hyka et al., 2013). In conventional cytometers, cells suspended in a liquid sample are aspirated and swiped in front of an illumination source with the subsequent detection of light scatter (forward scatter (FSC); side scatter (SSC)) and the fluorescence responses of cells in the sample. Cell or event classification is performed according to their size (FSC), internal complexity (SSC) and through fluorescence emissions (given by cell staining or autofluorescence). The data obtained for analysing the cell or event are plotted from empirical correlations among FSC, SSC and fluorescence and two dimensional cytograms. Due to the sample complexity, these correlations should be previously determined by a calibration procedure using standard samples as well as negative and positive controls. By way of example, Foladori et al. (Foladori et al., 2010), Luo et al. (Luo et al., 2020a) and Petrini et al. (Petrini et al., 2020) combined FCM with fluorescent molecular probes for rapid quantification of microalgal and bacterial cells and to assess their physiological state for wastewater treatment purposes.

The main limitation of FCM is given by cell aggregation and multicellular organisms. Bacteria cells can live attached to microalgal (Li et al., 2017) and some microalgae genera such as *Scenedesmus* or *Coelastrum* can develop a coenobia structure, thus underestimating the analysed populations. Non-ionic surfactants (Vasseur et al., 2012) and sonication (Coggins et al., 2020) are also feasible options to pre-treat the samples and disperse cell aggregates.

Conventional flow cytometer also features Fluorescence Activated Cell Sorting (FACS). This is a powerful tool for the rapid identification, separation and recovery of targeted

cells from a heterogeneous cell suspension, based on the signal detected (Morais, 2018). It is widely used for microalgae strain selection and further sequencing of microalgae (Lee et al., 2013) and combined with FISH, AOB cells can be identified, stored and isolated (Morais, 2018).

7.5.6.2. Imaging Flow Cytometry (IFC)

Imaging Flow Cytometry (IFC) combines single-cell identification and high FCM throughput with cellular image acquisition of fluorescence microscopy (Han et al., 2016). The images captured can be visualised and analysed by an image processor. IFC is recommended for analysing samples containing cellular aggregates and multicellular organisms, since the true nature of every event read can be verified from the 2D images obtained. IFC has been used to determine the relative abundance of microalgae species; to analyse microalgae cell size; to determine their viability and metabolic activity; and to define different life stages of microalgae (Dashkova et al., 2017; Harmon et al., 2020). Despite all its advantages, the taxonomic resolution provided by image acquisition is relatively low. In addition, to asses different microalgae cell sizes it is necessary to use a combination of magnification objectives and working modes (Dashkova et al., 2017; Haridas et al., 2017). IFC is not used to quantify free bacteria such as AOB in wastewater as it is complicated and provides no significant information other than that obtained by FCM (Haridas et al., 2017).

7.5.7. Sequencing-based techniques

7.5.7.1. Polymerase Chain Reaction (PCR)

Molecular analyses are the most sensitive and specific method for microorganism identification. They are based on targeted sequencing of amplified gene regions or "amplicon sequencing", i.e. they consist of Polymerase Chain Reaction (PCR) amplification of a target gene, followed by short-read sequencing of the obtained amplicon. The PCR technique has been widely used to identify bacteria and archaea (Davis, 2014; Jalali et al., 2017).

7.5.7.2. Quantitative real time PCR (qPCR)

The microbial community can be classified and detected by PCR, but not quantified. Quantitative real time PCR (qPCR) is a DNA amplification and quantification technique using specific fluorescent dyes to combine PCR amplification and detection stages, allowing the quantification of the concentration of genetic material in samples (Jalali et al., 2017). qPCR measures the DNA produced through the increase in the fluorescent signal after fluorescent staining.

7.5.7.3. Next Generation Sequencing (NGS)

PCR and qPCR require previous knowledge of the organisms of interest and provide little information on the general dynamics of the microbial community, while the emergence of NGS helps to understand complex microbial communities. NGS involves a variety of high-throughput nucleic acid sequencing technique which can retrieve millions of DNA or RNA sequences from environmental samples (Garner et al., 2021).

7.5.7.4. Application of sequencing-based techniques

Most studies of AOB populations target the 16S rRNA gene as amplicon sequencing, as it is a universal gene for bacteria and archaea and can determine the taxonomy or phylogeny of microbial population members. The 16S rRNA gene is about 1500-bases long and has relatively conserved regions and nine variable regions (from V1 to V9) which range from 50 to 100 bp in length (Johnson et al., 2019). Analyses of AOB populations have amplified segments of the following variable regions: V2 (Deng et al., 2018; Islam et al., 2019), V3-V4 (Lin et al., 2020; Sarvajith et al., 2020), V6 (Ye et al., 2012) and V7-V8 (Orschler et al., 2019) with the primers listed in the Supplementary Data. Although the 16S rRNA gene has been widely used to study AOB at the phylogenetic level, the amoA gene has also been applied as a molecular marker for AOB organisms through the primers described by Rotthauwe et al. (Rotthauwe et al., 1997) and compiled in the Supplementary Data. The amoA gene encoding the alpha-subunit of ammonia monooxygenase, which is the metalloenzyme responsible for catalysing

ammonia oxidation to hydroxylamine (Gilch et al., 2009). This gene is thus involved in the first step of nitrification and has been found only in organisms capable of oxidising ammonia, such as AOB.

Unlike AOB, no universal standard DNA sequence has been found for microalgae identification and quantification. Intensive research on microalgae identification is currently focused on the search for molecular markers that can be used to successfully identify and/or quantify a wide spectrum of microalgae. However, a universal sequence to establish a single sequence DNA barcode system is apparently not possible. However, in the case of specific taxonomic groups with different phylogenetic positions, the identification of microalgal populations would be performed with different sets of target sequences (Mirek et al., 2007).

Most molecular research on microalgae has used a rather limited set of markers, such as 18S rDNA, rbcL (large subunit of plasma Rubisco), internal transcribed spacers (ITS) or plastid elongation factor (tufA) (Kowalska et al., 2019; Vieira et al., 2016).

Fawley and Fawley (2020) recommended starting with sequencing of the 18S rDNA gene for identifying the higher taxonomic groups such as order or class because the available sequences set for this gene is a very large database. The primers selected should include the most variable region of the target gene such as the V4 and V9 region of the 18S rRNA (Amaral-Zettler et al., 2009).

In case of microalgae genus (or family), more specific primers based on specific protein-coding genes can be selected for species-level identification (Leliaert et al., 2014; Mann et al., 2010; Vieira et al., 2016).

As the gene region between the large (rbcL spacer) and small (rbcS spacer) subunits of RuBisCO is not variable enough to identify all strains (Hall et al., 2010). Chase et al. (Chase et al., 2007) proposed that the rbcL marker be combined with others. ITS1 and ITS2 markers are sufficiently variable to differentiate algal strains within species (Hall et

al., 2010; Mann et al., 2010; Moniz and Kaczmarska, 2009). However, few ITS sequences are available in the databases. The tufA marker appears to be a promising specific marker for class-level classification (Vieira et al., 2016).

At present there is no general classification technique that identifies all microalgal species, so that when a single area of the genetic material is not enough to address questions related to a specific group, it is recommended to combine two or more regions. For this it is necessary to choose the appropriate marker set, based not only on the genetic divergence of the group and the existence of reference sequences in databases, but also on the previous experience of other researchers to facilitate the selection of the appropriate markers for each group. The most commonly used markers (and their combinations) to identify indigenous microalgae from WWTPs are listed in the Supplementary Data.

7.5.8. Simultaneous measurement of microalgae and AOB concentration

The most promising methods of accurately determining the proportion of microalgae and AOB in a sample are: I) the combination of FISH and autofluorescence of microalgae; II) the combination of FISH and flow cytometry; III) sequencing-based techniques and; IV) respirometries (Section 7.4.4).

FISH and autofluorescence of microalgae: by combining FISH probe fluorescence for AOB and microalgae autofluorescence, the proportion of AOB (%AOB) and microalgae (%MA) in a sample can be estimated. An image processing system can be used to determine the area occupied by photosynthetic organisms, AOB and the rest of the bacteria (determined by *Eubacteria* FISH probes (Daims et al., 1999)). This method measures the proportion of AOB and MA in terms of area, which is supposed to be equivalent to the volume and biomass of the populations.

FISH technique and flow cytometry: by combining fluorescence signals and FSC and SSC measurements, the proportion of microalgae and AOB in a biological sample can

be quantified. The technique can discriminate not only by colour but also by size and complexity (Kalyuzhnaya et al., 2006), although there are some technical limitations. The main drawback is that to differentiate between both populations the flow cytometer must be calibrated with standard samples (usually pure cultures of the target organism). In samples with high biodiversity, calibration of the flow cytometer is complex, time-consuming and depends on the sample to be analysed in each case. Accurate quantification by cytometry requires the complete disaggregation of the samples (as the cytometer counts events) and there may be a high degree of bias if the aggregates are estimated as single cells instead of a group of cells. In biological samples, inorganic compounds (e.g. debris) can interfere with the signal of the instrument. The results of this technique are given in an event (hopefully cells) basis instead of cell basis, which could be controversial when applying this data directly to mathematical models.

Sequencing-based techniques: The results obtained from metagenomic techniques should be interpreted with caution, since the measured genetic material is not usually correlated to the real sample concentration. The main factors that influence the quantitative results are: the efficiency of the sample extraction process; the kind of primers used for DNA amplification; the different ratios between initial DNA concentration and final concentration after amplification, the sequences available in databases; and the algorithms used for data processing (Di Caprio, 2020). Depending on the target population, it is recommended to use a different extraction kit, introducing more uncertainty in the biological taxa comparison. The sequencing of microalgae and AOB is carried out separately, i.e., one sample is sequenced to obtain the information related to the Bacterial domain and another sample for the Eukaryotic domain. The results obtained are the relative abundance of AOB compared to bacteria abundance and the relative abundance of microalgae and compared to eukaryotic organisms abundance (Steichen and Brown, 2019). The results obtained are thus not comparable and at present it is not possible to determine the ratio of AOB to microalgae in a sample. The main drawback is

that these techniques quantify gene copies instead of organisms. As the number of gene copies varies between genes and organisms it is hard to correlate the obtained results with the real number of organisms present in the sample.

Respirometries: The main advantage of this technique is that it is the only one that measures activity instead of the number of microorganisms, which avoids the bias due to the presence of non-active AOB or microalgae in the sample. The results can be applied directly in mathematical models.

7.6. NITRIFICATION CONTROL STRATEGIES

Microalgae normally outcompete AOB due to their greater capacity to uptake nitrogen (Marcilhac et al., 2014). However, nitrifying bacteria can proliferate faster than microalgae depending on operational and environmental conditions (Sánchez-Zurano et al., 2020). In fact, nitrifiers can surpass microalgae as the dominant microorganism in the competence. In some cases microalgae can even collapse (González-Camejo et al., 2019a), so that nitrification has to be controlled. Other options can minimise nitrifying bacteria growth, hence minimising the decay in microalgae performance.

7.6.1. Temperature control

As commented in Section 7.3.1, temperature is essential in regulating nitrification. González-Camejo et al. (González-Camejo et al., 2019a) reported that microalgae-nitrifying bacteria remained in equilibrium in flat-panel PBRs when temperature was around 20 ºC, but nitrification was favoured when peak temperatures went over 30 ºC. When cultivating microalgae-bacteria cultures in open ponds the temperatures are usually regulated by evaporation. However, closed PBRs can reach temperatures 10 ºC higher than their surroundings (Yeo et al., 2018). Including cooling systems (González-Camejo et al., 2019a; Mazzelli et al., 2020) can reduce temperature in closed PBRs although it involves a drastic increase in the process costs.

7.6.2. BRT/HRT control

As explained in Section 7.3.6, BRT (or HRT) plays a significant role in microalgae-AOB competition. In terms of process efficiency, BRT (or HRT) tends to be operated for as short as possible to reduce costs. However, a too short BRT (around 2 days) can favour NO_2 accumulation due to higher AOB activity than microalgae and NOB, which can reduce microalgae activity significantly (Marazzi et al., 2019). On the other hand, longer BRTs tend to increase NOB activity (Munz et al., 2011), favouring nitrification at the expense of lower microalgae growth. Microalgae have been found to be favoured over nitrifiers at mid-range BRT values. (González-Camejo et al., 2020c) reported this range to be 2-4.5 d for an outdoor flat-panel MPBR system treating AnMBR effluent.

The most appropriate values of BRT/HRT depend on the culture characteristics (mainly biomass concentration and pigment content) as they affect the average light irradiance of the culture (Section 7.3.2). These characteristics will in turn be related to other factors such as ambient conditions and nutrient availability (González-Camejo et al., 2018). Mathematical models can predict the most appropriate BRT/HRT for variable conditions (De-luca et al., 2018; Fernández et al., 2016).

7.6.3. Temporary increase of dilution rate

Once a consistent nitrifying bacteria population has been established within the culture, microalgae usually reduce their performance. To change this trend the dilution rate can be increased to wash out the excess bacteria (Luo et al., 2020b). Raising the dilution rate will also reduce microalgae biomass and pigment concentrations, which can favour microalgae by reducing light attenuation in the reactor (Section 7.3.2). González-Camejo et al. (González-Camejo et al., 2020c) found a significant reduction in the nitrification rate of a microalgae-nitrifying bacteria system when the dilution rate was temporarily raised from 0.3 d^{-1} to 0.5 d^{-1}. However, the higher dilution rate only benefits the microalgae for a short time. If the operating and ambient conditions favour nitrifying bacteria growth, the nitrification rate will be dominant in the long-term.

7.6.4. Control of nutrient loads

Nutrient loading is related to the BRT/HRT/dilution rate. However, the competition between microalgae and nitrifying bacteria does not only depend on the influent flow rates but also on the distribution of nutrients, as previously explained in Section 7.3.3. For instance, if the ammonium loading rate is negligible, AOB growth will be inhibited. However, microalgae will still be able to grow using nitrite or nitrate (although at a lower growth rate). This behaviour was reported by González-Camejo et al. (González-Camejo et al., 2020a), who observed an equilibrium between microalgae and bacteria when the ammonium loading rate was under 30-35 mg $N \cdot L^{-1} \cdot d^{-1}$, but a significant proliferation of nitrifying bacteria when it went over 40 mg $N \cdot L^{-1} \cdot d^{-1}$. Other authors have also reported nitrification control by adjusting the N/P ratio of the influent (Bellucci et al., 2020). If phosphorus is scarce in the medium, nitrifying bacteria will not be able to grow. However, microalgae can use their intracellular phosphorus when P is lacking in the medium (Solovchenko et al., 2019).

7.6.5. Addition of nitrification inhibitors

Nitrification can be easily inhibited by adding selective inhibitors. ATU has been reported as a transient inhibitor of AOB activity when the concentration in the medium is around 5-10 $mg \cdot L^{-1}$ (González-Camejo et al., 2019a; Lu et al., 2020; Sánchez-Zurano et al., 2020), while potassium chlorate ($KClO_3$) inhibit the second step of nitrification (Rossi et al., 2020b). ATU does not affect microalgae significantly. As AOB growth is inhibited when ATU is added, nitrite will not be produced and NOB will thus be limited indirectly due to nutrient scarcity, favouring microalgae growth.

7.7. CONCLUSIONS

When operating mixed microalgae-bacteria systems using feeding media where ammonium is the main nitrogen source, the competition between microalgae and AOB for ammonium uptake is expected. Depending on the final goal of the wastewater

treatment process, the growth of one organism or another will be pursued. When nutrient removal and biomass productivity are to be maximised, microalgae activity will be favoured. On the other hand, significant nitrification will be desired when ammonium influent concentration is high (as in centrates) in order to reduce ammonium toxicity and the overall aeration needs of the treatment plant.

The activity of both microalgae and nitrifying bacteria can vary significantly with different medium characteristics and ambient and operational conditions, affecting equilibrium. Some of the important factors that influence (either directly or indirectly) microalgae-AOB competition are: temperature, light, nitrogen concentration (and the distribution of nitrogen species), pH, and dilution rate. Modifying these factors can thus help to improve process performance by maximising/minimising microalgae activity and/or nitrification. In this respect, some system control options are the following: I) control of culture temperature; II) control of SRT/HRT; III) temporary increase of dilution rate; IV) control of nutrient loading rates; and V) adding nitrification inhibitors to the culture. However, some of these operations can increase operating costs and affect the microalgae cultivation system and should be carefully evaluated.

To assess microalgae-nitrifying bacteria competition, most of the commonly used methods focus on measuring either microalgae or nitrifying bacteria activity (or concentration). For instance, photosynthetic efficiency and Chlorophyll fluorescence parameters are specific indicators of microalgae activity, while NO_2/NO_3 concentrations and nitrification rate are indicators of nitrifying bacteria activity. With respect to nutrient removal, biomass productivity, optical density and pH dynamics, despite being a result of both microalgae and bacteria activities, they are strongly influenced by microalgae in most microalgae-based systems, while respirometries can clearly distinguish between the activity of both microorganisms. Several of these methods should be combined to improve the wastewater treatment process by microalgae-AOB cultivation. Similarly, most methods of analysing the culture biomass concentration are based on either

microalgae (Chlorophyll concentration, cell counting and optical density) or bacteria (FISH, flow cytometry and DNA analysis).

REFERENCES

Acién, F.G., Gómez-Serrano, C., Morales-Amaral, M.M., Fernández-Sevilla, J.M., Molina-Grima, E., 2016. Wastewater treatment using microalgae: how realistic a contribution might it be to significant urban wastewater treatment? Appl. Microbiol. Biotechnol. 2016 10021 100, 9013–9022. https://doi.org/10.1007/S00253-016-7835-7

Akizuki, S., Cuevas-rodríguez, G., Toda, T., 2020a. Jo ur na l P re of. ECSN 127948. https://doi.org/10.1016/j.chemosphere.2020.127948

Akizuki, S., Cuevas-Rodríguez, G., Toda, T., 2021. Nitrification of anaerobic digestate using a consortium of microalgae and nitrifiers in an open photobioreactor with moving bed carriers. Chemosphere 263, 127948. https://doi.org/10.1016/J.CHEMOSPHERE.2020.127948

Akizuki, S., Kishi, M., Cuevas-Rodríguez, G., Toda, T., 2020b. Effects of different light conditions on ammonium removal in a consortium of microalgae and partial nitrifying granules. Water Res. https://doi.org/10.1016/j.watres.2019.115445

Alcántara, C., Muñoz, R., Norvill, Z., Plouviez, M., Guieysse, B., 2015. Nitrous oxide emissions from high rate algal ponds treating domestic wastewater. Bioresour. Technol. 177, 110–117. https://doi.org/10.1016/j.biortech.2014.10.134

Amaral-Zettler, L.A., McCliment, E.A., Ducklow, H.W., Huse, S.M., 2009. A method for studying protistan diversity using massively parallel sequencing of V9 hypervariable regions of small-subunit ribosomal RNA Genes. PLoS One 4. https://doi.org/10.1371/journal.pone.0006372

Andrade, G.A. De, Berenguel, M., Guzmán, J.L., Pagano, D.J., Acién, F.G., 2016. Optimization of biomass production in outdoor tubular photobioreactors. J. Process Control 37, 58–69. https://doi.org/10.1016/j.jprocont.2015.10.001

Anthonisen, A.C., Loehr, R.C., Prakasam, T.B.S., Srinath, E.G., 1976. Inhibition of Nitrification by Ammonia and Nitrous Acid. J. (Water Pollut. Control Fed. 48, 835–852.

APHA, AWWA, WEF, 2005. Standard Methods for the Examination of Water and Wastewater, 21st ed, American Public Health Association. Washington, DC.

Arbib, Z., Ruiz, J., Álvarez-díaz, P., Garrido-pérez, C., Barragan, J., Perales, J.A., 2013. Long term outdoor operation of a tubular airlift pilot photobioreactor and a high rate algal pond as tertiary treatment of urban wastewater. Ecol. Eng. 52, 143–153. https://doi.org/10.1016/j.ecoleng.2012.12.089

Assunção, J., Malcata, F.X., 2020. Enclosed “non-conventional” photobioreactors for microalga production: A review. Algal Res. 52. https://doi.org/10.1016/j.algal.2020.102107

Baker, N.R., 2008. Chlorophyll fluorescence: A probe of photosynthesis in vivo. Annu. Rev. Plant Biol. https://doi.org/10.1146/annurev.arplant.59.032607.092759

Bankston, E., Wang, Q., Higgins, B.T., 2020. Algae support populations of heterotrophic, nitrifying, and phosphate-accumulating bacteria in the treatment of poultry litter anaerobic digestate. Chem. Eng. J. 2020, Vol. 398, Page 125550 398, 125550. https://doi.org/10.1016/J.CEJ.2020.125550

Barbera, E., Sforza, E., Grandi, A., Bertucco, A., 2020. Uncoupling solid and hydraulic retention time in photobioreactors for microalgae mass production: A model-based analysis. Chem. Eng. Sci. 218. https://doi.org/10.1016/j.ces.2020.115578

Barceló-Villalobos, M., Fernández-del Olmo, P., Guzmán, J.L., Fernández-Sevilla, J.M., Acién Fernández, F.G., 2019. Evaluation of photosynthetic light integration by microalgae in a pilot-scale raceway reactor. Bioresour. Technol. 280, 404–411. https://doi.org/https://doi.org/10.1016/j.biortech.2019.02.032

Baroni, É.G., Yap, K.Y., Webley, P.A., Scales, P.J., Martin, G.J.O., 2019. The effect of nitrogen depletion on the cell size, shape, density and gravitational settling of Nannochloropsis salina, Chlorella sp. (marine) and Haematococcus pluvialis. Algal Res. 39, 101454. https://doi.org/10.1016/J.ALGAL.2019.101454

Barreiro-Vescovo, S., González-Fernández, C., Ballesteros, M., de Godos, I., 2020. Activity determination of an algal-bacterial consortium developed during wastewater treatment based on oxygen evolution. J. Water Process Eng. 36, 101278. https://doi.org/10.1016/j.jwpe.2020.101278

Bellucci, M., Marazzi, F., Ficara, E., Mezzanotte, V., 2020. Effect of N:P ratio on microalgae/nitrifying bacteria community in agro-digestate treatment. Environ. Clim. Technol. 24, 136–148. https://doi.org/10.2478/rtuect-2020-0061

Blackburne, R., Vadivelu, V.M., Yuan, Z., Keller, J., 2007. Kinetic characterisation of an enriched Nitrospira culture with comparison to Nitrobacter. Water Res. 41, 3033–3042. https://doi.org/10.1016/j.watres.2007.01.043

Caia, M., Bernard, O., Béchet, Q., 2018. Optimizing CO 2 transfer in algal open ponds. Algal Res. 35, 530–538. https://doi.org/10.1016/j.algal.2018.09.009

Chase, M.W., Cowan, R.S., Hollingsworth, P.M., Van Den Berg, C., Madriñán, S., Petersen, G., Seberg, O., Jørgsensen, T., Cameron, K.M., Carine, M., Pedersen, N., Hedderson, T.A.J., Conrad, F., Salazar, G.A., Richardson, J.E., Hollingsworth, M.L., Barraclough, T.G., Kelly, L., Wilkinson, M., 2007. A proposal for a standardised protocol to barcode all land plants. Taxon. https://doi.org/10.1002/tax.562004

Chen, X., Goh, Q.Y., Tan, W., Hossain, I., Chen, W.N., Lau, R., 2011. Bioresource Technology Lumostatic strategy for microalgae cultivation utilizing image analysis and chlorophyll a content as design parameters. Bioresour. Technol. 102, 6005–6012. https://doi.org/10.1016/j.biortech.2011.02.061

Choi, O., Das, A., Yu, C.P., Hu, Z., 2010. Nitrifying bacterial growth inhibition in the presence of algae and cyanobacteria. Biotechnol. Bioeng. 107, 1004–1011. https://doi.org/10.1002/bit.22860

Claros, J., Jiménez, E., Aguado, D., Ferrer, J., Seco, A., Serralta, J., 2013. Effect of pH and HNO2 concentration on the activity of ammonia-oxidizing bacteria in a partial nitritation reactor. Water Sci. Technol. 67, 2587–2594. https://doi.org/10.2166/wst.2013.132

Coggins, L.X., Larma, I., Hinchliffe, A., Props, R., Ghadouani, A., 2020. Flow cytometry for rapid characterisation of microbial community dynamics in waste stabilisation ponds. Water Res. 169. https://doi.org/10.1016/j.watres.2019.115243

Cuevas-Castillo, G.A., Navarro-Pineda, F.S., Baz Rodríguez, S.A., Sacramento Rivero, J.C., 2020. Advances on the processing of microalgal biomass for energy-driven biorefineries. Renew. Sustain. Energy Rev. 125, 109606. https://doi.org/10.1016/j.rser.2019.109606

Daims, H., Brühl, A., Amann, R., Schleifer, K.H., Wagner, M., 1999. The domain-specific probe EUB338 is insufficient for the detection of all bacteria: Development and evaluation of a more comprehensive probe set. Syst. Appl. Microbiol. 22, 434–444. https://doi.org/10.1016/S0723-2020(99)80053-8

Dashkova, V., Malashenkov, D., Poulton, N., Vorobjev, I., Barteneva, N.S., 2017. Imaging flow cytometry for phytoplankton analysis. Methods 112, 188–200. https://doi.org/10.1016/j.ymeth.2016.05.007

Davis, C., 2014. Enumeration of probiotic strains: Review of culture-dependent and alternative techniques to quantify viable bacteria. J. Microbiol. Methods 103, 9–17. https://doi.org/10.1016/j.mimet.2014.04.012

Day, J.G., Gong, Y., Hu, Q., 2017. Microzooplanktonic grazers – A potentially devastating threat to the commercial success of microalgal mass culture. Algal Res. 27, 356–365. https://doi.org/10.1016/j.algal.2017.08.024

De-luca, R., Trabuio, M., Barolo, M., Bezzo, F., 2018. Microalgae growth optimization in open ponds with uncertain weather data. Comput. Chem. Eng. 117, 410–419. https://doi.org/10.1016/j.compchemeng.2018.07.005

Delattre, C., Pierre, G., Laroche, C., Michaud, P., 2016. Production , extraction and characterization of microalgal and cyanobacterial exopolysaccharides. Biotechnol. Adv. 34, 1159–1179. https://doi.org/10.1016/j.biotechadv.2016.08.001

Deng, M., Chen, J., Gou, J., Hou, J., Li, D., He, X., 2018. The effect of different carbon sources on water quality, microbial community and structure of biofloc systems. Aquaculture 482, 103–110. https://doi.org/10.1016/j.aquaculture.2017.09.030

Di Caprio, F., 2020. Methods to quantify biological contaminants in microalgae cultures. Algal Res. https://doi.org/10.1016/j.algal.2020.101943

Eze, V.C., Velasquez-Orta, S.B., Hernández-García, A., Monje-Ramírez, I., Orta-Ledesma, M.T., 2018. Kinetic modelling of microalgae cultivation for wastewater treatment and carbon dioxide sequestration. Algal Res. 32, 131–141. https://doi.org/10.1016/j.algal.2018.03.015

Faleschini, M., Esteves, J.L., Valero, M.A.C., 2012. The effects of hydraulic and organic loadings on the performance of a full-scale facultative pond in a temperate climate region (Argentine Patagonia). Water. Air. Soil Pollut. 223, 2483–2493. https://doi.org/10.1007/s11270-011-1041-0

Fallahi, A., Rezvani, F., Asgharnejad, H., Khorshidi, E., Hajinajaf, N., Higgins, B., 2021. Interactions of microalgae-bacteria consortia for nutrient removal from wastewater: A review. Chemosphere 272, 129878. https://doi.org/10.1016/J.CHEMOSPHERE.2021.129878

Fawley, M.W., Fawley, K.P., 2020. Identification of eukaryotic microalgal strains. J. Appl. Phycol. 32, 2699–2709. https://doi.org/10.1007/s10811-020-02190-5

Fernández, I., Acién, F.G., Guzmán, J.L., Berenguel, M., Mendoza, J.L., 2016. Dynamic model of an industrial raceway reactor for microalgae production. Algal Res. 17, 67–78. https://doi.org/10.1016/j.algal.2016.04.021

Foladori, P., Bruni, L., Tamburini, S., Ziglio, G., 2010. Direct quantification of bacterial biomass in influent, effluent and activated sludge of wastewater treatment plants by using flow cytometry. Water Res. 44, 3807–3818. https://doi.org/10.1016/j.watres.2010.04.027

Galès, A., Bonnafous, A., Carré, C., Jauzein, V., Lanouguère, E., Le, E., Pinoit, J., Poullain, C., Roques, C., Sialve, B., Simier, M., Steyer, J., Fouilland, E., 2019a. Importance of ecological interactions during wastewater treatment using High Rate Algal Ponds under di ff erent temperate climates. Algal Res. 40, 101508. https://doi.org/10.1016/j.algal.2019.101508

Galès, A., Bonnafous, A., Carré, C., Jauzein, V., Lanouguère, E., Le Floc'h, E., Pinoit, J., Poullain, C., Roques, C., Sialve, B., Simier, M., Steyer, J.P., Fouilland, E., 2019b. Importance of ecological interactions during wastewater treatment using High Rate Algal Ponds under different temperate climates. Algal Res. 40, 101508. https://doi.org/10.1016/j.algal.2019.101508

Garner, E., Davis, B.C., Milligan, E., Blair, M.F., Keenum, I., Maile-Moskowitz, A., Pan, J., Gnegy, M., Liguori, K., Gupta, S., Prussin, A.J., Marr, L.C., Heath, L.S., Vikesland, P.J., Zhang, L., Pruden, A., 2021. Next generation sequencing approaches to evaluate water and wastewater quality. Water Res. 194, 116907. https://doi.org/10.1016/j.watres.2021.116907

Gilch, S., Meyer, O., Schmidt, I., 2009. A soluble form of ammonia monooxygenase in Nitrosomonas europaea. Biol. Chem. 390, 863–873. https://doi.org/10.1515/BC.2009.085

González-Camejo, J., Aparicio, S., Jiménez-Benítez, A., Pachés, M., Ruano, M. V, Borrás, L., Barat, R., Seco, A., 2020a. Improving membrane photobioreactor performance by reducing light path: operating conditions and key performance indicators. Water Res. 172. https://doi.org/10.1016/j.watres.2020.115518

González-Camejo, J., Aparicio, S., Ruano, M. V., Borrás, L., Barat, R., Ferrer, J., 2019a. Effect of ambient temperature variations on an indigenous microalgae-nitrifying bacteria culture dominated by Chlorella. Bioresour. Technol. 290, 121788. https://doi.org/10.1016/j.biortech.2019.121788

González-Camejo, J., Barat, R., Aguado, D., Ferrer, J., 2020b. Continuous 3-year outdoor operation of a flat-panel membrane photobioreactor to treat effluent from an anaerobic membrane bioreactor. Water Res. 169. https://doi.org/10.1016/j.watres.2019.115238

González-Camejo, J, Barat, R., Pachés, M., Murgui, M., Seco, A., Ferrer, J., 2018. Wastewater nutrient removal in a mixed microalgae–bacteria culture: effect of light and temperature on the microalgae–bacteria competition. Environ. Technol. (United Kingdom) 39, 503–515. https://doi.org/10.1080/09593330.2017.1305001

González-Camejo, J., Barat, R., Ruano, M. V., Seco, A., Ferrer, J., 2018. Outdoor flat-panel membrane photobioreactor to treat the effluent of an anaerobic membrane bioreactor. Influence of operating, design, and environmental conditions. Water Sci. Technol. 78, 195–206. https://doi.org/10.2166/WST.2018.259

González-Camejo, J., Ferrer, J., Seco, A., Barat, R., 2021. Outdoor microalgae-based urban wastewater treatment: Recent advances, applications, and future perspectives. Wiley Interdiscip. Rev. Water. https://doi.org/10.1002/wat2.1518

González-Camejo, J., Jiménez-Benítez, A., Ruano, M.V., Robles, A., Barat, R., Ferrer, J., 2019b. Preliminary data set to assess the performance of an outdoor membrane photobioreactor. Data Br. 27. https://doi.org/10.1016/j.dib.2019.104599

González-Camejo, J., Jiménez-Benítez, A., Ruano, M. V., Robles, A., Barat, R., Ferrer, J., 2019c. Optimising an outdoor membrane photobioreactor for tertiary sewage treatment. J. Environ. Manage. 245, 76–85. https://doi.org/10.1016/j.jenvman.2019.05.010

González-Camejo, J., Montero, P., Aparicio, S., Ruano, M. V., Borrás, L., Seco, A., Barat, R., 2020c. Nitrite inhibition of microalgae induced by the competition between microalgae and nitrifying bacteria. Water Res. 172, 115499. https://doi.org/10.1016/j.watres.2020.115499

González-Camejo, J, Pachés, M., Marín, A., Jiménez-Benítez, A., Seco, A., Barat, R., 2020a. Production of microalgal external organic matter in a Chlorella-dominated culture: influence of temperature and stress factors. Environ. Sci. Water Res. Technol. 6, 1828–1841. https://doi.org/10.1039/D0EW00176G

González-Camejo, J, Robles, A., Seco, A., Ferrer, J., Ruano, M. V, 2020b. On-line monitoring of photosynthetic activity based on pH data to assess microalgae cultivation. J. Environ. Manage. 276. https://doi.org/10.1016/j.jenvman.2020.111343

Goswami, R.K., Mehariya, S., Verma, P., Lavecchia, R., Zuorro, A., 2021. Microalgae-based biorefineries for sustainable resource recovery from wastewater. J. Water Process Eng. 40, 101747. https://doi.org/10.1016/j.jwpe.2020.101747

Griffiths, M.J., Garcin, C., van Hille, R.P., Harrison, S.T.L., 2011. Interference by pigment in the estimation of microalgal biomass concentration by optical density. J. Microbiol. Methods 85, 119–123. https://doi.org/10.1016/j.mimet.2011.02.005

Guerrero, M.A., Jones, R.D., 1996. Photoinhibition of marine nitrifying bacteria. I. Wavelength-dependent response. Mar. Ecol. Prog. Ser. 141, 183–192. https://doi.org/10.3354/meps141183

Gupta, S., Pawar, S.B., Pandey, R.A., 2019. Current practices and challenges in using microalgae for treatment of nutrient rich wastewater from agro-based industries. Sci. Total Environ. 687, 1107–1126. https://doi.org/10.1016/j.scitotenv.2019.06.115

Hall, J.D., Fučíková, K., Lo, C., Lewis, L.A., Karol, K.G., 2010. An assessment of proposed DNA barcodes in freshwater green algae. Cryptogam. Algol. 31, 529–555.

Han, Y., Gu, Y., Zhang, A.C., Lo, Y.H., 2016. Review: Imaging technologies for flow cytometry. Lab Chip. https://doi.org/10.1039/c6lc01063f

Haridas, V., Ranjbar, S., Vorobjev, I.A., Goldfeld, A.E., Barteneva, N.S., 2017. Imaging flow cytometry analysis of intracellular pathogens. Methods. https://doi.org/10.1016/j.ymeth.2016.09.007

Harmon, J., Mikami, H., Kanno, H., Ito, T., Goda, K., 2020. Accurate classification of microalgae by intelligent frequency-division-multiplexed fluorescence imaging flow cytometry. OSA Contin. 3, 430. https://doi.org/10.1364/osac.387523

Havlik, I., Lindner, P., Scheper, T., Reardon, K.F., 2013. On-line monitoring of large cultivations of microalgae and cyanobacteria. Trends Biotechnol. https://doi.org/10.1016/j.tibtech.2013.04.005

Hosoi-Tanabe, S., Sako, Y., 2006. Development and application of fluorescence in situ hybridization (FISH) method for simple and rapid identification of the toxic dinoflagellates Alexandrium tamarense and Alexandrium catenella in cultured and natural seawater. Fish. Sci. 72, 77–82. https://doi.org/10.1111/j.1444-2906.2006.01119.x

Hosoi-Tanabe, S., Sako, Y., 2005. Rapid detection of natural cells of Alexandrium tamarense and A. catenella (Dinophyceae) by fluorescence in situ hybridization. Harmful Algae 4, 319–328. https://doi.org/10.1016/j.hal.2004.04.002

Huang, J., Hankamer, B., Yarnold, J., 2019. Design scenarios of outdoor arrayed cylindrical photobioreactors for microalgae cultivation considering solar radiation and temperature. Algal Res. 41, 101515. https://doi.org/10.1016/j.algal.2019.101515

Hussain, F., Shah, S.Z., Ahmad, H., Abubshait, S.A., Abubshait, H.A., Laref, A., Manikandan, A., Kusuma, H.S., Iqbal, M., 2021. Microalgae an ecofriendly and sustainable wastewater treatment option: Biomass application in biofuel and bio-fertilizer production. A review. Renew. Sustain. Energy Rev. 137, 110603. https://doi.org/10.1016/j.rser.2020.110603

Hyka, P., Lickova, S., Přibyl, P., Melzoch, K., Kovar, K., 2013. Flow cytometry for the development of biotechnological processes with microalgae. Biotechnol. Adv. https://doi.org/10.1016/j.biotechadv.2012.04.007

Islam, G.M., Vi, P., Gilbride, K.A., 2019. Functional relationship between ammonia-oxidizing bacteria and ammonia-oxidizing archaea populations in the secondary treatment system of a full-scale municipal wastewater treatment plant. J. Environ. Sci. (China) 86, 120–130. https://doi.org/10.1016/j.jes.2019.04.031

Jalali, Mehdi, Zaborowska, J., Jalali, Morteza, 2017. The Polymerase Chain Reaction: PCR, qPCR, and RT-PCR, in: Basic Science Methods for Clinical Researchers. Elsevier Inc., pp. 1–18. https://doi.org/10.1016/B978-0-12-803077-6.00001-1

Jiménez, E., 2010. Mathematical modelling of the two-stage nitrification process. Developement of modelling calibration methodologies for a SHARON reactor and activated sludge process. Polytechnic University of Valencia, Spain.

Jiménez, E., Giménez, J.B., Ruano, M. V., Ferrer, J., Serralta, J., 2011. Effect of pH and nitrite concentration on nitrite oxidation rate. Bioresour. Technol. 102, 8741–8747. https://doi.org/10.1016/j.biortech.2011.07.092

Johnson, J.S., Spakowicz, D.J., Hong, B.Y., Petersen, L.M., Demkowicz, P., Chen, L., Leopold, S.R., Hanson, B.M., Agresta, H.O., Gerstein, M., Sodergren, E., Weinstock, G.M., 2019. Evaluation of 16S rRNA gene sequencing for species and strain-level microbiome analysis. Nat. Commun. 10. https://doi.org/10.1038/s41467-019-13036-1

Kalyuzhnaya, M.G., Zabinsky, R., Bowerman, S., Baker, D.R., Lidstrom, M.E., Chistoserdova, L., 2006. Fluorescence in situ hybridization-flow cytometry-cell sorting-based method for separation and enrichment of type I and type II methanotroph populations. Appl. Environ. Microbiol. 72, 4293–4301. https://doi.org/10.1128/AEM.00161-06

Kowalska, Z., Pniewski, F., Latała, A., 2019. DNA barcoding – A new device in phycologist's toolbox. Ecohydrol. Hydrobiol. https://doi.org/10.1016/j.ecohyd.2019.01.002

Kumar, A., Bera, S., 2020. Jo ur l P re of. Bioresour. Technol. Reports 100584. https://doi.org/10.1016/j.biteb.2020.100584

Kwon, G., Kim, H., Song, C., Jahng, D., 2019. Co-culture of microalgae and enriched nitrifying bacteria for energy-efficient nitrification. Biochem. Eng. J. 152, 107385. https://doi.org/10.1016/j.bej.2019.107385

Lam, T.P., Lee, T.M., Chen, C.Y., Chang, J.S., 2018. Strategies to control biological contaminants during microalgal cultivation in open ponds. Bioresour. Technol. 252, 180–187. https://doi.org/10.1016/j.biortech.2017.12.088

Lee, J., Cho, D.H., Ramanan, R., Kim, B.H., Oh, H.M., Kim, H.S., 2013. Microalgae-associated bacteria play a key role in the flocculation of Chlorella vulgaris. Bioresour. Technol. 131, 195–201. https://doi.org/10.1016/j.biortech.2012.11.130

Lee, Y.J., Lei, Z., 2019. Microalgal-bacterial aggregates for wastewater treatment: A mini-review. Bioresour. Technol. Reports 8, 100199. https://doi.org/10.1016/j.biteb.2019.100199

Leliaert, F., Verbruggen, H., Vanormelingen, P., Steen, F., López-Bautista, J.M., Zuccarello, G.C., De Clerck, O., 2014. DNA-based species delimitation in algae. Eur. J. Phycol. 49, 179–196. https://doi.org/10.1080/09670262.2014.904524

Li, K., Liu, Q., Fang, F., Luo, R., Lu, Q., Zhou, W., Huo, S., Cheng, P., Liu, J., Addy, M., Chen, P., Chen, D., Ruan, R., 2019. Microalgae-based wastewater treatment for nutrients recovery: A review. Bioresour. Technol. 291, 121934. https://doi.org/10.1016/j.biortech.2019.121934

Li, X., Li, W., Zhai, J., Wei, H., Wang, Q., 2019. Effect of ammonium nitrogen on microalgal growth, biochemical composition and photosynthetic performance in mixotrophic cultivation. Bioresour. Technol. 273, 368–376. https://doi.org/10.1016/j.biortech.2018.11.042

Li, Y., Xu, Y., Liu, L., Li, P., Yan, Y., Chen, T., Zheng, T., Wang, H., 2017. Flocculation mechanism of Aspergillus niger on harvesting of Chlorella vulgaris biomass. Algal Res. 25, 402–412. https://doi.org/10.1016/j.algal.2017.06.001

Lin, Z., Huang, W., Zhou, Jiong, He, X., Wang, J., Wang, X., Zhou, Jian, 2020. The variation on nitrogen removal mechanisms and the succession of ammonia oxidizing archaea and ammonia oxidizing bacteria with temperature in biofilm reactors treating saline wastewater. Bioresour. Technol. 314. https://doi.org/10.1016/j.biortech.2020.123760

Lu, S., Liu, X., Liu, C., Cheng, G., Shen, H., 2020. Influence of photoinhibition on nitrification by ammonia-oxidizing microorganisms in aquatic ecosystems. Rev. Environ. Sci. Bio/Technology 19, 531–542. https://doi.org/10.1007/s11157-020-09540-2

Luo, Y., Le-Clech, P., Henderson, R.K., 2020a. Characterisation of microalgae-based monocultures and mixed cultures for biomass production and wastewater treatment. Algal Res. 49. https://doi.org/10.1016/j.algal.2020.101963

Luo, Y., Le-Clech, P., Henderson, R.K., 2020b. Assessing the performance of membrane photobioreactors (MPBR) for polishing effluents containing different types of nitrogen. Algal Res. 50, 102013. https://doi.org/https://doi.org/10.1016/j.algal.2020.102013

Luo, Y., Le-Clech, P., Henderson, R.K., 2018. Assessment of membrane photobioreactor (MPBR) performance parameters and operating conditions. Water Res. 138, 169–180. https://doi.org/10.1016/j.watres.2018.03.050

Manhaeghe, D., Allosserie, A., Rousseau, D.P.L., Van Hulle, S.W.H., 2021. Model based analysis of carbon fluxes within microalgae-bacteria flocs using respirometric-titrimetric data. Sci. Total Environ. 784, 147048. https://doi.org/10.1016/j.scitotenv.2021.147048

Mann, D.G., Sato, S., Trobajo, R., Vanormelingen, P., Souffreau, C., 2010. DNA barcoding for species identification and discovery in diatoms. Cryptogam. Algol. 31, 557–577.

Mantovani, M., Marazzi, F., Fornaroli, R., Bellucci, M., Ficara, E., Mezzanotte, V., 2020. Outdoor pilot-scale raceway as a microalgae-bacteria sidestream treatment in a WWTP. Sci. Total Environ. 710, 135583. https://doi.org/10.1016/J.SCITOTENV.2019.135583

Marazzi, F., Bellucci, M., Rossi, S., Fornaroli, R., Ficara, E., Mezzanotte, V., 2019. Outdoor pilot trial integrating a sidestream microalgae process for the treatment of centrate under non optimal climate conditions. Algal Res. 39, 101430. https://doi.org/10.1016/j.algal.2019.101430

Marcilhac, C., Sialve, B., Pourcher, A.M., Ziebal, C., Bernet, N., Béline, F., 2014. Digestate color and light intensity affect nutrient removal and competition phenomena in a microalgal-bacterial ecosystem. Water Res. 64, 278–287. https://doi.org/10.1016/j.watres.2014.07.012

Markou, G., Dao, L.H.T., Muylaert, K., Beardall, J., 2017. Influence of different degrees of N limitation on photosystem II performance and heterogeneity of Chlorella vulgaris. Algal Res. 26, 84–92. https://doi.org/10.1016/j.algal.2017.07.005

Martinez, C., Mairet, F., Martinon, P., Bernard, O., 2019. Dynamics and control of a periodically forced microalgae culture. IFAC-PapersOnLine 52, 922–927. https://doi.org/10.1016/j.ifacol.2019.06.180

Mazzelli, A., Cicci, A., Di Caprio, F., Altimari, P., Toro, L., Iaquaniello, G., Pagnanelli, F., 2020. Multivariate modeling for microalgae growth in outdoor photobioreactors. Algal Res. 45, 101663. https://doi.org/10.1016/j.algal.2019.101663

Medeiros, R.C., Sammarro Silva, K.J., Daniel, L.A., 2020. Wastewater treatment performance in microbiological removal and (oo)cyst viability assessed comparatively to fluorescence decay. Environ. Technol. (United Kingdom) 0, 1–9. https://doi.org/10.1080/09593330.2020.1811396

Meng, F., Xi, L., Liu, D., Huang, Weiwei, Lei, Z., Zhang, Z., Huang, Wenli, 2019. Effects of light intensity on oxygen distribution, lipid production and biological community of algal-bacterial granules in photo-sequencing batch reactors. Bioresour. Technol. 272, 473–481. https://doi.org/10.1016/j.biortech.2018.10.059

Merbt, S.N., Stahl, D.A., Casamayor, E.O., Martí, E., Nicol, G.W., Prosser, J.I., 2012. Differential photoinhibition of bacterial and archaeal ammonia oxidation. FEMS Microbiol. Lett. 327, 41–46. https://doi.org/10.1111/j.1574-6968.2011.02457.x

Mirek, Z., Bieniek, W., Sztorc, A., 2007. Barkoding DNA-nowe narzędzie do opisu bioróżnorodności.

Mohsenpour, S.F., Hennige, S., Willoughby, N., Adeloye, A., Gutierrez, T., 2021. Integrating micro-algae into wastewater treatment: A review. Sci. Total Environ. 752, 142168. https://doi.org/10.1016/j.scitotenv.2020.142168

Moniz, M.B.J., Kaczmarska, I., 2009. Barcoding diatoms: Is there a good marker? Mol. Ecol. Resour. 9, 65–74. https://doi.org/10.1111/j.1755-0998.2009.02633.x

Morais, C.C., 2018. Nitrification in wastewater treatment at its biological oxygen limit.

Morillas-España, A., Lafarga, T., Gómez-serrano, C., Acién-fernández, F.G., González-lópez, C.V., 2020. Year-long production of Scenedesmus almeriensis in pilot-scale raceway and thin-layer cascade photobioreactors. Algal Res. 51, 102069. https://doi.org/10.1016/j.algal.2020.102069

Munz, G., Lubello, C., Oleszkiewicz, J.A., 2011. Factors affecting the growth rates of ammonium and nitrite oxidizing bacteria. Chemosphere 83, 720–725. https://doi.org/10.1016/j.chemosphere.2011.01.058

Nagarajan, D., Lee, D.J., Chen, C.Y., Chang, J.S., 2020. Resource recovery from wastewaters using microalgae-based approaches: A circular bioeconomy perspective. Bioresour. Technol. 302, 122817. https://doi.org/10.1016/j.biortech.2020.122817

Nielsen, S.L., Hansen, B.W., 2019. Evaluation of the robustness of optical density as a tool for estimation of biomass in microalgal cultivation: The effects of growth conditions and physiological state. Aquac. Res. 50, 2698–2706. https://doi.org/10.1111/are.14227

Nwoba, E.G., Parlevliet, D.A., Laird, D.W., Alameh, K., Moheimani, N.R., 2019. Light management technologies for increasing algal photobioreactor efficiency. Algal Res. 39, 101433. https://doi.org/10.1016/j.algal.2019.101433

Orschler, L., Agrawal, S., Lackner, S., 2019. On resolving ambiguities in microbial community analysis of partial nitritation anammox reactors. Sci. Rep. 9. https://doi.org/10.1038/s41598-019-42882-8

Pachés, M., Martínez-Guijarro, R., González-Camejo, J., Seco, A., Barat, R., 2020. Selecting the most suitable microalgae species to treat the effluent from an anaerobic membrane bioreactor. Environ. Technol. (United Kingdom) 41. https://doi.org/10.1080/09593330.2018.1496148

Pachés, M., Romero, I., Hermosilla, Z., Martinez-Guijarro, R., 2012. PHYMED: An ecological classification system for the Water Framework Directive based on phytoplankton community composition. Ecol. Indic. 19, 15–23. https://doi.org/https://doi.org/10.1016/j.ecolind.2011.07.003

Petrini, S., Foladori, P., Donati, L., Andreottola, G., 2020. Comprehensive respirometric approach to assess photosynthetic, heterotrophic and nitrifying activity in microalgal-bacterial consortia treating real municipal wastewater. Biochem. Eng. J. 161. https://doi.org/10.1016/j.bej.2020.107697

Rada-Ariza, A.M., Fredy, D., Lopez-Vazquez, C.M., Van der Steen, N.P., Lens, P.N.L., 2019. Ammonium removal mechanisms in a microalgal-bacterial sequencing-batch photobioreactor at different solids retention times. Algal Res. 39, 101468. https://doi.org/10.1016/j.algal.2019.101468

Rada-Ariza, A.M., Lopez-Vazquez, C.M., van der Steen, N.P., Lens, P.N.L., 2017. Nitrification by microalgal-bacterial consortia for ammonium removal in flat panel sequencing batch photo-bioreactors. Bioresour. Technol. 245, 81–89. https://doi.org/10.1016/j.biortech.2017.08.019

Raeisossadati, M., Moheimani, N.R., Parlevliet, D., 2019. Luminescent solar concentrator panels for increasing the efficiency of mass microalgal production. Renew. Sustain. Energy Rev. 101, 47–59. https://doi.org/10.1016/J.RSER.2018.10.029

Rajesh Banu, J., Preethi, Kavitha, S., Gunasekaran, M., Kumar, G., 2020. Microalgae based biorefinery promoting circular bioeconomy-techno economic and life-cycle analysis. Bioresour. Technol. 302, 122822. https://doi.org/10.1016/j.biortech.2020.122822

Ras, M., Steyer, J.P., Bernard, O., 2013. Temperature effect on microalgae: A crucial factor for outdoor production. Rev. Environ. Sci. Biotechnol. 12, 153–164. https://doi.org/10.1007/s11157-013-9310-6

Reichert, P., Borchardt, D., Henze, M., Rauch, W., Shanahan, P., Somlyódy, L., Vanrolleghem, P., 2001. River Water Quality Model no. 1 (RWQM1): II. Biochemical process equations, in: Water Science and Technology. pp. 11–30. https://doi.org/10.2166/wst.2001.0241

Reynolds, C.S., 2006. The ecology of phytoplankton, The Ecology of Phytoplankton. Cambridge University Press, Cambridge. https://doi.org/10.1017/CBO9780511542145

Robles, Á., Capson-Tojo, G., Galès, A., Ruano, M.V., Sialve, B., Ferrer, J., Steyer, J.P., 2020. Microalgae-bacteria consortia in high-rate ponds for treating urban wastewater: Elucidating the key state indicators under dynamic conditions. J. Environ. Manage. 261. https://doi.org/10.1016/j.jenvman.2020.110244

Robles, Á., Capson-tojo, G., Gales, A., Viruela, A., Sialve, B., Seco, A., Steyer, J., Ferrer, J., 2019. Performance of a membrane-coupled high-rate algal pond for urban wastewater treatment at demonstration scale. Bioresour. Technol. 122672. https://doi.org/10.1016/j.biortech.2019.122672

Romero-Villegas, G.I., Fiamengo, M., Acién Fernández, F.G., Molina Grima, E., 2018. Utilization of centrate for the outdoor production of marine microalgae at pilot-scale in flat-panel photobioreactors. J. Biotechnol. 284, 102–114. https://doi.org/10.1016/j.jbiotec.2018.08.006

Romero Villegas, G.I., Fiamengo, M., Acién Fernández, F.G., Molina Grima, E., 2017. Outdoor production of microalgae biomass at pilot-scale in seawater using centrate as the nutrient source. Algal Res. 25, 538–548. https://doi.org/10.1016/j.algal.2017.06.016

Rossi, S., Bellucci, M., Marazzi, F., Mezzanotte, V., Ficara, E., 2018. Activity assessment of microalgal-bacterial consortia based on respirometric tests. Water Sci. Technol. 78, 207–215. https://doi.org/10.2166/wst.2018.078

Rossi, S., Casagli, F., Mantovani, M., Mezzanotte, V., Ficara, E., 2020a. Selection of photosynthesis and respiration models to assess the effect of environmental conditions on mixed microalgae consortia grown on wastewater. Bioresour. Technol. 305, 122995. https://doi.org/10.1016/J.BIORTECH.2020.122995

Rossi, Simone, Díez-Montero, R., Rueda, E., Castillo Cascino, F., Parati, K., García, J., Ficara, E., 2020. Free ammonia inhibition in microalgae and cyanobacteria grown in wastewaters: Photo-respirometric evaluation and modelling. Bioresour. Technol. 305, 123046. https://doi.org/10.1016/j.biortech.2020.123046

Rossi, S., Sforza, E., Pastore, M., Bellucci, M., Casagli, F., Marazzi, F., Ficara, E., 2020b. Photo-respirometry to shed light on microalgae-bacteria consortia—a review. Rev. Environ. Sci. Biotechnol. https://doi.org/10.1007/s11157-020-09524-2

Rotthauwe, J.H., Witzel, K.P., Liesack, W., 1997. The ammonia monooxygenase structural gene amoa as a functional marker: Molecular fine-scale analysis of natural ammonia-oxidizing populations. Appl. Environ. Microbiol. 63, 4704–4712. https://doi.org/10.1128/aem.63.12.4704-4712.1997

Ruiz, J., Álvarez-Díaz, P.D., Arbib, Z., Garrido-Pérez, C., Barragán, J., Perales, J.A., 2013. Performance of a flat panel reactor in the continuous culture of microalgae in urban wastewater: Prediction from a batch experiment. Bioresour. Technol. 127, 456–463. https://doi.org/10.1016/J.BIORTECH.2012.09.103

Sánchez-Zurano, A, Cárdenas, J.A.G., Serrano, C.G., Amaral, M.M., Acién-fernández, F.G., Sevilla, J.M.F., Grima, E.M., 2020. Year-long assessment of a pilot-scale thin-layer reactor for microalgae wastewater treatment . Variation in the microalgae-bacteria consortium and the impact of environmental conditions. Algal Res. 50, 101983. https://doi.org/10.1016/j.algal.2020.101983

Sánchez-Zurano, A., Gómez-Serrano, C., Acién-Fernández, F.G., Fernández-Sevilla, J.M., Molina-Grima, E., 2020. A novel photo-respirometry method to characterize consortia in microalgae-related wastewater treatment processes. Algal Res. 47, 101858. https://doi.org/10.1016/j.algal.2020.101858

Sanz, J.L., Köchling, T., 2007. Molecular biology techniques used in wastewater treatment: An overview. Process Biochem. https://doi.org/10.1016/j.procbio.2006.10.003

Sarvajith, M., Kiran Kumar Reddy, G., Nancharaiah, Y. V., 2020. Aerobic granular sludge for high-strength ammonium wastewater treatment: Effect of COD/N ratios, long-term stability and nitrogen removal pathways. Bioresour. Technol. 306. https://doi.org/10.1016/j.biortech.2020.123150

Sato, M., Murata, Y., Mizusawa, M., 2004. A Simple and Rapid Dual-fluorescence Viability Assay for Microalgae 20.

Sayedin, F., Kermanshahi-pour, A., He, Q.S., Tibbetts, S.M., Lalonde, C.G.E., Brar, S.K., 2020. Microalgae cultivation in thin stillage anaerobic digestate for nutrient recovery and bioproduct production. Algal Res. 47, 101867. https://doi.org/10.1016/j.algal.2020.101867

Seco, A., Aparicio, S., González-Camejo, J., Jiménez-Benítez, A., Mateo, O., Mora, J.F., Noriega-Hevia, G., Sanchis-Perucho, P., Serna-García, R., Zamorano-López, N., Giménez, J.B., Ruiz-Martínez, A., Aguado, D., Barat, R., Borrás, L., Bouzas, A., Martí, N., Pachés, M., Ribes, J., Robles, A., Ruano, M. V., Serralta, J., Ferrer, J., 2018. Resource recovery from sulphate-rich sewage through an innovative anaerobic-based water resource recovery facility (WRRF). Water Sci. Technol. 78, 1925–1936. https://doi.org/10.2166/wst.2018.492

Sepehri, A., Sarrafzadeh, M.H., Avateffazeli, M., 2020. Interaction between Chlorella vulgaris and nitrifying-enriched activated sludge in the treatment of wastewater with low C/N ratio. J. Clean. Prod. 247, 119164. https://doi.org/10.1016/J.JCLEPRO.2019.119164

Serra-Maia, R., Bernard, O., Gonçalves, A., Bensalem, S., Lopes, F., 2016. Influence of temperature on Chlorella vulgaris growth and mortality rates in a photobioreactor. Algal Res. 18, 352–359. https://doi.org/10.1016/j.algal.2016.06.016

Shahid, A., Malik, S., Zhu, H., Xu, J., Nawaz, M.Z., Nawaz, S., Asraful Alam, M., Mehmood, M.A., 2020. Cultivating microalgae in wastewater for biomass production, pollutant removal, and atmospheric carbon mitigation; a review. Sci. Total Environ. 704, 135303. https://doi.org/10.1016/j.scitotenv.2019.135303

Soares, R.B., Martins, M.F., Gonçalves, R.F., 2019. A conceptual scenario for the use of microalgae biomass for microgeneration in wastewater treatment plants. J. Environ. Manage. 252, 109639. https://doi.org/10.1016/j.jenvman.2019.109639

Solovchenko, A., Khozin-goldberg, I., Selyakh, I., Semenova, L., Ismagulova, T., Lukyanov, A., Mamedov, I., Vinogradova, E., Karpova, O., Konyukhov, I., Vasilieva, S., Mojzes, P., Dijkema, C., Vecherskaya, M., Zvyagin, I., Nedbal, L., Gorelova, O., 2019. Phosphorus starvation and luxury uptake in green microalgae revisited. Algal Res. 43, 101651. https://doi.org/10.1016/j.algal.2019.101651

Steichen, S.A., Brown, J.K., 2019. Real-time quantitative detection of Vampirovibrio chlorellavorus, an obligate bacterial pathogen of Chlorella sorokiniana. J. Appl. Phycol. 31, 1117–1129. https://doi.org/10.1007/s10811-018-1659-z

Straka, L., Rittmann, B.E., 2018. Light-dependent kinetic model for microalgae experiencing photoacclimation , photodamage , and photodamage repair. Algal Res. 31, 232–238. https://doi.org/10.1016/j.algal.2018.02.022

Su, Y., 2021. Revisiting carbon, nitrogen, and phosphorus metabolisms in microalgae for wastewater treatment. Sci. Total Environ. 762, 144590. https://doi.org/10.1016/j.scitotenv.2020.144590

Sutherland, D.L., Park, J., Ralph, P.J., Craggs, R.J., 2020. Improved microalgal productivity and nutrient removal through operating wastewater high rate algal ponds in series. Algal Res. 47, 101850. https://doi.org/10.1016/j.algal.2020.101850

Tan, X.B., Zhang, Y.L., Yang, L. Bin, Chu, H.Q., Guo, J., 2016. Outdoor cultures of Chlorella pyrenoidosa in the effluent of anaerobically digested activated sludge: The effects of pH and free ammonia. Bioresour. Technol. 200, 606–615. https://doi.org/10.1016/j.biortech.2015.10.095

Toledo-Cervantes, A., Posadas, E., Bertol, I., Turiel, S., Alcoceba, A., Muñoz, R., 2019. Assessing the influence of the hydraulic retention time and carbon/nitrogen ratio on urban wastewater treatment in a new anoxic-aerobic algal-bacterial photobioreactor configuration. Algal Res. 44, 101672. https://doi.org/10.1016/J.ALGAL.2019.101672

Umamaheswari, J., Shanthakumar, S., 2016. Efficacy of microalgae for industrial wastewater treatment: a review on operating conditions, treatment efficiency and biomass productivity. Rev. Environ. Sci. Biotechnol. https://doi.org/10.1007/s11157-016-9397-7

Vargas, G., Donoso-Bravo, A., Vergara, C., Ruiz-Filippi, G., 2016. Assessment of microalgae and nitrifiers activity in a consortium in a continuous operation and the effect of oxygen depletion. Electron. J. Biotechnol. 23, 63–68. https://doi.org/10.1016/J.EJBT.2016.08.002

Vasseur, C., Bougaran, G., Garnier, M., Hamelin, J., Leboulanger, C., Chevanton, M. Le, Mostajir, B., Sialve, B., Steyer, J.P., Fouilland, E., 2012. Carbon conversion efficiency and population dynamics of a marine algae-bacteria consortium growing on simplified synthetic digestate: First step in a bioprocess coupling algal production and anaerobic digestion. Bioresour. Technol. 119, 79–87. https://doi.org/10.1016/j.biortech.2012.05.128

Vieira, H.H., Bagatini, I.L., Guinart, C.M., Vieira, A.A.H., 2016. tufA gene as molecular marker for freshwater Chlorophyceae. Algae 31, 155–165. https://doi.org/10.4490/algae.2016.31.4.14

Vo, H.N.P., Ngo, H.H., Guo, W., Nguyen, T.M.H., Liu, Yiwen, Liu, Yi, Nguyen, D.D., Chang, S.W., 2019. A critical review on designs and applications of microalgae-based photobioreactors for pollutants treatment. Sci. Total Environ. 651, 1549–1568. https://doi.org/10.1016/j.scitotenv.2018.09.282

Wei, V., Elektorowicz, M., Oleszkiewicz, J.A., 2011. Influence of electric current on bacterial viability in wastewater treatment. Water Res. 45, 5058–5062. https://doi.org/10.1016/j.watres.2011.07.011

Weon, S.Y., Lee, S.I., Koopman, B., 2004. Effect of temperature and dissolved oxygen on biological nitrification at high ammonia concentrations. Environ. Technol. 25, 1211–1219. https://doi.org/10.1080/09593332508618369

Winkler, M.K., Straka, L., 2019. New directions in biological nitrogen removal and recovery from wastewater. Curr. Opin. Biotechnol. 57, 50–55. https://doi.org/10.1016/j.copbio.2018.12.007

Winkler, M.K.H., Boets, P., Hahne, B., Goethals, P., Volcke, E.I.P., 2017. Effect of the dilution rate on microbial competition: R-strategist can win over kstrategist at low substrate concentration. PLoS One 12, 1–12. https://doi.org/10.1371/journal.pone.0172785

Wollmann, F., Dietze, S., Ackermann, J.U., Bley, T., Walther, T., Steingroewer, J., Krujatz, F., 2019. Microalgae wastewater treatment: Biological and technological approaches. Eng. Life Sci. 19, 860–871. https://doi.org/10.1002/elsc.201900071

Wu, D., Cheng, M., Zhao, S., Peng, N., Hu, R., Hu, J., Liang, Y., 2020. Algal Growth Enhances Light-Mediated Limitation of Bacterial Nitrification in an Aquaculture System. Water, Air, Soil Pollut. 231, 73. https://doi.org/10.1007/s11270-020-4436-y

Xu, M., Li, P., Tang, T., Hu, Z., 2015. Roles of SRT and HRT of an algal membrane bioreactor system with a tanks-in-series configuration for secondary wastewater effluent polishing. Ecol. Eng. 85, 257–264. https://doi.org/10.1016/j.ecoleng.2015.09.064

Xu, X., Gu, X., Wang, Zhongyang, Shatner, W., Wang, Zhenjun, 2019. Progress, challenges and solutions of research on photosynthetic carbon sequestration efficiency of microalgae. Renew. Sustain. Energy Rev. 110, 65–82. https://doi.org/10.1016/j.rser.2019.04.050

Yang, S., Wang, J., Cong, W., Cai, Z., Ouyang, F., 2004. Utilization of nitrite as a nitrogen source by Botryococcus braunii. Biotechnol. Lett. 26, 239–243. https://doi.org/10.1023/B:BILE.0000013722.45527.18

Ye, L., Zhang, T., Wang, T., Fang, Z., 2012. Microbial structures, functions, and metabolic pathways in wastewater treatment bioreactors revealed using high-throughput sequencing. Environ. Sci. Technol. 46, 13244–13252. https://doi.org/10.1021/es303454k

Yeo, U., Lee, I., Seo, I., Kim, R., 2018. ScienceDirect Identification of the key structural parameters for the design of a large-scale PBR. Biosyst. Eng. 171, 165–178. https://doi.org/10.1016/j.biosystemseng.2018.04.012

SUPPLEMENTARY DATA FOR CHAPTER VII

Equations

Lambert-Beer equation:

$$I_{av} = \frac{I_0}{K_a \cdot C \cdot L} \cdot \left(1 - e^{-K_a \cdot C \cdot L}\right) \quad \text{(Equation. VII. S 1)}$$

where I_{av} is the light irradiance, I_0 is the light irradiance applied to the PBR surface (μmol·m^{-2}·s^{-1}), C is the biomass concentration (g·m^{-3}), K_a is the extinction coefficient (m^2·g^{-1}), and L is the culture depth (m).

Anthonisen equation (Anthonisen et al., 1976):

$$NH_3 = \frac{NH_4}{1+10^{-pH+0.09018+\frac{2729.92}{T+273}}} \quad \text{(Equation. VII. S 2)}$$

where NH_3 is the ammonia concentration (g N·m^{-3}); NH_4 is the ammonium concentration (mg N·L^{-1}); pH is the pH of the culture and T is the culture temperature (ºC).

Nutrient removal

$$NRE = \frac{N_{inf} - N_{ef}}{N_{inf}} \cdot 100 \quad \text{(Equation. VII. S 3)}$$

$$NRR = \frac{F \cdot (N_{inf} - N_{ef})}{V} \quad \text{(Equation. VII. S 4)}$$

where NRE is the nutrient removal efficiency (%); NRR nutrient removal rate (g·m^{-3}·d^{-1}); F is the treatment flow rate (m^3·d^{-1}); N_{inf} is the influent nutrient concentration (g·m^{-3}); N_{ef} is the effluent nutrient concentration (g·m^{-3}); and V is the reactor volume (m^3).

Biomass productivity

$$BP = \frac{F_w \cdot C_b}{V} \quad \text{(Equation. VII. S 5)}$$

where BP is the biomass productivity (g·m^{-3}·d^{-1}); F_w (L·d^{-1}) is the flow of the biomass wasted with the purge; C_b (g·m^{-3}) is the biomass concentration in the photobioreactors and; V is the volume of the photobioreactors (L).

Photosynthetic efficiency

$$\mathrm{PE} = \frac{\mathrm{BP_m \cdot H}}{\mathrm{I \cdot S \cdot 24 \cdot 3600}} \cdot 100 \qquad \text{(Equation. VII. S 6)}$$

where PE is the photosynthetic efficiency (%); BP_m is the biomass productivity measured as ($g \cdot d^{-1}$); H is the enthalpy of dry biomass (22.9 $KJ \cdot g^{-1}$); I is the total light irradiance ($KJ \cdot m^{-2} \cdot s^{-1}$); and S is the illuminated PBR surface (m^2).

Nitrification rate

$$\mathrm{NOxR} = \frac{\mathrm{F \cdot (NOx_e - NOx_i)}}{\mathrm{V}} \qquad \text{(Equation. VII. S 7)}$$

where NOxR represents the nitrification rate (g $N \cdot m^{-3} \cdot d^{-1}$); F is flow rate of influent wastewater ($m^3 \cdot d^{-1}$); NOx_e is the concentration of NO_2 plus NO_3 in the effluent (g $N \cdot m^{-3}$); NO_{xi} is the concentration of NO_2-N plus NO_3-N in the influent (g $N \cdot m^{-3}$); and V is the volume of the reactor (m^3).

Chlorophyll concentration

$$\mathrm{Chl\ a}\left(\frac{\mathrm{mg}}{\mathrm{L}}\right) = (11.85 \cdot \mathrm{OD}_{664} - 1.54 \cdot \mathrm{OD}_{647} - 0.08 \cdot \mathrm{OD}_{630}) \cdot \frac{\mathrm{Vsolvent}}{\mathrm{Vsample}} \qquad \text{(Equation. VII. S 8)}$$

Where Chl *a* is the concentration of chlorophyll a; OD_{664}, OD_{647} and OD_{630} correspond to optical density at 664, 647 and 630 nm, respectively; V is the volume of solvent or sample.

Tables

Table VII. S. 1. Total and viability stains for bacteria and microalgae. Parameters λex and λem are the maximum excitation and emission wavelength respectively.

Fluorescent dyes	λ_{ex} - λ_{em} (nm)
SYBR Green	495 - 525
SYTO 9	
- for DNA	485 - 498
- for RNA	486 - 501
SYTO 16	
- for DNA	488 - 518
- for RNA	494 - 525
4′,6-diamidino-2-phenylindole or DAPI	358 - 461
Acridine orange	495 - 522
SYTOX Green	504 - 523
Propidium iode or PI	493 - 636
Fluorescein diacetate or FDA	490 - 526

Table VII. S 2. FISH probes used to identify bacteria and AOB.

Probes	Specific	Sequence (5′ → 3′)	References
Eubacteria			
EUB338	Most bacteria	GCTGCCTCCCGTAGGAGT	(Daims et al., 1999)
EUB338-II	Planctomycetales	GCAGCCACCCGTAGGTGT	
EUB338-III	Verrucomicrobiales	GCTGCCACCCGTAGGTGT	
Proteobacteria			
ALF1b	α-Proteobacteria (including Nitrobacter)	CGTTCGYTCTGAGCCAG	(Manz et al., 1992)
BET42a	β-Proteobacteria	GCCTTCCCACTTCGTTT	
GAM42a	γ-Proteobacteria	GCCTTCCCACATCGTTT	
AOB			
Cluster6a192	*Nitrosomonas oligotropha lineage*	CTTTCGATCCCCTACTTTCC	(Adamczyk et al., 2003)
NEU	*Nitrosomonas* spp. Most *halophilic and halotolerant* members	CCCCTCTGCTGCACTCTA	(Wagner et al., 1995)
Nmn657	*Nitrosomonas* spp.	TGGAATTCCACTCCCCTCTG	(Araki et al., 1999)
Nmo218	*Nitrosomonas oligotropha*	CGGCCGCTCCAAAAGCAT	(Gieseke et al., 2001)
NmV	*Nitrosococcus mobilis*	TCCTCAGAGACTACGCGG	(Pommerening-Röser et al., 1996)
Nse1472	*Nitrosomonas europea*, *N. halophila, N. eutropha, Kraftisried*-Isolat Nm103	ACC CCA GTCATG ACC CCC	(Juretschko et al., 1998)

Table VII. S 2. Continued

Probes	**Specific**	**Sequence (5′ → 3′)**	**References**
Nsm156	*Nitrosomonas C-56, Nitrosomonas europaea, Nitrosomonas eutropha, Nitrosococcus mobilis*	TATTAGCACATCTTTCGAT	(Mobarry et al., 1996)
NSMR34	*Nitrosospira tenius*-like	TCCCCCACTCGAAGATACG	(Burrell et al., 2001)
NSMR76	*Nitrosomonas marina*-like	CCCCCCTCTTCTGGATAC	(Burrell et al., 2001)
NSO1225	*β-Subdivision* of AOB	CGCCATTGTATTACGTGTGA	(Mobarry et al., 1996)
NSO190	*β-Subdivision* of AOB	CGATCCCCTGCTTTTCTCC	(Mobarry et al., 1996)
Nsv443	*Nitrosolobus multiformis*	CCGTGACCGTTTCGTTCCG	(Mobarry et al., 1996)

Table VII. S 3. Primers used to identify bacteria and AOB.

Target gene (region)	Primer	Sequence (5'-3')	Reference
16S rRNA (V2)	CTO 189fA/B	GGAGRAAAGCAGGGGATCG	(Hermansson and Lindgren, 2001; Naseer et al., 2013)
16S rRNA (V2)	CTO 189fC	GGAGGAAAGTAGGGGATCG	(Hermansson and Lindgren, 2001; Naseer et al., 2013)
16S rRNA (V2)	RT1R	CGTCCTCTCAGACCARCTACTG	(Hermansson and Lindgren, 2001)
16S rRNA (V2)	CTO 189F CTO654r	GGAGRAAAGYAGGGGATCG CTAGCYTTGTAGTTTCAAACGC	(Deng et al., 2018; Islam et al., 2019)
16S rRNA (V3-V4)	V3F V4R	ACTCCTACGGGAG GCAGCAG TACNVGGGTATCTAATCC	(Wang et al., 2014)
16S rRNA (V3-V4)	338F 806R	ACTCCTACGGGAGGCAGCAG GTGGACTACHVGGGTWTCTAAT	(Lin et al., 2020; Pan et al., 2018)
16S rRNA (V3-V4)	338F 518R	ACTCCTACGGGAGGCAGCAG ATTACCGCGGCTGCTGG	(Orschler et al., 2019)
16S rRNA (V3-V4)	V3F V4R	TCGTCGGCAGCGTCAGATGTGTATAAGAGACAG GTCTCGTGGGCTCGGAGATGTGTATAAGAGACAG	(Sarvajith et al., 2020)
16S rRNA (V6)	985F 1046R	CAACGCGAAGAACCTTACC CGACAGCCATGCANCACCT	(Ye et al., 2012)

Table VII. S 3. Continued

Target gene (region)	Primer	Sequence (5'-3')	Reference
16S rRNA (V7-V8)	1055F 1392R	ATGGCTGTOGTCAGCT ACGGGCGGTGTGTAC	(Orschler et al., 2019)
AOB amoA	amoA-1F amoA-2R	GGGGTTTCTACTGGTGGT CCCCTCKGSAAAGCCTTCTTC	(Islam et al., 2019; Lin et al., 2020; Orschler et al., 2019; Pan et al., 2018; Rotthauwe et al., 1997; Song et al., 2020; Wang et al., 2014; Yang et al., 2018; Ye et al., 2012; Zhang et al., 2011)

Table VII. S 4. Primers used to identify different taxonomic groups of microalgae.

Microalgae	Taxonomic Level (primer set)	Target gene(s)	Primer	Sequence (5'-3')	Reference
Chaetopeltidales	Order	18S rRNA	Chloro-F	TGGCCTATCTTGTTGGTCTGT	(Maza-Márquez et al., 2017)
			Chloro-R	GAATCAACCTGACAAGGCAAC	
Chaetophorales	Order	18S rRNA	Chloro-F	TGGCCTATCTTGTTGGTCTGT	(Maza-Márquez et al., 2017)
			Chloro-R	GAATCAACCTGACAAGGCAAC	
Chlamydomonadales	Order	18S rRNA	Chloro-F	TGGCCTATCTTGTTGGTCTGT	(Maza-Márquez et al., 2017)
			Chloro-R	GAATCAACCTGACAAGGCAAC	
Chlorellales	Order	18S rRNA	Chloro-F	TGGCCTATCTTGTTGGTCTGT	(Maza-Márquez et al., 2017)
			Chloro-R	GAATCAACCTGACAAGGCAAC	
Chlorodendrales	Order	18S rRNA	Chloro-F	TGGCCTATCTTGTTGGTCTGT	(Maza-Márquez et al., 2017)
			Chloro-R	GAATCAACCTGACAAGGCAAC	
Prasiolales	Order	18S rRNA	Chloro-F	TGGCCTATCTTGTTGGTCTGT	(Maza-Márquez et al., 2017)
			Chloro-R	GAATCAACCTGACAAGGCAAC	
Sphaeropleales	Order	18S rRNA	Chloro-F	TGGCCTATCTTGTTGGTCTGT	(Maza-Márquez et al., 2017)
			Chloro-R	GAATCAACCTGACAAGGCAAC	
Tetrasporales	Order	18S rRNA	Chloro-F	TGGCCTATCTTGTTGGTCTGT	(Maza-Márquez et al., 2017)
			Chloro-R	GAATCAACCTGACAAGGCAAC	
Chlorophyceae	Family	tufA	tufA F	GGNGCNGCNCAAATGGAYGG	(Vieira et al., 2016)
			tufA R	CCTTCNCGAATMGCRAAWCGC	
Characium	Genus	18S rRNA	574*F	CGGTAAYTCCAGCTCYV	(Ferro et al., 2020)
			1132R	CCGTCAATTHCTTYAAR	
Chlamydomonas	Genus	18S rRNA	574*F	CGGTAAYTCCAGCTCYV	(Ferro et al., 2020)
			1132R	CCGTCAATTHCTTYAAR	
			ITS4R	TCCTCCGCTTATTGATATGC	
		rbcL	RH1	TGTCACCACAAACAGAAACTAAAGC	
			rbcL 1385	AATTCAAATTTAATTTCTTTCC	

Table VII. S 4. Continued.

Microalgae	Taxonomic Level (primer set)	Target gene(s)	Primer	Sequence (5'-3')	Reference
Chlorella	Genus (1st primer set)	18S rRNA	574*F 1132R	CGGTAAYTCCAGCTCYV CCGTCAATTHCTTYAAR	(Ferro et al., 2020)
	Genus (2nd primer set)	18S rRNA	27F 518R 165F 1780R	AGAGTTTGATCCTGGCTCGA ATTACCGCGGCTGCTGG CGACTTCTGGAAGGGACGTA CTAGGTGGGAGGGTTTAATG	(Cho et al., 2017)
	Genus (3rd primer set)	18S rRNA	3NDF V4_euk_R2	GGCAAGTCTGGTGCCAG ACGGTATCT(AG)ATC(AG)TCTTCG	(Xie et al., 2018)
	Genus (4th primer set)	ITS2	ITS1 ITS4R	AGGAGAAGTCGTAAC AAGGT TCCTCCGCTTATTGATATGC	(Michelon et al., 2010)
		rbcL	RH1 rbcL 1385	TGTCACCACAAACAGAAACTAAAGC AATTCAAATTTAATTTCTTTCC	
Coelastrella	Genus	18S rRNA	574*F 1132R	CGGTAAYTCCAGCTCYV CCGTCAATTHCTTYAAR	(Ferro et al., 2020)
Desmodemus	Genus (1st primer set)	18S rRNA	574*F 1132R	CGGTAAYTCCAGCTCYV CCGTCAATTHCTTYAAR	(Ferro et al., 2020)
	Genus (2nd primer set)	18S rRNA	27F 518R 165F 1780R	AGAGTTTGATCCTGGCTCGA ATTACCGCGGCTGCTGG CGACTTCTGGAAGGGACGTA CTAGGTGGGAGGGTTTAATG	(Cho et al., 2017)
Oocystis	Genus	18S rRNA	574*F 1132R	CGGTAAYTCCAGCTCYV CCGTCAATTHCTTYAAR	(Ferro et al., 2020)
Paraphysomonas	Genus	18S rRNA	574*F 1132R	CGGTAAYTCCAGCTCYV CCGTCAATTHCTTYAAR	(Ferro et al., 2020)

Table VII. S 4. Continued.

Microalgae	Taxonomic Level (primer set)	Target gene(s)	Primer	Sequence (5'-3')	Reference
Polytoma	Genus	18S rRNA	574*F 1132R	CGGTAAYTCCAGCTCYV CCGTCAATTHCTTYAAR	(Ferro et al., 2020)
Pseudocharaciopsis	Genus	18S rRNA	574*F 1132R	CGGTAAYTCCAGCTCYV CCGTCAATTHCTTYAAR	(Ferro et al., 2020)
Scenedesmus	Genus (1st primer set)	18S rRNA	574*F 1132R	CGGTAAYTCCAGCTCYV CCGTCAATTHCTTYAAR	(Ferro et al., 2020)
	Genus (2nd primer set)	18S rRNA	27F 518R 165F 1780R	AGAGTTTGATCCTGGCTCGA ATTACCGCGGCTGCTGG CGACTTCTGGAAGGGACGTA CTAGGTGGGAGGGTTTAATG	(Cho et al., 2017)
	Genus (3rd primer set)	ITS1, 5.8S	F	GAAGTCGTAACAAGGTTTCC	(Moreno-García et al., 2021)
		ITS2	R	TCCTGGTTAGTTTCTTTTCC	
Spumella	Genus	18S rRNA	574*F 1132R	CGGTAAYTCCAGCTCYV CCGTCAATTHCTTYAAR	(Ferro et al., 2020)
Chlorella chlorelloides	Specie	18S rRNA	18SF 18SR 402–23F 1323–44F 898–919R 1308–39R	AACCTGGTTGATCCTGCCAGT TGATCCTTCTGCAGGTTCACCTACG GCTACCACATCCAAGGAAGGCA CGAACGAGACCTCAGCCTGCTA TAAATCCAAGAATTTCACCTCT CTCGTTCGTTAACGGAATTAACC	(Krivina and Temraleeva, 2020)
		ITS1, 5.8S	ITS-AF ITS-BR	CGTTTCCGTAGGTGAACCTGC CATATGCTTAAGTTCAGCGGG	
		ITS2	ITS3 ITS4	GCATCGATGAAGAACGCAGC TCCTCCGCTTATTGATATGC	

Table VII. S 4. Continued.

Microalgae	Taxonomic Level (primer set)	Target gene(s)	Primer	Sequence (5'-3')	Reference
Chlorella heliozoae	Specie	18S rRNA	18SF	AACCTGGTTGATCCTGCCAGT	(Krivina and Temraleeva, 2020)
			18SR	TGATCCTTCTGCAGGTTCACCTACG	
			402–23F	GCTACCACATCCAAGGAAGGCA	
			1323–44F	CGAACGAGACCTCAGCCTGCTA	
			898–919R	TAAATCCAAGAATTTCACCTCT	
			1308–39R	CTCGTTCGTTAACGGAATTAACC	
		ITS1, 5.8S	ITS-AF	CGTTTCCGTAGGTGAACCTGC	
			ITS-BR	CATATGCTTAAGTTCAGCGGG	
		ITS2	ITS3	GCATCGATGAAGAACGCAGC	
			ITS4	TCCTCCGCTTATTGATATGC	
Chlorella pituita	Specie	18S rRNA	18SF	AACCTGGTTGATCCTGCCAGT	(Krivina and Temraleeva, 2020)
			18SR	TGATCCTTCTGCAGGTTCACCTACG	
			402–23F	GCTACCACATCCAAGGAAGGCA	
			1323–44F	CGAACGAGACCTCAGCCTGCTA	
			898–919R	TAAATCCAAGAATTTCACCTCT	
			1308–39R	CTCGTTCGTTAACGGAATTAACC	
		ITS1, 5.8S	ITS-AF	CGTTTCCGTAGGTGAACCTGC	
			ITS-BR	CATATGCTTAAGTTCAGCGGG	
		ITS2	ITS3	GCATCGATGAAGAACGCAGC	
			ITS4	TCCTCCGCTTATTGATATGC	

Table VII. S 4. Continued.

Microalgae	Taxonomic Level (primer set)	Target gene(s)	Primer	Sequence (5'-3')	Reference
Chlorella sorokiniana	Specie	18S rRNA	18SF 18SR	CCAACCTGGTTGATCCTGCCAGTA CCTTGTTACGACTTCACCTTCCTCT	(Tale et al., 2014)
	Specie	rbcL	F R	CTTTCCAAGGTCCTCCTCAC TCTCTCCAACGCATAAATGG	(Singh et al., 2017)
Chlorella sorokiniana NKH15	Specie	18S rRNA	ss5 ss3	GGTGA TCCTG CCAGT AGTCA TATGC TTG GATCC TTCCG CAGGT TCACC TACGG AAACC	(Aketo et al., 2020)
		DNA polymerase	Prime STAR Max		
Chlorella sorokiniana NKH6	Specie	18S rRNA	ss5 ss3	GGTGA TCCTG CCAGT AGTCA TATGC TTG GATCC TTCCG CAGGT TCACC TACGG AAACC	(Aketo et al., 2020)
		DNA polymerase	Prime STAR Max		
Chlorella variabilis	Specie	18S rRNA	18SF 18SR 402–23F 1323–44F 898–919R 1308–39R	AACCTGGTTGATCCTGCCAGT TGATCCTTCTGCAGGTTCACCTACG GCTACCACATCCAAGGAAGGCA CGAACGAGACCTCAGCCTGCTA TAAATCCAAGAATTTCACCTCT CTCGTTCGTTAACGGAATTAACC	(Krivina and Temraleeva, 2020)
		ITS1, 5.8S	ITS-AF ITS-BR	CGTTTCCGTAGGTGAACCTGC CATATGCTTAAGTTCAGCGGG	
		ITS2	ITS3 ITS4	GCATCGATGAAGAACGCAGC TCCTCCGCTTATTGATATGC	

Table VII. S 4. Continued.

Microalgae	Taxonomic Level (primer set)	Target gene(s)	Primer	Sequence (5'-3')	Reference
Chlorella vulgaris	Specie (1st primer set)	18S rRNA	18SF	AACCTGGTTGATCCTGCCAGT	(Krivina and Temraleeva, 2020)
			18SR	TGATCCTTCTGCAGGTTCACCTACG	
			402–23F	GCTACCACATCCAAGGAAGGCA	
			1323–44F	CGAACGAGACCTCAGCCTGCTA	
			898–919R	TAAATCCAAGAATTTCACCTCT	
			1308–39R	CTCGTTCGTTAACGGAATTAACC	
		ITS1, 5.8S	ITS-AF	CGTTTCCGTAGGTGAACCTGC	
			ITS-BR	CATATGCTTAAGTTCAGCGGG	
		ITS2	ITS3	GCATCGATGAAGAACGCAGC	
			ITS4	TCCTCCGCTTATTGATATGC	
	Specie (2nd primer set)	18S rRNA	Euk1A	CTGGTTGATCCTGCCAG	(Cheung et al., 2020)
			Euk516r	ACCAGACTTGCCCTCC	
Chlorella sp. IFRPD 1018	Specie	18S rRNA	18SF	CCAACCTGGTTGATCCTGCCAGTA	(Tale et al., 2014)
			18SR	CCTTGTTACGACTTCACCTTCCTCT	
Chlorella sp. ZJU0204	Specie	18S rRNA	18SF	CCAACCTGGTTGATCCTGCCAGTA	(Tale et al., 2014)
			18SR	CCTTGTTACGACTTCACCTTCCTCT	
Chloroidium saccharophilum NKH13	Specie	18S rRNA	ss1	GGTGA TCCTG CCAGT AGTCA TATGC TTG	(Aketo et al., 2020)
			ss1	GATCC TTCCG CAGGT TCACC TACGG AAACC	
		DNA polymerase	Prime STAR Max		

Table VII. S 4. Continued.

Microalgae	Taxonomic Level (primer set)	Target gene(s)	Primer	Sequence (5'-3')	Reference
Desmodesmus sp. Mary 6/3 T-2d	Specie	18S rRNA	18S rDNA FW 18S0 rDNA RV	AAGTATAAACTGCTTATACTGTGAA CCTACGGAAACCTTGTTACGACT	(Ji et al., 2014)
		ITS1	ITS1 FW ITS2 RV	AGTCGTAACAAGGTTTCCGTAGG TATGCTTAAGTTCAGCGGGTAAT	
Desmodesmus sp. NKH10	Specie	18S rRNA	ss3 ss5	GGTGA TCCTG CCAGT AGTCA TATGC TTG GATCC TTCCG CAGGT TCACC TACGG AAACC	(Aketo et al., 2020)
		DNA polymerase	Prime STAR Max		
Desmodesmus sp. NKH8	Specie	18S rRNA	ss3 ss5	GGTGA TCCTG CCAGT AGTCA TATGC TTG GATCC TTCCG CAGGT TCACC TACGG AAACC	(Aketo et al., 2020)
		DNA polymerase	Prime STAR Max		
Desmodesmus sp. Tow 10/11 T-2W	Specie	18S rRNA	18S rDNA FW 18S0 rDNA RV	AAGTATAAACTGCTTATACTGTGAA CCTACGGAAACCTTGTTACGACT	(Ji et al., 2014)
		ITS1	ITS1 FW ITS2 RV	AGTCGTAACAAGGTTTCCGTAGG TATGCTTAAGTTCAGCGGGTAAT	
Desmodesmus sp., EJ9-6	Specie	18S rRNA	18S rDNA FW 18S0 rDNA RV	AAGTATAAACTGCTTATACTGTGAA CCTACGGAAACCTTGTTACGACT	(Ji et al., 2014)
		ITS1	ITS1 FW ITS2 RV	AGTCGTAACAAGGTTTCCGTAGG TATGCTTAAGTTCAGCGGGTAAT	
Jaagichlorella luteoviridis NKH7	Specie	18S rRNA	ss1 ss1	GGTGA TCCTG CCAGT AGTCA TATGC TTG GATCC TTCCG CAGGT TCACC TACGG AAACC	(Aketo et al., 2020)
		DNA polymerase	Prime STAR Max		

Table VII. S 4. Continued.

Microalgae	Taxonomic Level (primer set)	Target gene(s)	Primer	Sequence (5'-3')	Reference
Monoraphidium neglectum	Specie	18S rRNA	18SF 18SR	CCAACCTGGTTGATCCTGCCAGTA CCTTGTTACGACTTCACCTTCCTCT	(Tale et al., 2014)
Scenedesmus acuminatus	Specie	18S rRNA	18SF 18SR	CCAACCTGGTTGATCCTGCCAGTA CCTTGTTACGACTTCACCTTCCTCT	(Tale et al., 2014)
Scenedesmus almeriensis	Specie	18S rRNA	UnivF UnivR UnivProbe	TTGGAGGGCAAGTCTGGT CGAGCTTTTTAACTGCAACAA VIC-CGGTAATTCCAGCTCC	(Beatrice-Lindner et al., 2018)
		ITS2	SalmF SalmR SalmProbe	ACCCTCACCCCTCTTTCCTTT TTGGGAAAGCCAGATCCACC 6FAM-GTTAGCTTCTCAGCTGG	
Scenedesmus bajacalifornicus	Specie	rbcL	RbcL_13F RbcL_8R RbcL_14R	AATGGCTCCACAAACAGAAAC TCACAAGCAGCAGCTAATTC ATCAAGACCACCACGTAAACA	(Beatrice-Lindner et al., 2018)
		ITS1, 5.8S	ITS1	TCCGTAGGTGAACCTGCGG	
		ITS2	ITS4	TCCTCCGCTTATTGATATGC	
Scenedesmus obliquus	Specie (1st primer set)	rbcL	RbcL_13F RbcL_8R RbcL_14R	AATGGCTCCACAAACAGAAAC TCACAAGCAGCAGCTAATTC ATCAAGACCACCACGTAAACA	(Beatrice-Lindner et al., 2018)
		ITS1, 5.8S	ITS1	TCCGTAGGTGAACCTGCGG	
		ITS2	ITS4	TCCTCCGCTTATTGATATGC	
	Specie (2nd primer set)	18S rRNA	Euk1A Euk516r	CTGGTTGATCCTGCCAG ACCAGACTTGCCCTCC	(Cheung et al., 2020)

REFERENCES SUPPLEMENTARY DATA

Adamczyk, J., Hesselsoe, M., Iversen, N., Horn, M., Lehner, A., Nielsen, P.H., Schloter, M., Roslev, P., Wagner, M., 2003. The Isotope Array, a New Tool that Employs Substrate-Mediated Labeling of rRNA for Determination of Microbial Community Structure and Function. Appl. Environ. Microbiol. 69, 6875–6887. https://doi.org/10.1128/AEM.69.11.6875-6887.2003

Aketo, T., Hoshikawa, Y., Nojima, D., Yabu, Y., Maeda, Y., Yoshino, T., Takano, H., Tanaka, T., 2020. Selection and characterization of microalgae with potential for nutrient removal from municipal wastewater and simultaneous lipid production. J. Biosci. Bioeng. 129, 565–572. https://doi.org/10.1016/j.jbiosc.2019.12.004

Anthonisen, A.C., Loehr, R.C., Prakasam, T.B.S., Srinath, E.G., 1976. Inhibition of Nitrification by Ammonia and Nitrous Acid. J. (Water Pollut. Control Fed. 48, 835–852.

Araki, N., Ohashi, A., Machdar, I., Harada, H., 1999. Behaviors of nitrifiers in a novel biofilm reactor employing hanging sponge-cubes as attachment site, in: Water Science and Technology. pp. 23–31. https://doi.org/10.1016/S0273-1223(99)00146-8

Beatrice-Lindner, P., Garrido-Cardenas, J.A., Sepulveda, C., Acien-Fernandez, F.G., 2018. A new approach for detection and quantification of microalgae in industrial-scale microalgal cultures. Appl. Microbiol. Biotechnol. 102, 8429–8436. https://doi.org/10.1007/s00253-018-9268-y

Burrell, P.C., Phalen, C.M., Hovanec, T.A., 2001. Identification of Bacteria Responsible for Ammonia Oxidation in Freshwater Aquaria. Appl. Environ. Microbiol. 67, 5791–5800. https://doi.org/10.1128/AEM.67.12.5791-5800.2001

Cheung, S.L., Allen, D.G., Short, S.M., 2020. Specific quantification of Scenedesmus obliquus and Chlorella vulgaris in mixed-species algal biofilms. Bioresour. Technol. 295. https://doi.org/10.1016/j.biortech.2019.122251

Cho, D.H., Choi, J.W., Kang, Z., Kim, B.H., Oh, H.M., Kim, H.S., Ramanan, R., 2017. Microalgal diversity fosters stable biomass productivity in open ponds treating wastewater. Sci. Rep. 7. https://doi.org/10.1038/s41598-017-02139-8

Daims, H., Brühl, A., Amann, R., Schleifer, K.H., Wagner, M., 1999. The domain-specific probe EUB338 is insufficient for the detection of all bacteria: Development and evaluation of a more comprehensive probe set. Syst. Appl. Microbiol. 22, 434–444. https://doi.org/10.1016/S0723-2020(99)80053-8

Deng, M., Chen, J., Gou, J., Hou, J., Li, D., He, X., 2018. The effect of different carbon sources on water quality, microbial community and structure of biofloc systems. Aquaculture 482, 103–110. https://doi.org/10.1016/j.aquaculture.2017.09.030

Ferro, L., Hu, Y.O.O., Gentili, F.G., Andersson, A.F., Funk, C., 2020. DNA metabarcoding reveals microbial community dynamics in a microalgae-based municipal wastewater treatment open photobioreactor. Algal Res. 51. https://doi.org/10.1016/j.algal.2020.102043

Gieseke, A., Purkhold, U., Wagner, M., Amann, R., Schramm, A., 2001. Community Structure and Activity Dynamics of Nitrifying Bacteria in a Phosphate-Removing Biofilm. Appl. Environ. Microbiol. 67, 1351–1362. https://doi.org/10.1128/AEM.67.3.1351-1362.2001

Hermansson, A., Lindgren, P.E., 2001. Quantification of ammonia-oxidizing bacteria in arable soil by real-time PCR. Appl. Environ. Microbiol. 67, 972–976. https://doi.org/10.1128/AEM.67.2.972-976.2001

Islam, G.M., Vi, P., Gilbride, K.A., 2019. Functional relationship between ammonia-oxidizing bacteria and ammonia-oxidizing archaea populations in the secondary treatment system of a full-scale municipal wastewater treatment plant. J. Environ. Sci. (China) 86, 120–130. https://doi.org/10.1016/j.jes.2019.04.031

Ji, F., Liu, Y., Hao, R., Li, G., Zhou, Y., Dong, R., 2014. Biomass production and nutrients removal by a new microalgae strain Desmodesmus sp. in anaerobic digestion wastewater. Bioresour. Technol. 161, 200–207. https://doi.org/10.1016/j.biortech.2014.03.034

Juretschko, S., Timmermann, G., Schmid, M., Schleifer, K.-H., Pommerening-Ro¨ser, A., Ro¨ser, R., Koops, H.-P., Wagner, M., 1998. Combined Molecular and Conventional Analyses of Nitrifying Bacterium Diversity in Activated Sludge: Nitrosococcus mobilis and Nitrospira-Like Bacteria as Dominant Populations, APPLIED AND ENVIRONMENTAL MICROBIOLOGY.

Krivina, E.S., Temraleeva, A.D., 2020. Identification Problems and Cryptic Diversity of Chlorella-Clade Microalgae (Chlorophyta). Microbiol. (Russian Fed. 89, 720–732. https://doi.org/10.1134/S0026261720060107

Lin, Z., Huang, W., Zhou, Jiong, He, X., Wang, J., Wang, X., Zhou, Jian, 2020. The variation on nitrogen removal mechanisms and the succession of ammonia oxidizing archaea and ammonia oxidizing bacteria with temperature in biofilm reactors treating saline wastewater. Bioresour. Technol. 314. https://doi.org/10.1016/j.biortech.2020.123760

Manz, W., Amann, R., Ludwig, W., Wagner, M., Schleifer, K.H., 1992. Phylogenetic Oligodeoxynucleotide Probes for the Major Subclasses of Proteobacteria: Problems and Solutions. Syst. Appl. Microbiol. 15, 593–600. https://doi.org/10.1016/S0723-2020(11)80121-9

Maza-Márquez, P., González-Martínez, A., Rodelas, B., González-López, J., 2017. Full-scale photobioreactor for biotreatment of olive washing water: Structure and diversity of the microalgae-bacteria consortium. Bioresour. Technol. 238, 389–398. https://doi.org/10.1016/j.biortech.2017.04.048

Michelon, W., Luis Busi Da Silva, M., Paola Mezzari, M., Pirolli, M., Michel Prandini, J., Moreira Soares, H., 2010. Effects of Nitrogen and Phosphorus on Biochemical Composition of Microalgae Polyculture Harvested from Phycoremediation of Piggery Wastewater Digestate. Appl. Biochem. Biotechnol. 178, 1407–1419. https://doi.org/10.1007/s12010-015-1955-x

Mobarry, B.K., Wagner, M., Urbain, V., Rittmann, B.E., Stahl, D.A., 1996. Phylogenetic Probes for Analyzing Abundance and Spatial Organization of Nitrifying Bacteria, APPLIED AND ENVIRONMENTAL MICROBIOLOGY.

Moreno-García, A.F., Neri-Torres, E.E., Mena-Cervantes, V.Y., Altamirano, R.H., Pineda-Flores, G., Luna-Sánchez, R., García-Solares, M., Vazquez-Arenas, J., Suastes-Rivas, J.K., 2021. Sustainable biorefinery associated with wastewater treatment of Cr (III) using a native microalgae consortium. Fuel 290. https://doi.org/10.1016/j.fuel.2020.119040

Naseer, R., Abualhail, S., Xiwu, L., 2013. Biological nutrient removal with limited organic matter using a novel anaerobic-anoxic/oxic multi-phased activated sludge process. Saudi J. Biol. Sci. 20, 11–21. https://doi.org/10.1016/j.sjbs.2012.09.002

Orschler, L., Agrawal, S., Lackner, S., 2019. On resolving ambiguities in microbial community analysis of partial nitritation anammox reactors. Sci. Rep. 9. https://doi.org/10.1038/s41598-019-42882-8

Pan, K.L., Gao, J.F., Fan, X.Y., Li, D.C., Dai, H.H., 2018. The more important role of archaea than bacteria in nitrification of wastewater treatment plants in cold season despite their numerical relationships. Water Res. 145, 552–561. https://doi.org/10.1016/j.watres.2018.08.066

Pommerening-Röser, A., Rath, G., Koops, H.P., 1996. Phylogenetic diversity within the genus Nitrosomonas. Syst. Appl. Microbiol. 19, 344–351. https://doi.org/10.1016/S0723-2020(96)80061-0

Rotthauwe, J.H., Witzel, K.P., Liesack, W., 1997. The ammonia monooxygenase structural gene amoa as a functional marker: Molecular fine-scale analysis of natural ammonia-oxidizing populations. Appl. Environ. Microbiol. 63, 4704–4712. https://doi.org/10.1128/aem.63.12.4704-4712.1997

Sarvajith, M., Kiran Kumar Reddy, G., Nancharaiah, Y. V., 2020. Aerobic granular sludge for high-strength ammonium wastewater treatment: Effect of COD/N ratios, long-term stability and nitrogen removal pathways. Bioresour. Technol. 306. https://doi.org/10.1016/j.biortech.2020.123150

Singh, P., Kumari, S., Guldhe, A., Singh, G., Bux, F., 2017. ACCase and rbcL gene expression as a function of nutrient and metal stress for enhancing lipid productivity in Chlorella sorokiniana. Energy Convers. Manag. 148, 809–819. https://doi.org/10.1016/j.enconman.2017.06.054

Song, Z., Zhang, X., Sun, F., Ngo, H.H., Guo, W., Wen, H., Li, C., Zhang, Z., 2020. Specific microbial diversity and functional gene (AOB amoA) analysis of a sponge-based aerobic nitrifying moving bed biofilm reactor exposed to typical pharmaceuticals. Sci. Total Environ. 742. https://doi.org/10.1016/j.scitotenv.2020.140660

Tale, M., Ghosh, S., Kapadnis, B., Technology, S.K.-B., 2014, U., 2014. Isolation and characterization of microalgae for biodiesel production from Nisargruna biogas plant effluent. Bioresour. Technol. 169, 328–335. https://doi.org/https://doi.org/10.1016/j.biortech.2014.06.017

Vieira, H.H., Bagatini, I.L., Guinart, C.M., Vieira, A.A.H., 2016. tufA gene as molecular marker for freshwater Chlorophyceae. Algae 31, 155–165. https://doi.org/10.4490/algae.2016.31.4.14

Wagner, M., Rath, G., Amann, R., Koops, H.P., Schleifer, K.H., 1995. In situ Identification of Ammonia-oxidizing Bacteria. Syst. Appl. Microbiol. 18, 251–264. https://doi.org/10.1016/S0723-2020(11)80396-6

Wang, Z., Zhang, X.X., Lu, X., Liu, B., Li, Y., Long, C., Li, A., 2014. Abundance and diversity of bacterial nitrifiers and denitrifiers and their functional genes in tannery wastewater treatment plants revealed by high-throughput sequencing. PLoS One 9. https://doi.org/10.1371/journal.pone.0113603

Xie, B., Gong, W., Tian, Y., Qu, F., Luo, Y., Du, X., Tang, X., Xu, D., Lin, D., Li, G., Liang, H., 2018. Biodiesel production with the simultaneous removal of nitrogen, phosphorus and COD in microalgal-bacterial communities for the treatment of anaerobic digestion effluent in photobioreactors. Chem. Eng. J. 350, 1092–1102. https://doi.org/10.1016/j.cej.2018.06.032

Yang, Y.D., Ren, Y.F., Wang, X.Q., Hu, Y.G., Wang, Z.M., Zeng, Z.H., 2018. Ammonia-oxidizing archaea and bacteria responding differently to fertilizer type and irrigation frequency as revealed by Illumina Miseq sequencing. J. Soils Sediments 18, 1029–1040. https://doi.org/10.1007/s11368-017-1792-3

Ye, L., Zhang, T., Wang, T., Fang, Z., 2012. Microbial structures, functions, and metabolic pathways in wastewater treatment bioreactors revealed using high-throughput sequencing. Environ. Sci. Technol. 46, 13244–13252. https://doi.org/10.1021/es303454k

Zhang, T., Ye, L., Tong, A.H.Y., Shao, M.F., Lok, S., 2011. Ammonia-oxidizing archaea and ammonia-oxidizing bacteria in six full-scale wastewater treatment bioreactors. Appl. Microbiol. Biotechnol. 91, 1215–1225. https://doi.org/10.1007/s00253-011-3408-y

CHAPTER VIII

8. Microalgae-bacteria consortia dynamics in a long term operated membrane-coupled high-rate algal pond (MHRAP)

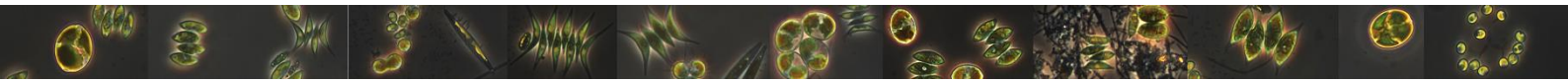

8. Microalgae-bacteria consortia dynamics in a long term operated membrane-coupled high-rate algal pond (MHRAP)

ABSTRACT

Bacterial and microalgal community composition has been widely studied through 16S rDNA and 18S rDNA sequencing, respectively. The influence of the hydraulic retention time (HRT) and the incoming wastewater stream on bacterial and microalgal communities established in membrane high rate algal pond (MHRAP) was investigated. The MHRAP was operated with two incoming wastewaters streams: effluent from primary settler (EPS) and from pre-treatment (EPT). EPS-fed MHRAP was operated at 6, 4 and 2 days of HRT. The bacterial community at 6 days HRT showed lower diversity than operating periods at 4 and 2 days. During MHRAP operation at 6 days HRT, the bacterial and microalgal community was dominated by *Verrucomicrobiota* phylum and *Desmodesmus* genus. MHRAP performance at 4 and 2 days of HRT resulted in a shift of bacterial community composition, with the *Proteobacteria* phylum dominating. At 6 d HRT, AOB and NOB communities were dominated by *Nitrosomonas* and *Nitrospira*, respectively, while when reducing HRT to 4 and 2 days *Candidatus Nitrotoga* outcompeted *Nitrospira*. EPT-fed MHRAP was operated at 2 and 1 days of HRT. Bacterial community was dominated by *Proteobacteria* phylum, regardless of HRT. *Ellin6067* spp. was the dominant AOB genus and *Nitrospira* the dominant NOB. *Ellin6067* spp. is not a typical AOB genus but it is associated with microalgae-bacteria systems. Denitrifying organisms from *Caldilineaceae* family, were detected when daily oxygen fluctuations appeared promoted by high organic loading rate. Regarding *Eukarya* organisms, microalgal biodiversity was similar, regardless of HRT and the incoming wastewater streams. *Coelastrella* was the main genus developed in this system, except in the period operated at 6 days HRT using EPS when *Desmodesmus* was better adapted to environmental and operational conditions. The abiotic stress factors, such as light intensity, pH, nitrite accumulation and free ammonia nitrogen concentration determined the bacterial and microalgal community structure rather than HRT. The effect of the microbial diversity on nitrogen removal mechanisms was also evaluated. Low relative abundances of NOB were associated to partial-nitrification. High nitrogen removal efficiencies were reached by growth of denitrifying bacteria within *Chloroflexy* phylum, with an important contribution of *Caldilineaceae* family

Keywords

16S/18S rDNA, microalgae-bacteria consortia, hydraulic retention time (HRT), wastewater stream, microbial ecology

Authors

Stéphanie Aparicio, Ángel Robles, José Ferrer, Aurora Seco and Luis Borrás Falomir.

8.1. INTRODUCTION

Activated sludge-based wastewater technologies have some drawbacks, such as high energy requirements, poor nutrient recovery performance and environmental impact associated with greenhouse gas emissions (Chai et al., 2015; Ozgun et al., 2013; Rahman et al., 2016; Sabeen et al., 2018). In the last two decades, low-cost and environmentally friendly alternatives to conventional activated sludge processes have emerged, especially those using microalgae processes (Acién et al., 2016; González-Camejo et al., 2020; Seco et al., 2018). Microalgae genera used for wastewater treatment are characterized by their rapid growth and tolerance to high light intensity and high temperatures (Bernard and Rémond, 2012). *Scenedesmus* and *Chlorella*-like morphologies are the most commonly microalgae described in wastewater treatment systems (González-Camejo et al., 2020; Mantovani et al., 2020; Marazzi et al., 2019). Applying microalgae to wastewater treatment involves their association with bacteria (Chapter 5).

Microalgae-bacteria interactions cover a wide range of ecological relationships (mutualism, amensalism, competition, etc.), which can be both beneficial and detrimental to microalgal growth (Ramanan et al., 2016; Zhang et al., 2020). Microalgae and bacteria can enhance nutrient removal and recovery in wastewater processes through mutualistic relationships (Zhang et al., 2020). The most widely described mutualistic relationship in microalgae-bacteria consortia is the self-sustaining gas exchange (Foladori et al., 2018; Zhang et al., 2020). Microalgae provide oxygen to aerobic bacteria and in exchange, heterotrophic bacteria supply inorganic carbon for photosynthesis (Zhang et al., 2020). As mentioned above, interactions between microalgae and bacteria are not only restricted to mutualism relationship, but also to amensalism and competition, which can negatively affect microalgae growth. Some bacterial population can influence microalgae activity through the synthesis of strong algaecidal metabolites (Lian et al., 2018). In addition, nitrifying bacteria can compete with microalgae for ammonium (Chapter 5).

It is therefore evident that microorganisms in the microalgae-bacteria consortium could have unpredictable and sometimes detrimental effects on microalgae growth and on effective wastewater pollutant removal from wastewater. Interrelationship between microalgae and bacteria is strongly affected by the reactor operating conditions and the ever-changing environmental conditions, as described in Chapter 5. Identifying the main groups of microalgae and bacteria involved in wastewater treatment, along with analyzing the impact of operational and environmental parameters on the ecological structure, could contribute to improve the performance of the treatment process. Few scientific researchers have focused on relating the biological diversity obtained with the operating parameters and pollutant removal efficiencies of the microalgae-bacteria wastewater treatment systems (Sánchez-Zurano et al., 2020; Ye et al., 2016).

In view of this, the aim of this chapter is to assess microalgae-bacteria community diversity and structure developed in a membrane high rate algal pond (MHRAP), with the operating conditions described in Chapter 5. Thereby, the changes in diversity and structure of microalgae and bacteria population at different hydraulic retention time (HRT) and wastewater influent are here evaluated. This microbial approach will improve our understanding of complex biological processes described in Chapter 5.

8.2. MATERIALS AND METHODS

8.2.1. MHRAP pilot plant

For this study, a continuous pilot-scale MHRAP plant located in the “Cuenca del Carraixet” WWTP (39°30′04.0’’N 0°20′00.1’’W, Valencia, Spain) was operated outdoors, i.e. culture temperature and sunlight irradiance were weather conditions dependent. The MHRAP pilot plant mainly consisted of a HRAP connected to one membrane tank (MT) module. The high rate algal pond (HRAP) had a working volume of 318.75 L, a solar irradiance area of 1.275 m^2 (2.55 x 0.5 m) and a liquid depth of 0.25 m. The reactor was continuously stirred by a single paddle wheel. The volume of the MT module was 14 L

and had a filtration surface of 3.4 m^2 given by a hollow-fiber membrane system (PURON® Koch Membrane Systems (PUR-PSH31), with 0.03 µm pore size). To reduce membrane fouling, air-sparging was used.

Various on-line sensors were installed in the MHRAP pilot plant to obtain real-time information on the process performance: a pH sensor (pHD sc DPD1R1, Hach Lange); a dissolved oxygen-temperature sensor (LDO Hach Lange); an AN-ISE sensor (AN-ISE LXV440.99.00001, Hach Lange) to record NH4-N and NOX-N (sum of NO2-N and NO3-N); and a light irradiance sensor (Apogee Quantum SQ-200) set up on the surface of the HRAP for measuring the photosynthetic active radiation (PAR).

8.2.2. MHRAP pilot plant operation

The MHRAP was not inoculated. Instead, a natural process of initial ecological succession of the indigenous microorganisms occurred. It was first operated in batch mode until reaching pseudo-stationary phase (i.e. biomass concentration measured as volatile suspended solids (VSS) did not significantly vary) and then a continuous feeding was maintained at the desired HRT. The biomass retention time (BRT) was set at 6 days, since, as described in Chapter 5, 6 days of BRT is the suitable time that maximizes biomass growth. The HRAP was fed with two wastewater streams from the “Cuenca del Carraixet” WWTP: effluent from primary settling (EPS) and effluent from pre-treatment (screening, degritter, and grease removal) (EPT). Table VIII. 1 shows the main characteristics of both wastewater streams. Five different HRT were evaluated: when feeding with effluent from the primary settling unit, 6, 4 and 2 days were studied; feeding directly from the pre-treatment was studied at 2 and 1 days HRT (Table VIII. 2). The following nomenclature was used to refer and identify each period: HRT_(operating HRT)_EP(S for effluent from primary settling or T for pre-treatment effluent), so that the period operated at 6 days of HRT using effluent form primary settling was referred as HRT_6_EPS.

Table VIII. 1. Average composition of effluent from primary settling and pre-treatment supplied to MHRAP pilot plant. Abbreviations: total suspended solids (TSS), volatile suspended solids (VSS), total and soluble chemical oxygen demand (T-COD and S-COD, respectively), total and soluble biological oxygen demand (T-BOD and S-BOD, respectively), total nitrogen (T-N), ammonium nitrogen (NH_4-N), total phosphorus (T-P) and phosphate phosphorus (PO_4-P).

Parameter		Effluent from primary settling (EPS)	Effluent from pre-treatment (EPT)
pH		7.7 ± 0.5	7.9 ± 0.3
TSS	(g TSS·m^{-3})	107 ± 61	308 ± 86
VSS	(g VSS·m^{-3})	92 ± 46	258 ± 73
T-COD	(g COD·m^{-3})	252 ± 71	692 ± 139
S-COD	(g COD·m^{-3})	100 ± 27	123 ± 29
T-BOD	(g BOD·m^{-3})	105 ± 18	290 ± 30
S-BOD	(g BOD·m^{-3})	36 ± 5	106 ± 21
T-N	(g N·m^{-3})	40 ± 10	47 ± 4
NH_4-N	(g N·m^{-3})	37 ± 8	39 ± 3
T-P	(g P·m^{-3})	4.2 ± 1.2	7.7 ± 1.4
PO_4-P	(g P·m^{-3})	3.7 ± 0.9	4.4 ± 1.3

8.2.3. Sampling and analytical methods

For each pseudo-stationary state, samples from the MHRAP culture, influent and permeate were collected in duplicate. Ammonium (NH_4-N), nitrite (NO_2-N), nitrate (NO_3-N) and phosphate (PO_4-P) were analysed according to the Standard Methods (APHA-AWWA-WPCF, 2012): 4500- NH3-G, 4500-NO2-B, 4500-NO3-H and 4500-P-F respectively, with an automatic analyser (Smartchem 200, WestcoScientifi Instruments, Westco). Total suspended solids (TSS), VSS, total and soluble COD (T-COD and S-COD) and total and soluble biological oxygen demand (T-BOD and S-BOD) were measured according 2540-TSS-D, VSS 2540-VSS-E, 5220-COD-C, 522-COD-D and 5210-BOD-C, respectively (APHA-AWWA-WPCF, 2012).

8.2.4. Nucleic material extraction and sequencing of 16S and 18S rDNA genes

A total of 29 samples (Table VIII. 2) were extracted from the MHRAP plus two more: for the experiments working with the primary settling effluent and pre-treatment effluent. For each pseudo-stationary state, samples from the HRAP culture were collected in duplicate/triplicate (biological replicates). Aliquots of 1 mL sample were stored in 2 mL cryotubes at −20 °C. For bacteria, the E.Z.N.A® DNA Extraction Kit for Soil (Omega-

Biotek, USA) was used to extract nucleic acid material from 1 g of biomass, in accordance with the manufacturer's protocol. For microalgae, the E.Z.N.A® Plant DNA Kit (Omega-Biotek, USA) was used. Samples analysed for bacteria were labelled as BRW, while those for microalgae were labelled as ARW. DNA concentration and purity were measured at wavelengths of 260, 230 and 280 nm with a Nanodrop 2000 spectrophotometer (Thermo Scientific, USA). Samples with a A260/280 ratio below 1.8 and a A260/230 ratio out of the range 2.0 - 2.2 were discarded, to avoid humic acids or other compounds contamination.

16S rDNA gene analysis of bacteria and archaea microorganisms was performed through amplicon sequencing using specific primers for the v3-4 hyper variable region of the target gene (341F 5′-CCTACGGGNGGCWGCAG-3′ and 805R 5′-GACTACHVGGGTATCTAATCC-3′) (Klindworth et al., 2013). The V4 hyper-variable region of the 18S rDNA gene was amplified using the universal primers set TAReuk454FWD1 (5′-CCAGCASCYGCGGTAATTCC-3′) and TAReukREV3_modified (5′-ACTTTCGTTCTTGATYRATGA-3′) to identify microalgal communities within the eukarya domain (Tragin and Vaulot, 2018). The sequencing run was carried out in a 2×300 base pairs paired-end run using v3 chemistry in an Illumina MiSeq Sequencer (FISABIO, Valencia, Spain).

8.2.5. Illumina data processing and statistical analysis

The resulting raw sequences were downstream processed following the MiSeq_SOP pipeline (website accession data 5th September 2021) using open-source mothur software (v.1.46.1) (Schloss et al., 2009). The taxonomy was assigned according to the v138.1 release of SILVA database. The contingency table generated was used as the input for microbial ecology analysis using R-studio v.2021.09.0 software and vegan packages. For bacteria quantification, chloroplasts were not considered for microbial ecology analysis as they were supposed to belong to eukaryotic microalgae and not to the bacteria domain.

Alpha diversity was calculated through the evenness and richness index indicators (Shannon-Wiener and Simpson) using R-studio v.2021.09.0 software and vegan packages.. A principal co-ordinate analysis (PCoA) based on the Bray-Curtis distances matrix was performed in mothur to explore the beta diversity of the different samples processed for bacteria and microalgae quantification.

The microbial and operational results obtained were statistically analysed by IBM SPSS Statistics 26 software (Armonk, NY: IBM Corp). An analysis of variance (ANOVA) was performed to evaluate the significance of the differences in the mean values. Differences were considered statistically significant when p-value was below 0.01.

8.3. RESULTS AND DISCUSSION

Table VIII. 2 details the samples analysed as well as the operational and environmental values. The analysis of the sequences obtained revealed very shallow depth in samples BRW122 and 123, were only 466 and 3858 sequences were detected respectively. Thus, both samples were discarded for further analysis. After rejecting this samples with extremely low reads, subsampling was applied to the minimum level of sequences obtained (94204 sequences for bacteria and 59919 for eukarya).

8.3.1. Diversity and operational parameters

To understand and analyze bacterial and microalgal structure of samples, diversity was measured using two indices, inverse Simpson and Shannon-Wiener. Diversity is the number of different microorganism types present in the sample and their evenness. i.e the relative abundance. The Shannon-Wiener index focuses on species richness and can present any value, being higher the more taxonomic levels there are in the sample and the more uniform its distribution. The inverse Simpson index is focused on species uniformity and give values between 0 and 1, the greater the value the higher the diversity. Figure VIII. 1 shows the Simpson and Shannon-Wiener diversity indexes for bacteria and eukarya domains, for all the samples, together with the number of genera found. In the

case of bacteria (Figure VIII. 1A), it seems that both, diversity and number of genera grow as HRT decreases. This trend is not observed for eukarya domain (Figure VIII. 1B).

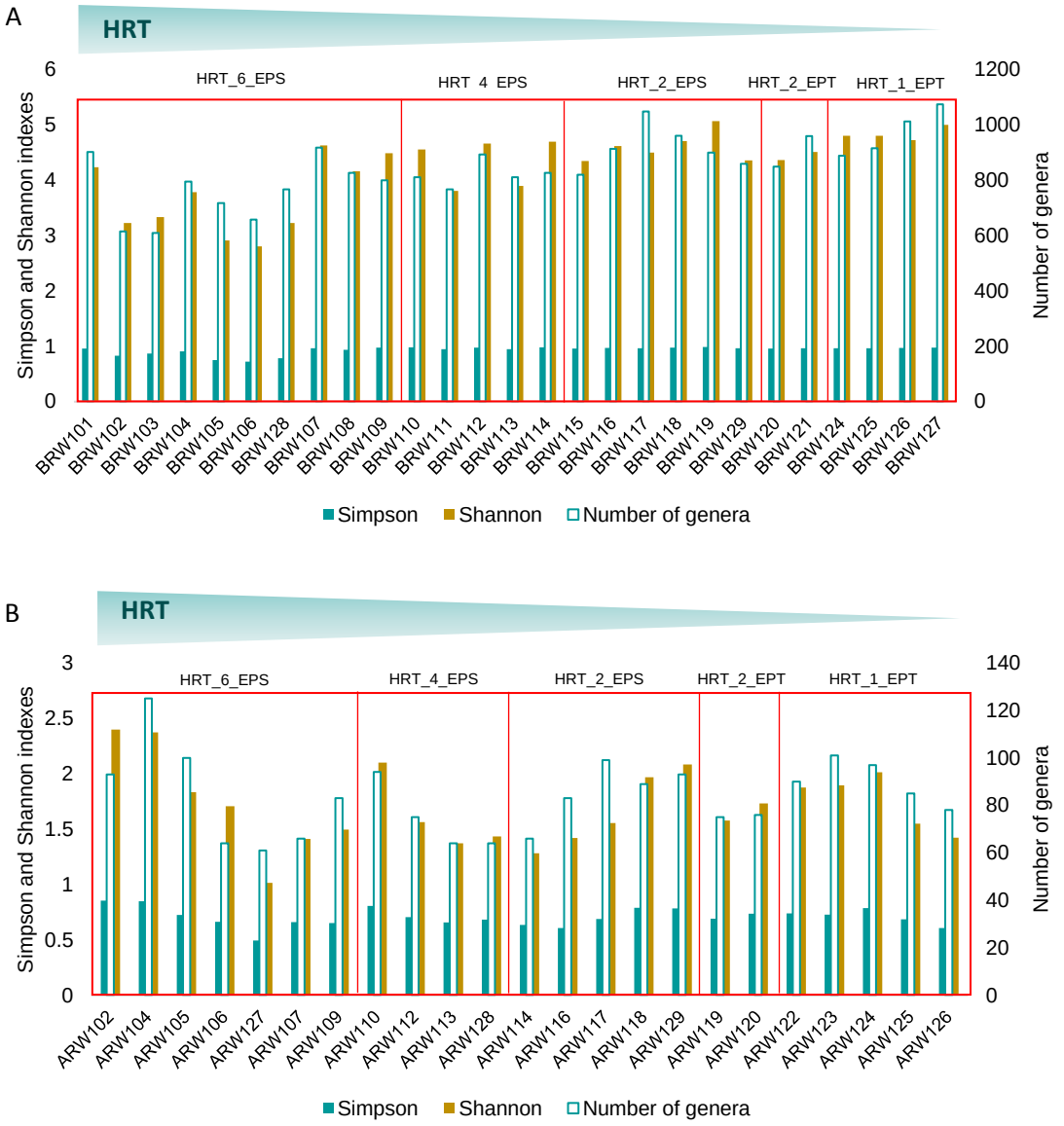

Figure VIII. 1. Diversity (inverse Simpson and Shannon-Wiener) and number of genera of bacteria (A) and eukarya (B)

Genera diversity can be related to both interspecific and intraspecific competition. The conventional theory of competition and niche differentiation assumes that competitive interactions can modify community structures by limiting a number of genus that can exploit the available resources/substrates. The role of competition is based on the competitive exclusion principle, i.e. if two or more genera compete for the same limiting resource, the genus best adapted to the boundary conditions will outcompete the

remaining genera. The ANOVA test for diversity and operational parameters revealed that for every bacteria taxonomic level, diversity increases as HRT decrease ($p < 0.01$). The lower the HRT, the higher the availability of substrate (organic matter, nutrients, micronutrients) for bacteria, which can increase both genera richness and relative abundance. The test also revealed that as this diversity increases, the effluent COD decreases ($p < 0.01$), proving that the more diverse bacteria community is, the more capable of consuming de COD despite its form. In addition, it was also observed that bacterial diversity decreases with increasing nitrite concentration ($p < 0.01$), since as mentioned in Chapter 6, NO_2-N not only affects microalgae growth but also some bacterial taxonomic groups (Blackburne et al., 2007; Claros et al., 2013; Pijuan et al., 2010).

Regarding eukarya domain, when looking at phylum or class levels, the ANOVA test revealed that when PAR increases, the diversity also increases ($p<0.01$). As PAR increases, more microalgae can grow, increasing not only its amount but its diversity. This rise is also related with the temperature ($p<0.01$). Another finding was that when the eukarya diversity decreases the effluent phosphorus content increase ($P<0.01$). It can be therefore assumed that phosphorus uptake by biomass is mainly due to microalgae.

In order to explore the beta diversity of the different samples processed for bacteria and microalgae quantification a PCoA based on Bray-Curtis distances matrix was performed (Figure VIII. 2 andFigure VIII. 3). This procedure allows to group samples based on the dissimilarity between samples and calculate a distance matrix. From Figure VIII. 2, it seems clear that the HRT and the incoming wastewater stream shape the bacterial populations. Bacterial structure of samples analyzed can be divided in 5 clusters. Biological community of the EPT-fed samples were similar regardless of operating HRT. However, significant differences in biological community can be observed in EPS-fed sampled. As in the biological activity measured in Chapter 5, the HRT_6_EPS period

shows a biological community different from the other HRTs. The main differences between these three periods is the concentration of NO_2-N, alkaline pH (and the consequent increase in free ammonia nitrogen (FAN)), which could specialize the bacterial groups towards a nitrite- and high pH-tolerant community. The specialization of the biological community against these abiotic factors explains the lower diversity observed from the Shannon-Wiener and Simpson indexes. Fewer genera are adapted to grow in these conditions, reducing the biological community diversity at 6 days of HRT (Figure VIII. 1).

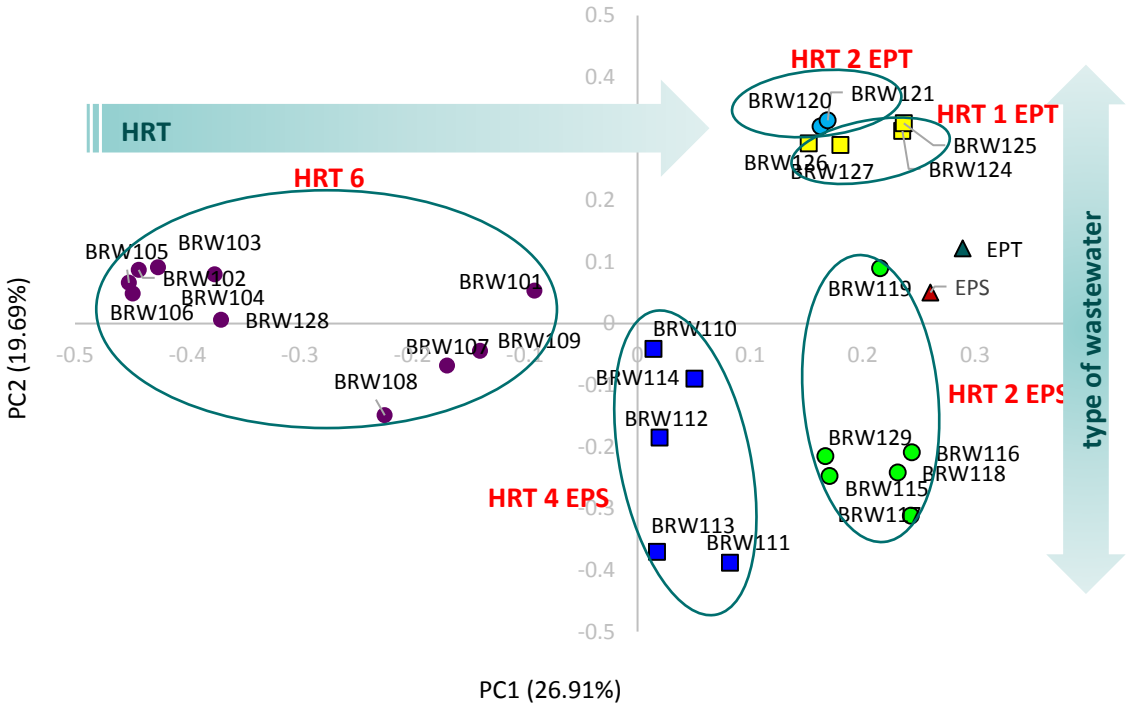

Figure VIII. 2. Principal Co-ordinates Analysis (PCoA) based on the Bray-Curtis distances matrix for 16S rDNA sequenced samples. Explained variance by each component is indicated in each axis in percentages.

Eukaryotic organisms seemed not be affected by the type of incoming wastewater stream and the operating HRT (Figure VIII. 3). Eukaryotic composition can be grouped into two main clusters: 6 days HRT and the rest of the samples. Oxygen production rate measured in Chapter 5 was significantly lower at 6 days of HRT, indicating that microalgae activity was limited. Furthermore, photosynthesis inhibition by NO_2-N was

verified and assessed in Chapter 6, when working at 6 days HRT. This sharp division between both clusters (Figure VIII. 3) could therefore be due to NO_2-N accumulation.

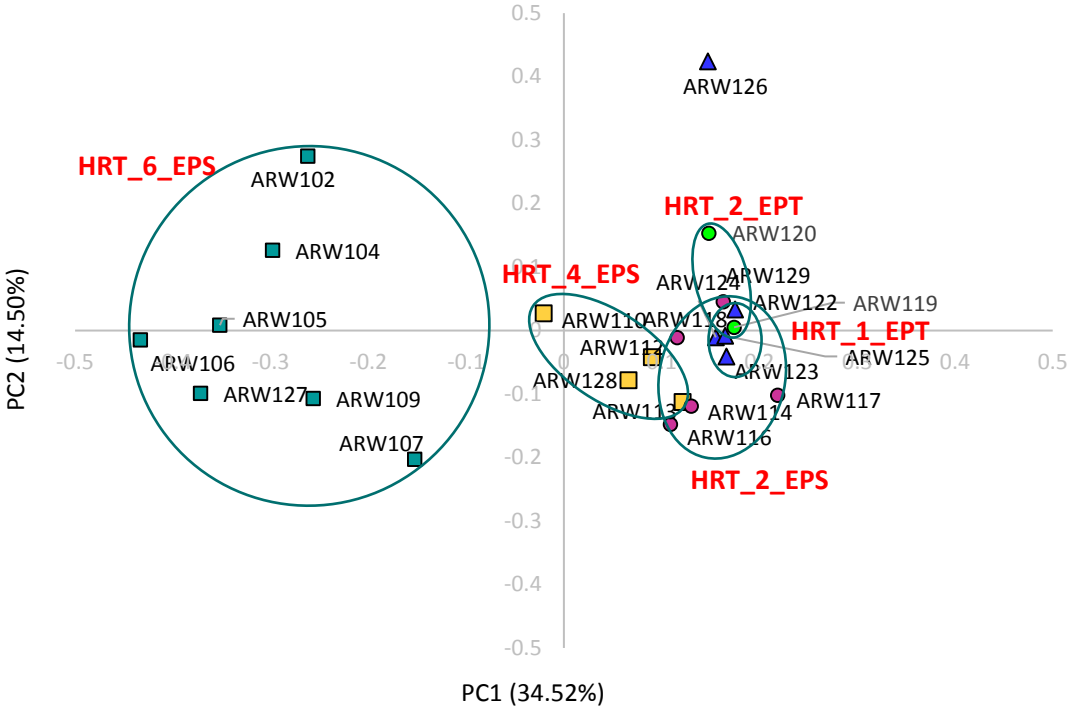

Figure VIII. 3. Principal Co-ordinates Analysis (PCoA) based on the Bray-Curtis distances matrix for 18S rDNA sequenced samples. Explained variance by each component is indicated in each axis in percentages.

However, although the optimal pH for microalgae range between 8 to 9 (Barceló-Villalobos et al., 2019; Rossi et al., 2020a), the slightly higher pH measured when working at 6 days HRT, could negatively affect microalgae, being also responsible for the division of both groups observed in Figure VIII. 3.

Table VIII. 2. Samples analyzed and characterization of the main abiotic parameters for each sample. Abbreviations: photosynthetically active radiation (PAR), temperature (T), average light intensity (I_{av}), dissolved oxygen (DO), organic loading rate (OLR), ammonium, nitrite and nitrate (NH_4-N, NO_2-N and NO_3-N, respectively) in the effluent, total nitrogen and ammonium removal efficiencies (T-N-RE and T-NH_4-RE).

Steady state group	Date	Bacteria sample code	Microalgae sample code	Wastewater stream	TRH (d)	T (ºC)	PAR ($\mu mol \cdot m^{-2} \cdot s^{-1}$)	Average I_{av} ($\mu mol \cdot m^{-2} \cdot s^{-1}$)	Maximum I_{av} ($\mu mol \cdot m^{-2} \cdot s^{-1}$)	pH	DO	OLR ($g \cdot m^{-3} \cdot d^{-1}$)	NH_4-N ($g\ N \cdot m^{-3}$)	NO_2-N ($g\ N \cdot m^{-3}$)	NO_3-N ($g\ N \cdot m^{-3}$)	T-N-RE (%)	T-NH_4-RE (%)
HRT_6_EPS	19/08/2019	BRW101		EPS	6	30.3	281.5	16 ± 5	186 ± 33	8.56	6.15	41.0	25.0	0.0	0.0	26.3 ± 0.6	75 ± 2
	16/10/2019	BRW102	ARW102		6	17.5	276.1			8.27	10.24	44.0	0.2	10.8	1.5		
	18/10/2019	BRW103			6	21.1	227.2			8.85	8.83	39.0	0.3	9.2	2.0		
	23/10/2019	BRW104	ARW104		6	15.4	136.7			8.53	9.03	46.0	0.0	6.9	0.0		
	25/10/2019	BRW105	ARW105		6	22.0	245.7			8.57	8.05	42.0	0.8	9.4	0.0		
	28/10/2019	BRW106	ARW106		6	22.8	99.6			8.55	7.42	48.0	0.4	5.5	0.0		
	06/11/2020	BRW128	ARW127		6	16.5	132.1			8.33	4.02	40.0	9.6	15.1	2.8		
	18/11/2019	BRW107	ARW107		6	16.4	132.0			8.22	3.91	38.0	10.5	16.2	2.8		
	20/11/2019	BRW108			6	16.4	152.0			8.25	2.82	52.0	9.0	16.5	8.5		
	25/11/2019	BRW109	ARW109		6	19.0	145.7			8.03	2.51	32.0	10.6	16.0	0.4		
HRT_4_EPS	20/12/2019	BRW110	ARW110	EPS	4	18.9	152.5	13 ± 5	91 ± 73	7.30	8.25	62.0	0.0	1.2	39.3	5.5 ± 0.9	98 ± 3
	23/12/2019	BRW111			4	19.1	165.2			7.56	8.63	59.0	0.0	1.4	39.1		
	26/12/2019	BRW112	ARW112		4	16.9	123.7			7.26	5.74	61.0	0.0	1.6	38.7		
	27/12/2019	BRW113	ARW113		4	16.1	140.2			7.57	8.79	60.0	0.5	1.1	42.8		
	02/01/2020	BRW114	ARW128		4	14.7	24.5			7.32	4.13	61.0	0.0	1.0	47.7		
HRT_2_EPS	13/01/2020	BRW115	ARW114	EPS	2	12.9	144.2	12 ± 2	105 ± 40	7.69	6.15	137.0	15.7	0.8	24.0	5.5 ± 0.8	99 ± 4
	15/01/2020	BRW116			2	12.8	81.0			7.70	5.86	128.0	16.7	0.8	22.5		
	20/01/2020	BRW117	ARW116		2	9.6	43.5			7.31	8.92	120.0	1.6	0.8	28.1		
	31/01/2020	BRW118	ARW117		2	20.3	145.5			7.19	4.49	132.0	0.5	1.6	42.7		
	11/02/2020	BRW119	ARW118		2	18.6	152.0			7.23	4.35	127.0	0.0	0.4	42.0		
	30/02/2020	BRW129	ARW129		2	17.7	151.1			7.14	4.26	118.0	0.0	0.4	30.2		
HRT_2_EPT	03/07/2020	BRW120	ARW119	EPT	2	28.4	117.8	4.3 ± 0.8	19.7 ± 0.6	7.35	2.54	339.0	1.5	0.0	3.8	91 ± 10	95 ± 6
	08/07/2020	BRW121	ARW120		2	30.8	269.5			7.43	1.00	337.0	34.6	0.0	1.9		
HRT_1_EPT	10/07/2020	BRW122	ARW122	EPT	1	29.8	259.6	3.1 ± 1.2	7.2 ± 0.8	7.64	0.13	678.0	31.4	0.4	1.0	1.12 ± 0.7	1.1 ± 0.5
	13/07/2020	BRW123			1	28.6	193.1			7.41	0.16	641.0	33.9	0.5	0.8		
	15/07/2020	BRW124	ARW123		1	27.6	265.6			7.36	0.17	666.0	30.1	2.1	2.0		
	17/07/2020	BRW125	ARW124		1	28.6	269.1			7.39	0.16	672.0	32.7	0.4	0.9		
	12/08/2020	BRW126	ARW125		1	29.6	253.4			7.42	0.15	681.0	30.1	0.4	0.2		
	17/08/2020	BRW127	ARW126		1	28.9	246.8			7.38	0.29	672.0	30.2	0.0	0.5		

8.3.2. Characterization of bacteria and microalgae communities

8.3.2.1. Bacteria community structure

Bacteria and microalgae communities were characterized and quantified by means of Illumina MiSeq platform. Figure VIII. 4 shows a barplot where relative abundances of bacteria are represented at phylum level. Microbial characterization of influent wastewaters has been also included, which have the same microbial composition. Dominant phylum differences are observed between the samples obtained from HRT_6_EPS and the rest of the periods. While in HRT_6_EPS the dominant phylum was *Verrucomicrobiota* (relative abundance between 18 – 56% without taking into account sample BRW101), in the other periods it was *Proteobacteria* (relative abundance between 28 – 44%) regardless of the operating conditions.

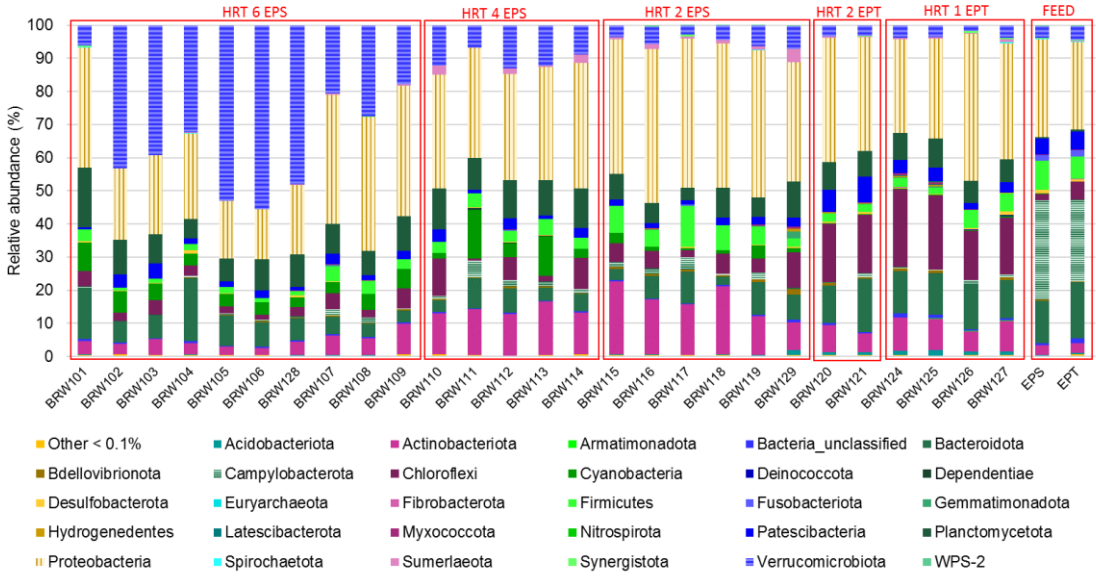

Figure VIII. 4. Relative abundance barplot of bacteria at phylum level. The series “Other” contains phyla with abundances below 0.1%. Samples are grouped by HRT and influent wastewater (EPS or EPT). Last columns represent the main phyla found in the effluent from the primary settler (EPS) and the effluent form the pre-treatment (EPT).

Phylum *Verrucomicrobiota* forms cytoplasmic appendages called protists, which are involved in attachment to surfaces and respiration. This morphological feature of this phylum could have induced the floc formation observed during most of the experimental period in our HRAP. The phylum *Verrucomicrobiota* has been widely reported in the

upper layer of aquatic ecosystems due to its high resistance to UV irradiation (Ferrero et al., 2012). The maximum average light intensity (I_{av}) was reported at HRT_6_EPS (186 ± 33 $\mu mol \cdot m^{-2} \cdot s^{-1}$, Chapter 5). Light intensity might therefore have acted as a microbial selection factor through UV tolerance. When reducing HRT to 4 days and also maximum average irradiance (91 ± 73 $\mu mol \cdot m^{-2} \cdot s^{-1}$, Chapter 5), *Verrucomicrobiota* decreased dramatically (7-13%) and *Proteobacteria* become the main bacteria phylum (32-35%). This shift between *Verrucomicrobiota* and *Proteobacteria* could be due to suppression of the "selective pressure". However, although the maximum I_{av} was significantly higher in HRT_6_EPS, the average I_{av} was similar in the three operating periods using EPS (16 ± 5, 13 ± 5, 12 ± 2 $\mu mol \cdot m^{-2} \cdot s^{-1}$, at 6, 4 and 2 days of HRT, Chapter 5). The distribution of the phylum cannot therefore be assumed to result of punctually high light intensities, but may also be influenced by NO_2-N accumulation and pH values close to 9. Taxonomic classification at the phylum level covers a wide range of organisms, which makes it unfeasible to establish tolerance ranges for pH and NO_2-N.

The rest of the phyla also increased, but *Actinobacteriota* (12-16%) experimented the highest increase in HRT_4_EPS and HRT_2_EPS. It is also worth noting the appearance of *Cyanobacteria*, reaching 15% in HRT_4_EPS. No major changes were observed in populations when decreasing the HRT to 2 days. *Proteobacteria* maintained its dominance (36-47%) and *Firmicutes* slightly increased (3-13%).

Next change was to feed the reactor with EPT instead of using EPS. Incoming wastewater stream increased markedly the relative abundance of *Chloroflexy* (15-24%). In wastewater systems, phylum *Chloroflexy* usually coexist with annamox bacteria. They grow due to intake of organic substrates such as soluble microbial products and extracellular polymeric substances that are derived from anammox bacteria (Kindaichi et al., 2012; Nierychlo et al., 2019). The ever-aerobic conditions of EPS-periods, due to low OLR (Table VIII. 2), limited anammox bacteria growth, and thus, bacteria of phylum *Chloroflexy*. This is why this phylum was hardly detected when using EPS.

To take a closer look at the evolution of microbial community structure along operating HRT and incoming wastewater stream, the metagenomics data was further analysed and compared at genus level. Genus LD29, belonging to the *Verrucomicrobiota* phylum, was the most abundant genera determined (up to 52%) in HRT_6_EPS. Although, the physiology of LD29 is unclear, it has been observed widely distributed in sea water and lakes, associated with high oxygen concentration and phytoplankton, suggesting their involvement in the utilization of phytoplankton-derived organic matter (Bergen et al., 2014; Zhao et al., 2021). Once the HRT was decreased, LD29 almost disappeared, the diversity increased and the main part of the genera (between 26 and 60%) were in abundances below 1%. Abiotic stress controlled the relative abundance and diversity of bacterial community. *Mycobacterium* (3-14%), from phylum *Actinobacteriota*, was the only genus with higher abundance in HRT_2_EPS. *Mycobacterium* genus could be potentially pathogenic bacteria and harmful to humans (Ye and Zhang, 2013), although it is difficult to know whether these *Mycobacterium* bacteria in these samples were pathogens since not all species in these genera are pathogenic bacteria. Some strains of *Mycobacterium* were closely related to degrade organic carbon, such as polycyclic aromatic ring (Jiang et al., 2021). Indeed, Warshawsky et al. (2007) reported that the consortium of *Mycobacterium* and microalgal *Selanastrum capricornutum* was able to degrade large recalcitrant polycyclic aromatic hydrocarbons.

After feeding pre-treated wastewater, an uncultured genus from *Caldilineaceae* family became the most abundant (10-18%). Members of *Caldilineaceae* are positively correlated with nitrite and nitrate removal rate (Cao et al., 2020; Liu and Li, 2019), indicating that this genus is a key active denitrifier. Zero oxygen concentrations were recorded during nighttime hours, promoting denitrification processes. Torres-Franco et al. (2021) also detected *Caldilineaceae* in an anoxic-aerobic microalgal-bacterial system treating digestate. In addition, genus *Ahniella*, from phylum *Proteobacteria*, also experimented an important increase (3-13%). However, members of this genus are not

commonly observed in activated sludge systems or microalgae-bacteria consortia and their role is almost unknown. They are considered heterotrophic bacteria that are not involved in nitrate reduction (Hwang et al., 2018).

Regarding bacteria related with phosphorous removal processes, it must be noted that no enhance biological phosphorous removal (EBPR) processes related bacteria, i.e. *Candidatus Accumulibacter Phosphatis*, were found in the MHARP, which highlights the absence of proper conditions for its growth, i.e. anaerobic conditions with the presence of soluble phosphorous and volatile fatty acids (AVG).

Ammonia-oxidizing bacteria (AOB)

One of the common threads between the previous chapters has been the role of nitrifying bacteria in microalgae-bacteria systems. Ammonia-oxidizing bacteria (AOB) not only compete with microalgae for ammonium, but also their metabolic product, NO_2-N, can inhibit microalgal photosynthesis. Regarding AOB genus detection, only genus *Nitrosomonas* was found in samples obtained when treating primary effluent (Figure VIII. 5). Neither *Nitrosospira* nor *Nitrosococcus* genera were detected.

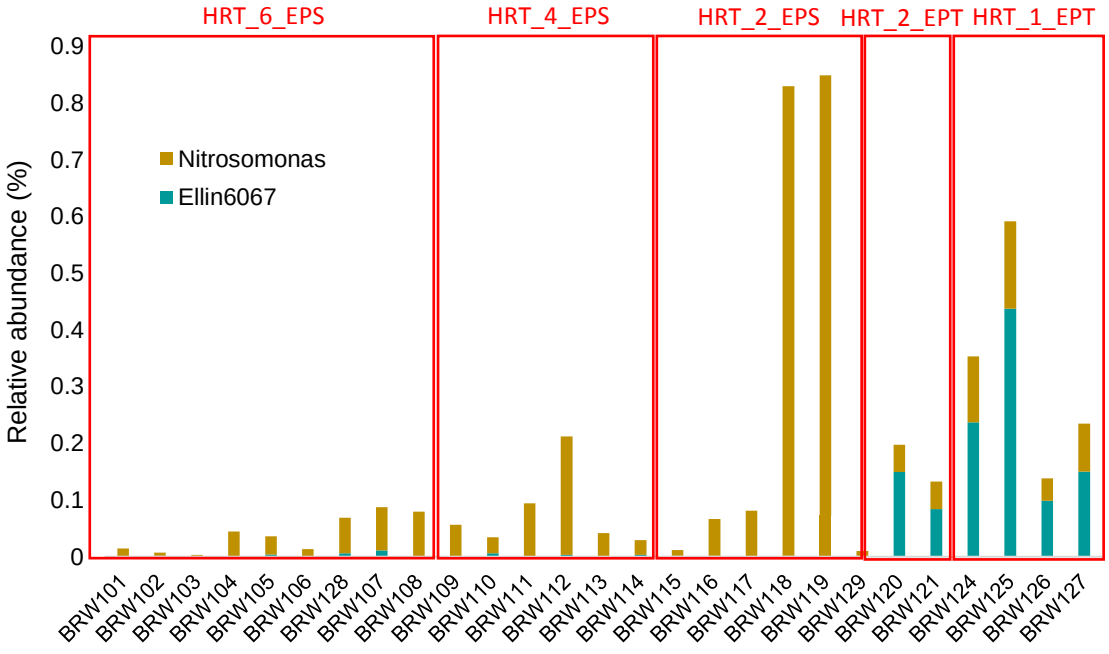

Figure VIII. 5. Ammonia-oxidizing bacteria relative abundance in each sample.

Nitrosococcus are commonly described associated to marine ecosystems and salt lakes. Furthermore, this genus has also been identified to cooperate as the dominant AOB with anammox bacteria in hypoxic layers (Campbell et al., 2011). The absence of genus *Nitrosococcus* in the EPS-period samples was therefore consistent with ever-aerobic conditions previously described.

Nitrosomonas and *Nitrosospira* are the most important genera of AOB activated sludge (Park and Noguera, 2004). Of the two genera, *Nitrosomonas* has been reported to be the dominant AOB in many bioreactors (Limpiyakorn et al., 2006; Wells et al., 2009), since *Nitrosomonas* has the potential to grow more than twice as fast as *Nitrospira* in the optimum abiotic boundary conditions (Siripong and Rittmann, 2007).

The most noticeable change between EPS- and EPT-fed MHRAP was the occurrence of genus *Ellin6067* spp. *Ellin6067* spp. is not a typical AOB genus in biological nitrogen removal systems. However, Wang et al. (2021) observed that its abundance gradually increased in lighted systems, behaving considerably tolerant and/or acclimated to light irradiation, ensuring the process of NH_4-N oxidation to NO_2-N in microalgae-bacteria systems. Although the light intensity measured at the reactor surface was higher in EPT and EPS periods, the I_{av} was higher in the periods using EPS (Table VIII. 2). Despite light-acclimation, it could therefore be photoinhibited at I_{av} of 12 $\mu mol \cdot m^{-2} \cdot s^{-1}$. In addition, inhibition of *Nitrosomonas* can be more strongly regulated by instantaneous incident light than by average light intensity, being *Ellin6067* spp. more competitive in EPT periods and outcompeting *Nitrosomonas*. However, scientist literature is limited for *Ellin6067* spp. High temperatures could also have promoted the growth of *Ellin6067* genus.

Although the AOB percentages of abundance obtained are very low (between 0 and 0.9%), it should be remembered that sequencing techniques detect copies of the gene and not individual organisms. More relevant is the observed trend, where it can be seen that when HRT decreases, the AOB population increases. Furthermore, it can also be noted that feeding with pre-treated wastewater (rather than primary settled wastewater)

leads to the proliferation of not only more AOB but also more AOB genera (*Nitrosomonas* + *Ellin6067*).

Nitrite-oxidizing bacteria (NOB)

As shown in Figure VIII. 6, NOB genera had different evolution trends under the different experimental periods. The main NOB genera found in the MHRAP were *Candidatus Nitrotoga*, *Nitrobacter* and *Nitrospira*. *Nitrospira*-like microorganisms generally dominate in activated sludge systems because of their high affinity for NO_2-N. The sequencing results of HRT_6_EPS revealed that *Nistrospira* was the only NOB present in the system although at quite low proportion overall, which is consistent with the NO_2-N accumulation (Figure VIII. 6).

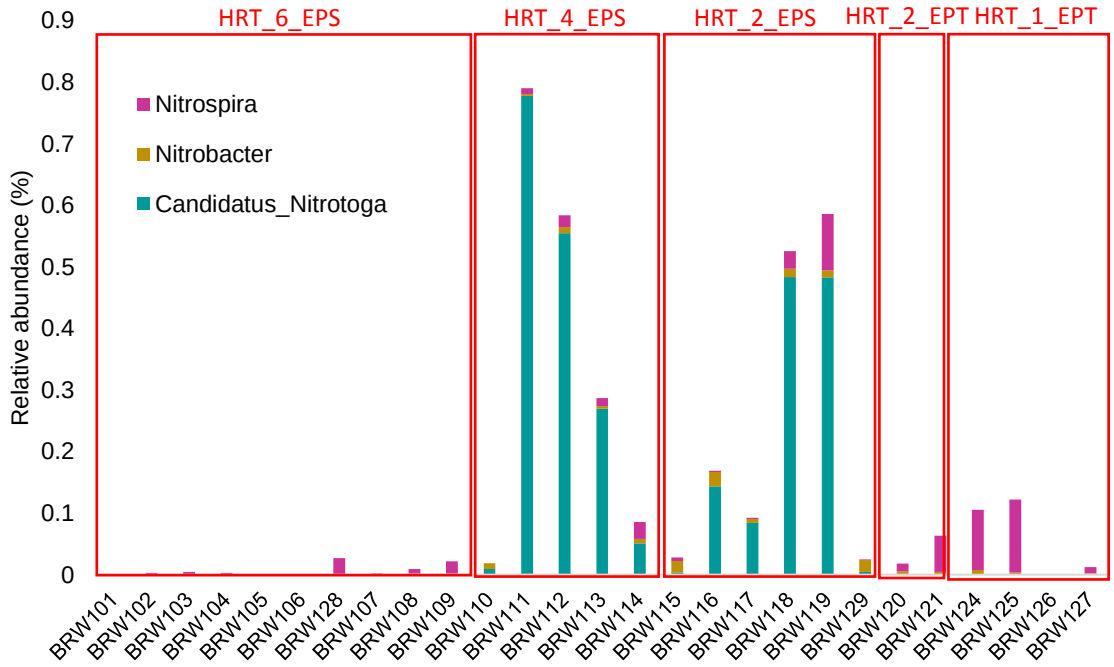

Figure VIII. 6. Nitrite-oxidizing bacteria relative abundance in each sample.

The dominant NOB in the ecological community changed from *Nitrospira* to *Candidatus Nitrotoga* in HRT_4_EPS and HRT_2_EPS (Figure VIII. 6). Zheng et al. (2020) elucidated the key factors that affect NOB community composition. This study demonstrated that *Nitrospira* are the dominant NOB under regular exposure to FAN. The culture pH was reduced (from approximately 9 to 7.5 (Table VIII. 2)) by decreasing HRT,

and therefore, the FAN concentration also decreased. The different NOB community structures observed in these three periods suggested that *Candidatus Nitrotoga* may indeed be more sensitive than *Nitrospira*. Comparing HRT_6_EPS with HRT_4_EPS and HRT_2_EPS, a sharp increase in relative abundance of NOB was observed, as well as for AOB. The higher relative abundance of NOB was 0.02% at HRT_6_EPS, while a 0.77 and a 0.50% of NOB was reached in HRT_4_EPS and HRT_2_EPS, respectively. It is assumed that higher NOB relative abundance in HRT_4_EPS and HRT_2_EPS is responsible for NO_2-N oxidation to NO_3-N, avoiding the accumulation of the former.

In EPT-fed MHRAP samples *Candidatus Nitrotoga* did not grow and the NOB community structures were dominated by *Nitrospira*. *Candidatus Nitrotoga* are less competitive than *Nitrospira* during oxygen deficiency. Although oxygen concentrations close to 8 were reached during daylight hours, oxygen concentration was zero at night, which could limit growth of *Candidatus Nitrotoga* in period HRT_2_EPT. In addition, oxygen concentration in period HRT_1_EPT was nearly zero, which resulted in a decrease in NOB relative abundance (0.01%) at the end of the period.

8.3.2.2. Microalgae community structure

Figure VIII. 7 depicts de relative abundance of eukarya organisms in the analysed samples at genus level. Working al HRT 6 days led to a higher abundance of green microalage *Desmodesmus* (30-69%) over *Coelastrella* (11-44%), both from order *Sphaeropleales*.

As in the bacterial community structure, abiotic stress in the HRT_6_EPS period samples conditioned the microalgae growth. *Desmodesmus* could be less sensitive than *Coelastrella* to alkaline pH, high nitrite and FAN concentrations. However, no data describing the suitable growth conditions for both genera have been found in literature.

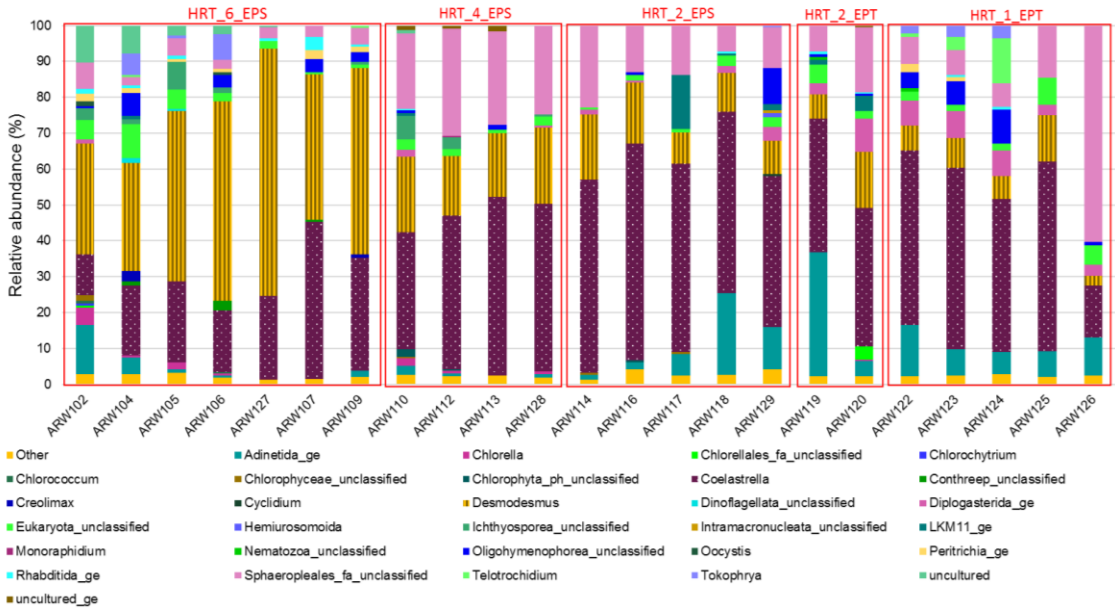

Figure VIII. 7. Relative abundance barplot of eukarya at genus level. The series “Other” contains genus with abundances below 0.5%. Samples are grouped by HRT and influent wastewater (EPS or EPT).

By decreasing HRT, algal community structure was dominated by *Coelastrella*, regardless of the incoming wastewater stream. *Coelastrella* genus accounted for over 50%. Previous studies revealed that *Chlorophyta* has been widely used in treating wastewater (Abinandan and Shanthakumar, 2015). It was thus reasonable to consider that *Coelastrella*, which belongs to *Chlorophyta* phylum, contributed to nitrogen removal. Luo et al. (2016) showed that NH_4-N removal efficiency of *Coelastrella* was relatively high (over 90%). Abe et al. (2007) reported a high nitrate removal, with nitrate uptake rate reaching 0.4 $mg \cdot h^{-1}$. However, according to nitrogen mass balance (Chapter 5) the main mechanism of NH_4-N removal was nitrification. In addition, NO_3-N uptake rate by microalgae was not observed. Thus, microalgae had a support role, providing oxygen to aerobic bacteria, regardless of operating HRT and the type of incoming wastewater. In the present study, microalgae composition was not affected by environmental parameters. Even the increase of PAR or temperature did not affected to *Coelastrella* dominance.

To date, the identification of microalgae in these chapters has been based on their morphology. Populations have traditionally been found to vary between *Scenedesmus*-

and *Chlorella*-like organisms. However, the sequencing data of the present study show that the abundance of the *Chlorellales* order barely reaches 7% of the eukarya domain (sample BRW101). Almost all the microalgae found in this study belong to the *Sphaeropleales* order, in which the *Scenedesmus*-like microalgae are included.

8.3.3. In-depth analysis of the evolution of the microbiota community structure and the relationship with MHRAP performance

The effect of bacterial and microalgal community structure on MHRAP performance was analysed according to the operating periods described in Chapter 5. Partial-nitrification accounted for 48.6%, resulting in a final NO_2-N concentration of 21 ± 3 $g \cdot m^{-3}$ in HRT_6_EPS. Relative abundance of NOB community in the period barely achieved a 0.03%, showing an oxygen uptake rate of NOB of 0.6 ± 0.2 mg $O_2 \cdot g\ VSS^{-1} \cdot h^{-1}$, indicating that NOB could be inhibited. However, abiotic stress of this period, e.g. alkaline pH, FAN concentration and even NO_2-N accumulation, not only limited NOB growth but also other groups of bacteria and microalgae. Biodiversity indexes (Figure VIII. 1) along with relative abundance of bacteria phylum (Figure VIII. 4) showed a reduction of organisms diversity (compared with other periods). Selective microalgae genus of *Desmodesmus* was dominant in period HRT_6_EPS, but strains of this genus only provide oxygen to aerobic bacteria. Reducing operating HRT reduces abiotic stress, as was indicated above. Partial nitrification was avoided in both HRT_4_EPS and HRT_2_EPS, which is consistent to the increase in NOB relative abundance (reaching values up to 0.7% in some samples) and activity (approximately 1.1 mg $O_2 \cdot g\ VSS^{-1} \cdot h^{-1}$ in both periods). MHRAP performance was similar in both periods (HRT_4_EPS and HRT_2_EPS), registering values of ammonium removal (T-NH_4-RE)) over 95%. This is consistent with microbial dynamics, as Figure VIII. 4 Figure VIII. 7 revealed similar bacterial and microalgal community composition. Both periods were dominated by the same bacterial and microalgal groups.

The main difference between EPS- and EPT-fed MHRAP was the oxygen fluctuation. In HRT_2_EPT, oxygen concentration near to saturation was recorded in lighting

conditions, while dark periods (night-time hours) provide anoxic conditions. As a result of this oxygen dynamic, denitrifying bacteria belonging to *Chloroflexy* phylum grew. Indeed a 91 ± 10% of T-N was removed by the coupled nitrification-denitrification process. Nitrifying activity was higher in EPT-operated periods (2.5 ± 0.4 mg O_2·g VSS^{-1}·h^{-1}) than in the EPS-operated periods, despite the lower relative NOB abundances in HRT_2_EPT. It should be noted, that relative abundance measured number of copies of each group but did not provide information about biological activity. Indeed, similar microbial composition was observed in HRT_2_EPT and HRT_1_EPT, but Nitrogen removal eficiency accounted for 91 ± 1% and 1.1 ± 0.7%, respectively. Oxygen demand under this conditions (HRT_1_EPT) surpass oxygen supply by microalgae, thus aerobic processes, as nitrification, were limited. Relative abudance of AOB and NOB genera in some samples of EPS- fed periods are higher than in HRT_2_EPT. However, nitrifiying activity was significantly lower, 0.3 mg O_2·g VSS^{-1}·h^{-1} compared to 1.3 mg O_2·g VSS^{-1}·h^{-1}, respectively. Again, metagenomic analysis is based in the number of copies of a tarjet gene, which is not necessarily related to the activity of the organisms.

Microalgal composition did not show significant differences between periods, indicating that microalgae selection was largely unaffected by HRT operation, (in the range of 4-1 days), and type of wastewater stream, under the abiotic conditions described in Table VIII. 2. The major role of microalgae was to provide oxygen to aerobic bacteria. Thus, as it was concluded in Chapter 5, bacteria are the cornerstone of the microalgae-bacteria consortium. Bacterial composition, rather than microalgal structure, determined MHRAP performance.

8.4. CONCLUSIONS

The study represents a powerful initial work for improving knowledge regarding microalgae-bacteria interactions in wastewater treatments. HRT and the incoming wastewater stream are the main responsible for shaping bacterial populations. Abiotic

stress conditions, such as light intensity, free ammonia nitrogen, pH and nitrite accumulation, reduced bacteria diversity. The observed shifts in bacterial composition, including AOB community, suggests that photoinhibtion processes could be taking place, which could regulate ecological structure of bacteria.

The NOB community was dominated by *Nitrospira* and *Candidatus Nitrotoga*. This study revealed that *Nitrospira* is the dominant NOB genera under regular exposure to free ammonia nitrogen and low average oxygen concentration. *Desmodesmus* and *Coelastrella* were the dominant genus in the five periods studied. Microalgal community was dominated by *Desmodesmus* under alkaline pH and exposure of nitrite and free ammonia nitrogen. The results suggest that microalgae biodiversity was not affected by the hydraulic retention time or influent wastewater composition.

The main abiotic stress conditions seem to be, light intensity, free ammonia nitrogen, pH and nitrite accumulation. The effect of these possible inhibiting factors will be evaluated in Chapter 10 using a mathematical model.

Nitrogen removal efficiencies were affected by bacterial community composition but not by microalgae composition. Low relative abundances of NOB resulted in partial-nitrification. Daily fluctuations of oxygen concentration resulted in *Chloroflexy* and *Caldilineaceae* growth, leading to nitrogen removal by coupled nitrification-denitrification process. The key role of microalgae was to support aerobic bacterial processes.

REFERENCES

Abe, K., Hattori, H., Hirano, M., 2007. Accumulation and antioxidant activity of secondary carotenoids in the aerial microalga Coelastrella striolata var. multistriata. Food Chem. 100, 656–661. https://doi.org/10.1016/j.foodchem.2005.10.026

Abinandan, S., Shanthakumar, S., 2015. Challenges and opportunities in application of microalgae (Chlorophyta) for wastewater treatment: A review. Renew. Sustain. Energy Rev. 52, 123–132. https://doi.org/10.1016/J.RSER.2015.07.086

Acién, F.G., Gómez-Serrano, C., Morales-Amaral, M.M., Fernández-Sevilla, J.M., Molina-Grima, E., 2016. Wastewater treatment using microalgae: how realistic a contribution might it be to significant urban wastewater treatment? Appl. Microbiol. Biotechnol. 2016 10021 100, 9013–9022. https://doi.org/10.1007/S00253-016-7835-7

APHA-AWWA-WPCF, 2012. Standard Methods for the Examination of Water and Wastewater, 22nd edition, American P. ed. Washington DC, USA.

Barceló-Villalobos, M., Serrano, C.G., Zurano, A.S., García, L.A., Maldonado, S.E., Peña, J., Fernández, F.G.A., 2019. Variations of culture parameters in a pilot-scale thin-layer reactor and their influence on the performance of Scenedesmus almeriensis culture. Bioresour. Technol. Reports 6, 190–197. https://doi.org/10.1016/J.BITEB.2019.03.007

Bergen, B., Herlemann, D.P.R., Labrenz, M., Jürgens, K., 2014. Distribution of the verrucomicrobial clade Spartobacteria along a salinity gradient in the Baltic Sea. Environ. Microbiol. Rep. 6, 625–630. https://doi.org/10.1111/1758-2229.12178

Bernard, O., Rémond, B., 2012. Validation of a simple model accounting for light and temperature effect on microalgal growth. Bioresour. Technol. 123, 520–527. https://doi.org/10.1016/j.biortech.2012.07.022

Blackburne, R., Vadivelu, V.M., Yuan, Z., Keller, J., 2007. Kinetic characterisation of an enriched Nitrospira culture with comparison to Nitrobacter. Water Res. 41, 3033–3042. https://doi.org/10.1016/j.watres.2007.01.043

Campbell, M.A., Chain, P.S.G., Dang, H., El Sheikh, A.F., Norton, J.M., Ward, N.L., Ward, B.B., Klotz, M.G., 2011. Nitrosococcus watsonii sp. nov., a new species of marine obligate ammonia-oxidizing bacteria that is not omnipresent in the world's oceans: calls to validate the names 'Nitrosococcus halophilus' and 'Nitrosomonas mobilis.' FEMS Microbiol. Ecol. 76, 39–48. https://doi.org/10.1111/J.1574-6941.2010.01027.X

Cao, J., Zhang, T., Wu, Y., Sun, Y., Zhang, Y., Huang, B., Fu, B., Yang, E., Zhang, Q., Luo, J., 2020. Correlations of nitrogen removal and core functional genera in full-scale wastewater treatment plants: Influences of different treatment processes and influent characteristics. Bioresour. Technol. 297, 122455. https://doi.org/10.1016/J.BIORTECH.2019.122455

Chai, C., Zhang, D., Yu, Y., Feng, Y., Wong, M.S., 2015. Carbon footprint analyses of mainstream wastewater treatment technologies under different sludge treatment scenarios in China. Water (Switzerland) 7, 918–938. https://doi.org/10.3390/w7030918

Claros, J., Jiménez, E., Aguado, D., Ferrer, J., Seco, A., Serralta, J., 2013. Effect of pH and HNO2 concentration on the activity of ammonia-oxidizing bacteria in a partial nitritation reactor. Water Sci. Technol. 67, 2587–2594. https://doi.org/10.2166/wst.2013.132

Ferrero, E.M., de Godos, I., Rodríguez, E.M., García-Encina, P.A., Muñoz, R., Bécares, E., 2012. Molecular characterization of bacterial communities in algal–bacterial photobioreactors treating piggery wastewaters. Ecol. Eng. 40, 121–130. https://doi.org/10.1016/J.ECOLENG.2011.10.001

Foladori, P., Petrini, S., Andreottola, G., 2018. Evolution of real municipal wastewater treatment in photobioreactors and microalgae-bacteria consortia using real-time parameters. Chem. Eng. J. 345, 507–516. https://doi.org/10.1016/J.CEJ.2018.03.178

González-Camejo, J., Aparicio, S., Jiménez-Benítez, A., Pachés, M., Ruano, M. V, Borrás, L., Barat, R., Seco, A., 2020. Improving membrane photobioreactor performance by reducing light path: operating

conditions and key performance indicators. Water Res. 172. https://doi.org/10.1016/j.watres.2020.115518

Hwang, W.M., Ko, Y., Kim, J.H., Kang, K., 2018. Ahniella affigens gen. Nov., sp. nov., a gammaproteobacterium isolated from sandy soil near a stream. Int. J. Syst. Evol. Microbiol. 68, 2478–2484. https://doi.org/10.1099/IJSEM.0.002859/CITE/REFWORKS

Jiang, Y., Shi, X., Ng, H.Y., 2021. Aerobic granular sludge systems for treating hypersaline pharmaceutical wastewater: Start-up, long-term performances and metabolic function. J. Hazard. Mater. 412, 125229. https://doi.org/10.1016/J.JHAZMAT.2021.125229

Kindaichi, T., Yuri, S., Ozaki, N., Ohashi, A., 2012. Ecophysiological role and function of uncultured Chloroflexi in an anammox reactor. Water Sci. Technol. 66, 2556–2561. https://doi.org/10.2166/WST.2012.479

Lian, J., Wijffels, R.H., Smidt, H., Sipkema, D., 2018. The effect of the algal microbiome on industrial production of microalgae. Microb. Biotechnol. https://doi.org/10.1111/1751-7915.13296

Limpiyakorn, T., Kurisu, F., Yagi, O., 2006. Quantification of ammonia-oxidizing bacteria populations in full-scale sewage activated sludge systems and assessment of system variables affecting their performance. Water Sci. Technol. 54, 91–99. https://doi.org/10.2166/WST.2006.376

Liu, X., Li, H., 2019. Nitrogen removal performance and microorganism community of an A/O-MBBR system under extreme hydraulic retention time. undefined 158, 105–113. https://doi.org/10.5004/DWT.2019.24268

Luo, L., He, H., Yang, C., Wen, S., Zeng, G., Wu, M., Zhou, Z., Lou, W., 2016. Nutrient removal and lipid production by Coelastrella sp. in anaerobically and aerobically treated swine wastewater. Bioresour. Technol. 216, 135–141. https://doi.org/10.1016/j.biortech.2016.05.059

Mantovani, M., Marazzi, F., Fornaroli, R., Bellucci, M., Ficara, E., Mezzanotte, V., 2020. Outdoor pilot-scale raceway as a microalgae-bacteria sidestream treatment in a WWTP. Sci. Total Environ. 710, 135583. https://doi.org/10.1016/J.SCITOTENV.2019.135583

Marazzi, F., Bellucci, M., Rossi, S., Fornaroli, R., Ficara, E., Mezzanotte, V., 2019. Outdoor pilot trial integrating a sidestream microalgae process for the treatment of centrate under non optimal climate conditions. Algal Res. 39, 101430. https://doi.org/10.1016/j.algal.2019.101430

Nierychlo, M., Miłobędzka, A., Petriglieri, F., McIlroy, B., Nielsen, P.H., McIlroy, S.J., 2019. The morphology and metabolic potential of the Chloroflexi in full-scale activated sludge wastewater treatment plants. FEMS Microbiol. Ecol. 95. https://doi.org/10.1093/FEMSEC/FIY228

Ozgun, H., Dereli, R.K., Ersahin, M.E., Kinaci, C., Spanjers, H., Van Lier, J.B., 2013. A review of anaerobic membrane bioreactors for municipal wastewater treatment: Integration options, limitations and expectations. Sep. Purif. Technol. https://doi.org/10.1016/j.seppur.2013.06.036

Park, H.D., Noguera, D.R., 2004. Evaluating the effect of dissolved oxygen on ammonia-oxidizing bacterial communities in activated sludge. Water Res. 38, 3275–3286. https://doi.org/10.1016/J.WATRES.2004.04.047

Pijuan, M., Ye, L., Yuan, Z., 2010. Free nitrous acid inhibition on the aerobic metabolism of poly-phosphate accumulating organisms. Water Res. 44, 6063–6072. https://doi.org/10.1016/j.watres.2010.07.075

Rahman, S.M., Eckelman, M.J., Onnis-Hayden, A., Gu, A.Z., 2016. Life-Cycle Assessment of Advanced Nutrient Removal Technologies for Wastewater Treatment. Environ. Sci. Technol. 50, 3020–3030. https://doi.org/10.1021/acs.est.5b05070

Ramanan, R., Kim, B.H., Cho, D.H., Oh, H.M., Kim, H.S., 2016. Algae–bacteria interactions: Evolution, ecology and emerging applications. Biotechnol. Adv. 34, 14–29. https://doi.org/10.1016/J.BIOTECHADV.2015.12.003

Rossi, S., Casagli, F., Mantovani, M., Mezzanotte, V., Ficara, E., 2020. Selection of photosynthesis and respiration models to assess the effect of environmental conditions on mixed microalgae consortia grown on wastewater. Bioresour. Technol. 305, 122995.

https://doi.org/10.1016/J.BIORTECH.2020.122995

Sabeen, A.H., Noor, Z.Z., Ngadi, N., Almuraisy, S., Raheem, A.B., 2018. Quantification of environmental impacts of domestic wastewater treatment using life cycle assessment: A review. J. Clean. Prod. https://doi.org/10.1016/j.jclepro.2018.04.053

Sánchez-Zurano, A., Cárdenas, J.A.G., Serrano, C.G., Amaral, M.M., Acién-fernández, F.G., Sevilla, J.M.F., Grima, E.M., 2020. Year-long assessment of a pilot-scale thin-layer reactor for microalgae wastewater treatment . Variation in the microalgae-bacteria consortium and the impact of environmental conditions. Algal Res. 50, 101983. https://doi.org/10.1016/j.algal.2020.101983

Seco, A., Aparicio, S., González-Camejo, J., Jiménez-Benítez, A., Mateo, O., Mora, J.F., Noriega-Hevia, G., Sanchis-Perucho, P., Serna-García, R., Zamorano-López, N., Giménez, J.B., Ruiz-Martínez, A., Aguado, D., Barat, R., Borrás, L., Bouzas, A., Martí, N., Pachés, M., Ribes, J., Robles, A., Ruano, M. V., Serralta, J., Ferrer, J., 2018. Resource recovery from sulphate-rich sewage through an innovative anaerobic-based water resource recovery facility (WRRF). Water Sci. Technol. 78, 1925–1936. https://doi.org/10.2166/wst.2018.492

Siripong, S., Rittmann, B.E., 2007. Diversity study of nitrifying bacteria in full-scale municipal wastewater treatment plants. Water Res. 41, 1110–1120. https://doi.org/10.1016/J.WATRES.2006.11.050

Torres-Franco, A.F., Zuluaga, M., Hernández-Roldán, D., Leroy-Freitas, D., Sepúlveda-Muñoz, C.A., Blanco, S., Mota, C.R., Muñoz, R., 2021. Assessment of the performance of an anoxic-aerobic microalgal-bacterial system treating digestate. Chemosphere 270, 129437. https://doi.org/10.1016/J.CHEMOSPHERE.2020.129437

Wang, L., Qiu, S., Guo, J., Ge, S., 2021. Light Irradiation Enables Rapid Start-Up of Nitritation through SuppressingnxrBGene Expression and Stimulating Ammonia-Oxidizing Bacteria. Environ. Sci. Technol. 55, 13297–13305. https://doi.org/10.1021/ACS.EST.1C04174/SUPPL_FILE/ES1C04174_SI_001.PDF

Warshawsky, D., LaDow, K., Schneider, J., 2007. Enhanced degradation of benzo[a]pyrene by Mycobacterium sp. in conjunction with green alga. Chemosphere 69, 500–506. https://doi.org/10.1016/J.CHEMOSPHERE.2007.03.031

Wells, G.F., Park, H.D., Yeung, C.H., Eggleston, B., Francis, C.A., Criddle, C.S., 2009. Ammonia-oxidizing communities in a highly aerated full-scale activated sludge bioreactor: betaproteobacterial dynamics and low relative abundance of Crenarchaea. Environ. Microbiol. 11, 2310–2328. https://doi.org/10.1111/J.1462-2920.2009.01958.X

Ye, J., Song, Z., Wang, L., Zhu, J., 2016. Metagenomic analysis of microbiota structure evolution in phytoremediation of a swine lagoon wastewater. Bioresour. Technol. 219, 439–444. https://doi.org/10.1016/J.BIORTECH.2016.08.013

Ye, L., Zhang, T., 2013. Bacterial communities in different sections of a municipal wastewater treatment plant revealed by 16S rDNA 454 pyrosequencing. Appl. Microbiol. Biotechnol. 97, 2681–2690. https://doi.org/10.1007/S00253-012-4082-4/FIGURES/5

Zhang, B., Li, W., Guo, Y., Zhang, Z., Shi, W., Cui, F., Lens, P.N.L., Tay, J.H., 2020. Microalgal-bacterial consortia: From interspecies interactions to biotechnological applications. Renew. Sustain. Energy Rev. 118, 109563. https://doi.org/10.1016/J.RSER.2019.109563

Zhao, D., Gao, P., Xu, L., Qu, L., Han, Y., Zheng, L., Gong, X., 2021. Disproportionate responses between free-living and particle-attached bacteria during the transition to oxygen-deficient zones in the Bohai Seawater. Sci. Total Environ. 791, 148097. https://doi.org/10.1016/J.SCITOTENV.2021.148097

Zheng, M., Li, S., Ni, G., Xia, J., Hu, S., Yuan, Z., Liu, Y., Huang, X., 2020. Critical Factors Facilitating Candidatus Nitrotoga to Be Prevalent Nitrite-Oxidizing Bacteria in Activated Sludge. Environ. Sci. Technol. 54, 15414–15423. https://doi.org/10.1021/ACS.EST.0C04192/SUPPL_FILE/ES0C04192_SI_001.PDF

CHAPTER IX

9. Global sensitivity and uncertainty analysis of a microalgae model for wastewater treatment.

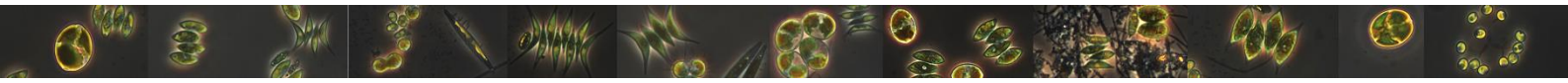

9. Global sensitivity and uncertainty analysis of a microalgae model for wastewater treatment.

ABSTRACT

The results of a global sensitivity and uncertainty analysis of a microalgae model applied to a Membrane Photobioreactor (MPBR) pilot plant were assessed. The main goals of this study were: (I) to identify the sensitivity factors of the model through the Morris screening method, i.e. the most influential factors; (II) to calibrate the influential factors online or offline; and (III) to assess the model's uncertainty. Four experimental periods were evaluated, which encompassed a wide range of environmental and operational conditions. Eleven influential factors (e.g. maximum specific growth rate, light intensity and maximum temperature) were identified in the model from a set of 34 kinetic parameters (input factors). These influential factors were preferably calibrated offline and alternatively online. Offline/online calibration provided a unique set of model factor values that were used to match the model results with experimental data for the four experimental periods. A dynamic optimization of these influential factors was conducted, resulting in an enhanced set of values for each period. Model uncertainty was assessed using the uncertainty bands and three uncertainty indices: p-factor, r-factor and ARIL. Uncertainty was dependent on both the number of influential factors identified in each period and the model output analyzed (i.e. biomass, ammonium and phosphate concentration). The uncertainty results revealed a need to apply offline calibration methods to improve model performance.

Keywords

Dynamic optimization; Microalgae model; MPBR; Municipal wastewater; Sensitivity analysis; Uncertainty analysis.

Authors

Stéphanie Aparicio, Rebecca Serna García, Aurora Seco, José Ferrer, Luis Borrás Falomir and Ángel Robles. Aparicio, S., García, R.S., Seco, A., Ferrer, J., Falomir, L.B., Robles, Á., 2022. Global sensitivity and uncertainty analysis of a microalgae model for wastewater treatment. Sci. Total Environ. 806, 150504. https://doi.org/10.1016/J.SCITOTENV.2021.150504

9.1. INTRODUCTION

Microalgae-based wastewater treatment represents a promising biological system to treat different wastewater sources in a way that can transform conventional wastewater treatment plants (WWTPs) into water resource recovery facilities (WRRFs) (Seco et al., 2018). Photoautotrophic microalgae use light energy, inorganic carbon and nutrients (inorganic nitrogen and phosphorus) for growth. Solar energy and nutrients are harvested in form of microalgae biomass while inorganic carbon is biofixed. Microalgae-based wastewater treatment can reduce treatment costs, generate clean water and reduce the environmental impact of the process (Seco et al., 2018).

An in-depth knowledge of the processes involved in microalgae metabolism is required to better understand how to operate microalgae-based technologies, how to optimize processes associated, how to improve reactor design and how to select the best control strategies to enhance pollutant removal efficiency. Microalgae and traditional activated sludge systems are intrinsically complex, since both depend on environmental variables such as temperature, pH, substrate availability, etc. However, it should be noted that photoautotrophic microalgae metabolism is not only affected by the environmental factors that influence activated sludge but also by seasonal and daily fluctuations in light intensity (González-Camejo et al., 2018). The correct operation of microalgae-based wastewater treatments thus demands a robust, feasible and efficient tool to forecast the culture development and its compliance with increasingly stringent regulations. Mathematical models can help to study the main processes and variables that influence algal metabolism in different culture media, including municipal wastewater.

An array of mathematical models for predicting microalgae growth has been developed in the last ten years (Costache et al., 2013; Eze et al., 2018; Ndiaye et al., 2018; Ruiz et al., 2013; Solimeno et al., 2015, 2017; Wágner et al., 2016). This process cannot be considered a well-characterized system, since some model factors are uncertain and speciation-dependent. The ammonium semi-saturation constant has been reported to

range from 0.1 to 31.5 g $N \cdot m^{-3}$ (Aslan and Kapdan, 2006; Solimeno et al., 2017), and is a perfect example of the intrinsic variability and uncertainty of model factors, so that the application of these models requires a great number of assumptions regarding the simplification of biological processes and model factors. These assumptions are sources of uncertainty that could propagate through the model thus generating uncertainty in the model outputs. The resulting uncertainty in the model results could lead to misleading decisions during process design and/or optimization. Hence, performing a global sensitivity and uncertainty analysis (GSA and UA, respectively) would help to deal with these issues by analyzing and understanding model performance. GSA involves identifying the most important model factors to be calibrated, while UA entails determining the model output uncertainty derived from uncertain model input factors (Rajabi et al., 2020). GSA and UA should be performed concurrently, as both are essential parts of the model development process in design optimization, reliability analysis, and data-worth analysis (Rajabi et al., 2020). To the best of the authors' knowledge, both GSA and UA have not been performed concurrently in mathematical models for wastewater treatment with microalgae. Therefore, no information is available on the microalgae models' most influential factors and the variability of the uncertainty of model output.

Although, the mechanistic microalgae model proposed by Viruela et al. (2021) was validated using 4 experimental periods, which combine key environmental and operational conditions characteristic of a microalgae-based wastewater treatment, the uncertainty of model parameters could lead to uncertainty propagations on modelling results, reducing its practical application. Thus, this study tends to address data gaps related to uncertainty on microalgae-based wastewater treatment models, based on Viruela et al. (2021), by performing a GSA and UA. The Morris screening method was applied as GSA method to identify the most influential factors of the model, which were calibrated through offline (obtained from experimental assays) and online (variation of

model parameters to match model predictions to experimental results) methodologies. For further enhancing the model performance, the calibrated values for the influential factors were dynamically optimized using online data. Model uncertainty was analyzed and quantified from Monte Carlo simulations and three uncertainty coefficients: the p-factor, the r-factor and the Average Relative Interval Length (ARIL). A calibration protocol was also recommended to reduce model uncertainty by means of prioritizing different calibration methodologies.

Hence, this work could be seen as the first study to simultaneously perform GSA and UA in the field of microalgae-based wastewater treatment modelling, while proposing a set of input factors to be calibrated by a given protocol.

9.2. MATERIAL AND METHODS

9.2.1. The mathematical model

The model used in this work (Viruela et al., 2021) simulated microalgae growth from different phosphorus and nitrogen sources. Regarding phosphorus source, the microalgae had two different metabolic pathways: under phosphorus-replete conditions, microalgae uptake dissolved extracellular phosphate (S_{PO4}) to support their vital metabolic functions and stored part of the excess in form of intracellular polyphosphate ($X_{PP\text{-}ALG}$) while under phosphorus-starved conditions they consumed their $X_{PP\text{-}ALG}$ reservoirs to grow. In terms of nitrogen source, microalgae can use ammonium-ammonia (S_{NHX}, both are considered in chemical equilibrium) and nitrate (S_{NO3}), although different authors state that microalgae prefer S_{NHX} over S_{NO3} when both are present simultaneously (Kim et al., 2013; Markou et al., 2014; Nagase et al., 2001; Pastore et al., 2020). To represent the microalgae's preference for the nitrogen-reduced form, an inhibition switching function of S_{NHX} was included for microalgae growth on S_{NO3}. González-Camejo et al. (2019) and Shoener et al. (2019) reported that S_{NO3} uptake rate was lower than S_{NHX}, so that nitrate related growth kinetic expressions have a specific

growth rate reduction factor. Microalgae growth was modeled as a biomass of non-specific photosynthetic organisms (X_{ALG}) by combining Monod-type kinetics for five components: S_{PO4}, X_{PP-ALG}, $S_{NHX,}$ S_{NO3}, and inorganic carbon source ($S_{Ig,C}$) (Table IX. 1). The storage of X_{PP-ALG} was modeled through the Hill equation and Monod kinetics for S_{PO4}, potassium (S_K) and magnesium (S_{Mg}), since X_{PP-ALG} composition was assumed as $(K_{0.34}Mg_{0.33}PO_3)_n$. The five processes described above are influenced by three environmental factors: light, pH and temperature factor (described below in Section 9.2.4.1). The endogenous respiration and decay processes of the particulate components (X_{ALG} and X_{PP-ALG}) were also considered in the model. These were light intensity and pH-independent, being affected only by thermal variations. As the storage product of X_{PP-ALG} was considered separately from X_{ALG}, this component was subjected to a separate decay process. The model included the stripping processes for free ammonia ($S_{[NH3]}$), oxygen (S_{O2}) and carbon dioxide ($S_{[CO2]}$). The processes described above together gave rise to a model comprising a total of 11 different processes: X_{ALG} growth on S_{NHX} and S_{PO4}, X_{ALG} growth on S_{NO3} and S_{PO4}, X_{ALG} growth on S_{NHX} and X_{PP-ALG}, X_{ALG} growth on S_{NO3} on X_{PP-ALG}, X_{PP-ALG} storage, X_{ALG} endogenous respiration, X_{ALG} lysis, X_{PP-ALG} lysis, $S_{[CO2]}$ stripping, S_{O2} stripping and $S_{[NH3]}$ stripping. The model process kinetics are summarized in Table XI. 1.

The 13 components considered for the model were classified as soluble (described with S-index) and particulate (described with X-index): soluble oxygen S_{O2}, soluble ammonia-ammonium nitrogen S_{NHX}, soluble nitrate nitrogen S_{NO3}, soluble phosphate S_{PO4}, soluble inorganic carbon $S_{Ig,C,}$ proton S_H, soluble magnesium S_{Mg}, soluble potassium S_K, readily biodegradable soluble organic matter S_S, inert soluble organic matter S_I, microalgae biomass X_{ALG}, inert particulate organic matter X_I and polyphosphates stored by microalgae X_{PP-ALG}.

Microalgae biomass (X_{ALG}) was quantified as volatile suspended solids (VSS). In order to compare experimental and simulated results, two additional components were

included: total suspended solids (X_{TSS}, g TSS·m^{-3}) and volatile suspended solids (X_{VSS}, g VSS·m^{-3}). X_{TSS} was considered as the sum of X_{ALG}, X_I, and X_{PP-ALG} while X_{VSS} was the sum of X_{ALG} and X_I. The modeled and experimental data were thus compared through X_{VSS}. For stoichiometry matrix, conversion factors and further details of the microalgae model the reader is referred to the literature (Viruela et al., 2021).

Table XI. 2. Processes kinetics included in microalgae model developed by Viruela et al. (2021).

2

Processes j	Processes rate [M L^{-3} T^{-1}]
1. X_{ALG} growth on S_{NHX} and S_{PO4}	$\mu_{ALG} \cdot \frac{S_{Ig,C}}{K_{Ig,C}+S_{Ig,C}} \cdot \frac{S_{NHX}}{K_{NHX}+S_{NHX}} \cdot \frac{S_{PO4}}{K_{PO4}+S_{PO4}} \cdot X_{ALG} \cdot f_L \cdot f_{pH} \cdot f_T$
2. X_{ALG} growth on S_{NO3} and S_{PO4}	$\mu_{ALG} \cdot \eta_{NO3} \cdot \frac{S_{Ig,C}}{K_{Ig,C}+S_{Ig,C}} \cdot \frac{K_{NHX}}{K_{NHX}+S_{NHX}} \cdot \frac{S_{PO4}}{K_{PO4}+S_{PO4}} \cdot \frac{S_{NO3}}{K_{NO3}+S_{NO3}} \cdot X_{ALG} \cdot f_L \cdot f_{pH} \cdot f_T$
3. X_{ALG} growth on S_{NHX} and $X_{PP\text{-}ALG}$	$\mu_{ALG} \cdot \frac{S_{Ig,C}}{K_{Ig,C}+S_{Ig,C}} \cdot \frac{S_{NHX}}{K_{NHX}+S_{NHX}} \cdot \frac{K_{I,PO4}}{K_{I,PO4}+S_{PO4}} \cdot \frac{\frac{X_{PP-ALG}}{X_{ALG}}}{K_{XPP-ALG}+\frac{X_{PP-ALG}}{X_{ALG}}} \cdot X_{ALG} \cdot f_L \cdot f_{pH} \cdot f_T$
4. X_{ALG} growth on S_{NO3} on $X_{PP\text{-}ALG}$	$\mu_{ALG} \cdot \eta_{NO3} \cdot \frac{S_{Ig,C}}{K_{Ig,C}+S_{Ig,C}} \cdot \frac{K_{NHX}}{K_{NHX}+S_{NHX}} \cdot \frac{K_{I,PO4}}{K_{I,PO4}+S_{PO4}} \cdot \frac{S_{NO3}}{K_{NO3}+S_{NO3}} \cdot \frac{\frac{X_{PP-ALG}}{X_{ALG}}}{K_{XPP-ALG}+\frac{X_{PP-ALG}}{X_{ALG}}} \cdot X_{ALG} \cdot f_L \cdot f_{pH} \cdot f_T$
5. $X_{PP\text{-}ALG}$ storage	$q_{PP-ALG} \cdot \frac{S_{PO4}}{K_{PO4}+S_{PO4}} \cdot \frac{S_{Mg}}{K_{Mg}+S_{Mg}} \cdot \frac{S_K}{K_K+S_K} \cdot \frac{{K_{XPP-qXPP}}^n}{{K_{XPP-qXPP}}^n+\left(\frac{X_{PP-ALG}}{X_{ALG}}\right)^n} \cdot X_{ALG} \cdot f_L \cdot f_{pH} \cdot f_T$
6. X_{ALG} endogenous respiration	$b_{ALG,1} \cdot X_{ALG} \cdot f_T$
7. X_{ALG} lysis	$b_{ALG,2} \cdot X_{ALG} \cdot f_T$
8. $X_{PP\text{-}ALG}$ lysis	$b_{ALG,2} \cdot X_{PP-ALG} \cdot f_T$
9. $S_{[CO2]}$ stripping	$K_{La,CO2} \cdot \left(S_{[CO2]} - S^*_{[CO2]}\right)$
10. S_{O2} stripping	$K_{La,O2} \cdot (S_{O2} - S^*_{O2})$
11. $S_{[NH3]}$ stripping	$K_{La,NH3} \cdot \left(S_{[NH3]} - S^*_{[NH3]}\right)$

9.2.2. Case studies

The outdoor MPBR pilot plant under study was located in the “Cuenca del Carraixet” WWTP (39°30′04.0’’N 0°20′00.1’’W, Valencia, Spain). The MPBR pilot plant was fed with effluent from an anaerobic membrane bioreactor (AnMBR) system on the same premises. The MPBR consisted of two 0.25-m and two 0.10-m wide flat panel photobioreactors (PBRs), all with a surface area of 2.3 m^2 (1.15 x 2 m; H x L), and a 14-L working volume membrane tank (MT) equipped with one commercial ultrafiltration hollow-fiber membrane system (PURON® Koch Membrane Systems (PUR-PSH31), 0.03 µm pore) with a filtration area of 3.4 m^2. The PBRs were air-stirred to promote complete mixing of culture medium. Stirring the PBR also promotes carbon stripping as carbon dioxide. Pure CO_2 was injected into the stirring system to set pH to 7.5, ensuring not only an inorganic carbon-rich culture, but also to reduce uncontrolled phosphorus precipitation and ammonia stripping. The temperature of the biomass culture was controlled by a cooling device and thermostat (Daikin R410A inverter). Besides natural light, twelve LED lamps (Unique Led IP65 WS-TP4S-40W-ME) placed at the back of the PBRs continuously illuminated the microalgae culture at a constant irradiance of 300 $\mu mol \cdot m^{-2} \cdot s^{-1}$. Allylthiourea (ATU) was added to keep a constant concentration of 5 $mg \cdot L^{-1}$ to inhibit nitrifying bacteria. For further details of the MPBR pilot plant see González-Camejo et al. (2020).

Real-time information on the process operation and conditions was obtained from a control network consisting of pH sensors (pHD sc DPD1R1, Hach Lange), dissolved oxygen-temperature sensors (LDO Hach Lange) and light irradiance sensors (Apogee Quantum SQ-200) to measure only photosynthetically active radiation (PAR). Data acquisition from the online sensors was previously described in Viruela et al. (2018).

Four operation periods were selected from the MPBR pilot plant performance. This analysis is divided into these 4 periods, which are the guiding threads to perform GSA and UA. The 4 periods represent the key variations observed during the three years of

the MPBR pilot plant operation, i.e. daily variations in light intensity and temperature, phosphorus-replete and phosphorus-starved conditions in the culture medium, and different operational conditions. Datasets related to the periods selected are shown in Table IX. 2. There were remarkable changes in the daily PAR averages in Periods 1 and 2, reaching minimum values of 10 and 67 $\mu mol \cdot m^{-2} \cdot s^{-1}$ and maximum values of 406 and 394 $\mu mol\ m^{-2}\ s^{-1}$ for Period 1 and Period 2, respectively. The difference between the PBR widths and VSS concentration in Period 1 (0.10-m reactor width and VSS of 1063 ± 141 g $VSS \cdot m^{-3}$) and Period 2 (0.25-m reactor width and VSS of 445 g $VSS \cdot m^{-3}$) revealed significant information on the model sensitivity and uncertainty towards the light intensity constants. Period 3 was mainly characterized by negligible S_{PO4} concentrations (phosphorus-starved conditions). As the model approach stipulates that microalgae should grow in this period by consuming the stored $X_{PP\text{-}ALG}$, the model factors related to $X_{PP\text{-}ALG}$ consumption could have influenced the simulation results. Although PBR temperature was controlled, thermal fluctuations of up to 8°C in culture medium were recorded during warm periods, as in experimental Period 4. Bearing in mind that all kinetic expressions of biological processes are regulated by a thermal factor (explained and developed in Section 9.2.4.1), the model should have been sensitive to cardinal temperatures.

The following parameters were monitored (APHA, 2005) in the influent, the algae culture medium and the permeate: total suspended solids (TSS) 2540-TSS-D, VSS 2540-VSS-E, soluble chemical oxygen demand (sCOD) 5220-COD-D, ammonium nitrogen (NH_4-N), nitrate nitrogen (NO_3-N) 4500-NO3-H, and phosphate (PO_4-P) 4500-P-F). The optical density at 680nm (OD_{680}) was measured with a portable fluorometer AquaPen-C AP-C 100 (Photon Systems Instruments). For more specific details on the analytical procedures see Viruela et al. (2021).

Table IX. 3. Environmental and operational conditions for the 4 selected experimental periods. VSS: volatile suspended solids in PBRs; PO_4-P soluble phosphate in PBRs; PAR: photosynthetically active radiation recorded on PBR surface area; T: culture temperature; and pH: culture pH. The MIN, MAX and AVG sub-indexes refer to the minimum, maximum and average values respectively.

		Period 1	**Period 2**	**Period 3**	**Period 4**
PBR width	m	0.10	0.25	0.10	0.25
VSS	g VSS $\cdot m^{-3}$	1063 ± 141	445 ± 80	830 ± 136	252 ± 36
NH_4-N	g N$\cdot m^{-3}$	16 ± 6	34 ± 4	11 ± 7	42 ± 6
PO_4-P	g P$\cdot m^{-3}$	3.7 ± 0.9	3.2 ± 0.9	0.14 ± 0.11	4.74 ± 1.12
PAR_{MIN}	µmol$\cdot m^{-2}\cdot s^{-1}$	10	67	284	112
PAR_{MAX}	µmol$\cdot m^{-2}\cdot s^{-1}$	406	394	394	290
PAR_{AVG}	µmol$\cdot m^{-2}\cdot s^{-1}$	214 ± 133	258 ± 114	345 ± 36	259 ± 50
T_{MIN}	ºC	20	24.82	23.2	24
T_{MAX}	ºC	26	28.18	24.30	32
T_{AVG}	ºC	24 ± 2	26.14 ± 1.03	23.8 ± 0.4	27 ± 2
pH_{MIN}	-	7.32	7.00	7.08	7.36
pH_{MAX}	-	7.55	7.40	7.37	7.68
pH_{AVG}	-	7.40 ± 0.06	7.2 ± 0.2	7.18 ± 0.08	7.50 ± 0.08

9.2.3. Sensitivity analysis

GSA was performed through the Morris screening method (Morris, 1991) to identify the model's most influential factors, reducing the size of parameter set to be calibrated. The Morris screening method was selected from other classical methodologies (e.g. Standardized Regression Coefficients, Sobol indices, or Fourier amplitude sensitivity testing) since it is widely used for GSA in the field of wastewater treatment (see e.g. Corominas and Neumann, 2014; Robles et al., 2014a, Robles et al., 2014b; Ruano et al., 2011; Sin et al., 2011; Solimeno et al., 2016; Sun et al., 2015), it represents a well-stablished methodology for data processing, and it is characterized by a relative simple interpretation.

The Morris screening method is a one-factor-at-a-time (OAT) GSA method that evaluates the distribution of the elementary effects (EE_i) of each input factor upon model outputs, used to calculate the statistical parameters that provide sensitivity results. The scaled elementary effect (SEE_i) proposed by Sin and Gernaey (2009) was applied. The finite

distribution of SEE_i associated with each input factor (i.e. F_i) is usually obtained by sampling different coordinates (X) from the parameter space at random. However, this random sampling of X could only cover a reduced part of the space. Campolongo et al. (2007) proposed a modification of the Morris screening method by improving the sampling strategy. In this study, the trajectory-based sampling strategy proposed in Ruano et al. (2012) was applied. From the generated matrices, it determines the distribution of SEE_i of each input factor on the model output. Finally, the distribution of SEE_i is analyzed to determine the relative importance of the input factors and obtain a good approximation of a GSA. Specifically, the selected statistical parameters to evaluate these distributions were: the absolute mean (μ^*, Equation IX. 1) and the standard deviation (σ, Equation IX. 2) (see e.g. Saltelli et al. (2004) and Campolongo et al. (2007)). μ^* estimates the input factor influence on the output and σ assesses the ensemble of higher order factor effects on the output, i.e. nonlinear effect and/or interactions among factors. Relatively low μ^* and σ values refer to negligible effects, high μ^* and low σ values indicate linear and additive effects, and low μ^* and high σ values are the nonlinear or interactions effects. The method is composed of individually randomized OAT screening experiments which consist of varying one factor at a time and measuring the variance of the output. Each model input factor is presumed to be varied across *p* selected levels in the input factor space. In this case study, the input factor variation for each factor was set at ±20% of the initial conditions, through 4 *p* levels. GSA was performed for the 4 experimental periods described in Section 9.2.2. A GSA based on these 4 periods gave a wider variability range in the environmental factors.

$$\mu_i^* = \frac{\sum_{n=1}^{r} |SEE_n|}{r} \qquad \text{Equation XI. 1}$$

$$\sigma_i = \sqrt{\frac{1}{r}\sum_{n=1}^{r} (SEE_n - \mu_i)^2} \qquad \text{Equation XI. 2}$$

where *r* is the number of repetitions of EE calculation, SEE_i is the scaled elementary effect and μ is the mean.

The software used for the GSA was the MATLAB/Simulink platform. The total number of simulations required in Morris's method is denoted as N and is calculated from Equation IX. 3:

$$N = r(k + 1)$$ Equation XI. 3

where *r* is the number of repetitions of EE calculation and *k* is the input factor number.

Croop & Braddock (2002) established that a good choice of *r* is critical to obtain a good estimation of the effects. In the model developed, an *r* = 100 setting was sought with a constant resolution of *p* = 4 (Campolongo et al., 1999). The input factor values used are listed in Table IX. 3, resulting in *k* = 34, so that the overall model evaluation costs were 3500 simulations.

The effects of these input factors were evaluated with respect to three model outputs: S_{NHx}, S_{PO4} and X_{ALG} concentrations. The simulation time period was set at 7 days to reach a pseudo-steady state and avoid excessive simulation costs.

Table IX. 3. Default and offline/online calibrated values for the model parameters.

Parameters	Description	Value	Unit	Source
μ_{ALG}	Maximum growth rate of X_{ALG}	1.8	d^{-1}	Calibrated
$b_{ALG,1}$	Maximum inactivation rate of X_{ALG}	0.1	d^{-1}	(Reichert et al., 2001)
$b_{ALG,2}$	Maximum decay rate of X_{ALG}	0.15	d^{-1}	Calibrated
q_{XPP}	Rate constant for storage of $X_{PP\text{-}ALG}$	0.01	d^{-1}	Calibrated
K_{O2}	Half saturation parameter for S_{O2}	0.2	g $O_2 \cdot m^{-3}$	(Reichert et al., 2001)
$K_{lg,C}$	Half saturation parameter for $S_{lg,C}$	$4.32 \cdot 10^{-3}$	g $C \cdot m^{-3}$	(Solimeno et al., 2015)
K_{NHX}	Half saturation parameter for S_{NHX} in a phosphorus-replete medium	0.1	g $N \cdot m^{-3}$	Calibrated
$K_{NHX\text{-}qXPP}$	Half saturation parameter for S_{NHX} in a phosphorus-deplete medium	3	g $N \cdot m^{-3}$	Calibrated
K_{NO3}	Half saturation parameter for S_{NO3}	12.61	g $N \cdot m^{-3}$	(Wágner et al., 2016)
η_{NO3}	Reduction factor for X_{ALG} growth of S_{NO3}	0.59	–	(Eze et al., 2018)

Table IX. 3. Continued.

Parameters	Description	Value	Unit	Source
K_{PO4}	Half saturation parameter for S_{PO4}	0.05	g P·m^{-3}	Calibrated
$K_{I,PO4}$	Inhibition parameter for X_{PP-ALG} use in a phosphorus-replete medium	0.15	g P·m^{-3}	Calibrated
K_{XPP}	Half saturation parameter of X_{ALG} growth for X_{PP-ALG}	0.0027	g P·m^{-3}	(Ruiz-Martinez et al., 2014)
K_{XPP_qXPP}	Half saturation parameter of X_{PP} storage for X_{PP-ALG}	0.003	g P·m^{-3}	(Ruiz-Martínez et al., 2015)
n	Regulation coefficient or Hill number	0.006	–	(Ruiz-Martínez et al., 2015)
K_{Mg}	Half saturation parameter for S_{Mg}	0.13	g Mg·m^{-3}	(Sydney et al., 2010)
K_K	Half saturation parameter for S_K	8.78	g K·m^{-3}	(Sydney et al., 2010)
T_{MIN}	Minimum temperature for microalgae growth	2	°C	Calibrated
T_{MAX}	Maximum temperature for microalgae growth	40	°C	Calibrated
b	Intrinsic model parameter	87.13	–	Calibrated
c	Intrinsic model parameter	1.46	–	Calibrated
I_{OPT}	Optimal light intensity for X_{ALG} growth	230	µmol·m^{-2}·s^{-1}	Calibrated
k_w	Attenuation coefficient due to water	1.97	m^{-3}	(Sun et al., 2016)
K_I	Attenuation coefficient due to particulate components	0.025	m^2 g·TSS^{-1}	Calibrated
$K_{I,H}$	Lower half saturation parameter for S_H	0.00001	mol H$^+$·L^{-1}	(Siegrist et al., 1993)
$K_{S,H}$	Upper half saturation parameter for S_H	0.00063	mol H$^+$·L^{-1}	(Siegrist et al., 1993)
$S_{H,opt}$	Optimal pH for X_{ALG} growth	7.50	pH	Calculated
$K_{La,O2}$	Mass transfer coefficient for oxygen	16.2	h^{-1}	Calibrated
$K_{La,CO2}$	Mass transfer coefficient for dioxide carbon	16.2	h^{-1}	Calibrated
$K_{La,NH3}$	Mass transfer coefficient for free ammonia	16.2	h^{-1}	Calibrated
k	Constants of mass transfer coefficient equation	0.05	-	Calibrated
r	Constants of mass transfer coefficient equation	1	-	Calibrated
F_{XI}	Fraction of X_I generated microalgae decay	0.25	g COD·g COD^{-1}	Calculated
F_{SI}	Fraction of S_I generated microalgae decay	0.6	g C·gCOD^{-1}	Calculated

A more precise description of the GSA method applied in this study can be found elsewhere (Robles et al., 2014a).

9.2.4. Model calibration

The model was calibrated preferably with data from photo-respirometric tests and MPBR performance (offline calibration), and alternatively matching model predictions to dynamic experimental MPBR data (online calibration). Offline and online calibration were only applied to determine the values of the most influential model input factors (influential GSA factors). The rest of the input factors were set to their default values (Table IX. 3) based on expert knowledge and the scientific literature.

9.2.4.1. Offline calibration

Photo-respirometric test

Offline calibration consisted of isolating specific microalgae biomass processes and measuring Oxygen Production Rate (OPR) and Oxygen Uptake Rate (OUR). Photo-respirometric tests were made to calibrate the model factors related to environmental conditions, i.e. light intensity and thermal factor. For this, a respirometer system was set up consisting of: a conical flask bioreactor (500 mL transparent glass flask), a dissolved oxygen probe (WTW CellOx 330i) recording both dissolved oxygen and temperature data every 30 s, an on-off electrovalve to add pure carbon dioxide to set pH at 7.5 and to avoid inorganic carbon limitation, a cooling-heating system connected to a heating coil for temperature control, a LED lighting system (SevenON LED 8 x 11W), and a magnetic stirrer system running at 100 rpm to ensure homogeneous conditions, prevent microalgae sedimentation, and minimize the oxygen mass transfer. The following protocol was conducted:

1. Microalgae biomass was collected from the MPBR pilot plant. Samples were centrifuged at 5000xg (Eppendorf AG 22331, Hamburg) and resuspended with AnMBR effluent to set OD_{680} at a fixed interval ranging from 0.4 to 0.6, giving

comparable biomass light attenuation and nutrients concentration. An aliquot of 500 mL was transferred into the photo-respirometric system.

2. Dissolved oxygen concentration was monitored online in two differentiated phases: light and dark. The light phase was set to 20 min and the dark phase to 10 min. In the light phase, oxygen production was expected due to photosynthesis, but oxygen was also consumed due to respiration of microalgae and other possible aerobic organisms. In the dark phase the bioreactor was covered to ensure darkness and that OUR was only due to microalgae and aerobic organism respiration. The net oxygen production rate (nOPR) was thus the result of the following contributions (Equation XI. 4):

$$\mathrm{nOPR} = \mathrm{OPR} - \mathrm{OUR} \qquad \text{Equation XI. 4}$$

Different temperature (10, 20.5, 25, 30, 35 and 40 ºC) and light conditions (87, 172, 229, 314, 374, 462, 534 and 607 µmol m^{-2} s^{-1}) were tested, all runs performing under non-limiting nutrients concentration. Each temperature test (6 bioreactors) was acclimatized for 24 hours at the selected temperature and at a reference light intensity of 229 µmol m^{-2} s^{-1}. Each light intensity test (8 bioreactors) was acclimatized for 24 hours at the selected light intensity and at a reference temperature of 25 ºC. Temperature and light intensity were calibrated in triplicate, i.e. 18 and 24 trials were conducted to calibrate the effect of both temperature and light intensity on oxygen production, respectively.

The experimental nOPR was matched by the following mathematical models to calibrate cardinal temperatures (Ratkowski model) and light intensity (Steele model) using the Solver tool in Microsoft Excel.

The Ratkowski model was used to describe the temperature dependence of biokinetics and to obtain the two cardinal temperatures (minimum and maximum), together with the thermic factor (F_T), which modifies kinetic rates (Equation IX. 5).

$$F_T = (b \cdot (T_0 - T_{MIN}))^2 \cdot (1 - e^{c \cdot (T_0 - T_{MAX})}) \quad \text{Equation XI. 5}$$

where T_0 (ºC) is the culture medium temperature; T_{MIN} (ºC) is the lowest limiting temperature for growth and the expected growth rate below which is zero; b is a model parameter; T_{MAX} (ºC) is the upper temperature limit above which the expected growth rate is zero; and c is a model parameter allowing the model to fit the data at a temperature approaching and exceeding the optimum temperature for growth.

The light factor (F_L) included in light-dependent model processes was calculated by Steele's function (Equation IX. 6), which was selected for modeling microalgae growth according to light intensity because it includes photoinhibition and the shallow effect in photobioreactors (Steele, 1965):

$$F_L = \frac{I_{AV}}{I_{OPT}} \cdot e^{\left(1 - \frac{I_{AV}}{I_{OPT}}\right)} \quad \text{Equation XI. 6}$$

where I_{OPT} (µmol·m^{-2}·s^{-1}) is the optimal light intensity and I_{AV} (µmol·m^{-2}·s^{-1}) is the average light intensity. I_{AV} was obtained using Lambert-Beer's Law. The incident light intensity is attenuated by TSS (g TSS·m^{-3}) concentration in the photobioreactor depth (m) (Equation IX. 7).

$$I_{AV} = \frac{I_{0,s} \cdot \left(1 - e^{-(k_w + K_I \cdot TSS) \cdot d}\right)}{(k_w + K_I \cdot TSS) \cdot d} \quad \text{Equation XI. 7}$$

where $I_{0,s}$ (µmol·m^{-2}·s^{-1}) is the incident light intensity and k_w (m^{-3}) is the attenuation coefficient due to water, K_I (m^2 g·TSS^{-1}) is the extinction coefficient associated to particulate components and d is the photobioreactor depth (m).

MPBR pilot plant

As in Ruiz et al. (2013), the PBRs were operated in two successive stages: batch and continuous operation. After microalgae inoculation with the AnMBR effluent, the PBR culture was grown in batch stage until the pseudo-stationary phase was reached (according to TSS), obtaining the batch growth kinetics and achieving a high microalgae biomass concentration. The batch stage datasets were calibrated by matching experimental data with two models: the Verhulst logistic kinetic model and Michaelis-Menten expression rate. Experimental data were matched to the corresponding model by minimizing the sum of squared residuals using Microsoft Excel Solver.

The Verhulst logistic kinetic model (Verhulst, 1838) was used to describe the PBR microalgae growth curve under batch operation and to obtain the kinetic growth factors. This model is a substrate-independent equation widely used to describe biomass growth in ecological studies, mainly because it can accurately describe biomass evolution under different culture conditions using a simple mathematical and biological definition. According to the Verhulst model, biomass growth can be expressed as sinusoidal (Equation IX. 8):

$$\frac{\partial X}{\partial t} = \mu_{max} X[1 - \frac{X}{X_{max}}] \qquad \text{Equation XI. 8}$$

Integrating Equation IX. 8, Equation IX. 9 was derived, where μ_{max} is the maximum specific growth rate (d^{-1}), X_0, X_{max} and X are biomass concentrations (g VSS·m^{-3}) at an operating time equal to zero, infinity and t, respectively.

$$X = \frac{X_0 X_{max} e^{t\mu_{max}}}{X_{max} - X_0 + X_0 e^{t\mu_{max}}} \qquad \text{Equation XI. 9}$$

The Michaelis-Menten relationship (Equation IX. 10) is an ecological model which can be applied to nutrient removal kinetics (Aslan and Kapdan, 2006):

$$r_0 = \frac{r_{max} S_0}{K_m + S_0}$$ Equation XI. 10

where r_0 is the nutrients uptake rate [$g \cdot m^{-3} \cdot d^{-1}$], r_{max} is the maximum removal rate of nutrients [d^{-1}], S_0 is the nutrient concentration at time equal zero [$g \cdot m^{-3}$] and Km is the Michaelis-Menten constant [$g \cdot m^{-3}$]. The kinetic coefficients r_{max} and Km were fitted and calibrated by use of the Lineweaver-Burk equation (Equation IX. 11).

$$\frac{1}{r_0} = \frac{K_m}{r_{max}} \frac{1}{S_0} + \frac{1}{r_{max}}$$ Equation XI. 11

9.2.4.2. Online calibration

Online calibration with mid-term pseudo-steady periods consisted of matching the modeling results to the experimental data and entailed 35 days of dynamics in nitrogen, phosphorus, VSS and sCOD concentration obtained from the MPBR system. The 0.10-m wide PBR was operated with an HRT and BRT of 1.25 ± 0.03 and 4.5 ± 0.2 days, respectively. Medium temperature and incident PAR were 25.6 ± 1.4 ºC and 290 ± 47 $\mu mol \cdot m^{-2} \cdot s^{-1}$, respectively. This period was long enough to enable the effect of both phosphorus-starved and -replete culture conditions. From this data, different model factors ($b_{ALG,2}$, $K_{NHX\text{-}QPP}$, $K_{I,PO4}$ and K_La) were adjusted using the Matlab® Curve Fitting App. To compare and determine whether there was a significant difference between the experimental data and the modeling results, the t-test and F-test, and a non-continuous level test (i.e. the Mann-Whitney U-test) were performed on Statgraphics® Centurion v.19.

A mass transfer coefficient K_La function (Equation IX. 12) was used to describe gas transport between liquid and gas phases.

$$K_La = k \cdot \left(\frac{G_F}{V_L}\right)^r$$ Equation XI. 12

where G_F is the gas flow rate ($L \cdot h^{-1}$), V_L is the liquid volume (L) and k and r are fitting parameters. Constants k (K_La_k) and r (K_La_r) were therefore the input factors calibrated to match simulated results.

9.2.4.3. Dynamic optimization

After offline/online calibration of the influential factors, these parameters were dynamically optimized to improve model performance throughout each experimental period. The optimization algorithm aimed at matching experimental data with the modeled results, using a standardized residuals function (Equation IX. 13) as objective function to be minimized. To this aim, a constrained optimization using genetic algorithm (GA) was applied through the function implemented on Matlab® software. Specifically, a global GA optimization was conducted for a predefined set of lower and upper bounds on the design variables, i.e. the influential model input factors. Bound constraints for variations of model inputs were set to ±20%. The influencing factors were fed to the GA with the same order of magnitude (unity) and later reconverted in the model function, e.g. optimal light intensity for X_{ALG} growth was 230 $\mu mol \cdot m^{-2} \cdot s^{-1}$, then a 10^{-2} factor was applied for seeding the GA; and μ_{ALG} was 1.8 d^{-1}, so that it was not necessary to apply a correction factor. The termination tolerance on fitness function value ("TolFun" option) was set to 10^{-3} (it was confirmed for a given experimental period (Period 1) that the optimized results did not vary statistically when this option was reduced from 10^{-3} to 10^{-6}).

$$\sum \frac{\left|S_{NHx_{sim}} - S_{NHx_{exp}}\right|}{\sqrt{\text{std}\left(S_{NHx_{exp}}\right)}} + \sum \frac{\left|S_{PO4_{sim}} - S_{PO4_{exp}}\right|}{\sqrt{\text{std}\left(S_{PO4_{exp}}\right)}} + \sum \frac{\left|X_{ALG_{sim}} - X_{ALG_{exp}}\right|}{\sqrt{\text{std}\left(X_{ALG_{exp}}\right)}}$$ Equation XI. 13

Bound constraints for variations of model inputs were set to ±20% of default or offline/online calibrated values.

9.2.5. Uncertainty analysis

UA was conducted to assess the propagation of different uncertainty sources to the model output. Only the influential input factors were considered during UA implementation, while non-important factors were set to their default values. 3500 Monte Carlo runs were performed with a 20% variance rate of the influencing factors. The Latin hypercube sampling method was used to generate the matrix for the Monte Carlo runs. The matrix for the Monte Carlo simulations was generated using the "maximin" criteria from Matlab® software, which maximize minimum distance between points. To try to optimize the Latin hypercube sampling design, the default number of interactions to be applied during the Monte Carlo design was increased from 5 to 100.

Results were assessed on different indices: (i) the 5th and 95th percentiles (Mannina et al., 2017), (ii) the p-factor (Yang et al., 2008), (iii) the r-factor (Mannina et al., 2018; Yang et al., 2008) and (iv) the Average Relative Interval Length (ARIL) (Mannina et al., 2018; Yang et al., 2008).

The p-factor, or the percentage of observations within the 95% prediction uncertainty (95PPU). The 95PPU was calculated at the 2.5% and 97.5% levels of the cumulative distribution of the model output. The closer the p-factor approaches 100%, the lower the uncertainty of the model predictions (Mannina et al., 2018; Yang et al., 2008). The r-factor was calculated from Equation IX. 14 (Mannina et al., 2018; Yang et al., 2008). The closer the r-factor is to 1, the narrower the uncertainty bands are.

$$\mathrm{r-factor} = \frac{\frac{1}{n}\sum_{i=1}^{n}\left(y_{sim,97.5\%,i} - y_{sim,2.5\%,i}\right)}{\sigma_{obs}} \qquad \text{Equation XI. 14}$$

where $y_{sim,97.5\%,i}$ and $y_{sim,2.5\%,i}$ are the upper and lower boundary value of 95PPU, respectively; n is the number of observation; and σ_{obs} represents the standard deviation of the measured data.

The ARIL index was calculated according to Equation IX. 15 (Jin et al., 2010). The lower the ARIL value the lower the model uncertainty.

$$\mathrm{ARIL} = \frac{1}{n}\sum_{i=1}^{n}\frac{(y_{sim,97.5\%,i} - y_{sim,2.5\%,i})}{y_{obs}} \qquad \text{Equation XI. 15}$$

The model uncertainty was assessed by combining the indices described above. High p-factor values, an r-factor values close to 1 and low ARIL values indicate low uncertainty in the model's prediction.

9.3. RESULTS AND DISCUSSION

9.3.1. Global sensitivity analysis

9.3.1.1. S_{NHX} output

S_{NHX} concentration decreases due to microalgae uptake for growth and S_{NH3} stripping. Conversely, S_{NHX} concentration increases due to microalgae lysis and endogenous respiration. Processes 1 (X_{ALG} growth on S_{NHX} and S_{PO4}), 3 (X_{ALG} growth on S_{NHX} and $X_{PP\text{-}ALG}$), 6 (X_{ALG} endogenous respiration), 7 (X_{ALG} lysis) and 11 ($S_{[NH3]}$ stripping) in Table IX. 1 therefore affect S_{NHX} concentration.

Figure IX. 1 gives the sensitivity measurements (μ* and σ) calculated from each input factor on the S_{NHX} output for the 4 periods.

Maximum growth rate of X_{ALG} (μ_{ALG}), optimal light intensity (I_{OPT}) and maximum temperature (T_{MAX}) were the most sensitive input factors for Period 1 (Figure IX. 1A). Specifically, μ_{ALG} ($\mu^* = 4.31$, $\sigma = 1.09$), I_{OPT} ($\mu^* = 2.99$, $\sigma = 0.75$) and K_I ($\mu^* = 1.72$, $\sigma = 0.50$) exhibited a linear and additive effect on S_{NHX} output, while T_{MAX} ($\mu^* = 1.68$, $\sigma = 1.31$) showed a nonlinear effect. S_{NHX} model output was mainly influenced by environmental factors, i.e. light intensity and temperature, which had a direct effect on photosynthesis and thus on net microalgae growth rate. This model output was also sensitive, although to a lesser extent, to the following input factors: K_{NHX}, $b_{ALG,2}$, K_{PO4}, $K_{I,PO4}$, $b_{ALG,1}$, $K_{NHX\text{-}QPP}$, K_{XPP}, q_{XPP} and K_La,r. All these influential input factors were

involved in microalgae growth and decay rate, except K_La,r which refers to free ammonia stripping.

GSA results for S_{NHX} in Period 2 are represented in Figure IX. 1B. Similar results to the ones obtained in Period 1 were observed in Period 2: μ_{ALG} (μ^* = 11.58, σ = 2.40) and I_{OPT} (μ^* = 6.80, σ = 1.26) showed a linear effect, while T_{MAX} (μ^* = 6.58, σ = 7.32) exhibited a nonlinear or interactive effect on S_{NHX} output. However, the fundamental difference between the two periods was in the factors described as less influential. Whereas in Period 1 input factors related to nutrient uptake, such as half saturation constants or maximum phosphate uptake rate, had a relatively important effect on the model output, in Period 2 only one minor input, K_I (μ^* = 4.68, σ = 0.93), was identified. This difference between the GSA results could be due to the available S_{NHX} concentration in the culture medium. The S_{NHX} concentrations in Periods 1 and 2 were 16 ± 6 mg N L^{-1} and 34 ± 4 mg N L^{-1}, respectively. The determination of S_{NHX} removal rate depends on external nitrogen concentrations. At high S_{NHX} concentrations, microalgae should remove ammonium-ammonia species at the maximum rate (r_{MAX}); thus, despite increasing the substrate concentration, the removal rate will not vary where the Michaelis-Menten equation becomes independent of S_{NHX} concentration, so that the Michaelis-Menten kinetics factors were irrelevant in Period 2. As mentioned previously, the reduced S_{NHX} concentration in the culture medium was mainly due to the growth of microalgae. Growth kinetics were dependent on the global computation of the nutrients uptake, including phosphorus sources (S_{PO4} and $X_{PP\text{-}ALG}$). Given that microalgae growth was limited in Period 1 by the S_{NHX} concentration, input factors involved in nutrient uptake had a relatively significant effect in Period 1 as compared to Period 2.

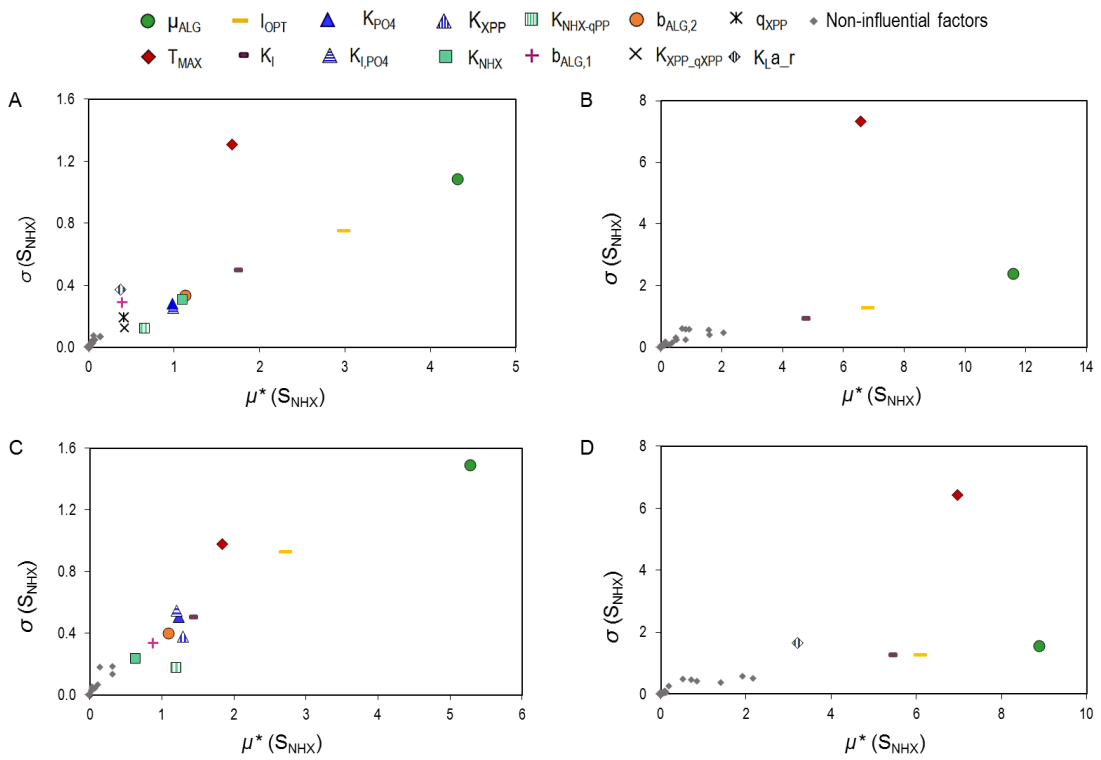

Figure IX. 1. Sensitivity measures μ^* versus σ for the model outputs S_{NHX} for Period 1 (A), Period 2 (B), Period 3 (C) and Period 4 (D).

Period 3 was operated in P-starved conditions. The GSA results from this period are reported in Figure IX. 1C. μ_{ALG}, (μ^* = 5.28, σ = 1.49) had a relatively higher influence than the remaining input factors and a nonlinear or interactive effect on S_{NHX} model output. I_{OPT} (μ^* = 2.71, σ = 0.92) and T_{MAX} (μ^* = 1.84, σ = 0.98) presented a linear or additive effect on the model output. K_I, K_{XPP}, K_{PO4}, $K_{NHX-qPP}$, $b_{ALG,2}$, and $K_{I,PO4}$ were included in the factors classified as influential, but to a lesser extent.

GSA results for Period 4 are shown in Figure IX. 1D. As this figure shows, there was a significant dependence of S_{NHX} concentration on microalgae growth rate, light intensity and temperature. μ_{ALG} (μ^* = 8.88, σ = 1.55), I_{OPT} (μ^* = 6.09, σ = 1.25) and K_I (μ^* = 5.39, σ = 1.25) exhibited linear or additive effects, while T_{MAX} (μ^* = 6.96, σ = 6.43) showed nonlinear or interactive effects on the output. K_La_r (μ^* = 3.21, σ = 1.65) reflected that free ammonia stripping participated on S_{NHX} concentration balance, but to a lesser degree than microalgae growth.

Regarding S_{NHX}, 10 input factors were selected as influential. Among these factors, μ_{ALG}, I_{OPT} and T_{MAX} had the greatest influence on S_{NHX} model output with linear/additive or nonlinear/iterative effects. Indeed, the variation in S_{NHX} concentration was mainly due to light-affected processes (photosynthetic metabolism), since I_{OPT} is one of the most influential input factors in S_{NHX} output. K_I was a relatively influential factor on model output in the 4 periods studied because of its intrinsic relationship to the light intensity available for photosynthesis. On the other hand, the following factors were considered as influential due to their effect on the model output within two or more periods: K_{NHX}, $b_{ALG,2}$, K_La,r, K_{PO4}, $K_{I,PO4}$ and $K_{NHX\text{-}QPP}$.

According to the results of the S_{NHX} model output evaluation, it would thus be recommendable to calibrate the following model factors: μ_{ALG}, I_{OPT}, T_{MAX}, K_I, K_{NHX}, $b_{ALG,2}$, K_La,r, K_{PO4}, $K_{I,PO4}$ and $K_{NHX\text{-}QPP}$.

9.3.1.2. S_{PO4} output

S_{PO4} decreases due to microalgae uptake for growth and $X_{PP\text{-}ALG}$ storage. Conversely, S_{PO4} concentration increases due to microalgae endogenous respiration and $X_{PP\text{-}ALG}$ and microalgae lysis. Processes 1 (X_{ALG} growth on S_{NHX} and S_{PO4}), 2 (X_{ALG} growth on S_{NO3} and S_{PO4}), 5 ($X_{PP\text{-}ALG}$ storage), 6 (X_{ALG} endogenous respiration) and 7 (X_{ALG} lysis) in Table IX. 1 thus affect S_{PO4} concentration.

Figure IX. 2 gives the sensitivity measurements (μ* and σ) calculated from each input factor on the S_{PO4} output for the 4 periods.

Seven input factors were determined as influential on S_{PO4} output. The most influential input factors for Period 1 were: T_{MAX} (μ^* = 0.15, σ = 0.15) exhibiting a nonlinear or interactive effect, and q_{XPP} (μ^* = 0.24, σ = 0.11), I_{OPT} (μ^* = 0.20, σ = 0.10) and K_I (μ^* = 0.11, σ = 0.07) with a linear or additive effect on the model output. Contrary to S_{NHX} model output, microalgae growth processes were not the main pathway for S_{PO4} removal, since polyphosphate storage also affected S_{PO4} concentration. Figure IX. 2A discloses a higher

μ^* value of q_{XPP} (0.24) than μ_{ALG} (0.06), showing that S_{PO4} output was more influenced by the X_{PP}-$_{ALG}$ storage process than direct microalgae growth from S_{PO4} in Period 1. μ_{ALG}, $b_{ALG,2}$, and K_{PO4} were encompassed within the input factors cluster with a relatively minor influence in the model output.

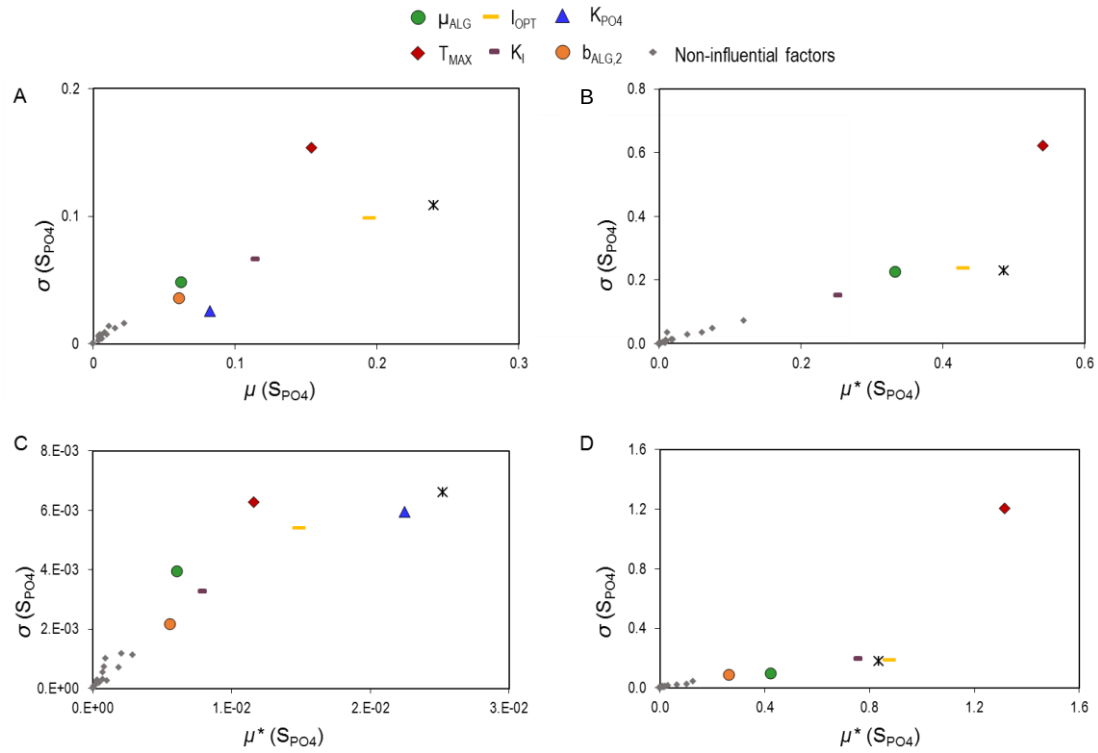

Figure IX. 2. Sensitivity measures μ^* versus σ for the model outputs S_{PO4} for Period 1 (A), Period 2 (B), Period 3 (C) and Period 4 (D).

Period 2 (Figure IX. 2B) highlighted T_{MAX}'s nonlinear or interactive significant effect on the model output (μ^* = 0.54, σ = 0.62), while q_{XPP} (μ^* = 0.49, σ = 0.23), I_{OPT} (μ^* = 0.43, σ = 0.24), μ_{ALG} (μ^* = 0.33, σ = 0.28) and K_I (μ^* = 0.25, σ = 0.15) showed a linear or additive effect. The higher μ^* of q_{XPP} than μ_{ALG} indicates that X_{PP-ALG} storage had a larger overall effect on the output, as well as in Period 1.

The effect of negligible soluble phosphorus concentration in the culture media (phosphorus-starved conditions) was assessed through Period 3 (Figure IX. 2C). The input factors q_{XPP} (μ^* = 0.025, σ = 0.007) and K_{PO4} (μ^* = 0.023, σ = 0.006) stand out, suggesting that X_{PP-ALG} storage was the main S_{PO4} removal pathway and that the storage rate was dependent on soluble phosphorus concentration, both with a nonlinear or

interactive effect. S_{PO4} removal by $X_{PP\text{-}ALG}$ storage process was influenced by environmental input factors, I_{OPT} (μ^* = 0.015, σ = 0.005) and T_{MAX} (μ^* = 0.012, σ = 0.006), with a nonlinear or interactive effect. K_I (μ^* = 0.008, σ = 0.003), μ_{ALG} (μ^* = 0.006, σ = 0.004) and $b_{ALG,2}$ (μ^* = 0.006, σ = 0.002) showed a relatively low μ^* values and could suggest a less influence on the model output. S_{PO4} uptake and release by microalgae absorption and lysis was thus not significant in Period 3.

Period 4 (Figure IX. 2D) showed a nonlinear or interactive effect of T_{MAX} (μ^* = 1.31, σ = 1.20) on S_{PO4} output. Input factors related to light availability for photosynthesis – I_{OPT} (μ^* = 0.87, σ = 0.18) and K_I (μ^* = 0.75, σ = 0.19) – exhibited a lower μ^* than T_{MAX}, indicating that Period 4 was governed by temperature fluctuations and their effect on microalgae kinetics. Figure IX. 2D differentiates three processes involved in the S_{PO4} balance: $X_{PP\text{-}ALG}$ storage, and growth and decay of microalgae. The input factor q_{XPP} (μ^* = 0.84, σ = 0.18) concerning $X_{PP\text{-}ALG}$ storage had a linear or additive effect and a higher μ^*, suggesting that the $X_{PP\text{-}ALG}$ storage process was the main pathway for S_{PO4} removal, similarly to previous periods. The relatively low μ^* value of μ_{ALG} (μ^* = 0.42, σ = 0.10) and $b_{ALG,2}$ (μ^* = 0.26, σ = 0.09), regarding microalgae growth and decay respectively, had a negligible overall effect on model output.

Regarding S_{PO4}, 7 input factors were hence selected as influential. Among these factors, T_{MAX} had the greatest influence on S_{PO4} concentration in the PBR. Indeed, this factor influences $X_{PP\text{-}ALG}$ storage, microalgae growth, and decay processes. The GSA results obtained here suggest that S_{PO4} balance was mainly affected by $X_{PP\text{-}ALG}$ storage since q_{XPP} along with T_{MAX} were the most influential input factors on S_{PO4} model output. On the other hand, the following factors were considered as influential due to their effect on the model output within two or more periods: I_{OPT}, K_I, μ_{ALG}, K_{PO4} and $b_{ALG,2}$.

Therefore, according to GSA of S_{PO4} concentration model output, the following factors must be calibrated: T_{MAX}, q_{XPP}, I_{OPT}, K_I, μ_{ALG}, K_{PO4} and $b_{ALG,2}$.

9.3.1.3. X_{ALG} output

X_{ALG} decreases due to microalgae lysis and endogenous respiration. Conversely, X_{ALG} increases due to microalgae growth. Processes 1 (X_{ALG} growth on S_{NHX} and S_{PO4}), 2 (X_{ALG} growth on S_{NO3} and S_{PO4}), 3 (X_{ALG} growth on S_{NHX} and X_{PP-ALG}), 4 (X_{ALG} growth on S_{NO3} and X_{PP-ALG}), 6 (X_{ALG} endogenous respiration) and 7 (X_{ALG} lysis) in Table 1 thus affect X_{ALG} concentration.

Figure IX. 3 shows the sensitivity measurements (μ* and σ) calculated from each input factor on the X_{ALG} output for the 4 periods.

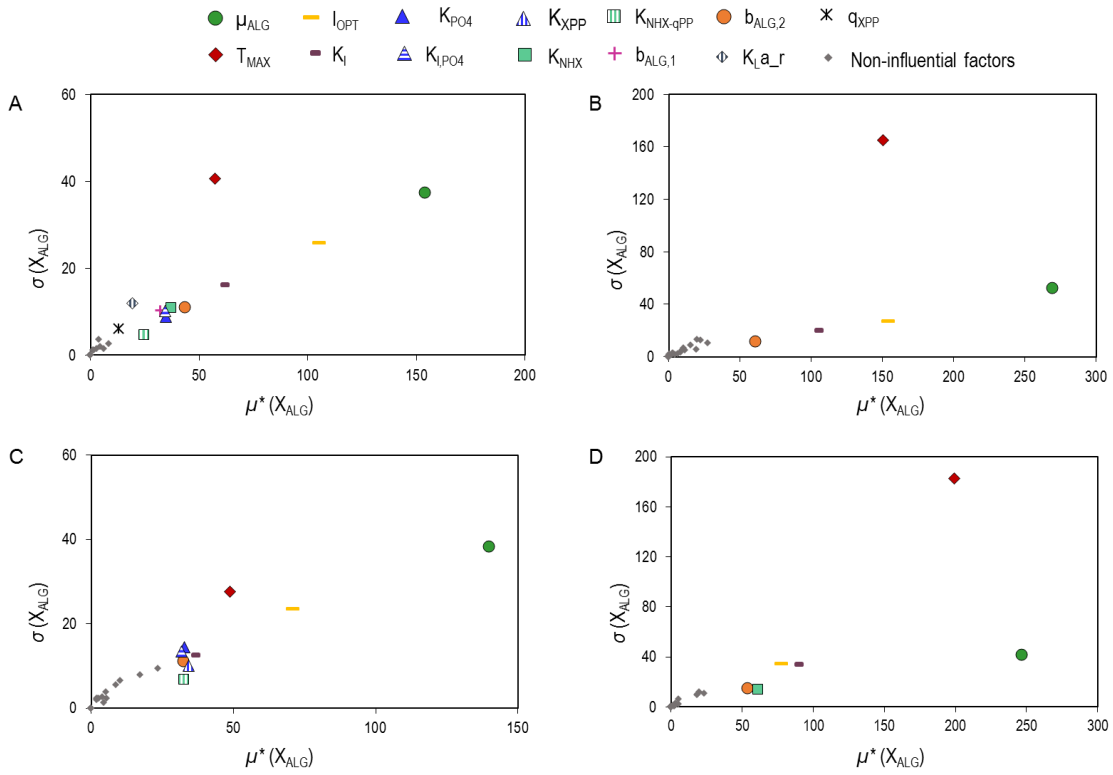

Figure IX. 3. Sensitivity measures μ^* versus σ for the model outputs X_{ALG} for Period 1 (A), Period 2 (B), Period 3 (C) and Period 4 (D).

In Period 1 (Figure IX. 3A), four input factors represented the greatest influence on the model output: μ_{ALG} (μ^* = 153.76, σ = 37.47) and T_{MAX} (μ^* = 57.24, σ = 40.62) with nonlinear or interactive effects, and I_{OPT} (μ^* = 105.17, σ = 25.64) and K_I (μ^* = 60.50, σ = 16.12) with linear or additive effects. Microalgae growth depended firstly on μ_{ALG} and secondly on the environmental factors (temperature, light intensity, nutrients

concentration, etc.) conditioning biomass growth rate. Indeed, the high μ^* for μ_{ALG} indicates that it was the input factor with the most important overall effect on the model output. The higher values of μ^* and σ for I_{OPT} suggested that microalgae growth rate was subjected to average light intensity, which is in agreement with the main growth pathway of microalgae: photosynthesis. However, although microalgae productivity was due to biomass growth, cell lysis and endogenous respiration represented by input factors $b_{ALG,2}$ (μ^* = 43.04, σ = 11.20) and $b_{ALG,1}$ (μ^* = 32.13, σ = 10.24), respectively, played a relatively minor role compared to μ_{ALG}. Influential input factors on X_{ALG} output for Period 2 were thus: μ_{ALG} (μ^* = 268.76, σ = 57.78), I_{OPT} (μ^* = 153.85, σ = 26.79), K_I (μ^* = 103.53, σ = 19.83), $b_{ALG,2}$ (μ^* = 60.44, σ = 12.06) with a linear or additive effect, and T_{MAX} (μ^* = 150.66, σ = 165.04) having a nonlinear or interactive effect.

GSA results for Period 3 are shown in Figure IX. 3C. μ_{ALG} (μ^* = 139.71, σ = 38.41) was the input with the greatest influence on X_{ALG} model output and had a nonlinear or interactive effect. Kinetic processes were mainly affected by I_{OPT} (μ^* = 70.77, σ = 23.45) and T_{MAX} to a lesser extent (μ^* = 48.77, σ = 27.60). Period 3 provided P-starved culture conditions, which explained why input factors associated with X_{PP-ALG} storage and assimilation processes (K_{XPP}, μ^* = 34.23, σ = 10.08; K_{PO4}, μ^* = 32.67, σ = 14.47; $K_{NHX-qPP}$, μ^* = 32.58, σ = 6.79; and $K_{I,PO4}$, μ^* = 31.85, σ = 13.05) stood out as relatively influential.

The influence of input factors in Period 4 followed the same pattern for nutrients removal outputs as for biomass production output. The higher μ^* of μ_{ALG} (μ^* = 246.47, σ = 41.84) indicated an important overall effect on biomass productivity. Figure IX. 3D reports that μ_{ALG} had a linear and additive effect on X_{ALG} output, while T_{MAX} (μ^* = 199.29, σ = 182.49) had a nonlinear or interactive effect. These two input factors, μ_{ALG} and T_{MAX}, were the most influential in comparison with K_I (μ^* = 88.09, σ = 33.54), I_{OPT} (μ^* = 77.38, σ = 33.94), K_{NHX} (μ^* = 60.88, σ = 14.08) and $b_{ALG,2}$ (μ^* = 53.41, σ = 15.46) which were encompassed in the cluster of input factors with a relatively minor influence. These results suggest that

the input factors related to microalgae productivity were mainly regulated by PBR temperature variations and the average available light intensity did not limit microalgae growth during Period 4.

X_{ALG} model output was sensitive to 10 inputs: μ_{ALG}, T_{MAX}, $I_{OPT,}$ K_I, $b_{ALG,2}$, K_{NHX}, K_{PO4}, and $K_{NHX\text{-}qPP}$. GSA results suggested that biomass concentration balance was dominated by microalgae growth and not by endogenous respiration and microalgae lysis. The four-kinetic rates of microalgae growth were influenced by light availability and temperature. The most influential factors related to X_{ALG} biomass concentration were thus μ_{ALG}, T_{MAX}, and I_{OPT}. The remaining factors, although they had a relative influence on X_{ALG} output, were less influential.

9.3.1.4. Overall GSA results

Overall, 11 of the 34 model parameters were classified as influential factors: μ_{ALG}, T_{MAX}, I_{OPT}, K_I, K_{NHX}, $b_{ALG,2}$, q_{XPP}, K_{PO4}, $K_{I,PO4}$, $K_{NHX\text{-}qPP}$, and K_La_r. The four input factors with the most important overall effect on the outputs analyzed were μ_{ALG}, q_{XPP}, T_{MAX}, and I_{OPT}. The input factor μ_{ALG} showed a strong influence on the S_{NHX} and X_{ALG} output, whereby the nitrogen and biomass concentrations in the PBRs were mainly due to microalgae growth processes. Conversely, the main phosphorus removal pathway was $X_{PP\text{-}ALG}$ storage by q_{XPP}. T_{MAX} and I_{OPT} indicated that the growth and storage kinetic rates were mainly influenced by temperature and light intensity fluctuations. The model was also sensitive to nitrogen half saturation constants, K_{NHX} and $K_{NHX\text{-}qPP}$ for Period 1 and Period 3, characterized by a low nitrogen and negligible phosphorus concentration, respectively.

9.3.2. Model calibration

9.3.2.1. Offline calibration

T_{MAX}, I_{OPT}, K_I, μ_{ALG}, K_{NHX} and K_{PO4} (Table IX. 3) were calibrated offline using experimental data from both photo-respirometric tests and the MPBR pilot plant.

Figure IX. 4A shows the normalized nOPR values following a typical temperature response characterized by a slow rise from cold to optimum temperature before a rapid drop for higher temperatures. The Ratkowski model provided a good fit with the experimental data (variance > 94%), providing T_{MIN} and T_{MAX} values of 0 ± 0.01 and 40.1 ± 0.2 ºC, respectively. These results were within the range of values compiled by Bernard & Rémond (2012) for 15 different algal species.

Figure IX. 4B shows that Steele's equation was able to describe the normalized nOPR evolution with light intensity with a variance of 95%. The light curve showed the typical increase in photosynthesis light response with rising light availability and a drop at high light intensities due to photoinhibition. The calibrated optimal light intensity for X_{ALG} growth and attenuation coefficient were 230 ± 30 µmol m^{-2} s^{-1} and 0.025 ± 0.002 m^2 g TSS^{-1}. The values reported in the literature range from 80 (Khalili et al., 2015) to 413 µmol m^{-2} s^{-1} (Barbera et al., 2020). This wide variation is probably due to differences in the environmental and operating conditions of the experimental set-up (Bernard, 2011) and microalgae speciation (Ouyang et al., 2010). The obtained attenuation coefficient of 0.025 m^2 g TSS^{-1} was in agreement with the observations made by Ruiz-Martinez et al. (2014).

Figure IX. 4C shows the microalgae growth kinetic curve. The experimental data was described by the logistic Verhulst model to quantify microalgae growth, resulting in a match with a variance above 99% in all regressions. The average μ_{ALG} obtained was 1.8 ± 0.3 d^{-1}, similar to the rates of 2, 1.6, 1.5 and 1.6 d^{-1} used by most integrated microalgae models, i.e. Reichert et al. (2001), Zambrano et al. (2016), Solimeno et al. (2017), and Sánchez-Zurano et al. (2021), respectively. According to the values reported in the literature, a maximum growth rate of 1.8 d^{-1} is suitable for modeling microalgae growth and development in a wastewater medium.

K_{NHX} and K_{PO4} were determined by the Michaelis-Menten kinetic relationship. Experimental data from 4 batch periods were linearized by the Lineweaver-Burk function

(see Figure IX. 4D). Kinetic coefficients of S_{NHX} and S_{PO4} were determined from the intercept and the slope. The observed K_{NHX} was 0.10 ± 0.02 g N m^{-3} and K_{PO4} was 0.050 ± 0.011 g P m^{-3}. The kinetic relationship proposed was able to adjust the experimental data to the model results at a variance above 96%. The calibrated KNHX value was consistent with the 0.10 g N m^{-3} adopted by Reichert et al. (2001). Zambrano et al. (2016) and Solimeno et al. (2017) both used the value proposed by Reichert et al. (2001) for model calibration and validation. As phosphorus was not usually considered a limiting nutrient, the K_{PO4} factor was not normally included in mathematical models, which limits the comparison between K_{PO4} values in the wastewater culture medium. Reichert et al. (2001) determined a phosphorus saturation constant of 0.02 g P m^{-3} for continental water bodies.

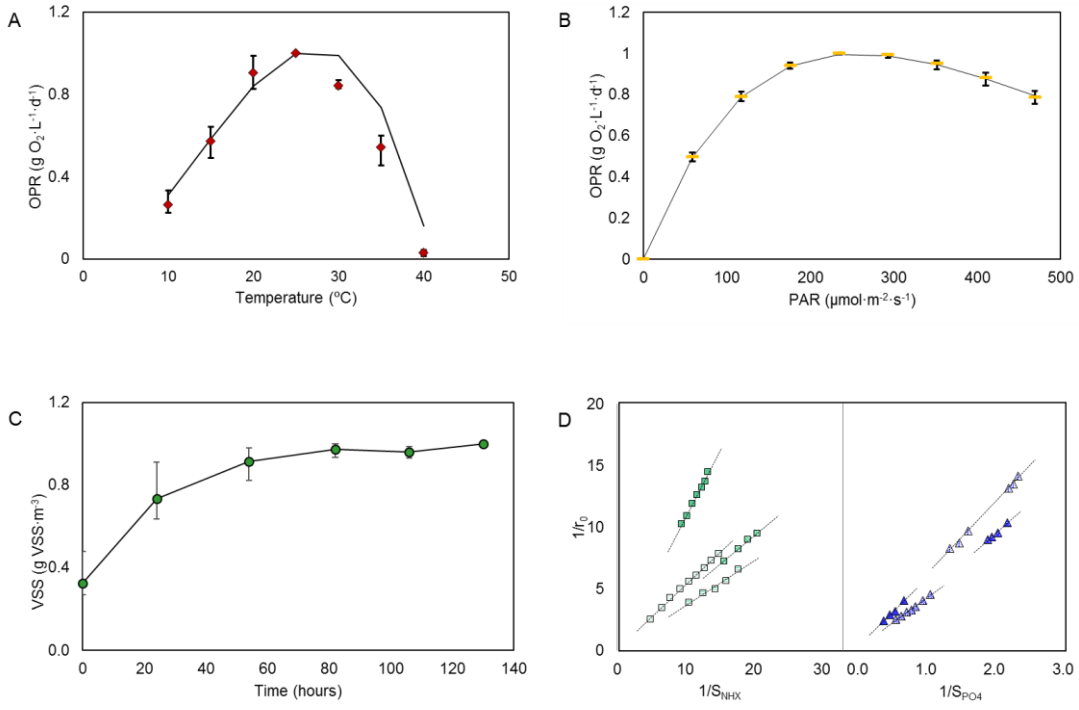

Figure IX. 4. Influence of temperature (A) and light intensity (B) on normalized oxygen production rate of microalgae, biomass growth (C) and nitrogen and phosphorus consumption linearizer by Lineweaver-Burk function. Experimental and modeled data are represented by markers and lines, respectively.

9.3.2.2. Online calibration and dynamic optimization

$K_{NHX-qPP}$, $K_{I,PO4}$, $b_{ALG,2}$, q_{XPP}, and K_La_r factors were calibrated online after setting the calibrated values of μ_{ALG}, T_{MAX}, I_{OPT}, K_I, K_{NHX}, and K_{PO4} using data from a 35-day pseudo-stationary operating period of the MPBR pilot plant. By means of the Curve Fitting tool implemented in Matlab® software and expert knowledge, the modeling results were matched with the experimental data. $K_{NHX-qPP}$ and K_La_r parameters were calibrated using the S_{NHX} concentration as a reference, while q_{XPP} and $K_{I,PO4}$ were calibrated from S_{PO4} and total suspended phosphorus (X_P, g $P \cdot m^{-3}$) concentrations. $b_{ALG,2}$ was calibrated from sCOD, X_{TSS} and X_{VSS} data. The resulting data set was calibrated by evaluating the combined effect of the following 6 model outputs: S_{NHX}, S_{PO4}, X_P, X_{TSS}, X_{VSS} and sCOD. Graphical representation of the experimental results and the modeled data obtained by the calibrated factors compiled in Table IX. 3 are reported in supplementary material.

Ruiz-Martinez et al. (2014) reported that N removal rate was higher in P-replete than in P-starved culture conditions. $K_{NHX-QPP}$ (i.e. the half saturation parameter for S_{NHX} in a phosphorus-starved medium) was included in the model to represent this approach. The calibrated value of $K_{NHX-QPP}$ was 3 g $N \cdot m^{-3}$, while that of K_{NHX} was 0.1. A higher value of the half saturation constant under P-deficient culture conditions is in agreement with the observations of Ruiz-Martinez et al. (2014). Parameters $b_{ALG,2}$ and $q_{XPP-ALG}$ were calibrated at 0.15 and 0.01 d^{-1} respectively. The $b_{ALG,2}$ calibrated value was in agreement with the range reported in the literature of 0.012 to 0.21 d^{-1} (Ruiz-Martinez et al., 2014; Wágner et al., 2016).The value obtained was in agreement with the maximum rate used by the ExPIM model (Singh et al., 2018). The fitting parameter K_La_r is physically meaningless and cannot be compared with the scientific literature.

Statistical tests were performed to find any significant differences between the experimental and simulated results.

The t-test revealed a confidence interval for the difference between the means of the experimental and modeled data from -57.50 to 58.93. As this confidence interval contains

the value 0, thus it can be assumed that there is no significant difference between these means, with a confidence level of 95%. Furthermore, since the calculated p-value was 0.9808 (> 0.05), the null hypothesis cannot be rejected. The means of the experimental and modeled data thus do not differ significantly from each other.

The confidence interval of the F-test ranged from 0.77 to 1.32. Since the confidence interval contained the value of 1, it can be assumed that there are no significant differences between the standard deviations of experimental and modeled data, with a confidence level of 95%. Since the calculated p-value was 0.9562 (> 0.05), the null hypothesis cannot be rejected and the standard deviations of the experimental and modeled data can be said not to differ significantly from each other.

The p-value of the Mann-Whitney U-test was 0.9184 (> 0.05), so that the null hypothesis cannot be rejected either and it can be assumed that there are no statistically significant differences between the medians of the experimental and modelled data, at a 95% confidence level.

Although, the statistical tests revealed the goodness of the results obtained with the offline/online calibration, it was decided to carry out a dynamic optimization of the 11 most influencing factors (μ_{ALG}, T_{MAX}, I_{OPT}, K_I, K_{NHX}, $b_{ALG,2}$, q_{XPP}, K_{PO4}, $K_{I,PO4}$, $K_{NHX\text{-}qPP}$ and K_La_r), to see if it was possible to obtain even better results for each period. The remaining factors were set to default values (Table IX. 3).

Table IX. 4 shows the calibrated values by offline/online methods, the dynamically optimized values for each operating period, and the rounded values of optimized parameters. The model accurately predicted microalgae performance using the calibrated offline/online values: an adequate correlation coefficient (R^2) of 0.9954 was obtained between the experimental and simulated data. It also obtained the following correlation coefficients (R^2) when using the optimized values: 0.9969, 0.9980, 0.9976 and 0.9982 for Periods 1, 2, 3 and 4, respectively (average R^2 of 0.9977). The model

accuracy using the sets of model parameters values obtained from both the offline/online calibration and the dynamic optimization was also assessed by Root Mean Square Error (RMSE) and Sum of Squares due to error (SSE). RMSE and SSE were reduced by 47% and 27%, respectively, when using the dynamically optimized values for the model parameters over the offline/online calibrated ones.

The model performance can thus be said to have only slightly improved by dynamically optimizing the model's influential parameters, validating the values obtained from the offline/online calibrated values from experimental data.

Table IX. 4. Offline/online calibrated and dynamically optimized values for the influential model parameters. SD was not specified in online and dynamically calibrated factors because they were set to a single specific value. Abbreviation: P. 1, P. 2, P. 3 and P. 4 are Periods 1, 2, 3 and 4, respectively.

Parameter		Offline/Online Calibrated value	Dynamic Optimization values				
			P. 1	P. 2	P. 3	P. 4	Mean ± SD
μ_{ALG}	d^{-1}	1.8 ± 0.3[a]	1.63	1.45	2.14	2.00	1.8 ± 0.3
K_{NHX}	g $N \cdot m^{-3}$	0.10 ± 0.02[a]	0.11	0.12	0.095	0.10	0.109 ± 0.012
$K_{NHX-QPP}$	g $N \cdot m^{-3}$	3[b]	3.55	3.57	2.54	3.56	3.3 ± 0.5
K_{PO4}	g $P \cdot m^{-3}$	0.050 ± 0.011[a]	0.04	0.05	0.04	0.06	0.049 ± 0.008
$K_{I,PO4}$	g $P \cdot m^{-3}$	0.15[b]	0.17	0.12	0.13	0.12	0.14 ± 0.02
I_{opt}	$\mu mol \cdot m^{-2} \cdot s^{-1}$	230 ± 30[a]	187.47	199.23	184.78	215.56	197 ± 14
K_I	m^2 g·TSS^{-1}	0.025 ± 0.002[a]	0.028	0.020	0.022	0.027	0.024 ± 0.004
T_{max}	°C	40.1 ± 0.2[a]	33.76	44.89	34.69	42.90	39 ± 6
$b_{ALG,2}$	d^{-1}	0.15[b]	0.15	0.14	0.16	0.17	0.156 ± 0.013
q_{XPP}	d^{-1}	0.010[b]	0.0096	0.011	0.011	0.012	0.0110 ± 0.0010
K_La_r	-	1[b]	0.86	1.00	1.19	0.81	1.0 ± 0.2

[a]Offline calibrated

[b]Online calibrated

9.3.3. Uncertainty analysis

9.3.3.1. S_{NHX} output

The results for S_{NHX} output from Monte Carlo simulations in the 4 periods are reported as supplementary material. There were 3500 lines (spaghettis), each one referring to the results of one simulation. The varying spread of the band in the multiple probability density function plot indicated the extent of the uncertainty in the simulated S_{NHX} at different sampling times. The 5^{th} and 95^{th} Monte Carlo percentiles (uncertainty bands) were calculated; the further away the uncertainty bands from the mean value, the greater the uncertainty.

Figure IX. 5 shows the experimental and calibrated model results, as well as the uncertainty bands for the 4 periods. It can be seen that the uncertainty bandwidths change with the period considered. This could be due to variations in the influencing factors of each period, the role they played in the variation of the model output and the interlinkage between the model outputs. The uncertainty bandwidths can be quantified from the r-factor (Table IX. 5). The closer the r-factor to 1, the narrower the uncertainty bands. According to this uncertainty factor, the uncertainty in Periods 3 and 4 is therefore lower than in Periods 1 and 2. UA results should be complemented with other indices such as the p-factor and the ARIL value. The closer to 100% the p-factor, the lower the uncertainty of the model predictions. Conversely, the lower the ARIL value, the lower the model uncertainty. The p-factor value was above 90% In all the periods because the wide bands obtained embrace most of the data. However, in this specific case, the large values obtained for the p-factor did not reflect low model uncertainty but rather the great width of the uncertainty bands and therefore a high degree of uncertainty. For the ARIL value (Table IX. 5), Period 4 had the lowest uncertainty of all the remaining periods. As the uncertainty of the periods varied according to the target coefficient, it was required to combine the three uncertainty coefficients analysis together with the uncertainty bandwidth for a critical UA.

Compiling the three coefficients, Period 4 showed low uncertainty (r-factor: 1.56, p-factor: 100% and ARIL: 0.22). From the 11 influential parameters, only T_{MAX} showed a strong influence on S_{NHX} output in Period 4, while the remaining factors had a relatively less influential effect, so that the model was mainly influenced by T_{MAX}, reducing the range of the simulation uncertainty bands.

A larger bandwidth and uncertainty coefficient values were obtained for Periods 1, 2 and 3 (Table IX. 5). Four (μ_{ALG}, T_{MAX}, I_{OPT} and K_I) and 9 (μ_{ALG}, T_{MAX}, I_{OPT}, K_I, K_{NHX}, K_{PO4}, $K_{NHX-qPP}$, $K_{I,PO4}$ and $b_{ALG,2}$) of the influencing parameters were identified in Periods 2 and 3, respectively, while all of them were identified in Period 1. Comparing the uncertainty bandwidth and coefficients obtained for the 4 periods, the results suggest that the model uncertainty is influenced by the number of influential input factors involved in each period. As expected, the more the influencing input factors involved, the greater the uncertainty of the model appears to be.

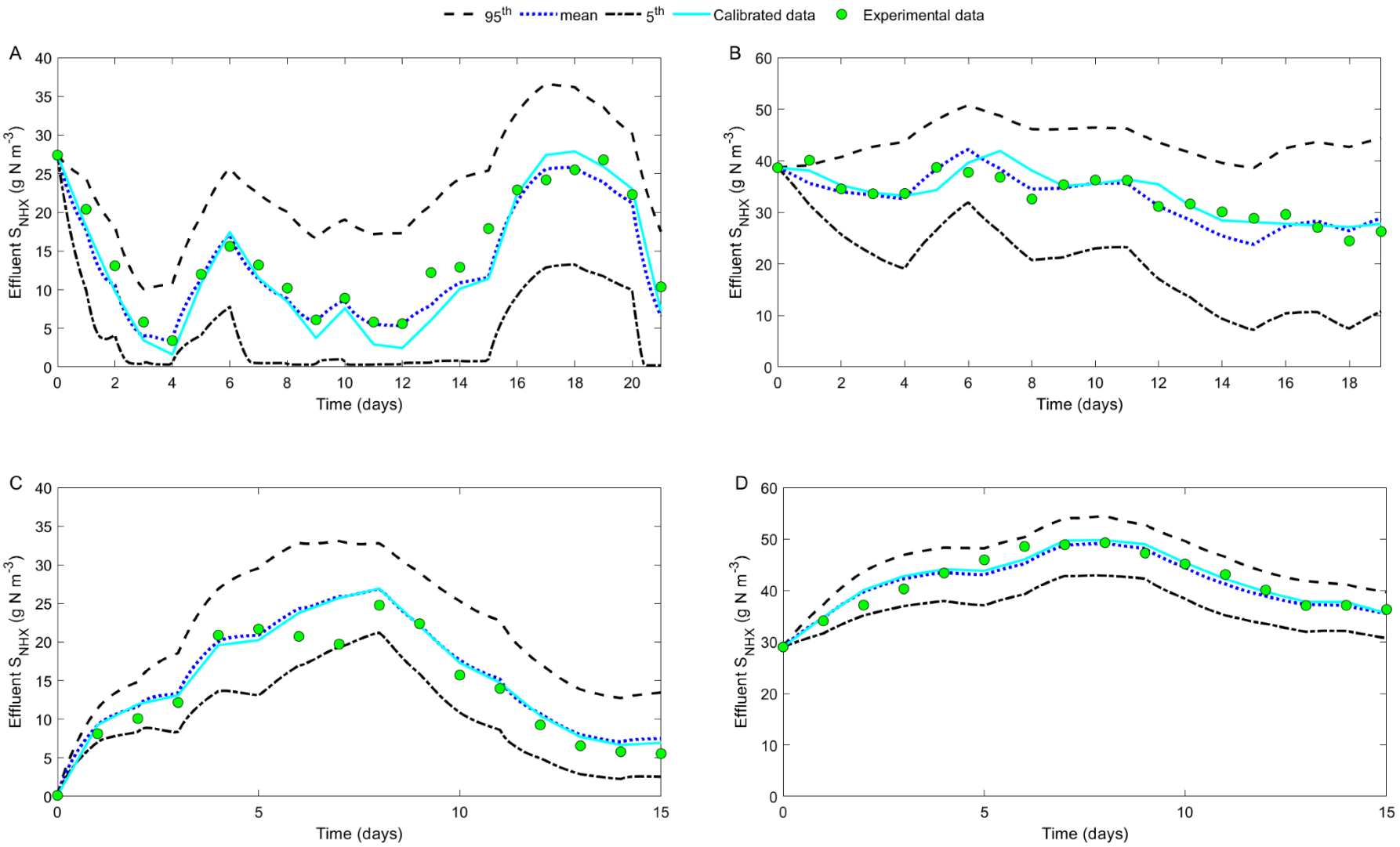

Figure IX. 5. Calibrated, experimental data, 95th and 5th percentiles for S_{NHX} concentration in the MPBR effluent for Period 1 (A), Period 2 (B), Period 3 (C) and Period 4 (D).

9.3.3.2. S_{PO4} output

The results for S_{PO4} output from the Monte Carlo simulation are also reported as supplementary material. The results of the S_{PO4} model output showed the model's good response in terms of uncertainty for Periods 1, 2 and 4. Nearly all the experimental data (p-factor value > 70%) lay inside the uncertainty bands (Figure IX. 6A, B and D, Table IX. 5). All the experimental data obtained for Period 2 were inside the 5^{th} and 95^{th} percentiles with a p-factor value of 100%, because this period presented the widest bandwidth with an r-factor value of 2.10. According to the uncertainty coefficient values reported by Mannina et al. (2018), the r-factor value for Period 2 showed a degree of uncertainty in the model output, although the low ARIL value (0.69) suggested a good response of the model in terms of uncertainty.

In Periods 1 and 4, the r-factor values close to 1 (1.72 and 0.58, respectively) and the low ARIL values (0.46 and 0.11, respectively), combined with the high p-factor value (75 and 71%, respectively), suggested an acceptable model response in uncertainty terms.

In contrast to the preceding periods, Period 3 showed high uncertainty in terms of S_{PO4} output. Although most experimental data fell within the uncertainty bands (p-factor value of 86%), the high ARIL value and r-factor provided high uncertainty in the S_{PO4} output. According to GSA, the more influential input factors were related to $X_{PP\text{-}ALG}$ storage. The higher level of uncertainty than the other periods could be due to the fact that storage and assimilation of $X_{PP\text{-}ALG}$ played a more significant role in Period 3. The results suggested that the uncertainty propagation through the model output was due to parameters related to $X_{PP\text{-}ALG}$.

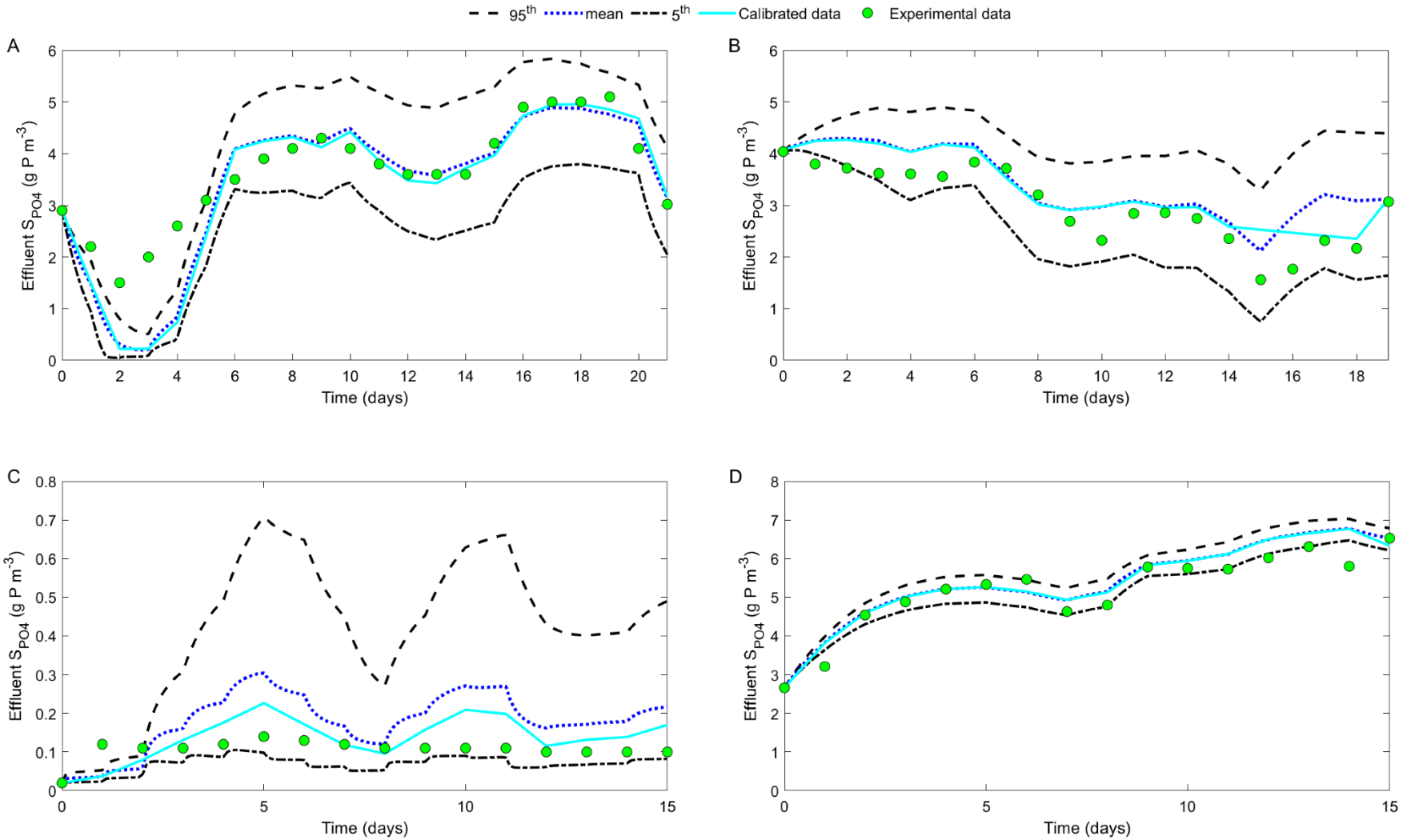

Figure IX 6. Calibrated, experimental data, 95th and 5th percentiles for S_{PO4} concentration in the MPBR effluent for Period 1 (A), Period 2 (B), Period 3 (C) and Period 4 (D).

9.3.3.3. X_{ALG} output

The results of X_{ALG} output from the Monte Carlo simulation are reported as supplementary material and the uncertainty coefficient values are shown in Table IX. 5. In X_{ALG}, all the experimental data lay inside the uncertainty bands (Figure IX. 7) and the p-factor was 100% for each period. As ARIL values were lower than 1, given the high p-factor values and low ARIL values, a good model response in terms of uncertainty would be obtained for the X_{ALG} output. However, the r-factor values on average were not near 1, with the closest being 2.06 in Period 3. As detailed above, the wider the bandwidth, the greater the probability of the experimental data being inside the uncertainty bands. Consequently, although the p-factor value mathematically provided low uncertainty, the model response should be analyzed as a whole, considering the overall computation of the uncertainty coefficients and Monte Carlo simulations.

Table IX. 5. Uncertainty coefficient for each Period and model output: p-factor, r-factor and ARIL.

Output - #Period	p-factor	r-factor	ARIL
S_{NHX} - 1	100	2.42	1.61
S_{NHX} - 2	94.44	5.70	0.73
S_{NHX} - 3	100	1.51	0.84
S_{NHX} - 4	100	1.56	0.22
S_{PO4} - 1	75.00	1.72	0.46
S_{PO4} - 2	100	2.10	0.69
S_{PO4} - 3	85.71	12.63	2.94
S_{PO4} - 4	71.43	0.58	0.11
X_{ALG} - 1	100	3.45	0.50
X_{ALG} - 2	100	4.35	0.74
X_{ALG} - 3	100	2.06	0.31
X_{ALG} - 4	100	4.49	0.65

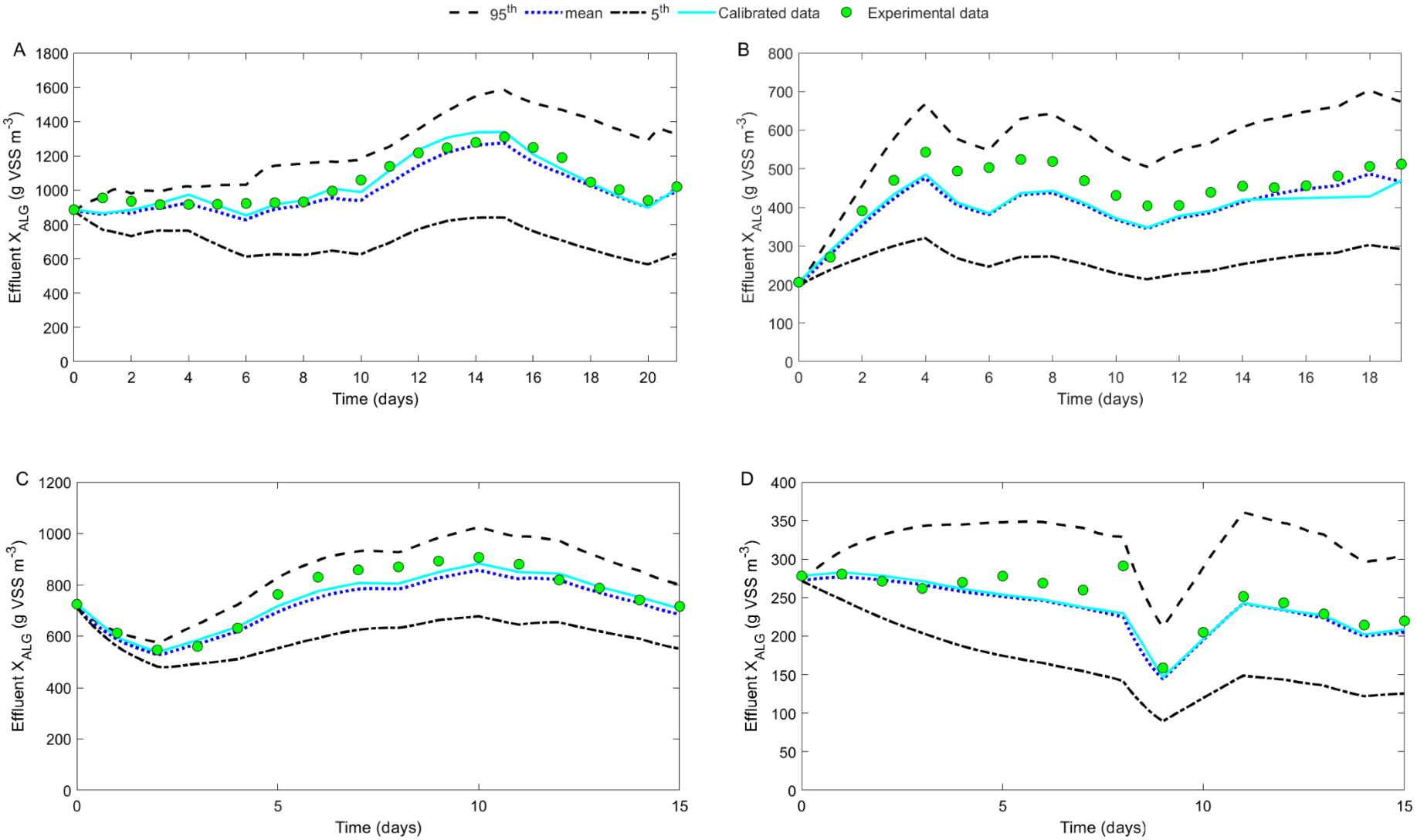

Figure IX. 7. Calibrated, experimental data, 95th and 5th percentiles for X_{ALG} concentration in the MPBR effluent for Period 1 (A), Period 2 (B), Period 3 (C) and Period 4 (D).

9.3.3.4. Overall uncertainty analysis

The Monte Carlo simulation and uncertainty coefficients show different responses in terms of uncertainty for each period. This result is probably due to two main reasons: (I) the number of sensitive factors involved and (II) the processes involved in each period. The results obtained for the S_{NHX} model output suggested that the uncertainty bandwidth depended on the number of influential input factors involved. S_{PO4} output suggested that the processes involved in each period had different effects on model output variations and on the interrelationship between model outputs. On the other hand, although p-factor and ARIL values for X_{ALG} output suggested a good response in terms of uncertainty, an integrated analysis of all uncertainty indices (bandwidth, p-factor, r-factor and ARIL value) showed high uncertainty in the model output.

The high uncertainty response of the 3 model outputs could be attributed to online calibrated factors. The reproducibility of this online calibration approach may be questionable and could introduce uncertainty into the model. The problem with online calibration is the non-identifiability of the parameters, which leads to accepting the possible "equifinality" of the models, i.e. there is no one "optimal" set of calibrated parameters to represent microalgae culture, although there are multiple combinations of parameter values for a chosen model structure that can be equally valid for matching data (Sin et al., 2005). These model parameter sets can be distributed over a wide range of values for each parameter, introducing high uncertainty into the model. Offline calibration is an alternative method to online calibration. In this respect, offline calibration enables kinetic processes to be isolated and the variables involved to be controlled. In this study, offline calibration was performed by: (I) photo-respirometry tests with biomass adapted from the MPBR pilot plant; and (II) microalgae growth in batch conditions, so that the offline calibrated data agree with the intrinsic characteristics of microalgae culture and operating conditions and thus provide more reliable values. Since a subset of the parameters was calibrated online, an optimization algorithm was used to match

the model parameters within a realistic data range. The offline method can thus be recommended over online calibration, as can the dynamic optimization of all the influential parameters.

9.4. CONCLUSIONS

This paper presents a GSA, an offline/online calibration, a dynamic optimization, and a UA of a previously proposed and validated microalgae model. Eleven out of 34 influential factor were identified from the GSA. The four factors with the most important overall effect on the three outputs evaluated (S_{NHX}, S_{PO4} and X_{ALG}) were μ_{ALG}, q_{XPP}, T_{MAX} and I_{OPT}. S_{NHX} and X_{ALG} model outputs were influenced by kinetic input factors related to microalgae growth, while S_{PO4} model output was affected by $X_{PP\text{-}ALG}$ storage. A single data set was achieved by offline/online calibration methods able to reproduce the model outputs for the 4 experimental periods evaluated, regardless of the operational and environmental conditions. A dynamic optimization of the calibrated model parameter values was conducted to improve the model's output response. The UA results revealed different responses according to the model output and the operating period considered and were dependent on the processes and the number of influencing input factors involved in each period. Uncertainty indices were analyzed together with uncertainty bands to avoid erroneous conclusions. The model's uncertainty results showed the need to prioritize offline calibration to improve model performance.

REFERENCES

APHA, AWWA, WEF, 2005. Standard Methods for the Examination of Water and Wastewater, 21st ed, American Public Health Association. Washington, DC.

Aslan, S., Kapdan, I.K., 2006. Batch kinetics of nitrogen and phosphorus removal from synthetic wastewater by algae. Ecol. Eng. 28, 64–70. https://doi.org/10.1016/j.ecoleng.2006.04.003

Barbera, E., Sforza, E., Grandi, A., Bertucco, A., 2020. Uncoupling solid and hydraulic retention time in photobioreactors for microalgae mass production : A model-based analysis. Chem. Eng. Sci. 218, 115578. https://doi.org/10.1016/j.ces.2020.115578

Bernard, O., 2011. Hurdles and challenges for modelling and control of microalgae for CO 2 mitigation and biofuel production, in: Journal of Process Control. pp. 1378–1389. https://doi.org/10.1016/j.jprocont.2011.07.012

Bernard, O., Rémond, B., 2012. Validation of a simple model accounting for light and temperature effect on microalgal growth. Bioresour. Technol. 123, 520–527. https://doi.org/10.1016/j.biortech.2012.07.022

Campolongo, F., Cariboni, J., Saltelli, A., 2007. An effective screening design for sensitivity analysis of large models. Environ. Model. Softw. 22, 1509–1518. https://doi.org/10.1016/j.envsoft.2006.10.004

Campolongo, F., Tarantola, S., Saltelli, A., 1999. Tackling quantitatively large dimensionality problems. Comput. Phys. Commun. 117, 75–85. https://doi.org/10.1016/S0010-4655(98)00165-9

Corominas, L., Neumann, M.B., 2014. Ecosystem-based management of a Mediterranean urban wastewater system: A sensitivity analysis of the operational degrees of freedom. J. Environ. Manage. 143, 80–87. https://doi.org/10.1016/J.JENVMAN.2014.04.021

Costache, T.A., Gabriel Acien Fernandez, F., Morales, M.M., Fernández-Sevilla, J.M., Stamatin, I., Molina, E., 2013. Comprehensive model of microalgae photosynthesis rate as a function of culture conditions in photobioreactors. Appl. Microbiol. Biotechnol. 97, 7627–7637. https://doi.org/10.1007/s00253-013-5035-2

Davison, I.R., 1991. ENVIRONMENTAL EFFECTS ON ALGAL PHOTOSYNTHESIS: TEMPERATURE. J. Phycol. https://doi.org/10.1111/j.0022-3646.1991.00002.x

Eze, V.C., Velasquez-Orta, S.B., Hernández-García, A., Monje-Ramírez, I., Orta-Ledesma, M.T., 2018. Kinetic modelling of microalgae cultivation for wastewater treatment and carbon dioxide sequestration. Algal Res. 32, 131–141. https://doi.org/10.1016/j.algal.2018.03.015

González-Camejo, J., Aparicio, S., Ruano, M. V., Borrás, L., Barat, R., Ferrer, J., 2019. Effect of ambient temperature variations on an indigenous microalgae-nitrifying bacteria culture dominated by Chlorella. Bioresour. Technol. 290, 121788. https://doi.org/10.1016/j.biortech.2019.121788

González-Camejo, J., Barat, R., Aguado, D., Ferrer, J., 2020. Continuous 3-year outdoor operation of a flat-panel membrane photobioreactor to treat effluent from an anaerobic membrane bioreactor. Water Res. 169. https://doi.org/10.1016/j.watres.2019.115238

González-Camejo, J., Barat, R., Ruano, M.V., Seco, A., Ferrer, J., 2018. Outdoor flat-panel membrane photobioreactor to treat the effluent of an anaerobic membrane bioreactor. Influence of operating, design, and environmental conditions. Water Sci. Technol. 78. https://doi.org/10.2166/wst.2018.259

Jin, X., Xu, C.Y., Zhang, Q., Singh, V.P., 2010. Parameter and modeling uncertainty simulated by GLUE and a formal Bayesian method for a conceptual hydrological model. J. Hydrol. 383, 147–155. https://doi.org/10.1016/j.jhydrol.2009.12.028

Khalili, A., Najafpour, G.D., Amini, G., Samkhaniyani, F., 2015. Influence of nutrients and LED light intensities on biomass production of microalgae Chlorella vulgaris. Biotechnol. Bioprocess Eng. 20, 284–290. https://doi.org/10.1007/s12257-013-0845-8

Kim, S., Lee, Y., Hwang, S.J., 2013. Removal of nitrogen and phosphorus by Chlorella sorokiniana cultured heterotrophically in ammonia and nitrate. Int. Biodeterior. Biodegrad. 85, 511–516.

https://doi.org/10.1016/j.ibiod.2013.05.025

Mannina, G., Cosenza, A., Ekama, G.A., 2017. Greenhouse gases from membrane bioreactors: Mathematical modelling, sensitivity and uncertainty analysis. Bioresour. Technol. 239, 353–367. https://doi.org/10.1016/j.biortech.2017.05.018

Mannina, G., Cosenza, A., Viviani, G., Ekama, G.A., 2018. Sensitivity and uncertainty analysis of an integrated ASM2d MBR model for wastewater treatment. Chem. Eng. J. 351, 579–588. https://doi.org/10.1016/j.cej.2018.06.126

Markou, G., Vandamme, D., Muylaert, K., 2014. Microalgal and cyanobacterial cultivation: The supply of nutrients. Water Res. https://doi.org/10.1016/j.watres.2014.07.025

Morris, M.D., 1991. Factorial sampling plans for preliminary computational experiments. Technometrics 33, 161–174. https://doi.org/10.1080/00401706.1991.10484804

Nagase, H., Yoshihara, K. ichi, Eguchi, K., Okamoto, Y., Murasaki, S., Yamashita, R., Hirata, K., Miyamoto, K., 2001. Uptake pathway and continuous removal of nitric oxide from flue gas using microalgae. Biochem. Eng. J. 7, 241–246. https://doi.org/10.1016/S1369-703X(00)00122-4

Ndiaye, M., Gadoin, E., Gentric, C., 2018. CO2 gas–liquid mass transfer and kLa estimation: Numerical investigation in the context of airlift photobioreactor scale-up. Chem. Eng. Res. Des. 133, 90–102. https://doi.org/10.1016/j.cherd.2018.03.001

Ouyang, Z.-R., Wen, X.-B., Geng, Y.-H., Mei, H., Hu, H.-J., Zhang, G.-Y., Li, Y.-G., 2010. The Effects of Light Intensities, Temperatures, pH and Salinities on Photosynthesis of Chlorella. Plant Sci. J. 30, 49–55. https://doi.org/10.3724/sp.j.1142.2010.00049

Pastore, M., Barbera, E., Panichi, A., Sforza, E., 2020. Application of photorespirometry to unravel algal kinetic parameters of nitrogen consumption in complex media. Algal Res. 47, 101837. https://doi.org/10.1016/j.algal.2020.101837

Rajabi, M.M., Fahs, M., Panjehfouladgaran, A., Ataie-Ashtiani, B., Simmons, C.T., Belfort, B., 2020. Uncertainty quantification and global sensitivity analysis of double-diffusive natural convection in a porous enclosure. Int. J. Heat Mass Transf. 162, 120291. https://doi.org/10.1016/j.ijheatmasstransfer.2020.120291

Reichert, P., Borchardt, D., Henze, M., Rauch, W., Shanahan, P., Somlyódy, L., Vanrolleghem, P., 2001. River Water Quality Model no. 1 (RWQM1): II. Biochemical process equations . Water Sci. Technol. 43, 11–30. https://doi.org/10.2166/wst.2001.0241

Robles, A., Ruano, M. V., Ribes, J., Seco, A., Ferrer, J., 2014a. Global sensitivity analysis of a filtration model for submerged anaerobic membrane bioreactors (AnMBR). Bioresour. Technol. 158, 365–373. https://doi.org/10.1016/j.biortech.2014.02.087

Robles, A., Ruano, M. V., Ribes, J., Seco, A., Ferrer, J., 2014b. Model-based automatic tuning of a filtration control system for submerged anaerobic membrane bioreactors (AnMBR). J. Memb. Sci. 465, 14–26. https://doi.org/10.1016/J.MEMSCI.2014.04.012

Ruano, M. V., Ribes, J., Ferrer, J., Sin, G., 2011. Application of the Morris method for screening the influential parameters of fuzzy controllers applied to wastewater treatment plants. Water Sci. Technol. 63, 2199–2206. https://doi.org/10.2166/wst.2011.442

Ruano, M. V., Ribes, J., Seco, A., Ferrer, J., 2012. An improved sampling strategy based on trajectory design for application of the Morris method to systems with many input factors. Environ. Model. Softw. 37, 103–109. https://doi.org/10.1016/J.ENVSOFT.2012.03.008

Ruiz-Martinez, A., Serralta, J., Pachés, M., Seco, A., Ferrer, J., 2014. Mixed microalgae culture for ammonium removal in the absence of phosphorus: Effect of phosphorus supplementation and process modeling. Process Biochem. 49, 2249–2257. https://doi.org/10.1016/j.procbio.2014.09.002

Ruiz-Martínez, A., Serralta, J., Romero, I., Seco, A., Ferrer, J., 2015. Effect of intracellular P content on phosphate removal in Scenedesmus sp. Experimental study and kinetic expression. Bioresour. Technol. 175, 325–332. https://doi.org/10.1016/j.biortech.2014.10.081

Ruiz, J., Álvarez-Díaz, P.D., Arbib, Z., Garrido-Pérez, C., Barragán, J., Perales, J.A., 2013. Performance of a flat panel reactor in the continuous culture of microalgae in urban wastewater: Prediction from a batch experiment. Bioresour. Technol. 127, 456–463. https://doi.org/10.1016/j.biortech.2012.09.103

Ruiz, J, Arbib, Z., Álvarez-Díaz, P.D., Garrido-Pérez, C., Barragán, J., Perales, J.A., 2013. Photobiotreatment model (PhBT): A kinetic model for microalgae biomass growth and nutrient removal in wastewater. Environ. Technol. (United Kingdom). https://doi.org/10.1080/09593330.2012.724451

Saltelli, A., Tarantola, S., Campolongo, F., Ratto, M., 2004. Sensitivity Analysis in Practice: A Guide to Assessing Scientific Models.

Sánchez-Zurano, A., Rodríguez-miranda, E., Guzmán, J.L., Acién-fernández, F.G., Fernández-sevilla, J.M., Grima, E.M., 2021. Abaco: A new model of microalgae-bacteria consortia for biological treatment of wastewaters. Appl. Sci. 11, 1–24. https://doi.org/10.3390/app11030998

Seco, A., Aparicio, S., González-Camejo, J., Jiménez-Benítez, A., Mateo, O., Mora, J.F., Noriega-Hevia, G., Sanchis-Perucho, P., Serna-García, R., Zamorano-López, N., Giménez, J.B., Ruiz-Martínez, A., Aguado, D., Barat, R., Borrás, L., Bouzas, A., Martí, N., Pachés, M., Ribes, J., Robles, A., Ruano, M. V., Serralta, J., Ferrer, J., 2018. Resource recovery from sulphate-rich sewage through an innovative anaerobic-based water resource recovery facility (WRRF). Water Sci. Technol. 78, 1925–1936. https://doi.org/10.2166/wst.2018.492

Shoener, B.D., Schramm, S.M., Béline, F., Bernard, O., Martínez, C., Plósz, B.G., Snowling, S., Steyer, J.P., Valverde-Pérez, B., Wágner, D., Guest, J.S., 2019. Microalgae and cyanobacteria modeling in water resource recovery facilities: A critical review. Water Res. X. https://doi.org/10.1016/j.wroa.2018.100024

Siegrist, H., Renggli, D., Gujer, W., 1993. Mathematical modelling of anaerobic mesophilic sewage sludge treatment, in: Water Science and Technology. pp. 25–36. https://doi.org/10.2166/wst.1993.0070

Sin, G., Gernaey, K. V., 2009. Improving the Morris method for sensitivity analysis by scaling the elementary effects. Comput. Aided Chem. Eng. 26, 925–930. https://doi.org/10.1016/S1570-7946(09)70154-3

Sin, G., Gernaey, K. V., Neumann, M.B., van Loosdrecht, M.C.M., Gujer, W., 2011. Global sensitivity analysis in wastewater treatment plant model applications: Prioritizing sources of uncertainty. Water Res. 45, 639–651. https://doi.org/10.1016/J.WATRES.2010.08.025

Sin, G., Van Hulle, S.W.H., De Pauw, D.J.W., Van Griensven, A., Vanrolleghem, P.A., 2005. A critical comparison of systematic calibration protocols for activated sludge models: A SWOT analysis. Water Res. 39, 2459–2474. https://doi.org/10.1016/J.WATRES.2005.05.006

Singh, D., Nedbal, L., Ebenhöh, O., 2018. Modelling phosphorus uptake in microalgae. Biochem. Soc. Trans. https://doi.org/10.1042/BST20170262

Solimeno, A., Parker, L., Lundquist, T., García, J., 2017. Integral microalgae-bacteria model (BIO_ALGAE): Application to wastewater high rate algal ponds. Sci. Total Environ. 601–602, 646–657. https://doi.org/10.1016/j.scitotenv.2017.05.215

Solimeno, A., Samsó, R., García, J., 2016. Parameter sensitivity analysis of a mechanistic model to simulate microalgae growth. Algal Res. 15, 217–223. https://doi.org/10.1016/J.ALGAL.2016.02.027

Solimeno, A., Samsó, R., Uggetti, E., Sialve, B., Steyer, J.P., Gabarró, A., García, J., 2015. New mechanistic model to simulate microalgae growth. Algal Res. https://doi.org/10.1016/j.algal.2015.09.008

Steele, J.H., 1965. Notes on some theoretical problems in production ecology. Goldman, C. R. (ed.), Prim. Product. Aquat. Environ. (Mem. Ist. Ital. Idrobiol., 18 Suppl.) 383–398.

Sun, H., Zhu, Y., Yang, J., Wang, X., 2015. Global sensitivity analysis for an integrated model for simulation of nitrogen dynamics under the irrigation with treated wastewater. Environ. Sci. Pollut. Res. 2015 2221 22, 16664–16675. https://doi.org/10.1007/S11356-015-4860-5

Sun, Y., Huang, Y., Liao, Q., Fu, Q., Zhu, X., 2016. Enhancement of microalgae production by embedding hollow light guides to a flat-plate photobioreactor. Bioresour. Technol. 207, 31–38. https://doi.org/10.1016/j.biortech.2016.01.136

Sydney, E.B., Sturm, W., de Carvalho, J.C., Thomaz-Soccol, V., Larroche, C., Pandey, A., Soccol, C.R., 2010. Potential carbon dioxide fixation by industrially important microalgae. Bioresour. Technol. 101, 5892–5896. https://doi.org/10.1016/j.biortech.2010.02.088

Verhulst, P.-F., 1838. Notice sur la loi que la population suit dans son accroissement. Correspondance Mathématique et Physique Publiée par A. Quetelet 10, 113–121.

Viruela, A., Aparicio, S., Robles, Á., Falomir, L.B., Serralta, J., Seco, A., Ferrer, J., 2021. Kinetic modeling of autotrophic microalgae mainline processes for sewage treatment in phosphorus-replete and -deplete culture conditions. Sci. Total Environ. 149165. https://doi.org/10.1016/J.SCITOTENV.2021.149165

Viruela, A., Robles, Á., Durán, F., Ruano, M.V., Barat, R., Ferrer, J., Seco, A., 2018. Performance of an outdoor membrane photobioreactor for resource recovery from anaerobically treated sewage. J. Clean. Prod. 178, 665–674. https://doi.org/10.1016/j.jclepro.2017.12.223

Wágner, D.S., Valverde-Pérez, B., Sæbø, M., Bregua de la Sotilla, M., Van Wagenen, J., Smets, B.F., Plósz, B.G., 2016. Towards a consensus-based biokinetic model for green microalgae – The ASM-A. Water Res. 103, 485–499. https://doi.org/10.1016/j.watres.2016.07.026

Yang, J., Reichert, P., Abbaspour, K.C., Xia, J., Yang, H., 2008. Comparing uncertainty analysis techniques for a SWAT application to the Chaohe Basin in China. J. Hydrol. 358, 1–23. https://doi.org/10.1016/j.jhydrol.2008.05.012

Zambrano, J., Krustok, I., Nehrenheim, E., Carlsson, B., 2016. A simple model for algae-bacteria interaction in photo-bioreactors. Algal Res. 19, 155–161. https://doi.org/10.1016/j.algal.2016.07.022

SUPPLEMENTARY DATA FOR CHAPTER IX

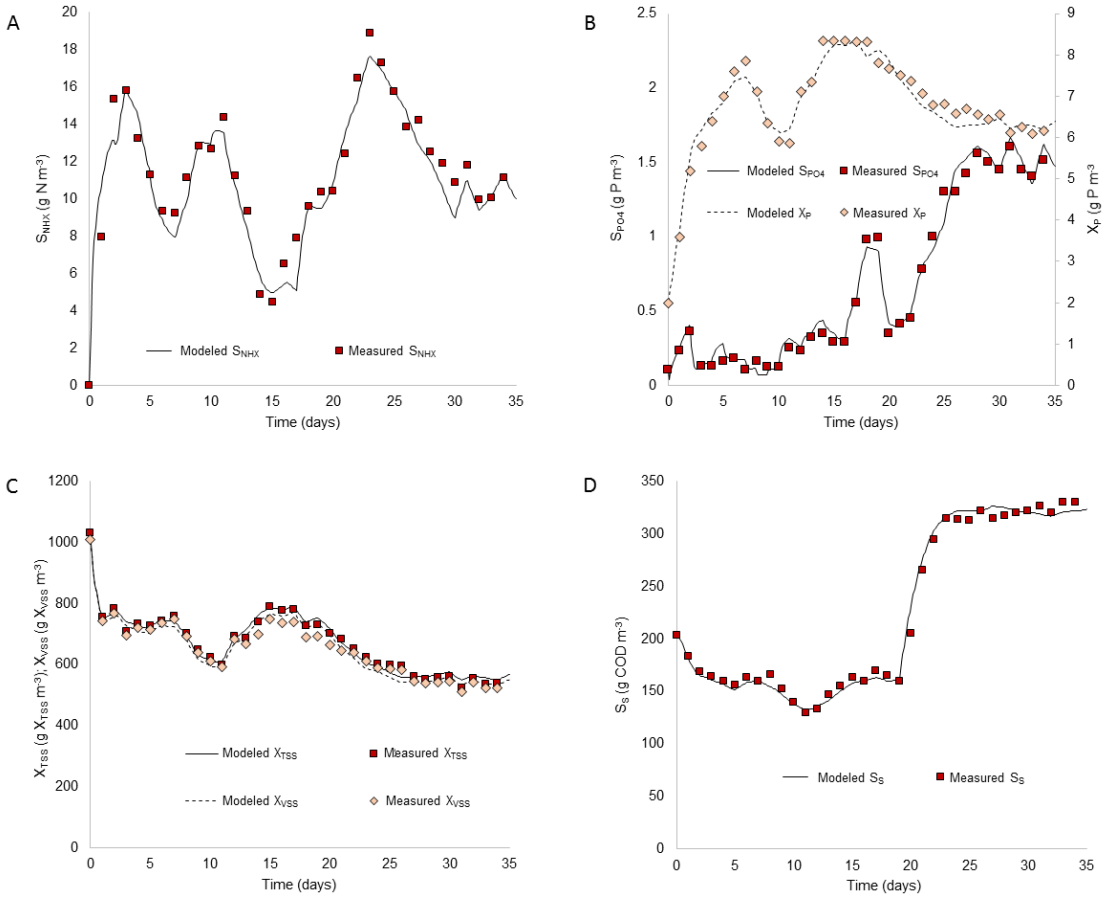

Figure IX. S1. Online simulation of: (A) SNHX concentration (g N m-3) in the PBR culture medium; (B) SPO4 concentration (g P m-3) and XP [g P m-3] in the PBR culture medium; (C) XTSS (g TSS m-3) and XVSS (g VSS m-3) and (D) SS (g COD m-3) concentrations in the PBR culture medium. Experimental and modeled data are represented by markers and lines, respectively.

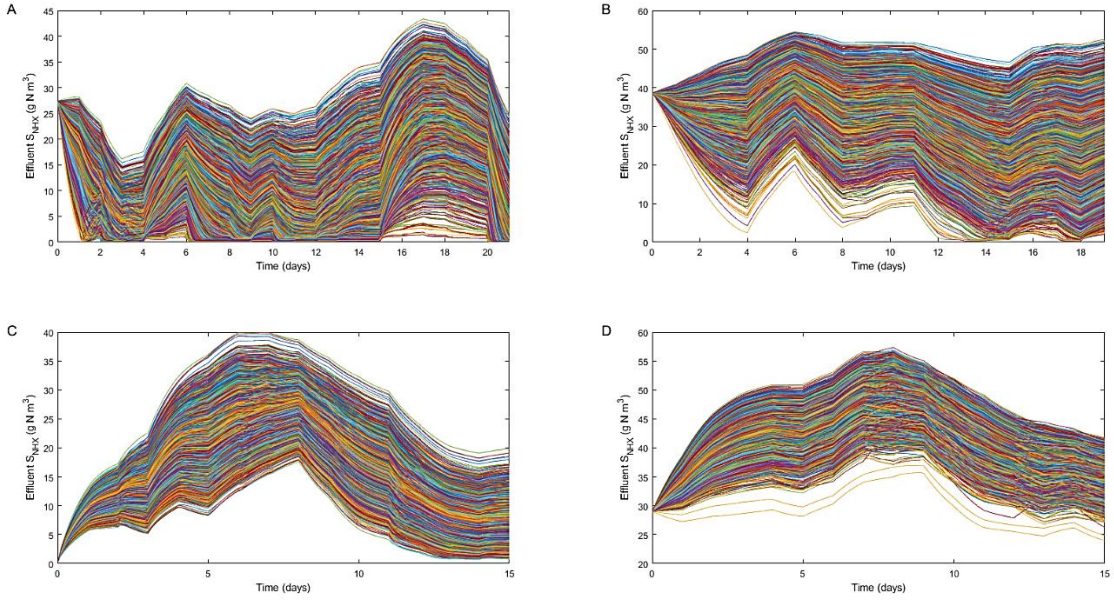

Figure IX. S2. Computed time series of S_{NHX} concentration in Membrane Photobioreactor (MPBR) pilot plant effluent obtained from the Monte Carlo simulation (3300 runs) for periods: (A) Period 1, (B) Period 2, (C) Period 3 and (D) Period 4.

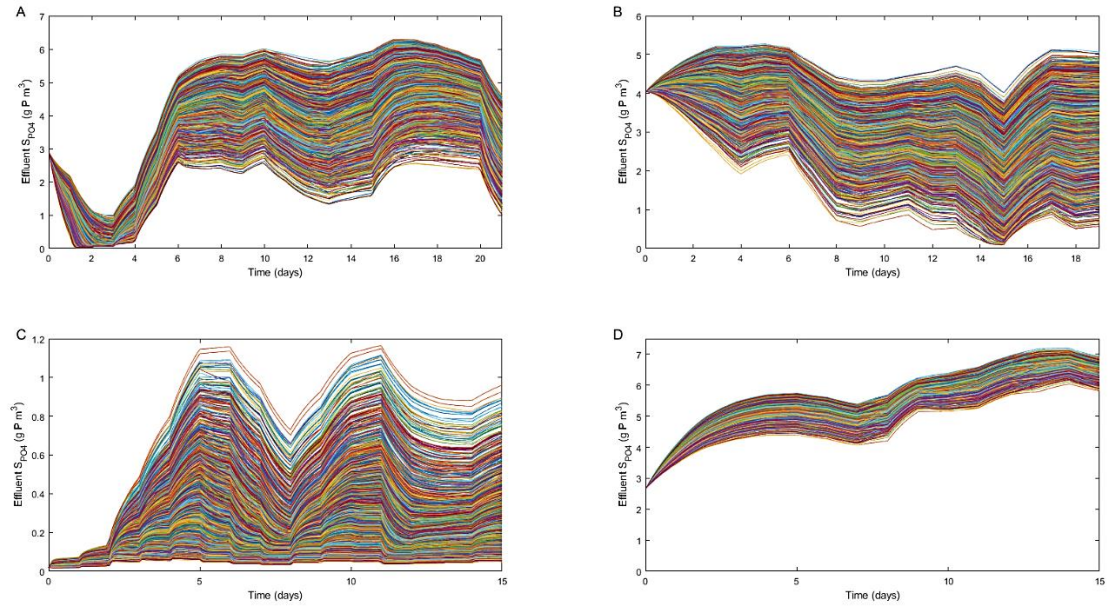

Figure IX. S3. Computed time series of S_{PO4} concentration **in** MPBR pilot plant effluent obtained from the Monte Carlo simulation (3300 runs) for periods: (A) Period 1, (B) Period 2, (C) Period 3 and (D) Period 4.

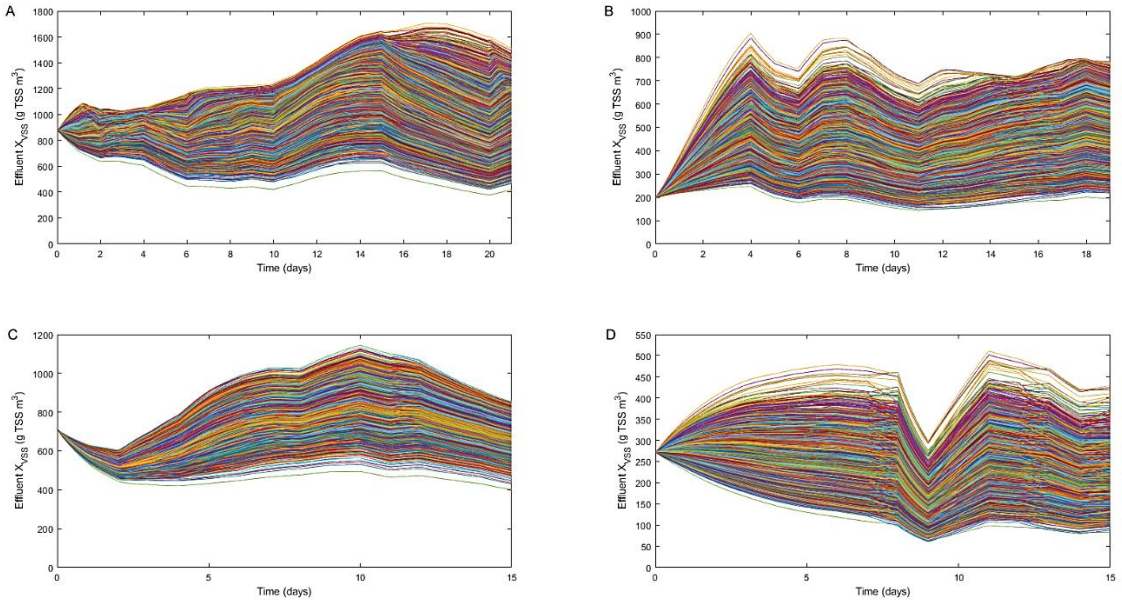

Figure IX. S3. Computed time series of X_{VSS} concentration in MPBR pilot plant effluent obtained from the Monte Carlo simulation (3300 runs) for periods: (A) Period 1, (B) Period 2, (C) Period 3 and (D) Period 4.

CHAPTER X

10. Integrated microalgae-bacteria modelling: application to an outdoor membrane photobioreactor (MPBR)

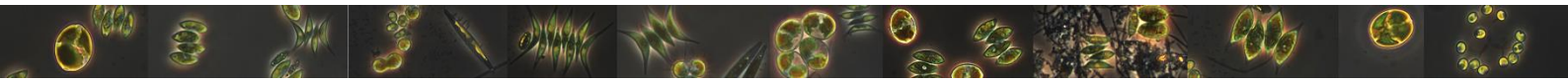

10. Integrated microalgae-bacteria modelling: application to an outdoor membrane photobioreactor (MPBR)

ABSTRACT

A mechanistic model describing the key interactions occurring in microalgae-bacteria consortia systems was developed and validated. The proposed model includes the most relevant features of microalgae, such as light dependence, endogenous respiration, growth and nutrient consumption for different nutrient sources. The model is coupled to the plant-wide model BNRM2, including heterotrophic and nitrifying bacteria, and chemical precipitation processes, among others. A major novelty of the model is microalgae growth inhibition by nitrite. Validation was conducted using experimental data from a pilot-scale membrane photobioreactor (MPBR) fed with permeate from an anaerobic membrane bioreactor (AnMBR). Three experimental periods dealing with different interactions between nitrifying bacteria and microalgae were validated. The model was able to accurately represent the dynamics occurring in the MPBR, predicting the relative abundance of microalgae and bacteria over time. Specifically, more than 500 pairs of experimental and modelled data were evaluated, giving an average R2 coefficient of 0.9902. The validated model was also used to evaluate different offline control strategies for enhancing process performance. Partial-nitrification resulting in NO_2-N accumulation (i.e. microalgae growth inhibition) could be avoided by increasing biomass retention time from 2.0 to 4.5 days. Microalgae biomass growth rate could be also enhanced by punctually increasing the dilution rate, allowing to outcompete nitrifying bacteria.

Keywords

Microalgae, Bacteria, Wastewater treatment, Nitrogen, Mathematical model

Authors

Stéphanie Aparicio, Ángel Robles, Luis Borrás Falomir, José Ferrer and Aurora Seco.

10.1. INTRODUCTION

Microalgae-based technology for wastewater treatment was first studied in the 60 s (Oswald et al., 1957) and more recently revisited in view of a more sustainable approach to bioremediation (Chapter 5, Acién et al., 2018; Van Den Hende et al., 2016). However, until now, this technology has not been fully exploited at industrial scale. Research is usually focused to accomplish requirements of industry, reducing the hydraulic retention time (HRT) and meeting with European Union (EU) regulation on discharged water quality (Directive 98/15/CEE). The interest on microalgae-based technologies is also due to potential total cost savings compared to conventional wastewater treatment plants (WWTP), including savings in energy requirements related to external aeration due to photosynthetic oxygenation (Acién et al., 2016; Karya et al., 2013). Thus, there is a change for the wastewater industry for shifting from “standard WWTP” to a sustainable “water resource recovery facilities (WRRFs)” (Seco et al., 2018), which are also able to remove wastewater pollutant and recover nutrient from microalgae biomass.

Microalgae-based wastewater treatment processes are performed by consortia of different microalgae and bacteria communities (Chapter 8, Acién et al., 2016; Sánchez-Zurano et al., 2020). Ecological interactions in the consortia are highly dependent on operating and environmental conditions (abiotic conditions) (Chapter 5, (García et al., 2018). Optimizing design of microalgae-bacteria consortia-based wastewater treatment systems requires the development of mathematical models, which integrate biochemistry along with physical-chemical processes.

Different plant-wide models have been developed for conventional wastewater treatment systems, such as Biological Nutrient Removal Model No. 2 (BNRM2) (Barat et al., 2013). Nonetheless, a gap in integrating microalgae metabolism in plant-wide models exists still. Oxygen and pH fluctuation resulting from photosynthesis activity can affect bacteria metabolism, thus the performance of bacteria under these specific conditions should also be reanalyzed. Integrated mechanistic models for microalgae-based wastewater

treatment systems are necessary to better understand interactions between microalgae and bacteria (Chapters 5 and 8) and control the performance of the system. An accurate model represents a powerful tool to overcome the bottlenecks of this promising technology. Few models have already been developed for simulating microalgae-bacteria interactions. The River Water Quality Model 1 (RWQM1) of the International Water Association (Reichert et al., 2001) was developed for modelling wastewater discharge in river ecosystems. Similar models, such as BIO_ALGAE 2 (Solimeno et al., 2019), ABACO (Sánchez-Zurano et al., 2021) and ALBA (Casagli et al., 2021) have been developed with the aim of becoming the fundamental basis for modeling approach that integrates the biological, chemical, and physical processes occurring in microalgae-bacteria consortia. However, previous models did not include the luxury uptake and the use of intracellular polyphosphate as phosphorus source (Ruiz et al., 2013; Viruela et al., 2021). In addition, phosphorus precipitation due to alkaline pH achieved by photosynthesis (Acién et al., 2018; Barat et al., 2011; Xu et al., 2021) was neither included, although it can be the main phosphorus removal mechanism (see Chapter 5).

The aim of this Chapter is to complete the microalgae model previously developed by the authors (Viruela et al., 2021) with biological, chemical and physical processes related to microalgae and bacteria in wastewater treatment systems. The model was mainly built by coupling the microalgal model of the authors (Viruela et al., 2021) with the model BNRM2 (Barat et al., 2013). Combination of both models has been used as the basis to represent microalgae-bacteria interactions. The most relevant feature of the model proposed is the inclusion of phosphorus precipitation, which can affect microalgae growth due to the reduction in the bioavailable phosphorus concentration. In addition, other relevant feature is nitrite (NO_2-N) inhibition effect on photosynthesis, described in Chapter 5. The key objective of the work shown in this chapter was to validate the model under different operating and environmental conditions with experimental data from an outdoor pilot plant.

10.2. MODEL DESCRIPTION

10.2.1. Conceptual model

A general schematic representation of the conceptual model is shown in Figure X. 1. Photosynthesis is activated in lighting conditions. Microalgae grow with nitrogen (N) and phosphorus (P) present in the culture media (i.e. wastewater), while they fix inorganic carbon and supply oxygen required by heterotrophic bacteria to oxidize biodegradable organic matter. From organic matter oxidation, dissolved inorganic carbon (DIC) is produced and it is consumed by microalgae and nitrifying bacteria. Nitrification is developed in a two-step process: first, ammonium is oxidized to nitrite by ammonium-oxidizing bacteria (AOB); then, nitrite is oxidized to nitrate by nitrite-oxidizing bacteria (NOB). Micronutrients are not considered limiting factors in the proposed model, as they are considered to be present in wastewater in a wide extend. Microalgae can grow with both ammonium-ammonia (they are considered to be in chemical equilibrium) and nitrate, although ammonium-ammonia is considered the preferred form of nitrogen source since its assimilation and incorporation is energetically more efficient (Barbera et al., 2018; Eustance et al., 2013).

Because of microalgal photosynthesis, pH increases and bicarbonate-carbonate equilibrium shifts towards the formation of carbonate, boosting free ammonia nitrogen (FAN) stripping and phosphorus precipitation. In terms of phosphorus assimilation, the luxury uptake concept was applied. Microalgae can uptake phosphorus above their metabolic needs and store it as acid-insoluble polyphosphate granules, which can be used for cell growth when external phosphorus concentration becomes limiting (Powell et al., 2009; Ruiz-Martinez et al., 2014; Ruiz-Martínez et al., 2015).

In darkness, both microalgae and heterotrophic bacteria have a net DIC release through respiration and organic matter oxidation, respectively. With this DIC release, hydrogen ion concentration increases and pH decreases, and the bicarbonate-carbonate equilibrium shifts and carbonate is turned into bicarbonate, which can be used again as

DIC in lighting conditions. Microalgae respiration along with heterotrophic and nitrifying bacteria growth reduce oxygen concentration, and aerobic conditions can shift to anoxic conditions or, in some cases, to anaerobic conditions (Chapter 5). Nitrate can be used as electron acceptor for denitrifying bacteria in anoxic conditions. Denitrification reduce nitrate to nitrogen gas, releasing it into the atmosphere. Denitrifying bacteria are considered the same heterotrophic bacteria that used oxygen as electron acceptor in aerobic conditions, but under anoxic conditions can facultatively use nitrate instead of oxygen. Respiration and cell lysis release nitrogen, phosphorus and organic matter compounds, which are hydrolyzed by heterotrophic bacteria. Microalgae and bacteria processes are influenced by temperature, which also affects pH, gas solubility and chemical equilibrium. Excess of oxygen, DIC and FAN are transferred from the liquid phase to the gaseous phase, and vice versa.

The model BNRM2, besides the heterotrophic and nitrifying bacteria, also includes polyphosphate-accumulating organisms (PAOs), methanogenic acetoclastic organisms and methanogenic hydrogenotrophic organisms. The environmental conditions, i.e. aerobic, anoxic or anaerobic, will determine the bacterial communities that can proliferate. In this chapter, microalgae-bacteria model description did not include PAOs, methanogenic acetoclastic organisms and methanogenic hydrogenotrophic organisms, since they were not detected in the microbial structure (Chapter 8). However, it should be highlighted that microalgae can lead to aerobic and anaerobic conditions cycling through the light-dark cycle and could potentially lead to phosphate accumulation by PAOs (Bankston et al., 2020). The proposed model was mainly built by coupling the microalgae model developed by Viruela et al. (2021) with an adaptation of BNRM2 applied to heterotrophic bacteria and nitrifiers, and of chemical precipitation.

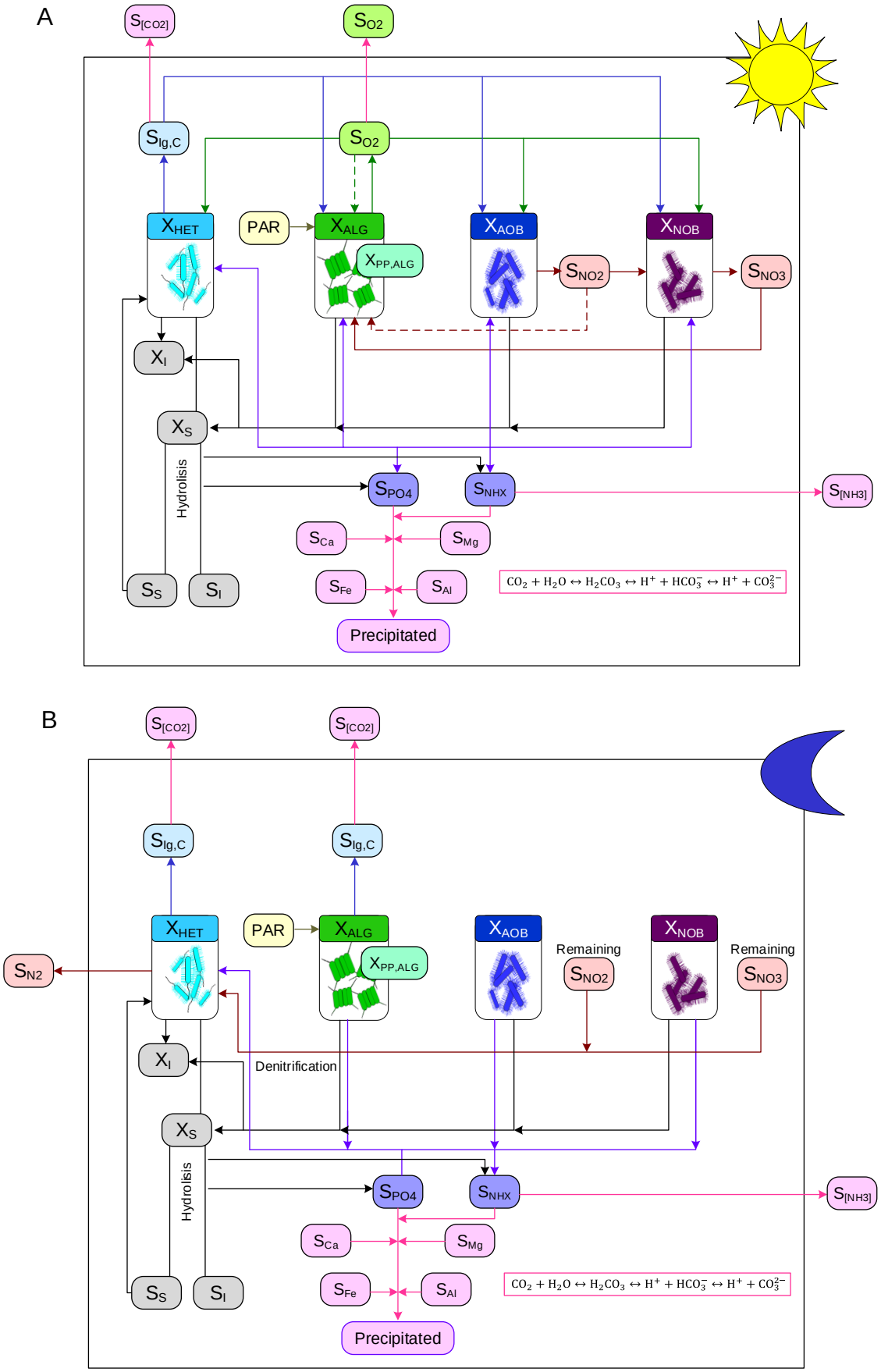

Figure X. 1. Simplified schematic representation of the conceptual model showing the main processes in light (A) and dark conditions (B). The nomenclature of the dissolved and particulate components is described in 10.2.3 as are the model processes. The dashed line indicated inhibition process.

10.2.2. Model assumptions

Some simplification were adopted to reduce the complexity of this mechanistic model. Readily biodegradable soluble organic matter (S_S) was consumed only by heterotrophic bacteria, although microalgae can growth mixotrophically or heterotrophycally (Pang et al., 2019). However, heterotrophic and mixotrophic metabolism are restricted to few microalgae and, therefore, the most common pathway is the photoautotrophic metabolism (Perez-Garcia et al., 2011; Shandilya and Pattarkine, 2019). Hydrolysis processes are performed only by heterotrophic bacteria. Micronutrients in wastewater were considered not limiting for biomass growth.

10.2.3. Model components and connection between simulated outputs and experimental data

Nomenclature used for model components distinguishes between soluble "S_j" and particulates "X_j". Particulate components are electrically neutral, i.e. no ionic charges, while soluble components can carry ionic charge. The model considers 15 soluble and 17 suspended components.

10.2.3.1. Soluble components

S_{O2}: (g $O_2 \cdot m^{-3}$): dissolved oxygen. Dissolved oxygen concentration in the liquid phase produced by microalgae growth through photosynthesis. It is consumed by aerobic bacteria growth and endogenous respiration. Dissolved oxygen can also be transferred to/from gas phase.

S_{NHx}: (g $N \cdot m^{-3}$): ammonium plus free ammonia nitrogen (S_{NH4} + S_{NH3}). Nitrogen present in liquid phase as ammonium and FAN. S_{NHX} is produced by hydrolysis, respiration and microorganism lysis. It is consumed as essential nutrient by microorganism and during the first step of nitrification by AOB. FAN stripping is also considered.

S_{NO2}: (g $N \cdot m^{-3}$): nitrite nitrogen. It is produced in the first step of nitrification and consumed by NOB, heterotrophic bacteria during denitrification and by microalgae as nitrogen source.

S_{NO3}: (g $N \cdot m^{-3}$): nitrate nitrogen. It is produced in the second step of nitrification and consumed by heterotrophic bacteria (X_{HET}) during denitrification and by microalgae as nitrogen source.

S_{PO4}: (g $P \cdot m^{-3}$): total soluble inorganic phosphorous. Phosphorous present in liquid phase. To balance the electrical charges, S_{PO4} is assumed to consist of $H_2PO_4^-$, regardless of pH. S_{PO4} concentration increases due to hydrolysis, respiration and lysis of both biomass and the intracellular phosphorous component (polyphosphate). It is consumed by biomass growth and phosphorous storage processes in microalgae biomass. Precipitation is also involved in the reduction of inorganic phosphorous bioavailability.

$S_{Ig,C}$: (kmol $C \cdot m^{-3}$): total inorganic carbon consists of CO_2, HCO_3^- and CO_3^{2-}. It is produced by heterotrophic growth and respiration along with lysis of all microorganisms. $S_{Ig,C}$ concentration decreases as a result of the combination of microalgae and nitrifying bacteria growth. It can also be transferred to/from gas phase. For all stoichiometric computations it is assumed that $S_{Ig,C}$ is CO_2.

S_H: (kmol $H \cdot m^{-3}$): proton representing the analytical summary of all the species in which the H^+ component participates (Equation X. 1). Instead of using the charge balance, the BNRM2 considers a mass-balance for proton component as proposed in the software MINTEQA2 Conversion factors i_{H_i} are defined to apply the continuity equation. It should be highlighted that the consideration of the acid-base and the ion-paring interactions as equilibrium governed processes hugely simplifies the numerical solution and the model calibration due to the absence of kinetic parameters to solve the aqueous equilibrium.

$$S_H = [H^+] - [HCO_3^-] + 2[H_2CO_3] + [HPO_4^{2-}] + 2[H_2PO_4^-] + 3[H_3PO_4] - [NH_3] - [OH^-] \quad \text{Equation X. 1}$$

S_{Mg} (g $Mg \cdot m^{-3}$): total soluble inorganic magnesium. Magnesium concentration present in liquid phase, which is consumed by bacteria growth, storage of intracellular phosphorous compound and chemical precipitation. It is released to culture medium by hydrolysis, respiration and both intracellular phosphorous and bacteria lysis.

S_K (g $K \cdot m^{-3}$): total soluble inorganic potassium. Potassium concentration present in liquid phase, which is consumed by bacteria growth storage of intracellular phosphorous compound and chemical precipitation. It is released to culture medium by hydrolysis, respiration and both intracellular phosphorous and bacteria lysis.

S_{Ca} (g $Ca \cdot m^{-3}$): Total soluble inorganic calcium. Calcium concentration present in liquid phase, which is consumed as a nutrient by bacteria and it is released in hydrolysis, respiration and bacteria lysis. Calcium concentration also depend on precipitation and dissolution processes.

S_{Fe} (g $Fe \cdot m^{-3}$): Total soluble inorganic iron. Iron concentration present in liquid phase, which is consumed as a nutrient by bacteria and it, is released in hydrolysis, respiration and bacteria lysis. Iron concentration also depend on precipitation and dissolution processes.

S_{Al} (g $Al \cdot m^{-3}$): Total soluble inorganic aluminum. Aluminum concentration present in liquid phase. Its concentration depends on bacteria growth and lysis and respiration, along with precipitation and dissolution processes.

S_S (g $COD \cdot m^{-3}$): readily biodegradable soluble organic matter. Fraction of the biodegradable soluble organic matter in liquid phase directly available for heterotrophic bacteria. It is produced during the hydrolysis of biodegradable particulate organic matter.

S_I (g $COD \cdot m^{-3}$): inert soluble organic matter. Fraction of the inert soluble organic matter in liquid phase. It is produced during the hydrolysis of biodegradable particulate organic matter.

S_{N2} (g N·m^{-3}): dinitrogen. It is produced in the denitrification process.

10.2.3.2. Particulate components

X_{ALG} (g COD·m^{-3}): microalgae biomass. Concentration of microalgae in liquid phase that increases with growing processes and is reduced by respiration and lysis. The common composition for microalgae cell $C_{106}H_{181}O_{45}N_{17}P$ is assumed for stoichiometric considerations (Oswald, 1988).

X_{HET} (g COD·m^{-3}): Heterotrophic bacteria. They can grow aerobically and anoxically and decrease by lysis. These bacteria are responsible for the hydrolysis processes.

X_{AOB} (g COD·m^{-3}): Ammonium-oxidizing bacteria. Autotrophic bacteria responsible for the first step of nitrification. These bacteria growth in aerobic conditions and decrease by lysis.

X_{NOB} (g COD·m^{-3}): Nitrite-oxidizing bacteria. Autotrophic bacteria responsible for the second step of nitrification. These bacteria growth in aerobic conditions and decrease by lysis.

X_S (g COD·m^{-3}): Slowly biodegradable particulate organic matter. Fraction of organic matter that can be hydrolyzed to S_S and S_I by heterotrophic bacteria. It is increased by lysis of biomass.

X_I (g COD·m^{-3}): inert particulate organic matter. It increases by lysis of microorganisms.

$X_{PP,ALG}$ (g P·m^{-3}): polyphosphates stored by microalgae. Concentration of inorganic intracellular polyphosphates but not included in the microalgae mass. For stoichiometric considerations, $X_{PP,ALG}$ is assumed to have the composition of $(K_{0.34}Mg_{0.33}PO_3)_n$. Polyphosphate is consumed by microalgae and is also reduced as a result of $X_{PP,ALG}$ lysis. Intracellular polyphosphates increase with storage of polyphosphates process.

X_{ACP} (kmol ACP·m^{-3}): amorphous calcium phosphate. It is assumed to have the composition of $Ca_3(PO_4)_2 \cdot xH_2O$. Its concentration depends on precipitation and dissolution process.

X_{HAP} (kmol HAP·m^{-3}): hydroxyapatite. It is assumed to have the composition of $Ca_5(PO_4)_3 \cdot OH$. Its concentration depends on precipitation and dissolution process.

X_{MAP} (kmol MAP·m^{-3}): struvite. It is assumed to have the composition of $MgNH_4PO_4 \cdot 6H_2O$. Its concentration depends on precipitation and dissolution process.

X_{NEW} (kmol New·m^{-3}): Newberite. It is assumed to have the composition of $MgHPO_4 \cdot 3H_2O$. Its concentration depends on precipitation and dissolution process.

X_{VIV} (kmol Viv·m^{-3}): Vivianite. It is assumed to have the composition of $Fe_3(PO_4)_2 \cdot 8H_2O$. Its concentration depends on precipitation and dissolution process.

X_{STR} (kmol Str·m^{-3}): Strengite. It is assumed to have the composition of $FePO_4$. Its concentration depends on precipitation and dissolution process.

X_{VAR} (kmol Var·m^{-3}): Variscite. It is assumed to have the composition of $AlPO_4$. Its concentration depends on precipitation and dissolution process.

X_{CAL} (kmol Cal·m^{-3}): Calcium carbonate. It is assumed to have the composition of $CaCO_3$. Its concentration depends on precipitation and dissolution process.

X_{TSS} (g TSS·m^{-3}): total suspended solids. Experimental data and modeled results were compared by total suspended solids. It was considered as the sum of all particulate compounds (microalgae and bacteria biomass, particulate organic matter, polyphosphate and precipitates). Since phosphorous removal and precipitation process introduce mineral fraction into the reactor, prediction of X_{TSS} is important.

X_{NVSS} (g TSS·m^{-3}): influent non-volatile suspended solids. This component does not include non-volatile suspended solids related to $X_{PP,ALG}$ and precipitated.

10.2.4. Connection between simulated outputs and experimental data

Experimental data of volatile suspended solids (VSS) were compared with simulate variables computed (Equation X. 2). Equation of total suspended solids was reported in Supplementary Data (Equation X. S 1).

$$X_{VSS} = X_{ALG} \cdot i_{TSS,ALG} + X_{HET} \cdot i_{TSS,B} + X_{AOB} \cdot i_{TSS,B} + X_{NOB} \cdot i_{TSS,B} + X_I \cdot i_{TSS,XI} + X_S \cdot i_{TSS,XS} \quad \text{Equation X. 2}$$

where X_{VSS} is the volatile suspended solids concentration (g TSS·m^{-3}), X_{ALG} is the microalgae biomass (g COD·m^{-3}), X_{HET} is the heterotrophic bacteria biomass (g COD·m^{-3}), X_{AOB} is the AOB biomass (g COD·m^{-3}), X_{NOB} is the NOB biomass (g COD·m^{-3}), X_I is the inert particulate organic matter (g COD·m^{-3}), X_S is the slowly biodegradable particulate organic matter (g COD·m^{-3}), and $i_{TSS,ALG}$ (g TSS·g COD^{-1}), $i_{TSS,B}$, $i_{TSS,XI}$ and $i_{TSS,XS}$ (g TSS·g COD^{-1}) are TSS contained in bacterial biomass (nitrifiers and heterotrophs) X_I and X_S, respectively. Conversion factors are listed in Supplementary Data of this Chapter (Table X. S 1).

Polyphosphate can be quantified by different analytical methods, but these are time consuming and require many reagents. Total suspended phosphorus was proposed as an indirect measure of X_{PP-ALG}. The comparison and validation of the experimental and simulated results were performed from the total suspended phosphorus concentrations: X_P (g P·m^{-3}). It was not included in the stoichiometric matrix, but was obtained from the sum of polyphosphate, phosphorus content in suspended fraction and precipitates (see Equation X. S 2. in Supplementary Data).

10.2.5. Processes and Stoichiometry

In this model, 4 groups of microorganisms are assumed to represent the wide variety of indigenous wastewater organisms. It is assumed that microalgae, heterotrophic bacteria, AOB and NOB can simulate biological processes described in Chapter 5. The analysis of ecological structure (Chapter 7) showed that indigenous bacteria, such as PAO, were not abundant and did not play a key role in the evaluated microalgae-bacteria consortia.

The proposed model considers 19 biological and 19 physical kinetically-governed processes (Tables X. 1, 2, 3 and 4). Conversion factors to be applied in the continuity equations for COD N, P, Mg, K, Ca, mass, carbon and proton of the model are described in Table X. and 6. The production rate [M L^{-3} T^{-1}] of each component (r_i) in all processes was computed from Equation X. 3:

$$r_i = \sum v_{ji} \cdot \rho_j$$ Equation X. 3

where i is the component considered and j is the transformation process; v_{ji} is the stoichiometric coefficient and ρ_j is the process rate for each process j.

10.2.5.1. Microalgae processes

Photosynthesis inhibition by nitrite was assessed and calibrated in Chapter 5. This effect was considered in the 4 microalgae growth kinetics proposed.

ρ_1: Microalgae phototrophic growth using S_{NHX} and S_{PO4} as nitrogen and phosphorus sources, respectively. $S_{Ig,C}$ is consumed and S_{O2} is produced.

ρ_2: Microalgae phototrophic growth using S_{NHX} and $X_{PP,ALG}$ as nitrogen and phosphorus sources, respectively. Intracellular phosphorus is used as phosphorus source when extracellular phosphorus concentration is limiting. To represent this phenomenon a non-competitive inhibition function for S_{PO4} is considered. $S_{Ig,C}$ is consumed and S_{O2} is produced.

ρ_3: Microalgae phototrophic growth using S_{NO3} and S_{PO4} as nitrogen and phosphorus sources, respectively. $S_{Ig,C}$ is consumed and S_{O2} is produced. Nitrate assimilation is energetically less efficient and ammonium/ammonia is generally preferred by microalgae. To represent this phenomenon a non-competitive inhibition function for S_{NHX} is introduced when nitrate is the nitrogen source for microalgae growth. Moreover, González-Camejo et al. (2019a) and Shoener et al. (2019) observed that nitrate uptake was lower than ammonium, since it has to be intracellularly reduced to ammonium before

being assimilated and incorporated into the cellular matter. The rate for microalgae growth with nitrate is introduced by the factor η_{NO3}.

ρ_4: Microalgae phototrophic growth using S_{NO3} and $X_{PP,ALG}$ as nitrogen and phosphorus sources, respectively. Intracellular phosphorus is used as phosphorus source when extracellular phosphorus concentration is limiting. To represent this phenomenon a non-competitive inhibition function for S_{PO4} is considered. Ratio of microalgae able to grow with nitrate was introduce by η_{NO3}. $S_{lg,C}$ is used and S_{O2} y produced.

ρ_5: Intracellular phosphorus storage. Polyphosphate ($X_{PP,ALG}$) is storaged by microalgae, which is used for microalgae growth under deplete phosphorus conditions.

ρ_6: Microalgae endogenous respiration. This process accounts for biomass loss due to microalgae maintenance, with S_{O2} consumption and production of $S_{lg,C}$. In the proposed model, respiration and lysis processes are distinguished for microalgae, assuming that S_{O2} consumption occurs only during respiration.

ρ_7: Microalgae lysis. Nutrient and organic matter are released to the external environment. In this process, intracellular polyphosphates are dissolved forming soluble phosphates. The proposed model assumes that lysis of microalgae and polyphosphates occurs at the same rate, $b_{ALG,2}$.

ρ_8: $X_{PP,ALG}$ lysis. The storage of $X_{PP,ALG}$ is considered separately from X_{ALG} growth, thus this component should therefore be subject to a separate decay process. It is assumed that composition of microalgae does not change due to microalgae decay, thus the rate constants for X_{ALG} and $X_{PP,ALG}$ lysis are equal.

Table X. 1. Stoichiometric matrix soluble and particulate components-processes of microalgae (Viruela et al., 2021).

Components → i Processes ↓ j	S_{O2} g O_2 m^{-3}	S_{NHx} g N m^{-3}	S_{NO3} g N m^{-3}	S_{PO4} g P m^{-3}	S_H mol H m^{-3}	S_{Mg} g Mg m^{-3}	S_K g K m^{-3}	$S_{Ig,C}$ mol C m^{-3}	X_I g COD m^{-3}	X_S g COD m^{-3}	X_{ALG} g COD m^{-3}	$X_{ALG,PP}$ g P m^{-3}	X_{TSS} g TSS m^{-3}
ρ_1	1	$-i_{N,ALG}$		$-i_{P,ALG}$	$v_{5,1}$			$-i_{C,ALG}$			1		$i_{TSS,ALG}$
ρ_2	1	$-i_{N,ALG}$			$v_{5,2}$			$-i_{C,ALG}$			1	$-i_{P,ALG}$	$v_{13,2}$
ρ_3	1		$-i_{N,ALG}$	$-i_{P,ALG}$	$v_{5,3}$			$-i_{C,ALG}$			1		$i_{TSS,ALG}$
ρ_4	1		$-i_{N,ALG}$		$v_{5,4}$			$-i_{C,ALG}$			1	$-i_{P,ALG}$	$v_{13,4}$
ρ_5				-1	$v_{5,5}$	$-i_{Mg,XPPALG}$	$-i_{K,XPPALG}$					1	3.23
ρ_6	-1	$i_{N,ALG}$		$i_{P,ALG}$	$v_{5,6}$			$i_{C,ALG}$			-1		$i_{TSS,ALG}$
ρ_7		$v_{2,7}$		$v_{4,7}$	$v_{5,7}$			$v_{8,7}$	f_{XI}	$1-f_{XI}$	-1		$v_{13,7}$
ρ_8				1	$v_{5,8}$	$i_{Mg,XPPALG}$	$i_{K,XPPALG}$					-1	-3.23

10.2.5.2. Heterotrophic bacteria processes

ρ_9: Aerobic hydrolysis of X_S. This process is performed by heterotrophic bacteria under aerobic conditions. X_S is hydrolyzed to S_S and S_I.

ρ_{10}: Anoxic hydrolysis of X_S. This process is performed by heterotrophic bacteria under anoxic conditions. X_S is hydrolyzed to S_S and S_I. This process is typically slower than aerobic hydrolysis.

ρ_{11}: Anaerobic hydrolysis of X_S. This process is performed by heterotrophic bacteria under anaerobic conditions. X_S is hydrolyzed to S_S and S_I. This process is typically slower than aerobic hydrolysis.

ρ_{12}: Aerobic growth of heterotrophic bacteria over S_S and S_{O2}. In aerobic conditions, heterotrophic bacteria oxidize S_S for growing, consuming S_{NHX} and S_{PO4}.

ρ_{13}: Anoxic growth of heterotrophic bacteria over S_S and S_{NO3}. The S_{NO3} is the electron acceptor rather than oxygen. The stoichiometry for S_{NO3} is computed based on the assumption that S_{NO3} is reduced to nitrogen gas S_{N2} (denitrification). Denitrification is assumed to be inhibited by S_{O2} (non-competitive inhibitions function) and the ratio of heterotrophic bacteria can growth with nitrate was introduce by $\eta_{\mu H,Ax3}$

ρ_{14}: Anoxic growth of heterotrophic bacteria over S_S and S_{NO2} (same assumption as denitrification process over S_{NO3}, using $\eta_{\mu H,Ax2}$ as reduction factor).

ρ_{15}: Lysis of heterotrophic bacteria is modelled similarly to microalgae lysis.

Table X. 2. Stoichiometric matrix soluble and particulate components-processes of heterotrophic bacteria (Barat et al., 2012).

Components → i Processes ↓ j	S_{O2} g O_2 m^{-3}	S_S g COD m^{-3}	S_{NHx} g N m^{-3}	S_{NO2} g N m^{-3}	S_{NO3} g N m^{-3}	S_{N2} g N m^{-3}	S_{PO4} g P m^{-3}	S_I g COD m^{-3}	S_H mol H m^{-3}
ρ_9		$1-f_{SI}$	$v_{1,9}$				$v_{2,9}$	f_{SI}	$v_{3,9}$
ρ_{10}		$1-f_{SI}$	$v_{1,10}$				$v_{2,10}$	f_{SI}	$v_{3,10}$
ρ_{11}		$1-f_{SI}$	$v_{1,11}$				$v_{2,11}$	f_{SI}	$v_{3,11}$
ρ_{12}	$-\frac{1-Y_H}{Y_H}$	$-\frac{1}{Y_H}$	$v_{1,12}$				$v_{2,12}$		$v_{3,12}$
ρ_{13}		$-\frac{1}{Y_{H,Ax3}}$	$v_{1,13}$		$\frac{1-Y_{H,Ax3}}{1.14\,Y_{H,Ax3}}$	$-\frac{1-Y_{H,Ax3}}{1.14\,Y_{H,Ax3}}$	$v_{2,13}$		$v_{3,13}$
ρ_{14}		$-\frac{1}{Y_{H,Ax2}}$	$v_{1,14}$	$-\frac{1-Y_{H,Ax2}}{1.71\,Y_{H,Ax2}}$		$\frac{1-Y_{H,Ax2}}{1.71\,Y_{H,Ax2}}$	$v_{2,14}$		$v_{3,14}$
ρ_{15}			$v_{1,18}$				$v_{2,18}$		$v_{3,18}$

Table X. 2. Continued.

Components → i Processes ↓ j	S_{Mg} g Mg m^{-3}	S_K g K m^{-3}	S_{Ca} g Ca m^{-3}	S_{Fe} g Fe m^{-3}	$S_{Ig,C}$ mol C m^{-3}	X_I g COD m^{-3}	X_S g COD m^{-3}	X_H mol COD m^{-3}	X_{TSS} g TSS m^{-3}
ρ_9	$v_{4,9}$	$v_{5,9}$	$v_{6,9}$	$v_{7,9}$	$v_{8,9}$		-1		$-i_{TSS,XS}$
ρ_{10}	$v_{4,10}$	$v_{5,10}$	$v_{6,10}$	$v_{7,10}$	$v_{8,10}$		-1		$-i_{TSS,XS}$
ρ_{11}	$v_{4,11}$	$v_{5,11}$	$v_{6,11}$	$v_{7,11}$	$v_{8,11}$		-1		$-i_{TSS,XS}$
ρ_{12}	$v_{4,12}$	$v_{5,12}$	$v_{6,12}$	$v_{7,12}$	$v_{8,12}$			1	$i_{TSS,B}$
ρ_{13}	$v_{4,13}$	$v_{5,13}$	$v_{6,13}$	$v_{7,13}$	$v_{8,13}$			1	$i_{TSS,B}$
ρ_{14}	$v_{4,14}$	$v_{5,14}$	$v_{6,14}$	$v_{7,14}$	$v_{8,14}$			1	$i_{TSS,B}$
ρ_{15}	$v_{4,18}$	$v_{5,18}$	$v_{6,18}$	$v_{7,18}$	$v_{8,18}$	f_{XI}	$1-f_{XI}$	-1	$v_{9,18}$

10.2.5.3. Nitrifying bacteria processes

ρ_{16}: Aerobic growth of AOB. The two-step nitrification process has been implemented to reproduce S_{NO2} accumulation observed in Chapter 5. S_{O2} is consumed by AOB to oxidize S_{NH4} to S_{NO2}. $S_{Ig,C}$ is used as carbon source and S_{NHX} is also assimilated as nutrient along with S_{PO4}.

ρ_{17}: Lysis of AOB is modelled similarly to microalgae lysis.

ρ_{18}: Aerobic growth of NOB. S_{NO2} is oxidize to S_{NO3} consuming S_{O2}. $S_{Ig,C}$ is used as carbon source and S_{NHX} is also assimilated as nutrient along with S_{PO4}, as well as AOB.

ρ_{19}: Lysis of NOB is modelled similarly to microalgae lysis.

Table X. 3. Stoichiometric matrix soluble and particulate components-processes of nitrifying bacteria (Barat et al., 2012).

Components → i Processes ↓ j	S_{O2} g O_2 m^{-3}	S_{NHx} g N m^{-3}	S_{NO2} g N m^{-3}	S_{NO3} g N m^{-3}	S_{PO4} g P m^{-3}	S_H mol H m^{-3}	S_{Mg} g Mg m^{-3}	S_K g K m^{-3}	S_{Ca} g Ca m^{-3}
ρ_{16}	$-\frac{3.43-Y_{AOB}}{Y_{AOB}}$	$-\frac{1}{Y_{AOB}}-i_{N,B}$	$\frac{1}{Y_{AOB}}$		$-i_{P,B}$	$v_{12,19}$	$-i_{Mg,B}$	$-i_{K,B}$	$-i_{Ca,B}$
ρ_{17}		$v_{10,21}$			$v_{11,21}$	$v_{12,21}$	$v_{13,21}$	$v_{14,21}$	$v_{15,21}$
ρ_{18}	$-\frac{1.14-Y_{NOB}}{Y_{NOB}}$	$-i_{N,B}$	$-\frac{1}{Y_{NOB}}$	$-\frac{1}{Y_{NOB}}$	$-i_{P,B}$	$v_{12,22}$	$-i_{Mg,B}$	$-i_{K,B}$	$-i_{Ca,B}$
ρ_{19}		$v_{10,24}$			$v_{11,24}$	$v_{12,24}$	$v_{13,24}$	$v_{14,24}$	$v_{15,24}$

Table X. 3. Continued.

Components → i Processes ↓ j	S_{Fe} g Fe m^{-3}	$S_{Ig,C}$ mol C m^{-3}	X_I g COD m^{-3}	X_S g COD m^{-3}	X_{AOB} g COD m^{-3}	X_{NOB} g COD m^{-3}	X_{TSS} g COD m^{-3}
ρ_{16}	$-i_{Fe,B}$	$-i_{C,B}$			1		$i_{TSS,B}$
ρ_{17}	$v_{16,21}$	$v_{17,21}$	f_{XI}	$1-f_{XI}$	-1		$v_{18,21}$
ρ_{18}	$-i_{Fe,B}$	$-i_{C,B}$				1	$i_{TSS,B}$
ρ_{19}	$v_{17,24}$	$v_{17,24}$	f_{XI}	$1-f_{XI}$		-1	$v_{18,24}$

10.2.5.4. Stripping and chemical precipitation

Gas-liquid mas transfer of CO_2, O_2, N_2 and FAN (NH_3) is considered in the model (ρ_{20}, ρ_{21}, ρ_{22}, and ρ_{23}, respectively. The general expression for mas transfer kinetics is described by Equation X. 4**¡Error! No se encuentra el origen de la referencia.**:

$$K_{La,j} \cdot \left(S_j - S_j^*\right) \qquad \text{Equation X. 4}$$

where $K_{La,j}$ is the surface mass transfer coefficient of the gas j gas (d^{-1}), S_j is the j gas concentration in liquid phase ($g \cdot m^{-3}$) and S_j^* is the saturation concentration of j gas in the liquid phase ($g \cdot m^{-3}$).

In order to model the phosphorus removal observed in Chapter 5, which are partly due to chemical precipitation, 15 process (including precipitation and dissolution) are included in the proposed model. The precipitation kinetics expressions (extracted from Barat et al., 2012) are based on the assumption that the precipitation and dissolution are reverse processes except for hydroxyapatite (X_{HAP}).

ρ_{24} and ρ_{25}: Precipitation and dissolution of amorphous calcium phosphate (X_{ACP}).

ρ_{26} and ρ_{27}: Precipitation and dissolution of strengite (X_{STR}).

ρ_{28} and ρ_{29}: Precipitation and dissolution of struvite (X_{MAP}).

ρ_{30} and ρ_{31}: Precipitation and dissolution of newberite (X_{NEW}).

ρ_{32} and ρ_{33}: Precipitation and dissolution of vivianite (X_{VIV}).

ρ_{34} and ρ_{35}: Precipitation and dissolution of varscite (X_{VAR}).

ρ_{36} and ρ_{37}: Precipitation and dissolution of calcium carbonate (X_{CAL}).

ρ_{38}: Precipitation of X_{HAP}.

Table X. 4. Stoichiometric matrix soluble and particulate components-processes of stripping and chemical precipitation (Barat et al., 2012).

Components → i Processes ↓ j	S_{O2} g O_2 m^{-3}	S_{NHx} g N m^{-3}	S_{N2} g N m^{-3}	S_{PO4} g P m^{-3}	S_H mol H m^{-3}	S_{Mg} g Mg m^{-3}	S_{Ca} g Ca m^{-3}	S_{Fe} g Fe m^{-3}	S_{Al} g Al m^{-3}
ρ_{20}					$-1 \cdot 2$				
ρ_{21}	-1								
ρ_{22}			-1						
ρ_{23}		-1			$-1 \cdot \left(-\frac{1}{14}\right)$				
ρ_{24}				-62	$-62 \cdot \left(\frac{3}{31}\right) - 120.3 \cdot \left(\frac{-2}{40.1}\right)$		-120.3		
ρ_{25}				62	$62 \cdot \left(\frac{3}{31}\right) + (120.3) \cdot \left(\frac{-2}{40.1}\right)$		120.3		
ρ_{26}				-31	$-31 \cdot \left(\frac{3}{31}\right) - 55.8 \cdot \left(\frac{-3}{55.8}\right)$			-55.8	
ρ_{27}				31	$31 \cdot \left(\frac{3}{31}\right) + 55.8 \cdot \left(\frac{-3}{55.8}\right)$			55.8	
ρ_{28}		-14		-31	$-14 \cdot \left(\frac{-1}{14}\right) - 31 \cdot \left(\frac{3}{31}\right) - 24.3 \cdot \left(\frac{-2}{24.3}\right)$	-24.3			
ρ_{29}		14		31	$14 \cdot \left(\frac{-1}{14}\right) + 31 \cdot \left(\frac{3}{31}\right) + 24.3 \cdot \left(\frac{-2}{24.3}\right)$	24.3			
ρ_{30}				-31	$-31 \cdot \left(\frac{3}{31}\right) - 24.3 \cdot \left(\frac{-2}{24.3}\right)$	-24.3			
ρ_{31}				31	$31 \cdot \left(\frac{3}{31}\right) + 24.3 \cdot \left(\frac{-2}{24.3}\right)$	24.3			
ρ_{32}				-62	$-62 \cdot \left(\frac{3}{31}\right) - 167.4 \cdot \left(\frac{-3}{55.8}\right)$			-167.4	
ρ_{33}				62	$62 \cdot \left(\frac{3}{31}\right) + 167.4 \cdot \left(\frac{-3}{55.8}\right)$			167.4	
ρ_{34}				-31	$-31 \cdot \left(\frac{3}{31}\right) - 26.9 \cdot \left(\frac{-3}{26.9}\right)$				-26.9
ρ_{35}				31	$31 \cdot \left(\frac{3}{31}\right) + 26.9 \cdot \left(\frac{-3}{26.9}\right)$				26.9
ρ_{36}					$-40.1 \cdot \left(\frac{-2}{40.1}\right) - 2$		-40.1		
ρ_{37}					$40.1 \cdot \left(\frac{-2}{40.1}\right) + 2$		40.1		
ρ_{38}				-31	$-31 \cdot \left(\frac{3}{31}\right) - 80.2 \cdot \left(\frac{-2}{40.1}\right)$		-80.2		

Table X. 4. Continued.

Components → i Processes ↓ j	$S_{Ig,C}$ mol C m^{-3}	X_{TSS} g TSS m^{-3}	X_{ACP} Kmol ACP m^{-3}	X_{HAP} Kmol HAP m^{-3}	X_{MAP} Kmol MAP m^{-3}	X_{New} Kmol New m^{-3}	X_{Viv} Kmol Viv m^{-3}	X_{Str} Kmol Str m^{-3}	X_{Var} Kmol Var m^{-3}	X_{Cal} Kmol Cal m^{-3}
ρ_{20}	-1									
ρ_{21}										
ρ_{22}										
ρ_{23}										
ρ_{24}		364.2	1							
ρ_{25}		-364.2	-1							
ρ_{26}		186.8						1		
ρ_{27}		-186.8						-1		
ρ_{28}		245.3			1					
ρ_{29}		-245.3			-1					
ρ_{30}		174.3				1				
ρ_{31}		-174.3				-1				
ρ_{32}		501.6					1			
ρ_{33}		-501.6					-1			
ρ_{34}		157.9							1	
ρ_{35}		-157.9							-1	
ρ_{36}	-1	100.1								1
ρ_{37}	1	-100.1								-1
ρ_{38}		$502.3 - 364.2$	-1	1						

Table X. 5. Conversion factors to be applied in the continuity equations for N, P, magnesium (Mg), potassium (K), calcium (Ca), iron (Fe), aluminium (Al), mass, carbon and proton of the model for soluble components.

Conservation for	S_{O2} gO_2	S_S gCOD	S_{NHx} gN	S_{NO2} gN	S_{NO3} gN	S_{N2} gN	S_{PO4} gP	S_I gCOD	S_H molH	S_{Mg} gMg	S_K gK	S_{Ca} gCa	S_{Fe} gFe	S_{Al} gAl	$S_{Ig,C}$ molC
COD	-1	1		$\frac{-48}{14}$	$\frac{-64}{14}$	$\frac{-24}{14}$		1							
N (g N)		$i_{N,SS}$	1	1	1	1		$i_{N,SI}$							
P (g P)		$i_{P,SS}$					1	$i_{P,SI}$							
Mg (g Mg)		$i_{Mg,SS}$						$i_{Mg,SI}$		1					
K (g K)		$i_{K,SS}$						$i_{K,SI}$			1				
Ca (g Ca)		$i_{Ca,SS}$						$i_{Ca,SI}$				1			
Fe (g Fe)		$i_{Fe,SS}$						$i_{Fe,SI}$					1		
Al (g Al)		$i_{Al,SS}$						$i_{Al,SI}$						1	
Mass (g TSS)															
C (mol C)		$i_{C,SS}$						$i_{C,SI}$							1
H^+ (mol H)			$\frac{-1}{14}$	$\frac{1}{14}$	$\frac{1}{14}$		$\frac{3}{31}$		-1	$\frac{-2}{24.3}$	$\frac{-1}{39.1}$	$\frac{-2}{40}$	$\frac{-3}{55.8}$	$\frac{-3}{26.9}$	2

Table X. 6. Conversion factors to be applied in the continuity equations for N, P, Mg, K, Ca, Fe, Al, mass, carbon and proton of the model for particulate components.

Conservation for	X_I gCOD	X_S gCOD	X_{ALG} gCOD	X_H gCOD	X_{AOB} gCOD	X_{NOB} gCOD	X_{PP-ALG} gP	X_{TSS} gTSS	X_{NVSS} gNVSS	X_{ACP} kmol ACP	X_{HAP} kmol HAP	X_{MAP} kmol MAP	X_{New} kmol New	X_{Viv} kmol Viv	X_{Str} kmol Str	X_{Var} kmol Var	X_{Cal} kmol Cal
COD	1	1	1	1	1												
N (g N)	$i_{N,XI}$	$i_{N,XS}$	$i_{N,ALG}$	$i_{N,B}$	$i_{N,B}$	$i_{N,B}$						14					
P (g P)	$i_{P,XI}$	$i_{P,XS}$	$i_{P,ALG}$	$i_{P,B}$	$i_{P,B}$	$i_{P,B}$	1			62	93	31	31	62	31	31	
Mg (g Mg)	$i_{Mg,XI}$	$i_{Mg,XS}$	$i_{Mg,ALG}$	$i_{Mg,B}$	$i_{Mg,B}$	$i_{Mg,B}$	$i_{Mg,XPP,ALG}$					24.3	24.3				
K (g K)	$i_{K,XI}$	$i_{K,XS}$	$i_{K,ALG}$	$i_{K,B}$	$i_{K,B}$	$i_{K,B}$	$i_{K,XPP,ALG}$										
Ca (g Ca)	$i_{Ca,XI}$	$i_{Ca,XS}$	$i_{Ca,ALG}$	$i_{Ca,B}$	$i_{Ca,B}$	$i_{Ca,B}$				120.3	200.5						
Fe (g Fe)	$i_{Fe,XI}$	$i_{Fe,XS}$												167.4	55.8		
Al (g Al)	$i_{Al,XI}$	$i_{Al,XS}$														26.9	
Mass (g TSS)	$i_{TSS,XI}$	$i_{TSS,XS}$	$i_{TSS,ALG}$	$i_{TSS,B}$	$i_{TSS,B}$	$i_{TSS,B}$	3.23	-1	1	364.2	502.3	245.3	174.3	501.6	186.8	157.9	100.1
C (mol C)	$i_{C,XI}$	$i_{C,XS}$	$i_{C,ALG}$	$i_{C,B}$	$i_{C,B}$	$i_{C,B}$											1
H^+ (mol H)																	

10.2.5.5. Bioprocess kinetics

The kinetics described in Section 10.2.5 (ρ_i, where *i* is the process number) account for the effect of nutrient concentration (limitation or inhibition) and the ever-changing environmental conditions inherent in outdoors microalgae-bacteria cultivation (light intensity, pH and temperature) through the product of Monod function and dedicated relationship (f_L, f_{pH}, f_T, and f_{O2}, detailed in the following paragraph).

- Nutrients. The kinetics and stoichiometry used to describe biological processes have been chosen as simply as possible, based mainly on Monod functions for model parameters that influence reaction rates. Preferences among different nitrogen source (i.e. S_{NHX} and S_{NO3}) was introduced by a non-competitive inhibition function. The Hill-type function proposed to simulate the inhibition process is included in kinetic rates related to microalgae growth.

Storage of $X_{PP,ALG}$ stops if the intracellular phosphorous content of microalgae becomes too high (Ruiz-Martínez et al., 2015). This observation leads to an $X_{PP,ALG}$ storage inhibition term, which is activated by the $X_{PP,ALG}/X_{ALG}$ ratio. The Hill-type function (Equation X.) is proposed to simulate the influence of $X_{PP,ALG}$ on phosphorous storage process.

$$\frac{K_{XPP-qXPP}{}^{n}}{K_{XPP-qXPP}{}^{n} + \left(\frac{X_{PP,ALG}}{X_{ALG}}\right)^{n}}$$ Equation X. 5

where $X_{PP,ALG}/X_{ALG}$ is the intracellular stored polyphosphate (g P·g TSS^{-1}), $K_{XPP-qXPP}$ is the half saturation parameter of $X_{PP,ALG}/X_{ALG}$ in the storage $X_{PP,ALG}$ process (g P·g TSS^{-1}), and *n* is the Hill number or the regulation coefficient.

- Light intensity (I) (µmol·m^{-2}·s^{-1}). Light intensity was measured as photosynthetically active radiation (PAR), which is responsible for providing energy for light-dependent reactions and comprises wavelengths in the range of 400 to 700 nm. The influence of light factor (f_L) in photosynthetic organisms has been modeled by

Steele's equation (Equation X.). This model considers microalgae photoinhibition and is suitable for modeling microalgae growth in shallow photobioreactors (Steele, 1965):

$$f_L = \frac{I_{av}}{I_{opt}} \cdot e^{\left(1-\frac{I_{av}}{I_{opt}}\right)}$$ Equation X. 6

where I_{opt} (µmol $m^{-2} \cdot s^{-1}$) is the optimal light intensity for microalgae growth and I_{av} (µmol $m^{-2} \cdot s^{-1}$) is the average light intensity.

I_{av} (µmol $m^{-2} \cdot s^{-1}$) is obtained using Lambert-Beer's Law and is attenuated by particulate components and reactor depth (Equation X.).

$$I_{av} = \frac{I_{0,s} \cdot \left(1 - e^{-(k_w + K_I \cdot Xtss) \cdot d}\right)}{(k_w + K_I \cdot X_{TSS}) \cdot d}$$ Equation X. 7

where $I_{0,s}$ (µmol $m^{-2} \cdot s^{-1}$) is the incident light intensity, and k_w (m^{-3}) and k_b (m^2 $gTSS^{-1}$) are the extinction coefficient of water and particulate components, respectively.

- pH. Culture pH is obtained from mass-balance for S_H. MINTEQA2 software is used for calculating both pH and chemical equilibrium. Two different pH inhibition functions are considered in the model BNRM2: a combination of Monod and non-competitive inhibition switching functions (f_{pH1}, Equation X.) and a sigmoidal function (f_{pH2}, Equation X.).

$$f_{pH1} = \frac{\frac{S_H}{S_H + K_{S,H}} \cdot \frac{K_{I,H}}{S_H + K_{I,H}}}{\frac{S_{H,opt}}{S_{H,opt} + K_{S,H}} \cdot \frac{K_{I,H}}{S_{H,opt} + K_{I,H}}}$$ Equation X. 8

$$f_{pH2} = \frac{1}{1 + e^{\left(A_H \cdot (K_{S,H} - pH)\right)}}$$ Equation X. 9

where S_H represents free proton concentration (mol $H^+ \cdot L^{-1}$), $K_{S,H}$ and $K_{I,H}$ the half-saturation and inhibition constants for S_H (mol $H^+ \cdot L^{-1}$), A_H is the fitting parameter, and $S_{H,opt}$ represents the optimal S_H concentration (mol $H^+ \cdot L^{-1}$), obtained as $\sqrt{K_{I,H} \cdot K_{S,H}}$. This last factor is used to cancel pH inhibition under optimal pH conditions.

The sigmoidal function shown Equation X. (f_{pH2}) is only used to model the growth of X_{NOB} since f_{pH1} type function was not able to reproduce the sharp activity decrease observed at low pH values (Jiménez et al., 2011).

- Temperature (ºC). Biokinetic dependence on culture temperature was modeled by the Ratkowski and Arrhenius thermics factors ($f_{T\text{-}R}$ and $f_{T\text{-}A}$) for microalgae and bacteria, respectively (Equation X. and 11)

$$f_{T-R} = (b \cdot (T_0 - T_{MIN}))^2 \cdot (1 - e^{c\cdot(T_0 - T_{MAX})}) \quad \text{Equation X. 10}$$

$$f_{T-A} = \theta^{T_0 - T_{OPT}} \quad \text{Equation X. 11}$$

where T_0 (ºC) is the temperature of culture medium, θ is the temperature coefficient, T_{OPT} is the optimal temperature for bacteria (ºC), T_{MIN} (ºC) is the lowest temperature limit for biomass growth below which the expected growth rate is zero, b is a model parameter defined as the square root regression coefficient of the rate versus the suboptimal temperature, T_{MAX} (ºC) is the upper temperature limit above which the expected growth rate is zero, c is a model parameter that enables the model to fit data at a temperature near, and above the optimal temperature for biomass growth.

- Oxygen (g $O_2 \cdot m^{-3}$). High dissolved oxygen concentration can negatively affect photosynthetic activity (Reynolds, 2006). The influence of dissolved oxygen (f_{O2}) in photosynthetic organisms is modeled by Equation X. 12.

$$f_{O2} = 1 - \left(\frac{S_{O2}}{S_{O2,MAX}}\right)^m \quad \text{Equation X. 12}$$

where S_{O2} is the culture dissolved oxygen (g $O_2 \cdot m^{-3}$), $S_{O2,MAX}$ is the maximum amount of dissolved oxygen for microalgae growth (g $O_2 \cdot m^{-3}$), and m is a fitting parameter.

The kinetics expressions described in Section 10.2.5 are shown in Table X. . In this table, Monod function for component *i* has been denoted by M_i and non-competitive inhibition function have been denoted by I_i.

Table X. 7. Kinetics expressions of the processes.

Processes	Processes rate [M L^{-3} T^{-1}]
ρ_1: X_{ALG} growth over S_{NHX} and S_{PO4}	$\mu_{ALG} \cdot M_{Ig,C} \cdot M_{NHX} \cdot M_{PO4} \cdot X_{ALG} \cdot f_L \cdot f_{pH1} \cdot f_T \cdot f_{O2}$
ρ_2: X_{ALG} growth over S_{NO3} and S_{PO4}	$\mu_{ALG} \cdot \eta_{NO3} \cdot M_{Ig,C} \cdot M_{NO3} \cdot M_{PO4} \cdot I_{NHX} \cdot X_{ALG} \cdot f_L \cdot f_{pH1} \cdot f_T \cdot f_{O2}$
ρ_3: X_{ALG} growth over S_{NHX} and $X_{PP,ALG}$	$\mu_{ALG} \cdot M_{Ig,C} \cdot M_{NHX} \cdot \frac{\frac{X_{PP,ALG}}{X_{ALG}}}{K_{XPP,ALG} + \frac{X_{PP,ALG}}{X_{ALG}}} \cdot I_{PO4} \cdot X_{ALG} \cdot f_L \cdot f_{pH1} \cdot f_T \cdot f_{O2}$
ρ_4: X_{ALG} growth over S_{NO3} on $X_{PP,ALG}$	$\mu_{ALG} \cdot \eta_{NO3} \cdot M_{Ig,C} \cdot M_{NO3} \cdot \frac{K_{NHX}}{K_{NHX-qXPP} + S_{NHX}} \cdot \frac{\frac{X_{PP,ALG}}{X_{ALG}}}{K_{XPP-ALG} + \frac{X_{PP,ALG}}{X_{ALG}}} \cdot I_{PO4} \cdot X_{ALG} \cdot f_L \cdot f_{pH1} \cdot f_T \cdot f_{O2}$
ρ_5: $X_{PP,ALG}$ storage	$q_{PP-ALG} \cdot M_{PO4} \cdot M_{Mg} \cdot M_K \cdot \frac{{K_{XPP-qXPP}}^n}{{K_{XPP-qXPP}}^n + \left(\frac{X_{PP,ALG}}{X_{ALG}}\right)^n} \cdot X_{ALG} \cdot f_L \cdot f_{pH1} \cdot f_T \cdot f_{O2}$
ρ_6: X_{ALG} respiration	$b_{ALG,1} \cdot X_{ALG} \cdot f_T \cdot f_{pH1}$
ρ_7: X_{ALG} lysis	$b_{ALG,2} \cdot X_{ALG} \cdot f_T \cdot f_{pH1}$
ρ_8: $X_{PP,ALG}$ lysis	$b_{ALG,2} \cdot X_{PP,ALG} \cdot f_T \cdot f_{pH1}$
ρ_9: Aerobic hydrolysis	$q_{HET,XS} \cdot M_{O2} \cdot \frac{X_I/X_{HET}}{K_X + X_I/X_{HET}} \cdot f_{pH1} \cdot f_T \cdot X_{HET}$
ρ_{10}: Anoxic hydrolysis	$q_{HET,XS} \cdot \eta_{\mu H,Ax} \cdot I_{O2} \cdot M_{NO3} \cdot \frac{X_I/X_{HET}}{K_X + X_I/X_{HET}} \cdot f_{pH1} \cdot f_T \cdot X_{HET}$
ρ_{11}: Anaerobic hydrolysis	$q_{HET,XS} \cdot \eta_{\mu H,An} \cdot I_{O2} \cdot I_{NO3} \cdot \frac{X_I/X_{HET}}{K_X + X_I/X_{HET}} \cdot f_{pH1} \cdot f_T \cdot X_{HET}$

Table X. 7. Continued.

Processes	Processes rate [M L^{-3} T^{-1}]
ρ_{12}: Aerobic growth of X_H over S_S	$\mu_{HET} \cdot M_{O2} \cdot M_{S_S} \cdot M_{NHX} \cdot M_{PO4} \cdot X_{HET} \cdot f_{pH1} \cdot f_T$
ρ_{13}: Anoxic growth of X_H over S_S and S_{NO3}	$\mu_{HET} \cdot \eta_{\mu HET,Ax3} \cdot I_{O2} \cdot M_{S_S} \cdot M_{NHX} \cdot M_{PO4} \cdot M_{NO3} \cdot \frac{S_{NO3}}{S_{NO2} + S_{NO3}} \cdot X_{HET} \cdot f_{pH1} \cdot f_T$
ρ_{14}: Anoxic growth of X_H over S_S and S_{NO2}	$\mu_{HET} \cdot \eta_{\mu HET,Ax2} \cdot I_{O2} \cdot M_{S_S} \cdot M_{NHX} \cdot M_{PO4} \cdot M_{NO2} \cdot \frac{S_{NO2}}{S_{NO2} + S_{NO3}} \cdot X_{HET} \cdot f_{pH1} \cdot f_T$
ρ_{15}: Lysis of X_H	$b_{HET} \cdot X_{HET} \cdot f_{pH1} \cdot f_T$
ρ_{16}: Aerobic growth of X_{AOB}	$\mu_{AOB} \cdot M_{O2} \cdot M_{Ig,C} \cdot M_{NHX} \cdot M_{PO4} \cdot I_{HNO2} \cdot X_{AOB} \cdot f_{pH1} \cdot f_T$
ρ_{17}: Lysis of X_{AOB}	$b_{AOB} \cdot X_{AOB} \cdot f_T \cdot f_{pH1}$
ρ_{18}: Aerobic growth of X_{NOB}	$\mu_{NOB} \cdot M_{O2} \cdot M_{Ig,C} \cdot M_{NO2} \cdot M_{NHX} \cdot M_{PO4} \cdot I_{HNO2} \cdot X_{NOB} \cdot f_{pH2} \cdot f_T$
ρ_{19}: Lysis of X_{NOB}	$b_{NOB} \cdot X_{NOB} \cdot f_T \cdot f_{pH2}$
ρ_{20}: $S_{[CO2]}$ stripping	$K_{La,CO2} \cdot \left(S_{[CO2]} - S^*_{[CO2]}\right)$
ρ_{21}: S_{O2} stripping	$K_{La,O2} \cdot (S_{O2} - S^*_{O2})$
ρ_{22}: S_{N2} stripping	$K_{La,N2} \cdot \left(S_{[N2]} - S^*_{[N2]}\right)$
ρ_{23}: $S_{[NH3]}$ stripping	$K_{La,NH3} \cdot \left(S_{[NH3]} - S^*_{[NH3]}\right)$

Table X. 7. Continued.

Processes	Processes rate [M L^{-3} T^{-1}]
ρ_{24}: Precipitation of X_{ACP}	$q_{ACP,p} \cdot \frac{K_{I,ACP}}{K_{I,ACP} + \frac{X_{ACP}}{X_{TSS}}} \cdot \left(S_{[Ca^{2+}]}^{\frac{3}{5}} \cdot S_{[PO_4^{3-}]}^{\frac{2}{5}} - \left(\frac{K_{ACP,SP}}{\gamma_d^3 \cdot \gamma_t^2} \right)^{\frac{1}{5}} \right)^2 \cdot \frac{1 + sign(SI_{ACP})}{2}$
ρ_{25}: Dissolution of X_{ACP}	$q_{ACP,d} \cdot \frac{X_{ACP}}{K_{S,ACP} + X_{ACP}} \cdot \left(S_{[Ca^{2+}]}^{\frac{3}{5}} \cdot S_{[PO_4^{3-}]}^{\frac{2}{5}} - \left(\frac{K_{ACP,SP}}{\gamma_d^3 \cdot \gamma_t^2} \right)^{\frac{1}{5}} \right)^2 \cdot \frac{1 - sign(SI_{ACP})}{2}$
ρ_{26}: Precipitation of X_{Str}	$q_{STR,p} \cdot \frac{K_{I,Str}}{K_{I,Str} + \frac{X_{Str}}{X_{TSS}}} \cdot \left(S_{[Fe^{3+}]}^{\frac{1}{2}} \cdot S_{[PO_4^{3-}]}^{\frac{1}{2}} - \left(\frac{K_{Str,SP}}{\gamma_t^2} \right)^{\frac{1}{2}} \right)^2 \cdot \frac{1 + sign(SI_{Str})}{2}$
ρ_{27}: Dissolution of X_{Str}	$q_{Str,d} \cdot \frac{X_{Str}}{K_{S,Str} + X_{Str}} \cdot \left(S_{[Fe^{3+}]}^{\frac{1}{2}} \cdot S_{[PO_4^{3-}]}^{\frac{1}{2}} - \left(\frac{K_{Str,SP}}{\gamma_t^2} \right)^{\frac{1}{2}} \right)^2 \cdot \frac{1 - sign(SI_{Str})}{2}$
ρ_{28}: Precipitation of X_{MAP}	$q_{MAP,p} \cdot \frac{K_{I.MAP}}{K_{I,MAP} + \frac{X_{MAP}}{X_{TSS}}} \cdot \left(S_{[Mg^{2+}]}^{\frac{1}{3}} \cdot S_{[NH_4^+]}^{\frac{1}{3}} \cdot S_{[PO_4^{3-}]}^{\frac{1}{3}} - \left(\frac{K_{MAP,SP}}{\gamma_m \gamma_d \cdot \gamma_t} \right)^{\frac{1}{3}} \right)^3 \cdot \frac{1 + sign(SI_{MAP})}{2}$
ρ_{29}: Dissolution of X_{MAP}	$q_{MAP,d} \cdot \frac{X_{MAP}}{K_{S,MAP} + X_{MAP}} \cdot \left(S_{[Mg^{2+}]}^{\frac{1}{3}} \cdot S_{[NH_4^+]}^{\frac{1}{3}} \cdot S_{[PO_4^{3-}]}^{\frac{1}{3}} - \left(\frac{K_{MAP,SP}}{\gamma_m \gamma_d \cdot \gamma_t} \right)^{\frac{1}{3}} \right)^3 \cdot \frac{-1 + sign(SI_{MAP})}{2}$

Table X. 7. Continued.

Processes	Processes rate [M L^{-3} T^{-1}]
ρ_{30}: Precipitation of X_{New}	$q_{New,p} \cdot \frac{K_{I,New}}{K_{I,New} + \frac{X_{New}}{X_{TSS}}} \cdot \left(S_{[Mg^{2+}]}^{\frac{1}{2}} \cdot S_{[HPO_4^{2-}]}^{\frac{1}{2}} - \left(\frac{K_{New,SP}}{\gamma_d^2} \right)^{\frac{1}{2}} \right)^2 \cdot \frac{1 + sign(SI_{New})}{2}$
ρ_{31}: Dissolution of X_{New}	$q_{New,d} \cdot \frac{X_{New}}{K_{S,New} + X_{New}} \cdot \left(S_{[Mg^{2+}]}^{\frac{1}{2}} \cdot S_{[HPO_4^{2-}]}^{\frac{1}{2}} - \left(\frac{K_{New,SP}}{\gamma_d^2} \right)^{\frac{1}{2}} \right)^2 \cdot \frac{1 - sign(SI_{New})}{2}$
ρ_{32}: Precipitation of X_{Viv}	$q_{Viv,p} \cdot \frac{K_{I,Viv}}{K_{I,Viv} + \frac{X_{Viv}}{X_{TSS}}} \cdot \left(S_{[Fe^{2+}]}^{\frac{3}{5}} \cdot S_{[PO_4^{3-}]}^{\frac{2}{5}} - \left(\frac{K_{Viv,SP}}{\gamma_d^3 \cdot \gamma_t^2} \right)^{\frac{1}{2}} \right)^2 \cdot \frac{1 + sign(SI_{Viv})}{2}$
ρ_{33}: Dissolution of X_{Viv}	$q_{Viv,d} \cdot \frac{X_{Viv}}{K_{S,Viv} + X_{Viv}} \cdot \left(S_{[Fe^{2+}]}^{\frac{3}{5}} \cdot S_{[PO_4^{3-}]}^{\frac{2}{5}} - \left(\frac{K_{Viv,SP}}{\gamma_d^3 \cdot \gamma_t^2} \right)^{\frac{1}{2}} \right)^2 \cdot \frac{1 - sign(SI_{Viv})}{2}$
ρ_{34}: Precipitation of X_{Var}	$q_{Var,p} \cdot \frac{K_{I,Var}}{K_{I,Var} + \frac{X_{Var}}{X_{TSS}}} \cdot \left(S_{[Al^{3+}]}^{\frac{1}{2}} \cdot S_{[PO_4^{3-}]}^{\frac{1}{2}} - \left(\frac{K_{Var,SP}}{\gamma_t^2} \right)^{\frac{1}{2}} \right)^2 \cdot \frac{1 + sign(SI_{Var})}{2}$
ρ_{35}: Dissolution of X_{Var}	$q_{Var,d} \cdot \frac{X_{Var}}{K_{S,Var} + X_{Var}} \cdot \left(S_{[Al^{3+}]}^{\frac{1}{2}} \cdot S_{[PO_4^{3-}]}^{\frac{1}{2}} - \left(\frac{K_{Var,SP}}{\gamma_t^2} \right)^{\frac{1}{2}} \right)^2 \cdot \frac{1 - sign(SI_{Var})}{2}$

Table X. 1. Continued.

Processes	Processes rate [M L^{-3} T^{-1}]

ρ_{36}: Precipitation of X_{Cal}	$q_{Cal,p} \cdot \frac{K_{I,Cal}}{K_{I,Cal} + \frac{X_{Cal}}{X_{TSS}}} \cdot \left(S_{[Ca^{2+}]}^{\frac{1}{2}} \cdot S_{[CO_3^{2-}]}^{\frac{1}{2}} - \left(\frac{K_{Cal,SP}}{\gamma_d^2} \right)^{\frac{1}{2}} \right)^2 \cdot \frac{1 + sign(SI_{Cal})}{2}$
ρ_{37}: Dissolution of X_{Cal}	$q_{Cal,d} \cdot \frac{X_{Cal}}{K_{S,Cal} + X_{Cal}} \cdot \left(S_{[Ca^{2+}]}^{\frac{1}{2}} \cdot S_{[CO_3^{2-}]}^{\frac{1}{2}} - \left(\frac{K_{Cal,SP}}{\gamma_d^2} \right)^{\frac{1}{2}} \right)^2 \cdot \frac{1 - sign(SI_{Cal})}{2}$
ρ_{38}: Precipitation of X_{HAP}	$q_{HAP} \cdot \frac{X_{ACP}}{K_{S,HAP} + X_{ACP}} \cdot \frac{S_{[PO_4^{3-}]}}{K_{S,PO4} + S_{[PO_4^{3-}]}} \cdot \frac{S_{[Ca^{2+}]}}{K_{S,Ca} + S_{[Ca^{2+}]}}$

10.3. EXPERIMENTAL SETUP

10.3.1. Analysis scenario

Two scenarios can be analyzed to validate the microalgae-bacteria model. In this respect, according to the degree of accuracy of the fitting between experimental and model data, it could be concluded whether or not a given environmental conditions can explain microalgae-bacteria interactions. To this aim, microalgae and nitrifying bacteria were cultivated in an outdoor membrane photobioreactor (MPBR) pilot plant.

The first scenario is focused on interactions between microalgae and nitrifying bacteria. The negative effects of nitrifying bacteria on the activity of microalgae were reported and analyzed in Chapters 5, 6, and 7. In this respect, the proposed model aims to represent a powerful tool to assess: (I) the competition and amensalism interactions between both AOB and microalgae, (II) the most efficient competitor under favorable growth conditions, and (III) the photoinhibition of nitrifying bacteria. For instance, a decrease in NOB activity resulting in NO_2-N accumulation was observed in Chapter 5, which was mainly related to NOB growth inhibition due to light intensity. However, light inhibition was not included in the model's kinetic expressions (see Table X.) since there are no scientific sources providing calibration results for this inhibition process. Moreover, although the inhibition constant could have been calibrated online, it would have also contributed to model output uncertainty (Chapter 9). For assessment of this first scenario, environmental parameters such as pH, temperature, and nitrogen sources were controlled, thus competitive interactions were not affected by external factors to the competitive ability of microorganisms. In addition, the calibrated parameters related to NO_2-N inhibition (Chapter 6) can be validated.

The second scenario is focused on modeling inorganic carbon and pH dynamics (along with oxygen), since it is the cornerstone of microalgae-bacteria interactions. This second scenario has not been developed in this chapter and will be evaluated in future work.

However, the integrated model of microalgae and bacteria is fully described for representing both analysis scenarios.

10.3.2. MPBR pilot plant

The model was validated using data gathered from an outdoor MPBR pilot plant at the "Cuenca del Carraixet" WWTP (39°30′04.0''N 0°20′00.1''W, Valencia, Spain) fed with effluent from an anaerobic membrane bioreactor (AnMBR) pilot plant. The AnMBR effluent consisted of a nutrient-rich permeate with a negligible concentration of TSS (0 g $TSS \cdot m^{-3}$) and a BOD concentration of 14 ± 4 g $BOD \cdot m^{-3}$, characteristics that make this permeate a suitable culture medium for microalgae growth, limiting the development of heterotrophic bacteria population. Further details on the AnMBR plant can be found in Seco et al. (2018). The MPBR plant mainly consisted of two flat-panel photobioreactors (PBRs) connected to one membrane tank (MT) module. The PBRs had a sun-exposed surface area of 2.3 m^2 (1.15 x 2 m) and a 0.10-m width. The PBRs were continuously air-stirred for mixing the culture medium while reducing wall fouling.

The total working volume of the MT module was 14L with a filtration area of 3.4 m^2. It included one bundle extracted from one commercial ultrafiltration hollow-fiber membrane system (PURON® Koch Membrane Systems PUR-PSH31, 0.03-µm pores). Membrane scouring was conducted by air sparging.

PBR and MT stirring conditions have a remarkable effect on K_{La} coefficient, and therefore on gas stripping. Pure CO_2 (99.9%) was injected into the air system to set pH at 7.5 and ensure culture conditions rich in inorganic carbon. Thus, decreases on microalgae and nitrifying activity due to lack of inorganic carbon and/or uncontrolled pH was minimized, which allows focusing on the competition for nitrogen source and nitrite inhibition (Chapter 7). Chemical phosphorous precipitation and FAN stripping were therefore also minimized. On the other hand, a temperature control system was implemented, consisting of a cooling device equipped with a thermostat (Daikin R410A inverter). The

temperature set point was 20ºC. The cooled fluid was supplied to the MPBR plant through a 20-m long spiral tube immersed in the PBRs.

Online sensors were installed in the MPBR plant to obtain real-time information on process performance. One dissolved oxygen-temperature sensor (LDO Hach Lange) and one pH sensor (pHD sc DPD1R1, Hach Lange) were installed in each PBR. A light irradiance sensor (Apogee QuantIm SQ-200) was set up on the surface of the PBRs to measure incident PAR. Besides sunlight, PBRs were constantly illuminated by twelve LED lamps (Unique Led IP65 WS-TP4S–40W-ME) placed on the back of the PBRs, providing a continuous light irradiation of 300 $\mu mol \cdot m^{-2} \cdot s^{-1}$ (measured on the PBR surface).

10.3.3. Analytical methods

Besides the information provided by the online sensors, samples were taken from influent, effluent, and biomass culture. The streams were sampled in duplicate three times a week to monitor MPBR plant performance. Ammonium (NH_4-N), nitrite (NO_2-N) nitrate (NO_3-N), phosphate (PO_4^{3-}), TSS and VSS were determined according to Standard Methods (APHA, 2005): methods 4500-NH3-G, 4500-NO2-B, 4500-NO3-H, 4500-P-F, 2540-TSS-D, and 2540-VSS-E, respectively. Total nitrogen (T-N) concentration of biomass culture was measured by a commercial total nitrogen test kit (1.14537.001, Merck Millipore). Sample was digested at 150ºC for 2 hours, followed by PO_4^{3-} determination, 4500-P-F according to the Standard Methods, to quantify total phosphorous (T-P) concentration. Soluble organic matter was estimated once a week in duplicate through soluble chemical oxygen demand (S-COD) and soluble biological oxygen demand (S-BOD) according to Standard Methods (APHA, 2005): methods 5220-COD-D and 5210-BOD-C, respectively.

10.4. MODEL SETUP

The model was run on MATLAB®. The PBRs were considered as completely stirred tanks. The MPBR plant was operated in a contentious regime, i.e. the recorded influent dynamics, effluent (membrane permeate), and MPBR wastage were considered. The initial component concentrations used to run the model corresponded to experimental data from the MPBR, varying therefore depending on the data set validated.

As proposed in the model BNRM2, the simulation procedure involves a sequential iteration among the differential equations obtained from the kinetically-governed processes (biological and precipitation model) and the algebraic equations obtained from the equilibrium-governed processes (chemical model). The total concentration of each component (e.g. S_{PO4} and S_{NHx}) needed for applying the chemical model, is provided by the solution of the corresponding mass-balance equations. The concentrations of the species (e.g. $S_{[PO4^{3-}]}$, $S_{[HPO4^{2-}]}$, $S_{[H2PO4^{1-}]}$, $S_{[H3PO4]}$, $S_{[FeHPO4]}$, $S_{[FeH2PO4^{+}]}$, $S_{[FeHPO4^{+}]}$, $S_{[FeH2PO4^{2+}]}$, $S_{[MgPO4^{-}]}$, $S_{[MgHPO4]}$, $S_{[MgH2PO4^{+}]}$, $S_{[CaPO4^{-}]}$, $S_{[CaHPO4]}$, $S_{[CaH2PO4^{+}]}$, $S_{[KHPO4^{-}]}$, $S_{[Al2PO4^{+3}]}$ and $S_{[AlHPO4^{+}]}$ related to S_{PO4}; and $S_{[NH4^{+}]}$, $S_{[NH3]}$, $S_{[CaNH3^{2+}]}$,$S_{[Ca(NH3)2^{2+}]}$ and $S_{[FeNH3^{2+}]}$ related to S_{NHx}) involved in the kinetic expressions are provided by the solution of the chemical equilibrium.

MINTEQA2 software was used to compute the chemical equilibrium, including the calculation of the ionic species. The main advantages of using MINTEQA2 can be summarized as:

- The chemical algebraic equations are already implemented in the software.
- The equilibrium composition is thoroughly calculated: temperature variations of equilibrium constants are taken into account, ion strength and activity coefficients of each specie are calculated to apply the law of mass action.
- The model can be easily enlarged because the equations required to calculate the equilibrium composition considering new components are already implemented.

10.4.1. Model validation

The microalgae-bacteria model was validated through three operating periods: P_AOB, P_NOB, and P_Microalgae. These periods were selected to cover different microbial structures, thus assessing the first analysis scenario described in Section 10.3.1. Nitrite inhibition and NOB photoinhibition were analyzed throughout the period P_AOB, as nitrite accumulated during reactor operation. In period P_NOB, ammonium was oxidized to NO_3-N (i.e. NO_2-N did not accumulate). Period P_Microalgae was dominated by microalgae and NO_2-N nor NO_3-N were less than 2 g $N \cdot m^{-3}$. All periods were preceded by chemical cleaning of the membranes and a start-up phase (as explained in detail in González-Camejo et al., 2019b). The MPBR pilot plant was inoculated with a microalgae suspension where morphologies similar to *Coelastrella* and *Desmodesmus* genus were the dominant microalgae.

Model outputs selected for model validation were X_{TSS}, X_{VSS}, S_{NHX}, S_{NO2}, S_{NO3} and S_{PO4}. The model seed concentrations along with the main abiotic parameters for each evaluated period are shown in Table X. 2. Initial ratio of X_{ALG}, X_H, X_{AOB}, X_{NOB}, and X_S concentrations were quantified from initial X_{TSS}, based on previous simulation tests to match initial pattern trend of X_{TSS}, S_{NHX}, S_{NO2}, S_{NO3}, and S_{PO4}.

Model prediction performance was evaluated through correlation coefficients (R^2). In addition, the t-test and F-test, and a non-continuous level test (i.e. the Mann-Whitney I-test) were performed on Statgraphics® Centurion v.19 to compare and determine whether or not there was significant differences between experimental and modeling data.

Table X. 2. Main model seed concentrations and main abiotic parameters values for each evaluated period.

Parameters		P_AOB	P_NOB	P_Microalga
S_{O2}	g $O_2 \cdot m^{-3}$	13.43	14.15	11.56
S_{NHX}	g $N \cdot m^{-3}$	1.32	20.30	23.55
S_{NO3}	g $N \cdot m^{-3}$	0	1.61	0
S_{NO2}	g $N \cdot m^{-3}$	0.025	0	0
S_{PO4}	g $P \cdot m^{-3}$	0.03	0.05	3.44
X_P	g $P \cdot m^{-3}$	3.0	2.66	4.7
S_{Mg}	g $Mg \cdot m^{-3}$	52	52	52
S_K	g $K \cdot m^{-3}$	22	22	22
S_{Fe}	g $Fe \cdot m^{-3}$	10	10	10
S_{Al}	g $Al \cdot m^{-3}$	10	10	10
S_{Ca}	g $Ca \cdot m^{-3}$	197	197	197
X_I	g $COD \cdot m^{-3}$	10	10	10
S_S	g $COD \cdot m^{-3}$	0	0	0
S_I	g $COD \cdot m^{-3}$	44	40	41
X_{ALG}	g $COD \cdot m^{-3}$	950	1100	1000
X_{HET}	g $COD \cdot m^{-3}$	0.1	0.1	0.1
X_{AOB}	g $COD \cdot m^{-3}$	0.1	0.1	0.1
X_{NOB}	g $COD \cdot m^{-3}$	0.1	0.1	0.1
BRT	days	2.0 ± 0.3	5.88 ± 1.01	4.8 ± 1.6
HRT	days	1.24 ± 0.08	1.3 ± 0.2	1.58 ± 0.05
PAR	$\mu mol \cdot m^{-2} \cdot s^{-1}$	241 ± 120	262 ± 47	245 ± 153
T	ºC	18 ± 2	20.5 ± 1.3	24 ± 2
pH		7.52 ± 0.09	7.45 ± 0.03	7.49 ± 0.04

10.4.2. Case study

Practical case study was conducted to evaluate the effect of nitrification control strategies proposed in Chapter 7. Total and volatile suspended solids, ammonium, nitrite, nitrate and phosphate concentration, along with the relative proportion of microalgae and bacteria as a function of different BRT, dilution rate, incoming nitrogen speciation, and temperature was investigated.

The effect of BRT was assessed in period P_AOB, keeping constant the values for the environmental parameters, HRT, and seed and influent component concentrations. The experimental BRT was 2.0 ± 0.3 days and it was increased to 4.5 days.

Dilution rate and incoming nitrogen speciation effect on microalgae and bacteria interaction were studied separately in period P_NOB. The experimental dilution rate was 0.21 ± 0.04 $days^{-1}$ and it was increased punctually up to 0.85 $days^{-1}$. The main source of nitrogen was also simulated to be NO_3-N instead of NH_4-N, which would be similar to microalgae growth with secondary treatment effluent. The remaining abiotic conditions were kept constant as in P_AOB.

10.5. RESULTS AND DISCUSSION

10.5.1. Model validation

Validation step was conducted using the previous calibrated parameter values obtained from Chapter 9 (Supplementary Data, Table X. S 1). Values for the chemical equilibrium, physical and stoichiometric parameters are supplied in the Supplementary Data of this chapter. Figures X. 3, 4 and 5 show the comparison between the experimental data (markers) and the model predictions (lines).

10.5.1.1. P_AOB validation

Figure X. 2 shows the results of P_AOB, during which AOB and NOB growth were uncoupled, accumulating NO_2-N to values of 17 ± 2 g $N \cdot m^{-3}$. Modeled X_{TSS} and X_{VSS} concentrations fitted well with the experimental data (R^2 of 0.9521 and 0.9509, respectively). Nutrient concentrations were reproduced with a high degree of accuracy (R^2 of 0.9484 and 0.9509, respectively). Similarly, the model was able to reproduce the nitrification processes, since the simulated concentrations matched accurately experimental data for S_{NO2} and S_{NO3} (R^2 of 0.9925 and 0.9906, respectively).

Microalgae concentration along with AOB and NOB biomass were estimated over the 27 days of simulation (Figure X. 2D). The trend in microalgae biomass concentration was downward decreasing from 79 to 47 % of TSS, while AOB and NOB gradually increased throughout the simulated period until reaching values of 4.5 and 1% of TSS. This period was operated at BRT and HRT of 2.0 ± 0.3 and 1.24 ± 0.08 days, respectively. According to Chapter 7, low BRTs favor the growth of AOB over NOB, resulting in NO_2-N accumulation. The downward trend of microalgae could therefore be related to photosynthesis inhibition due to the presence of NO_2-N (see Chapter 6). Hence, the mathematical model could be used as a tool to analyze the factors affecting microalgae-bacteria consortia.

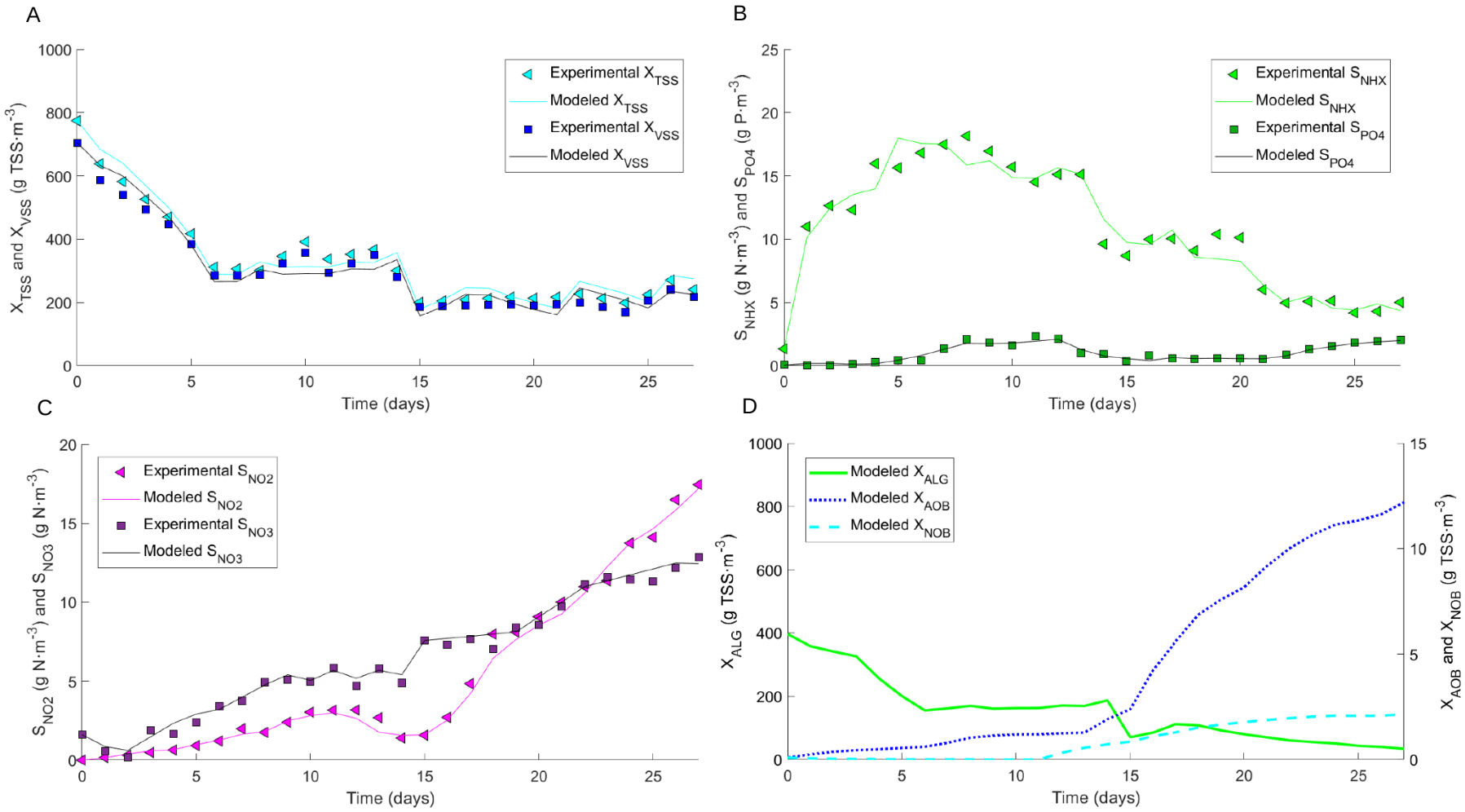

Figure X. 2. Dynamic simulation of period P_AOB. Evolution of: (A) X_{TSS} and X_{VSS} (g TSS·m^{-3}), (B) S_{NHX} (g N·m^{-3}) and S_{PO4} (g P·m^{-3}), (C) S_{NO2} and S_{NO3} (g N·m^{-3}), and (D) X_{ALG}, X_{AOB} and X_{NOB} (gTSS·m^{-3}).

The same period was simulated without the nitrite inhibition kinetics, so that it was possible both to evaluate whether microalgae are really inhibited by NO_2-N and to validate the calibrated value obtained in Chapter 6. Figure X. shows the evolution of X_{VSS} and X_{ALG} model outputs with and without nitrite kinetic inhibition.

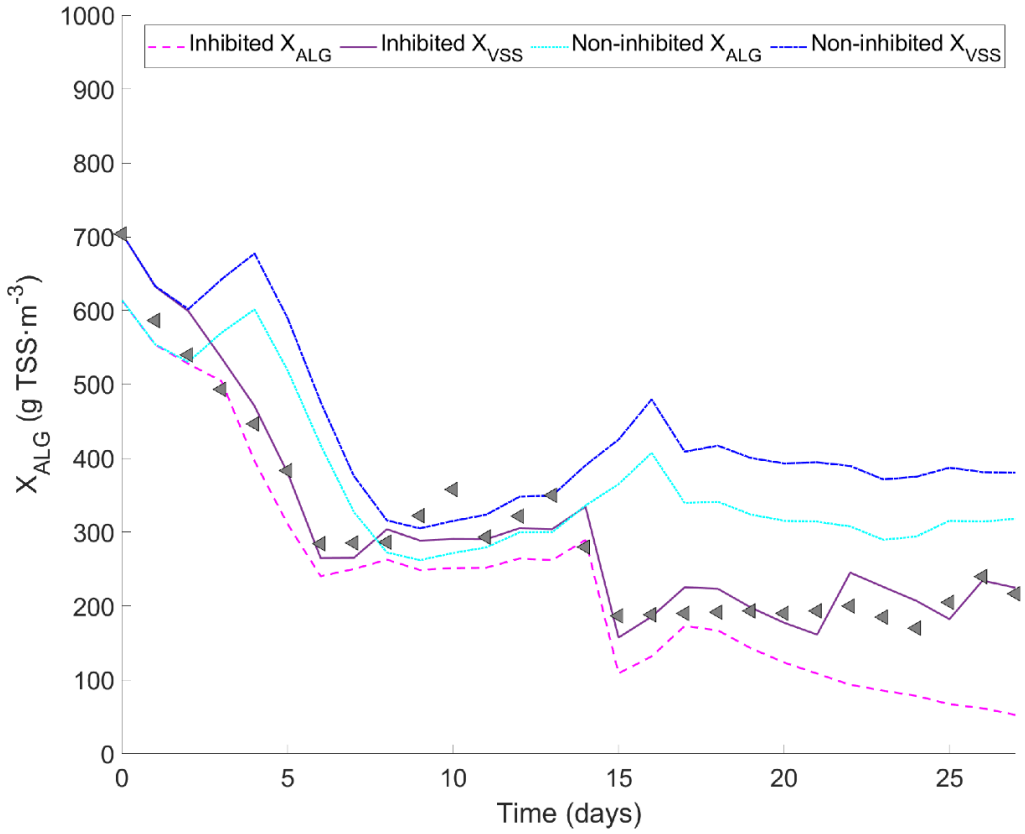

Figure X. 3. Dynamic simulation of X_{VSS} and X_{ALG} model outputs with and without taking into accournt the nitrite kinetic inhibition funcion for NO_2-N. Markers represents experimental data for VSS concentration from period P_AOB.

Correlation degree between experimental VSS concentration and X_{VSS} output with no NO_2-N inhibition decreased to 0.5442 (R^2 between experimental and modeled results with NO_2-N inhibition was 0.9521), indicating that microalgae growth was clearly inhibited by NO_2-N. In addition, inhibition kinetics obtained from Chapter 6 can accurately reproduce the experimental data. Relatively low concentration of AOB (barely 5%) can significantly reduce microalgae growth (Chapter 8). Simulated concentration of both S_{NO2} and S_{NO3} match with experimental results without a photoinhibition kinetics for NOB. Uncoupled activity of nitrifying bacteria could be therefore due to the operating BRT. However, this assumption will be analyzed in Section 10.5.2.

10.5.1.2. P_NOB validation

Figure X. shows the simulation results for period P_NOB, operated at 5.88 ± 1.01 days of BRT and 1.3 ± 0.2 days of HRT. Once more, the modeled data matched the trend of experimental X_{TSS} and X_{VSS} concentration (R^2 of 0.9488 and 0.9198, respectively) (Figure X. A). The experimental and modeled nutrient concentrations are depicted in Figure X. B, showing adequate data set fittings (R^2 of 0.9569 and 0.9272, respectively). In this period, NO_2-N concentration was nearly zero, being the model able to reproduce this situation (R^2 of 0.9190). The zero nitrite concentration was due to NOB growth. The model results also successfully represented S_{NO3} (R^2 of 0.9071) (Figure X. C).

Figure X. D shows the simulated curve of microalgae (X_{ALG}) and nitrifying bacteria (X_{AOB} and X_{NOB}). As this figure shows, NOB biomass represented only a 5% of TSS, being enough to nitrify the 53% of the incoming S_{NHX}. Microalgae biomass was apparently not affected by NOB activity, since X_{ALG} remained stable at 650 ± 26 g TSS·m^{-3}.

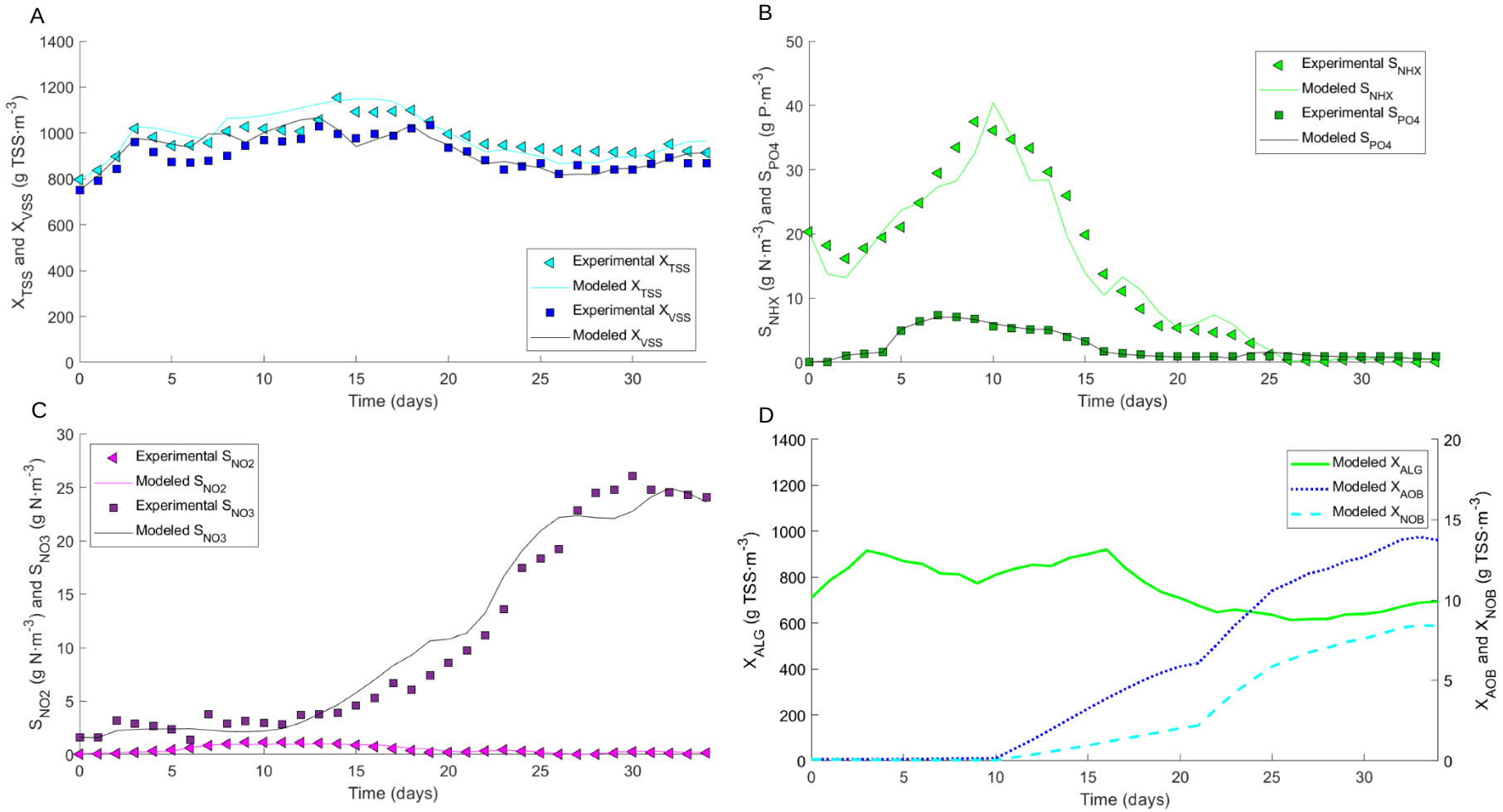

Figure X. 4. Dynamic simulation of period P_NOB. Evolution of: (A) X_{TSS} and X_{VSS} (g TSS·m^{-3}), (B) S_{NHX} (g N·m^{-3}) and S_{PO4} (g P·m^{-3}), (C) S_{NO2} and S_{NO3} (g N·m^{-3}), and (D) X_{ALG}, X_{AOB} and X_{NOB} (gTSS·m^{-3}).

10.5.1.3. P_Microalgae validation

Figure X. shows the modelling results for period P_Microalgae, during which microbial community was dominated by microalgae and interaction with bacteria was not significant. As this figure shows, the model was able to reproduce X_{TSS} and X_{VSS} dynamics (Figure X. A) with a good degree of accuracy (R^2 of 0.9131 and 0.9323, respectively). The modeled data followed the experimental trend for S_{NH4}, S_{NO2}, S_{NO3}, and S_{PO4} measurements (Figure X. B and C) with a good degree of success (R^2 of 0.9229, 0.9620, 0.9808 and 0.9888, respectively). Culture media concentrations for S_{NO2} and S_{NO3} were just the result of the nitrification process, since denitrification was avoided by the ever-aerobic conditions in the PBR. The abiotic conditions from this experimental period (see Table X. 2) favor microalgae growth instead of nitrifying bacteria. Low S_{NHX} concentration (< 2 g $N \cdot m^{-3}$) indicated competition between microalgae and AOB for the substrate, with AOB being outcompeted in this case.

The model also allowed estimating microalgal (X_{ALG}) and bacterial biomass (X_{AOB} and X_{NOB}) dynamics (see Figure X. D). Above 70% of the average biomass corresponded to microalgae (74 ± 7% in average of TSS), while nitrifying bacteria resulted in very low concentrations (<0.1%).

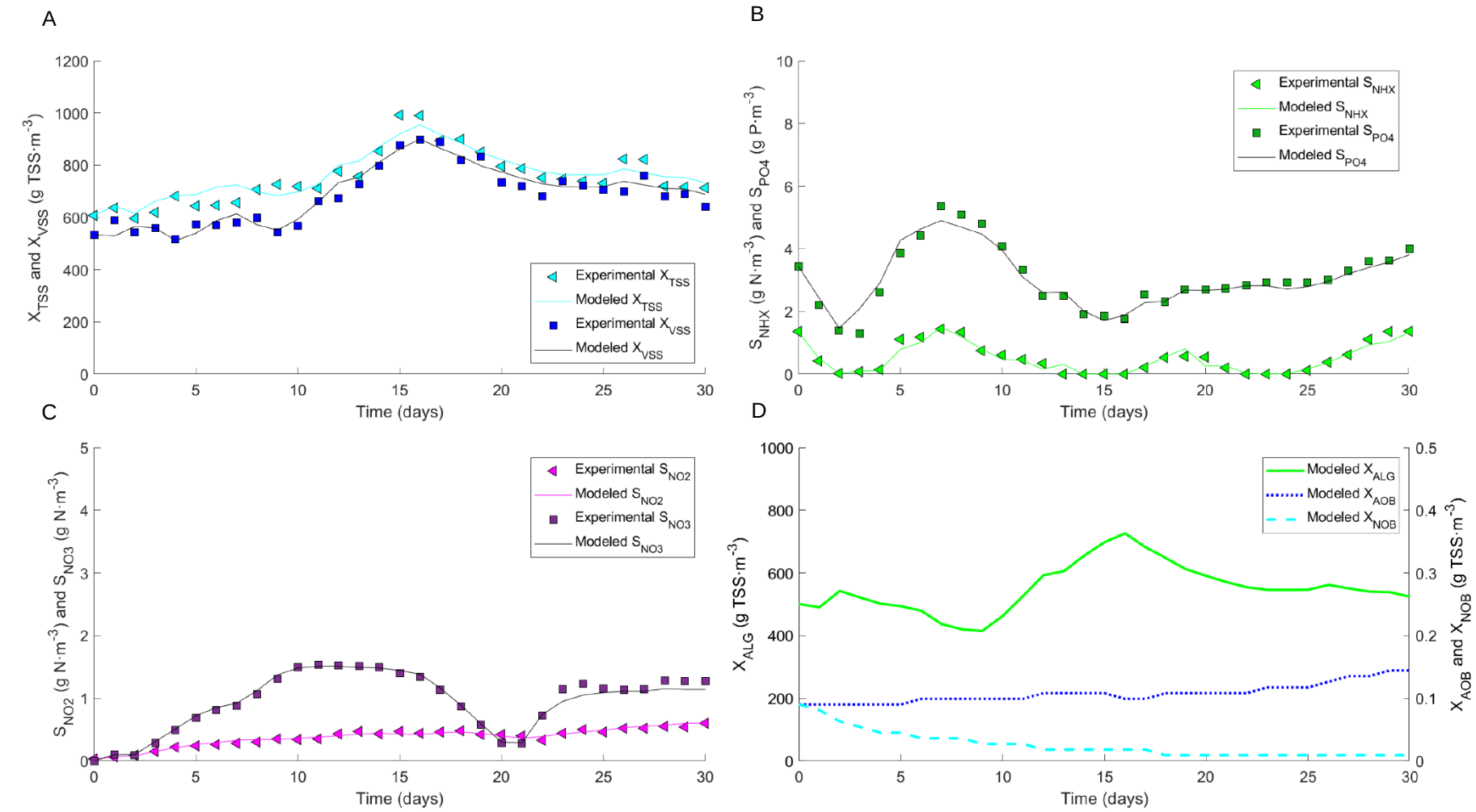

Figure X. 5. Dynamic simulation of period P_Microalgae. Evolution of: (A) X_{TSS} and X_{VSS} (g TSS·m^{-3}), (B) S_{NHX} (g N·m^{-3}) and S_{PO4} (g P·m^{-3}), (C) S_{NO2} and S_{NO3} (g N·m^{-3}), and (D) X_{ALG}, X_{AOB} and X_{NOB} (gTSS·m^{-3}).

10.5.1.4. Overall model performance

More than 500 pairs of data were evaluated, which resulted in an average R^2 coefficient of 0.9902, highlighting the capability of the proposed microalgae-bacteria model for assessing microalga and nitrifying bacteria interactions. The t-test was used to compare the means of the experimental and simulated data: the experimental data mean was 317.7 and for the modeled data was 323.3. This test also constructs confidence intervals, or confidence limits, for each mean and the differences between means. The confidence interval of the difference between the means, which extends from 30.12 to 58.73, is of particular interest, given that it resulted in a value of zero, indicating no significant difference between the means of the two data samples, with a confidence level of 95.0%. The t-test can also be used to evaluate specific hypotheses on the difference between the means of the experimental and simulated data. The test was constructed to determine whether the difference between the two means is equal to zero, versus the alternate hypothesis that the difference is not equal to zero. Since the calculated P-value of 0.8214 is not less than 0.05, the null hypothesis cannot be rejected, which specifies that the means of both data sets are statistically equal.

These results assume that the variances of the two samples are equal. In this case, this assumption seems reasonable based on the F-test results, since the standard deviation obtained for the experimental and modeled data were 443.3 and 451.8, respectively. The F-test also constructs confidence intervals or confidence limits for each standard deviation and for the ratio of variances. The confidence interval for the variance ratio is of interest, which ranges from 0.9624 to 1.5071. Since the interval has the value of one, there is no statistically significant difference between the standard deviations of the experimental and modeled data at a 95.0% confidence level.

Similarly to the T-test, an F-test can also be run to evaluate a specific hypothesis on the SD of the populations from which the two samples are drawn. In this case, the test was constructed to determine whether the SD ratio was equal to 1.0, versus the alternative hypothesis by which the ratio was not equal to 1.0. Since the calculated P-value (0.6208)

was not less than 0.05, the null hypothesis cannot be rejected, which means that the means of both data sets are statistically equal.

Finally, a Mann-Whitney U-test was run to compare the medians of two samples, combining the two samples with the data from smallest to largest and comparing the average rankings of the two samples in the combined data. The median for the experimental data was 7.38 and for the simulated data 9.87. Since the p-value was 0.8653, there was no statistically significant difference between the medians, at 95.0%.

10.5.2. Case study

According to the results presented in previous sections (Section 10.5.1, and Chapters 5 and 6), microalgae activity can be negatively affected by nitrifying bacteria activity; especially when AOB and NOB activities are uncoupled and nitrite accumulates in the culture. In Chapter 6, different nitrification control strategies were proposed. Therefore, the implementation of these strategies has been analyzed. To this aim, the results of the baseline scenarios for the model validation have been compared to the model results from varying BRT, dilution rate, and nitrogen speciation.

Period P_AOB was used to evaluate the effect of BRT on microalgae-bacteria culture. BRT was increased from 2.0 ± 0.3 to 4.5 days to favor microalgae growth (Chapter 7). Longer BRT results in increased concentrations for both NOB and AOB, increasing from 2.15 to 4.75 g $TSS \cdot m^{-3}$ and from 12.19 to 17.20 g $TSS \cdot m^{-3}$ (Figure X. A), respectively. The biomass ratio for AOB to NOB was 5.7 and 3.6 for 2 and 4.5 days of BRT, respectively. Yao and Peng (2017) also observed that the abundance of AOB was higher than NOB in active sludge samples. Theoretically, AOB/NOB ratio in a balanced nitrifying system should be 2/1 according to thermodynamics and electron transfer (Winkler et al., 2012). Therefore, AOB should be the dominant bacteria in a nitrifying community. The biomass ratio AOB/NOB obtained by You et al. (2003) was in the range of 2.0-3.5 for an efficient coupled nitrification process. The AOB/NOB ratio at 2 days BRT from this chapter is higher than the one observed by Winkler et al. (2012), Yao and Peng (2017)

and You et al. (2003), leading to NO_2-N accumulation and microalgae inhibition. Increasing BRT resulted in an AOB/NOB ratio of 3.6, which is much closer to the ratio found by You et al. (2003).

The combined effect of increasing BRT and ahieving non-NO_2-N accumulating situations (Figure X. B) results in enhanced microalgae growth and X_{VSS} model ouput (Figure X. C). Microalgae biomass increased from 113 to 1378 g TSS·m^{-3} at 2 and 4.5 days of BRT, respectively. The increase in microalgae concentration in the system also increased phosphorus removal rate (P-RR) from 0.87 to 2.37 g P·m^{-3}·d^{-1}, resulting in an effluent concentration of 2.00 and 0.19 g P·m^{-3} at 2 and 4.5 days of BRT, respectively, at the end of the period simulated. Nitrogen removal rate (NRR) also increased from 8.75 to 15.61 g N·m^{-3}·d^{-1}, resulting in an effluent concentration of 21.53 and 29.65 g N·m^{-3} at 2 and 4.5 days BRT, respectively. Nutrient removal rate was in the range of the values reported by González-Camejo et al. (2020), thus it is assumed that the removal efficiency of microalgae was not overestimated by the model.

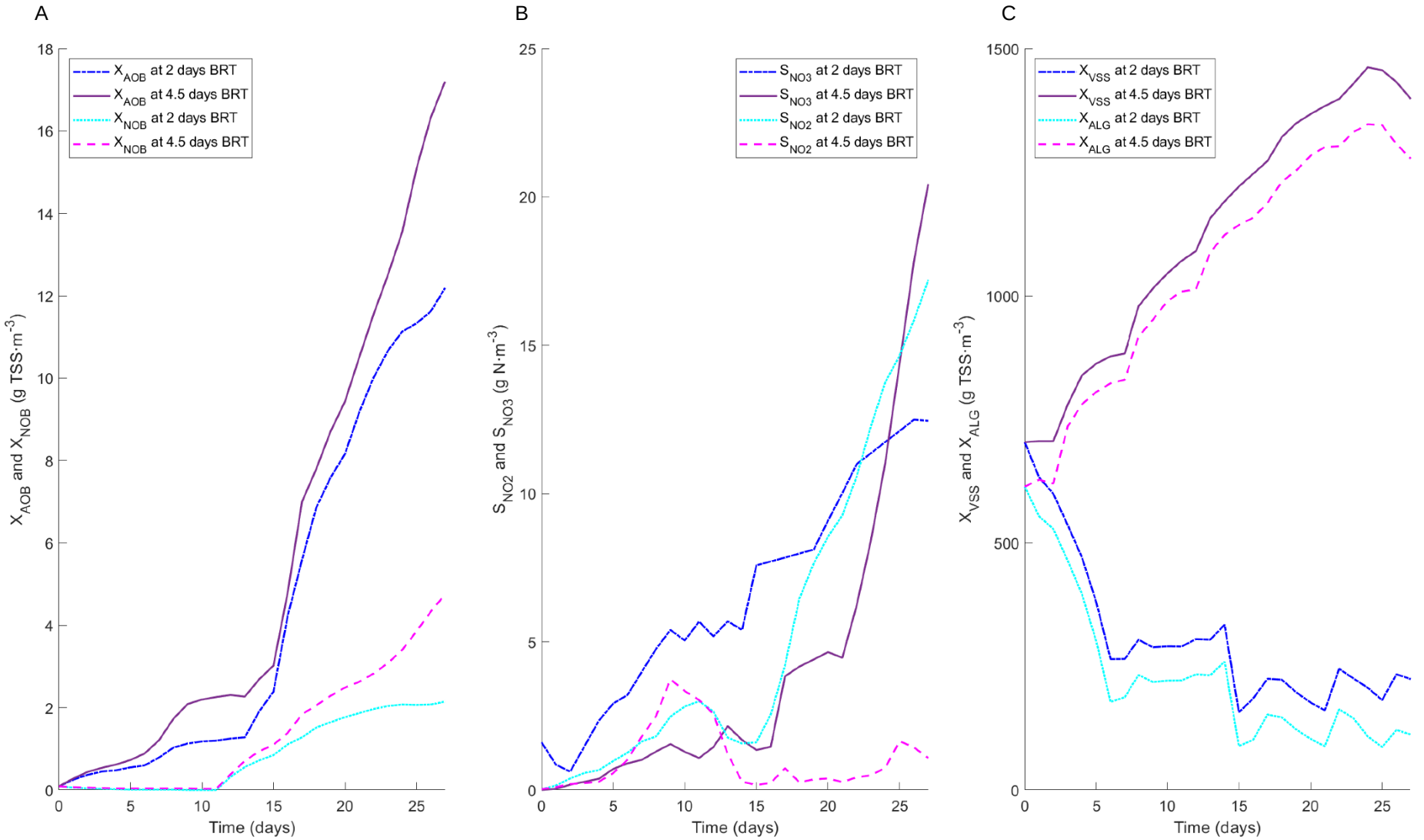

Figure X. 6. Dynamic simulation of period P_AOB at 2 and 4.5 days of BRT. Evolution of: (A) X_{AOB} and X_{NOB} (g TSS·m^{-3}), (B) S_{NO2} and S_{NO3} (g N·m^{-3}), and (C) X_{VSS} and X_{ALG} (gTSS·m^{-3}).

The second nitrification control strategy may consist in increasing the dilution rate from 0.21 to 0.85 $days^{-1}$. In this study, the dilution rate change was performed at mid-term (day 19) to compare the growth of biomass. Figure X. shows the modelling results from applying this strategy. Concentration of particulate components decreases significantly due to the punctual increase of dilution rate, resulting in an increase in average light intensity within PBR and microalgae growth. More lighting-conditions for phototrophic organisms (from 14.39 to 29.77 $\mu mol \cdot m^{-2} \cdot s\text{-}1$) provokes that microalgae outcompete AOB. Indeed, the final concentration of AOB is reduced from 13.80 to 2.14 g $TSS \cdot m^{-3}$ after changing the dilution rate. NOB concentration is also decreased from 8.40 to 0.80 g $TSS \cdot m^{-3}$ (see Figure X. A). Nitrification is therefore reduced, resulting in S_{NO2} and S_{NO3} effluent concentrations of 1.39 and 4.65 g $N \cdot m^{-3}$, respectively, in contrast to the S_{NO3} concentration of 23.60 g $N \cdot m^{-3}$ obtained for the baseline scenario working at constant dilution rate (Figure X. 7B). Increasing the dilution rate appears as a useful nitrification control strategy not only to reduce nitrifying activity but also to increase microalgal biomass. The model simulates a final X_{VSS} concentration of 1315 g $TSS \cdot m^{-3}$, mainly consisting of microalgal biomass (76% of TSS) (Figure X. 7C). This concentration was higher than the one achieved in the baseline scenario (913 g $TSS \cdot m^{-3}$).

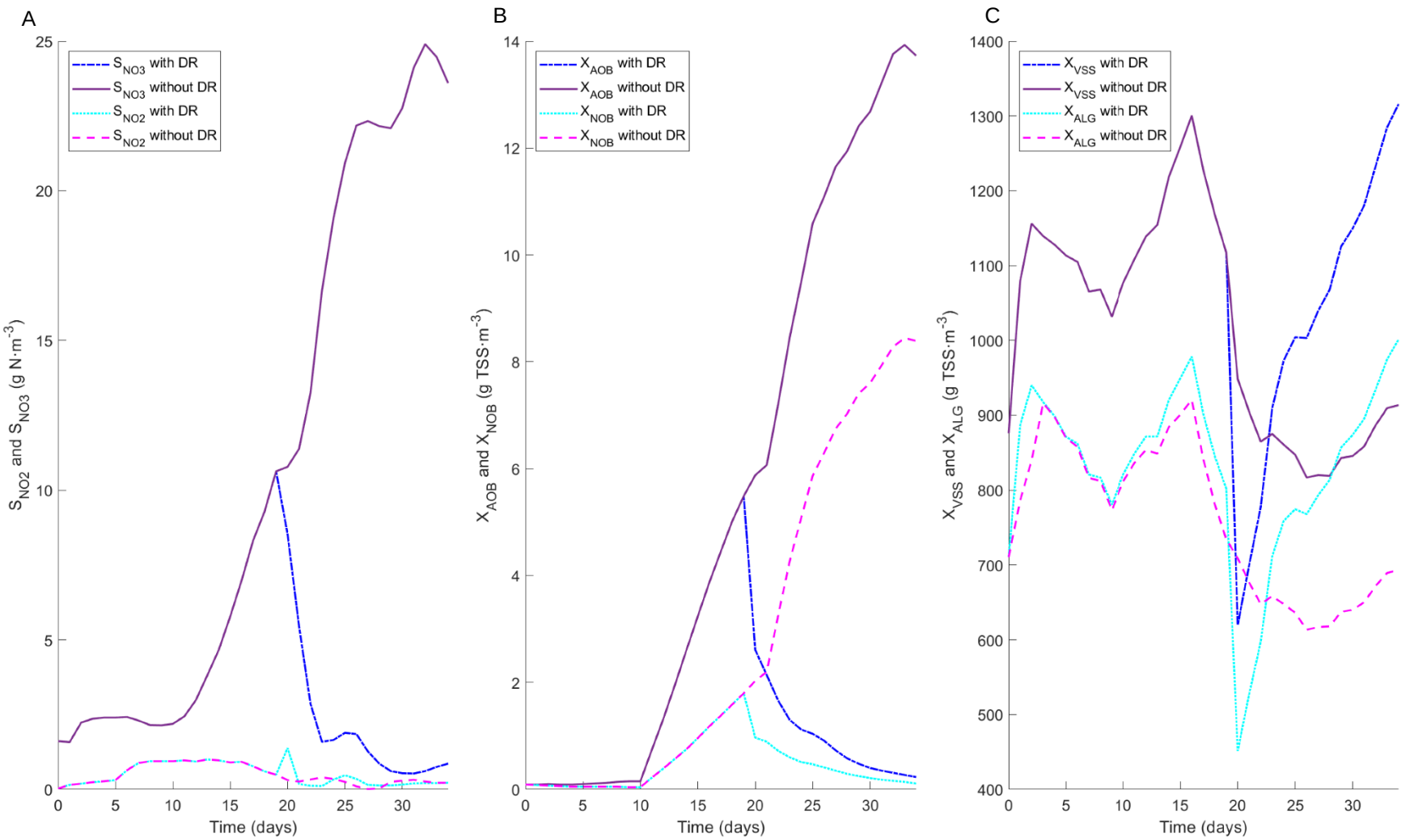

Figure X. 7. Dynamic simulation of period P_NOB with and without modifying the dilution rate. Evolution of: (A) S_{NO2} and S_{NO3} (g N·m^{-3}), (B) X_{AOB} and X_{NOB} (g TSS·m^{-3}) and (C) X_{VSS} and X_{ALG} (gTSS·m^{-3}).

The third simulation was performed to analyze microalgae growth with a simulated secondary effluent i.e. a wastewater stream with negligible concentrations of NH_4-N and COD. The NH_4-N preference by microalgae is reflected in Figure X. . Concentration of VSS, and microalgae biomass is reduced compared to simulated results using NH_4-N as the main nitrogen source.

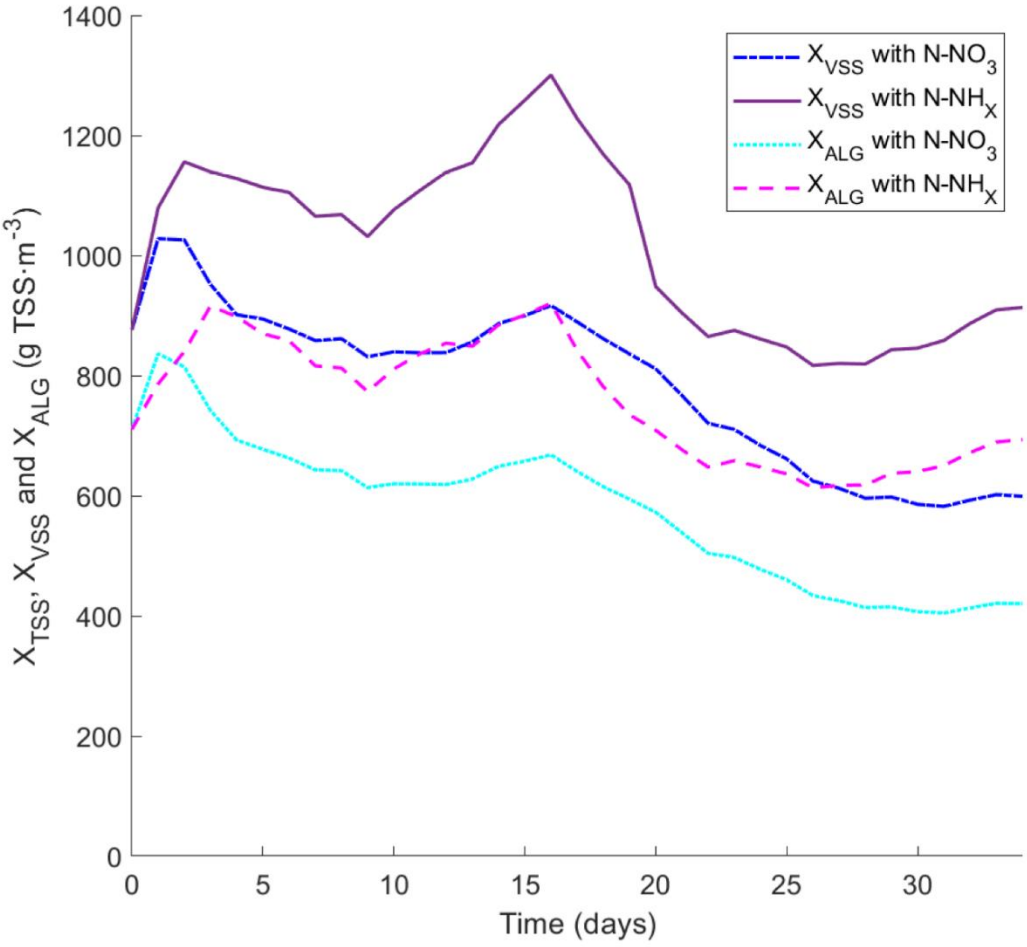

Figure X. 8. Dynamic simulation of X_{VSS} and X_{ALG} using S_{NHX} or S_{NO3} as nitrogen source.

10.5.3. Future research prospects

In this Chapter, the microalgae-bacteria model has been validated at controlled temperature, pH, and dissolved oxygen concentration, since it has been applied to model a MPBR pilot plant operating at controlled conditions. In addition, the low biodegradable organic content in the influent did not promote heterotrophic bacteria growth. Thus, only interactions between nitrifying bacteria and microalgae have been evaluated (the first analysis scenario). In this respect, a comprehensive study is needed in a more complex culture system, in which temperature, pH, and dissolved oxygen concentration fluctuate depending on environmental conditions and microbial activity.

10.6. CONCLUSIONS

The model was validated using data from three operating periods in a pilot-scale MPBR plant. Despite the dynamics on operating conditions and ecological structure developed in the MPBR plant, the model was able to reproduce process performance and effluent quality (no statistically significant differences were found between the model and the experimental results). Nitrite inhibition kinetics obtained in Chapter 6 were successfully validated and it was confirmed that nitrite had a negative impact on microalgae growth. In addition, through the simulation of different periods, it was observed that the nitrite accumulation in the system could be explained without adding the NOB photoinhibition. The developed model has demonstrated to be a useful tool to infer the relative proportion of microalgae and bacteria. The model was also applied to investigate the nitrification control strategies proposed in Chapter 7. Increasing biomass retention time from 2 to 4.5 days and increasing the dilution rate from 0.21 to 0.85 $days^{-1}$ promote microalgae growth. Nitrate as nitrogen source decreases microalgae concentration as expected due to the model structure. Future research will evaluate the model performance under variations in temperature, pH, and dissolved oxygen concentration, as well as including heterotrophic bacterial growth from organic matter oxidation.

REFERENCES

Acién, F.G., Gómez-Serrano, C., Morales-Amaral, M.M., Fernández-Sevilla, J.M., Molina-Grima, E., 2016. Wastewater treatment using microalgae: how realistic a contribution might it be to significant urban wastewater treatment? Appl. Microbiol. Biotechnol. 2016 10021 100, 9013–9022. https://doi.org/10.1007/S00253-016-7835-7

Acién Fernández, F.G., Gómez-Serrano, C., Fernández-Sevilla, J.M., 2018. Recovery of Nutrients From Wastewaters Using Microalgae. Front. Sustain. Food Syst. 2, 59. https://doi.org/10.3389/FSUFS.2018.00059/BIBTEX

Aparicio, S., García, R.S., Seco, A., Ferrer, J., Falomir, L.B., Robles, Á., 2022a. Global sensitivity and uncertainty analysis of a microalgae model for wastewater treatment. Sci. Total Environ. 806, 150504. https://doi.org/10.1016/J.SCITOTENV.2021.150504

Aparicio, S., Robles, Á., Ferrer, J., Seco, A., Borrás Falomir, L., 2022b. Assessing and modeling nitrite inhibition in microalgae-bacteria consortia for wastewater treatment by means of photo-respirometric and chlorophyll fluorescence techniques. Sci. Total Environ. 808, 152128. https://doi.org/10.1016/J.SCITOTENV.2021.152128

APHA, AWWA, WEF, 2005. Standard Methods for the Examination of Water and Wastewater, 21st ed, American Public Health Association. Washington, DC.

Bankston, E., Wang, Q., Higgins, B.T., 2020. Algae support populations of heterotrophic, nitrifying, and phosphate-accumulating bacteria in the treatment of poultry litter anaerobic digestate. Chem. Eng. J. 2020, Vol. 398, Page 125550 398, 125550. https://doi.org/10.1016/J.CEJ.2020.125550

Barat, R., Montoya, T., Seco, A., Ferrer, J., 2011. Modelling biological and chemically induced precipitation of calcium phosphate in enhanced biological phosphorus removal systems. Water Res. 45, 3744–3752. https://doi.org/10.1016/j.watres.2011.04.028

Barat, R., Serralta, J., Ruano, M. V., Jiménez, E., Ribes, J., Seco, A., Ferrer, J., 2013. Biological Nutrient Removal Model No. 2 (BNRM2): a general model for wastewater treatment plants. Water Sci. Technol. 67, 1481–1489. https://doi.org/10.2166/WST.2013.004

Barbera, E., Bertucco, A., Kumar, S., 2018. Nutrients recovery and recycling in algae processing for biofuels production. Renew. Sustain. Energy Rev. https://doi.org/10.1016/j.rser.2018.03.004

Casagli, F., Zuccaro, G., Bernard, O., Steyer, J.P., Ficara, E., 2021. ALBA: A comprehensive growth model to optimize algae-bacteria wastewater treatment in raceway ponds. Water Res. 190, 116734. https://doi.org/10.1016/J.WATRES.2020.116734

Eustance, E., Gardner, R.D., Moll, K.M., Menicucci, J., Gerlach, R., Peyton, B.M., 2013. Growth, nitrogen utilization and biodiesel potential for two chlorophytes grown on ammonium, nitrate or urea. J. Appl. Phycol. 25, 1663–1677. https://doi.org/10.1007/s10811-013-0008-5

Eze, V.C., Velasquez-Orta, S.B., Hernández-García, A., Monje-Ramírez, I., Orta-Ledesma, M.T., 2018. Kinetic modelling of microalgae cultivation for wastewater treatment and carbon dioxide sequestration. Algal Res. 32, 131–141. https://doi.org/10.1016/j.algal.2018.03.015

Foley, J., de Haas, D., Hartley, K., Lant, P., 2010. Comprehensive life cycle inventories of alternative wastewater treatment systems. Water Res. 44, 1654–1666. https://doi.org/10.1016/j.watres.2009.11.031

García, D., Posadas, E., Blanco, S., Acién, G., García-Encina, P., Bolado, S., Muñoz, R., 2018. Evaluation of the dynamics of microalgae population structure and process performance during piggery wastewater treatment in algal-bacterial photobioreactors. Bioresour. Technol. 248, 120–126.

https://doi.org/10.1016/j.biortech.2017.06.079

González-Camejo, J., Aparicio, S., Jiménez-Benítez, A., Pachés, M., Ruano, M. V, Borrás, L., Barat, R., Seco, A., 2020. Improving membrane photobioreactor performance by reducing light path: operating conditions and key performance indicators. Water Res. 172. https://doi.org/10.1016/j.watres.2020.115518

González-Camejo, J., Aparicio, S., Ruano, M. V., Borrás, L., Barat, R., Ferrer, J., 2019a. Effect of ambient temperature variations on an indigenous microalgae-nitrifying bacteria culture dominated by Chlorella. Bioresour. Technol. 290, 121788. https://doi.org/10.1016/j.biortech.2019.121788

González-Camejo, J., Jiménez-Benítez, A., Ruano, M. V., Robles, A., Barat, R., Ferrer, J., 2019b. Optimising an outdoor membrane photobioreactor for tertiary sewage treatment. J. Environ. Manage. 245, 76–85. https://doi.org/10.1016/j.jenvman.2019.05.010

Jiménez, E., Giménez, J.B., Ruano, M. V., Ferrer, J., Serralta, J., 2011. Effect of pH and nitrite concentration on nitrite oxidation rate. Bioresour. Technol. 102, 8741–8747. https://doi.org/10.1016/j.biortech.2011.07.092

Karya, N.G.A.I., van der Steen, N.P., Lens, P.N.L., 2013. Photo-oxygenation to support nitrification in an algal–bacterial consortium treating artificial wastewater. Bioresour. Technol. 134, 244–250. https://doi.org/10.1016/J.BIORTECH.2013.02.005

Oswald, A.W.J., Gotaas, H.B., Golueke, C.G., Kellen, W.R., Gloyna, E.F., Sewage, S., Wastes, I., Apr, N., Oswald, J., Kellen, R., 1957. Algae in Waste Treatment [with Discussion] All use subject to JSTOR Terms and Conditions IN WASTE. Sewage Ind. Waste. 29, 437–457.

Oswald, W.J., 1988. Micro-algae and wastewater treatment. Microalgal Biotechnol. 305–328.

Pang, N., Gu, X., Chen, S., Kirchhoff, H., Lei, H., Roje, S., 2019. Exploiting mixotrophy for improving productivities of biomass and co-products of microalgae. Renew. Sustain. Energy Rev. 112, 450–460. https://doi.org/10.1016/J.RSER.2019.06.001

Perez-Garcia, O., Escalante, F.M.E., de-Bashan, L.E., Bashan, Y., 2011. Heterotrophic cultures of microalgae: Metabolism and potential products. Water Res. 45, 11–36. https://doi.org/10.1016/J.WATRES.2010.08.037

Powell, N., Shilton, A., Chisti, Y., Pratt, S., 2009. Towards a luxury uptake process via microalgae - Defining the polyphosphate dynamics. https://doi.org/10.1016/j.watres.2009.06.011

Reichert, P., Borchardt, D., Henze, M., Rauch, W., Shanahan, P., Somlyódy, L., Vanrolleghem, P., 2001. River Water Quality Model no. 1 (RWQM1): II. Biochemical process equations, in: Water Science and Technology. pp. 11–30. https://doi.org/10.2166/wst.2001.0241

Reynolds, C.S., 2006. The ecology of phytoplankton, The Ecology of Phytoplankton. Cambridge University Press, Cambridge. https://doi.org/10.1017/CBO9780511542145

Ruiz-Martinez, A., Serralta, J., Pachés, M., Seco, A., Ferrer, J., 2014. Mixed microalgae culture for ammonium removal in the absence of phosphorus: Effect of phosphorus supplementation and process modeling. Process Biochem. 49, 2249–2257. https://doi.org/10.1016/j.procbio.2014.09.002

Ruiz-Martínez, A., Serralta, J., Romero, I., Seco, A., Ferrer, J., 2015. Effect of intracellular P content on phosphate removal in Scenedesmus sp. Experimental study and kinetic expression. Bioresour. Technol. 175, 325–332. https://doi.org/10.1016/j.biortech.2014.10.081

Ruiz, J., Arbib, Z., Álvarez-Díaz, P.D., Garrido-Pérez, C., Barragán, J., Perales, J.A., 2013. Photobiotreatment model (PhBT): A kinetic model for microalgae biomass growth and nutrient removal in wastewater. Environ. Technol. (United Kingdom). https://doi.org/10.1080/09593330.2012.724451

Sánchez-Zurano, A., Cárdenas, J.A.G., Serrano, C.G., Amaral, M.M., Acién-fernández, F.G., Sevilla, J.M.F., Grima, E.M., 2020. Year-long assessment of a pilot-scale thin-layer reactor for microalgae wastewater treatment . Variation in the microalgae-bacteria consortium and the impact of environmental conditions. Algal Res. 50, 101983. https://doi.org/10.1016/j.algal.2020.101983

Sánchez-Zurano, A., Rodríguez-miranda, E., Guzmán, J.L., Acién-fernández, F.G., Fernández-sevilla, J.M., Grima, E.M., 2021. Abaco: A new model of microalgae-bacteria consortia for biological treatment of wastewaters. Appl. Sci. 11, 1–24. https://doi.org/10.3390/app11030998

Seco, A., Aparicio, S., González-Camejo, J., Jiménez-Benítez, A., Mateo, O., Mora, J.F., Noriega-Hevia, G., Sanchis-Perucho, P., Serna-García, R., Zamorano-López, N., Giménez, J.B., Ruiz-Martínez, A., Aguado, D., Barat, R., Borrás, L., Bouzas, A., Martí, N., Pachés, M., Ribes, J., Robles, A., Ruano, M. V., Serralta, J., Ferrer, J., 2018. Resource recovery from sulphate-rich sewage through an innovative anaerobic-based water resource recovery facility (WRRF). Water Sci. Technol. 78, 1925–1936. https://doi.org/10.2166/wst.2018.492

Shandilya, K.K., Pattarkine, V.M., 2019. Using microalgae for treating wastewater, in: Advances in Feedstock Conversion Technologies for Alternative Fuels and Bioproducts: New Technologies, Challenges and Opportunities. Woodhead Publishing, pp. 119–136. https://doi.org/10.1016/B978-0-12-817937-6.00007-2

Shoener, B.D., Schramm, S.M., Béline, F., Bernard, O., Martínez, C., Plósz, B.G., Snowling, S., Steyer, J.P., Valverde-Pérez, B., Wágner, D., Guest, J.S., 2019. Microalgae and cyanobacteria modeling in water resource recovery facilities: A critical review. Water Res. X 2, 100024. https://doi.org/10.1016/j.wroa.2018.100024

Siegrist, H., Renggli, D., Gujer, W., 1993. Mathematical modelling of anaerobic mesophilic sewage sludge treatment, in: Water Science and Technology. pp. 25–36. https://doi.org/10.2166/wst.1993.0070

Solimeno, A., Gómez-Serrano, C., Acién, F.G., 2019. BIO_ALGAE 2: improved model of microalgae and bacteria consortia for wastewater treatment. Environ. Sci. Pollut. Res. 2019 2625 26, 25855–25868. https://doi.org/10.1007/S11356-019-05824-5

Solimeno, A., Samsó, R., Uggetti, E., Sialve, B., Steyer, J.P., Gabarró, A., García, J., 2015. New mechanistic model to simulate microalgae growth. Algal Res. https://doi.org/10.1016/j.algal.2015.09.008

Steele, J.H., 1965. Notes on some theoretical problems in production ecology. Goldman, C. R. (ed.), Prim. Product. Aquat. Environ. (Mem. Ist. Ital. Idrobiol., 18 Suppl.) 383–398.

Sun, Y., Huang, Y., Liao, Q., Fu, Q., Zhu, X., 2016. Enhancement of microalgae production by embedding hollow light guides to a flat-plate photobioreactor. Bioresour. Technol. 207, 31–38. https://doi.org/10.1016/j.biortech.2016.01.136

Sydney, E.B., Sturm, W., de Carvalho, J.C., Thomaz-Soccol, V., Larroche, C., Pandey, A., Soccol, C.R., 2010. Potential carbon dioxide fixation by industrially important microalgae. Bioresour. Technol. 101, 5892–5896. https://doi.org/10.1016/j.biortech.2010.02.088

Van Den Hende, S., Beelen, V., Julien, L., Lefoulon, A., Vanhoucke, T., Coolsaet, C., Sonnenholzner, S., Vervaeren, H., Rousseau, D.P.L., 2016. Technical potential of microalgal bacterial floc raceway ponds treating food-industry effluents while producing microalgal bacterial biomass: An outdoor pilot-scale study. Bioresour. Technol. 218, 969–979. https://doi.org/10.1016/J.BIORTECH.2016.07.065

Viruela, A., Aparicio, S., Robles, Á., Falomir, L.B., Serralta, J., Seco, A., Ferrer, J., 2021. Kinetic modeling of autotrophic microalgae mainline processes for sewage treatment in phosphorus-replete and -deplete culture conditions. Sci. Total Environ. 149165. https://doi.org/10.1016/J.SCITOTENV.2021.149165

Wágner, D.S., Valverde-Pérez, B., Sæbø, M., Bregua de la Sotilla, M., Van Wagenen, J., Smets, B.F., Plósz,

B.G., 2016. Towards a consensus-based biokinetic model for green microalgae – The ASM-A. Water Res. 103, 485–499. https://doi.org/10.1016/j.watres.2016.07.026

Winkler, M.K.H., Bassin, J.P., Kleerebezem, R., Sorokin, D.Y., Van Loosdrecht, M.C.M., 2012. Unravelling the reasons for disproportion in the ratio of AOB and NOB in aerobic granular sludge. Appl. Microbiol. Biotechnol. 94, 1657–1666. https://doi.org/10.1007/S00253-012-4126-9/FIGURES/6

Xu, K., Zou, X., Xue, Y., Qu, Y., Li, Y., 2021. The impact of seasonal variations about temperature and photoperiod on the treatment of municipal wastewater by algae-bacteria system in lab-scale. Algal Res. 54, 102175. https://doi.org/10.1016/J.ALGAL.2020.102175

Yao, Q., Peng, D.C., 2017. Nitrite oxidizing bacteria (NOB) dominating in nitrifying community in full-scale biological nutrient removal wastewater treatment plants. AMB Express 7, 1–11. https://doi.org/10.1186/S13568-017-0328-Y/FIGURES/5

You, S.J., Hsu, C.L., Chuang, S.H., Ouyang, C.F., 2003. Nitrification efficiency and nitrifying bacteria abundance in combined AS-RBC and A2O systems. Water Res. 37, 2281–2290. https://doi.org/10.1016/S0043-1354(02)00636-X

SUPPLEMENTARY DATA FOR CHAPTER IX

Table X. S 1. Values for the kinetic and physical parameters considered in the model.

Parameters	Description	Value	Unit	Source
μ_{ALG}	Maximum growth rate of X_{ALG}	1.5	d^{-1}	(Aparicio et al., 2022a)
$b_{ALG,1}$	Maximum inactivation rate of X_{ALG}	0.1	d^{-1}	(Reichert et al., 2001)
$b_{ALG,2}$	Maximum decay rate of X_{ALG}	0.15	d^{-1}	(Aparicio et al., 2022a)
q_{XPP}	Rate constant for storage of $X_{PP\text{-}ALG}$	0.01	d^{-1}	(Aparicio et al., 2022a)
K_{O2}	Half saturation parameter for S_{O2}	0.2	g O_2 m^{-3}	(Reichert et al., 2001)
$S_{O2,MAX}$	Maximum amount of dissolved oxygen for X_{ALG} growth	32	g O_2 m^{-3}	(Sánchez-Zurano et al., 2021)
m	Intrinsic model parameter	4.15	-	(Sánchez-Zurano et al., 2021)
$K_{Ig,C}$	Half saturation parameter for $S_{Ig,C}$	$4.32 \cdot 10^{-3}$	g C m^{-3}	(Solimeno et al., 2015)
K_{NHX}	Half saturation parameter for S_{NHX} in a phosphorus-replete medium	0.1	g N m^{-3}	(Aparicio et al., 2022a)
$K_{NHX\text{-}qXPP}$	Half saturation parameter for S_{NHX} in a phosphorus-deplete medium	3	g N m^{-3}	(Aparicio et al., 2022a)
K_{NO3}	Half saturation parameter for S_{NO3}	12.61	g N m^{-3}	(Wágner et al., 2016)
η_{NO3}	Reduction factor for X_{ALG} growth of S_{NO3}	0.59	–	(Eze et al., 2018)
K_{PO4}	Half saturation parameter for S_{PO4}	0.05	g P m^{-3}	(Aparicio et al., 2022a)
$K_{I,PO4}$	Inhibition parameter for $X_{PP\text{-}ALG}$ use in a phosphorus-replete medium	0.15	g P m^{-3}	(Aparicio et al., 2022a)
K_{XPP}	Half saturation parameter of X_{ALG} growth for $X_{PP\text{-}ALG}$	0.0027	g P m^{-3}	(Ruiz-Martinez et al., 2014)
K_{XPP_qXPP}	Half saturation parameter of X_{PP} storage for $X_{PP\text{-}ALG}$	0.003	g P m^{-3}	(Ruiz-Martínez et al., 2015)
n_{XPP}	Regulation coefficient or Hill number for X_{PP} storage	0.006	–	(Ruiz-Martínez et al., 2015)
K_{Mg}	Half saturation parameter for S_{Mg}	0.13	g Mg m^{-3}	(Sydney et al., 2010)
K_K	Half saturation parameter for S_K	8.78	g K m^{-3}	(Sydney et al., 2010)
T_{MIN}	Minimum temperature for X_{ALG} growth	2	°C	(Aparicio et al., 2022a)
T_{MAX}	Maximum temperature for X_{ALG} growth	40	°C	(Aparicio et al., 2022a)
b	Intrinsic model parameter	87.13	–	(Aparicio et al., 2022a)
c	Intrinsic model parameter	1.46	–	(Aparicio et al., 2022a)
I_{OPT}	Optimal light intensity for X_{ALG} growth	230	µmol m^{-2} s^{-1}	(Aparicio et al., 2022a)
k_w	Attenuation coefficient due to water	1.97	m^{-3}	(Sun et al., 2016)
K_I	Attenuation coefficient	0.025	m^2 g TSS^{-1}	(Aparicio et al., 2022a)
$K_{I,H}$	Lower half saturation parameter for S_H	0.00001	mol H^+ L^{-1}	(Siegrist et al., 1993)
$K_{S,H}$	Upper half saturation parameter for S_H	0.00063	mol H^+ L^{-1}	(Siegrist et al., 1993)

Table X. S 1. Continued.

Parameters	Description	Value	Unit	Source
$S_{H,opt}$	Optimal pH for X_{ALG} growth	7.50	pH	(Aparicio et al., 2022a)
$K_{La,O2}$	Mass transfer coefficient for oxygen	16.2	h^{-1}	(Aparicio et al., 2022a)
$K_{La,CO2}$	Mass transfer coefficient for dioxide carbon	16.2	h^{-1}	(Aparicio et al., 2022a)
$K_{La,NH3}$	Mass transfer coefficient for free ammonia	16.2	h^{-1}	(Aparicio et al., 2022a)
$K_{La,N2}$	Mass transfer coefficient for nitrogen	16.2	h^{-1}	(Aparicio et al., 2022a)
S_{CO2atm}	Saturation parameter for CO_2	0.23	g CO_2 m^3	(Barat et al., 2013)
S_{O2atm}	Saturation parameter for O_2	0.01	g O_2 m^3	(Barat et al., 2013)
S_{N2atm}	Saturation parameter for N_2	14.61	g N_2 m^3	(Barat et al., 2013)
S_{NH3atm}	Saturation parameter for NH_3	0.01	g NH_3 m^3	(Barat et al., 2013)
k	Constants of mass transfer coefficient equation	0.05	-	(Aparicio et al., 2022a)
r	Constants of mass transfer coefficient equation	1	-	(Aparicio et al., 2022a)
$K_{I,NO2}$	Nitrite value associated to 50% algae growth reduction	23.7	g N m^{-3}	(Aparicio et al., 2022b)
n	Regulation coefficient or Hill number for nitrite inhibition	1.82	-	(Aparicio et al., 2022b)
$q_{HET,XS}$	Maximum specific hydrolysis rate	3	d^{-1}	(Barat et al., 2013)
$K_{O,HET}$	Half saturation parameter for S_{O2}	0.2	g COD m^{-3}	(Barat et al., 2013)
K_X	Half saturation parameter for X_S	0.1	g X_S g X_H^{-1}	(Barat et al., 2013)
$K_{SpH,HET}$	Upper half saturation parameter for S_H	9.698970004	pH	(Barat et al., 2013)
$K_{IpH,HET}$	Lower half saturation parameter for S_H	5.361510743	pH	(Barat et al., 2013)
$\eta_{\mu H,Ax}$	Reduction factor for Anoxic hydrolysis rate of X_{HET}	0.6	-	(Barat et al., 2013)
$\eta_{\mu H,An}$	Reduction factor for anaerobic hydrolysis rate of X_{HET}	0.1	-	(Barat et al., 2013)
$K_{NO2,HET}$	Half saturation parameter for S_{NO2}	0.5	g N m^{-3}	(Barat et al., 2013)
$K_{NO3,HET}$	Half saturation parameter for S_{NO3}	0.5	g N m^{-3}	(Barat et al., 2013)
$\mu_{H,Max}$	Maximum growth rate	6	d^{-1}	(Barat et al., 2013)
$K_{NHx,HET}$	Half saturation parameter for S_{NHx}	0.05	g N m^{-3}	(Barat et al., 2013)
$K_{PO4,HET}$	Half saturation parameter for S_{PO4}	0.01	g P m^{-3}	(Barat et al., 2013)
$\eta_{\mu H,Ax3}$	Reduction factor for Anoxic endogenous respiration of S_{NO3}	0.4	-	(Barat et al., 2013)
$\eta_{\mu H,Ax2}$	Reduction factor for anaerobic endogenous respiration of S_{NO2}	0.4	-	(Barat et al., 2013)

Table X. S 1. Continued.

Parameters	Description	Value	Unit	Source
b_{HET}	Decay rate	0.4	d^{-1}	(Barat et al., 2013)
$K_{PO4,HET}$	Half saturation parameter for S_{PO4}	0.01	g P m^{-3}	(Barat et al., 2013)
$\mu_{AOB,Max}$	Maximum growth rate	1	d^{-1}	(Barat et al., 2013)
$K_{O,AOB}$	Half saturation parameter for S_{O2}	0.52	g COD m^{-3}	(Barat et al., 2013)
$K_{NHx,AOB}$	Half saturation parameter for S_{NH3}	0.54	g N m^{-3}	(Barat et al., 2013)
$K_{PO4,AOB}$	Half saturation parameter for S_{PO4}	0.01	g P m^{-3}	(Barat et al., 2013)
$K_{HNO2,AOB}$	Half saturation parameter for S_{HNO2}	0.013	g N m^{-3}	(Barat et al., 2013)
$K_{IpH,AOB}$	Upper half saturation parameter for S_H	5.522878745	pH	(Barat et al., 2013)
$K_{SpH,AOB}$	Lower half saturation parameter for S_H	9.15490196	pH	(Barat et al., 2013)
b_{AOB}	Decay rate	0.15	d^{-1}	(Barat et al., 2013)
$\mu_{NOB,Max}$	Maximum growth rate	0.5	d^{-1}	(Barat et al., 2013)
$K_{O,NOB}$	Half saturation parameter for S_{O2}	0.67	g COD m^{-3}	(Barat et al., 2013)
$K_{NO2,NOB}$	Half saturation parameter for S_{NO2}	0.26	g N m^{-3}	(Barat et al., 2013)
$K_{NHx,NOB}$	Half saturation parameter for S_{NHx}	0.01	g N m^{-3}	(Barat et al., 2013)
$K_{PO4,NOB}$	Half saturation parameter for S_{PO4}	0.01	g P m^{-3}	(Barat et al., 2013)
$K_{HNO2,NOB}$	Half saturation parameter for S_{HNO2}	1000	g N m^{-3}	(Barat et al., 2013)
$A_{H,NOB}$	Constant in the logarithmic equation for S_H	6.9	-	(Barat et al., 2013)
$K_{S,pHNOB}$	Constant in the logarithmic equation for S_H	6.903089987	pH	(Barat et al., 2013)
b_{NOB}	Decay rate	0.075	d^{-1}	(Barat et al., 2013)
Y_d	Activity coefficient for the specie	0.5	-	(Barat et al., 2013)
Y_t	Activity coefficient for the specie	0.5	-	(Barat et al., 2013)
Y_m	Activity coefficient for the specie	0.5	-	(Barat et al., 2013)
$q_{ACP,p}$	Rate constant for precipitation	6.00E+08	l mol^{-1} d^{-1}	(Barat et al., 2013)
$K_{I,ACP}$	Half saturation parameter for X_{ACP}/X_{TSS} ratio	6.00E-10	X_{ACP} X_{TSS}^{-1}	(Barat et al., 2013)
$K_{ACP,SP}$	Parameter in the precipitate equation	1.00E-26	$(mol\ l^{-1})^5$	(Barat et al., 2013)
$q_{ACP,d}$	Rate constant for redissolution	2.00E+08	l mol^{-1} d^{-1}	(Barat et al., 2013)
$K_{S,ACP}$	Half saturation parameter for X_{ACP}	2.00E-04	X_{ACP} (kmol ACP m^{-3})	(Barat et al., 2013)
$q_{Str,p}$	Rate constant for precipitation	6.00E+08	l mol^{-1} d^{-1}	(Barat et al., 2013)
$K_{I,Str}$	Half saturation parameter for X_{Str}/X_{TSS} ratio	6.00E-10	X_{Str} X_{TSS}^{-1}	(Barat et al., 2013)
$K_{Str,SP}$	Parameter in the precipitate equation	3.98E-27	$(mol\ l^{-1})^2$	(Barat et al., 2013)
$q_{Str,d}$	Rate constant for redissolution	2.00E+08	l mol^{-1} d^{-1}	(Barat et al., 2013)

Table X. S 1. Continued.

Parameters	Description	Value	Unit	Source
$K_{S,Str}$	Half saturation parameter for X_{Str}	2.00E-04	X_{Str} (kmol Str m^{-3})	(Barat et al., 2013)
$q_{MAP,p}$	Rate constant for precipitation	6.00E+08	l^2 mol^{-2} d^{-1}	(Barat et al., 2013)
$K_{I,MAP}$	Half saturation parameter for X_{MAP}/X_{TSS} ratio	6.00E-10	X_{MAP} X_{TSS}^{-1}	(Barat et al., 2013)
$K_{MAP,SP}$	Parameter in the precipitate equation	5.50E-14	$(mol\ l^{-1})^3$	(Barat et al., 2013)
$q_{MAP,d}$	Rate constant for redissolution	2.00E+08	l^2 mol^{-2} d^{-1}	(Barat et al., 2013)
$K_{S,MAP}$	Half saturation parameter for X_{MAP}	2.00E-04	X_{MAP} (kmol MAP m^{-3})	(Barat et al., 2013)
$q_{New,p}$	Rate constant for precipitation	6.00E+08	l mol^{-1} d^{-1}	(Barat et al., 2013)
$K_{I,New}$	Half saturation parameter for X_{New}/X_{TSS} ratio	6.00E-10	X_{New} X_{TSS}^{-1}	(Barat et al., 2013)
$K_{New,SP}$	Parameter in the precipitate equation	1.59E-06	$(mol\ l^{-1})^2$	(Barat et al., 2013)
$q_{New,d}$	Rate constant for redissolution	2.00E+08	l mol^{-1} d^{-1}	(Barat et al., 2013)
$K_{S,New}$	Half saturation parameter for X_{New}	2.00E-04	X_{New} (kmol New m^{-3})	(Barat et al., 2013)
$q_{Viv,p}$	Rate constant for precipitation	6.00E+08	l mol^{-1} d^{-1}	(Barat et al., 2013)
$K_{I,Viv}$	Half saturation parameter for X_{Viv}/X_{TSS} ratio	6.00E-10	X_{Viv} X_{TSS}^{-1}	(Barat et al., 2013)
$K_{Viv,SP}$	Parameter in the precipitate equation	1.00E-36	$(mol\ l^{-1})^5$	(Barat et al., 2013)
$q_{Viv,d}$	Rate constant for redissolution	2.00E+08	l mol^{-1} d^{-1}	(Barat et al., 2013)
$K_{S,Viv}$	Half saturation parameter for X_{Viv}	2.00E-04	X_{Viv} (kmol Viv m^{-3})	(Barat et al., 2013)
$q_{Var,p}$	Rate constant for precipitation	6.00E+08	l mol^{-1} d^{-1}	(Barat et al., 2013)
$K_{I,Var}$	Half saturation parameter for X_{Var}/X_{TSS} ratio	6.00E-10	X_{Var} X_{TSS}^{-1}	(Barat et al., 2013)
$K_{Var,SP}$	Parameter in the precipitate equation	1.00E-21	$(mol\ l^{-1})^2$	(Barat et al., 2013)
$q_{Var,d}$	Rate constant for redissolution	2.00E+08	l mol^{-1} d^{-1}	(Barat et al., 2013)
$K_{S,Var}$	Half saturation parameter for X_{Var}	2.00E-04	X_{Var} (kmol Var m^{-3})	(Barat et al., 2013)
$q_{Cal,p}$	Rate constant for precipitation	6.00E+08	l mol^{-1} d^{-1}	(Barat et al., 2013)
$K_{I,Cal}$	Half saturation parameter for X_{Cal}/X_{TSS} ratio	6.00E-10	X_{Cal} X_{TSS}^{-1}	(Barat et al., 2013)
$K_{Cal,SP}$	Parameter in the precipitate equation	3.31E-09	$(mol\ l^{-1})^2$	(Barat et al., 2013)
$q_{Cal,d}$	Rate constant for redissolution	2.00E+08	l mol^{-1} d^{-1}	(Barat et al., 2013)
$K_{S,Cal}$	Half saturation parameter for X_{Cal}	2.00E-04	X_{Cal} (kmol Cal.m^{-3})	(Barat et al., 2013)

Table X. S 1. Continued.

Parameters	Description	Value	Unit	Source
q_{HAP}	Rate constant for precipitation	2.00E-03	d^{-1}	(Barat et al., 2013)
$K_{S,HAP}$	Half saturation parameter for X_{HAP}	5.00E-04	X_{ACP} (kmol ACPm^{-3})	(Barat et al., 2013)
$K_{S,PO4}$	Half saturation parameter for S_{PO4e}	0.01	S_{PO4e} (mol/l)	(Barat et al., 2013)
$K_{S,Ca}$	Half saturation parameter for S_{Cae}	0.03	S_{Cae} (mol/l)	(Barat et al., 2013)

Table X. S 2. Values for conversion factors for conservation equation.

Parameters	Description	Value	Unit	Source
$i_{N,ALG}$	Fraction of nitrogen in microalgae	0.060	g N g COD^{-1}	Calculated from Oswald (1988)
$i_{P,ALG}$	Fraction of phosphorus in microalgae	0.0016	g P g COD^{-1}	(Ruiz-Martínez et al., 2015)
$i_{C,ALG}$	Fraction of carbon in microalgae	0.3372	g C g COD^{-1}	Calculated from Oswald (1988)
$i_{TSS,ALG}$	Fraction of total suspended solids in microalgae	0.646	g TSS g COD^{-1}	Calculated from Oswald (1988)
$i_{N,XI}$	Fraction of nitrogen in X_I	0.01	g N g COD^{-1}	(Aparicio et al., 2022a)
$i_{P,XI}$	Fraction of phosphorus in X_I	0.005	g P g COD^{-1}	(Aparicio et al., 2022a)
$i_{C,XI}$	Fraction of carbon in X_I	0.025	g C g COD^{-1}	(Aparicio et al., 2022a)
$i_{TSS,XI}$	Fraction of total suspended solids in X_I	0.60	g TSS g COD^{-1}	(Aparicio et al., 2022a)
$i_{Mg,XPP-ALG}$	Fraction of magnesium in X_{PP-ALG}	0.26	g Mg g P^{-1}	Calculated from $(K_{0.34}Mg_{0.33}PO_3)n$
$i_{K,XPP-ALG}$	Fraction of potassium in X_{PP-ALG}	0.42	g K g P^{-1}	Calculated from $(K_{0.34}Mg_{0.33}PO_3)n$
$i_{TSS,XPP-ALG}$	Fraction of total suspended solids in X_{PP-ALG}	3.23	g TSS g P^{-1}	Calculated from $(K_{0.34}Mg_{0.33}PO_3)n$
$i_{N,SS}$	Fraction of nitrogen in S_S	0.01	g N g COD^{-1}	(Aparicio et al., 2022a)
$i_{P,SS}$	Fraction of phosphorus in S_S	0.001	g P g COD^{-1}	(Aparicio et al., 2022a)
$i_{C,SS}$	Fraction of carbon in S_S	0.025	g C g COD^{-1}	(Aparicio et al., 2022a)
$i_{N,SI}$	Fraction of nitrogen in S_I	0.001	g N g COD^{-1}	(Aparicio et al., 2022a)
$i_{P,SI}$	Fraction of phosphorus in S_I	0.001	g P g COD^{-1}	(Aparicio et al., 2022a)
$i_{C,SI}$	Fraction of carbon in S_I	0.03	g C g COD^{-1}	(Aparicio et al., 2022a)
F_{XI}	Fraction of X_I generated biomass decay	0.1	g COD g COD^{-1}	(Barat et al., 2013)
F_{SI}	Fraction of S_I generated biomass decay	0.6	g C g COD^{-1}	(Aparicio et al., 2022a)

Table X. S 2. Continued.

Parameters	Description	Value	Unit	Source
$i_{Al,Bio}$	Al content of biomass	0.0000	g Al g COD^{-1}	(Barat et al., 2013)
$i_{Al,SS}$	Al content of S_F	0.0000	g Al g COD^{-1}	(Barat et al., 2013)
$i_{Al,SI}$	Al content of S_U	0.0000	g Al g COD^{-1}	(Barat et al., 2013)
$i_{Al,XS}$	Al content of X_S	0.0000	g Al g COD^{-1}	(Barat et al., 2013)
$i_{Al,XI}$	Al content of X_U	0.0000	g Al g COD^{-1}	(Barat et al., 2013)
$i_{Ca,Bio}$	Ca content of biomass	0.0035	g Ca g COD^{-1}	(Barat et al., 2013)
$i_{Ca,SS}$	Ca content of S_S	0.0000	g Ca g COD^{-1}	(Barat et al., 2013)
$i_{Ca,SI}$	Ca content of S_I	0.0000	g Ca g COD^{-1}	(Barat et al., 2013)
$i_{Ca,XS}$	Ca content of X_S	0.0000	g Ca g COD^{-1}	(Barat et al., 2013)
$i_{Ca,XI}$	Ca content of X_I	0.0000	g Ca g COD^{-1}	(Barat et al., 2013)
$I_{C,Bio}$	C content of biomass	0.0310	mol C g COD^{-1}	(Barat et al., 2013)
$i_{C,SS}$	C content of S_S	0.0250	mol C g COD^{-1}	(Barat et al., 2013)
$i_{C,SI}$	C content of S_I	0.0300	mol C g COD^{-1}	(Barat et al., 2013)
$i_{C,XS}$	C content of X_S	0.0250	mol C g COD^{-1}	(Barat et al., 2013)
$i_{C,XI}$	C content of X_I	0.0300	mol C g COD^{-1}	(Barat et al., 2013)
$i_{Fe,Bio}$	Fe content of biomass	0.0000	g Fe g COD^{-1}	(Barat et al., 2013)
$i_{Fe,SS}$	Fe content of S_S	0.0000	g Fe g COD^{-1}	(Barat et al., 2013)
$i_{K,SS}$	K content of S_S	0.0008	g K g COD^{-1}	(Barat et al., 2013)
$i_{K,SI}$	K content of S_I	0.0008	g K g COD^{-1}	(Barat et al., 2013)
$i_{K,XS}$	K content of X_S	0.0008	g K g COD^{-1}	(Barat et al., 2013)
$i_{K,XI}$	K content of X_I	0.0008	g K g COD^{-1}	(Barat et al., 2013)
$i_{K,SS}$	K content of S_S	0.0008	g K g COD^{-1}	(Barat et al., 2013)
$i_{Mg,Bio}$	Mg content of biomass	0.0015	g Mg g COD^{-1}	(Barat et al., 2013)
$i_{Mg,SS}$	Mg content of S_S	0.0015	g Mg g COD^{-1}	(Barat et al., 2013)
$i_{Mg,SI}$	Mg content of S_I	0.0015	g Mg g COD^{-1}	(Barat et al., 2013)
$i_{Mg,XS}$	Mg content of X_S	0.0015	g Mg g COD^{-1}	(Barat et al., 2013)
$i_{Mg,Bio}$	Mg content of biomass	0.0015	g Mg g COD^{-1}	(Barat et al., 2013)
$i_{TSS,Bio}$	TSS content of biomass	0.9000	g TSS g COD^{-1}	(Barat et al., 2013)
$i_{TSS,XS}$	TSS content of X_S	0.7500	g TSS g COD^{-1}	(Barat et al., 2013)
$i_{TSS,XI}$	TSS content of X_I	0.7500	g TSS g COD^{-1}	(Barat et al., 2013)

Table X. S 2. Continued.

Parameters	Description	Value	Unit	Source
Y_{AOB}	Yield for X_{AOB} growth	0.170	g X_{AOB} g N^{-1}	(Barat et al., 2013)
Y_{NOB}	Yield for X_{NOB} growth	0.070	g X_{NOB} g N^{-1}	(Barat et al., 2013)
Y_{HET}	Yield for X_{HET} growth	0.630	g X_{HET} g COD^{-1}	(Barat et al., 2013)
$Y_{HET,Ax2}$	Yield for X_{HET} growth (Anoxic)	0.479	g X_{HET} g COD^{-1}	(Barat et al., 2013)
$Y_{HET,Ax3}$	Yield for X_{HET} growth (Anaerobic)	0.479	g X_{HET} g COD^{-1}	(Barat et al., 2013)
Y_{NOB}	Yield for X_{NOB} growth	0.070	g X_{NOB} g N^{-1}	(Barat et al., 2013)

EQUATIONS

Equation X. S 1

$$X_{TSS} = X_{ALG} \cdot i_{TSS,ALG} + X_{HET} \cdot i_{TSS,B} + X_{AOB} \cdot i_{TSS,B} + X_{NOB} \cdot i_{TSS,B} + X_I \cdot i_{TSS,XI} + X_S \cdot i_{TSS,XS} + X_{PP,ALG} \cdot i_{TSS,XPP,ALG} + TSS_{PREC}$$

where X_{TSS} is the total suspended solids concentration (g TSS·m^{-3}), X_{ALG} is the microalgae biomass (g COD·m^{-3}), X_I is the inert particulate organic matter (g COD·m^{-3}), X_S is the slowly biodegradable particulate organic matter (g COD·m^{-3}), X_{HET} is the heterotrophic bacteria biomass (g COD·m^{-3}), X_{AOB} is the AOB bacteria biomass (g COD·m^{-3}), X_{NOB} is the NOB bacteria biomass (g COD·m^{-3}), $X_{PP,ALG}$ is polyphosphates stored by X_{ALG} (g P·m^{-3}), TSS_{PREC} is the total suspended solids content of precipitates (g TSS·m^{-3}) and $i_{TSS,ALG}$ (g TSS·g COD^{-1}), $i_{TSS,XI}$ (g TSS·g COD^{-1}), $i_{TSS,XS}$ (g TSS·g COD^{-1}), $i_{TSS,XPP,ALG}$ (g TSS·g P^{-1}) and $i_{TSS,BIO}$ (g TSS·g COD^{-1}) are total suspended solids content in X_{ALG}, X_I, X_S, $X_{PP,ALG}$ and in bacteria biomass, respectively.

Equation X. S 2

$$X_P = X_{PP-ALG} + X_{ALG} \cdot i_{P,ALG} + X_I \cdot i_{P,XI} + X_S \cdot i_{P,XS} + X_{HET} \cdot i_{P,XBIO} + X_{AOB} \cdot i_{P,XBIO} + X_{NOB} \cdot i_{P,BIO} + P_{PREC}$$

where X_P is the total suspended phosphorus concentration (g P·m^{-3}), $X_{PP,ALG}$ is polyphosphates stored by X_{ALG} (g P·m^{-3}), X_{ALG} is the microalgae biomass (g COD·m^{-3}), X_I is the inert particulate organic matter (g COD·m^{-3}), X_S is the slowly biodegradable particulate organic matter (g COD·m^{-3}), X_{HET} is the heterotrophic bacteria biomass (g COD·m^{-3}), X_{AOB} is the AOB bacteria biomass (g COD·m^{-3}), X_{NOB} is the NOB bacteria biomass (g COD·m^{-3}), P_{REC} is the phosphorus content of precipitates (g P·m^{-3}) and $i_{P,ALG}$ (g P·g COD^{-1}), $i_{P,XI}$ (g P g COD^{-1}), $i_{P,XS}$ (g P g COD^{-1}), and $i_{P,BIO}$ (g P g COD^{-1}) are phosphorus content in X_{ALG}, X_I, X_S and in bacteria biomass, respectively.

REFERENCES OF SUPPLEMENTARY DATA

Aparicio, S., García, R.S., Seco, A., Ferrer, J., Falomir, L.B., Robles, Á., 2022a. Global sensitivity and uncertainty analysis of a microalgae model for wastewater treatment. Sci. Total Environ. 806, 150504. https://doi.org/10.1016/J.SCITOTENV.2021.150504

Aparicio, S., Robles, Á., Ferrer, J., Seco, A., Borrás Falomir, L., 2022b. Assessing and modeling nitrite inhibition in microalgae-bacteria consortia for wastewater treatment by means of photo-respirometric and chlorophyll fluorescence techniques. Sci. Total Environ. 808, 152128. https://doi.org/10.1016/J.SCITOTENV.2021.152128

Barat, R., Serralta, J., Ruano, M. V., Jiménez, E., Ribes, J., Seco, A., Ferrer, J., 2013. Biological Nutrient Removal Model No. 2 (BNRM2): a general model for wastewater treatment plants. Water Sci. Technol. 67, 1481–1489.

Ruiz-Martínez, A., Serralta, J., Romero, I., Seco, A., Ferrer, J., 2015. Effect of intracellular P content on phosphate removal in Scenedesmus sp. Experimental study and kinetic expression. Bioresour. Technol. 175, 325–332. https://doi.org/10.1016/j.biortech.2014.10.081

Sánchez-Zurano, A., Rodríguez-miranda, E., Guzmán, J.L., Acién-fernández, F.G., Fernández-sevilla, J.M., Grima, E.M., 2021. Abaco: A new model of microalgae-bacteria consortia for biological treatment of wastewaters. Appl. Sci. 11, 1–24. https://doi.org/10.3390/app11030998

CHAPTER XI

11. Overall discussion

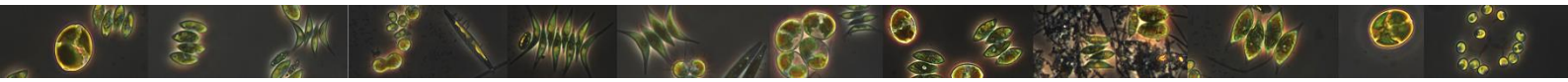

11. OVERALL DISCUSSION

This research work aimed at deepening the understanding of the urban wastewater treatment based on microalgae-bacteria consortia. The initial hypothesis of this work stated that urban wastewater treatment systems employing microalgae-bacteria consortia have the potential to remove wastewater pollutants and enhance nutrient removal efficiency. The knowledge of the effects of operational and environmental parameters on the biological consortium and the ecological interactions between both communities could highly improve system operation and performance. For this purpose, urban wastewater treatment using microalgae-bacteria consortia was studied from different approaches and scientific areas, including biochemical engineering, ecology, microbiology and mathematical modeling.

11.1. Overview

The core of this dissertation is based on the analysis of the main interactions between microalgae and bacteria and the pathways of wastewater pollutant removal. The study of how feasible is the treatment process based on microalgae and bacteria appears as the first step to better address this work. An outdoor membrane high rate algal pond (MHRAP) pilot plant was assessed and operated at fixed 6-days biomass retention time (BRT) and a variable hydraulic retention time (HRT) using two urban wastewater streams (Chapter 5). Negative interactions, such as amensalism and competition processes between microalgae and nitrifying bacteria, were detected through the optimization of the system. Nitrite inhibition of photosynthesis (amensalism interaction) has already been reported by González-Camejo et al. (2020) and has been also observed in Chapter 5. Nitrite inhibition mechanism in photosynthesis was assessed and modeled in Chapter 6. Microalgal activity was measured by *Chlorophyll a* (*Chl a*) fluorescence and photo-respirometric analysis, obtaining the inhibition constant (Chapter 10). Since nitrifying bacteria can outcompete microalgae for nitrogen source and the metabolic product of ammonium-oxidizing bacteria (AOB) reduce photosynthetic efficiency, a manual to

identify and reduce these negative interactions was developed in Chapter 7. In addition, microbial community of this outdoor MHRAP pilot plant has been explored in Chapter 8. This chapter is a good example of how molecular ecology studies can be integrated during the development of technical solutions for microalgae-bacteria systems for wastewater treatment. Indeed, different biostatistical analyses have been implemented in the analysis of microbial communities, including principal coordinates analysis and ANOVA test). In this way, the effect of certain operational parameters such as, HRT, chemical and biological oxygen demand (COD and BOD, respectively) load rates, light intensity, temperature has been determined and analyzed. All the information obtained from Chapter 5 to Chapter 8 was exploited and used to develop an integrated microalgae-bacteria mechanistic model and to evaluate the sensitivity and uncertainty of the integrated model outputs in Chapters 9 and 10. Chapter 9 was focused on identify the most influential parameters and uncertainty sources in microalgae kinetic expressions. Once calibrated the most influential parameters, microalgae-bacteria model was validated with data from an outdoor membrane photobioreactor (MPBR) pilot plant fed with effluent from an anaerobic membrane bioreactor (AnMBR) plant.

11.2. Can microalgae-bacteria consortia effectively remove wastewater pollutants? Assessing urban wastewater treatment using microalgae and bacteria at different hydraulic retention times and using different wastewater streams

Microalgae-bacteria consortia application to wastewater can play a major role in WRRFs due to ecological relationships and synergic effects between microalgae and bacteria (Morillas-España et al., 2021; Robles et al., 2020). Self-sustaining oxygen-carbon dioxide gas exchange constitutes the basis of the main mutualistic relationship between microalgae and aerobic heterotrophic bacteria. Photosynthesis can also support nitrification process and enhance free ammonia nitrogen (FAN) stripping and

phosphorus precipitation. Nutrient and BOD removal mechanism resulted from biological interaction between microalgae and bacteria communities. Equilibrium between both algae and bacteria communities is highly affected by environmental parameters (light intensity, temperature, etc.), which cannot be controlled in outdoor systems. The operating parameters are therefore the key tool to achieve a biological system that can effectively remove COD, nitrogen and phosphorus from wastewater. By establishing an operating HRT, requirements of nitrogen, phosphorus and light can be identified to support desirable biological communities. The HRAP pilot plant, located in the wastewater treatment plant (WWTP) “Cuenca del Carraixet”, was fed with effluents from primary settling and from pre-treatment and operated at different HRTs in Chapter 5. Wastewater treatment systems performance was assessed by pollutant removal efficiencies. Activities of microalgae and the indigenous wastewater bacteria (heterotrophic and nitrifying bacteria) were also determined.

11.2.1. Effluent from primary settling

In the experimental set performed with primary settling effluent, MHRAP pilot plant was operated at 6, 4 and 2 days HRT. The biological community achieved using primary settled incoming wastewater was not able to remove nitrogen and phosphorus, regardless the operating HRT. Although nitrifying bacteria activity was less than 10%, the equilibrium among microorganisms reached was fully dominated by these autotrophic bacteria, in the three operating HRTs studied.

Abiotic boundary conditions reached at operating 6 days HRT favored AOB activity over nitrite-oxidizing bacteria (NOB). The difference between nitritation and nitratation activity was barely 3%. According to Philips et al. (2002), this small margin is enough to promote significant nitrite (NO_2-N) accumulation. Partial nitrification accounted for 48 ± 3% of ammonium removal efficiency (NH_4-N-RE), resulting in a nitrite NO_2-N accumulation of 21 ± 3 g $N \cdot m^{-3}$. NO_2-N can be highly toxic, not only to microalgae (González-Camejo et

al., 2020) but also to a wide range of bacteria, such as AOB and NOB (Philips et al., 2002).

Photosynthesis efficiency (measured as oxygen production) was lower at 6 days HRT compared with 4 and 2 days HRT (17 ± 2, 32 ± 4 and 31 ± 4 mg O_2·g VSS^{-1}·h^{-1}, respectively). NO_2-N accumulation along with high pH, limited dissolved inorganic carbon (DIC) concentration and competition with AOB for NH_4-N can inhibit photosynthetic activity and nutrient assimilation. Indeed, total nitrogen and phosphorus removal efficiencies (TN-RE and TP-RE, respectively) by biomass assimilation were 1.7 ± 0.6 and 5.2 ± 0.9%, respectively. Value of pH increased during daylight hours, reaching values near 9 (8.7 ± 0.3) due to DIC uptake via photosynthesis. Consequently, FAN stripping accounted for 25 ± 4% of T_N-RE, being the main nitrogen removal mechanism. Abiotic boundary conditions also provided phosphorus precipitation, which was the main phosphorus removal pathway, accounting for 20% of total phosphorous removed. Permeate total nitrogen and phosphorus concentrations were 32 ± 3 g N m^{-3} and 2.2 ± 0.8 g P m^{-3}, respectively, therefore the effluent obtained in the experimental period of 6 days HRT did not met European Union (EU) nutrient discharge limits.

Partial-nitrification was avoided and complete oxidation of NH_4-N to NO_3-N was achieved at 4 and 2 days HRT. Reducing HRT from 6 to 4 and 2 days increased significantlly the oxygen uptake rate of AOB and NOB (OUR_{AOB} and OUR_{NOB}, respectively). OUR_{AOB} increased from 1.12 ± 0.09 to 1.7 ± 0.6 and 1.5 ± 0.5 mg O_2·g VSS^{-1}·h^{-1} at 6, 4 and 2 days HRT, respectively. OUR_{NOB} was 0.6 ± 0.2, 1.1 ± 0.2 and 1.0 ± 0.2 mg O_2·g VSS^{-1}·h^{-1} at 6, 4 and 2 days HRT, respectively. This slight increase in NOB activity, avoided NO_2-N accumulation. Indeed, NH_4-N-RE were higher than 98% in both operating HRTs and NO_2-N concentrations were 1.1 ± 0.7 and 1.6 ± 0.5 g N·m^{-3}, respectively. However, TN-RE barely reached 5%, since FAN stripping was reduced due to culture pH, which dropped to 7.4 ± 0.2 and 7.3 ± 0.3 in experimental periods operated at 4 and 2 days respectively. Since phosphorus precipitation was not promoted by high pH, phosphorus

removal also deteriorate: TP-REs were 1.07 ± 0.02 and 1.6 ± 0.4 % for 4 and 2 days HRT. Again, nutrient concentration in the final permeate were far above the EU discharge limit in experimental periods operated at 4 and 2 days HRT.

The COD removal efficiencies (COD-REs) at 6, 4 and 2 days HRT were, respectively, 89 ± 10, 88 ± 6 and 86 ± 9%. Final COD permeate concentrations in all HRT studied were lower than 125 g $O_2 \cdot m^{-3}$, which is the maximum concentration of COD established for wastewater discharge into the environment according to the EU Directive 98/15/CEE. However, the analysis of COD concentration in supernatant of a 0.45 µm membrane filter and in the permeate from membrane tank (MT) module showed that MT removed a significant portion of COD. COD-REs using a 0.45 µm membrane filter at 6, 4 and 2 days HRT were, respectively, 59 ± 15, 64 ± 11 and 58 ± 13%. COD-REs differences between filtration systems indicated that the mixed liquor in MHRAP reactor contained a significant portion of colloidal and particulate COD, which was effectively retained by the 0.03 µm hollow fiber membrane.

11.2.2. Effluent from pre-treatment

Experimental period operated at 4 days HRT with pre-treatment effluent showed similar results to those obtained using primary settling effluent at 4 and 2 days HRT.

Reducing HRT from 4 to 2 days did not promote nutrients uptake by biomass and nitrification was the main NH_4-N removal pathway. Nitrification activity did not showed differences between working at 2 and 4 days HRT (3 ± 0.2 and 2.5 ± 0.4 mg O_2 $g \cdot VSS^{-1} \cdot h^{-1}$, respectively), indicating that nitrification potential was largely unaffected by HRT operation in the range of 4-2 days under these abiotic boundary conditions. The photosynthetic activity at 2 days HRT (58 ± 10 mg O_2 $g \cdot VSS^{-1} \cdot h^{-1}$) was comparable to that in culture produced using agricultural leachate wastes, considered a good microalgae substrate (Sánchez-Zurano et al., 2020). Phosphorus removal was increased by the assimilation capacity of biomass. N/P uptake ratio was 11.7 ± 1.4 (on a mass basis), which is similar to N/P ratio reported by Gardner-Dale et al. (2017) and Reynolds

(2006). The decrease in HRT from 4 to 2 days and thus the increase in BOD load (from 73 ± 6 to 145 ± 10 $g \cdot m^{-3} \cdot d^{-1}$) resulted in a shift from aerobic to anoxic conditions during daylight hours and nighttime, respectively. Under these conditions, the coupled nitrification-denitrification process was the main nitrogen removal mechanism and accounted for 87% of total nitrogen removal. Nitrogen assimilation by biomass was a minor removal mechanism. Microalgae role was therefore, to support nitrification during daytime.

Overall, the decrease in the HRT from 2 to 1 days increased heterotrophic activity (from 3.0 ± 0.6 to 5.1 ± 0.2 mg O_2 $g \cdot VSS^{-1} \cdot h^{-1}$, respectively) due to BOD loading (from 145 ± 10 to 290 ± 30 $g \cdot m^{-3} \cdot d^{-1}$). Nitrogen removal by nitrification represented less than 5% due to zero DO concentration that prevailed throughout day. Growth of heterotrophic bacteria increased total suspended solids (TSS) concentration and reduced the maximum average light intensity, photolimiting microalgae photosynthesis (1.2 ± 0.8 mg O_2 $g \cdot VSS^{-1} \cdot h^{-1}$). The OPR_{NET} of biomass was not able to match O_2 demand by hetetrotrophic (5.1 ± 0.2 mg O_2 $g \cdot VSS^{-1} \cdot h^{-1}$) and nitrifyng bacteria (1.1 ± 0.4 mg O_2 $g \cdot VSS^{-1} \cdot h^{-1}$), suggesting a shift in ecological community structure to heterotrophic bacteria at 1 day HRT. TN-RE and TP-RE were 1.12 ± 0.7 and 0.70 ± 0.13 %, respectively.

The average COD-REQ was 96 ± 1.4 %, regardless of HRT due to filtration process by MT module.

Feeding the reactor with pre-treatment effluent and operating at 2 days HRT were the only operating conditions studied that met the COD, nitrogen and phosphorus discharge limits in accordance with European Directive 98/15/EEC. Since the main nitrogen removal mechanism was de coupled nitrification-denitrification process, it is recommended to determine the operational conditions that promote aerobic conditions at daytime and anoxic conditions at night.

11.3. Assessing and modeling nitrite inhibition in microalgae-bacteria consortia for wastewater treatment by means of photo-respirometric and chlorophyll fluorescence techniques.

In Chapter 5, it was observed that photosynthesis activity could be negatively affected by inhibitory abiotic conditions, including NO_2-N accumulation. González-Camejo et al. (2020) reported that an NO_2-N concentrations ranging from 5 to 20 g $N \cdot m^{-3}$ inhibits microalgae metabolism in terms of biomass productivity and nutrient removal. Chapter 6 of this work focuses on determining the mechanism of NO_2-N inhibition due to the scientific evidence that suggests that nitrite is a toxic component for microalgal photochemistry. The inhibition was assessed combining photo-respirometric tests with *Chlorophyll a* (*Chl a*) fluorescence measures (Rossi et al., 2018; Sánchez-Zurano et al., 2020; Strasser et al., 2004).

Exposure to NO_2-N produced a partial inhibition of the primary photosynthetic process mainly due to hindrance of the electron transport chain. Under non-stress conditions, i.e. no NO_2-N accumulation, the excitation energy obtained from light is absorbed by the reaction center (RC) of PS II, (P_{680}). The excited P_{680} is oxidized by releasing an electron which is transported across the membrane to the first electron acceptor, Q_A. Then the electron passes to the second acceptor, Q_B, and finally reduces plastoquinone (PQ) to PQH_2. Electrons passing through the electron transport chain loose energy that is used to pump H^+ ions by complex Cytochrome b6f. These concentrated ions store potential energy forming an electrochemical gradient. The H^+ ions "slide" down their concentration gradient. As they flow, the ion channel/enzyme adenosine triphosphate (ATP) synthase uses its energy to produce ATP. At the end of the chain, electrons bind H^+ ions to nicotinamide adenine dinucleotide phosphate ($NADP^+$) to produce NADPH (non-cyclic photophosphorylation). The excited electrons can take an alternative path called cyclic electron flow, which only is involved the Photosystem I (PS I). Electrons flow from the electron acceptor ferredoxin to Cytochrome b6f, with ATP being the only product (cyclic

photophosphorylation). However, under NO_2-N stress conditions, the electron transport chain between Photosystem II (PS II) and PS I is hindered and the probability of an electron being transported to PS I is reduced. The reduced Q_A is not able to reoxidize and cannot efficiently transfer electrons to Q_B, accumulating oxidized P_{680} and PQ. Therefore, the oxidized P_{680} cannot be re-reduced and the oxidative splitting of water into four protons and molecular oxygen is limited, resulting in a decrease in oxygen release as was observed in Chapter 5. ATP and NADPH production are negatively affected, reducing sugar building in the second stage of photosynthesis. The preceding energy of excited electrons is accumulated and damages RCs of PS II. As a self-protective mechanism, the excess of intracellular energy is dissipated as heat.

The NO_2-N inhibition constants were determined by minimizing the root mean square error between model prediction (Hill-type model) and experimental data of OPR_{NET}, non-photochemical quenching (NPQ), maximum photosynthetic rate (ETR_{MAX}) and the performance index (PI_{ABS}). The inhibitor concentration that produce 50% inhibition ($K_{I,NO2}$) resulted in 24.10, 26.99, 40.54, and 27.55 g $N \cdot m^{-3}$ and the Hill parameter (n) was 1.82, 5.3, 2.4 and 4.2 for the above four parameters, respectively.

Nitrite inhibition modeling has been included in the integrated microalgae-bacteria mechanistic model described in Chapter 10.

11.4. Comprehensive assessment of the microalgae-nitrifying bacteria competition in microalgae-based wastewater treatment systems: relevant factors, evaluation methods and control strategies

From MHRAP operation at different HRT and incoming wastewater streams (Chapter 5) competition between AOB and microalgae for nitrogen source was evidenced. AOB outcompete microalgae and NH_4-N is fully oxidized to NO_2-N and NO_3-N. However, for the suitable integration of microalgae-bacteria consortia in a circular economy framework, resource recovery should be promoted. The main nutrient removal

mechanism should therefore be assimilation by biomass, which made a minor contribution to nutrient removal in Chapter 5.

In addition, NO_2-N inhibition of microalgal photochemistry was assessed and quantified in Chapter 6. Philips et al. (2002) reported that differences between nitritation and nitration activity of barely 3% results in significant NO_2-N accumulation. NOB are more light- and alkaline pH-sensitive than AOB (Park et al., 2007; Vergara et al., 2016). The increase in pH and high light intensity exposition are intrinsic features of microalgae and bacterial cultures, therefore, the NOB inhibition and the consequent accumulation of nitrite is highly probable.

Chapter 7 compile the main abiotic and biotic factors involved in microalgae-AOB competition, the available methodology to quantify AOB and microalgae concentration and activity, along with control strategies based on our own experience and knowledge to reduce competitive pressure on microalgal community. This is expected to be useful to wastewater treatment systems based on microalgae-AOB cultures as it could help to improve the process performance by maximising/minimising microalgae activity and/or nitrification, respectively.

11.4.1. Factors influencing microalgae-nitrifying bacteria cultivation

Different medium characteristics and environmental and operational conditions can greatly affect microalgae or nitrifying bacteria, and shift their equilibrium (Bellucci et al., 2020; Sánchez-Zurano et al., 2020). The most important factors related to both microalgae and nitrifying bacteria activity are temperature, light pH BRT, HRT and oxygen concentration.

Temperature

Temperatures above the optimum value, even by only 2-4 ºC, drastically reduce microalgae growth (Mazzelli et al., 2020). In the case of a mixed microalgae culture dominated by microalgae with a *Chlorella*-like morphology, González-Camejo et al.

(2019a) reported that microalgae viability fell significantly when temperature was over 30 ºC. The AOB growth rate sharply increases at higher temperatures. In this respect, AOB growth has been reported to be 0.9 d^{-1} at 20 ºC but reaches 2.9 d^{-1} at 30 ºC (Jiménez, 2010), showing that temperature peaks can have a noteworthy influence on microalgae-AOB competition.

Light

The importance of light irradiance on the MA-AOB competition is mainly due to microalgae as it is probably the main factor in phototrophic growth (Raeisossadati et al., 2019). Indeed, when a culture is light-irradiated under proper conditions, microalgae outcompete AOB.

Although nitrifying bacteria do not need light for their metabolism, excessive light irradiance can affect them negatively (Lu et al., 2020; Wu et al., 2020). For instance, Akizuki et al. (2020) reported nitrification inhibition at incident light intensities over 450 $\mu mol \cdot m^{-2} \cdot s^{-1}$, while Merbt et al. (2012) observed photoinhibition of AOB *Nitrosomonas europaea* and *Nitrosospira multiformis* at light irradiance of 500 $\mu mol \cdot m^{-2} \cdot s^{-1}$. Meng et al. (2019) found inhibition of NOB *Nitrospiraceae* under incident light irradiances over 180 $\mu mol \cdot m^{-2} \cdot s^{-1}$. NOB are usually more sensitive to light than AOB (Akizuki et al., 2020), as was observed in Chapter 5.

Nitrogen concentration

Distribution of nitrogen species, i.e. NH_4-N, NO_2-N and NO_3-N, in wastewater is highly relevant in microalgae-AOB interactions (Fallahi et al., 2021). The influence of NH_4-N is analogous in both microalgae and AOB and their growth rate is limited with low NH_4-N availability. In the case of microalgae, ammonium concentrations under 10 g $N \cdot m^{-3}$ have been found to significantly affect their growth (González-Camejo et al., 2019b; Pachés et al., 2020). However, AOB can support NH_4-N scarcity more efficiently than microalgae. NO_2-N can act as a nitrogen source for microalgae (Akizuki et al., 2021), although it can inhibit photosynthesis (Chapter 6). Microalgae assimilate NO_3-N less efficiently than

NH4-N, reducing algal growth rate (Kumar and Bera, 2020; Mohsenpour et al., 2021; Su, 2021).

pH

Culture pH regulated metabolic pathways of Microalgae and AOB, and therefore, both present an optimum pH value. Microalgae present optimum pH at around 7-8 (Caia et al., 2018; Eze et al., 2018), while the optimum pH is close to 8.5 and 7.9 for AOB and NOB, respectively (Park et al., 2007). In Chapter 5, pH was also detected as a potential inhibitor of NOB. Two steps of nitrification were decoupled, since NOB activity was limited by an alkaline pH, promoting NO_2-N accumulation and photosynthesis inhibition. In addition, pH is related to the acid-base equilibrium, so that it is related to the production of FAN. Nitrogen removal by FAN stripping reduces NH_4-N concentration available to microalgae (Chapter 5), which are worse competitors for NH_4-N than AOB.

BRT and HRT

BRT and HRT are essential operating parameters in continuous and semi-continuous operated reactors as they can be used to control factors related to microalgae-AOB systems (González-Camejo et al., 2020b; Rada-Ariza et al., 2017). Shorter BRTs boost the growth of the fastest microorganisms (Winkler et al., 2017), which can favor bacteria growth with respect to microalgae (González-Camejo et al., 2020c). HRT is responsible for the nutrient load to the system, thus being a key factor in the nutrient removal efficiency of the system and microalgae-AOB competition (Arbib et al., 2013; J. González-Camejo et al., 2018).

Oxygen concentration

In a microalgae-nitrifying bacteria culture, oxygen is mainly produced from microalgae photosynthesis. Depending on the microalgae activity within the culture, there will be four different situations (Akizuki et al., 2020b): (I) low microalgae activity, which produces insufficient oxygen to carry out nitrification (Chapter 5), (II) enough oxygen to develop the first step of nitrification (via nitrite), (III) sufficient oxygen to carry out full nitrification

via nitrate (Chapter 5), (IV) production of oversaturated dissolved oxygen, i.e. over 250% (around 20-25 g $N \cdot m^{-3}$), which can reduce microalgae performance (Barreiro-Vescovo et al., 2020).

11.4.2. Measuring culture activity and concentration

Although different techniques have been reported for quantification of microalgae and bacteria, an accurate method for determining the microalgae/bacteria ratio has not yet been developed.The most promising methods of accurately determining the proportion of microalgae and AOB in a sample are: (I) the combination of FISH and autofluorescence of microalgae, (II) the combination of FISH and flow cytometry, (III) sequencing-based techniques, and (IV) photo-respirometric tests.

FISH and autofluorescence of microalgae

Combining FISH probes for AOB and microalgae autofluorescence, the proportion of AOB and microalgae in a sample can be estimated. An image processing system can be used to determine the area occupied by photosynthetic organisms, AOB and the rest of the bacteria (determined by *Eubacteria* FISH probes (Daims et al., 1999)). This method measures the proportion of AOB and microalgae in terms of area, which is supposed to be equivalent to the volume and biomass of the populations.

FISH technique and flow cytometry

Combining fluorescence signals and forward scatter (FSC) and side scatter (SSC) measurements, the proportion of microalgae and AOB in a biological sample can be quantified. The technique can discriminate not only by color but also by size and complexity (Kalyuzhnaya et al., 2006), although there are some technical limitations. The main drawback is that to differentiate between both populations the flow cytometer must be calibrated with standard samples (usually pure cultures of the target organism). In samples with high biodiversity, calibration of the flow cytometer is complex, time-consuming and depends on the sample to be analyzed in each case. Accurate quantification by cytometry requires the complete disaggregation of the samples and

there may be a high degree of bias if the aggregates are estimated as single cells instead of a group of individual cells. In biological samples, inorganic compounds (e.g. debris) can interfere with the signal of the instrument. The results of this technique are given in an event (hopefully cells) basis instead of cell basis, which could be controversial when applying this data directly to mathematical models.

Sequencing-based techniques

The results obtained from metagenomic techniques should be interpreted with caution, since the measured genetic material is not usually correlated to the real sample concentration. The main factors that influence the quantitative results are: the efficiency of the sample extraction process; the kind of primers used for deoxyribonucleic acid (DNA) amplification; the different ratios between initial DNA concentration and final concentration after amplification, the sequences available in databases; and the algorithms used for data processing (Di Caprio, 2020). Depending on the target population, it is recommended to use a different extraction kits, introducing more uncertainty in the biological taxa comparison. The sequencing of microalgae and AOB is carried out separately, i.e., one sample is sequenced to obtain the information related to the Bacterial domain and another sample for the Eukaryotic domain. The results obtained are the relative abundance of AOB compared to bacteria abundance and the relative abundance of microalgae and compared to eukaryotic organisms abundance (Steichen and Brown, 2019). The results obtained are thus not comparable and at present, it is not possible to determine the ratio of AOB to microalgae in a sample. The main drawback is that these techniques quantify gene copies instead of organisms. As the number of gene copies varies between genes and organisms it is hard to correlate the obtained results with the real number of organisms present in the sample.

Photo-respirometric test

The main advantage of this technique is that it is the only one that measures activity instead of the number of microorganisms, which avoids the bias due to the presence of

non-active AOB or microalgae in the sample. The results can be applied directly in mathematical models.

11.4.3. Nitrification control strategies

Nitrifying bacteria can proliferate faster than microalgae depending on operational and environmental conditions (Sánchez-Zurano et al., 2020). Indeed, nitrifying bacteria can surpass microalgae as the dominant microorganism in the competence (Chapter 5). In some cases microalgae can even collapse (González-Camejo et al., 2019a), so that nitrification has to be controlled.

Temperature control

Temperatures in HRAP are usually regulated by evaporation. However, closed photobioreactors (PBRs) can reach temperatures 10 ºC higher than their surroundings (Yeo et al., 2018). Including cooling systems (González-Camejo et al., 2019a; Mazzelli et al., 2020) can reduce temperature in closed PBRs although it involves a drastic increase in process costs.

BRT and HRT

In terms of process efficiency, BRT (or HRT) tends to be operated for as short as possible to reduce costs and land use. However, shorter BRT (around 2 days) can favor NO_2-N accumulation due to higher AOB activity than microalgae and NOB, which can reduce microalgae activity significantly (Chapter 6). Longer BRTs increase NOB activity (Munz et al., 2011), favoring nitrification at the expense of lower microalgae growth. Microalgae have been found to be favored over nitrifying bacteria at mid-range BRT values. González-Camejo et al. (2020c) reported this range to be 2-4.5 d for an outdoor flat-panel MPBR pilot plant.

Once a consistent nitrifying bacteria population has been established within the culture, microalgae usually reduce their performance (Chapter 5). To change this trend the dilution rate can be increased to wash out the excess bacteria. Raising dilution rate also

reduces microalgae and TSS concentration, which can increase the remaining microalgae activity by reducing light attenuation.

Addition of nitrification inhibitors

Nitrification can be easily inhibited by adding allylthiourea (ATU), which did not affect photosynthesis activity (Chapter 6). As AOB growth is inhibited, NO_2-N will not be produced and NOB will thus be limited indirectly due to nutrient scarcity, favoring microalgae growth. However, ATU addition is not economically feasible on an industrial scale

11.5. Microalgae-bacteria consortia dynamics in a long term operated membrane-coupled high-rate algal pond (MHRAP)

Due to the abovementioned interactions between microalgae and bacteria (Chapter 5, 6 and 7), the discussion about the operational and environmental parameters influence over microbial communities is the main objective of Chapter 8. The samples used in this study were obtained from the MHRAP pilot plant operated in Chapter 5. The operational parameters evaluated in this work were: HRT and the influent wastewater streams (effluents from primary treatment and pre-treatment). The structure of the microbial communities retrieved from MHRAP were analyzed in a Principal Coordinates Analysis (PCoA) based on Bray-Curtis distances matrix. Bacterial community from the MHRAP operated at 6 days HRT and fed with effluent from primary treatment was substantially different from the rest of the periods studied. This specialization of bacterial community was also reproduced in microalgal structure, indicating that abiotic factors of this period were determinant for microorganisms' development. High light intensity, alkaline pH, nitrite accumulation and FAN concentration determined the reactor performance at 6 days of HRT. Phylum *Verrucomicrobiota* was less sensitive to stress conditions related to this period, as it was de predominant phylum under this conditions. Decreasing HRT along with the pH, nitrite and FAN concentrations shifted dominance from

Verrucomicrobiota to *Proteobacteria* phylum. Effluent from pre-treatment, with higher COD and nitrogen than primary settling effluent, promoted anoxic conditions and denitrifying bacteria growth. Among these, *Caldilineaceae* family, belonging to phylum *Chloroflexy*, increased markedly.

As pointed out in Chapters 5, nitrification rate was also affected by operating conditions. Regarding AOB genus classification, only *Nitrosomonas* was found in samples obtained when feeding primary effluent, while *Ellin6067* spp. dominated AOB community using effluent from pre-treatment. *Ellin6067* spp. is not commonly developed in activated sludge systems, but it has been previously detected in microalgae-bacteria systems behaving considerably tolerant and/or acclimated to light irradiation (Wang et al., 2021). The partial-nitrification observed at 6 days HRT was related to the low relative abundances of *Nitrospira*. Decrease of the abiotic stress on NOB community resulted in an increase in relative abundances of NOB genera and promoted *Candidatus Nitrotoga* growth at 4 and 2 days of HRT using effluent from primary treatment. This indicates that this genus was more sensitive to FAN and less competitive than *Nitrospira* in systems with low oxygen concentrations (Zheng et al., 2020).

Microbial specialization in period operated at 6 days HRT was also observed in microalgae composition. *Desmodesmus* genus was better adapted to stress factors of this period. However, reducing selective pressure resulted in a dominance of *Coelastrella*, regardless of HRT and wastewater stream. Microalgae described in Chapter 6 belonged therefore to *Desmodesmus* genus.

Nitrogen removal efficiency achieved at 2 days HRT with pre-treatment effluent was the combined effect of oxygen depletion at nighttime hours and proliferation of nitrifying bacteria along with denitrifying bacteria.

Conventional identification of microalgae in these microalgae-bacteria systems has been based on their morphology. Populations have traditionally been found to vary between

Scenedesmus- and *Chlorella*-like organisms. However, the sequencing data of the present study show that the abundance of the *Chlorellales* order barely reached 7% of the eukarya domain. Instead, almost all the microalgae found in this study belonged to the *Sphaeropleales* order, in which the *Scenedesmus*-like microalgae are included. *Sphaeropleales* order contains different morphologies that could be wrongly identified as Chlorella-like organism. Thus, this chapter remarks the importance of performing an appropriate identification of microalgae using sequencing techniques instead of using only morphological identification.

11.6. Global sensitivity and uncertainty analysis of a microalgae model for wastewater treatment

Microalgae metabolism cannot be considered a well-characterized process, since some mathematical model parameters are uncertain and speciation-dependent. Application of mathematical models requires therefore a great number of assumptions regarding the simplification of biological processes and model parameters. These assumptions are sources of uncertainty that could propagate through the model thus generating uncertainty in the model outputs. The resulting uncertainty in the model results could lead to misleading decisions during process design and/or optimization. Hence, performing a global sensitivity and uncertainty analysis (GSA and UA, respectively) would help to deal with these issues by analyzing and understanding model performance. Both analysis were performed over 4 operation periods obtained from the MPBR pilot plant performance. The 4 periods represent the key variations observed during the three years of the MPBR pilot plant operation, i.e. daily variations in light intensity and temperature, phosphorus-replete and phosphorus-starved conditions in the culture medium, and different operational conditions.

Overall, 11 of the 34 model parameters were classified as influential factors: maximum growth rate of microalgae (μ_{ALG}), minimum temperature for microalgae growth (T_{MAX}),

optimal light intensity for microalgae growth (I_{OPT}), attenuation coefficient due to particulate components (K_I), half saturation parameter for ammonium-ammonia in a phosphorus-replete medium (K_{NHX}), maximum decay rate of microalgae ($b_{ALG,2}$), rate constant for storage of intracellular phosphorus (q_{XPP}), half saturation parameter for phosphate (K_{PO4}), inhibition parameter for intracellular phosphorus use in a phosphorus-replete medium ($K_{I,PO4}$), half saturation parameter for ammonium-ammonia in a phosphorus-deplete medium ($K_{NHX-qPP}$), and constants of mass transfer coefficient equation (K_La_r). The four input factors with the most important overall effect on the outputs analyzed were μ_{ALG}, q_{XPP}, T_{MAX}, and I_{OPT}. The input factor μ_{ALG} showed a strong influence on the soluble ammonium-ammonia (S_{NHX}) and microalgal biomass (X_{ALG}) concentration output, whereby the nitrogen and biomass concentrations in the MPBR pilot plant were mainly due to microalgae growth processes. Conversely, the main phosphorus removal pathway was X_{PP-ALG} storage by q_{XPP}. T_{MAX} and I_{OPT} indicated that the growth and storage kinetic rates were mainly influenced by temperature and light intensity fluctuations.

The UA shows different responses for each period. This result is probably due to two main reasons: (I) the number of sensitive factors involved and (II) the processes involved in each period. The results obtained for the ammonium-ammonia concentration suggested that the uncertainty bandwidth depends on the number of influential input factors involved. Phosphate concentration suggested that the processes involved in each period had different effects on model output variations and on the interrelationship between model outputs. Although p-factor and ARIL values for microalgae concentration suggested a good response in terms of uncertainty, an integrated analysis of all uncertainty indices (bandwidth, p-factor, r-factor and ARIL value) showed high uncertainty in the model output.

The high uncertainty response could be attributed to online-calibrated factors. The reproducibility of this online calibration approach may be questionable and could introduce uncertainty into the model. These model parameter sets can be distributed

over a wide range of values for each parameter, introducing high uncertainty into the model. Offline calibration is an alternative method to online calibration. In this respect, offline calibration enables kinetic processes to be isolated and the variables involved to be controlled. Since a subset of the parameters was calibrated online, an optimization algorithm was used to match the model parameters within a realistic data range. The offline method can thus be recommended over online calibration, as can the dynamic optimization of all the influential parameters.

11.7. Integrated microalgae-bacteria modelling: application to an outdoor membrane photobioreactor (MPBR)

All the knowledge gathered in the previous chapters has been used in the development of an integral microalgae-bacteria model. Biological, chemical and physical processes described in Chapters 5, 6 and 8 were integrated to simulate microalgae-bacteria consortia based-wastewater treatment. Microalgae, heterotrophic bacteria, AOB and NOB growth, along with, chemical precipitation and stripping of nitrogen, ammonia, carbon dioxide and oxygen were the crucial kinetics included. The nitrite inhibition kinetics in the growth of microalgae is the most significant novelty introduced in the proposed model. Besides, to the best of the authors' knowledge, it is first microalgae-bacteria model that integrates phosphorus removal by chemical precipitation which was included because the pH fluctuations inherent to microalgal systems promote alkaline pH values that drive chemical phosphorus removal.

The proposed model demonstrated to be able to simulate, with a high degree of accuracy, the dynamics of total and volatile suspended solids, ammonium, nitrite, nitrate and phosphate concentrations in the photobioreactors. Relative abundance of microalgae, AOB and NOB were also obtained. However, results cannot be directly compared with relative abundance described in Chapter 8, since metagenomics analysis provide number of copies of genes, whereas model calculates biomass concentrations

in terms of mass units, which is more correlated with activity than with genomic abundances.

Validation was conducted with experimental data from a membrane photobioreactor (MPBR) fed with effluent from anaerobic membrane bioreactor (AnMBR). The AnMBR effluent consisted of a nutrient-rich permeate with a negligible concentration of organic matter, making it a suitable culture for microalgae and nitrifying growth and limiting the development of heterotrophic bacteria population. This chapter was focused on interaction between nitrifying bacteria and microalgae, as they have been the guiding thread of this research work.

Three periods according to microalgae-bacteria interactions were studied. The first period was selected to analyze inhibition of microalgae and NOB by NO_2-N and light intensity, respectively. The same period was simulated without the nitrite inhibition kinetics, so that it was possible both, to evaluate whether microalgae are really inhibited by NO_2-N and to validate the calibrated value obtained in Chapter 5. Correlation degree between experimental and simulated volatile suspended solids concentration with no NO_2-N inhibition decreased to 0.5442 (R^2 between experimental and modeled results with NO_2-N inhibition was 0.9521), indicating that microalgae growth was indeed inhibited by NO_2-N. Inhibition kinetics obtained from Chapter 5 can accurately reproduce the experimental data. In addition, the trend in NOB growth was reproduced without photoinhibition kinetics. Therefore, the low relative abundances of NOB reported in Chapter 8 were probably due to high pH, FAN and nitrite concentration, rather than light intensity.

The nitrifying control strategies proposed in Chapter 7 were investigated through practical case study. Partial-nitrification was avoided increasing biomass retention time from 2 to 4.5 days. Concentration of particulate components decreased significantly due to the punctual increase of dilution rate, resulting in an increase of average light intensity within PBR and microalgae growth. Microalgae and nitrifying bacteria compete for NH_4-N. However, microalgae can assimilate both NH_4-N and NO_3-N. Dynamics of total

suspended solids and nutrient were simulated using NO_3-N as nitrogen source instead of NH_4-N. A clear preference for NH_4-N over NO_3-N by microalgae was observed in simulated results. Microalgae biomass dropped from nearly 700 to 450 g TSS·m^{-3}.

The proposed model is an efficient tool for industry to predict the behaviors of microalgae and nitrifying bacteria, as well as the different nitrogen fractions in the effluents.

CHAPTER XII

12. Conclusions

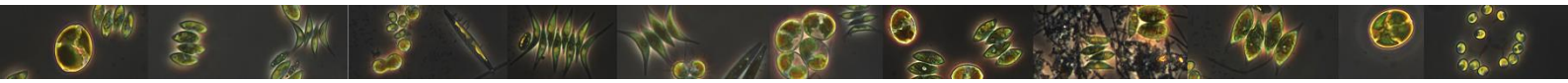

12. CONCLUSIONS

This research work has focused on the interaction between microalgae and bacteria for wastewater treatment. The main objectives were: (I) to assess the effect of hydraulic retention time and the incoming wastewater stream on microalgae-bacteria growth, (II) to identify and calibrate inhibition mechanism of nitrite on photosynthesis, (III) to develop a guide to reduce competitive interactions between nitrifiying bacteria and microalgae, (IV) to explore the influence of hydraulic retention time and incoming wastewater stream over microbial populations, (V) to perform a global sensitive and uncertainty analysis of microalgae model outputs, and (VI) to develop and validate an integrated microalgae-bacteria model.

I.1. The influence of hydraulic retention time over microalgae-bacteria growth was higher for systems fed with effluent from pre-treatment than from primary treatment, because of the higher biological oxygen demand content.

I.2. No external oxygen supply was needed due to photo-oxygenation of the system to remove wastewater pollutants from primary effluent. Microalgae provided the oxygen needed to nitrification but promoted ever-aerobic conditions (even at night) resulting in nitrate accumulation and low nitrogen removal rate. Organic matter supplied by this wastewater stream was not enough to achieve annoxic conditions and remove the oxidized nitrogen. Microalgae role was to supply oxygen for bacteria, since their contribution to nutrient removal was negligible.

The membrane high rate algal pond (MHRAP) pilot plant operated at an hydraulic retention time of 6 days was ammonium-oxidizing bacteria-dominated and nitrite accumulation was reported, since nitrite-oxidizing bacteria community was probably inhibited by a group of parameters, such as, pH, free ammonia and nitrite concentrations.

I.3. The membrane high rate algal pond (MHRAP) pilot plant operated at 2 days of hydraulic retention time was a suitable option to remove wastewater pollutant from

pre-treatment effluent, since meet European Union discharge limits (European Directive 98/15/CEE (10000 a 100000 p.e.). Oxygen fluctuations due to microalgae and heterotrophic bacteria activity promoted aerobic and anoxic conditions during daytime and nighttime hours, respectively. Coupled nitrification-denitrification process was therefore the main nitrogen removal mechanism. Microbial consortium shift from an oxygen-producing biomass to an oxygen-consuming biomass as the hydraulic retention time decreases to 1 day. Oxygen demand by heterotrophic bacteria surpassed oxygen production by photosynthesis. This system operated at 1 day of hydraulic retention time was not able to remove nutrients from pre-treatment effluent.

I.4. The use of membrane technology coupled with bacterial activity removed the organic matter in wastewater below the discharge limits, regardless operating hydraulic retention time and wastewater stream.

I.5. Heterotrophic activity is the cornerstone of the system. A bacteria-deficient consortium did not promote microalgae growth and anoxic conditions to remove nitrogen oxidized. An ecological structure dominated by heterotrophic bacteria reduced light for photosynthesis and resulted in zero oxygen concentration that allowed anoxic condiotions for denitrifying bacteria.

II.1. Nitrite, rather than the free nitrous acid, has an overall negative and rapid effect on photosynthesis. The nitrite inhibition mechanism was based on reducing light absorption and hindering the electron transport chain. The Q_A was not able to transfer electrons to Q_B, so that the primary photosynthetic process was limited and the maximum electron transfer yield was also reduced. The photosynthetic apparatus of microalgae responded to nitrite stress by increasing self-protective mechanism to avoid damage by the excess of intracellular energy.

II.2. The proposed Hill function was able to accurately reproduce the inhibitory effect of nitrite on four photosynthetic parameters.

II.3. Comparing the results obtained in this work with other scientific investigations, it is suggested that the inhibitory effect of nitrite could be species-dependent.

III.1. The activity of both microalgae and nitrifying bacteria can vary significantly with different medium characteristics and ambient and operational conditions, affecting equilibrium. Some of the important factors that influence (either directly or indirectly) microalgae-AOB competition are: temperature, light, nitrogen concentration (and the distribution of nitrogen species), pH, and dilution rate. Modifying these factors can thus help to improve process performance by maximising/minimising microalgae activity and/or nitrification. In this respect, some system control options are the following: I) control of culture temperature; II) control of biomass or hydraulic retention time; III) temporary increase of dilution rate; IV) control of nutrient loading rates; and V) adding nitrification inhibitors to the culture. However, some of these operations are unviable, since they can increase operating costs.

III.2. To assess microalgae-nitrifying bacteria competition, most of the commonly used methods focus on measuring either microalgae or nitrifying bacteria activity (or concentration). For instance, photosynthetic efficiency and Chlorophyll fluorescence parameters are specific indicators of microalgae activity, while nitrite/nitrate concentrations and nitrification rate are indicators of nitrifying bacteria activity. With respect to nutrient removal, biomass productivity, optical density and pH dynamics, despite being a result of both microalgae and bacteria activities, are strongly influenced by microalgae in most microalgae-based systems, while respirometries can clearly distinguish between the activity of both microorganisms. The most promising methods of accurately determining the proportion of microalgae and AOB in a sample is photo-respirometric test.

IV.1. HRT and the incoming wastewater stream are the main responsible factors that shape bacterial populations. Abiotic stress conditions, such as light intensity, free ammonia nitrogen, pH and nitrite accumulation, reduced bacteria diversity. The observed shifts in bacterial composition, including ammonium-oxidizing bacteria community, suggests that photoinhibtion processes could be taking place, which could regulate ecological structure of bacteria.

IV.2. The NOB community was dominated by *Nitrospira* and *Candidatus Nitrotoga*. This study revealed that *Nitrospira* is the dominant NOB genera under regular exposure to free ammonia nitrogen and low average oxygen concentration. *Desmodesmus* and *Coelastrella* were the dominant genus in the five periods studied. Microalgal community was dominated by *Desmodesmus* under alkaline pH and exposure of nitrite and free ammonia nitrogen. The results suggested that microalgae biodiversity was not affected by the hydraulic retention time or influent wastewater composition.

IV.3. Nitrogen removal efficiencies were affected by bacterial community composition but not by microalgae composition.

V.1. Eleven out of 34 influential factors were identified from the global sensitivity analysis. The four factors with the most important overall effect on the three outputs evaluated (ammonia-ammonium, phosphate and microalgae concentration) were maximum growth rate of microalgae, rate constant for phosphorus storage, maximum temperature and optimal light intensity for microalgae growth. A single data set was obtained by offline/online calibration methods, which was able to reproduce the model outputs for four experimental periods, regardless of the operational and environmental conditions. A dynamic optimization of the calibrated model parameter values was conducted to improve the model's output response.

V.2. The uncertainty analysis results revealed different responses according to the model output and the operating period considered and were dependent on the processes

and the number of influencing input factors involved in each period. Uncertainty indices were analyzed together with uncertainty bands to avoid erroneous conclusions. The model's uncertainty results showed the need to prioritize offline calibration to improve model performance.

VI.1. Despite the dynamics on operating conditions and ecological structure developed in a membrane photobioreactor plant, the model was able to reproduce process performance and effluent quality (no statistically significant differences were found between the model and the experimental results).

VI.2. Nitrite inhibition kinetics obtained in Chapter 6 were successfully validated and it was confirmed that nitrite had a negative impact on microalgae growth. The model reproduced the nitrite and nitrate concentrations without adding photoinhibition kinetics on NOB growth.

VI.3. The model was also applied to investigate the nitrification control strategies proposed in Chapter 7. Increasing biomass retention time from 2 to 4.5 days and increasing the dilution rate from 0.21 to 0.85 $days^{-1}$ promote microalgae growth. Nitrate as nitrogen source decreases microalgae concentration as expected due to the model structure.

APPENDIX A

RESUMEN EXTENDIDO

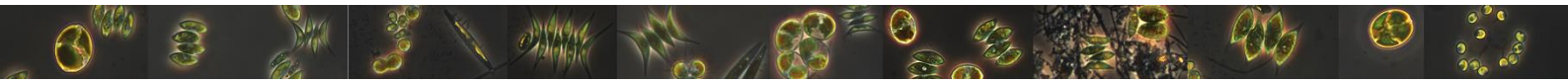

APPENDIX A: RESUMEN EXTENDIDO

1. INTRODUCCIÓN

Uno de los factores fundamentales de la vida es la disponibilidad de agua dulce. El aumento de la población mundial, la industrialización, la expansión de la agricultura de regadío en las últimas décadas han provocado un aumento drástico en la demanda de agua. La escasez de agua, junto con la demanda energética y el cambio climático son los principales problemas de este sigo. Desde la Unión Europea (UE) se han publicado diferentes Directivas con el fin de regular el uso y la conservación de las masas de agua, como, por ejemplo, la Directiva Marco del Agua 2000/60/CE y la Directiva 98/15/CE por la que se regulan los límites de vertido de las aguas residuales. Asimismo, la UE está adoptando diferentes medidas para desarrollar una economía competitiva cuyos principales pilares sean el uso sostenible de los recursos y la producción energética con bajas emisiones de dióxido de carbono (CO_2). Este nuevo planteamiento, revela la necesidad de un cambio de paradigma a nivel económico y social. Este cambio se ha hecho patente en el sector del tratamiento de las aguas residuales. Las aguas residuales han dejado de considerarse como una fuente de contaminantes para ser una fuente de recursos. Por ello, actualmente, se están evaluando y estudiando diferentes estrategias, económica y técnicamente viables, para maximizar la recuperación de recursos, como son la propia agua depurada o regenerada, nitrógeno, fósforo y energía.

En este sentido, el tratamiento de aguas residuales basado en consorcios de microalgas y bacterias han recibido un creciente interés por parte de la comunidad científica, ya que son capaces de eliminar contaminantes del agua residuales y recuperar nutrientes con un bajo consumo energético. Esta estrategia se enmarca en la economía circular del agua y en la que se centra este trabajo.

En las estaciones depuradoras de aguas residuales (EDAR) convencionales, las tecnologías de eliminación de nutrientes gastan aproximadamente el 50% de su demanda energética en el sistema de aireación, lo que implica un potencial de

calentamiento global de 0,6-0,9 kg de CO_2 eq·m^3. A partir de estas tecnologías, el nitrógeno se libera a la atmósfera y el fósforo se pierde dentro de los lodos como sal metálica, lo que evita su posible reutilización. En los consorcios de microalgas y bacterias, los organismos fotosintéticos suministran el oxígeno (O_2) necesario para los metabolismos aerobios, mientras asimilan y almacenen nitrógeno y fósforo intracelular. Las bacterias heterótrofas aerobias utilizan el oxígeno suministrado para degradar la materia orgánica presente en el agua residual, suministrando, a su vez, CO_2 que puede ser utilizado como fuente de carbono inorgánico por las microalgas. Sin embargo, además de esta relación sinérgica, entre las diferentes comunidades biológicas que componen el consorcio, se desarrollan otras interacciones ecológicas. La competencia e incluso el amensalismo son las principales relaciones ecológicas que pueden desequilibrar el correcto funcionamiento del consorcio, y con ello, la eficiencia en la depuración de las aguas residuales.

El análisis, desde diferentes áreas de conocimiento, de los consorcios de microalgas-bacterias, permiten desarrollar y mejorar el diseño de los sistemas de depuración basados en esta tecnología.

2. OBJETIVOS

Los objetivos de la presente tesis han sido: (I) evaluar el efecto del tiempo de retención hidráulico (TRH) y de las distintas corrientes de tratamiento de la EDAR en la eficacia de depuración de consorcios microalgas-bacterias, (II) evaluar e identificar el mecanismo de inhibición del nitrito sobre la fotosíntesis y describir un modelo matemático que reproduzca el efecto inhibitorio, (III) elaboración de un manual para identificar y reducir las interacciones competitivas entre las bacterias nitrificantes y las microalgas, (IV) comprender los cambios en las estructuras de la comunidad microalgal y bacteriana mediante la evaluación de diferentes parámetros operacionales, (V) realización de un análisis de sensibilidad e incertidumbre de un modelo de microalgas,

y (VI) desarrollo y validación de un modelo matemático integrado de microalgas y bacterias.

Este trabajo se ha estructurado como un compendio de artículos en los que los anteriores objetivos se han desarrollado. Cada objetivo se ha abordado en un capítulo distinto dando lugar a 6 capítulos centrados en la descripción y discusión de los resultados de este trabajo.

3. MATERIALES Y MÉTODOS

Se operaron dos plantas a escala piloto para la consecución de los objetivos descritos: raceway de membrana (MHRAP) y fotobiorreactor de membrana (MPBR). Ambas plantas pilotos estaban situadas en la EDAR “Cuenca del Carraixet”. La planta MHRAP piloto consistió en un reactor raceway conectado a un tanque de membranas de ultrafiltración. El volumen del reactor era 318,75 L, con una superficie expuesta a la luz solar de 1,275 m^2 y una profundidad de 0,25 m. Este reactor fue operado a distintos HRT y alimentado con agua procedente del decantador primario y del desarenador de la propia EDAR “Cuenca del Carraixet” (Capítulo 4). Por otro lado, la planta MPBR consistía en dos fotobiorreactores (FBR) conectados a un tanque de membrana de ultrafiltración. Cada FBR tenía una superficie expuesta al sol de 2,3 m^2. Durante el periodo de operación se operaron dos conjuntos de FBR con distinto espesor. Dos FBR con un espesor de 0,25 m (volumen 0,550 m^3) y otros dos FBR con 0,10 m (volumen de trabajo 0,220 m^3). Los resultados derivados de la operación de la planta piloto fueron utilizados para la calibración y análisis de sensibilidad e incertidumbre de un modelo matemático previamente publicado (Capítulo 8).

Para mantener unas condiciones ambientales de operación más estables también se operaron reactores a escala de laboratorio. El reactor consistió en un cilindro de metacrilato transparente de 8 L (con un diámetro interno de 20 cm). Se iluminó constantemente con lámparas LED, para suministrar una intensidad de luz de 150

$\mu mol \cdot m^{-2} \cdot s^{-1}$. El pH se monitorizaba y controlaba con una sonda de pH-temperatura y una bala de CO_2 puro (99,9%). Se suministraba CO_2 cada vez que el pH superaba el setpoint, que en este caso estaba fijado a 7,5. Además de la sonda de pH-temperatura, el reactor estaba equipado con una sonda de oxígeno. El cultivo resultante de la operación de este reactor fue utilizado para cuantificar los efectos inhibitorios del nitrito sobre la fotosíntesis (Capítulo 5). El proceso de inhibición fue modelado mediante foto-respirometrías.

Los ensayos foto-respirométricos fueron realizados en otro reactor cilíndrico de 0,5 L, iluminado por dos lámparas LED que suministraban 150 $\mu mol \cdot m^{-2} \cdot s^{-1}$. El pH se mantuvo a 7,5 siguiendo la misma filosofía de control descrita anteriormente. La producción y consumo de oxígeno fueron medidos y registrados a partir de una sonda de oxígeno. Mediante las pendientes de la producción de oxígeno neta (OPR_{NET}) y el consumo de oxígeno (OUR) se calibró la inhibición del nitrito en producción de oxígeno.

Asimismo, se han empleado técnicas de medición de la fluorescencia de la *Clorofila a* (*Chl a*) para analizar como el nitrito inhibe los procesos químicos del Fotosistema II (PS II). Con el AquaPen-C AP-C 100 (PSI (Photon Systems Instruments), 2017) se puede obtener una inmensa cantidad de información del PS II, véase la velocidad de transporte de electrones (ETR), el apagado no fotoquímico (NPQ) y la cinética de transitorios de fluorescencia.

Durante la operación de la planta piloto MHRAP se almacenaron muestras para analizar la estructura y diversidad microbiana dentro del reactor, mediante técnicas de secuenciación masivas (Capítulo 7). La extracción de ADN se realizó mediante dos kits comerciales, E.Z.N.A.® Soil DNA Kit (Omega-Biotek) y E.Z.N.A.® Plant DNA Kit (Omega-Biotek). El biomarcador estudiado para las comunidades bacterianas fue el gen 16S rDNA, empleando cebadores para la región V4 con secuencia 515F (5'-GTGCCAGCMGCCGCGGTAA-3') and 806R (5'-GGACTACHVGGGTWTCTAAT-3'). Para el análisis de las comunidades microalgales, el biomarcador estudiado fue el gen

18S rDNA empleando cebadores para la región V4 con secuencia TAReuk454FWD1 (5′- CCA GCA SCY GCG GTA ATT CC-3′) and TAReukREV3P (5′-ACT TTC GTT CTT GAT YRA-3′). A partir del análisis de coordenadas principales (PCoA) se correlacionaron la abundancia de los distintos microorganismos con las condiciones operacionales y ambientales.

Previamente a la confección del presente trabajo, se desarrolló un modelo matemático que describe las principales cinéticas de crecimiento de microalgas y asimilación de nutrientes. Se realizó un análisis general de sensibilidad (GSA) y de incertidumbre (UA) para determinar los parámetros del modelo más influyentes y calibrarlos e identificar las principales fuentes de incertidumbre del modelo, respectivamente (Capítulo 8). El GSA se realizó mediante el método de cribado de Morris y el UA mediante simulaciones de Monte Carlo. El software utilizado para ambos análisis fue la plataforma MATLAB/Simulink.

4. RESULTADOS Y DISCUSIÓN

4.1. ¿Pueden los consorcios de microalgas y bacterias eliminar realmente los contaminantes de las aguas residuales? Evaluación del tratamiento de aguas residuales urbanas con microalgas y bacterias a diferentes TRH y corrientes de aguas residuales.

La aplicación de consorcios de microalgas-bacterias en el tratamiento de las aguas residuales se basan en las relaciones ecológicas y los efectos sinérgicos entre comunidades biológicas. El intercambio gaseoso autosostenible de oxígeno y dióxido de carbono constituye la base de la principal relación mutualista entre las microalgas y las bacterias heterótrofas aerobias. La fotosíntesis también puede apoyar el proceso de nitrificación y mejorar la eliminación del nitrógeno amoniacal libre (FAN) y la precipitación de fósforo. El mecanismo de eliminación de nutrientes y demanda química de oxígeno (DQO) es el resultado de la interacción biológica entre las comunidades de

microalgas y bacterias. El equilibrio entre las comunidades de algas y bacterias se ve muy afectado por los parámetros ambientales (intensidad de la luz, temperatura, etc.), que no pueden controlarse en los sistemas exteriores. Los parámetros de funcionamiento son, por tanto, la herramienta clave para conseguir un sistema biológico que pueda eliminar eficazmente la DQO, el nitrógeno y el fósforo de las aguas residuales. Al definir un TRH de funcionamiento, se pueden identificar los requisitos de nitrógeno, fósforo y luz para mantener las comunidades biológicas deseadas. La planta piloto MHRAP, situada en la estación depuradora de aguas residuales (EDAR) "Cuenca del Carraixet", fue alimentada con efluentes procedentes de la decantación primaria y del pretratamiento y operada a diferentes TRH (Capítulo 5). Los sistemas de aguas residuales fueron evaluados por las eficiencias de eliminación de contaminantes junto con las actividades de las microalgas y las principales bacterias autóctonas de las aguas residuales (bacterias heterotróficas y nitrificantes).

Efluentes del decantador primario

En el conjunto experimental realizado con el efluente del decantado primario, la planta piloto MHRAP fue operada TRH de 6, 4 y 2 días. La comunidad biológica desarrollada con el agua residual primaria no fue capaz de eliminar el nitrógeno y el fósforo, independientemente del TRH de funcionamiento. Aunque la actividad de las bacterias nitrificantes era inferior al 10%, el equilibrio ecológico estaba totalmente dominado por estas bacterias autótrofas, en los tres TRH estudiados.

Las condiciones abióticas del periodo operado con un TRH de 6 días favorecieron la actividad de las AOB sobre las bacterias oxidantes de nitritos (NOB). La diferencia entre la actividad de nitritación y la de nitratación fue de apenas un 3%. Según Philips et al. (2002), este pequeño margen es suficiente para promover una acumulación significativa de nitritos (NO_2-N). La nitrificación parcial representó el 48 ± 3% de la eficiencia de eliminación de amonio (NH_4-N-RE), resultando en una acumulación de nitrito NO-N $_2$de 21 ± 3 g $N \cdot m^{-3}$. El NO_2-N puede ser altamente tóxico, no sólo para las microalgas

(Capítulo 5) sino también para una amplia gama de bacterias, como las AOB y las NOB (Philips et al., 2002).

La eficiencia fotosintética fue menor en la planta piloto MHRAP operada con un TRH de 6 días en comparación con los resultados obtenidos a 4 y 2 días de TRH (17 ± 2, 32 ± 4 y 31 ± 4 mg O_2·g VSS^{-1}·h^{-1}, respectivamente). La acumulación de NO_2-N junto con un pH elevado, una concentración limitada de carbono inorgánico disuelto (DIC) y la competencia por el NH_4-N con las AOB, pueden inhibir la actividad fotosintética y la asimilación de nutrientes. De hecho, las eficiencias de eliminación de nitrógeno total y fósforo (T_N-RE y T_P-RE, respectivamente) por asimilación de biomasa fueron de 1,7 ± 0,6 y 5,2 ± 0,9%, respectivamente. El pH aumentó durante las horas de luz, alcanzando valores cercanos a 9 (8,7 ± 0,3) debido a la captación de DIC por la fotosíntesis. En consecuencia, la volatilización de FAN representó el 25 ± 4% de la T_N-RE, siendo el principal mecanismo de eliminación de nitrógeno en el sistema. Las condiciones abióticas también proporcionaron la precipitación de fósforo, que fue la principal vía de eliminación de fósforo, representando el 20%. La concentración total de nitrógeno y fósforo en el permeado fue de 32 ± 3 g N·m^{-3} y 2,2 ± 0,8 g P·m^{-3}, respectivamente, por lo que el período experimental operado a 6 días de TRH no cumplió con los límites de vertido de nutrientes establecidos por la Unión Europea (UE).

Se limitó la nitrificación parcial y se logró la oxidación completa del NH_4-N a NO_3-N en los periodos operados a 4 y 2 días de TRH. La reducción del TRH de 6 a 4 y 2 días aumentó significativamente la tasa de consmo de oxígeno de AOB y NOB (OUR_{AOB} y OUR_{NOB}, respectivamente). El OUR_{AOB} aumentó de 1,12 ± 0,09 mg O_2·g VSS^{-1}·h^{-1} a 1,7 ± 0,6 y 1,5 ± 0,5 mg O_2·g VSS^{-1}·h^{-1} a TRH de 6, 4 y 2 días, respectivamente. La OUR_{NOB} fue de 0,6 ± 0,2, 1,1 ± 0,2 y 1,0 ± 0,2 mg O_2·g VSS^{-1}·h^{-1} a TRH de 6, 4 y 2 días, respectivamente. Este ligero aumento de la actividad de las NOB, evitó la acumulación de NO_2-N. De hecho, los NH_4-N-RE fueron superiores al 98% en ambos TRH de operación y la concentración de NO_2-N fue de 1,1 ± 0,7 y 1,6 ± 0,5 g N·m^{-3},

respectivamente. Sin embargo, la T_N-RE apenas alcanzó el 5%, ya que la volatilización de FAN se redujo debido a que el pH del cultivo fue de 7,4 ± 0,2 y 7,3 ± 0,3 para los periodos experimentales operados a TRH de 4 y 2 días respectivamente. La asimilación de la biomasa de nitrógeno fue de 4,8 ± 1,3 y 5 ± 2 % para el TRH de 4 y 2 días, respectivamente. Dado que la precipitación de fósforo no fue promovida por el alto pH, los TP-REs fueron 1,07 ± 0,02 y 1,6 ± 0,4 % para 4 y 2 días HRT. La concentración de nutrientes en el permeado final estaba muy por encima del límite de descarga de la UE en los periodos experimentales operados a 4 y 2 días HRT.

Las eficiencias de eliminación de la DQO (DQO-REs) en los periodos operados a 6, 4 y 2 días de TRH fueron, respectivamente, 89 ± 10, 88 ± 6 y 86 ± 9%. Las concentraciones finales de DQO en el permeado fueron inferiores a 125 g $O_2 \cdot m^{-3}$, que es la concentración máxima de DQO establecida para el vertido de aguas residuales al medio ambiente según la Directiva 98/15/CEE de la UE, independientemente del TRH de operación. Sin embargo, el análisis de la concentración de DQO en el sobrenadante de un filtro de membrana de 0,45 µm y en el permeado del módulo del tanque de membrana (MT), mostró que el MT eliminaba una parte significativa de la DQO. Los valores de DQO utilizando un filtro de membrana de 0,45 µm en los periodos de TRH de 6, 4 y 2 días fueron, respectivamente, 59 ± 15, 64 ± 11 y 58 ± 13%. Las diferencias de DQO-REs entre los sistemas de filtración indicaron que el licor mezclado en el reactor MHRAP contenía una porción significativa de DQO coloidal, que fue efectivamente retenida por la membrana de fibra hueca de 0,03 µm.

Efluentes del pretratamiento

El período experimental operado a TRH 4 días con efluente del pretratamiento mostró resultados similares a los obtenidos usando efluente del decantador primario a TRH de 4 y 2 días.

Reducir el TRH de 4 a 2 días no promovió la absorción de nutrientes por la biomasa y la nitrificación fue la principal vía de eliminación de NH_4-N. La actividad de las bacterias

nitrificantes no mostró diferencias entre 2 y 4 días de TRH (3 ± 0,2 y 2,5 ± 0,4 mg O_2·g VSS^{-1}·h^{-1}, respectivamente), lo que indica que el potencial de nitrificación no se vio afectado en gran medida por el TRH en el rango de 4-2 días bajo estas condiciones abióticas. La actividad fotosintética a 2 días de TRH (58 ± mg O_2 g·VSS^{-1}·h^{-1}) fue comparable a la de los cultivos producidos con residuos de lixiviados agrícolas, los cuales son considerados un buen sustrato para las microalgas (Sánchez-Zurano et al., 2020). La eliminación de fósforo se vio incrementada por la capacidad de asimilación de la biomasa. La relación de absorción de N/P fue de 11,7 ± 1,4 (en base a la masa), similar a la relación N/P reportada por Gardner-Dale et al. (2017) y Reynolds (2006). La reducción del TRH de 4 a 2 días y, por lo tanto, el aumento de la carga de la demanda biológica de oxígeno (DBO) (de 73 ± 6 a 145 ± 10 g·m^{-3}·d^{-1}) dieron lugar a un cambio de las condiciones aeróbicas a las anóxicas durante las horas de luz y la noche, respectivamente. El proceso acoplado de nitrificación-desnitrificación fue el principal mecanismo de eliminación de nitrógeno y representó el 87% de la eliminación total de nitrógeno. La asimilación de nitrógeno por la biomasa fue un mecanismo de eliminación menor. El papel de las microalgas fue, por tanto, apoyar la nitrificación durante el día.

En general, la disminución del TRH de 2 a 1 días aumentó la actividad heterotrófica (de 3,0 ± 0,6 a 5,1 ± 0,2 mg O_2 g·VSS^{-1}·h^{-1}, respectivamente) debido a la carga de DBO (de 145 ± 10 a 290 ± 30 g·m^{-3}·d^{-1}). La eliminación de nitrógeno por nitrificación representó menos del 5% debido a la nula concentración de oxígeno disuelto que prevaleció durante todo el día. El crecimiento de las bacterias heterótrofas aumentó la concentración de los sólidos suspendidos totales (SST) y redujo la intensidad luminosa media máxima, fotolimitando la fotosíntesis de las microalgas (1,2 ± 0,8 mg O_2 g·VSS^{-1}·h^{-1}). La OPR_{NET} de la biomasa no fue capaz de igualar la demanda de O_2 por parte de las bacterias heterótrofas (5,1 ± 0,2 mg O_2 g·VSS^{-1}·h^{-1}) y nitrificantes (1,1 ± 0,4 mg O_2 g·VSS^{-1}·h^{-1}), lo que sugiere un cambio en la estructura de la comunidad ecológica hacia las bacterias heterótrofas a 1 día de HRT. TN-RE y TP-RE fueron 1,12 ± 0,7 y 0,70 ± 0,13 %, respectivamente.

La media de DQO-RE fue del 96 ± 1,4 %, independientemente del TRH debido al proceso de filtración por el módulo MT.

El efluente del pretratamiento y la planta MHRAP operada a 2 días de TRH fueron las únicas condiciones de funcionamiento estudiadas que cumplían los límites de descarga de DQO, nitrógeno y fósforo de acuerdo con la Directiva Europea 98/15/CEE.

4.2. Evaluación y modelización de la inhibición de la fotosíntesis por nitrito mediante técnicas foto-respirometrías y de fluorescencia de la Clorofila.

En el Capítulo 5, se observó que la actividad fotosintética podría verse afectada negativamente por la concentración de DIC y nutrientes, el pH y la acumulación de NO_2-N. González-Camejo et al. (2020) informaron de que una concentraciones entre 5 y 20 g $N \cdot m^{-3}$ de NO_2-N inhibe el metabolismo de las microalgas en términos de productividad de biomasa y eliminación de nutrientes. El Capítulo 6 de este trabajo se centra en determinar el mecanismo de inhibición debido a la evidencia científica que sugiere que el nitrito es un componente tóxico para la fotoquímica microalgal. La inhibición se evaluó combinando pruebas de foto-respirometrías con medidas de fluorescencia de *Chl a* (Rossi et al., 2018; Sánchez-Zurano et al., 2020; Strasser et al., 2004).

La exposición al NO_2-N produjo una inhibición parcial del proceso fotosintético primario debido principalmente a la obstaculización de la cadena de transporte de electrones. En condiciones de no estrés, es decir, sin acumulación de NO_2-N, la energía de excitación obtenida de la luz es absorbida por el centro de reacción (CR) del PS II, (P_{680}). El P_{680} excitado se oxida liberando un electrón que es transportado a través de la membrana hasta el primer aceptor de electrones, Q_A, luego el electrón pasa al segundo aceptor, Q_B, y finalmente reduce la plastoquinona (PQ) a PQH_2. Los electrones que pasan por la cadena de transporte de electrones pierden energía que se utiliza para bombear iones H^+ por el complejo Citocromo b6f. Estos iones concentrados almacenan energía potencial formando un gradiente electroquímico. Los H^+ "deslizan" por su gradiente de

concentración. A medida que fluyen, el canal iónico/enzima adenosina trifosfato (ATP) sintasa utiliza su energía para producir ATP. Al final de la cadena, los electrones unen los iones H^+al nicotinamida adenina dinucleótido fosfato ($NADP^+$) para producir NADPH (fotofosforilación no cíclica). Los electrones excitados pueden tomar un camino alternativo llamado flujo cíclico de electrones, en el que sólo interviene el Fotosistema I (PS I). Los electrones fluyen desde el aceptor de electrones ferredoxina hasta el citocromo b6f, siendo el ATP el único producto (fotofosforilación cíclica). Sin embargo, en condiciones de estrés por NO_2-N, la cadena de transporte de electrones entre el PS II y el fotosistema I (PS I) se ve obstaculizada y la probabilidad de que un electrón sea transportado al PS I se reduce. El Q_A reducido no es capaz de reoxidarse y no puede transferir eficientemente electrones al Q_B, acumulando P_{680} oxidado y PQ. Por lo tanto, el P_{680} oxidado no puede volver a reducirse y el desdoblamiento oxidativo del agua en cuatro protones y oxígeno molecular es limitado, lo que da lugar a una disminución de la liberación de oxígeno como se observó en el Capítulo 5. La producción de ATP y NADPH se ve afectada negativamente, reduciendo la construcción de azúcares en la segunda etapa de la fotosíntesis. La energía precedente de los electrones excitados se acumula y daña los CR del PS II. Como mecanismo de autoprotección, el exceso de energía intracelular se disipa en forma de calor.

Las constantes de inhibición de NO_2-N se determinaron minimizando el error cuadrático medio entre la predicción del modelo (modelo tipo Hill) y los datos experimentales de OPR_{NET}, el apagado no fotoquímico (NPQ), la tasa fotosintética máxima (ETR_{MAX}) y el índice de rendimiento (PI_{ABS}). La concentración de inhibidor que produce el 50% de inhibición ($K_{I,NO2}$) resultó en 24,10, 26,99, 40,54 y 27,55 g $N \cdot m^{-3}$ y el parámetro de Hill (n) fue de 1,82, 5,3, 2,4 y 4,2 para los cuatro parámetros anteriores, respectivamente.

La modelización de la inhibición del nitrito se ha incluido en el modelo mecanicista integrado microalgas-bacterias descrito en el Capítulo 10.

4.3. Evaluación exhaustiva de la competencia entre microalgas y bacterias nitrificantes en sistemas de tratamiento de aguas residuales basados en microalgas: factores relevantes, métodos de evaluación y estrategias de control

A partir del funcionamiento del MHRAP a diferentes TRH y corrientes de aguas residuales entrantes (Capítulo 5) se evidenció la competencia entre las AOB y las microalgas por la fuente de nitrógeno. Las AOB superan a las microalgas y el NH_4-N se oxida completamente a NO_2-N y NO_3-N. Sin embargo, para la adecuada integración de los consorcios de microalgas-bacterias en un marco de economía circular, debe promoverse la recuperación de recursos. Por lo tanto, el principal mecanismo de eliminación de nutrientes debería ser la asimilación por parte de la biomasa, cuya contribución a la eliminación de nutrientes fue minoritaria en el Capítulo 5.

Además, en el Capítulo 6 se evaluó y cuantificó la inhibición del NO_2-N en la fotoquímica de las microalgas. Philips et al (2002) informaron de que las diferencias entre la actividad de nitritación y la de nitración de apenas un 3% dan lugar a una acumulación significativa de NO_2-N. Los NOB son más sensibles a la luz y al pH alcalino que los AOB (Park et al., 2007; Vergara et al., 2016). El aumento del pH y la exposición a una alta intensidad de luz son características intrínsecas de los cultivos de microalgas y bacterias, por lo que la inhibición de NOB y la consecuente acumulación de nitrito es altamente probable.

El Capítulo 7 recopila los principales factores abióticos y bióticos que intervienen en la competencia entre microalgas y AOB, la metodología disponible para cuantificar la concentración y la actividad de las AOB y las microalgas, junto con las estrategias de control basadas en nuestra propia experiencia y conocimientos para reducir la presión competitiva sobre la comunidad microalgal. Se espera que esto sea útil para los sistemas de tratamiento de aguas residuales basados en cultivos de microalgas-AOB, ya que podría ayudar a mejorar el rendimiento del proceso maximizando/minimizando la actividad de las microalgas y/o la nitrificación, respectivamente.

Factores que influyen en el cultivo de microalgas y bacterias nitrificantes

Las diferentes características del medio y las condiciones ambientales y operativas pueden afectar en gran medida a las microalgas o a las bacterias nitrificantes y modificar su equilibrio (Bellucci et al., 2020; Sánchez-Zurano et al., 2020). Los factores más importantes relacionados con la actividad de las microalgas y las bacterias nitrificantes son la temperatura, el pH de la luz, el TRH y la concentración de oxígeno.

Temperatura

Temperaturas superiores al valor óptimo, incluso en sólo 2-4 ºC, reducen drásticamente el crecimiento de las microalgas (Mazzelli et al., 2020). En el caso de un cultivo mixto de microalgas dominado por microalgas de morfología similar a *Chlorella*, González-Camejo et al. (2019a) informaron que la viabilidad de las microalgas disminuía significativamente cuando la temperatura era superior a 30 ºC. La tasa de crecimiento de AOB aumenta bruscamente a temperaturas más altas. En este sentido, se ha reportado que el crecimiento de la AOB es de 0,9 d^{-1}a 20 ºC pero alcanza los 2,9 d^{-1}a 30 ºC (Jiménez, 2010), mostrando que los picos de temperatura pueden tener una influencia notable en la competencia microalga-AOB.

Luz

La importancia de la irradiación de luz en la competencia microalgas-nitrificantes se debe principalmente a las microalgas, ya que es probablemente el principal factor de crecimiento fototrófico (Raeisossadati et al., 2019).

Aunque las bacterias nitrificantes no necesitan luz para su metabolismo, una irradiación lumínica excesiva puede afectarlas negativamente (Lu et al., 2020; Wu et al., 2020). Por ejemplo, Akizuki et al. (2020) informaron de la inhibición de la nitrificación a intensidades de luz incidente superiores a 450 $\mu mol \cdot m \cdot^{-2}\text{-}s^{-1}$, mientras que Merbt et al. (2012) observaron la fotoinhibición de AOB, *Nitrosomonas europaea* y *Nitrosospira multiformis,* a una irradiación de luz de 500 $\mu mol\text{-}m^{-2}\text{-}s^{-1}$. Meng et al. (2019) encontraron la inhibición de NOB, *Nitrospiraceae,* bajo irradiaciones de luz incidente superiores a 180

$\mu mol \cdot m^{-2} \cdot s \cdot^{-1}$. Las NOB suelen ser más sensibles a la luz que las AOB (Akizuki et al., 2020), como se observó en el Capítulo 4.

Concentración de nitrógeno

La distribución de las especies de nitrógeno, es decir, NH_4-N, NO_2-N y NO_3-N, en las aguas residuales es muy relevante en las interacciones microalgas-AOB (Fallahi et al., 2021). La influencia del NH_4-N es análoga tanto en las microalgas como en el AOB y su tasa de crecimiento está limitada con una baja disponibilidad de NH_4-N. En el caso de las microalgas, se ha encontrado que concentraciones de amonio por debajo de 10 g $N \cdot m^{-3}$ afectan significativamente su crecimiento (González-Camejo et al., 2019b; Pachés et al., 2020). Sin embargo, las AOB pueden soportar la escasez de NH_4-N de forma más eficiente que las microalgas. El NO_2 -N puede actuar como fuente de nitrógeno para las microalgas (Akizuki et al., 2021), aunque puede inhibir la fotosíntesis (Capítulo 5). Las microalgas asimilan el NO_3-N de forma menos eficiente que el NH4-N, reduciendo la tasa de crecimiento de las algas (Kumar y Bera, 2020; Mohsenpour et al., 2021; Su, 2021).

pH

El pH de los cultivos regula las vías metabólicas de las microalgas y los NOB, por lo que ambos presentan un valor de pH óptimo. Las microalgas presentan un pH óptimo en torno a 7-8 (Caia et al., 2018; Eze et al., 2018), mientras que el pH óptimo se acerca a 8,5 y 7,9 para AON y NOB, respectivamente (Park et al., 2007). En el Capítulo 4, el pH también se detectó como un potencial inhibidor de la NOB. Dos pasos de la nitrificación fueron desacoplados, ya que la actividad de NOB fue limitada por un pH alcalino, promoviendo la acumulación de NO_2-N y la inhibición de la fotosíntesis. Además, el pH está relacionado con el equilibrio ácido-base, por lo que está relacionado con la producción de FAN. La eliminación de nitrógeno mediante la volatilización de FAN reduce la concentración de NH_4-N disponible para las microalgas (Capítulo 4), que son peores competidores para el NH_4-N que el AOB.

TRC y HRT

El tiempo de retención celular (TRC) y el TRH son parámetros operativos esenciales en las operaciones continuas y semicontinuas, ya que pueden utilizarse para controlar factores relacionados con los sistemas de microalgas-AOB (González-Camejo et al., 2020b; Rada-Ariza et al., 2017). TRC más cortos potencian el crecimiento de los microorganismos más rápidos (Winkler et al., 2017), lo que puede favorecer el crecimiento de las bacterias respecto a las microalgas (González-Camejo et al., 2020c). Los TRH son responsables de la carga de nutrientes del sistema, siendo por tanto un factor clave en la eficiencia de eliminación de nutrientes del sistema y en la competencia microalgas-AOB (Arbib et al., 2013; J. González-Camejo et al., 2018).

Concentración de oxígeno

En un cultivo de microalgas y bacterias nitrificantes, el oxígeno se produce principalmente a partir de la fotosíntesis de las microalgas. Dependiendo de la actividad de las microalgas en el cultivo, habrá cuatro situaciones diferentes (Akizuki et al., 2020b) (I) baja actividad de las microalgas, que produce insuficiente oxígeno para llevar a cabo la nitrificación (Capítulo 4), (II) suficiente oxígeno para desarrollar el primer paso de la nitrificación (vía nitrito), (III) suficiente oxígeno para llevar a cabo la nitrificación completa (vía nitrato (Capítulo 4), (IV) producción de oxígeno disuelto sobresaturado, es decir, superior al 250% (alrededor de 20-25 g $N \cdot m^{-3}$), lo que puede reducir el rendimiento de las microalgas (Barreiro-Vescovo et al., 2020).

Medición de la actividad y la concentración del cultivo

Los métodos más prometedores para determinar con precisión la proporción de microalgas y AOB en una muestra son (I) la combinación de FISH y autofluorescencia de microalgas, (II) la combinación de FISH y citometría de flujo, (III) las técnicas basadas en la secuenciación, y (IV) las respirometrías.

FISH y autofluorescencia de microalgas

Combinando la fluorescencia de la sonda FISH para AOB y la autofluorescencia de las microalgas, se puede estimar la proporción de las AOB y de las microalgas en una muestra. Se puede utilizar un sistema de procesamiento de imágenes para determinar el área ocupada por organismos fotosintéticos, AOB y el resto de bacterias (determinado por las sondas FISH de *Eubacteria* (Daims et al., 1999)). Este método mide la proporción de AOB y microalgas en términos de área, lo que se supone que es equivalente al volumen y la biomasa de las poblaciones.

Técnica FISH y citometría de flujo

Combinando las señales de fluorescencia y las mediciones de dispersión frontal (FSC) y lateral (SSC), se puede cuantificar la proporción de microalgas y AOB en una muestra biológica. La técnica puede discriminar no sólo por el color, sino también por el tamaño y la complejidad (Kalyuzhnaya et al., 2006), aunque existen algunas limitaciones técnicas. El principal inconveniente es que, para diferenciar ambas poblaciones, el citómetro de flujo debe calibrarse con muestras estándar (normalmente cultivos puros del organismo objetivo). En muestras con alta biodiversidad, la calibración del citómetro de flujo es compleja, requiere mucho tiempo y depende de la muestra que se vaya a analizar en cada caso. La cuantificación precisa por citometría requiere la desagregación completa de las muestras (ya que el citómetro cuenta los eventos) y puede haber un alto grado de sesgo si los agregados se estiman como células individuales en lugar de un grupo de células. En las muestras biológicas, los compuestos inorgánicos (por ejemplo, el debris) pueden interferir con la señal del instrumento. Los resultados de esta técnica se dan en base a eventos (con suerte, células) en lugar de en base a células, lo que podría ser controvertido a la hora de aplicar estos datos directamente a modelos matemáticos.

Técnicas basadas en la secuenciación

Los resultados obtenidos con las técnicas metagenómicas deben interpretarse con precaución, ya que el material genético medido no suele estar correlacionado con la concentración real de la muestra. Los principales factores que influyen en los resultados cuantitativos son: la eficiencia del proceso de extracción de la muestra; el tipo de cebadores utilizados para la amplificación del ácido desoxirribonucleico (ADN); las diferentes relaciones entre la concentración inicial de ADN y la concentración final tras la amplificación, las secuencias disponibles en las bases de datos; y los algoritmos utilizados para el procesamiento de los datos (Di Caprio, 2020). Dependiendo de la población objetivo, se recomienda utilizar un kit de extracción diferente, introduciendo más incertidumbre en la comparación de los taxones biológicos. La secuenciación de microalgas y AOB se realiza por separado, es decir, se secuencia una muestra para obtener la información relativa al dominio Bacteria y otra muestra para el dominio Eucariota. Los resultados obtenidos son la abundancia relativa de AOB en comparación con la abundancia de bacterias y la abundancia relativa de microalgas y en comparación con la abundancia de organismos eucariotas (Steichen y Brown, 2019). Por lo tanto, los resultados obtenidos no son comparables y en la actualidad no es posible determinar la proporción de AOB y microalgas en una muestra. El principal inconveniente es que estas técnicas cuantifican copias de genes en lugar de organismos. Como el número de copias de genes varía entre los genes y los organismos, es difícil correlacionar los resultados obtenidos con el número real de organismos presentes en la muestra.

Foto-respirometrías

La principal ventaja de esta técnica es que es la única que mide la actividad en lugar del número de microorganismos, lo que evita el sesgo debido a la presencia de AOB o microalgas no activas en la muestra. Los resultados pueden aplicarse directamente en modelos matemáticos.

Estrategias de control de la nitrificación

Las bacterias nitrificantes pueden proliferar más rápidamente que las microalgas dependiendo de las condiciones operativas y ambientales (Sánchez-Zurano et al., 2020). De hecho, las bacterias nitrificantes pueden superar a las microalgas como microorganismo dominante en la competencia (Capítulo 4). En algunos casos las microalgas pueden incluso colapsar (González-Camejo et al., 2019a), por lo que la nitrificación debe ser controlada.

Control de la temperatura

Las temperaturas en los raceways suelen estar reguladas por la evaporación. Sin embargo, los FBR pueden alcanzar temperaturas 10 ºC más altas que su entorno (Yeo et al., 2018). Incluir sistemas de refrigeración (González-Camejo et al., 2019a; Mazzelli et al., 2020) puede reducir la temperatura en los PBRs cerrados aunque implica un aumento drástico de los costes del proceso.

TRC y TRH

En términos de eficiencia del proceso, el TRC (o TRH) tiende a ser operado durante el menor tiempo posible para reducir los costes y el uso de la tierra. Sin embargo, un TRC más corto (alrededor de 2 días) puede favorecer la acumulación de NO_2-N debido a una mayor actividad de AOB que de microalgas y NOB, lo que puede reducir la actividad de las microalgas de forma significativa (capítulo 5). Los TRC más largos aumentan la actividad del NOB (Munz et al., 2011), favoreciendo la nitrificación a expensas en valores de TRC de rango medio. González-Camejo et al. (2020c) informaron de que este rango era de 2-4,5 d para una planta piloto MPBR de panel plano al aire libre.

Una vez que se ha establecido una población consistente de bacterias nitrificantes en el cultivo, las microalgas suelen reducir su rendimiento (Capítulo 4). Para cambiar esta tendencia se puede aumentar la tasa de dilución para lavar el exceso de bacterias. El aumento de la tasa de dilución también reduce la concentración de microalgas y SST,

lo que puede aumentar la actividad de las microalgas restantes al reducir la atenuación de la luz.

Control de la carga de nutrientes

La competencia entre las microalgas y las bacterias nitrificantes no sólo depende de los caudales afluentes sino también de la distribución de las especies de nitrógeno. Una tasa de carga de NH_4-N insignificante limita el crecimiento de las AOB. Sin embargo, las microalgas podrán seguir creciendo utilizando NO_2-N o NO_3-N (aunque con una tasa de crecimiento menor).

Adición de inhibidores de la nitrificación

La nitrificación puede inhibirse fácilmente añadiendo aliltiourea (ATU), que no afectó a la actividad fotosintética (Capítulo 5). Al inhibirse el crecimiento de la AOB, no se producirá NO_2-N y, por tanto, la NOB estará limitada indirectamente debido a la escasez de nutrientes, favoreciendo el crecimiento de las microalgas.

4.4. Dinámica de los consorcios de microalgas y bacterias en un raceway acoplado a una membrana (MHRAP) operado a largo plazo

Debido a las mencionadas interacciones entre las microalgas y las bacterias (capítulos 5, 6 y 7), la discusión sobre la influencia de los parámetros operativos y ambientales sobre las comunidades microbianas es el principal objetivo del capítulo 8. Las muestras utilizadas en este estudio se obtuvieron de la planta piloto del MHRAP operada en el Capítulo 5. Los parámetros operativos evaluados en este trabajo fueron: TRH y las corrientes de aguas residuales entrantes (efluente del tratamiento primario y del pretratamiento). La estructura de las comunidades microbianas obtenidas del MHRAP se analizó en un PCoA basado en la matriz de distancias de Bray-Curtis. Se establecieron comunidades bacterianas diferentes durante el MHRAP operado a 6 días con el efluente del tratamiento primario, en comparación al resto de periodos. Esta especialización de la comunidad bacteriana se reprodujo también en la estructura

microalgal, indicando que los factores abióticos de este periodo fueron determinantes para el desarrollo de los microorganismos. La alta intensidad lumínica, el pH alcalino, la acumulación de nitritos y la concentración de amoniaco libre determinaron el rendimiento del reactor operado a 6 días de TRH. El filo *Verrucomicrobiota* fue menos sensible a las condiciones de estrés relacionadas con este periodo. La disminución del TRH junto con el pH, el nitrito y la concentración de FAN desplazó la dominancia de *Verrucomicrobiota* frente a *Proteobacterias*. El efluente procedente del pretratamiento aumentó notablemente la abundancia relativa de *Chloroflexy*. El efluente del pretratamiento promovió condiciones anóxicas para el crecimiento de bacterias desnitrificantes pertenecientes al filo *Chloroflexy*, como la familia *Caldilineaceae*.

Como se señala en el capítulo 5, la tasa de nitrificación también se vio afectada por las condiciones de funcionamiento. En cuanto a la clasificación de géneros de AOB, sólo se encontró *Nitrosomonas* en las muestras obtenidas con el efluente primario, mientras que *Ellin6067* spp. dominó la comunidad de AOB utilizando el efluente del pretratamiento. *Ellin6067* spp. no es un género comúnmente desarrollado en los sistemas de lodos activados, pero se ha detectado sistemas de microalgas y bacterias.

La nitrificación parcial estaba relacionada con la baja abundancia relativa de *Nitrospira* a 6 días de TRH. La disminución del estrés abiótico en la comunidad de NOB resultó en un aumento de la abundancia relativa de los géneros de NOB y propició condiciones favorables para el crecimiento del género *Candidatus Nitrotoga*. La proliferación de *Candidatus Nitrotoga* sólo a los 4 y 2 días de TRH utilizando efluentes del tratamiento primario indicó que, este género era más sensible al amoniaco libre y menos competitivo que *Nitrospira* en sistemas con baja concentración de oxígeno (Zheng et al., 2020).

La especialización microbiana en el periodo operado a los 6 días de TRH también se observó en la composición de géneros de microalgas. El género *Desmodesmus* se adaptó mejor a los factores de estrés de este periodo. Sin embargo, la reducción de la

presión selectiva dio lugar a un predominio de *Coelastrella*, independientemente del TRH y de la corriente de agua residual.

La eficiencia de eliminación de nitrógeno alcanzada a los 2 días de TRH con el efluente del pretratamiento fue el efecto combinado del agotamiento del oxígeno en las horas nocturnas y la proliferación de bacterias nitrificantes junto con las bacterias desnitrificantes.

4.5. Análisis global de sensibilidad e incertidumbre de un modelo de microalgas para el tratamiento de aguas residuales

El metabolismo de las microalgas no puede considerarse un proceso bien caracterizado, ya que algunos parámetros de los modelos matemáticos son inciertos y dependen de la especiación. La aplicación de modelos matemáticos requiere, por tanto, un gran número de suposiciones relativas a la simplificación de los procesos biológicos y los parámetros del modelo. Estas suposiciones son fuentes de incertidumbre que podrían propagarse a través del modelo, generando así incertidumbre en los resultados del mismo. La incertidumbre resultante en los resultados del modelo podría conducir a decisiones erróneas durante el diseño y/o la optimización del proceso. Por lo tanto, la realización de un GSA y UA ayudaría a tratar estas cuestiones mediante el análisis y la comprensión del rendimiento del modelo. Ambos análisis se realizaron sobre 4 periodos de operación obtenidos del rendimiento de la planta piloto MPBR. Los 4 periodos representan las variaciones clave observadas durante los tres años de funcionamiento de la planta piloto MPBR, es decir, las variaciones diarias de la intensidad de la luz y la temperatura, las condiciones de abundancia y escasez de fósforo en el medio de cultivo y las diferentes condiciones operativas.

En general, 11 de los 34 parámetros del modelo se clasificaron como factores influyentes tasa máxima de crecimiento de las microalgas (μ_{ALG}), temperatura mínima para el crecimiento de las microalgas (T_{MAX}), intensidad luminosa óptima para el

crecimiento de las microalgas (I_{OPT}), coeficiente de atenuación debido a los componentes de las partículas (K_I), parámetro de media saturación para el amonio-amoniaco en un medio rico en fósforo (K_{NHX}), tasa máxima de descomposición de las microalgas ($b_{ALG,2}$) constante de velocidad de almacenamiento del fósforo intracelular (q_{XPP}), parámetro de media saturación del fosfato (K_{PO4}), parámetro de inhibición de la utilización del fósforo intracelular en un medio rico en fósforo ($K_{I,PO4}$), parámetro de media saturación del amonio-amoniaco en un medio pobre en fósforo ($K_{NHX-qPP}$), y constantes de la ecuación del coeficiente de transferencia de masa (K_La_r). Los cuatro factores de entrada con el efecto global más importante sobre los resultados analizados fueron μ_{ALG}, q_{XPP}, T_{MAX}, e I_{OPT}. El factor de entrada μ_{ALG} mostró una fuerte influencia en los resultados de la concentración de amonio-amoniaco (S_{NHX}) y de la biomasa algal (X_{ALG}), por lo que las concentraciones de nitrógeno y biomasa en la planta piloto MPBR se debieron principalmente a los procesos de crecimiento de las microalgas. Por el contrario, la principal vía de eliminación de fósforo fue el almacenamiento de X_{PP-ALG} por q_{XPP}. T_{MAX} e I_{OPT} indicaron que las tasas cinéticas de crecimiento y almacenamiento estaban influidas principalmente por las fluctuaciones de la temperatura y la intensidad de la luz.

El UA muestra respuestas diferentes para cada periodo. Este resultado se debe probablemente a dos razones principales: (I) el número de factores sensibles implicados y (II) los procesos que intervienen en cada periodo. Los resultados obtenidos para la concentración de amonio-amoníaco sugieren que el ancho de banda de la incertidumbre depende del número de factores de entrada influyentes que intervienen. La concentración de fosfato sugirió que los procesos implicados en cada periodo tenían efectos diferentes en las variaciones de los resultados del modelo y en la interrelación entre los resultados del modelo. Aunque los valores del factor-p y del ARIL para la concentración de microalgas sugerían una buena respuesta en términos de incertidumbre, un análisis integrado de todos los índices de incertidumbre (ancho de

banda, factor-p, factor-r y valor ARIL) mostraba una elevada incertidumbre en la salida del modelo.

La elevada respuesta de incertidumbre podría atribuirse a los factores calibrados en línea. La reproducibilidad de este enfoque de calibración en línea puede ser cuestionable y podría introducir incertidumbre en el modelo. Estos conjuntos de parámetros del modelo pueden estar distribuidos en un amplio rango de valores para cada parámetro, introduciendo una alta incertidumbre en el modelo. La calibración fuera de línea es un método alternativo a la calibración en línea. En este sentido, la calibración offline permite aislar los procesos cinéticos y controlar las variables implicadas. Dado que un subconjunto de los parámetros se calibró en línea, se utilizó un algoritmo de optimización para ajustar los parámetros del modelo dentro de un rango de datos realista. Así pues, el método fuera de línea puede recomendarse sobre la calibración en línea, al igual que la optimización dinámica de todos los parámetros influyentes.

4.6. Modelo integral de microalgas-bacterias: Aplicación a un fotobiorreactor de membrana en condiciones outdoor

Todos los conocimientos recopilados en los capítulos anteriores se han utilizado en el desarrollo de un modelo integral de microalgas-bacterias. Los procesos biológicos, químicos y físicos descritos en los capítulos 5, 6 y 8 se integraron para simular el tratamiento de aguas residuales basado en consorcios de microalgas y bacterias. El crecimiento de las microalgas, las bacterias heterótrofas, el AOB y el NOB, junto con la precipitación química y la volatilización del nitrógeno, el amoníaco, el dióxido de carbono y el oxígeno fueron las cinéticas incluidas.

La cinética de inhibición del nitrito en el crecimiento de las microalgas es la novedad más significativa introducida en el modelo. Además, hasta donde saben los autores, es el primer modelo de microalgas-bacterias que integra la eliminación de fósforo por

precipitación química. Las fluctuaciones de pH inherentes a los sistemas de microalgas promueven valores de pH alcalinos que impulsan la eliminación química del fósforo.

El modelo fue capaz de simular con un alto grado de precisión la dinámica de los sólidos suspendidos totales y volátiles, la concentración de amonio, nitrito, nitrato y fosfato en los fotobiorreactores. También se obtuvo la abundancia relativa de microalgas, AOB y NOB. Sin embargo, los resultados no pueden compararse con la abundancia relativa descrita en el capítulo 8, ya que el análisis metagenómico proporciona el número de copias de un gen, mientras que el modelo calcula la concentración de biomasa en unidades de masa.

Se estudiaron tres periodos según las interacciones microalgas-bacterias. Se seleccionó P_AOB para analizar la inhibición de las microalgas y NOB por el NO_2-N y la intensidad de la luz, respectivamente. El mismo periodo fue simulado sin la cinética de inhibición por NO_2-N, de forma que se pudo evaluar tanto si las microalgas son realmente inhibidas por el NO_2-N como validar el valor calibrado obtenido en el capítulo 5. El grado de correlación entre la concentración de sólidos suspendidos volátiles experimental y la simulada sin inhibición por NO_2-N disminuyó a 0,5442 (el R^2 entre los resultados experimentales y los modelados con inhibición por NO_2-N fue de 0,9521), lo que indica que el crecimiento de las microalgas sí fue inhibido por el NO_2-N. La cinética de inhibición obtenida a partir del capítulo 5 puede reproducir con precisión los datos experimentales. La tendencia del crecimiento de NOB se reprodujo sin la cinética de fotoinhibición. Por lo tanto, las bajas abundancias relativas de NOB reportadas en el capítulo 8 se debieron probablemente a la alta concentración de pH, FAN y nitritos, más que a la intensidad de la luz.

Las estrategias de control de la nitrificación propuestas en el capítulo 7 se investigaron mediante casos prácticos de estudio. Se evitó la nitrificación parcial aumentando el tiempo de retención de la biomasa de 2 a 4,5 días. La concentración de componentes suspendidos disminuyó significativamente debido al aumento puntual de la tasa de dilución, lo que resultó en un aumento de la intensidad media de la luz dentro del PBR

y del crecimiento de las microalgas. Las microalgas y las bacterias nitrificantes compiten por el NH_4-N. Sin embargo, las microalgas pueden asimilar tanto el NH_4-N como el NO_3-N. Se simuló la dinámica de los sólidos suspendidos totales y de los nutrientes utilizando como fuente de nitrógeno el NO_3-N en lugar del NH_4-N. En los resultados simulados se observó una clara preferencia del NH_4-N sobre el NO_3-N por parte de las microalgas. La biomasa de microalgas se redujo de casi 700 a 450 g $TSS \cdot m^{-3}$.

El modelo propuesto podría ser una herramienta eficaz para la industria a la hora de predecir las microalgas y las bacterias nitrificantes.